

# **New Insights into Homo- and Heterometallic Alkali Metal Amide Chemistry**

by

Gemma Margaret Robertson

A thesis submitted to the Department of Pure and Applied Chemistry, University of Strathclyde, in part fulfilment of the requirements for the degree of Doctor of Philosophy.

June 2012

This thesis is the result of the author's original research. It has been composed by the author and has not been previously submitted for examination which has led to the award of a degree.

The copyright of this thesis belongs to the author under the terms of the United Kingdom Copyright Acts as qualified by the University of Strathclyde Regulation 3.49. Due acknowledgement must always be made to the use of any material contained in, or derived from, this thesis.

This thesis is dedicated to my mum, dad and late gran, who sadly passed away before the completion of this work. I must thank them collectively for their support and encouragement during the course of my university studies and individually for their unique contributions throughout. Mum, thank you for your financial support; the proof reading of various works; and the passing down of your great knowledge of English grammar in the process (a case of work in progress!). Dad, thank you for your daily cheery phone calls, and for the kind gift of a laptop for my birthday, which has made the writing of this thesis so much easier. Gran, thank you for letting me relax at your house; feeding me the best homemade food; and being there to listen to my worries. I know you are still listening.

Gemma

## Acknowledgements

First and foremost, I would like to thank my supervisor and fellow Lanarkshire comrade, Dr. Charlie O'Hara for giving me the opportunity to work on such an exciting and diverse research project. His infinite supply of ideas never ceases to amaze me and his continual enthusiasm and support have been a great source of encouragement to me throughout my studies. His guidance and assistance in conducting this research, whether it be in the lab or getting to grips with various software packages, was gratefully received, as, and above all, was his endearing friendship.

Secondly, I would like to thank Professor Robert Mulvey for his insight into the project, his fascinating stories of times gone by and his great sense of humour (even if he does make jibes at my home town of Carlisle and my eating habits!). I would also like to thank Dr. Eva Hevia for her intriguing thoughts into the project and for the heads up on when House of Fraser have a sale on (a girl after my own heart!). Particular thanks must go to my parents for their incessant support and providing me with all the necessities to achieve my goals in life.

I must also thank Dr. Alan Kennedy, Dr. Pablo García-Álvarez, Dr. Stuart Robertson and Dr. Jan Klett for solving my crystal structures – each must have the patience of a saint. A special thanks to Dr. David Armstrong, whose support and encouragement from the beginning has been great (as too have our discussions on the latest television talent contest). Thanks must also go to Dr. Chris Dodds and Janie-Anne Pickrell, without whom I would have no Schlenks, stoppers, tap adapters *etc.*. Their help in the maintenance and day to day running of the lab was greatly appreciated.

I would also like to thank the final year undergraduate students – Graham Fairweather, Kieran Reilly and Graeme McGrath – who have worked alongside me during this project.

It remains for me to thank my fellow students, past and present – Dr. Benjamin Conway, Dr. Victoria Blair, Matthew McCall, Liam Balloch, Ross Campbell, Sharon Baillie, Zoe Livingstone, Elaine Crosbie, Ben Fleming, Jennifer Garden, Sarah Leenhouts, Emma Herd and Donna Ramsay – for the hilarious banter in the lab and the good times out with. Memories of laughter shared, from Vicki's blonde moments to Ross's uncanny wit, will undoubtedly feature in Rab's stories for years to come.

## Abstract

Currently a hot topic in organometallic chemistry; bimetallic alkali metal magnesium (or zinc) reagents exhibit a unique ‘synergic’ chemistry which cannot be replicated by either monometallic component on its own. This research project focused on enhancing this chemistry by introducing chiral ligands into these bimetallic systems.

The metallate chemistry of achiral *cis*-2,6-dimethylpiperidide (*cis*-DMP) is explored through the synthesis and characterisation of a series of bimetallic bases which contain this ligand. The bis(alkyl)amido lithium and sodium zincates [(TMEDA)·Li(μ-*cis*-DMP)Zn(<sup>*t*</sup>Bu)<sub>2</sub>], **75** and [(TMEDA)·Na(μ-*cis*-DMP)(μ-<sup>*t*</sup>Bu)Zn(<sup>*t*</sup>Bu)], **76**, were successfully prepared and characterised in both the solid- and solution-states, along with the bis(amido)alkyl sodium zincate [(TMEDA)·Na(μ-*cis*-DMP)<sub>2</sub>Zn(<sup>*t*</sup>Bu)], **77**, which was prepared from **76** *via* a ligand reorganisation process. In addition, the tris(amido) sodium magnesiates [(TMEDA)·Na(μ-*cis*-DMP)<sub>2</sub>Mg(*cis*-DMP)], **79** and [{*cis*-DMP(H)}·Na(μ-*cis*-DMP)<sub>2</sub>Mg(*cis*-DMP)], **80**, are also presented. Surprisingly, little attention has been paid to *cis*-DMP despite its structural similarity to diisopropylamide (DA) and 2,2,6,6-tetramethylpiperidide (TMP). By comparison of the complexes produced herein with appropriate complexes from the literature, it has been possible to experimentally determine that the steric bulk of *cis*-DMP closely resembles that of DA but is considerably less bulky than TMP.

Focusing on introducing the chiral diamines (–)-sparteine and *N,N,N',N'*-(1*R*,2*R*)-tetramethylcyclohexane-1,2-diamine [(*R,R*)-TMCDA] into the molecular framework of bimetallic alkali metal zinc reagents, three bis(alkyl)amido sodium zincates were successfully prepared and characterised – two of the form [{chiral diamine}·Na(μ-TMP)(μ-<sup>*n*</sup>Bu)Zn(<sup>*t*</sup>Bu)] [chiral diamine = (–)-sparteine for **96**, (*R,R*)-TMCDA for **97**], and the third [{(*R,R*)-TMCDA}·Na(μ-TMP)(μ-<sup>*t*</sup>Bu)Zn(<sup>*t*</sup>Bu)], **98**. These complexes represent the first examples of (–)-sparteine or (*R,R*)-TMCDA being successfully incorporated within the molecular framework of an alkali metal/zinc synergic system [or indeed any alkali metal/divalent metal synergic system for (*R,R*)-TMCDA], and perhaps most significantly complex **98** is a chiral variant of a synthetically important utility ate base.

Having investigated heterobimetallic systems containing chiral diamines, it was also deemed important to study the alkali metal building blocks, specifically chiral diamine adducts of the synthetically important lithium and sodium bis(trimethylsilyl)amides. ‘Conventional’ (–)-sparteine adducts of lithium and sodium 1,1,1,3,3,3-hexamethyldisilazide (HMDS) were prepared and characterised, [MHMDS·(–)-sparteine] (M = Li for **106**, Na for **107**), along with

an unexpected and ‘unconventional’ hydroxyl-incorporated solvent-separated hexanuclear sodium sodiate,  $[(-)\text{-sparteine}\cdot\text{Na}(\mu\text{-HMDS})\text{Na}\cdot(-)\text{-sparteine}]^+[\text{Na}_4(\mu\text{-HMDS})_4(\mu_4\text{-OH})]^-$ , **108**. Following this unusual result, a similar complex containing (*R,R*)-TMCDA was prepared and characterised, namely the hydroxyl-incorporated solvent-separated pentanuclear sodium sodiate  $[\text{Na}\{(R,R)\text{-TMCDA}\}_2]^+[\text{Na}_4(\mu\text{-HMDS})_4(\mu_4\text{-OH})]^-$ , **109**.

Given that both of these diamine-NaHMDS systems have formally captured monomeric NaOH, we envisaged that similar systems could encapture substoichiometric quantities of other salts, particularly the Lewis amphoteric metal halides, and in doing so, develop a new Group 1 macrocyclic/supramolecular family of complexes. Initially concentrating on LiHMDS systems and investigating several approaches in reaching this goal, we successfully isolated four solvent-separated ion pair complexes; two of the form  $[\text{Li}\cdot\{(R,R)\text{-TMCDA}\}_2]^+[\text{Li}_5(\mu\text{-HMDS})_5(\mu_5\text{-X})]^-$  (where X = Cl for **115**, Br for **116**); and two of the form  $[\text{Me}_6\text{-TREN}\cdot\text{Li}(\mu\text{-X})\text{Li}\cdot\text{Me}_6\text{-TREN}]^+[\text{Li}_5(\mu\text{-HMDS})_5(\mu_5\text{-X})]^-$  [where Me<sub>6</sub>-TREN = tris[2-(dimethylamino)ethyl]amine and X = Cl for **117**, Br for **118**]. The former two complexes have captured one LiX unit and the latter two complexes two LiX units (bearing parallels with **108** where an additional monomeric NaHMDS unit has been trapped). The anions of these complexes – ten-membered (LiN)<sub>5</sub> rings (which host halide guests) – are unprecedented.

---

## Abbreviations

Ac <sub>2</sub> O	acetic anhydride
Ad	adamantyl
AMMM	alkali metal mediated metallation
AMMMg	alkali metal mediated magnesiation
AMMZn	alkali metal mediated zincation
9-BBN	borabicyclo[3.3.1]nonane
BINOL	1,1'-bi-2-naphthol
BIPHEN H2	5,5',6,6'-tetramethyl-3,3'-di- <i>tert</i> -butyl-1,1'-biphenyl-2,2'-diol
Bn	benzyl
Bu	butyl
<sup>n</sup> Bu	<i>n</i> -butyl
<sup>s</sup> Bu	<i>sec</i> -butyl
<sup>t</sup> Bu	<i>tert</i> -butyl
<sup>t</sup> BuH	isobutane
C <sub>6</sub> D <sub>6</sub>	d <sub>6</sub> -benzene
CH <sub>2</sub> O	formaldehyde
CCDC	Cambridge Crystallographic Data Centre
<i>cis</i> -DMP	<i>cis</i> -2,6-dimethylpiperidide
<i>cis</i> -DMP(H)	<i>cis</i> -2,6-dimethylpiperidine
COSY	Correlation Spectroscopy
cy	cyclo
<i>cyc</i>	cyclic
d <sub>8</sub> -THF	d <sub>8</sub> -tetrahydrofuran
DA	diisopropylamide
DA(H)	diisopropylamine
DAME	2-( <i>N,N</i> -dimethylamino)ethyl methyl ether
DBU	1,8-diazabicycloundec-7-ene
DFT	Density Functional Theory
DIBA	diisobutylamide
DIBA(H)	diisobutylamine
DIPAMP	ethane-1,2-diylbis[(2-methoxyphenyl)phenylphosphane]
Dipp	2,6-diisopropylphenyl
DMAP	4-dimethylaminopyridine

---

DME	1,2-dimethoxyethane
DoI	Directed <i>ortho</i> -Insertion
DoM	Directed <i>ortho</i> -Metallation
DOSY	Diffusion Ordered NMR Spectroscopy
<i>d. r.</i>	diastereomeric ratio
<i>e. e.</i>	enantiomeric excess
<i>e. r.</i>	enantiomeric ratio
ESI	electrospray ionisation
Et	ethyl
Et <sub>2</sub> O	diethylether
GOF	goodness of fit
Hal	halide
HCOOH	formic acid
Hetero	heteroatom
HMDS	1,1,1,3,3,3-hexamethyldisilazide
HMDS(H)	1,1,1,3,3,3-hexamethyldisilane
HMPA	hexamethylphosphoramide
HPP	hexahydropyrimidopyrimidide
HSQC	Heteronuclear Single Quantum Coherence
IPr	1,3-bis(2,6-di-isopropylphenyl)-imidazol-2-ylidene
LDA	lithium diisopropylamide
L-DOPA	( <i>S</i> )-2-amino-(3,4-dihydroxyphenyl) propanoic acid
LiTMP	lithium 2,2,6,6-tetramethylpiperidide
MAC	metal anionic crown
Me	methyl
MeLi	methyllithium
Me <sub>3</sub> SiCH <sub>2</sub>	(trimethylsilylmethyl)
Me <sub>3</sub> TACD	1,4,7-trimethyl-1,4,7,10-tetraazacyclododecane
Me <sub>6</sub> -TREN	tris[2-(dimethylamino)ethyl]amine
Mes	mesitylene
MIB	3- <i>exo</i> -morpholinoisoborneol
MgR <sub>2</sub>	di-(trimethylsilylmethyl)magnesium
MW	molecular weight
Naphthyl	naphthalene
NaTMP	sodium 2,2,6,6-tetramethylpiperidide

---



---

NMR	Nuclear Magnetic Resonance
Np	neopentyl
NPh <sub>2</sub>	diphenylamide
Ph <sub>2</sub> NH	diphenylamine
Ph	phenyl
PhNap	phenylnaphthalene
PMDETA	<i>N,N,N',N'',N'''</i> -pentamethyldiethylenetriamine
<sup>i</sup> Pr	<i>iso</i> -propyl
Pyr	pyridine
TADDOL	$\alpha,\alpha,\alpha,\alpha$ -tetraaryl-1,3-dioxolane-4,5-dimethanol
( <i>R,R</i> )-TECDA	<i>N,N,N',N'</i> -(1 <i>R</i> ,2 <i>R</i> )-tetraethylcyclohexane-1,2-diamine
TEEDA	<i>N,N,N',N'</i> -tetraethylethylenediamine
2-MeTHF	2-methyltetrahydrofuran
2,2-Me <sub>2</sub> THF	2,2-dimethyltetrahydrofuran
THF	tetrahydrofuran
THP	tetrahydropyran
( <i>R,R</i> )-TMCDA	<i>N,N,N',N'</i> -(1 <i>R</i> ,2 <i>R</i> )-tetramethylcyclohexane-1,2-diamine
TMEDA	<i>N,N,N',N'</i> -tetramethylethylenediamine
TMP	2,2,6,6-tetramethylpiperidide
TMP(H)	2,2,6,6-tetramethylpiperidine
TMPDA	<i>N,N,N',N'</i> -tetramethylpropanediamine
TMS	trimethylsilane
TMSCl	trimethylsilyl chloride
TMTA	1,3,5-trimethyl-1,3,5-triazinane
TMTCY	1,4,7-trimethyl-1,4,7-triazacyclononane
TPhNap	tetraphenylnaphthalene

---

## Papers Published

1. *Reactions of (-)-sparteine with alkali metal HMDS complexes: conventional meets the unconventional*; Natalie M. Clark, Pablo García-Álvarez, Alan R. Kennedy, Charles T. O'Hara and Gemma M. Robertson, *Chem. Commun.*, **2009**, 5835.
2. *cis-2,6-Dimethylpiperidide: a structural mimic for TMP or DA?*; Ross Campbell, Ben Conway, Graham S. Fairweather, Pablo García-Álvarez, Alan R. Kennedy, Jan Klett, Robert E. Mulvey, Charles T. O'Hara and Gemma M. Robertson, *Dalton. Trans.*, **2010**, 511.
3. *Structural elucidation of TMEDA-solvated alkali metal diphenylamide complexes*; Alan R. Kennedy, Jan Klett, Robert E. Mulvey, Charles T. O'Hara and Gemma M. Robertson, *Eur. J. Inorg. Chem.*, **2009**, 5029.
4. *Synthesis and structural chemistry of alkali metal tris(HMDS) magnesiates containing chiral diamine donor ligands*; Pablo García-Álvarez, Alan R. Kennedy, Charles T. O'Hara, Kieran Reilly and Gemma M. Robertson, *Dalton. Trans.*, **2011**, 5332.
5. *Mixed lithium amide-lithium halide compounds: unusual halide-deficient metal anionic crowns*; Alan R. Kennedy, Robert E. Mulvey, Charles T. O'Hara, Gemma M. Robertson and Stuart D. Robertson, *Angew. Chem. Int. Ed.*, **2011**, 50, 8378.

## Conference Presentations

1. *Chiral ligand incorporation in s-block organometallic complexes*; Poster presentation at the 42<sup>nd</sup> IUPAC Congress Chemistry Solutions 2009 in Glasgow, 5<sup>th</sup> August 2009; USIC 2009 at Heriot Watt, 3<sup>rd</sup> September 2009; and Dalton Main Group Meeting in Manchester, 11<sup>th</sup> September 2009.
2. *Chiral ligand incorporation in alkali metal amide complexes*; Oral presentation at the Inorganic and Analytical Section Postgraduate Talks in Glasgow, 11<sup>th</sup> June 2010; and USIC 2010 at Durham, 9<sup>th</sup> July 2010.
3. *Chiral ligands in s-block organometallic complexes*; Poster presentation at the Pacifichem 2010 conference in Hawaii, 16<sup>th</sup> December 2010.
4. *Molecular salt cellars: halide-deficient metal anionic crowns (MACs)*; Poster presentation at the USIC 2011 conference in Glasgow, 22<sup>nd</sup> July 2011.

---

**Table of Contents**

<b>Acknowledgements</b> .....	<b>I</b>
<b>Abstract</b> .....	<b>II</b>
<b>Abbreviations</b> .....	<b>IV</b>
<b>Papers Published</b> .....	<b>VII</b>
<b>Conference Presentations</b> .....	<b>VIII</b>
<b>Chapter 1: Introduction</b> .....	<b>1</b>
<b>1.1 Alkali Metal Amides</b> .....	<b>1</b>
1.1.1 Preparation of Alkali Metal Amide Complexes .....	1
1.1.2 Synthetic Applications of Alkali Metal Amides .....	2
1.1.3 Structures of Unsolvated Alkali Metal Amides .....	3
1.1.4 Structures of Solvated Alkali Metal Amides .....	14
1.1.5 Solution Structures of Alkali Metal Amides.....	19
<b>1.2 Chiral Metal Amides</b> .....	<b>22</b>
1.2.1 Synthetic Applications of Chiral Lithium Amides .....	23
1.2.2 Structural Chemistry of Chiral Lithium Amides .....	25
1.2.3 Chiral Magnesium Bis(amide) Complexes.....	27
<b>1.3 Mixed-Metal Synergy</b> .....	<b>28</b>
<b>1.4 Heterobimetallic Complexes and Inverse Crown Chemistry</b> .....	<b>31</b>
<b>1.5 Alkali Metal Mediated Metallations</b> .....	<b>34</b>
<b>1.6 Extensions to Chiral Mixed-Metal Systems</b> .....	<b>42</b>
1.6.1 (–)-Sparteine as a Chiral Auxiliary.....	43
1.6.2 ( <i>R,R</i> )-TMCDA as a Chiral Auxiliary.....	48
<b>1.7 Salt Effects in Organometallic Chemistry</b> .....	<b>51</b>
<b>Chapter 2: Enhancing the Scope of s-block Homo- and Heterobimetallic Amide Chemistry</b> .....	<b>58</b>

<b>2.1 <i>cis</i>-DMP Zincate and Magnesiate Complexes .....</b>	<b>59</b>
2.1.1 [(TMEDA)·Li(μ- <i>cis</i> -DMP)Zn( <sup><i>t</i></sup> Bu) <sub>2</sub> ], <b>75</b> .....	63
2.1.2 [(TMEDA)·Na(μ- <i>cis</i> -DMP)(μ- <sup><i>t</i></sup> Bu)Zn( <sup><i>t</i></sup> Bu)], <b>76</b> .....	68
2.1.3 [(TMEDA)·Na(μ- <i>cis</i> -DMP) <sub>2</sub> Zn( <sup><i>t</i></sup> Bu)], <b>77</b> .....	72
2.1.4 [(TMEDA)·Na(μ- <i>cis</i> -DMP) <sub>2</sub> Mg( <i>cis</i> -DMP)], <b>79</b> .....	74
2.1.5 [{ <i>cis</i> -DMP(H)}·Na(μ- <i>cis</i> -DMP) <sub>2</sub> Mg( <i>cis</i> -DMP)], <b>80</b> .....	79
<b>2.2 TMEDA-Solvated Alkali Metal Salts of HMDS.....</b>	<b>84</b>
2.2.1 [KHMDS·TMEDA] <sub>2</sub> , <b>83</b> .....	85
2.2.2 [(NaHMDS) <sub>2</sub> ·TMEDA] <sub>∞</sub> , <b>84</b> .....	87
<b>2.3 Alkali Metal Tris(HMDS) Magnesiates Containing TMEDA Donor Ligand .....</b>	<b>91</b>
2.3.1 [Na(TMEDA) <sub>2</sub> ] <sup>+</sup> [Mg(HMDS) <sub>3</sub> ] <sup>-</sup> , <b>88</b> .....	94
2.3.2 [Li(TMEDA) <sub>2</sub> ] <sup>+</sup> [Mg(HMDS) <sub>3</sub> ] <sup>-</sup> , <b>89</b> .....	96
<b>2.4 Diphenylamide TMEDA-Solvated Homobimetallic Complexes.....</b>	<b>98</b>
2.4.1 [(TMEDA)Li(NPh <sub>2</sub> ) <sub>2</sub> ], <b>90</b> .....	99
2.4.2 [(TMEDA)Na(NPh <sub>2</sub> ) <sub>2</sub> ], <b>91</b> .....	105
2.4.3 [(TMEDA) <sub>3/2</sub> K(NPh <sub>2</sub> ) <sub>2</sub> ], <b>92</b> .....	108
<b>2.5 Alkylmagnesium TMP Complexes .....</b>	<b>115</b>
2.5.1 [(Me <sub>3</sub> SiCH <sub>2</sub> )Mg(μ-TMP)] <sub>2</sub> , <b>94</b> .....	116
2.5.2 [(TMP)Mg(μ-TMP){μ-N(H)C(Me) <sub>2</sub> (CH <sub>2</sub> ) <sub>3</sub> C(Me)=CH <sub>2</sub> }Mg(μ-OCH <sub>2</sub> SiMe <sub>3</sub> ) <sub>2</sub> ], <b>95</b> .....	121
 <b>Chapter 3: Chiral Ligand Incorporation in Magnesiate and Zincate Chemistry .....</b>	<b>126</b>
<b>3.1 Sodium TMP Zincates Containing Chiral Diamine Donor Ligands.....</b>	<b>127</b>
3.1.1 [{(-)-sparteine}·Na(μ-TMP)(μ- <sup><i>n</i></sup> Bu)Zn( <sup><i>t</i></sup> Bu)], <b>96</b> .....	129
3.1.2 [{( <i>R,R</i> )-TMCDA}·Na(μ-TMP)(μ- <sup><i>n</i></sup> Bu)Zn( <sup><i>t</i></sup> Bu)], <b>97</b> .....	133
3.1.3 [{( <i>R,R</i> )-TMCDA}·Na(μ-TMP)(μ- <sup><i>t</i></sup> Bu)Zn( <sup><i>t</i></sup> Bu)], <b>98</b> .....	138
<b>3.2 Alkali Metal Tris(HMDS) Magnesiates Containing Chiral Diamine Donor Ligands</b> .....	<b>140</b>
<b>3.2.1 Complexes 100-103</b> .....	<b>141</b>

3.2.2 Complexes <b>104</b> and <b>105</b> .....	150
<b>3.3 Reactions of Chiral Diamine Donor Ligands with Alkali Metal HMDS Complexes: Conventional Meets the Unconventional</b> .....	<b>157</b>
3.3.1 (–)-Sparteine Complexes <b>106-108</b> .....	158
3.3.2 $[\text{Na}\{(R,R)\text{-TMCD A}\}_2]^+[\text{Na}_4(\mu\text{-HMDS})_4(\mu_4\text{-OH})]^-$ , <b>109</b> .....	166
3.3.3 $[(\text{NaHMDS})_2\{^n\text{Bu}_2\text{Mg}\cdot(R,R)\text{-TMCD A}\}]_\infty$ , <b>110</b> .....	170
 <b>Chapter 4: New Developments in Lithium and Sodium Amide Chemistry; Capturing Halides to Form Metal Anionic Crowns</b> .....	<b>176</b>
<b>4.1 Mixed Lithium Amide-Lithium Halide Compounds: Unusual Halide-Deficient Amido Metal Anionic Crowns</b> .....	<b>178</b>
4.1.1 Complexes <b>115</b> and <b>116</b> .....	179
4.1.2 Complexes <b>117</b> and <b>118</b> .....	184
<b>4.2 Unusual Halide-Deficient Amido Metal Anionic Crowns: Extensions to Mixed Sodium Amide-Sodium Halide Compounds</b> .....	<b>192</b>
4.2.1 $[\text{Me}_6\text{-TREN}\cdot\text{Na}(\mu\text{-Br})\text{Na}\cdot\text{Me}_6\text{-TREN}]^+[\text{Na}_5(\mu\text{-HMDS})_5(\mu_5\text{-Br})]^-$ , <b>127</b> .....	192
4.2.2 $[\text{Me}_6\text{-TREN}\cdot\text{Na}(\mu\text{-I})\text{Na}\cdot\text{Me}_6\text{-TREN}]^+[\text{Na}_5(\mu\text{-HMDS})_5(\mu_5\text{-I})]^-$ , <b>128</b> .....	195
<b>4.3 Non-MAC Mixed Alkali Metal Amide-Alkali Metal Halide Complexes</b> .....	<b>196</b>
4.3.1 $[\{(R,R)\text{-TMCD A}\cdot\text{LiI}\}_2(\text{LiHMDS})_2]_\infty$ , <b>129</b> .....	196
4.3.2 $[\text{Me}_6\text{-TREN}\cdot\text{LiI}]$ , <b>130</b> .....	198
4.3.3 $[\text{Me}_6\text{-TREN}\cdot\text{Na}(\mu\text{-I})\text{Na}(\mu\text{-HMDS})_2\text{Na}(\mu\text{-I})\text{Na}\cdot\text{Me}_6\text{-TREN}]$ , <b>131</b> .....	199
4.3.4 $[\{(R,R)\text{-TMCD A}\cdot\text{Li}(\text{SCN})\}_2(\text{LiHMDS})_2]_\infty$ , <b>132</b> .....	200
4.3.5 $[\text{Me}_6\text{-TREN}\cdot\text{K}(\mu\text{-HMDS})\text{K}(\mu\text{-HMDS})_2\text{K}(\mu\text{-HMDS})\text{K}\cdot\text{Me}_6\text{-TREN}]$ , <b>134</b> .....	203
4.3.6 $[\text{KHMDS}\cdot 12\text{-crown-4}]_2$ , <b>136</b> .....	206
 <b>Chapter 5: Experimental</b> .....	<b>210</b>
<b>5.1 General Experimental Techniques</b> .....	<b>210</b>
5.1.1 Schlenk Techniques .....	210
5.1.2 Glove Box Operation .....	210

---

5.1.3 Solvent and Liquid Reagent Purification.....	211
5.1.4 Preparation of Glassware.....	212
5.1.5 Reagents Used.....	212
5.1.6 Analytical Procedures.....	213
<b>5.2 Preparation of Starting Materials.....</b>	<b>214</b>
5.2.1 Preparation of <sup>n</sup> BuNa.....	214
5.2.2 Preparation of PhCH <sub>2</sub> K.....	214
5.2.3 Preparation of Me <sub>3</sub> SiCH <sub>2</sub> K.....	214
5.2.4 Preparation of (Me <sub>3</sub> SiCH <sub>2</sub> ) <sub>2</sub> Mg.....	215
5.2.5 Preparation of <sup>t</sup> Bu <sub>2</sub> Zn.....	215
5.2.6 Preparation of ( <i>R,R</i> )-TMCDA.....	216
5.2.7 Preparation of Me <sub>6</sub> -TREN.....	217
<b>5.3 Synthesis of Products.....</b>	<b>217</b>
5.3.1 Synthesis of [(TMEDA)·Li(μ- <i>cis</i> -DMP)Zn( <sup>t</sup> Bu) <sub>2</sub> ], <b>75</b> .....	217
5.3.2 Synthesis of [(TMEDA)·Na(μ- <i>cis</i> -DMP)(μ- <sup>t</sup> Bu)Zn( <sup>t</sup> Bu)], <b>76</b> .....	218
5.3.3 Synthesis of [(TMEDA)·Na(μ- <i>cis</i> -DMP) <sub>2</sub> Zn( <sup>t</sup> Bu)], <b>77</b> .....	219
5.3.4 Synthesis of [(TMEDA)·Na(μ- <i>cis</i> -DMP) <sub>2</sub> Mg( <i>cis</i> -DMP)], <b>79</b> .....	219
5.3.5 Synthesis of [{ <i>cis</i> -DMP(H)}·Na(μ- <i>cis</i> -DMP) <sub>2</sub> Mg( <i>cis</i> -DMP)], <b>80</b> .....	220
5.3.6 Synthesis of [KHMDS·TMEDA] <sub>2</sub> , <b>83</b> .....	221
5.3.7 Synthesis of [(NaHMDS) <sub>2</sub> ·TMEDA] <sub>∞</sub> , <b>84</b> .....	221
5.3.8 Synthesis of [KHMDS·( <i>R,R</i> )-TMCDA] <sub>2</sub> , <b>85</b> .....	222
5.3.9 Synthesis of [Na(TMEDA) <sub>2</sub> ] <sup>+</sup> [Mg(HMDS) <sub>3</sub> ] <sup>-</sup> , <b>88</b> .....	222
5.3.10 Synthesis of [Li(TMEDA) <sub>2</sub> ] <sup>+</sup> [Mg(HMDS) <sub>3</sub> ] <sup>-</sup> , <b>89</b> .....	223
5.3.11 Synthesis of [(TMEDA)Li(NPh <sub>2</sub> ) <sub>2</sub> ], <b>90</b> .....	223
5.3.12 Synthesis of [(TMEDA)Na(NPh <sub>2</sub> ) <sub>2</sub> ], <b>91</b> .....	224
5.3.13 Synthesis of [(TMEDA) <sub>3/2</sub> K(NPh <sub>2</sub> ) <sub>2</sub> ], <b>92</b> .....	225
5.3.14 Synthesis of [(Me <sub>3</sub> SiCH <sub>2</sub> )Mg(μ-TMP)] <sub>2</sub> , <b>94</b> .....	225

---

<b>5.3.15</b> Synthesis of $[(\text{TMP})\text{Mg}(\mu\text{-TMP})\{\mu\text{-N}(\text{H})\text{C}(\text{Me})_2(\text{CH}_2)_3\text{C}(\text{Me})=\text{CH}_2\}\text{Mg}(\mu\text{-OCH}_2\text{SiMe}_3)_2]$ , <b>95</b> .....	227
<b>5.3.16</b> Synthesis of $[\{(-)\text{-sparteine}\}\cdot\text{Na}(\mu\text{-TMP})(\mu\text{-}^n\text{Bu})\text{Zn}(^t\text{Bu})]$ , <b>96</b> .....	227
<b>5.3.17</b> Synthesis of $[\{(R,R)\text{-TMCDA}\}\cdot\text{Na}(\mu\text{-TMP})(\mu\text{-}^n\text{Bu})\text{Zn}(^t\text{Bu})]$ , <b>97</b> .....	228
<b>5.3.18</b> Synthesis of $[\{(R,R)\text{-TMCDA}\}\cdot\text{Na}(\mu\text{-TMP})(\mu\text{-}^t\text{Bu})\text{Zn}(^t\text{Bu})]$ , <b>98</b> .....	228
<b>5.3.19</b> Synthesis of $[\text{Li}\{(-)\text{-sparteine}\}_2]^+[\text{Mg}(\text{HMDS})_3]^-$ , <b>100</b> .....	229
<b>5.3.20</b> Synthesis of $[\text{Na}\{(-)\text{-sparteine}\}_2]^+[\text{Mg}(\text{HMDS})_3]^-$ , <b>101</b> .....	230
<b>5.3.21</b> Synthesis of $[\text{Li}\{(R,R)\text{-TMCDA}\}_2]^+[\text{Mg}(\text{HMDS})_3]^-$ , <b>102</b> .....	230
<b>5.3.22</b> Synthesis of $[\text{Na}\{(R,R)\text{-TMCDA}\}_2]^+[\text{Mg}(\text{HMDS})_3]^-$ , <b>103</b> .....	231
<b>5.3.23</b> Synthesis of $[\{\text{K}\cdot(-)\text{-sparteine}\}^+\{\text{Mg}(\text{HMDS})_3\}^-]_\infty$ , <b>104</b> .....	232
<b>5.3.24</b> Synthesis of $[\{\text{K}\cdot(R,R)\text{-TMCDA}\}^+\{\text{Mg}(\text{HMDS})_3\}^-]_\infty$ , <b>105</b> .....	233
<b>5.3.25</b> Synthesis of $[\text{LiHMDS}\cdot(-)\text{-sparteine}]$ , <b>106</b> .....	233
<b>5.3.26</b> Synthesis of “[NaHMDS·(-)-sparteine]”, <b>107</b> .....	234
<b>5.3.27</b> Synthesis of $[(-)\text{-sparteine}\cdot\text{Na}(\mu\text{-HMDS})\text{Na}\cdot(-)\text{-sparteine}]^+[\text{Na}_4(\mu\text{-HMDS})_4(\mu_4\text{-OH})]^-$ , <b>108</b> .....	234
<b>5.3.28</b> Synthesis of $[\text{Na}\{(R,R)\text{-TMCDA}\}_2]^+[\text{Na}_4(\mu\text{-HMDS})_4(\mu_4\text{-OH})]^-$ , <b>109</b> .....	235
<b>5.3.29</b> Synthesis of $[(\text{NaHMDS})_2\{^n\text{Bu}_2\text{Mg}\cdot(R,R)\text{-TMCDA}\}]_\infty$ , <b>110</b> .....	235
<b>5.3.30</b> Synthesis of $[\text{Li}\{(R,R)\text{-TMCDA}\}_2]^+[\text{Li}_5(\mu\text{-HMDS})_5(\mu_5\text{-Cl})]^-$ , <b>115</b> .....	236
<b>5.3.31</b> Synthesis of $[\text{Li}\{(R,R)\text{-TMCDA}\}_2]^+[\text{Li}_5(\mu\text{-HMDS})_5(\mu_5\text{-Br})]^-$ , <b>116</b> .....	237
<b>5.3.32</b> Synthesis of $[\text{Me}_6\text{-TREN}\cdot\text{Li}(\mu\text{-Cl})\text{Li}\cdot\text{Me}_6\text{-TREN}]^+[\text{Li}_5(\mu\text{-HMDS})_5(\mu_5\text{-Cl})]^-$ , <b>117</b> .....	239
<b>5.3.33</b> Synthesis of $[\text{Me}_6\text{-TREN}\cdot\text{Li}(\mu\text{-Br})\text{Li}\cdot\text{Me}_6\text{-TREN}]^+[\text{Li}_5(\mu\text{-HMDS})_5(\mu_5\text{-Br})]^-$ , <b>118</b> .....	240
<b>5.3.34</b> Synthesis of $[\text{Me}_6\text{-TREN}\cdot\text{Li}(\mu\text{-Br})\text{Li}\cdot\text{Me}_6\text{-TREN}]^+[\text{Li}_4(\mu\text{-HMDS})_4(\mu_4\text{-OH})]^-$ , <b>126</b> .....	240
<b>5.3.35</b> Synthesis of $[\text{Me}_6\text{-TREN}\cdot\text{Na}(\mu\text{-Br})\text{Na}\cdot\text{Me}_6\text{-TREN}]^+[\text{Na}_5(\mu\text{-HMDS})_5(\mu_5\text{-Br})]^-$ , <b>127</b> .....	241
<b>5.3.36</b> Synthesis of $[\text{Me}_6\text{-TREN}\cdot\text{Na}(\mu\text{-I})\text{Na}\cdot\text{Me}_6\text{-TREN}]^+[\text{Na}_5(\mu\text{-HMDS})_5(\mu_5\text{-I})]^-$ , <b>128</b> .....	242



---

5.3.37 Synthesis of $[\{(R,R)\text{-TMCDA}\cdot\text{LiI}\}_2(\text{LiHMDS})_2]_\infty$ , <b>129</b> .....	243
5.3.38 Synthesis of $[\text{Me}_6\text{-TREN}\cdot\text{LiI}]$ , <b>130</b> .....	243
5.3.39 Synthesis of $[\text{Me}_6\text{-TREN}\cdot\text{Na}(\mu\text{-I})\text{Na}(\mu\text{-HMDS})_2\text{Na}(\mu\text{-I})\text{Na}\cdot\text{Me}_6\text{-TREN}]$ , <b>131</b> .....	244
5.3.40 Synthesis of $[\{(R,R)\text{-TMCDA}\cdot\text{Li}(\text{SCN})\}_2(\text{LiHMDS})_2]_\infty$ , <b>132</b> .....	245
5.3.41 Synthesis of $[\text{Me}_6\text{-TREN}\cdot\text{K}(\mu\text{-HMDS})\text{K}(\mu\text{-HMDS})_2\text{K}(\mu\text{-HMDS})\text{K}\cdot\text{Me}_6\text{-TREN}]$ , <b>134</b> .....	246
5.3.42 Synthesis of $[\text{KHMDS}\cdot 12\text{-crown-4}]_2$ , <b>136</b> .....	247
<b>Chapter 6: Future Work</b> .....	<b>248</b>
<b>6.1 Further Extensions to the Work Contained Within Chapter 2</b> .....	<b>248</b>
6.1.1 <i>cis</i> -DMP .....	248
6.1.2 HMDS .....	250
6.1.3 Diphenylamide .....	250
6.1.4 TMP .....	251
<b>6.2 Further Extensions to the Work Contained Within Chapter 3</b> .....	<b>251</b>
6.2.1 (–)-Sparteine- and (R,R)-TMCDA-containing Sodium TMP Zincates .....	251
6.2.2 (–)-Sparteine- and (R,R)-TMCDA-containing Alkali Metal Tris(HMDS) Magnesiates .....	254
6.2.3 Conventional and Unconventional (–)-Sparteine- and (R,R)-TMCDA-containing Alkali Metal HMDS Complexes .....	255
<b>6.3 Further Extensions to the Work Contained Within Chapter 4</b> .....	<b>256</b>
6.3.1 Solid- and Solution-Structural Chemistry of MAC Complexes .....	256
6.3.2 Synthetic Chemistry of MAC Complexes .....	258
6.3.3 Non-MAC Mixed Alkali Metal Amide-Alkali Metal Halide Complexes .....	259
<b>Appendix I</b> .....	<b>261</b>
<b>References</b> .....	<b>267</b>

---

## Chapter 1: Introduction

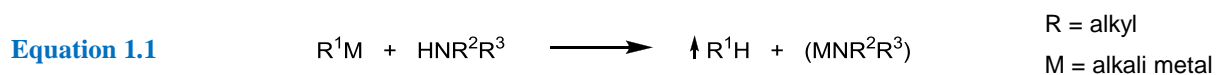
This chapter aims to provide a concise introduction into the structural and synthetic chemistry of the *s*-block metal amides. The initial focus will be on literature relating to single component alkali metal amides, as the development of this topical area of organometallic chemistry is the main basis of this PhD study, with particular attention to the increasing popularity of chiral alkali metal amides. Secondly, a review of the special co-operative chemistry observed when a specific alkali metal reagent is combined with a certain magnesium or zinc reagent within the same compound will be discussed, including how this special chemistry led to the unearthing of a new class of macrocyclic host-guest compounds which have been termed inverse crown ethers. Finally, a brief overview of the beneficial and detrimental effects of the addition of alkali metal halide salts to reactions of organometallic reagents will be discussed.

### 1.1 Alkali Metal Amides

The majority of the new compounds detailed within this thesis are derived from alkali metal amide complexes, and in particular from *secondary* amide species. Therefore, an in-depth review of how the Group 1 secondary amide complexes are prepared, along with their synthetic applications and structural chemistry will be presented.

#### 1.1.1 Preparation of Alkali Metal Amide Complexes

Numerous alkali metal amide complexes (in particular those of Li) are commercially available in various media and quantities.<sup>[1]</sup> They are generally prepared by the metallation of the corresponding amine using an alkali metal alkyl reagent, often of the form BuM (where M = alkali metal). The deprotonation of the acidic proton on the amine group generates a gaseous alkane, which escapes from the reaction mixture (thus driving the reaction to completion), leaving behind the amide product in high yield (Equation 1.1).



The heavier Group 1 alkali metal amide complexes are normally prepared by firstly preparing the Li amide complex *via* Equation 1.1 and then subsequent reaction with MO<sup>t</sup>Bu (where M = Na, K, Rb or Cs) to form the corresponding alkali metal amide product and lithium alkoxide by-product (Equation 1.2).

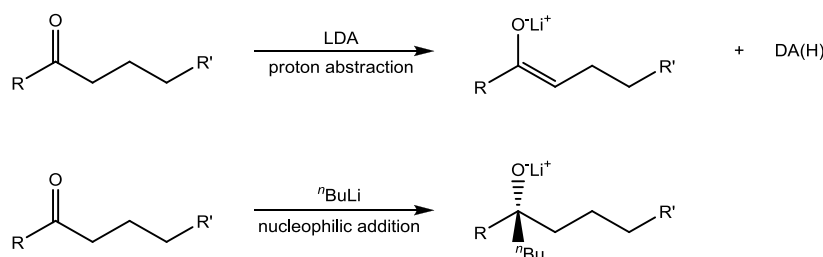


### 1.1.2 Synthetic Applications of Alkali Metal Amides

Alkyl and amido alkali metal reagents, in particular the respective lithium reagents, are amongst the most utilised compounds in synthesis, due to their efficiency in converting relatively unreactive C–H, C–Hal or C–C bonds into highly polar and synthetically useful C–Li bonds. Indeed, more than 95% of all natural product syntheses relevant to the pharmaceutical industry are thought to involve a lithium reagent at some stage.<sup>[2]</sup>

The main reason for the immense popularity and wide applicability of alkali metal amides as reagents in organic synthesis is due to their strong Lowry-Brønsted basicity coupled with their relatively poor nucleophilicity, making them ideal for regio/stereoselective deprotonations. Alkyl alkali metal reagents, on the other-hand, are even stronger Lowry-Brønsted bases; however, their strong nucleophilicity greatly compromises their regioselectivity and functional group tolerance, and they often attack common solvents unless reactions are carried out at sub-ambient temperatures (often below  $-78^{\circ}\text{C}$ ), a requirement which is of course a financial burden on the chemical industry.

The difference in reactivity of such reagents is illustrated well by looking at the reactions of the most utilised lithium amide,<sup>[3]</sup> lithium diisopropylamide, ( $\text{LiN}^i\text{Pr}_2$  or LDA) and the synthetically important alkyllithium, *n*-butyllithium,  $^n\text{BuLi}$  (Scheme 1.1).

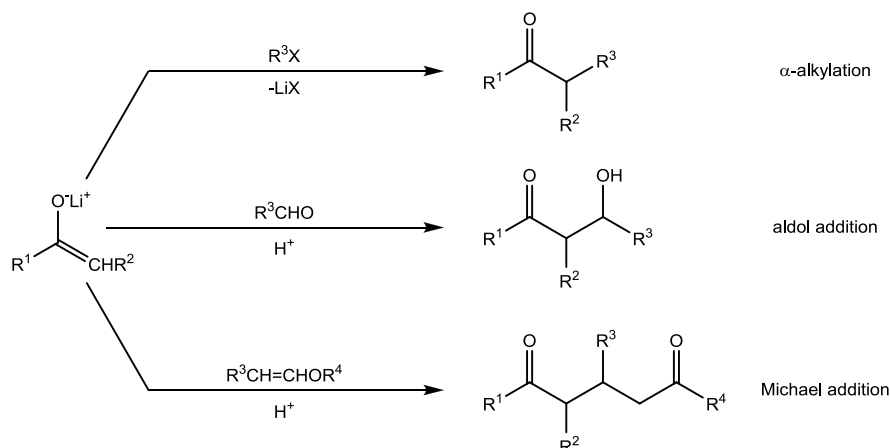


**Scheme 1.1** Differences in reactivity of LDA (top) and  $^n\text{BuLi}$  (bottom).

Due to the increased steric demand of the amide unit of LDA (in comparison to that of the straight chain alkyl group of  $^n\text{BuLi}$ ), addition across the carbonyl function generally does not occur.  $^n\text{BuLi}$  on the other hand, nucleophilically adds across susceptible groups, owing to its less sterically demanding alkyl unit.

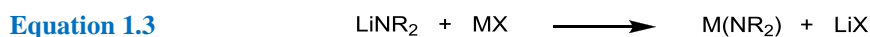
LDA can abstract acidic protons from a number of substrates, including aldehydes, ketones, esters,<sup>[4]</sup> nitrile-containing compounds<sup>[5]</sup> and nitrosamines,<sup>[6]</sup> forming carbanion intermediates. These intermediates can then react with electrophilic reagents, such as alkyl halides, to form new carbon-carbon bonds at the  $\alpha$ -position of such species, with the elimination of lithium halide salts.

As shown in [Scheme 1.1](#), the deprotonation of a ketone (or an aldehyde) with LDA results in the formation of a lithium enolate. As well as reacting with alkyl halides to give the  $\alpha$ -alkylated products, lithium enolates can react with aldehydes and  $\alpha,\beta$ -unsaturated ketones, to give aldol addition products and Michael addition products respectively ([Scheme 1.2](#)).



**Scheme 1.2** Fundamental C–C bond formation reactions involving lithium enolate intermediates.

Turning to an inorganic perspective, lithium amides have been found to be excellent transmetallating agents for the formation of other main group and transition metal amides ([Equation 1.3](#)),<sup>[7]</sup> where the driving force for the reaction is the formation of a lithium halide salt which possesses a large lattice energy of formation.



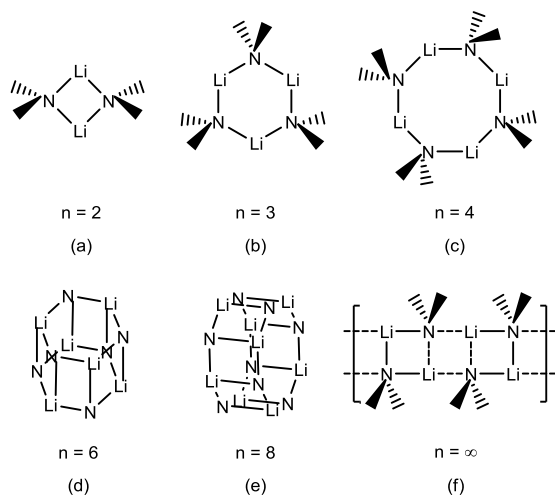
LDA, along with LiHMDS (lithium 1,1,1,3,3,3-hexamethyldisilazide) and LiTMP (lithium 2,2,6,6-tetramethylpiperidide), are amongst the most widely employed synthetic lithium amides, and, as structure is intimately linked to reactivity,<sup>[8]</sup> it is perhaps not surprising they have become (and remain) prime candidates for structural characterisation. An overview of the different structural aggregates which they can form – unsolvated and solvated – will follow.

### 1.1.3 Structures of Unsolvated Alkali Metal Amides

Of the numerous unsolvated alkali metal amide structures [of general formula  $(\text{MNR}^1\text{R}^2)_n$ , where M = alkali metal and  $\text{NR}^1\text{R}^2$  = secondary amide] which have been characterised thus far, lithium amides are by far the most prevalent.<sup>[9]</sup> These amides are based on rings composed of  $(\text{LiN})_n$  units and can form dimeric,<sup>[10]</sup> trimeric,<sup>[11]</sup> tetrameric,<sup>[12]</sup> hexameric<sup>[13]</sup> octameric<sup>[14]</sup> or even polymeric structures<sup>[15]</sup> ([Figure 1.1](#)).

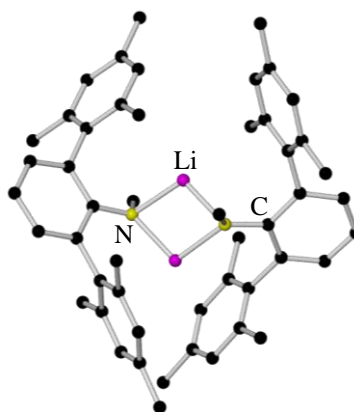
The monomeric Li–N units aggregate extensively as a result of the highly polar nature of the Li–N bonds [due to differences in electronegativity, Li 1.0, N 3.0 (Pauling scale)]<sup>[16]</sup> and the

presence of the lone pair of electrons on the nitrogen centre. The R groups of the amide project above and below the  $(\text{LiN})_n$  plane due to the approximate tetrahedral geometries at the amide N centres, which are thus  $\text{sp}^3$  hybridised. The amido rings can ‘self-associate’ laterally (edge to edge) and this has been termed *ring laddering* [Figure 1.1 (f)].<sup>[9b, 9c, 17]</sup> Laddering can occur when the R groups of the amide are small or flat, and is favourable when the coordination number of the metal atoms increases from two (in the parent ring) to three (for an internal position in the ladder).

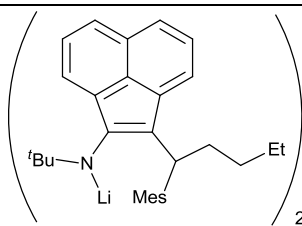


**Figure 1.1** Structural representations of known unsolvated lithium amides.

Of the fourteen lithium dimeric examples, all are silylamides, bar two,  $[\text{LiN}(\text{Me})\text{Ar}^{\text{mes}}]_2$ <sup>[18]</sup> (molecular structure shown in Figure 1.2) and lithium *N-tert-butyl-2-(1-mesitylpentyl)acenaphthylen-1-amide*<sup>[19]</sup> (Table 1.1). The Li centres in all these complexes are formally two coordinate, binding to the nitrogens of the two amide units; however, extra stabilisation is provided by several agostic-type interactions between the electron deficient Li and the H and C atoms of the amido substituents (when phenyl groups are present, Li- $\pi$  bonding also occurs). The bulky nature of these ligands prevents the formation of higher oligomers.



**Figure 1.2** Molecular structure of the dimeric lithium amide  $[\text{LiN}(\text{Me})\text{Ar}^{\text{mes}}]_2$ . H atoms are omitted for clarity.

Unsolvated Dimeric Lithium Amide	Reference
<i>trans</i> -[LiN(Dipp)(SiMe <sub>3</sub> ) <sub>2</sub> ]	[10a]
<i>trans</i> -[LiN{Si(SiMe <sub>3</sub> ) <sub>3</sub> }(SiMe <sub>3</sub> ) <sub>2</sub> ]	[10b]
[LiN(H){N(SiMe <sub>2</sub> Ph) <sub>2</sub> }] <sub>2</sub>	[10c]
<i>cis</i> -[LiN(Si <sup>t</sup> Bu <sub>2</sub> H)(SiMe <sub>3</sub> ) <sub>2</sub> ]	[10d]
<i>cis</i> -[LiN(Si <sup>t</sup> Bu <sub>2</sub> H)( <sup>t</sup> Bu)] <sub>2</sub>	[10d]
<i>trans</i> -[LiN(SiPh <sub>2</sub> H)(SiMe <sub>3</sub> ) <sub>2</sub> ]	[10d]
[LiN(SiMe <sub>2</sub> Ph) <sub>2</sub> ] <sub>2</sub>	[10e]
<i>cis</i> -[LiN(SiMe <sub>2</sub> Ph)(SiMe <sub>3</sub> ) <sub>2</sub> ]	[10f, 10g]
<i>cis</i> -[LiN(Si <sup>t</sup> Bu <sub>2</sub> O){SiF(2,4,6- <sup>t</sup> BuC <sub>6</sub> H <sub>2</sub> )}] <sub>2</sub>	[10h]
<i>cis</i> -[LiN(SiPh <sub>3</sub> )(SiMe <sub>3</sub> ) <sub>2</sub> ]	[10i]
<i>trans</i> -[LiN(SiPh <sub>2</sub> <sup>t</sup> Bu)(SiMe <sub>3</sub> ) <sub>2</sub> ]	[10i]
<i>trans</i> -[LiN{C(Ad)C(H)SiMe <sub>3</sub> }(SiMe <sub>3</sub> ) <sub>2</sub> ]	[10j]
<i>trans</i> -[LiN{Me(2,6-MeC <sub>6</sub> H <sub>3</sub> )}] <sub>2</sub>	[18]
	[19]

**Table 1.1** Known unsolvated dimeric lithium amides.

The first crystallographically characterised lithium amide was lithium 1,1,1,3,3,3-hexamethyldisilazide (LiHMDS), [LiN(SiMe<sub>3</sub>)<sub>2</sub>]<sub>3</sub>,<sup>[11a, 11b]</sup> **1** (Figure 1.3). It is composed of (LiN)<sub>3</sub> units, forming a six-membered trimeric planar ring, where each Li centre is two coordinate. For the other seven trimeric lithium amides, four of which are also silylamides (Table 1.2), the ligands adopt various arrangements to maximise Li···H and Li···C contacts. For example, in [LiN(SiMe<sub>2</sub>H)(SiMe<sub>2</sub><sup>t</sup>Bu)]<sub>3</sub>,<sup>[11j]</sup> four organic substituents belonging to two of the amido units are *cis* to one another, while the remaining two organic substituents belonging to the third amido unit are *trans* with respect to the former four substituents. This leads to Li···H interactions within the complex, and thus different coordination numbers for the three Li centres (two, three and four coordinate respectively). Li···C contacts come into play, for example in [LiN(CH<sub>2</sub>Ph)<sub>2</sub>]<sub>3</sub>,<sup>[11c, 11d]</sup> where the Ph groups are orientated in such a way that they are twisted towards the central ring to exploit Li···C interactions.

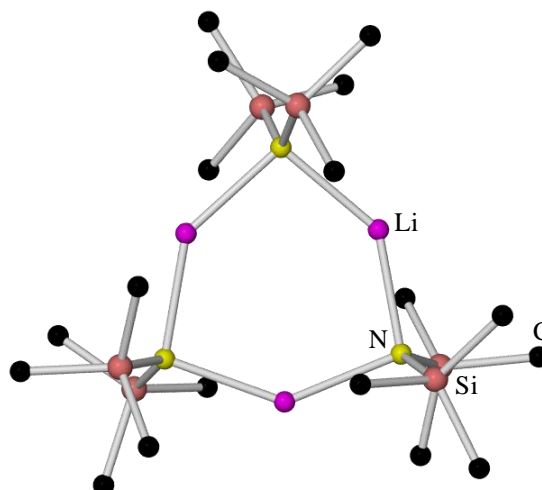


**Figure 1.3** Molecular structure of the trimeric lithium amide  $[\text{LiN}(\text{SiMe}_3)_2]_3$ , **1**. H atoms are omitted for clarity.

Unsolvated Trimeric Lithium Amide	Reference
$[\text{LiN}(\text{CH}_2\text{Ph})_2]_3$	[11c, 11d]
$[\text{LiN}(\text{GeMe}_3)_2]_3$	[11e]
$[\text{LiN}(\text{NPh}_2)(\text{SiMe}_3)]_3$	[11f]
<i>cis</i> - $[\text{LiN}(\text{CH}_2\text{Ph})(\text{SiMe}_3)]_3$	[11g]
<i>cis</i> - $[\text{LiN}(9\text{-BBN})(\text{SiMe}_3)]_3$	[11h]
$[\text{LiN}\{\text{CH}(\text{CH}_3)\text{Ph}\}_2]_3$	[11i]
$[\text{LiN}(\text{SiMe}_2\text{H})(\text{SiMe}_2^t\text{Bu})]_3$	[11j]

**Table 1.2** Known unsolvated trimeric lithium amides.

When the bulkier secondary amines 2,2,6,6-tetramethylpiperidine<sup>[12a]</sup> [TMP(H)] and dicyclohexylamine<sup>[12b]</sup> are utilised, larger eight-membered tetrameric rings are formed. The molecular structure of lithium 2,2,6,6-tetramethylpiperidide (LiTMP),  $[\text{Li}(\text{TMP})]_4$ , **2**, is shown in [Figure 1.4](#). Conventionally, aggregation decreases with increasing steric demand of the amide; however, these tetranuclear species are best considered as pseudo-dimers, where the N–Li–N angles tend to linearity, resulting in the complexes adopting a square-like appearance. When the primary amine  $\text{NHSi}^t\text{Bu}_2\text{Me}$ <sup>[12c]</sup> is employed (complex **3**, [Figure 1.5](#)), an eight-membered distorted cubane is formed, where the Li centre is three coordinate (in comparison to being two coordinate in the near planar tetrameric rings of the former two complexes, where, as for the previous complexes discussed, each Li centre augments its electron density needs through short  $\text{Li}\cdots\text{C}$  contacts).

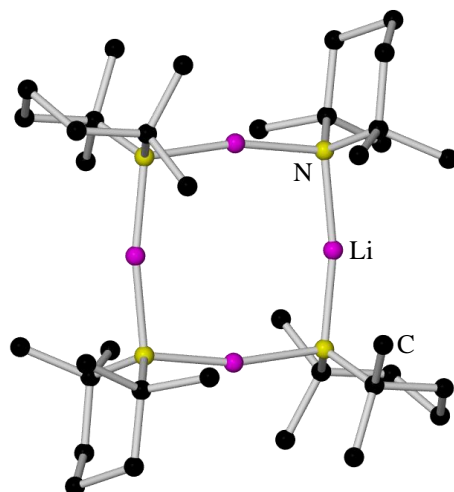


**Figure 1.4** Molecular structure of the tetrameric lithium amide  $[\text{Li}(\text{TMP})]_4$ , **2**. H atoms are omitted for clarity.

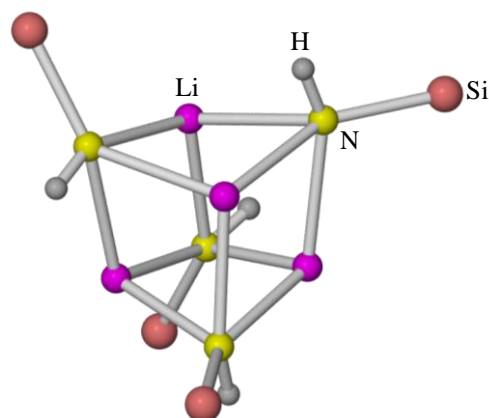


**Figure 1.5** Molecular structure of the cubic tetrameric lithium amide  $[\text{LiNH}(\text{Si}^t\text{Bu}_2\text{Me})]_4$ , **3**. Alkyl substituents are omitted for clarity.

Hexameric and octameric unsolvated lithium amides form through the process of *ring laddering* (*vide supra*).<sup>[9b, 9c, 17]</sup> The only donor-free hexameric lithium amide which has been reported thus far is the cyclic ladder hexamethyleneimidolithium  $[\text{Li}\{\text{cyc-N}(\text{CH}_2)_5\text{CH}_2\}]_6$ ,<sup>[13]</sup> **4** (Figure 1.6). The structure is created by planar  $(\text{LiN})_2$  rings which fuse together in an exclusively *cisoid* manner to give the hexamer, with each Li centre three coordinate (Figure 1.7). When the primary amine  $\text{NH}_2^t\text{Bu}$ <sup>[14]</sup> is employed (complex **5**, Figure 1.8), a cyclic octameric ladder is constructed in the same manner [*i.e.*, lateral fusion of four identical  $(\text{LiN})_2$  dimeric rings, where curving occurs to minimise van der Waals repulsions between substituents]. Note, when amines of higher denticity are employed, for example, the diamine  $[\{\text{N}(\text{H})(^t\text{Bu})\}_2\text{SiMe}_2]$ <sup>[20]</sup> or the triamine  $[\{\text{N}(\text{H})(^t\text{Bu})\}_3\text{SiPh}]$ ,<sup>[20]</sup> more complex aggregates are often obtained.<sup>[10f, 21]</sup>



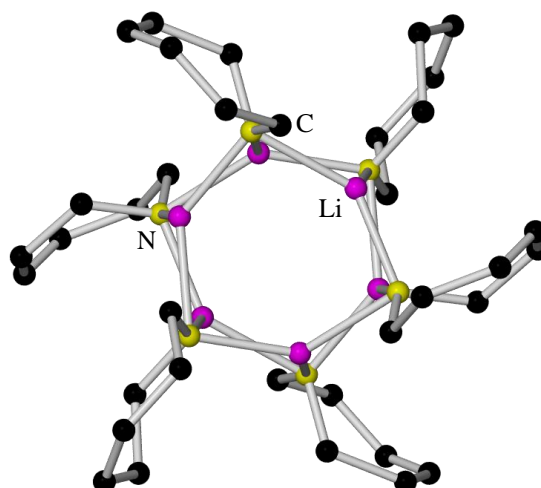


**Figure 1.6** Molecular structure of the cyclic hexameric lithium amide  $[\text{Li}\{\text{cyc-N}(\text{CH}_2)_5\text{CH}_2\}]_6$ , **4**. H atoms are omitted for clarity.

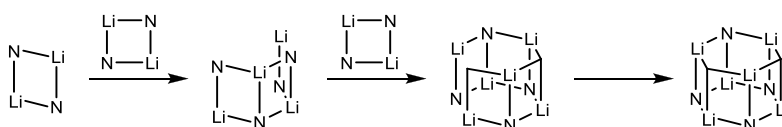


**Figure 1.7** Construction of  $[\text{Li}\{\text{cyc-N}(\text{CH}_2)_5\text{CH}_2\}]_6$ , **4**, from the lateral fusion of  $(\text{LiN})_2$  rings.

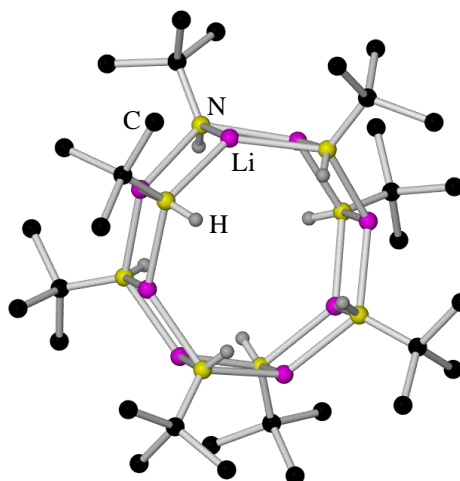


**Figure 1.8** Molecular structure of the cyclic octameric lithium amide  $[\text{LiNH}(\text{tBu})]_8$ , **5**. Alkyl H atoms are omitted for clarity.

Finally, the most synthetically important amide, lithium diisopropylamide (LDA),  $[\text{LiN}^i\text{Pr}_2]_\infty$ ,<sup>[15]</sup> **6**, is unique as it remains the only donor-free polymeric lithium amide to be characterised crystallographically. The structure is composed of a single-stranded helical polymer, with near linear N–Li–N bond angles. Further association is prevented by the bulky amide pendant arms projecting outwards from the Li–N spiral (Figure 1.9).

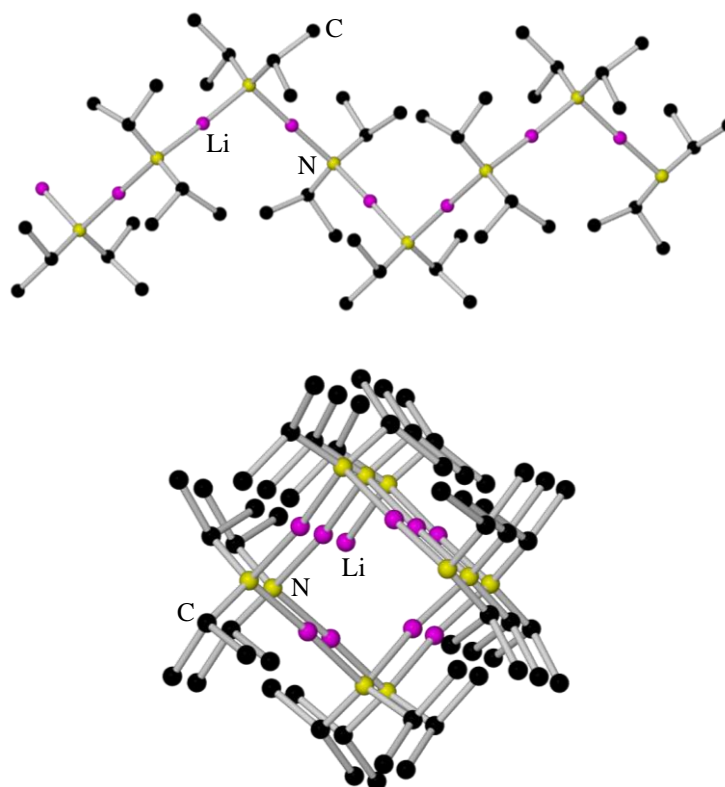


**Figure 1.9** Molecular structure of  $[\text{LiN}^i\text{Pr}_2]_\infty$ , **6**, side view (top) and axial view (bottom). H atoms are omitted for clarity.

Thus far only the amidolithiums have been considered. The remainder of this sub-section will focus on the heavier alkali metal analogues. Regarding sodium amides, only trimeric and polymeric compositions of  $(\text{NaNR}_2)_n$  units exist. The first unsolvated sodium amide to be crystallographically characterised was that of the polymeric sodium 1,1,1,3,3,3-hexamethyldisilazide (NaHMDS),  $[\text{NaN}(\text{SiMe}_3)_2]_\infty$ ,<sup>[22]</sup> **7**, in 1977. Two decades later, a polymorph of the same complex was crystallised – a six-membered trimeric ring (Figure 1.10) – which initially appears to be isostructural with its lithium congener, **1**.<sup>[23]</sup>

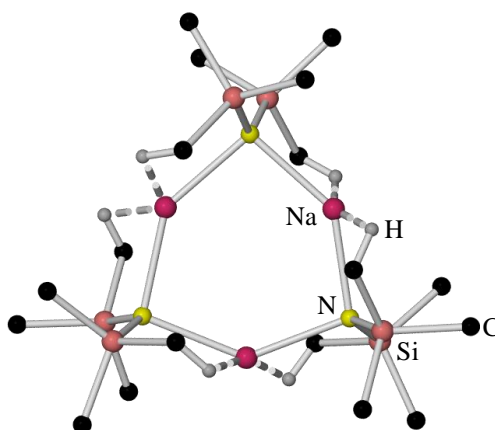


**Figure 1.10** Discrete asymmetric unit of **7**, showing the intramolecular  $\text{Na}\cdots\text{H}$  interactions (represented by dashed bonds). All other H atoms are omitted for clarity.

Each Na centre in the trimeric motif shows C···H intramolecular agostic interactions to two methyl groups originating from different N(SiMe<sub>3</sub>)<sub>2</sub> groups (Figure 1.10). Additionally, the trimeric units are associated *via* two comparatively short intermolecular Na···H interactions (~2.6 Å per molecule) which result in the formation of a loosely connected polymer. This leads to the intermolecularly-bridging Na centres being five coordinate and the non-bridging Na centres four coordinate (Figure 1.11). Although the lithium analogue **1** adopts a planar (MN)<sub>3</sub> ring, as is the case here, it does not require intramolecular interactions to stabilise the metal centre and does not form a polymeric structure through intermolecular interactions.

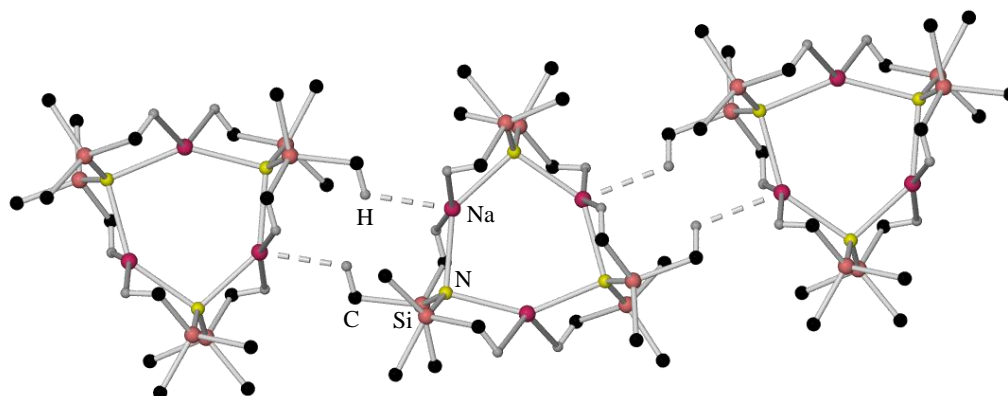


**Figure 1.11** Expanded structure of **7** showing the intermolecular Na···H interactions (represented by dashed bonds). The only other H atoms shown are those involved in the intramolecular Na···H interactions.

The bond distances and bond angles of the trimeric and polymeric forms of **7** are in good agreement, with the exception of the endocyclic N–Na–N angles (139.7° *vs.* 150.2°) and the Na–N distances (2.381 Å *vs.* 2.355 Å). Two other polymeric sodium amides exist; one has a similar composition to that of **7**, namely [NaN(SiMe<sub>2</sub>H)<sub>2</sub>]<sub>∞</sub>,<sup>[24]</sup> **8** (Figure 1.12), which consists of an infinite zig-zag chain of sodium and amide ions, and the other *trans*-[NaN(SiMe<sub>2</sub>Ph)(SiMe<sub>3</sub>)]<sub>∞</sub>,<sup>[10f, 10g]</sup> **9**, is composed of linked dinuclear units which associate to one another *via* intermolecular Na···C contacts (Figure 1.13). In both **7** and **8**, the Na centres are formally two coordinate; however, it has been proposed that in **8** a long range Na···N contact exists due to the less hindered nature of the ligand.

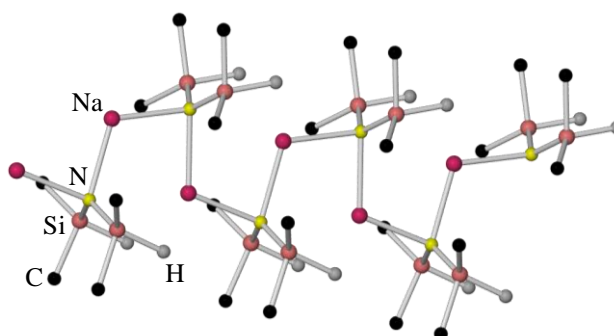


**Figure 1.12** Polymeric structure of [NaN(SiMe<sub>2</sub>H)<sub>2</sub>]<sub>∞</sub>, **8** (long range Na···N contacts not shown). Me H atoms are omitted for clarity.

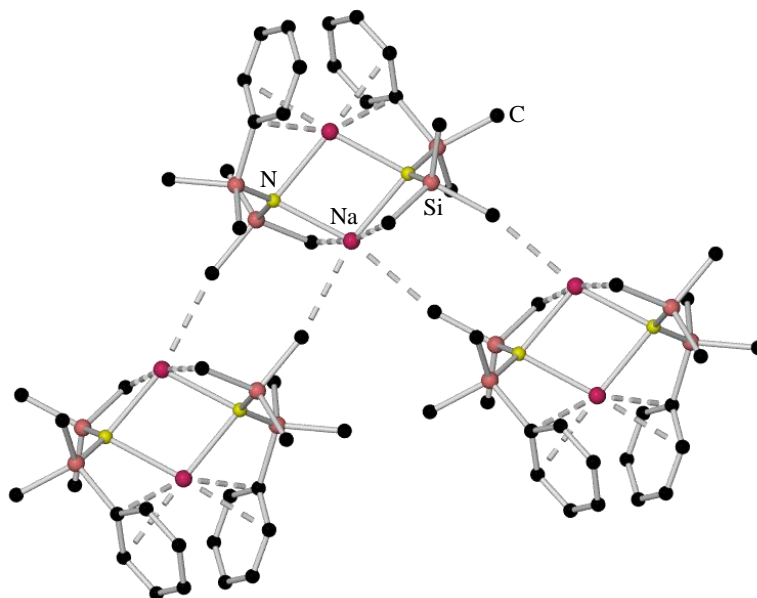


**Figure 1.13** Polymeric structure of *trans*-[NaN(SiMe<sub>2</sub>Ph)(SiMe<sub>3</sub>)]<sub>∞</sub>, **9**, showing the dinuclear units linked *via* intermolecular Na...C contacts (represented by dashed bonds). H atoms are omitted for clarity.

The only truly ‘discrete’ unsolvated sodium amides reported thus far are two trimeric complexes; namely [Na(TMP)]<sub>3</sub>,<sup>[25]</sup> **10** (Figure 1.14) and [NaN(*t*Bu)(SiMe<sub>3</sub>)]<sub>3</sub>,<sup>[26]</sup> **11**. There are no intermolecular contacts between individual trimers in these complexes as found in **7-9**, however, there are still some intermolecular agostic interactions. Comparing **10** with its tetrameric lithium analogue, **2**, the smaller metal cation in the latter complex causes contraction of the M–N bond lengths, resulting in increased steric repulsion between the methyl groups of the bulky TMP ligands; and hence, formation of a cyclic trimer is prohibited.

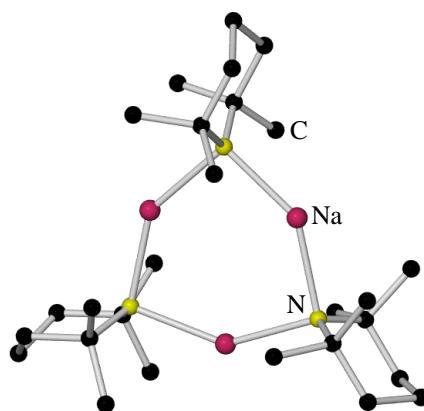


**Figure 1.14** Molecular structure of the trimeric sodium amide [Na(TMP)]<sub>3</sub>, **10**. H atoms are omitted for clarity.

Progressing to unsolvated potassium amides, six complexes have thus far been crystallographically characterised – the highly ionic silylamides, potassium 1,1,1,3,3,3-hexamethyldisilazide (KHMDS), [KN(SiMe<sub>3</sub>)<sub>2</sub>]<sub>∞</sub>,<sup>[27]</sup> **12**, [KN(SiMe<sub>2</sub>H)<sub>2</sub>]<sub>∞</sub>,<sup>[28]</sup> **13**,

$[\text{KN}(\text{SiPh}_2\text{Me})_2]_\infty$ ,<sup>[29]</sup> **14**,  $[\text{KN}\{\text{SiMe}_3\}\{\text{Si}(\text{SiMe}_3)(1,2\text{-C}_6\text{H}_4(\text{Np})_2)\}]_\infty$ ,<sup>[30]</sup> **15**, *trans*- $[\text{KN}(\text{SiMe}_2\text{Ph})(\text{SiMe}_3)]_\infty$ ,<sup>[10g]</sup> **16** and *trans*- $[\text{KN}(\text{SiMe}_2^t\text{Bu})(\text{SiMe}_3)]_\infty$ ,<sup>[31]</sup> **17**. Complexes **12**, **14**, **16** and **17**, all adopt dimeric arrangements which orientate themselves so that the potassium cations are stabilised by both intra- and intermolecular interactions with the methyl and/or phenyl substituents, thus leading to the formation of a polymeric complex through the aggregation of the dinuclear units (molecular structure of complex **17** shown in Figure 1.15). The mononuclear units of complex **15** also arrange themselves so as to maximise intermolecular interactions with the methyl and phenyl substituents. Complex **13** is isomorphous to its sodium analogue (complex **8**), consisting of an infinite zig-zag chain of potassium and amide ions.

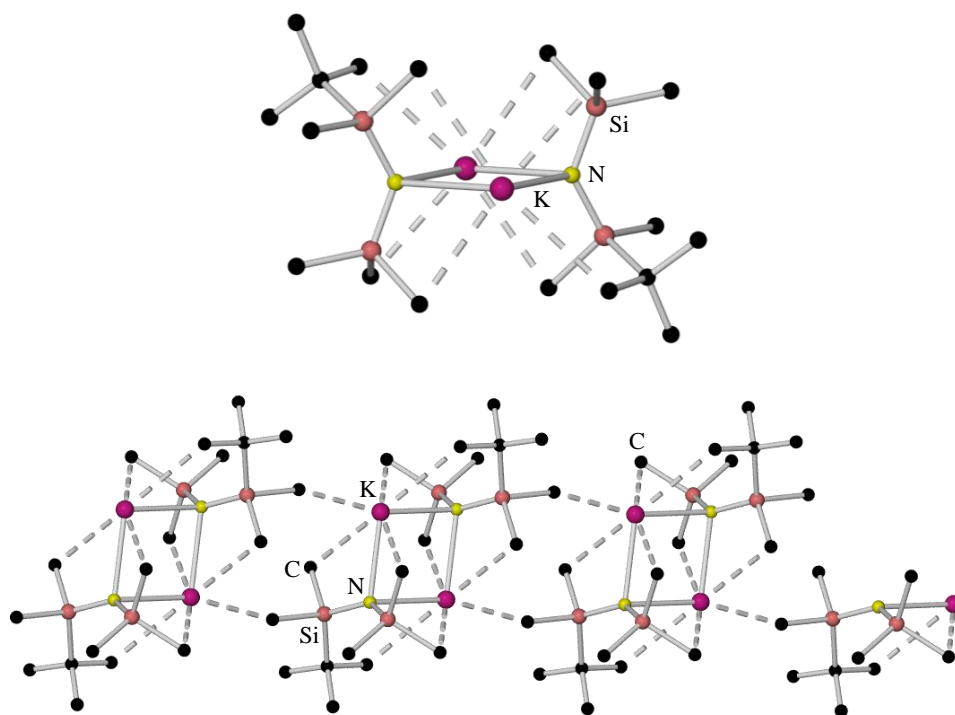


**Figure 1.15** The molecular structure of *trans*- $[\text{KN}(\text{SiMe}_2^t\text{Bu})(\text{SiMe}_3)]_\infty$ , **17**, showing the dimeric unit (top) and the association of these units to form the polymeric complex (bottom) (agostic contacts represented by dashed bonds). H atoms are omitted for clarity.

Rubidium and caesium analogues of both **12** and **16** have been prepared and characterised in the solid-state, as well as a rubidium analogue of complex **14**. Rubidium 1,1,1,3,3,3-hexamethyldisilazide (RbHMDS),  $[\text{RbN}(\text{SiMe}_3)_2]_2$ ,<sup>[32]</sup> **18**, is one of only two truly ‘discrete’ unsolvated heavier alkali metal amides to be reported thus far (of dimeric composition), whilst  $[\text{RbN}(\text{SiPh}_2\text{Me})_2]_\infty$ ,<sup>[29]</sup> **19** and *trans*- $[\text{RbN}(\text{SiMe}_2\text{Ph})(\text{SiMe}_3)]_\infty$ ,<sup>[10g]</sup> **20**, are essentially isostructural to their potassium analogues, *i.e.*, a polymeric array of dimeric units. The caesium equivalents of complexes **18** and **20** (complexes **21**<sup>[32]</sup> and **22**<sup>[10g]</sup> respectively) are isostructural to the rubidium complexes. On progressing down the Group 1 bis(trimethylsilyl)amide and (trimethylsilyl)(dimethylphenylsilyl)amide complexes, the

coordination number at the metal centre increases (by means of a greater number of agostic-type interactions with the methyl and/or phenyl substituents of the respective amide) as the ionic size of the alkali metal increases in order to stabilise the more diffuse electron density of the heavier metals.

A caesium tetrameric example exists when the primary amine  $\text{NHSiMe}_3$ <sup>[33]</sup> is employed (complex **23**, Figure 1.16). Here, an eight-membered cubane, or equivalently a  $\text{Cs}_4$  tetrahedron with a  $\mu_3$ -amido group over each face forms, where the  $(\text{CsN})_4$  units polymerise through intermolecular  $\text{Cs}\cdots\text{C}$  contacts. Interestingly, the space group which was assigned to this complex was revised 15 years after its publication from the original space group  $P23$  to its amended space group  $P\bar{4}3m$ .<sup>[34]</sup> The change in space group involves an increase in the Laue symmetry of the structure, which modifies the bond lengths and angles which were severely distorted in the original space group.

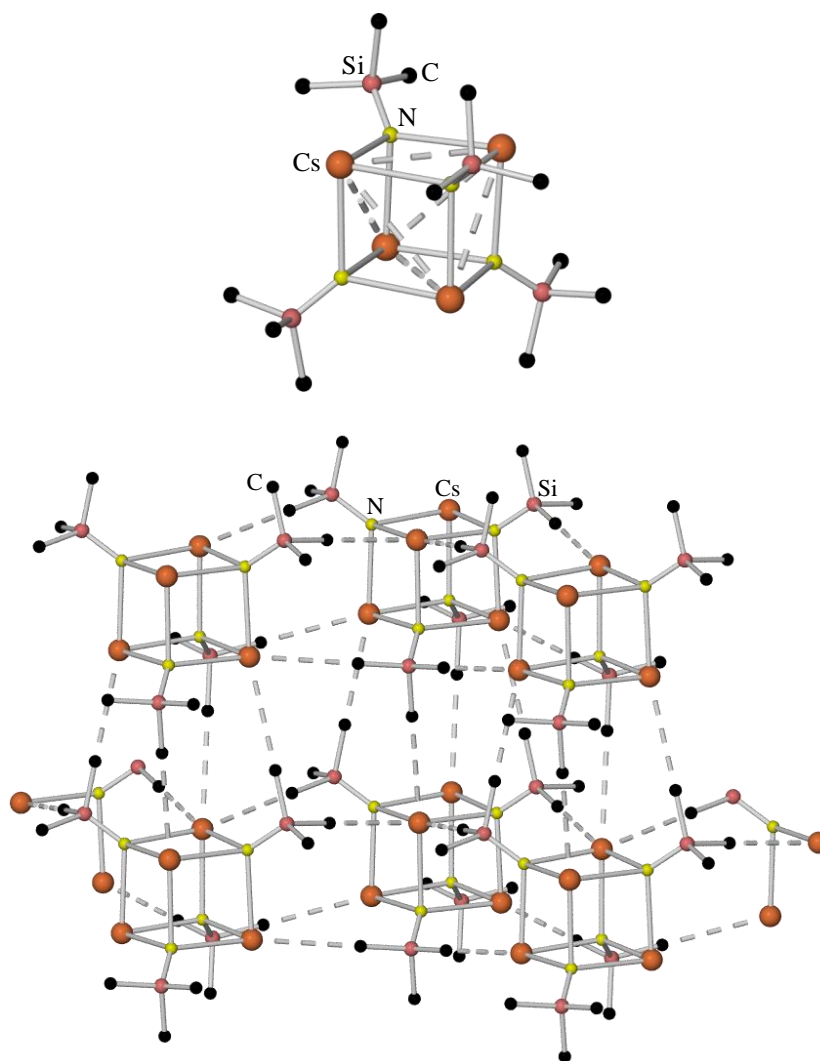


**Figure 1.16** Molecular structure of  $[\text{CsNH}(\text{SiMe}_3)]_x$ , **23**, showing the discrete asymmetric unit (top) and the polymeric structure (bottom). The dashed lines between the Cs atoms in the discrete asymmetric unit illustrate the description of the compound as a  $\text{Cs}_4$  tetrahedron capped on each face with  $\mu_3$ -amido groups. For clarity, these bonds have been removed from the polymeric view of the complex. All H atoms are omitted for clarity.

Unsolvated alkali metal amides are largely insoluble in hydrocarbon solvents due to their oligomeric or more usually polymeric nature, making crystals suitable for X-ray analysis difficult to obtain. If electron rich donor solvents (Lewis bases) are added, the deaggregation of the material often produces homogeneous solutions from which crystals can be grown and analysed. The following sub-section will briefly illustrate some of the common solvated alkali metal amide structural motifs which are encountered, and a select few representative examples will be described.

#### 1.1.4 Structures of Solvated Alkali Metal Amides

All solvated alkali metal amides can be represented by the general formula  $[(\text{MNR}'')_x \cdot (\text{D})_y]_z$ , but the structures vary depending on the metal cation (M), the donor solvent (D), and the steric nature of the amide R groups (NRR').<sup>[17b]</sup> The vast majority of the heavier solvated alkali metal amides (Na, K, Rb or Cs) which have been characterised are monomeric or dimeric, although some ladder structures are known for solvated lithium, sodium and potassium amides, with lithium amides being far the most prevalent. To compensate for the loss of bonding on deaggregation, new dative bonds form between the alkali metal and donor solvent. The different structures which can form are shown below (Figure 1.17).

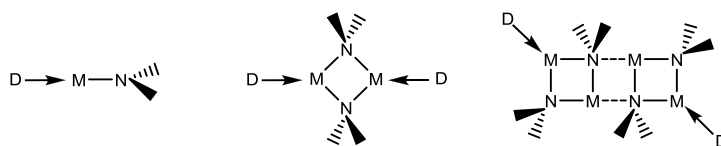


**Figure 1.17** Generalised structures of solvated alkali metal amides.

Focusing on solvated lithium amides, monomeric amides tend to form when multidentate donors such as *N,N,N',N'',N''*-pentamethyldiethylenetriamine<sup>[35]</sup> (PMDETA) or 12-crown-4<sup>[36]</sup> are employed. A prime example is  $[\text{LiHMDS} \cdot 12\text{-crown-4}]$ , **24** (Figure 1.18). Here, the coordination number of the Li centre is five, due to its complexation with the crown ether.

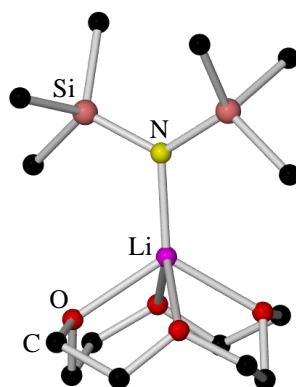


**Figure 1.18** Molecular structure of the monomeric lithium amide,  $[\text{LiHMDS} \cdot 12\text{-crown-4}]$ , **24**. H atoms are omitted for clarity.

When the alkali metal centres become three or four coordinate (depending on the donor solvent used) dimers tend to form. Three coordinate amides form when the complex is prepared in the presence of ethereal<sup>[11c, 12a, 37]</sup> and amine solvents<sup>[38]</sup> or strongly coordinating monodentate donors, such as hexamethylphosphoramide<sup>[11c]</sup> (HMPA) (complex **25**, Figure 1.19). Four coordinate amides by and large only form when the amide ligand has a low steric demand and in this instance, the use of a bidentate donor such as *N,N,N',N'*-tetramethylethylenediamine<sup>[35, 39]</sup> (TMEDA) (complex **26**, Figure 1.19) becomes useful (Table 1.3).

As alluded to earlier, LDA is polymeric when crystallised from hexane. When TMEDA is introduced, a polymer complex is still obtained  $[(\text{LDA})_2 \cdot \text{TMEDA}]_\infty$ ,<sup>[40]</sup> **27**, *i.e.*, deaggregation on the addition of donor has not completely succeeded. In this instance, the polymer is composed of an infinite array of dimers linked by bridging TMEDA ligands (Figure 1.20). As the TMEDA ligands act as bridging ligands and thus only coordinate to each Li centre through one of their available N atoms, the Li centres are rendered three coordinate (*i.e.*, an increase in coordination number from two to three has occurred at the metal centre on the introduction of the donor).

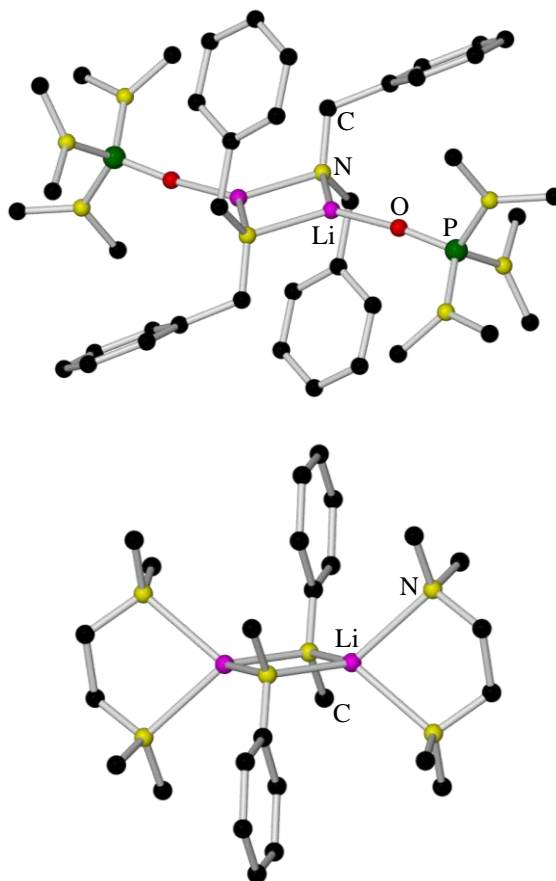


**Figure 1.19** Molecular structures of the dimeric lithium amides  $[\text{LiN}(\text{PhCH}_2)_2 \cdot \text{HMPA}]_2$ , **25** (top) and *trans*- $[\text{LiN}(\text{Me})\text{Ph} \cdot \text{TMEDA}]_2$ , **26** (bottom). H atoms are omitted for clarity.



Solvated Dimeric Lithium Amide	Reference
$[\text{LiN}(\text{PhCH}_2)_2 \cdot \text{Et}_2\text{O}]_2$	[11c]
$[\text{LiHMDS} \cdot \text{Et}_2\text{O}]_2$	[12a, 37a]
<i>trans</i> - $[\text{LiNH}(2,4,6\text{-}^t\text{Bu}_3\text{C}_6\text{H}_2) \cdot \text{Et}_2\text{O}]_2$	[37b]
$[\text{LiHMDS} \cdot \text{THF}]_2$	[37c, 37d]
$[\text{LDA} \cdot \text{THF}]_2$	[37e]
$[\text{LiTMP} \cdot \text{THF}]_2$	[37f]
$[\text{LiN}(\text{PhCH}_2)_2 \cdot \text{HMPA}]_2$	[11c]
$[\text{LiHMDS} \cdot \text{pyridine}]_2$	[38]
<i>trans</i> - $[\text{LiN}(\text{Me})\text{Ph} \cdot \text{TMEDA}]_2$	[35]
$[\text{LiN}=\text{C}=\text{C}(\text{H})\text{Ph} \cdot \text{TMEDA}]_2$	[39a]
$[\text{LiTMP} \cdot \text{TMEDA}]_2$	[39b]

**Table 1.3** A representative selection of known solvated dimeric lithium amides.

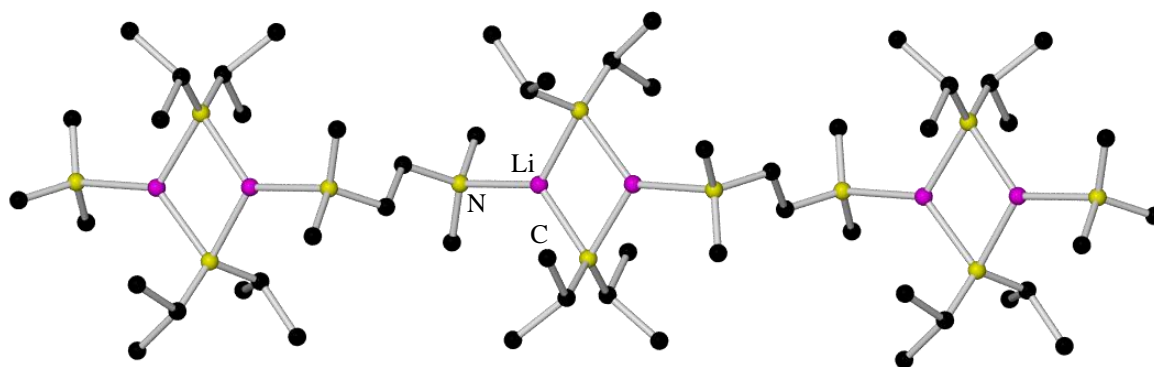


**Figure 1.20** Polymeric structure of  $[(\text{LDA})_2 \cdot \text{TMEDA}]_\infty$ , **27**.

As with unsolvated alkali metal amides, solvated alkali metal amides can aggregate laterally to form ladder structures providing the R groups of the amide are small and flat. Three such ladder structures have been crystallographically characterised –  $[\{\text{LiNH}(\text{PhCH}_2)\}_2 \cdot \text{THF}]_\infty$ ,<sup>[41]</sup> **28**,  $[\text{Li}_2\{\text{cyc-N}(\text{CH}_2)_3\text{CH}_2\}_2 \cdot \text{TMEDA}]_2$ ,<sup>[17b]</sup> **29** and  $[\text{Li}_3\{\text{cyc-N}(\text{CH}_2)_3\text{CH}_2\}_3 \cdot \text{PMDETA}]_2$ ,<sup>[17]</sup> **30**. Focusing on the lithium pyrrolidine complexes **29** and **30** (Figure 1.21), each structure is a finite stepped-ladder consisting of four Li–N rungs. In **29** the outermost lithium atoms are complexed by TMEDA and are therefore four coordinate, while the lithium atoms in the inner rungs remain uncomplexed and three coordinate. In contrast, in **30** the outermost lithium atoms are uncomplexed by the donor solvent, and instead extra rungs at either end of the ladder are present, which are partially broken so as to accommodate the bulky tridentate PMDETA donor ligand. This allows the lithium centres to achieve their more favoured four coordination.

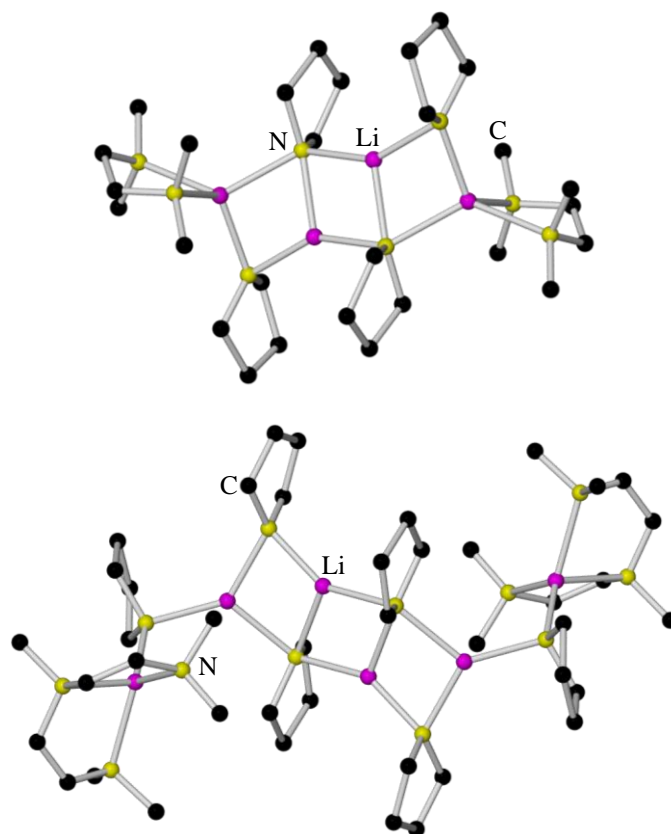


**Figure 1.21** Molecular structures of  $[\text{Li}_2\{\text{cyc-N}(\text{CH}_2)_3\text{CH}_2\}_2\cdot\text{TMEDA}]_2$ , **29** (top) and  $[\text{Li}_3\{\text{cyc-N}(\text{CH}_2)_3\text{CH}_2\}_3\cdot\text{PMDETA}]_2$ , **30** (bottom). H atoms are omitted for clarity.

As a result of strong donor solvents being required to deaggregate the highly ionic, polymeric unsolvated amides of the heavier alkali metals, the majority of Na, K, Rb and Cs solvated amides which have been reported in the literature are monomeric or dimeric, although a few scarce ladder structures are known. Of the heavier alkali metal amides, sodium amides are by far the most frequently encountered. A recent example of a sodium dimer is the THF-solvated NaTMP complex  $[\text{NaTMP}\cdot\text{THF}]_2$ ,<sup>[37f]</sup> **31** (Figure 1.22), which is isostructural to its lithium congener (*vide supra* Table 1.3).<sup>[37e]</sup>

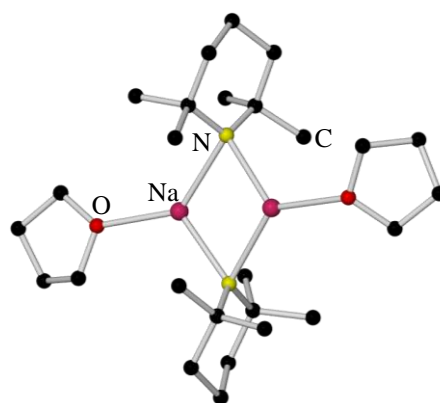


**Figure 1.22** Molecular structure of the dimeric sodium amide  $[\text{NaTMP}\cdot\text{THF}]_2$ , **31**. H atoms are omitted for clarity.

Ladder structures of TMEDA-solvated sodium dimethylamides, with aggregation numbers of 10-12, have been reported by Weiss.<sup>[42]</sup> One such example is  $[\{\text{Na}(\text{NMe}_2)\}_{12} \cdot (\text{TMEDA})_4]$ , **32**. The increased aggregation state arises due to the highly electrostatic Na–N bonding and the low steric demand of the amide.

Moving to solvated potassium amides, a recent example of a dimeric species is the TMEDA-solvated KTMP,  $[\text{KTMP} \cdot \text{TMEDA}]_2$ ,<sup>[43]</sup> **33** (Figure 1.23), prepared by treating KTMP (made from a metathesis reaction between LiTMP and potassium *tert*-butoxide) with an excess of TMEDA in a hexane solution. As is the case with the previously discussed sodium dimer, the high steric demand of the TMP ligand causes the donor molecules (THF in **31** and TMEDA in **33**) to bind to the metal centres in an asymmetric manner. The coordination sphere of the K centres is completed by agostic  $\text{K} \cdots \text{C}$  interactions to a methyl group of the TMP ligands.

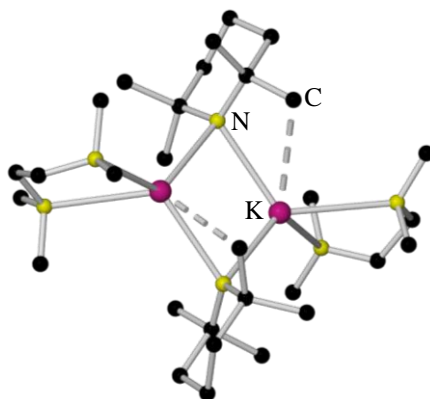


**Figure 1.23** Molecular structure of the dimeric potassium amide  $[\text{KTMP} \cdot \text{TMEDA}]_2$ , **33** (agostic contacts represented by dashed bonds). H atoms are omitted for clarity.

Reported in 2003, the only oligomeric potassium amide possessing a ladder structure is the benzene-solvated potassium (*t*-butyl)(trimethylsilyl)amide  $\text{trans}-[\{\text{KN}(t\text{Bu})(\text{SiMe}_3)\}_4(\eta^6\text{-C}_6\text{H}_6)_2]$ ,<sup>[10g]</sup> **34** (Figure 1.24). It is believed that the use of benzene as the crystallisation solvent, which is  $\eta^6$ -bound to each terminal K centre, causes the partial rupture of the probable infinite polymeric chain adopted by the unsolvated analogue, which, as yet, has only been obtained as a powder.

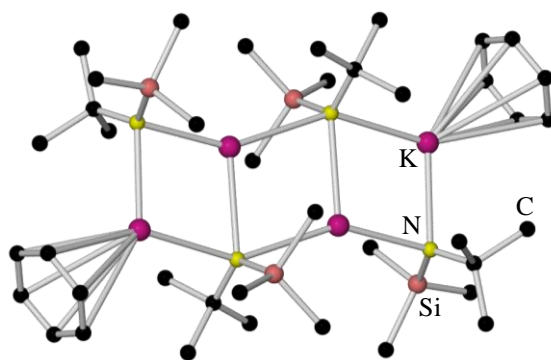


**Figure 1.24** Molecular structure of  $\text{trans}-[\{\text{KN}(t\text{Bu})(\text{SiMe}_3)\}_4(\eta^6\text{-C}_6\text{H}_6)_2]$ , **34**. H atoms are omitted for clarity.

Evident from the wide variety of solid-state structures discussed thus far, one can imagine that the solution-state structures of the alkali metal amides are even more diverse and complex. This is indeed the case, with coexistence of – and dynamic equilibria between – different oligomeric states. The next sub-section will detail the various solution-state structures of the synthetically important lithium amides LDA, LiHMDS and LiTMP.

### 1.1.5 Solution Structures of Alkali Metal Amides

Although the solid-state structures of the alkali metal amides are highly informative, they do not necessarily represent the ‘true’ composition of the base in solution, and as most organometallic reactions are performed in this state, evidence of the various oligomeric states adopted by said bases in solution is highly desirable. Spectroscopic and kinetic studies come to the fore here and hold the key to divulging the ‘real’ active form of the base in the reaction media employed.

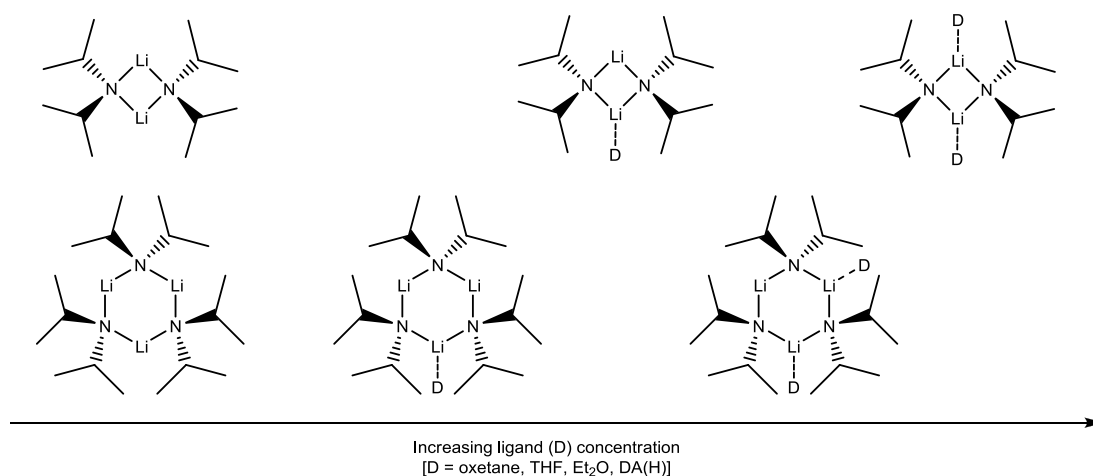
The solution-state structures of the highly important lithium amides LDA, LiHMDS and LiTMP have been extensively studied by two of the pioneers of NMR spectroscopic studies of organolithium species; Williard<sup>[44]</sup> and Collum.<sup>[2, 45]</sup>

NMR analysis of LDA conducted in hexane revealed evidence of an equilibrium mixture of at least three cyclic oligomers; a dimeric, trimeric and un-clarified higher-state oligomeric species.<sup>[46]</sup> On investigating the solution-state structure of the same amide over a wide range of concentrations in THF, the <sup>6</sup>Li and <sup>15</sup>N NMR spectra showed single resonances displaying multiplicities in accordance with a cyclic aggregate assigned to a di-solvated dimer, which is identical to its crystallographically characterised solid-state structure.<sup>[37e, 44, 47]</sup> Di-solvated dimeric arrangements were also observed in Et<sub>2</sub>O, dimethoxymethane and -ethane, and diethoxymethane,<sup>[48]</sup> as well as in the presence of <sup>n</sup>BuOMe, <sup>t</sup>BuOMe, 2-MeTHF, 2,2-Me<sub>2</sub>THF, THP, TMEDA and MeOCH<sub>2</sub>CH<sub>2</sub>NR<sub>2</sub> (NR<sub>2</sub> = NMe<sub>2</sub>, NEt<sub>2</sub>, pyrrolidino) in a 2 : 1 toluene-pentane solution.<sup>[49]</sup> Addition of 1,2-dipyrrolidinoethane and (2-pyrrolidinoethyl)dimethylamine afforded a monomer-dimer mixture, whilst treatment with *trans*-TMEDA or *trans*-1-(dimethylamino)-2-isopropoxycyclohexane provided exclusively mono-solvated monomers.<sup>[49]</sup> Sparteine bound reluctantly, giving a monomer along with substantial concentrations of unsolvated oligomers.<sup>[49]</sup>

The importance of carrying out spectroscopic studies of lithium amides at low ligand concentrations was noted as details of lithium-ligand interactions not available when the ligand is used as the medium can be detected.<sup>[50]</sup> Indeed, progressive addition of ethereal ligands such as oxetane, THF, Et<sub>2</sub>O or DA(H) to a solution of LDA in a 3 : 2 pentane-toluene

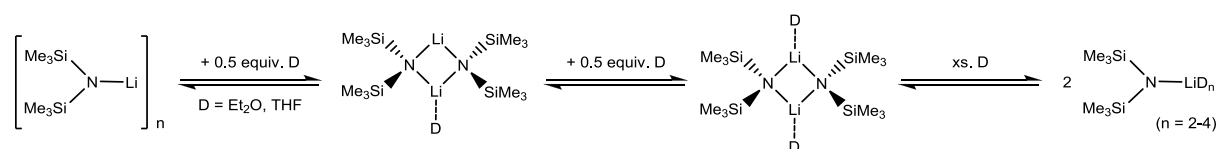
solution (which reveals mixtures of unsolvated cyclic oligomers) shows progressive formation of mono- and di-solvated dimers and trimers, the proportion of each species depending on the ligand type and concentration. In all cases, the di-solvated dimer became the favoured species on addition of a large excess of base (Scheme 1.3).

Spectroscopic studies of LDA in neat TMEDA also displayed a cyclic dimer bearing a single  $\eta^1$ -coordinated diamine ligand on each lithium centre.<sup>[40]</sup> This diamine proved a poor ligand for LDA, being easily and rapidly replaced by THF. The addition of HMPA was found to displace the THF and afforded the di-solvated HMPA-dimeric species.<sup>[51]</sup>



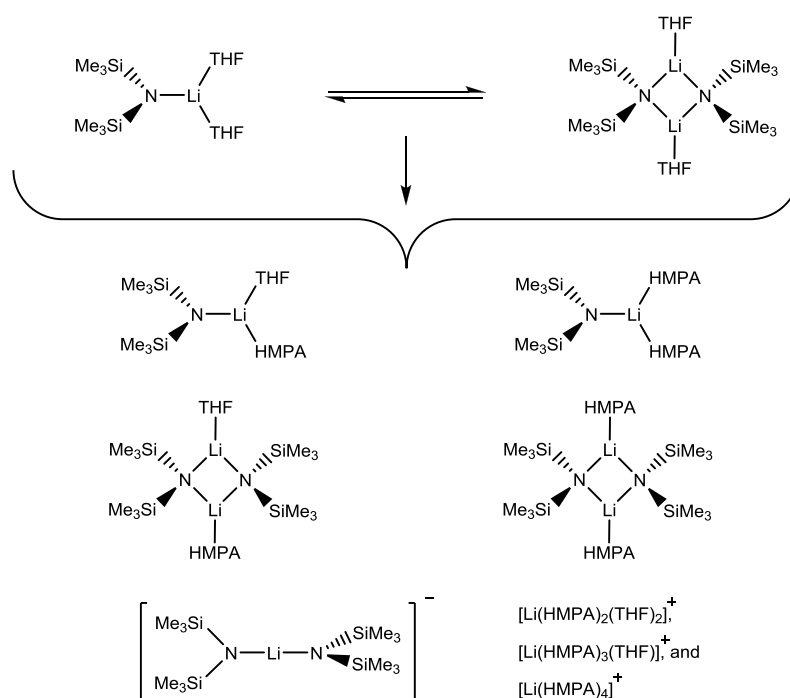
**Scheme 1.3** Oligomers of LDA observed at variable ligand concentration.

Turning to the structure of LiHMDS in solution, it is found to exist as a cyclic dimer in toluene, and in THF a monomer-dimer mixture occurs.<sup>[2]</sup> The changing aggregation states of LiHMDS is once again observed on the progressive addition of Et<sub>2</sub>O or THF to a hydrocarbon solution of this amide (toluene<sup>[52]</sup> or pentane<sup>[52a, 52c]</sup>). The developments noted, were as follows (Scheme 1.4): i) pure LiHMDS in a pentane media was shown to exist as a mixture of unsolvated dimer and higher cyclic oligomer; ii) addition of 0.5 equivalents of ethereal ligand afforded mono-solvated dimers as the major species, along with low concentrations of di-solvated dimers and the original unsolvated oligomers; iii) increasing the ligand concentration to that of LiHMDS (1 : 1 stoichiometric ratio) favoured the exclusive formation of di-solvated dimers; vi) monomeric solvates started to form once an excess of ligand was introduced.<sup>[52b, 52c]</sup> Solvation by monodentate amine ligands has also been examined and was shown to undergo a similar evolution.<sup>[53]</sup>



**Scheme 1.4** Oligomeric changes of LiHMDS on the progressive addition of ethers.

The affinity in solution of LiHMDS for the diamine TMEDA and the triamine PMDETA was brought to light by a comprehensive study on the influence of polydentate amines and ether solvates.<sup>[2, 54]</sup> The addition of TMEDA to pure LiHMDS in toluene afforded a monomeric structure (where the Li centre was coordinated to the two nitrogens of the diamine), along with an unsolvated dimer, with the monomeric species being favoured once an excess of TMEDA had been introduced. On treatment with PMDETA a tetra-coordinated monomer was observed. Complex equilibria were observed on the progressive addition of HMPA to the monomer-dimer mixture of LiHMDS in THF.<sup>[52a]</sup> An excess of this ligand afforded a di-solvated monomer and a tetra-solvated triple ion (Scheme 1.5).



**Scheme 1.5** Monomer-dimer mixture of LiHMDS in THF and the various oligomers observed on incremental addition of ligand.

Examining LiTMP, a 1 : 9 monomer/dimer mixture of this lithium amide was found to exist in THF, with both oligomers containing two THF ligands,<sup>[2, 55]</sup> while in hydrocarbon solvents, two isomeric planar trimers and four isomeric cyclic tetramers were observed (Figure 1.25).<sup>[55a, 56]</sup> Addition of TMEDA to a 2 : 1 toluene-pentane solution of LiTMP afforded a mixture of an open dimer and a monomer, along with a mixture of unsolvated cyclic oligomers. When the THF was present in excess, the monomer became the sole observable species.<sup>[56b]</sup> Upon progressive addition of HMPA to a THF solution of LiTMP, seven new solvates evolved in the following manner (Scheme 1.6): i) addition of 0.3 equivalents of HMPA afforded the appearance of a mixed solvated monomer and the corresponding mixed solvated dimer; ii) as one exceeded 0.5 equivalents of HMPA, a di-solvated dimer and an open dimer were observed; iii) as the HMPA content exceeded stoichiometric values, the

formation of a tri-solvated ion triplet and a tetra-solvated ion triplet were detected; vi) a di-solvated monomeric species started to form once an excess of ligand was introduced.<sup>[51, 57]</sup>

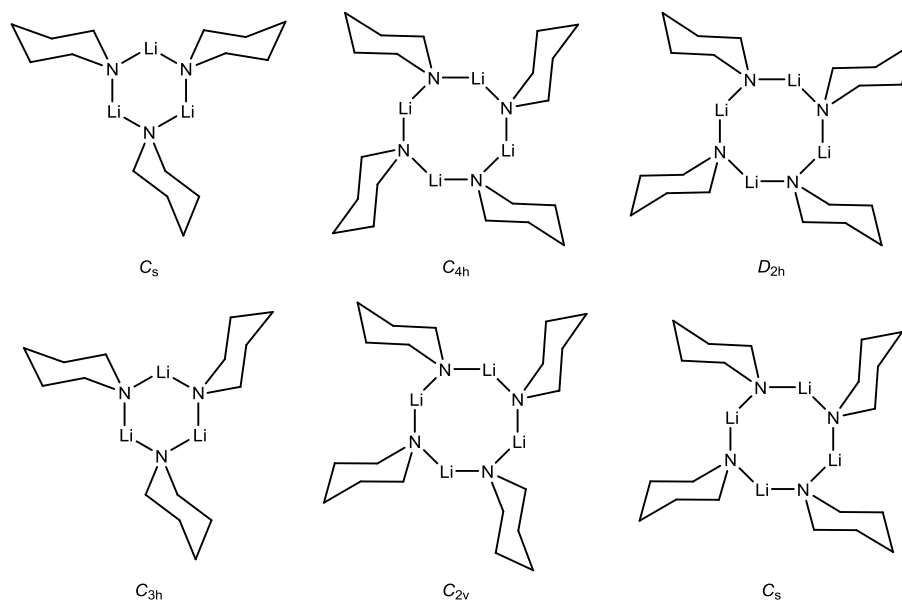
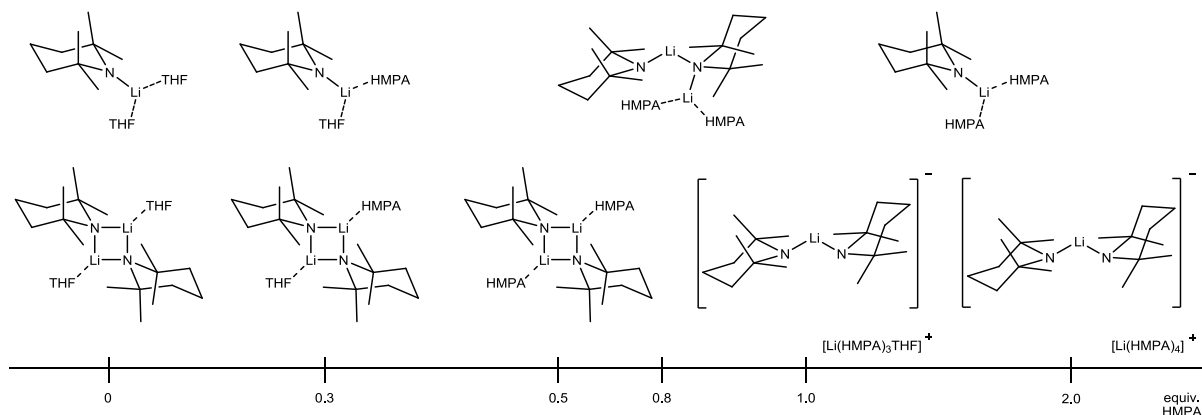


**Figure 1.25** Structural representations of the two isomeric planar trimers and four isomeric cyclic tetramers of LiTMP found in hydrocarbon solvents (Me groups omitted for clarity).



**Scheme 1.6** Oligomers of LiTMP observed at variable ligand concentration.

It is evident from the wide variety of structures adopted by the alkali metal amides, both in the solid- and solution-state, that by making subtle changes to the metal cations, the amide and auxiliary ligands, a vast range of new synthetic reagents can be formed with high regio- and stereoselective potential.

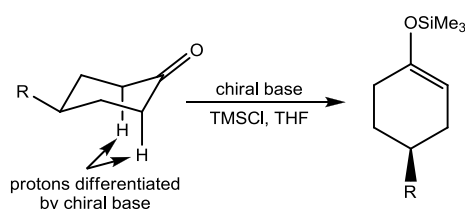
## 1.2 Chiral Metal Amides

With the constant demand for more selective reagents in organic chemistry, the employment of chiral amines to create chiral bases with high levels of chemo-, regio-, stereo- and enantioselectivities has become increasingly popular. Therefore, an in-depth review of the synthetic applications of chiral lithium amide complexes, along with their structural and

solution chemistry will be presented. Developments in the area of chiral magnesium bis(amide) complexes will also be briefly discussed.

### 1.2.1 Synthetic Applications of Chiral Lithium Amides

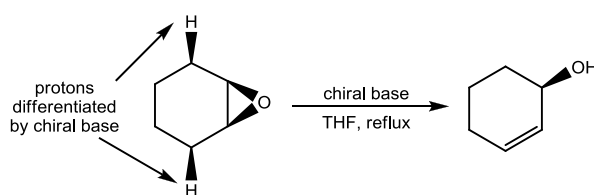
The pioneering work of the independent research groups of Simpkins<sup>[58]</sup> and Koga<sup>[59]</sup> in the late 1980s to early 1990s, in identifying the use of chiral lithium amide bases in the enantioselective deprotonation of prochiral cyclic ketones (Scheme 1.7), initiated extensive research into the uses, structures and intermediates formed during the reactions of chiral lithium amides.



**Scheme 1.7** Enantioselective deprotonation of a prochiral ketone.

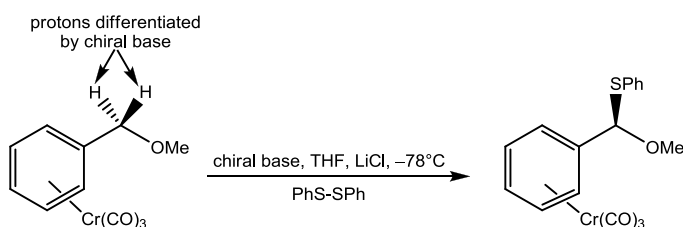
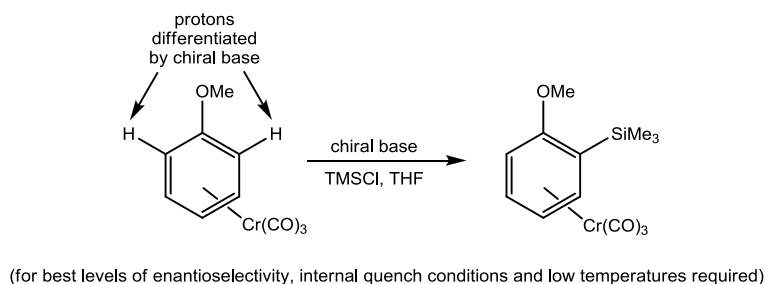
Chiral lithium amides have been used successfully in three main types of asymmetric reactions: (i) deprotonation of conformationally locked prochiral cyclic ketones or steroids containing keto functionality (Scheme 1.7),<sup>[58-60]</sup> (ii) rearrangement of epoxides to allylic alcohols (Scheme 1.8);<sup>[58d, 61]</sup> and (iii) aromatic and benzylic functionalisation of ( $\eta^6$ -arene)chromium(tricarbonyl) complexes (Scheme 1.9).<sup>[62]</sup> All three are examples of asymmetric desymmetrisation: the chiral base discriminates between a pair of protons in a substrate possessing a plane of symmetry to produce an enantiomerically enriched chiral product.

Chiral lithium amides are also used as non-covalently bound chiral auxiliaries, whereby they initially deprotonate a substrate to give a prochiral carbanion (such as an enolate and generate a chiral amine) and on subsequent reaction with an electrophile, the amine directs the electrophile to one enantiotopic face preferentially over the other. Example reactions include the alkylation of cyclic ketones (Scheme 1.10)<sup>[59b, 63]</sup> and aldol reactions<sup>[64]</sup> of esters (Scheme 1.11).

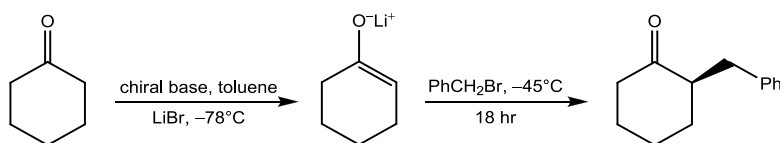


**Scheme 1.8** Rearrangement of an epoxide to an allylic alcohol.

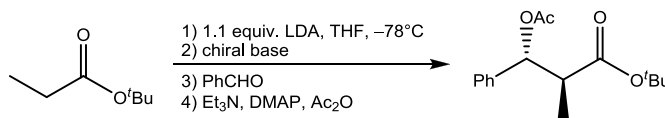




**Scheme 1.9** Aromatic (top) and benzylic (bottom) functionalisation of a ( $\eta^6$ -arene)chromium(tricarbonyl) complex.



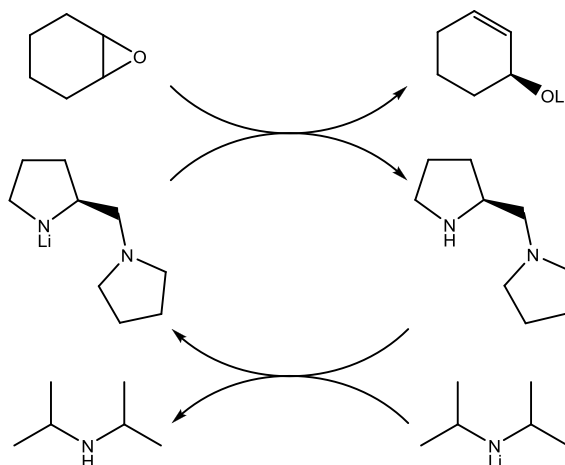
**Scheme 1.10** Alkylation of a cyclic ketone.



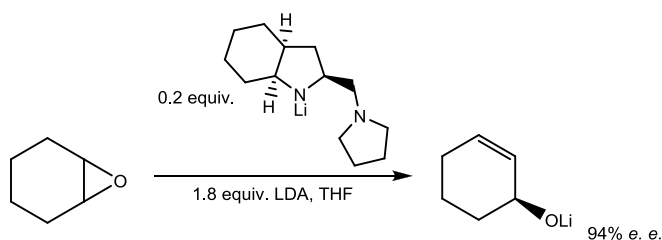
**Scheme 1.11** Aldol reaction of an ester.

Research into chiral amides in asymmetric synthesis has continued to grow and it is now possible to carry out a range of chiral base-mediated asymmetric transformations with high enantioselectivity. Reactions include deprotonation,<sup>[60a, 60m, 65]</sup> desymmetrisation,<sup>[60a, 60m, 61a, 62a, 62b, 66]</sup> alkylation,<sup>[59b, 63b, 67]</sup> reduction<sup>[68]</sup> and conjugate addition reactions,<sup>[69]</sup> alongside kinetic resolution abilities.<sup>[70]</sup>

Attention has recently turned to the possibility of carrying out such reactions catalytically.<sup>[71]</sup> If the chiral amide can be regenerated after the reaction from its protonated form, it can be re-used, allowing for more economical use of the amide.<sup>[72]</sup> The first example, reported by Asami in 1994, was the rearrangement of cyclohexene oxide into an allylic alcohol of 75% *e. e.*<sup>[72a]</sup> Here, the chiral amide is regenerated by reaction with LDA in the presence of excess DBU (1,8-diazabicycloundec-7-ene) (**Scheme 1.12**). Further research showed that by changing the chiral amide used, 94% *e. e.* could be achieved, and excess DBU was no longer required (**Scheme 1.13**).<sup>[72c]</sup>



**Scheme 1.12** Catalytic rearrangement of cyclohexene oxide into an allylic alcohol, with regeneration of the amine.

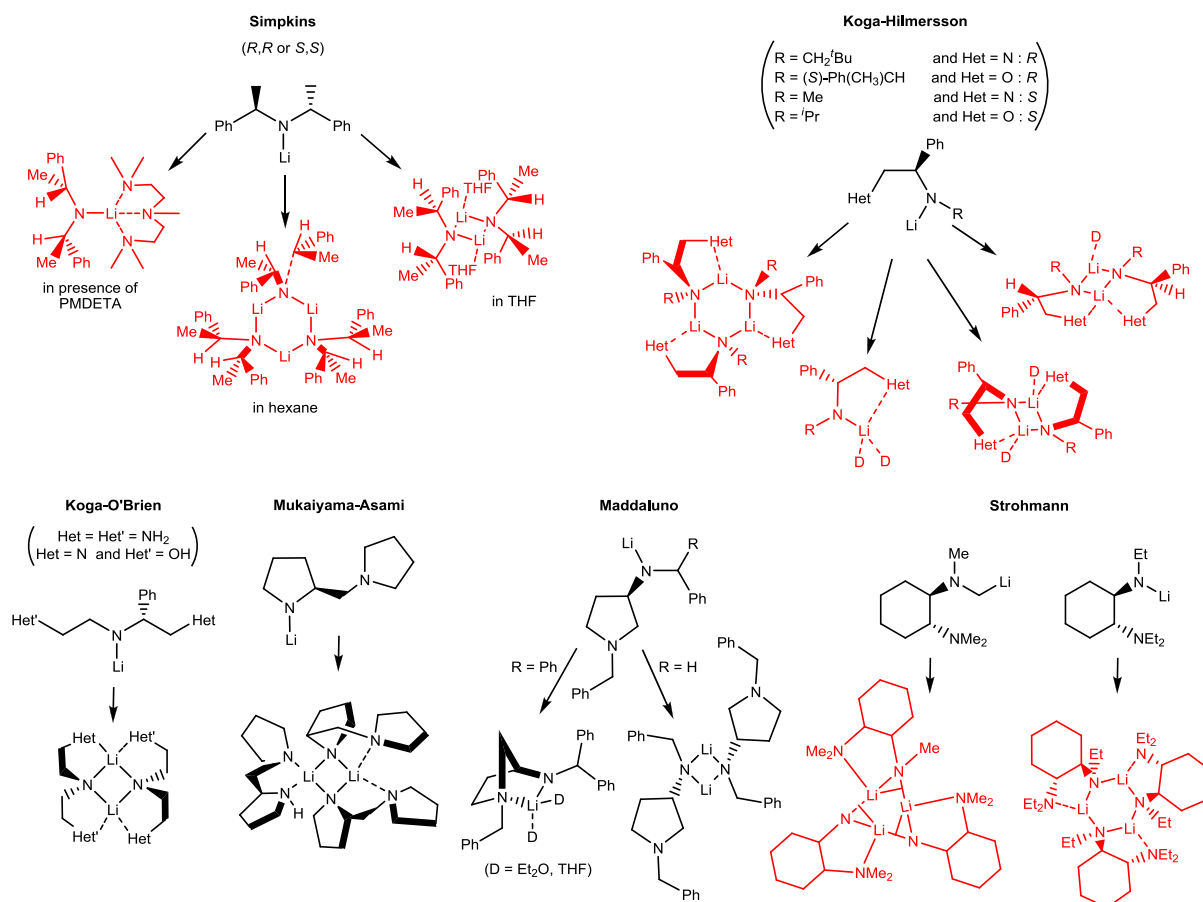


**Scheme 1.13** Catalytic rearrangement of cyclohexene oxide into an allylic alcohol, with increased *e. e.*, using the chiral lithium amide shown.

Knowledge of the conformations adopted by chiral lithium amides, both in the solid- and solution-state, is paramount to understanding the stereochemical outcome of the reaction process in which they are involved. An overview of the different structural aggregates which they can form (both in the solid- and solution-state) will follow.

### 1.2.2 Structural Chemistry of Chiral Lithium Amides

Of the vast array of chiral lithium amides employed in synthesis, six categories have been structurally characterised by crystallography and NMR spectroscopy analyses. They are classified according to the research groups which unearthed such discoveries: Simpkins,<sup>[11i, 73]</sup> Koga-Hilmersson,<sup>[60d, 74]</sup> Koga-O'Brien,<sup>[75]</sup> Mukaiyama-Asami,<sup>[61f, 76]</sup> Maddaluno<sup>[77]</sup> and Strohmann (Scheme 1.14).



**Scheme 1.14** Structural representations of chiral lithium amides and the motifs they adopt in the solid- (red) or solution-state (black).

Taking the six categories in turn, Simpkins' chiral lithium amide crystallised as an unsolvated trimer when grown from a hexane solution,<sup>[11i]</sup> and when the donor PMDETA was introduced or crystals grown from a THF solution, a mono-solvated monomer<sup>[73b]</sup> and di-solvated<sup>[73a]</sup> dimer were formed respectively. The Li centres are two coordinate in the unsolvated form, three coordinate in the di-solvated dimer, and four coordinate in the mono-solvated monomer owing to the tridentate nature of the PMDETA ligand (Scheme 1.14).

Koga-Hilmersson's chiral lithium amides stem from Simpkins' work, where an additional heteroatom is now present, which can intramolecularly chelate to the metal.<sup>[60d, 74]</sup> These amides form trimers in the absence of donor solvents and a mixture of di-solvated monomers, mono-solvated dimers and di-solvated dimers in the presence of etheral solvents.<sup>[74b, 74f]</sup> In the unsolvated complex the Li centres are three coordinate, bridging between two amide units and receiving extra stabilisation through the coordination of the intramolecular heteroatom. The Li centres are four coordinate in the di-solvated monomer and the di-solvated dimer, binding to the amide N, the other heteroatom and two molecules of donor in the di-solvated monomer and bridging between two amide units and coordinating to one donor molecule and

heteroatom respectively in the di-solvated dimer. In the mono-solvated dimer the Li centres are in different coordination environments. One Li is four coordinate, being surrounded by two amide units, where the heteroatoms of both intramolecularly coordinate to the Li centre. The other Li is three coordinate, bridging between the two amide units and coordinating to one molecule of donor. Competitive Li...H agostic interactions with the various R groups of the amide prevented the interaction with more donor solvent (Scheme 1.14). Recently a cyclic dimer in toluene has been observed in hydrocarbon solution with the sterically hindered lithium amide analogue derived from (*S*)-*N*-isopropyl-*O*-triisopropylsilyl valinol.<sup>[74h]</sup>

NMR spectroscopic studies of Koga-O'Brien's chiral lithium amides revealed evidence of an unsolvated symmetrical dimer, where the nitrogen of the amide bears two substituents, each with a chelating heteroatom, thus affording tetra-coordination around the Li centres (Scheme 1.14).<sup>[75]</sup>

The Mukaiyama-Asami chiral lithium amide is composed of a pyrrolidine lithium amide with a methyl-pyrrolidine side arm at the  $\alpha$ -position. NMR spectroscopic analysis indicated intramolecular interactions between the Li cation and the  $\gamma$ -heteroatom and the formation of a four-membered Li<sub>2</sub>N<sub>2</sub> ring complex, where each Li centre is four coordinate. One Li centre is coordinated to two amide units (interacting with the  $\gamma$ -heteroatom of both) and one Li centre is coordinated to the two aforementioned amides with a chelating amine providing extra electron density (Scheme 1.14).<sup>[61f, 76]</sup>

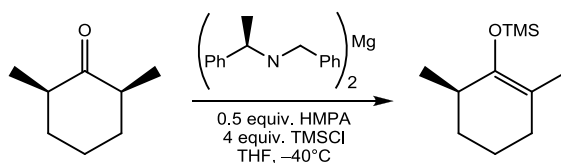
Solution studies in d<sub>8</sub>-THF of Maddaluno's chiral lithium amides, based on disubstituted-3-aminopyrrolidines, showed that when a relatively bulky group (such as a CHPh<sub>2</sub> group) was on the 3-amido moiety, a norbornyl-like rigid conformation was adopted in which the Li cation is chelated by both nitrogen atoms of the amide, thus imposing folding of the ring. When the amido substituent was the less rigid CH<sub>2</sub>Ph group, a dimer formed, in which both Li centres are two coordinate (Scheme 1.14).<sup>[77]</sup>

Finally, the recent crystallographic data obtained by Strohmamm working on lithiated *N,N,N',N'*-(1*R*,2*R*)-tetramethylcyclohexane-1,2-diamine [(*R,R*)-TMCD] <sup>[78]</sup> and *N,N,N',N'*-(1*R*,2*R*)-tetraethylcyclohexane-1,2-diamine [(*R,R*)-TECD] <sup>[79]</sup> disclosed trimer complexes, where the Li centres are three coordinate due to the bidentate nature of the chiral amides (Scheme 1.14).

### 1.2.3 Chiral Magnesium Bis(amide) Complexes

Over the past few years, chiral magnesium amides have also shown promise as effective reagents in asymmetric synthesis, both as homo- and heteroleptic species.<sup>[80]</sup> Complementing

their more reactive lithium counterparts, they have an enhanced degree of functional group tolerance, good selectivity (due to their poor nucleophilicity) and the ability to carry out reactions at ambient temperatures (Scheme 1.15).



**Scheme 1.15** Enantioselective deprotonation of *cis*-2,6-dimethylcyclohexanone and silyl enol formation.

As with alkali metal amides, magnesium amide complexes can form unsolvated and solvated complexes (Figure 1.26). However, whereas only one anion is required to achieve neutral organo-alkali metal complexes, two anions are required for neutral organomagnesium complexes. Magnesium bis(amide) complexes are commonly based on rings composed of  $(\text{MgN})_n$  units and as such have great potential to bridge, resulting in insoluble polymeric material. To inhibit aggregation to either monomers or dimers, bulky amides or donor solvents are utilised.<sup>[81]</sup> In general, monomers and dimers form in highly polar solvent media or in the presence of strongly Lewis basic donor ligands. Higher aggregation complexes can be achieved using specialised ligand systems such as dianionic amides and imides ( $\text{RN}^{2-}$ ).<sup>[82]</sup>

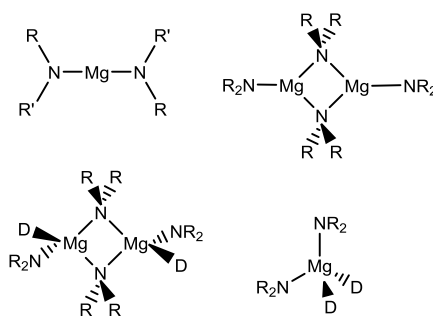


**Figure 1.26** Structural representations of unsolvated (top) and solvated (bottom) magnesium bis(amide) complexes.

Although chiral magnesium amides have been studied to a great extent, the use of chiral mixed-metal synergic bases containing active, anionic magnesium (or zinc) has thus far been largely neglected. Given the relevance to this project of the synergic effects shown by mixed-metal bases, some background information into the phenomenon of synergy and the structural motifs adopted by the arising co-operative heterobimetallic complexes will be given, before going on to discuss chiral mixed-metal systems.

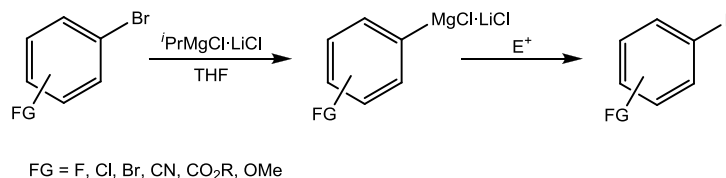
### 1.3 Mixed-Metal Synergy

Synergy – “interaction or cooperation of two or more agents to produce a combined effect greater than the sum of their separate effects”.<sup>[83]</sup>

The special ‘synergic’ chemistry which results when a specific alkali metal reagent is combined with a particular magnesium (or zinc) reagent is an extremely important developing area of organometallic chemistry. The resulting bimetallic alkali metal magnesium (or zinc) reagents are found to cohere with the above definition and exhibit a chemistry which cannot be replicated by either monometallic ‘agent’ on its own.<sup>[84]</sup>

This emerging class of compounds is currently being intensively studied by several independent groups, both here in the UK, but also worldwide (including in particular France, Germany and Japan). The studies which have been undertaken in these research laboratories have unearthed a number of very interesting and important results.

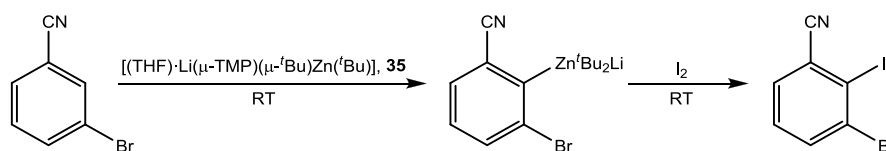
In the past few years, Mulvey has documented that alkali metal-mediated metallations (magnesiations, zincations or manganations) can occur when arenes, metallocenes or heterocycles are treated with an appropriate synergic base.<sup>[85]</sup> Focusing on magnesiates, Knochel has discovered two new classes of magnesium bases (‘turbo-Grignard’ reagents and ‘turbo-Hauser’ reagents), with the composition  $\text{RMgCl}\cdot\text{LiCl}$  or  $\text{R}_2\text{Mg}\cdot\text{LiCl}$  (where  $\text{R} = ^i\text{Pr}$ ) and  $\text{TMPMgCl}\cdot\text{LiCl}$  or  $(\text{DA})_2\text{Mg}\cdot 2\text{LiCl}$  respectively, which can regioselectively generate functionalised aryl and heteroaryl magnesium compounds.<sup>[86]</sup> Historically, lithium bases (alkyl- or amidolithiums) would be used for such reactions; however, the resulting aryllithiums are generally highly reactive, which often prohibits the inclusion of functional groups such as esters or ketones within the arene molecule. Independently, magnesium bases have low kinetic basicity, but with Knochel’s mixed Li/Mg bases this property is greatly enhanced and allows selective magnesiation to occur with a wide variety of highly functionalised arenes and heterocycles (Scheme 1.16). Mongin has shown that a number of substrates, including fluoro-aromatics, chloro-pyridines, thiophenes and oxazoles, can undergo a deprotonation-electrophilic quench sequence at relatively high temperatures using lithium tri(*n*-butyl)magnesiates.<sup>[87]</sup> Oshima has revealed that it is possible to induce facile selective halogen-magnesium exchange reactions *via* lithium di(*n*-butyl)isopropylmagnesiates and tri(*n*-butyl)magnesiates.<sup>[88]</sup>



**Scheme 1.16** Turbo-Grignard reagents allow halogen-magnesium exchange to occur in the presence of many functional groups.

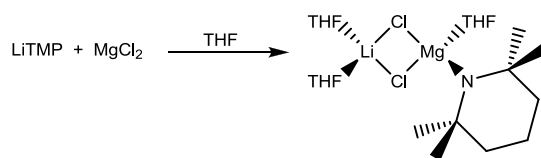
Turning to zincates, Kondo and Uchiyama have developed a bis(alkyl)amido lithium zincate, formulated as “ $\text{LiZn}^i\text{Bu}_2(\text{TMP})$ ”, which has demonstrated high levels of selectivity and

reactivity in Directed *ortho*-Metallation (DoM) reactions.<sup>[89]</sup> Structural evidence for this reagent came to the fore almost 15 years later when Mulvey *et al.* determined its X-ray structure [(THF)·Li(μ-TMP)(μ-<sup>t</sup>Bu)Zn(<sup>t</sup>Bu)],<sup>[90]</sup> **35**, (*vide infra*). The base has been shown to be highly chemoselective, achieving the direct zincation of a wide variety of highly functionalised aromatic and heteroaromatic substrates, including for example those with amine, cyano, ester and halogen functions as well as various substituted pyridine, thiophene, quinoline and isoquinoline heteroaromatics (Scheme 1.17).<sup>[89-90]</sup> Mongin and Uchiyama have revealed that a number of substrates, including pyrazine, pyridazine, pyrimidine, quinoxaline, various five-membered aromatic heterocycles and substituted aromatics and heteroaromatics, can undergo a deprotonation-electrophilic quench sequence at ambient temperatures using a mixed lithium-zinc species composed of ZnCl<sub>2</sub>·TMEDA and LiTMP in a 1 : 3 ratio in THF.<sup>[91]</sup> Recently, through the use of Diffusion Ordered NMR Spectroscopy (DOSY) studies, Mulvey and García-Álvarez have elucidated that with this mixture (which, when all components are considered can be represented by the empirical formula “(TMEDA)·LiTMP·Zn(TMP)<sub>2</sub>·2LiCl”) lithiation occurs first, followed by transmetalation with Zn(TMP)<sub>2</sub> (as proposed by Mongin) and have identified LiTMP·2LiCl±TMEDA as the possible active lithiating base.<sup>[92]</sup>



**Scheme 1.17** Deprotonation of 3-cyano-bromobenzene with [(THF)·Li(μ-TMP)(μ-<sup>t</sup>Bu)Zn(<sup>t</sup>Bu)], **35**, and subsequent iodine trapping.

The metallating reagents detailed above have been synthesised *in situ* by the mixing together of two or more distinct components to form various formulations. Apart from the synergic bases developed by Mulvey *et al.* and the lithium zincate synthesised by Kondo and Uchiyama, which have been characterised in both the solid- and solution-state, little or no knowledge of the exact structural composition of the actual reagent carrying out the deprotonation(s) or of key intermediates along the reaction pathway utilising the other aforementioned magnesiates is present. Mulvey *et al.* however, were successful in this uncharted area in 2008, where the molecular structure of Knochel’s “[TMP]MgCl·LiCl” base was determined by X-ray crystallography, and found to have a non-planar LiClMgCl ring with TMP strongly bound to Mg (and not Li). In addition, no less than three solvating THF molecules complete the coordination sphere of the metal centres (Scheme 1.18).<sup>[93]</sup>



**Scheme 1.18** Synthesis of Knochel's turbo-Hauser base.

Due to their ability to chemo-, regio- and stereoselectively deprotonate a diverse range of substrates, these remarkable compounds appeal not only to laboratory synthetic chemists (organometallic, inorganic or organic); but also to industrial chemists working in the fine chemical, pharmaceutical, and research and development sectors.

## 1.4 Heterobimetallic Complexes and Inverse Crown Chemistry

It is evident from the volume of literature discussed thus far, that the chemistry of the homometallic alkali metal amido complexes is a vast and ever growing research area. Likewise, the chemistry of mixed-metal alkyl/amido species is developing at a rapid rate.

In 1976, Hsieh and Wang found that when a dialkylzinc is complexed with an alkyllithium initiator, the initiation rate of the polymerisation of styrene or dienes was effectively increased.<sup>[94]</sup> A decade later, they presented similar results on the complexation of a dialkylmagnesium to the alkyllithium initiator. When simple homometallic compounds were used, polymerisation was found not to proceed.<sup>[95]</sup> Mixed lithium-magnesium amides, based around hexamethyleneimine, have also been found to act as polymerisation initiators of diene polymers and copolymer elastomers. This work was patented in 1996 by Hall and Antkowiak.<sup>[96]</sup> Richey and Farkas showed that on mixing solutions of alkyllithium and dialkylmagnesium reagents, the resultant homogeneous solution exhibited different alkylation behaviour towards pyridine, from either organometallic reagent on its own.<sup>[97]</sup>

The main driving force behind our interest in mixed metal alkyl/amido chemistry is in combining the metal components to generate beneficial *synergic effects*.<sup>[98]</sup> As mentioned previously, this could lead to the mixed-metal compounds having a unique chemical reactivity (different reactivity and/or selectivity towards various substrates), completely distinct from those of the parent homometallic compounds from which they are derived.

A considerable amount of progress has been made here at the University of Strathclyde centered on the chemistry of combining an alkali metal (lithium, sodium or potassium) with either magnesium or zinc.<sup>[85a]</sup> Most of this work has utilised the amido ligands HMDS, TMP and DA (Figure 1.27), and the resulting compounds have shown that the general order of



reactivity observed in homometallic chemistry, where organo-alkali metal compounds are orders of magnitude more reactive than organomagnesium or organozinc compounds, is not observed for heterometallic compounds. The seat of reactivity is transferred to the Mg or Zn and the reactivity of these compounds far outreaches those shown by  $R_2Mg$  or  $R_2Zn$ , with the mixed-metal zinc compounds being more reactive than the mixed-metal magnesium compounds. This is demonstrated by looking at the deprotonation of toluene – whereas the zincate  $KZn(HMDS)_3$  readily deprotonates toluene to give  $[KZn(HMDS)_2(CH_2Ph)]_\infty$ , the corresponding magnesiate  $KMg(HMDS)_3$  fails to deprotonate toluene under the same conditions.<sup>[99]</sup>

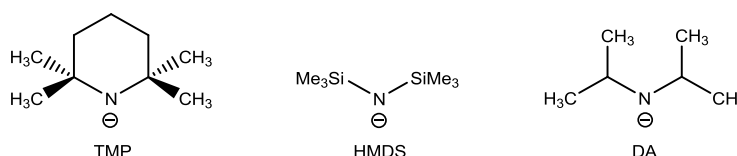


**Figure 1.27** Synthetically important amide reagents.

The lithium analogue of the aforementioned magnesiate,  $LiMg(HMDS)_3$ , was successfully synthesised by Mulvey *et al.* in 1998.<sup>[100]</sup> During attempts to re-prepare the compound, it was continually found that the reaction solutions crystallised as an oxygen-contaminated variant of the sought product, despite the reactions being carried out under conditions designed for the rigorous exclusion of moisture and oxygen. The macrocyclic complex was found to have the formula  $[Li_2Mg_2\{N(SiMe_3)_2\}_4(O_2)_x(O)_y]$ , **36**, and typical yields, although poor at 1-5%, were reproducible (Figure 1.28). The presence of oxygen in this compound, despite the extreme care taken to expel oxygen and moisture from the reaction vessel and chemical reagents, shows it to be an extremely efficient oxygen scavenger.

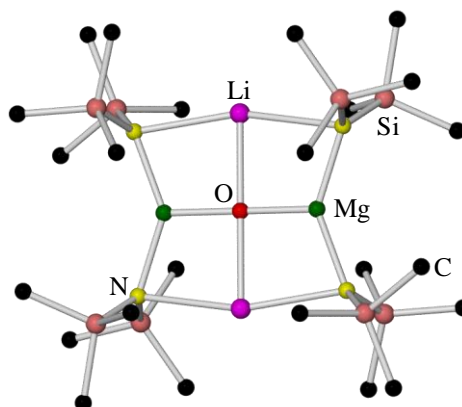


**Figure 1.28** Molecular structure of  $[Li_2Mg_2\{N(SiMe_3)_2\}_4(O_2)_x(O)_y]$ , **36**. H atoms are omitted for clarity.

The molecular structure of this complex reveals a discrete eight-membered ring composed of alternating nitrogen and metal centres. The metal centres alternate between lithium and magnesium. Oxo or peroxo anions are seen to occupy the core of the ring resulting in the

molecule obtaining charge neutrality. These peroxide- and oxide-containing molecules can be differentiated by performing  $^1\text{H}$  NMR spectroscopic studies in an arene solution.

This macrocyclic compound was the first in a new series of complexes to be formed, which are now termed ‘inverse crown ethers’ due to their inverse relationship to that of conventional crown ether complexes.<sup>[101]</sup> In conventional crown ether complexes, the Lewis basic oxygen centres play host to an electron-poor metal cation guest, but in inverse crown ether complexes, the Lewis acidic metal centres play host to an anionic Lewis basic oxide (Figure 1.29).

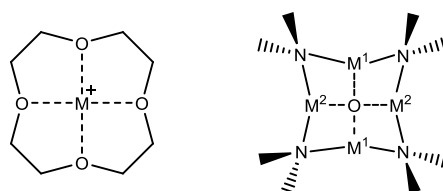
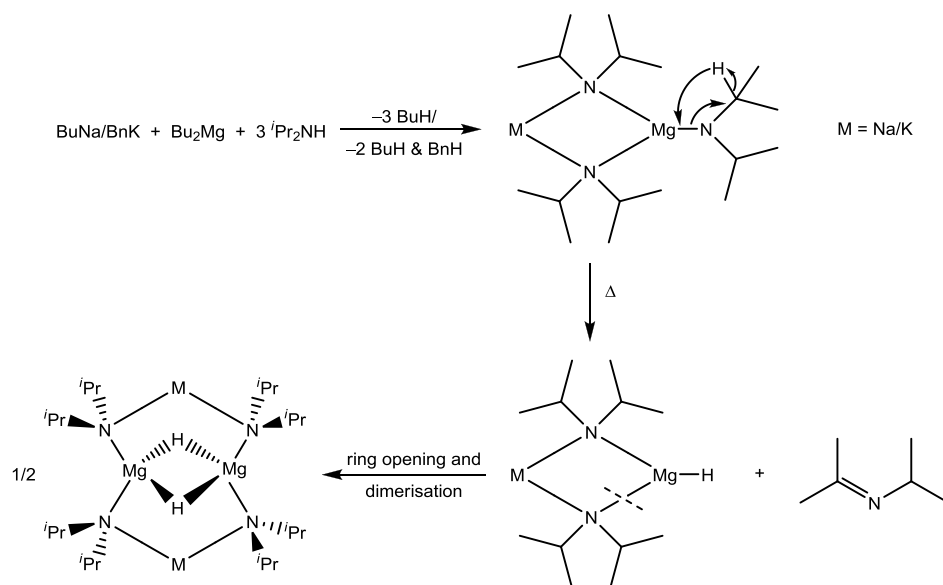


**Figure 1.29** Generalised structures of crown ether complexes (left) and inverse crown ether complexes (right).

Since the unintentional discovery of the first inverse crown ether, a selection of other inverse crown ethers (utilising the bulky amides TMP and HMDS along with the alkali metals lithium, sodium and potassium in combination with magnesium or zinc) have now been prepared and crystallographically characterised,<sup>[98, 102]</sup> indicating that the first inverse crown ether was not simply an anomalous result. These compounds can be represented by the general formula  $[\text{M}^{\text{I}}_2\text{M}^{\text{II}}_2(\text{amide})_4(\text{O}_2)_x(\text{O})_y]$ , where  $\text{M}^{\text{I}}$  represents an alkali metal and  $\text{M}^{\text{II}}$  represents Mg or Zn and the structures produced are similar to that shown in Figure 1.28. In the case of complexes derived from potassium, the inverse crown ethers are not discrete molecules but are linked by intermolecular  $\text{K}\cdots\text{C}$  contacts, forming linear polymeric chains. Recently Wu has extended this class of compounds to include the larger, more highly charged  $\text{Al}^{3+}$  ion (in combination with sodium), by the utilisation of bulky bisphenol ligands (*ie.*,  $\text{M}^{\text{III}}_2$  and two bisphenol ligands replace  $\text{M}^{\text{II}}_2$  and the four amide ligands in the above formula).<sup>[103]</sup>

When the amide utilised in the formation of these compounds is changed from TMP or HMDS to DA, a different type of inverse crown ether complex is formed.<sup>[104]</sup> Rather than trapping a peroxide or oxide anion, the inverse crown ethers contain hydride anions. With the general formula  $[\text{M}_2\text{Mg}_2(\text{DA})_4(\mu\text{-H})_2\cdot(\text{toluene})_2]$ , these ‘hydride-encapsulated’ inverse crown ether complexes are also based on eight-membered rings, although they adopt a chair conformation rather than the planar conformation adopted by the oxo/peroxide encapsulating analogues. The formation of these compounds is rationalised by an intramolecular  $\beta$ -hydride elimination transfer pathway, in which the  $^i\text{Pr}$  substituent of the DA ligand allows for this reaction pathway to occur (Scheme 1.19).



**Scheme 1.19** Proposed reaction pathway for the preparation of ‘hydride-encapsulated’ inverse crown ether complexes.

The aforementioned inverse crown ether complexes are generally synthesised in an alkane medium, but when prepared in the presence of an arene solvent, new categories of mixed-metal host-guest type complexes can be formed, which do not contain oxo, peroxy or hydride anions. As they are still composed of Lewis acidic metal centres playing host to Lewis basic guest anions, they retain the label ‘inverse crown’ but the suffix ‘ether’ is no longer required in describing them. These new mixed-metal inverse crowns are products of special magnesiations or zincations, and are therefore best regarded as *alkali metal mediated magnesiations* or *zincations* (*AMMMg* and *AMMZn* respectively).

## 1.5 Alkali Metal Mediated Metallations

The first mixed-metal inverse crown to be prepared in the presence of an arene solvent was reported in 1999.<sup>[105]</sup> Here, the inverse crown formed encapsulates regioselectively, two-fold deprotonated toluene or benzene. Toluene is normally more susceptible to mono-metallation at the methyl substituent, forming a benzylic carbanion and, although conventional homometallic reagents can remove more than one hydrogen atom from toluene and benzene, this occurs in a random unpredictable way. However here, in the inverse crown formed, the two-fold deprotonations are regioselective: toluene is metallated at the 2,5-positions and benzene at the 1,4-positions.

The di-metallated arenes are encapsulated in twelve-membered mixed-metal rings, of the general formula  $[\text{Na}_4\text{Mg}_2(\text{TMP})_6(\text{arene}^{2-})]$ , where  $\text{arene}^{2-}$  is  $\text{C}_6\text{H}_3\text{CH}_3$  or  $\text{C}_6\text{H}_4$  (Figure 1.30).

From this formula, it can be seen that the number of hydrogen atoms lost from the parent arenes (two) tallies exactly with the number of Mg atoms in the inverse crown products (two), whereas in contrast there are four Na atoms present. Thus, these two-fold deprotonations can be classified as magnesiations; however, more accurately, these can be termed as *alkali metal mediated magnesiations* as neither  $n^s\text{Bu}_2\text{Mg}$  nor  $\text{Mg}(\text{TMP})_2$  on their own can metallate benzene, requiring the mediation of the sodium component to carry out the di-metallation successfully.

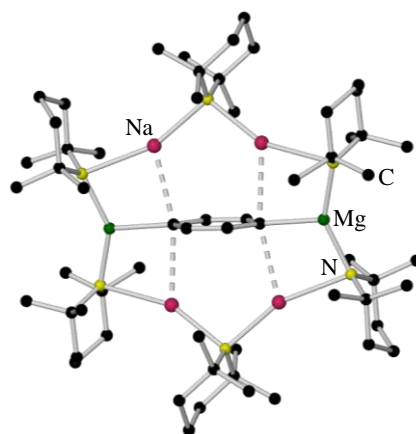


**Figure 1.30** Molecular structure of the inverse crown formed upon the metallation of benzene at the 1,4-positions. H atoms are omitted for clarity.

To try and identify the active base in the above system, the complexing ability of TMEDA was utilised by adding it stoichiometrically to the reaction which affords the above complex, but in the absence of arene. The expected tris(amide) product “ $\text{NaMg}(\text{TMP})_3 \cdot \text{TMEDA}$ ” however, was not obtained; and instead the reaction reproducibly affords the bis(amido)alkyl complex  $[(\text{TMEDA}) \cdot \text{Na}(\mu\text{-TMP})(\mu\text{-}n\text{Bu})\text{Mg}(\text{TMP})]$ ,<sup>[106]</sup> **37** (Figure 1.31), where one butyl ligand remains in the complex. The retention of the butyl ligand (even on refluxing the reaction solution for several hours) can be attributed to synergic effects, as both  $n\text{BuNa}$  and  $n^s\text{Bu}_2\text{Mg}$  on their own (when heated to reflux in toluene) react fully with  $\text{TMP}(\text{H})$ , with butane gas released from the reaction.

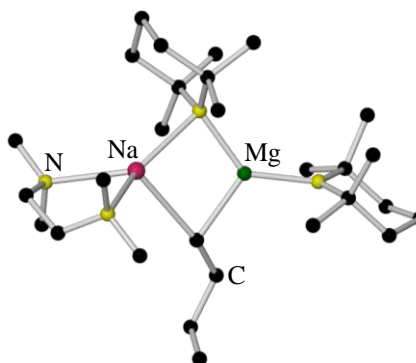


**Figure 1.31** Molecular structure of  $[(\text{TMEDA}) \cdot \text{Na}(\mu\text{-TMP})(\mu\text{-}n\text{Bu})\text{Mg}(\text{TMP})]$ , **37**. H atoms are omitted for clarity.

Possessing both alkyl and amido functionalities, the reactivity of **37** is highly intriguing. Initial deprotonation reactions carried out with benzene and toluene revealed that it behaves as a selective alkyl base, mono-metallating the ring and releasing butane, producing  $[(\text{TMEDA})\cdot\text{Na}(\mu\text{-TMP})(\mu\text{-Ph})\text{Mg}(\text{TMP})]^{[106]}$  and  $[(\text{TMEDA})\cdot\text{Na}(\mu\text{-TMP})(\mu\text{-C}_6\text{H}_4\text{CH}_3)\text{Mg}(\text{TMP})]^{[107]}$  respectively (Figure 1.32). Importantly, the latter reaction shows toluene to be metallated selectively at the *meta* position, which cannot be achieved by any known homometallic base.

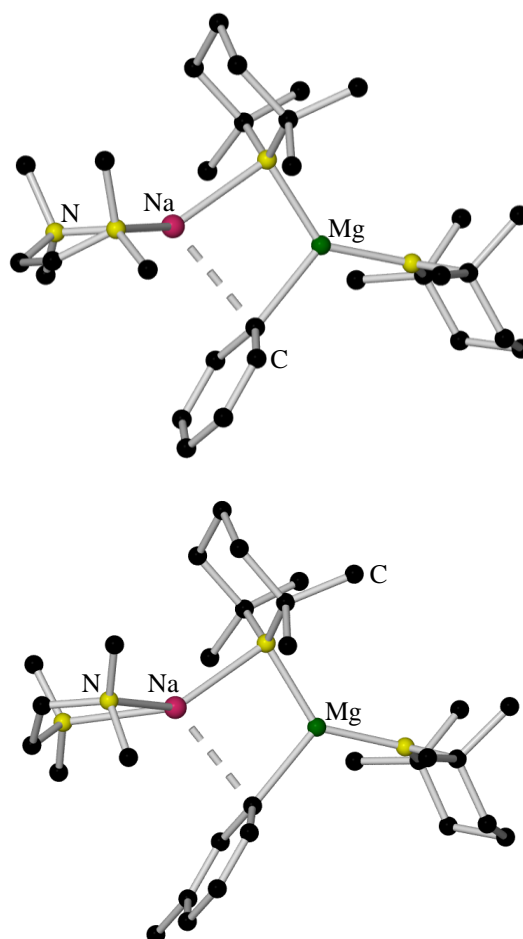


**Figure 1.32** The products of the deprotonation of benzene (top) and toluene (bottom) by the synergic base  $[(\text{TMEDA})\cdot\text{Na}(\mu\text{-TMP})(\mu\text{-}^n\text{Bu})\text{Mg}(\text{TMP})]$ , **37**. H atoms are omitted for clarity.

The diversity and importance of such synergic bases has been illustrated further by the reaction of **37** with the aromatic heterocyclic compound furan, producing a novel inverse crown architecture.<sup>[108]</sup> Moreover, the extraordinary power of these synergic mixed-metal inverse crown complexes is demonstrated in their ability to regioselectively metallate parent metallocene molecules such as ferrocene<sup>[109]</sup> and bis(benzene)chromium.<sup>[110]</sup>

When coupled with an alkali metal, zinc is also showing promise in alkali metal mediated metallations. Although zinc is in Group 12, due to its stable filled d shell and its reactivity being centred on its  $s^2$  valence shell, it has more in common with magnesium than it does with

the transition elements. Zinc and magnesium are of similar size, stable in the +2 oxidation state, able to assume trigonal planar (ate) coordination geometry, and have the propensity to form strong  $\sigma$ -bonds with carbon. However, due to zinc's greater electronegativity, Zn–C bonds are shorter and stronger than corresponding Mg–C bonds; hence, in theory, zinc could be even superior to magnesium in fulfilling the  $\sigma$ -bonding role within synergic  $\sigma/\pi$ -bonded divalent metal/alkali metal complexes (that is, the greater stability of the Zn–C  $\sigma$ -bonds would be transmitted to the overall stability of the complex).

The development of this alternative concept of *alkali metal mediated zincation* kick started in 1999, when Kondo and Uchiyama developed the alkali metal amino zincate “LiZn<sup>t</sup>Bu<sub>2</sub>(TMP)” and showed that it exhibited high levels of chemo- and regioselectivity towards the deprotonation of a series of functionalised aromatics<sup>[89a, 89c]</sup> and heteroaromatics<sup>[89b]</sup> (*vide supra*). However, no structural details of the zincate reagent or of any metallated intermediates were reported in these studies; and, wishing to investigate the synergic effects and structural chemistry of such reagents, Mulvey *et al.* (inspired by the novel chemistry of the sodium-magnesium system discussed earlier) prepared a sodium TMP-zincate as its TMEDA adduct [(TMEDA)·Na( $\mu$ -TMP)( $\mu$ -<sup>t</sup>Bu)Zn(<sup>t</sup>Bu)],<sup>[111]</sup> **38** (Figure 1.33). Unlike the lithium TMP-zincate, prepared in the bulk (polar) solvent THF, the sodium TMP-zincate was prepared in nonpolar hexane to aid crystallisation.

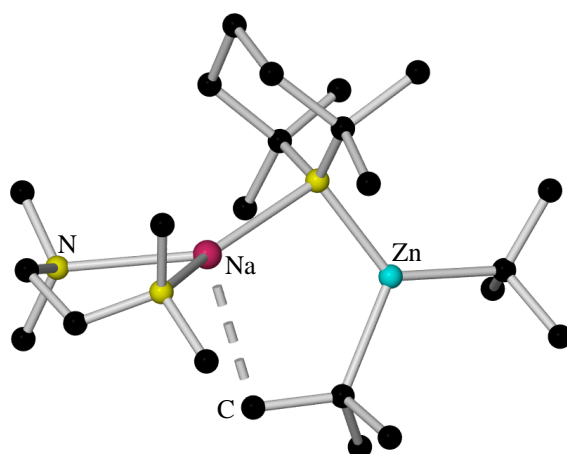


**Figure 1.33** Molecular structure of [(TMEDA)·Na( $\mu$ -TMP)( $\mu$ -<sup>t</sup>Bu)Zn(<sup>t</sup>Bu)], **38**. H atoms are omitted for clarity. From Figure 1.33, it can be seen that the structure, at least in a connectivity sense, bears a close resemblance to that of the sodium-magnesium bis(amido)alkyl complex shown earlier (Figure 1.31). A Na chelated by TMEDA bridges through TMP to a Zn or Mg carrying a terminal ligand, while an alkyl ligand forms a second bridge between Na and Zn or Mg. In both structures the Group 12/2 metal is in a trigonal planar coordination geometry with short Zn– $\mu$ -C or Mg– $\mu$ -C alkyl bonds; however, in contrast, the Na–C alkyl bridges are long and

weak and, moreover, distinct, involving an agostic Me contact in the zincate and an  $\alpha\text{-CH}_2^-$  atom in the magnesiate. As agostic contacts are inherently weak, the  $\text{Na}\cdots\text{Me}$  agostic contact within the zincate could be viewed as a potential reactivity hotspot and this appears to be the case in its reaction with benzene, affording the hetero(tri)leptic zincate  $[(\text{TMEDA})\cdot\text{Na}(\mu\text{-TMP})(\mu\text{-Ph})\text{Zn}(\text{tBu})]^{[111]}$  (Figure 1.34). The deprotonated benzene occupies the bridging site previously occupied by the  $\text{tBu}$  group, with  $\text{Na}\cdots\text{Ph}$   $\pi$ -contacts replacing the  $\text{Na}\cdots\text{Me}$  agostic contacts.

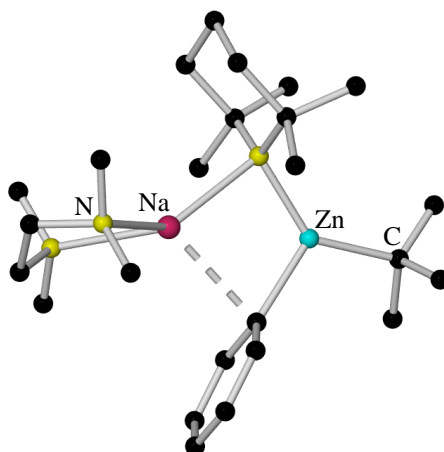
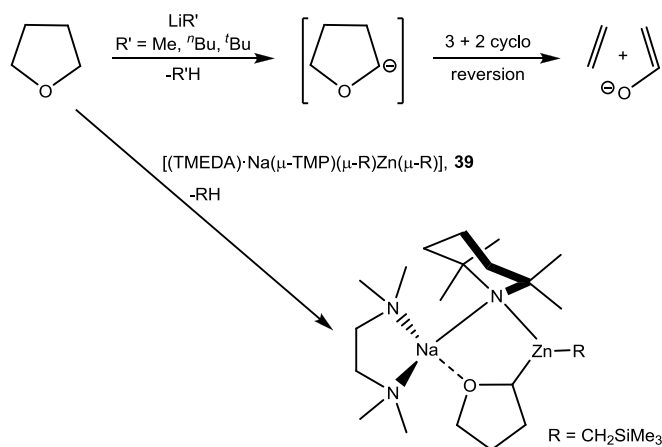


**Figure 1.34** The product of the deprotonation of benzene by the mixed-metal base  $[(\text{TMEDA})\cdot\text{Na}(\mu\text{-TMP})(\mu\text{-tBu})\text{Zn}(\text{tBu})]$ , **38**. H atoms are omitted for clarity.

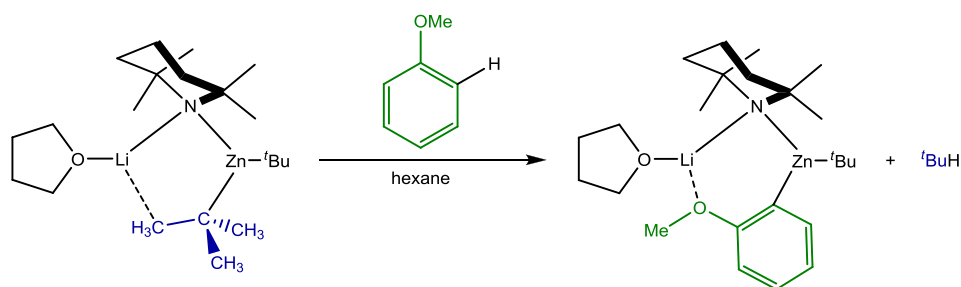
The observed deprotonation of benzene by the mixed-metal base **38** can be attributed to synergic effects as neither  $\text{tBu}_2\text{Zn}$  nor  $\text{Na}(\text{TMP})$  on their own can metallate benzene; hence, this metallation can be termed an *alkali metal mediated zincation*, or more specifically, a sodium-mediated zincation. The zincating power of **38** has recently been further exploited in the *AMMZn* of naphthalene<sup>[112]</sup> and trifluoromethyl benzene,<sup>[113]</sup> the direct meta-zincation of *N,N*-dimethylaniline and its 3-methyl derivative,<sup>[114]</sup> the *C*-zincation of *N*-heterocyclic aromatics,<sup>[115]</sup> the direct *meta*- and *para*-zincation of toluene,<sup>[116]</sup> and the direct *ortho*-zincation of benzylmethylether,<sup>[117]</sup> phenyl *O*-carbamate and benzamides.<sup>[118]</sup>

When the aggressive  $\text{tBu}^-$  anions were replaced with gentler trimethylsilyl ( $\text{Me}_3\text{SiCH}_2^-$ ) ligands in the above sodium TMP-zincate **38**, the resulting complex  $[(\text{TMEDA})\cdot\text{Na}(\mu\text{-TMP})(\mu\text{-CH}_2\text{SiMe}_3)\text{Zn}(\text{CH}_2\text{SiMe}_3)]$ ,<sup>[119]</sup> **39**, was successful in trapping and directly metallating (zincating) the sensitive cyclic ether THF at the  $\alpha$ -position at ambient temperature. This accomplishment is highly impressive as metallation at the  $\alpha$ -position of THF with strong bases such as organolithium reagents localises a high degree of negative charge on the  $\alpha$ -C atom adjacent to the electron rich O atom, causing a severe destabilisation that induces spontaneous ring-opening (Scheme 1.20).



**Scheme 1.20** Ring-opening of THF with conventional organolithium reagents and the trapping of  $\alpha$ -metallated THF within the framework of the sodium TMP-zincate **39**.

In the case of **38**, the zincate appears to be acting as an alkyl base, in contrast to the amido basicity<sup>[89a, 89b]</sup> exhibited by the lithium TMP-zincate developed by Kondo and Uchiyama in *DoM* reactions with a variety of aromatic and heteroaromatic substrates. On unveiling the X-ray structure of the lithium amido zincate, formulated as  $[(\text{THF})\cdot\text{Li}(\mu\text{-TMP})(\mu\text{-}^t\text{Bu})\text{Zn}({}^t\text{Bu})]$ , **35**, Mulvey *et al.* further explored its applications in *DoM* reactions, specifically investigating its reactivity towards the *ortho*-deprotonation of anisole,<sup>[120]</sup> revealing that overall the zincate acts as an alkyl base, where the  ${}^t\text{Bu}$  bridge of **35** is *ultimately* replaced by an *ortho*-deprotonated anisole fragment, with  ${}^t\text{BuH}$  as the co-product of the reaction (Scheme 1.21).

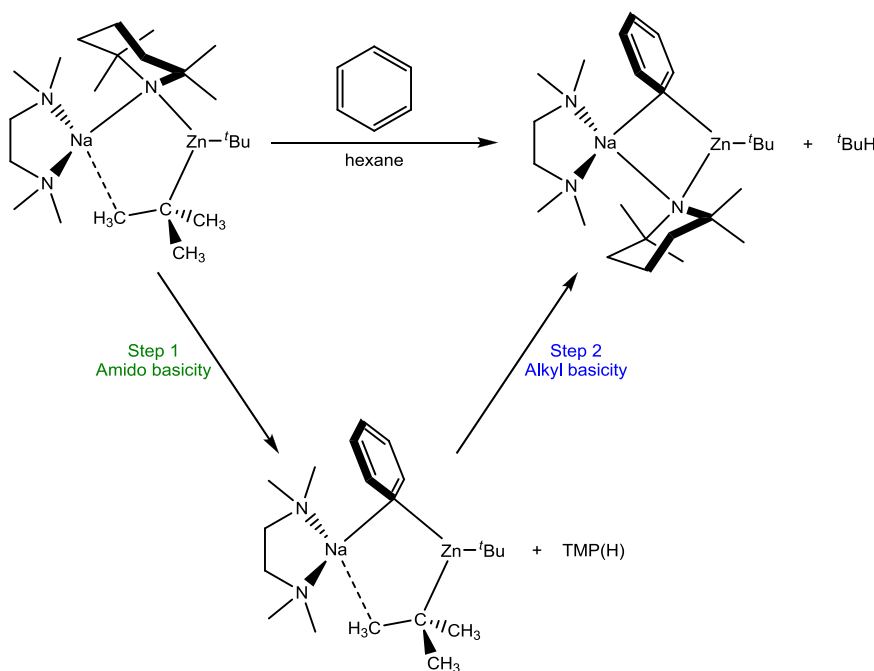


**Scheme 1.21** Selective *ortho*-deprotonation of anisole with the lithium TMP-zincate  $[(\text{THF})\cdot\text{Li}(\mu\text{-TMP})(\mu\text{-}^t\text{Bu})\text{Zn}({}^t\text{Bu})]$ , **35**.

Density Functional Theory (DFT) studies (which reveal the kinetic processes taking place along the reaction pathway of a given reaction) of several *DoM* substrates, conducted by Uchiyama,<sup>[89d, 121]</sup> in conjunction with Morokuma,<sup>[89d, 121a]</sup> Wheatley<sup>[121b]</sup> and Nobuto,<sup>[122]</sup> indicated that kinetically, amido basicity is preferred to the experimentally observed alkyl basicity due to the significantly lower activation energies for the cleavage of the Zn–N bonds in comparison to Zn–C bonds. To account for the structures found experimentally for the isolated intermediates (as in Scheme 1.21) they proposed a two-step mechanism where the arene is initially deprotonated by the amido ligand (due to the greater kinetic ability of the Zn–



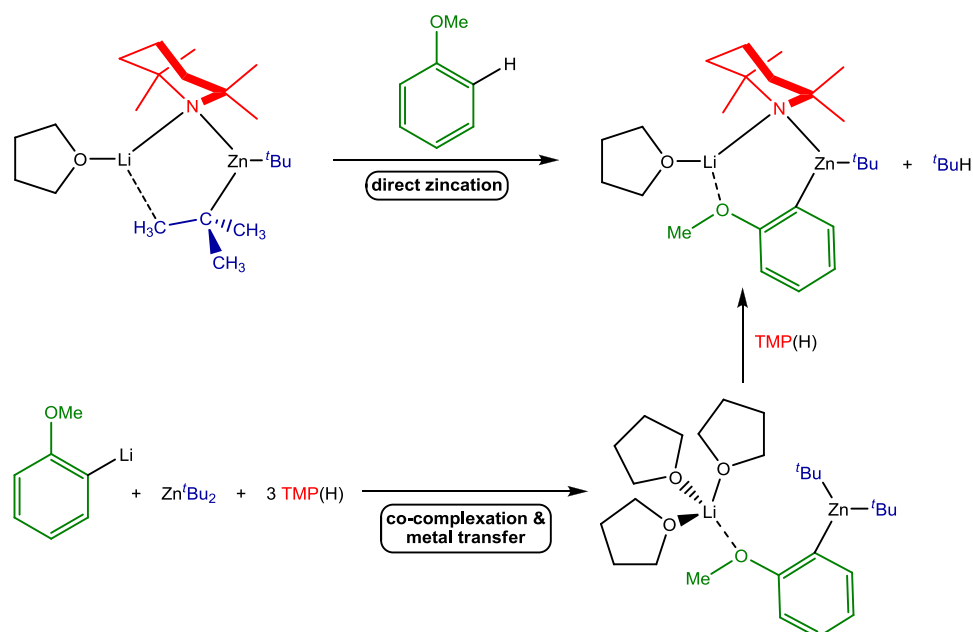
N bonds) affording a reaction intermediate (of the form “[ $(\text{THF})_3\cdot\text{Li}(\text{C}_6\text{H}_4\text{-OMe})(\mu\text{-}^t\text{Bu})\text{Zn}(^t\text{Bu})$ ]” when considering the reaction of anisole with the lithium-TMP zincate **35**), which can then react with concomitantly generated TMP(H) giving rise to the relevant *ortho*-zincated product and isobutane, in agreement with the aforementioned experimentally established overall alkyl basicity (Scheme 1.22).<sup>[122]</sup>



**Scheme 1.22** Proposed two-step mechanism for the deprotonation of benzene by the mixed-metal base [(TMEDA)·Na( $\mu$ -TMP)( $\mu$ -*t*Bu)Zn(*t*Bu)], **38**.

However, simplified models for zincates **35** and **38** were employed throughout these studies, namely [(Me<sub>2</sub>O)·M( $\mu$ -NMe<sub>2</sub>)( $\mu$ -Me)Zn(Me)] (M = Li or Na), which do not take into account the steric influence and the carbanionic nature that the bulky substituents *t*Bu and TMP play in these metallations. Furthermore, attempts by Hevia *et al.* to detect experimentally the proposed intermediates were unsuccessful, even when the metallations were carried out at low temperatures, indicating that if a two-step process was indeed taking place, the second step must be extremely fast.

Hevia *et al.* delved further into unearthing the true mechanism of the *AMMZn* of anisole by preparing and characterising the putative intermediates suggested by the theoretical studies in which the lithium-TMP zincate **35** was utilised.<sup>[123]</sup> These intermediates were prepared by an indirect route in which anisole was first metallated by *t*BuLi and then co-complexed with R<sub>2</sub>Zn (R = *t*Bu, Me). The complexes formed were subjected to the addition of TMP(H) to probe their reactivity and these studies provided the first experimental evidence of the possibility of a two-step mechanism for the *AMMZn* of anisole using zincate **35** (and thus for TMP-zincates in general), as predicted by the theoretical calculations (Scheme 1.23).



**Scheme 1.23** Preparation of the putative intermediate suggested by the theoretical studies and its reactivity with TMP(H), providing for the first time compelling experimental evidence of the possibility of a two-step mechanism for TMP-zincates.

A complementary lithium-zinc complex to the sodium-magnesium bis(amido)alkyl complex has also been recently synthesised and crystallographically characterised as [(TMEDA)·Li(μ-TMP)(μ-*n*-Bu)Zn(*n*-Bu)],<sup>[124]</sup> **40** (Figure 1.35). From the molecular structure, it can be seen that it is very similar to that of the magnesiate, having an ion-contacted ate arrangement, with the contact through a short Li–N(TMP) bond and a long (weak) Li–C(*n*-butyl) bond. Confirming the synergic power of these novel mixed-metal compounds, this complex can carry out direct zincation of ferrocene, in contrast to its homometallic component parts LiTMP and *n*Bu<sub>2</sub>Zn, which are both inert towards ferrocene – even in the presence of TMEDA.

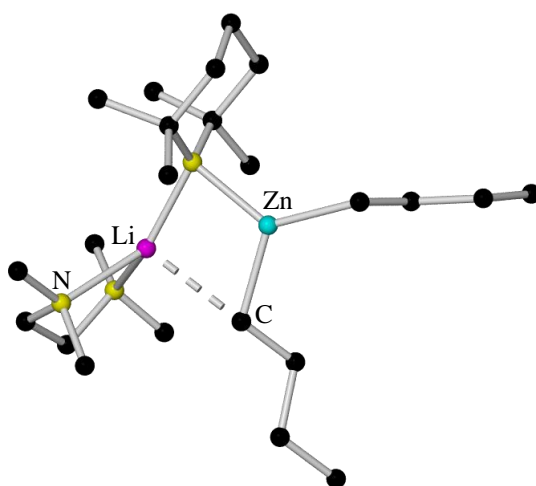


**Figure 1.35** Molecular structure of [(TMEDA)·Li(μ-TMP)(μ-*n*-Bu)Zn(*n*-Bu)], **40**. H atoms are omitted for clarity.

The captivating chemistry highlighted thus far has laid the foundations for the possible incorporation of chiral amides into mixed-metal compounds (an area which has thus far been largely neglected). The careful design of new synergic bases (*i.e.*, by modifying electronic, steric and chiral properties of the molecule) will undoubtedly deliver a series of high interest compounds which will not only appeal to laboratory synthetic chemists (organometallic, inorganic or organic), but also to industrial chemists working in the fine chemical, pharmaceutical, and research and development sectors.

## 1.6 Extensions to Chiral Mixed-Metal Systems

In 2008, the first chiral amido zincate  $(R,R)$ -[(TMEDA)·Na{ $\mu$ -N(CH<sub>2</sub>Ph)(CH(CH<sub>3</sub>)Ph)}( $\mu$ -<sup>t</sup>Bu)Zn(<sup>t</sup>Bu)]<sup>[125]</sup> **41** (Figure 1.36), was successfully prepared by carrying out a transamination reaction of **38** with the chiral amine (*R*)-*N*-benzyl- $\alpha$ -methylbenzylamine. This showed for the first time that chiral moieties could be incorporated successfully within the molecular framework of an alkali metal/zinc synergic system.

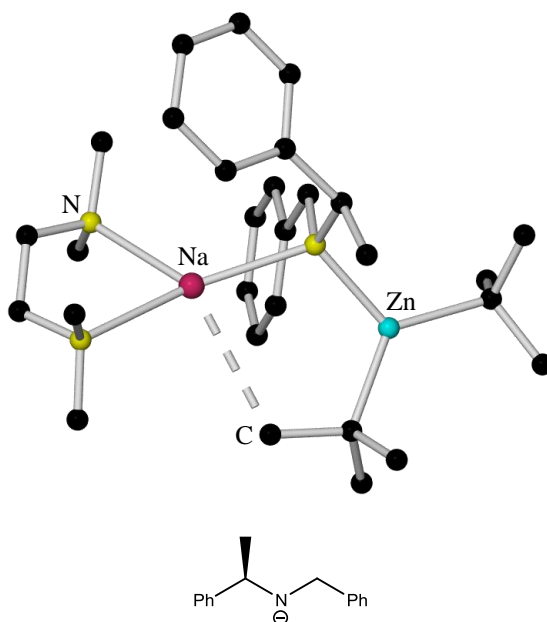


**Figure 1.36** Molecular structure of  $(R,R)$ -[(TMEDA)·Na{ $\mu$ -N(CH<sub>2</sub>Ph)(CH(CH<sub>3</sub>)Ph)}( $\mu$ -<sup>t</sup>Bu)Zn(<sup>t</sup>Bu)]<sup>[125]</sup>, **41**, showing the chiral amide utilised. H atoms are omitted for clarity.

The isolation and characterisation (by X-ray crystallography and NMR spectroscopy) of this complex has enhanced the prospect that other chiral amines may be exploited to form a new array of heterometallic asymmetric bases. Moreover, by varying the mono- and divalent metals an even larger assortment of complexes (and possibly unique structural chemistry) may be observed.

### 1.6.1 (–)-Sparteine as a Chiral Auxiliary

Another approach to synthesising a chiral synergic base is to utilise chiral amines in the formation of ‘chiral carbanions’. Here, alkyl metal amides are used in tandem with chiral ligands such as (–)-sparteine [C<sub>15</sub>H<sub>26</sub>N<sub>2</sub>] (an alkaloid which is widely used in synthesis to give a high degree of chiral recognition) (Figure 1.37).

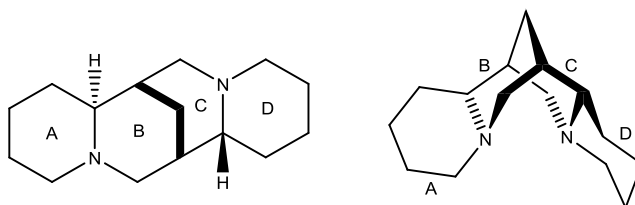


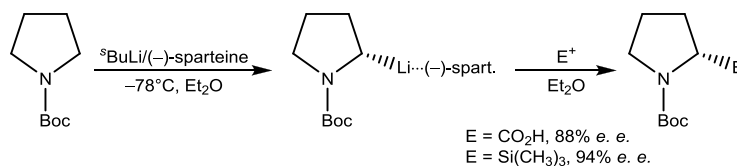
**Figure 1.37** Structure of (–)-sparteine, showing the conformation normally adopted on binding to a metal centre (right).

(–)-Sparteine is commercially available and obtained through the extraction of certain *papilionaceous* plants such as *Scotch broom*<sup>[1, 126]</sup> and although it deviates from  $C_2$ -symmetry, it is generally the chiral auxiliary of choice due to its ability to effect the enantioselective metallation of many key organic substrates,<sup>[127]</sup> generally in conjunction with alkyllithiums such as <sup>s</sup>BuLi.<sup>[5b, 128]</sup> These reagents commonly give products in high enantiomeric excess and yield, with the efficiency and breadth of application of these (–)-sparteine alkyllithium systems thus far unsurpassed, achieving high levels of reactivity and stereoselectivity in deprotonation, oxidation, reduction and addition reactions.<sup>[128-129]</sup>

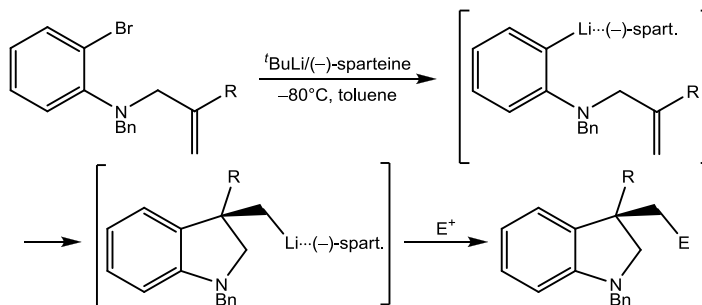
(–)-Sparteine was first studied as a possible chiral additive in carbanion reactions in 1968 by Nozaki *et al.*, who applied it in chiral organolithium and –magnesium compounds, although with limited success.<sup>[130]</sup> Greater success was achieved by Guetté *et al.* five years later, with high chiral induction of 98% *e. e.* in a Reformatzky aldolisation reaction in the presence of (–)-sparteine.<sup>[131]</sup> Use of (–)-sparteine to induce stereoselectivity in reactions became evident not long after, as (–)-sparteine-modified alkyllithium and alkylmagnesium complexes found early application in stereoselective anionic polymerisation.<sup>[132]</sup>

More recently, investigations by Hoppe with  $\alpha$ -oxygen dipole-stabilised carbanions have demonstrated high enantioselectivities for reactions in the presence of (–)-sparteine.<sup>[133]</sup> Hoppe’s work has stimulated a number of further developments in (–)-sparteine-mediated regio-, diastereo- and enantioselective carbolithiation reactions.<sup>[128-129]</sup> Examples include the asymmetric deprotonation of *N*-Boc-pyrrolidine with <sup>s</sup>BuLi/(–)-sparteine, which reacts with electrophiles to provide enantio-enriched products with enantiomeric excesses of 88-94% (Scheme 1.24);<sup>[134]</sup> (–)-sparteine-mediated preparation of enantio-enriched ferrocene derivatives;<sup>[135]</sup> ring-opening cyclisation of a *meso*-epoxide with <sup>i</sup>PrLi/(–)-sparteine;<sup>[136]</sup> chiral

deprotonation of a piperazine,<sup>[127c]</sup> and the enantioselective synthesis of 3,3-disubstituted indolines *via* asymmetric intramolecular carbolithiation in the presence of (–)-sparteine (Scheme 1.25).<sup>[127d]</sup>

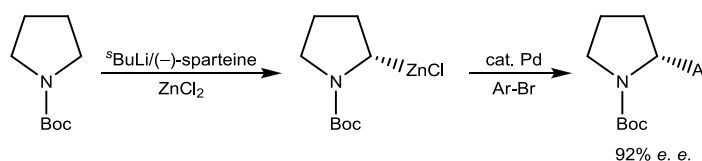


**Scheme 1.24** N-Boc-pyrrolidine carbolithiation/enantioselective electrophilic substitution reactions.



**Scheme 1.25** The enantioselective synthesis of a 3,3-disubstituted indoline *via* asymmetric intramolecular carbolithiation in the presence of (–)-sparteine.

The product of asymmetric deprotonation of *N*-Boc-pyrrolidine with <sup>s</sup>BuLi/(–)-sparteine can also be used in subsequent cross-coupling reactions. For example, the (–)-sparteine-mediated enantioselective lithiation of *N*-Boc-pyrrolidine followed by *in situ* transmetalation to zinc and Pd-catalysed Negishi cross-coupling with aryl bromides, provided 2-arylpyrrolidines in 92% *e. e.* with retention of stereo-integrity throughout the process (Scheme 1.26).<sup>[137]</sup>

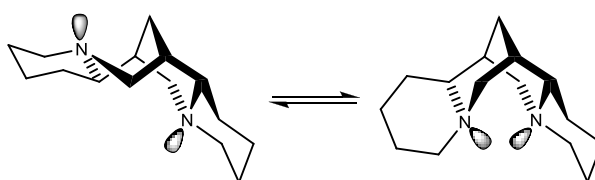


**Scheme 1.26** Enantioselective deprotonation of *N*-Boc-pyrrolidine, followed by transmetalation and subsequent Pd-catalysed Negishi cross-coupling with aryl bromides.

(–)-Sparteine can be used to induce chirality at C and P atoms. The latter is detailed by O’Brien in his communications on the (–)-sparteine-mediated asymmetric synthesis of P-stereogenic compounds *via*; the regioselective lithiation of silyl phosphine sulfides;<sup>[138]</sup> the asymmetric deprotonation of phosphine borane;<sup>[139]</sup> the kinetic resolution of P-stereogenic phosphine boranes;<sup>[140]</sup> the kinetic deprotonation and dynamic thermodynamic resolution of phosphine sulfides;<sup>[141]</sup> and the catalytic asymmetric deprotonation of phosphine borane (Scheme 1.27).<sup>[142]</sup> The development of these methodologies is highly important considering that chiral phosphane ligands are widely utilised in transition metal catalysed asymmetric hydrogenation, a process which is routinely employed in the pharmaceutical, agrochemical



From these structures it can also be seen that (–)-sparteine exclusively adopts the same conformation in each structure. (–)-Sparteine consists of four rings whose conformation alters upon complexation. When not coordinated to a metal centre, rings A, B and D exist in a chair conformation, while ring C adopts a boat conformation, with both the A/B ring junction and the C/D ring junction adopting the *trans* configuration. However on complexation, all rings adopt a chair conformation and the A/B ring junction remains in the *trans* configuration, while the C/D ring junction adopts the *cis* configuration (Scheme 1.28).<sup>[127a]</sup> The reason for the exclusive appearance of this latter conformation in the above complexes is believed to be due to the more favourable arrangement of the two nitrogen atoms which allow the (–)-sparteine to act as a bidentate donor towards the Lewis acidic metal centre.



**Scheme 1.28** Equilibrium of (–)-sparteine ring flipping.

Håkansson *et al.*, have determined the structures which exist in the solid-state when (–)-sparteine is combined with methyllithium and phenyllithium.<sup>[151]</sup> The 1 : 1 complex of methyllithium and (–)-sparteine forms a dimer  $[\text{MeLi}\cdot(\text{–})\text{-sparteine}]_2$ , **45** and the 2 : 1 complex of phenyllithium and (–)-sparteine displays a tetranuclear  $\text{Li}_4\text{Ph}_4$  core (with a twisted helical ladder arrangement) with one (–)-sparteine ligand at each end  $[\text{Ph}_4\text{Li}_4\cdot\{(\text{–})\text{-sparteine}\}_2]$ , **46**. On changing the ratio of phenyllithium and (–)-sparteine to 1 : 1, Strohmann discovered that as well as crystallising **46**, a small quantity of the simple dimer species was also isolated.<sup>[152]</sup>

Other examples of (–)-sparteine-complexed organolithium reagents which have been characterised in the solid-state include the allyllithium meso-1,3-diphenylallyllithium·(–)-sparteine,<sup>[153]</sup> and the chiral lithiosilanes  $[\text{PhMe}_2\text{SiLi}\cdot(\text{–})\text{-sparteine}\cdot\text{thf}]$ ,<sup>[154]</sup> **47**,  $[\text{Ph}_2(\text{Et}_2\text{N})\text{SiLi}\cdot(\text{–})\text{-sparteine}]$ ,<sup>[154]</sup> **48**,  $[\text{Ph}_2\text{MeSiLi}\cdot(\text{–})\text{-sparteine}\cdot\text{thf}]$ ,<sup>[154-155]</sup> **49**,  $[\text{Ph}(\text{Et}_2\text{N})_2\text{SiLi}\cdot(\text{–})\text{-sparteine}\cdot\text{thf}]$ ,<sup>[154-155]</sup> **50** and  $[\text{Me}_3\text{SiCH}_2\text{Li}\cdot(\text{–})\text{-sparteine}]_2$ ,<sup>[156]</sup> **51**.

Solution studies on alkylolithium/(–)-sparteine complexes have been conducted by Hilmersson,<sup>[157]</sup> Collum<sup>[158]</sup> and Beak,<sup>[159]</sup> where it has been noted that non-coordinating solvents such as toluene, pentane, or hexane must be employed for high enantioselective deprotonation processes utilising <sup>s</sup>BuLi or <sup>n</sup>BuLi and (–)-sparteine.<sup>[129b, 160]</sup> Negligible enantioselectivity is achieved when reactions are carried out in THF due to the THF preferentially complexing to the organolithium.<sup>[157a, 161]</sup>

In 2008, we successfully ligated (–)-sparteine to “[Na(μ-TMP)(μ-<sup>n</sup>Bu)Mg(TMP)]” as a chiral substitute for achiral TMEDA to form [{"(–)-sparteine"}·Na(μ-TMP)(μ-<sup>n</sup>Bu)Mg(TMP)],<sup>[162]</sup> **52** (Figure 1.39). A search of the Cambridge Crystallographic Data Centre (CCDC)<sup>[163]</sup> showed that no other (–)-sparteine adducts of sodium or magnesium compounds had been prepared prior to this. Indeed, complex **52** represented the first crystallographically characterised structure in which (–)-sparteine was attached to an alkali metal other than lithium – surprising considering the importance of this chiral ligand in asymmetric synthesis. Uchiyama and Wheatley<sup>[121b]</sup> have recently published a mechanism (supported by DFT calculations) which suggests that the auxiliary ligand stays attached to the alkali metal, in a related lithium zincate system, during the desired deprotonation reaction – a fundamental feature if these new chiral bases are to behave in an enantioselective manner.

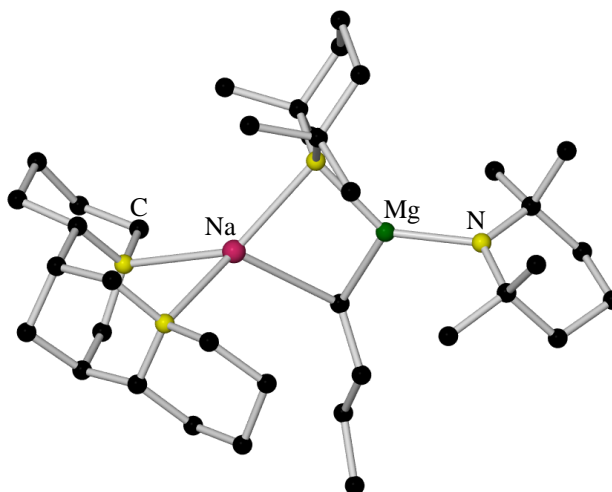


**Figure 1.39** Molecular structure of [{"(–)-sparteine"}·Na(μ-TMP)(μ-<sup>n</sup>Bu)Mg(TMP)], **52**. H atoms are omitted for clarity.

Until 2009, (–)-sparteine was readily available from most chemical suppliers at relatively low expense (approximately £1.80 per mL);<sup>[1]</sup> however, it has now been withdrawn from sale by many chemical suppliers. Other chiral diamine auxiliaries have been prepared in an attempt to better the performance of (–)-sparteine in enantioselective deprotonations and it has recently been emphasised that altering the chiral diamine can have a drastic effect on the outcome of the reaction.<sup>[157b]</sup> These include; (+)-sparteine,<sup>[164]</sup> (–)-isosparteine,<sup>[165]</sup> (*R,R*)-TMCDA,<sup>[166]</sup> (–/+)-sparteine surrogates<sup>[167]</sup> and bispidine derivatives<sup>[167c]</sup> (Figure 1.40).



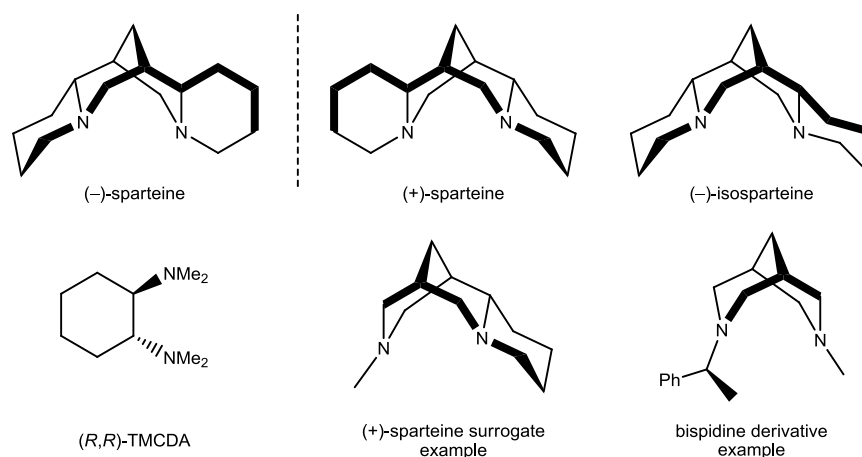
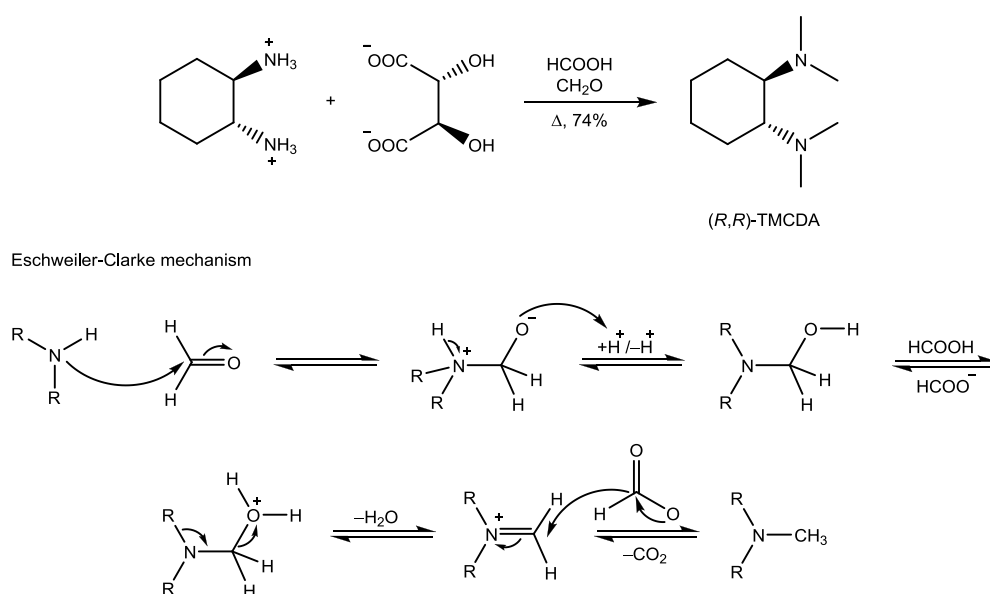


**Figure 1.40** Chiral diamines (-)-sparteine and (R,R)-TMCDA, along with other common chiral diamine auxiliaries.

### 1.6.2 (R,R)-TMCDA as a Chiral Auxiliary

As highlighted, another chiral auxiliary which is gaining interest for use in chiral diamine-alkyllithium asymmetric deprotonations is the  $C_2$ -symmetric  $N,N,N',N'$ -(1*R*,2*R*)-tetramethylcyclohexane-1,2-diamine [(*R,R*)-TMCDA], which in combination with  $^s\text{BuLi}$  is more reactive than  $^s\text{BuLi}/(-)\text{-sparteine}$ , but with modest enantioselectivity.<sup>[168]</sup>

(*R,R*)-TMCDA is prepared by performing an Eschweiler-Clarke reaction directly on the enantiomerically pure tartaric salt [(*R,R*)-1,2-diammoniumcyclohexane mono-(+)-tartrate salt] (Scheme 1.29).<sup>[166c]</sup>



**Scheme 1.29** Synthesis of (R,R)-TMCDA and the Eschweiler-Clarke mechanism.

Strohmann *et al.* have once again been at the forefront of structural characterisation of chiral diamine alkyllithium systems, preparing and characterising the (R,R)-TMCDA-coordinated

organolithium complexes of *t*-butyllithium [*t*BuLi·(*R,R*)-TMCDA],<sup>[78]</sup> **53**, methyllithium [MeLi·(*R,R*)-TMCDA]<sub>2</sub>,<sup>[169]</sup> **54**, *s*-butyllithium [*s*BuLi·(*R,R*)-TMCDA],<sup>[169]</sup> **55**, *iso*-propyllithium [*i*PrLi·(*R,R*)-TMCDA]<sub>2</sub>,<sup>[169]</sup> **56** and *n*-butyllithium, which can form a dimer [*n*BuLi·(*R,R*)-TMCDA]<sub>2</sub>,<sup>[170]</sup> **57** or an aggregate [(*n*BuLi)<sub>2</sub>·(*R,R*)-TMCDA]<sub>2</sub>,<sup>[170]</sup> **58**, (with a ladder arrangement) depending on the <sup>n</sup>BuLi/TMCDA ratio (Figure 1.41).

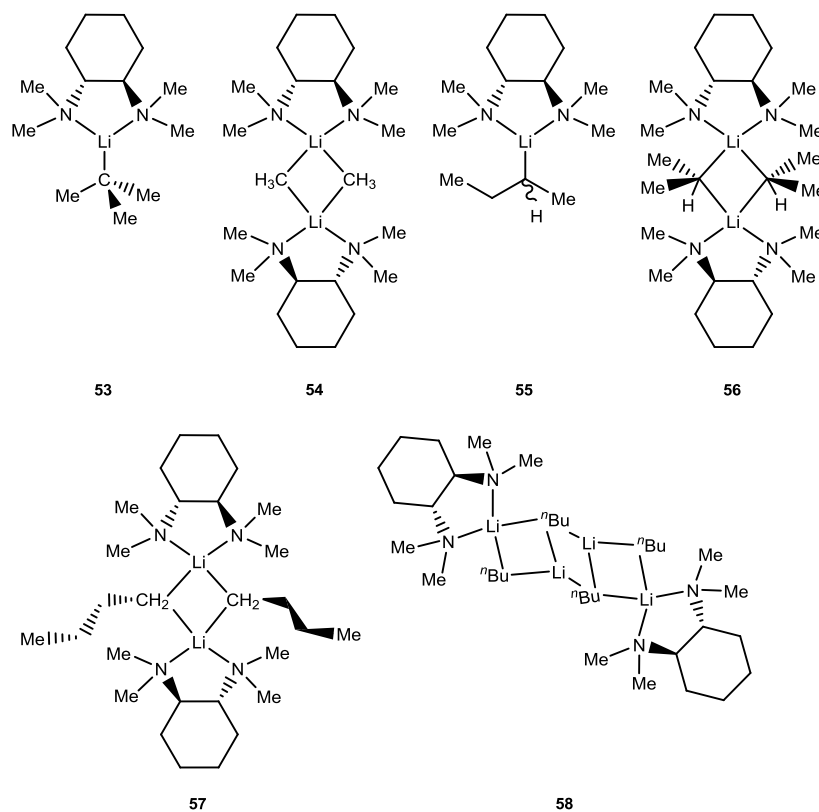


**Figure 1.41** Molecular structures of the (*R,R*)TMCDA adducts of *t*BuLi, MeLi, *s*BuLi, *i*PrLi and *n*BuLi respectively.

Monomer **53** is only the second structurally characterised monomeric alkyllithium compound bearing a saturated hydrocarbon, the first being the (–)-sparteine analogue, complex **42** (*vide supra*). On warming from  $-78^{\circ}\text{C}$  to room temperature, monomer **53** in *n*-pentane was found to undergo slow lithiation, yielding  $\alpha$ -lithiated (*R,R*)-TMCDA (molecular structure shown in Scheme 1.14).<sup>[78]</sup> Carrying out the same reaction as that used to prepare **53**, but this time with an excess of *t*-butyllithium present, resulted in the formation of a mixed aggregate with incorporation of a second equivalent of organolithium base into the  $\alpha$ -lithiated amine [*t*BuLi·(*R,R*)-TMCDA-Li]<sub>2</sub>,<sup>[171]</sup> **59** (Figure 1.42) (crystals forming at  $-30^{\circ}\text{C}$  and upon warming the solution to room temperature and subsequent cooling to  $-78^{\circ}\text{C}$ ).

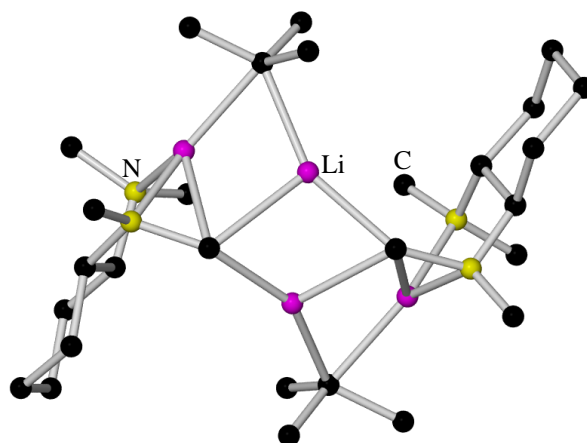
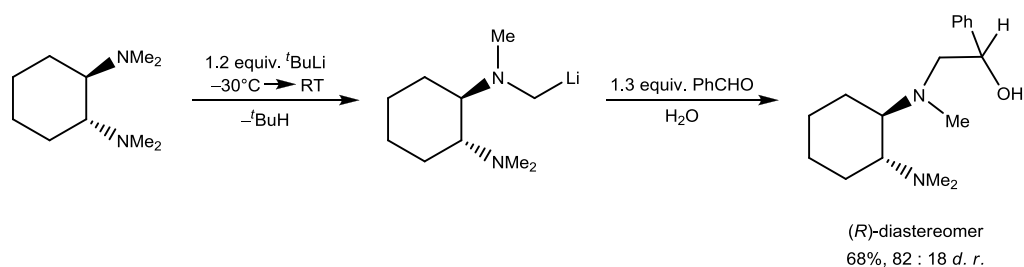


**Figure 1.42** Molecular structure of  $[t\text{BuLi}\cdot(R,R)\text{-TMCDA-Li}]_2$ , **59**. H atoms are omitted for clarity.

The  $\alpha$ -lithiated (*R,R*)-TMCDA has been effectively employed as a building block for the preparation of chiral N,N,O ligands by asymmetric 1,2-addition onto different ketones and aldehydes.<sup>[171]</sup> Depending on the carbonyl compound utilised, a new stereocentre can be introduced into the molecule at the  $\alpha$ -position with respect to the hydroxy function (Scheme 1.30). This methodology has been further extended to the preparation of aminomethyl functionalised silanes, with mono-, di- and tri-aminomethyl substituted systems being successfully synthesised; however, the di- and tri-functionalised systems do suffer from high sensitivity towards Si–C bond cleavage in solution, decomposing over 60 hours.<sup>[172]</sup>



**Scheme 1.30** Lithiation of (*R,R*)-TMCDA, followed by trapping with benzaldehyde and aqueous work-up to give the corresponding alcohol.

(*R,R*)-TMCDA has also been instrumental in the preparation of chiral phosphane ligands,<sup>[173]</sup> but unlike (–)-sparteine-alkyllithium mediated asymmetric deprotonation of prochiral dimethylphosphine boranes, where only one methyl group is deprotonated (*vide supra*), here, both methyl groups are deprotonated, providing access to novel ligands for transition metal complexes for their use in catalytic asymmetric hydrogenation. The dilithiation can be explained by computational studies which reveal stabilising  $\text{Li}\cdots\text{H}$  interactions with the borane moiety.

Space-filling models of **53** show the less sterically demanding nature of (*R,R*)-TMCDA in comparison to (–)-sparteine and highlight that the Li centre is barely shielded by the ligand and thus the positively polarised coordination site at the Li centre is quite exposed. This in turn demonstrates the structure-reactivity relationship of organolithium compounds, with this site of attack explaining the high reactivity of **53**.<sup>[78]</sup> Even more intriguing, monomer **55** is the first Lewis base-coordinated adduct of <sup>s</sup>BuLi, which again, owing to its monomeric structure, is highly reactive, deprotonating non-coordinating benzene and toluene in substoichiometric amounts of (*R,R*)-TMCDA.<sup>[169]</sup>

Turning to solution-state chemistry, only three aggregates containing (*R,R*)-TMCDA have been divulged thus far, all from spectroscopic studies conducted by Collum.<sup>[45, 49, 158, 174]</sup> NMR analysis of LDA in a 2 : 1 toluene-pentane solution containing (*R,R*)-TMCDA provided evidence of exclusive monomer formation,<sup>[45, 49]</sup> and when (*R,R*)-TMCDA was added to <sup>n</sup>BuLi or PhLi in toluene, dimers formed in solution.<sup>[158, 174]</sup>

Surprisingly, the synthetic and structural chemistry of chiral diamine complexes of alkali metal amides has been largely neglected,<sup>[175]</sup> despite increased deprotonative selectivity of an amidolithium *versus* an alkyllithium towards certain organic substrates (nucleophilic addition is a common competing reaction for the latter).

Addressing this deficiency, and following on from the successful preparation and isolation of the first chiral amidozincate (complex **41**, Figure 1.36) and chiral amidomagnesiate (complex **52**, Figure 1.39) we hope to develop this topical area of organometallic chemistry through the design of new, potentially enantioselective, bases by incorporating the chiral diamines (–)-sparteine and (*R,R*)-TMCDA into the molecular framework of alkali metal, and mixed alkali metal-magnesium/zinc amide complexes, and investigating the solid-state and solution structures of such bases, with the aim of utilising these ‘designer’ synergic reagents in heterometallic enantioselective synthesis.

## 1.7 Salt Effects in Organometallic Chemistry

Alkali metal halide salts, particularly those of lithium (when added intentionally or unintentionally), can produce substantial positive or negative effects on the reactivity and/or selectivity of organic transformations (Figure 1.43).<sup>[176]</sup> Although numerous chemical, spectroscopic and theoretical investigations have unveiled salt effects in specific systems, the reasons for them, and the structures and mechanisms involved are generally buried in complexity.<sup>[59b, 63b, 69b, 177]</sup> It is only over the past decade that progress has been made in uncovering the fundamental aspects of salt effects in organometallic chemistry and in how

this understanding can be exploited in new ways in stoichiometric and catalytic reactions with implications for laboratory and process chemistry.<sup>[86, 178]</sup> Selected examples of the dramatic influence, both beneficial and detrimental, of the addition of the most widely studied alkali metal halide salt – lithium chloride – to reactions of organometallic reagents will now be presented.

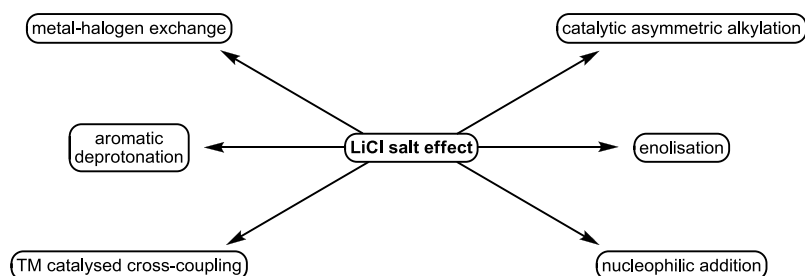
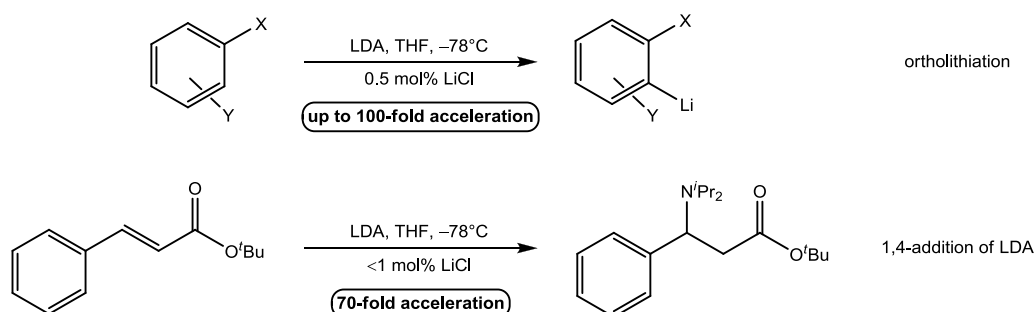


**Figure 1.43** Selected reactions in which LiCl has a profound effect.

Considering first the beneficial effects, Collum has established that LiCl plays a surprising and dominant role in a series of organic reactions.<sup>[178n, 178v, 178x, 178y]</sup> For example, *ortho*-lithiations of a range of arenes containing halogen-based directing groups (F, Cl or CF<sub>3</sub>), utilising the protocol commonly employed by organic chemists (LDA, THF, –78°C), can be greatly accelerated (up to 100-fold) by the addition of miniscule quantities of LiCl (as little as 0.5 mol%) (Scheme 1.31).<sup>[178n]</sup> The ‘striking accelerations’ elicited by such a minute quantity of LiCl is extraordinary, considering that the author draws attention to the fact that unpurified commercial samples of <sup>n</sup>BuLi used to prepare LDA are contaminated with sufficient quantities of LiCl to catalyse such reactions, an underlying point which may have gone unnoticed in previously reported lithiations. Rate variations were noted depending on the source and batch of commercial <sup>n</sup>BuLi utilised, which Collum highlights as potentially causing costly problems when processes are carried out on a larger scale in industry.

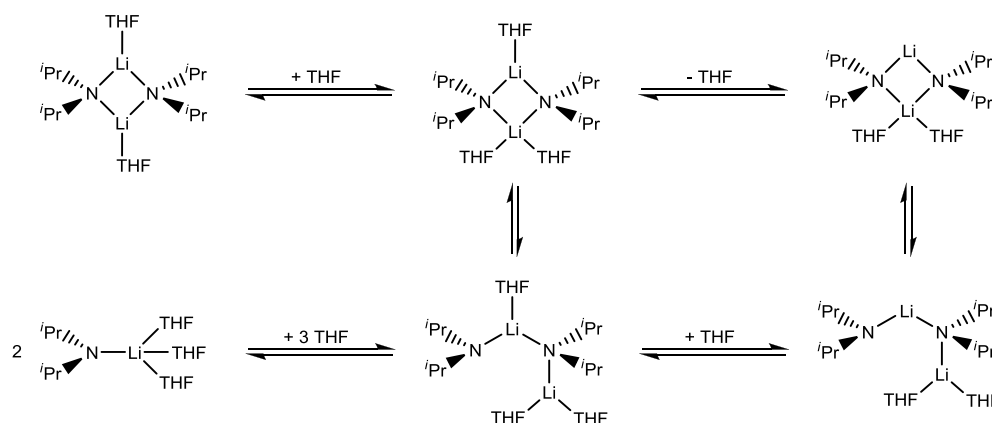


**Scheme 1.31** LiCl-catalysed reactions of LDA.

This LiCl catalysis phenomenon is not only applicable to deprotonation reactions but also to nucleophilic addition reactions. In a subsequent study investigating the 1,4-addition reactions of LDA to unsaturated esters, Collum detected similar rate accelerations (70-fold) provoked

by less than 1 mol% of LiCl (Scheme 1.31).<sup>[178v]</sup> The quantity of LiCl is crucial, as molar excesses can inhibit the reaction.

The same outcome from two distinct types of LDA-mediated reactions suggests a substrate independent process, which kinetic measurements thoroughly conducted by Collum indicate could involve the rate-limiting deaggregation of a THF di-solvated LDA dimer to a corresponding tri-solvated monomer (Scheme 1.32).<sup>[178v, 178x, 178y]</sup> The kinetics are highly complex, involving a combination of a range of process including for example a mixture of deaggregation, autocatalysis, homodimerisation and mixed dimerisation, hence, a lot of physical-organic work is still needed to untangle these interwoven pathways. However, what is clear is that it is these rates of aggregate exchange which dictate reactivity and the autocatalysis and catalysis by LiCl is extremely prominent in these LDA-mediated reactions.



**Scheme 1.32** Reaction pathway for the deaggregation of the di-solvated LDA dimer to the corresponding tri-solvated monomer.

LiCl influences the reaction rate by catalysing the deaggregation of the LDA dimer to a highly reactive LDA monomer, but quite how LiCl does this still remains unclear as under conditions of LiCl catalysis, LiCl exists exclusively as a 1 : 8 mixture of mixed aggregates (dimer and trimer) with LDA and the fate of these aggregates under the reaction conditions is unknown (Figure 1.44).<sup>[178v, 178x]</sup> Nevertheless, Collum does propose two possible routes, either an LDA rung breaks away from a mixed (LDA·LiCl)<sub>2</sub> ladder or a (LDA·THF)<sub>2</sub>Cl<sup>-</sup> ate releases monomeric LDA(THF)<sub>2</sub> and (LDA)Cl<sup>-</sup> (Scheme 1.33).<sup>[178x]</sup>

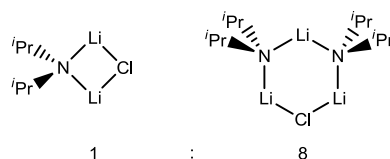
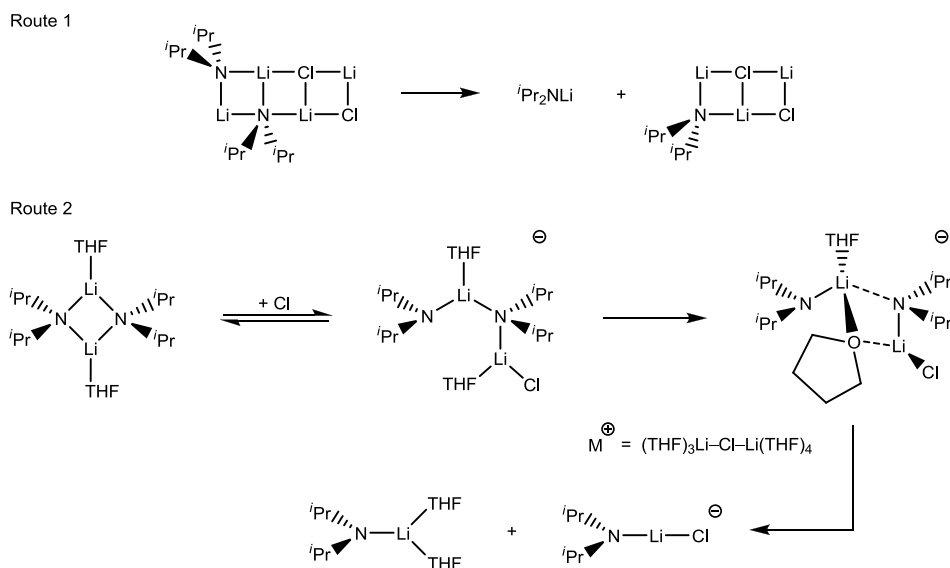


**Figure 1.44** 1 : 8 mixture of LiCl-LDA dimer and trimer formed at the low concentrations utilised in the rate studies conducted by Collum.



**Scheme 1.33** Proposed routes for the LiCl catalysed deaggregation of LDA dimer to LDA monomer. LDA rung breaking away from a mixed  $(\text{LDA}\cdot\text{LiCl})_2$  ladder (route 1) and a  $(\text{LDA}\cdot\text{THF})_2\text{Cl}^-$  ate releasing monomeric  $\text{LDA}(\text{THF})_2$  and  $(\text{LDA})\text{Cl}^-$  (route 2).

Solution evidence for LiCl-facilitated deaggregation of organolithium reagents comes from combined NMR and DFT studies conducted by Maddaluno,<sup>[178u]</sup> who, on mixing tetrameric MeLi with dimeric LiCl in a THF solution, found a single new species, in dinuclear  $[(\text{MeLi})(\text{LiCl})]$ , in the equilibrium mixture. DOSY experiments suggested that this dinuclear species was tri-solvated by THF, containing a monomeric fragment of MeLi.

The beneficial effects of the addition of LiCl have also been noted in metal base chemistry, where the exploitation of salt effects has led to reagents with improved synthetic performance. Knochel has excelled in this area (*vide supra*), adding stoichiometric LiCl to conventional Grignard or Hauser reagents [producing his turbo-Grignard/Hauser reagents *e.g.*,  $\alpha^i\text{PrMgCl}\cdot\text{LiCl}$ ],<sup>[86a, 86b, 86m]</sup>  $\alpha^i\text{Pr}_2\text{Mg}\cdot\text{LiCl}$ ,<sup>[86c]</sup>  $\alpha^i\text{Pr}(\text{TMP})\text{MgCl}\cdot\text{LiCl}$ ,<sup>[86d-f, 86i-n]</sup> and  $\alpha^i\text{Pr}(\text{TMP})_2\text{Mg}\cdot 2\text{LiCl}$ ,<sup>[86g, 86h, 86n]</sup> to induce an enhanced reactivity towards many aromatics and heterocycles generally inert towards ‘non-turbo’ prototypes. Turbo magnesiating reagents display a greater functional group tolerance (*e.g.*, to esters, nitriles and ketones) than conventional organolithium reagents but are intolerant of the most sensitive groups (*e.g.*, aldehydes or nitro).

Tolerance thresholds can be raised further by incorporating  $\text{ZnCl}_2$ , such as in the complex  $\alpha^i\text{Pr}(\text{TMP})_2\text{Zn}\cdot\text{MgCl}_2\cdot 2\text{LiCl}$ ,<sup>[86n, 178h, 178j]</sup> which can metallate triazoles and oxadiazoles.<sup>[178d]</sup>

The combination of salts promotes stability and high zinc reactivity, although, the order of addition is important. Adding  $\text{ZnCl}_2$  first to the substrate (*e.g.*, pyrazine) followed by  $\alpha^i\text{Pr}(\text{TMP})_2\text{Mg}\cdot 2\text{LiCl}$  produced faster deprotonation rates than the reverse order of addition or

with preformed “(TMP)<sub>2</sub>Zn·MgCl<sub>2</sub>·2LiCl”.<sup>[178i]</sup> As detailed in section 1.3, Mulvey *et al.* successfully determined the X-ray crystallographic structure of Knochel’s “[ (TMP)MgCl·LiCl ]” base,<sup>[93]</sup> indicating that ate species are implicated in turbo reagent chemistry, with further circumstantial evidence provided by DOSY NMR studies.<sup>[178r]</sup>

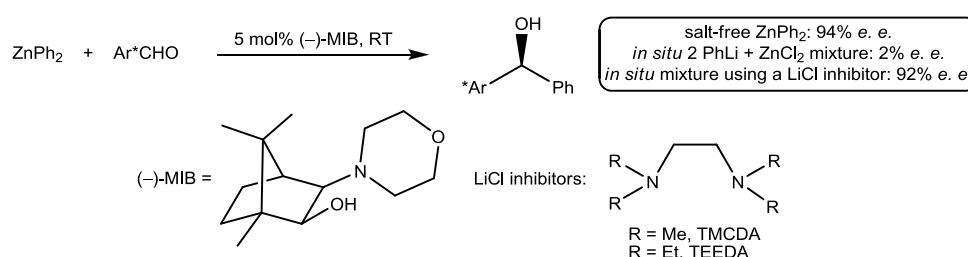
Knochel has also used Zn powder in conjunction with LiCl and THF to prepare a range of functionalised organozinc compounds by the direct insertion of zinc into alkyl, aryl and heteroaryl iodides and bromides<sup>[178a]</sup> and benzyl chlorides,<sup>[178f]</sup> including Directed *ortho*-Insertion (DoI) reactions performed on aromatic and heterocyclic systems.<sup>[178e]</sup> Extending this work further, he has induced chirality into a series of homoallylic alcohols by preparing di- and tri-substituted allylic zinc chlorides (starting from the corresponding allylic chlorides) and coupling these with various ketones.<sup>[178b]</sup> Recent findings by Oshima suggest that the addition of LiCl not only facilitates zinc insertion, but also enhances the reactivity of the resulting organozinc halides towards transmetallation.<sup>[178g]</sup> Anion-mode electrospray ionisation (ESI) mass spectrometry experiments, conducted by Koszinowski, on THF solutions of the products formed from LiCl-mediated zinc insertion reactions into various organic halides, revealed that mixed organozincate anions were observed, depending on the type of halide ion present.<sup>[178m]</sup> Their analysis revealed that reactions with organic bromides and iodides yielded predominantly mononuclear complexes, such as ZnRHalCl<sup>-</sup> and ZnRHal<sub>2</sub><sup>-</sup> (where Hal = halide), whereas reactions with organic chlorides, produced polynuclear complexes, such as Zn<sub>2</sub>Bn<sub>2</sub>Cl<sub>3</sub><sup>-</sup> and Zn<sub>3</sub>Bn<sub>3</sub>Cl<sub>4</sub><sup>-</sup> (where Bn = benzyl). These differences in aggregation states (which appear to be governed by the nature of the halide ion) may offer an explanation of the observed reactivity of the organozinc species described and the pronounced effect of LiCl in organozinc chemistry.

Moving to detrimental effects, studies conducted by Maddaluno of enantioselective nucleophilic alkylation reactions, showed that here, on the addition of LiCl to *o*-tolualdehyde with MeLi (in the presence of a chiral lithium amide) the *e. e.* of the resulting *o*-tolylethanol was significantly reduced (from 80% *e. e.* to 40% *e. e.*).<sup>[178c]</sup> Multinuclear NMR spectroscopy (carried out in THF) confirmed that the initial mixed aggregate of the chiral lithium amide and MeLi was rapidly, totally, and irreversibly replaced by a similar complex involving one lithium chloride and one lithium amide. The chiral inductor is thus trapped in an inactive complex, leaving only ‘naked’ MeLi to react with the aldehyde. DFT calculations supported the thermodynamic preference for the chiral lithium amide/LiCl aggregate and together these results rationalise the negative effect of the presence of LiCl on the *e. e.* of the studied reaction. Recently, Maddaluno has been able to achieve the first substoichiometric version of



this enantiomeric addition reaction by adding 0.33 equivalents of LiCl to the THF solution of the aldehyde before it is introduced onto the preformed chiral lithium amide/MeLi aggregate.<sup>[178z]</sup>

In many cases LiCl is not added deliberately, but instead forms *in situ* in a metathesis reaction and is often dismissed as an innocent by-product. For example, in the catalytic asymmetric synthesis of diarylmethanols,<sup>[179]</sup> prepared by the phenylation (with ZnPh<sub>2</sub>) of aromatic aldehydes in the presence of an enantioenriched catalyst [3-*exo*-morpholinoisoborneol (MIB)], the Lewis acidic LiCl by-product promotes an achiral background reaction, resulting in diarylmethanols with diminished *e. e.* Walsh overcame this inhibition by adding a Lewis base, such as TMEDA or *N,N,N',N'*-tetraethylethylenediamine (TEEDA) (Scheme 1.34).<sup>[178o]</sup>



**Scheme 1.34** LiCl inhibited catalytic asymmetric synthesis of diarylmethanols.

Similar negative effects have been observed by Marder and Lei,<sup>[178p]</sup> in Ni-catalysed oxidative homocouplings of PhZnCl, in which the arylzinc reagents were generated *in situ* via the salt-metathesis reaction between ZnCl<sub>2</sub> and either the aryl-Grignard reagent PhMgCl or the aryllithium reagent PhLi. When the aryl-Grignard reagent was utilised the yield was quantitative; however, when the aryllithium was employed the reaction only proceeded to 13% conversion. This marked difference in reactivity can be attributed to the *in situ* formation of LiCl in the latter process. Mixed-metal salt intermediates are implicated in this study and in related Negishi cross-couplings.<sup>[180]</sup>

The intriguing chemistry conferred thus far could be captured under the umbrella of ‘molecular salt chemistry’, with the Lewis acidic and Lewis basic properties of molecular LiCl at the hub of its complexity. It can be appreciated now, that if LiCl is present in a reaction solution, whether intentionally or unintentionally, then its possible influence must be explicitly explored before the chemistry can be confidently considered to be fully understood.

Despite the advances so far in this area, firm structural evidence of the crucial halide-incorporated species that may be involved in these reactions is rare.<sup>[177e, 177h, 178w]</sup> Work in our laboratory is thus currently focused on deconvoluting the complex chemistry at work when synthetically important alkali metal amides come into contact with a halide source.

Halide-incorporated species have recently come to the fore in the relatively new field of supramolecular anion coordination chemistry, an area of chemistry which covers a vast range of topics such as anion recognition, catalysis, anion sensors, ion-pair recognition, and anion templation and directed self-assembly. The expansion in understanding of how systems within these areas selectively bind, functionalise and transport negative anions, will undoubtedly be of high interest to environmental, biological and medicinal chemists worldwide.

## Chapter 2: Enhancing the Scope of *s*-block Homo- and Heterobimetallic Amide Chemistry

This chapter will be broken down into five sections. Firstly, the metallate chemistry of achiral *cis*-2,6-dimethylpiperidide (*cis*-DMP) is explored through its incorporation into structurally characterised alkali metal zincate and magnesiate complexes.<sup>[181]</sup> By comparison of the complexes produced with appropriate literature material, it has been possible to experimentally determine that the steric bulk of *cis*-DMP closely resembles that of diisopropylamide (DA) but is considerably less than that of 2,2,6,6-tetramethylpiperidide (TMP).

Focus then turns to the preparation and structural characterisation of two novel *N,N,N',N'*-tetramethylethylenediamine (TMEDA) adducts of sodium and potassium 1,1,1,3,3,3-hexamethyldisilazide (HMDS). The homometallic lithium compound of HMDS has long been a utility reagent in organic synthesis and its sodium and potassium congeners are becoming increasingly utilised due to their commercial availability; however, despite their importance in synthetic chemistry and the extensive employment of TMEDA as a co-ligand in organometallic chemistry, only the TMEDA adduct of LiHMDS has been crystallographically characterised.<sup>[182]</sup> Thus, the complexes reported herein allow the development of a homologues series of TMEDA-solvated alkali metal HMDS complexes.

Having successfully synthesised homometallic alkali metal salts of HMDS solvated by TMEDA, our attention turned to the possibility of incorporating the alkaline earth metal magnesium into these systems to afford HMDS-containing alkali metal magnesiates. Two new alkali metal tris(HMDS) magnesiate complexes, each containing the donor ligand TMEDA, were prepared and characterised. Both complexes have a solvent-separated ion pair composition of the form  $[M(TMEDA)_2]^+[Mg(HMDS)_3]^-$  (where M = Na or Li). The cation – with the sodium or lithium sequestered by the diamine, and the anion – consisting of three HMDS ligands coordinated to a magnesium centre, have previously been reported; however to date, they have not been synthesised within the same product.

The amide diphenylamide was then investigated as a possible newcomer to *alkali metal mediated metallation* (AMMM), as over the past few years Mulvey *et al.* have shown that DA, TMP and HMDS can be incorporated within these heterobimetallic alkali metal/divalent metal ate reagents.<sup>[85]</sup> As a prelude, the preparation and structural characterisation of three key monometallic building blocks: namely TMEDA adducts of  $MNPh_2$  (where M is Li, Na or K)

is reported.<sup>[183]</sup> This chemistry is being pursued as TMEDA has proved a useful co-ligand in reagents designed for *AMMM* applications.<sup>[84-85]</sup>

Finally, the chemistry of the synthetically-important utility amide TMP is explored through its incorporation into alkylmagnesium reagents. The magnesium reagent of choice to be utilised in these studies was  $(\text{Me}_3\text{SiCH}_2)_2\text{Mg}$ , as the more conventional and commercially available reagent of choice  $n\text{Bu}_2\text{Mg}$  has recently been shown to contain trace amounts of  $\text{Et}_3\text{Al}$  as a stabilising agent, the presence of which has unexpectedly been found to alter the course of reactions.<sup>[184]</sup> Two fundamental monometallic building blocks were isolated during these studies which are crucial in building up a greater understanding of the role neutral magnesium reagents play in magnesiate systems,<sup>[84-85]</sup> and also in the chemistry of macrocyclic inverse crown complexes.<sup>[98]</sup> A dimeric complex of the alkylmagnesium amide was prepared, which interestingly contains two different conformations of TMP ligand. One ligand adopts the usual chair conformation, which is adopted in the vast majority of *s*-block homo- and heterometallic complexes,<sup>[102d, 105-106, 185]</sup> while the second TMP ligand adopts a rarer, less thermodynamically-preferred twisted boat conformation.<sup>[186]</sup> It was hoped that by using a ‘cleaner’ magnesium reagent, crystals of the parent bis(amide)  $\text{Mg}(\text{TMP})_2$  (the solid-state structure of which has remained elusive despite its wide use in synthesis), could possibly be obtained. However on attempting to prepare the magnesium bis(amide), X-ray crystallographic analysis revealed that the crystalline material deposited was not representative of the simple formulation  $\text{Mg}(\text{TMP})_2$ , but was a tetranuclear triheteroanionic amide-alkoxide-amidoalkene complex. This complex contains two unusual and unexpected anions: an alkoxide, produced *via* oxygen insertion into a Mg–C bond; and a primary amidoalkene, produced *via* ring-opening of a TMP anion. To the best of our knowledge, this represents the first time that a ring-opened derivative of TMP has been captured within an organometallic product.

## 2.1 *cis*-DMP Zincate and Magnesiate Complexes

As highlighted earlier, there is currently worldwide interest surrounding the chemistry of alkali metal zincates and magnesiates.<sup>[84-85]</sup> Thus far, the amides which have drawn the most interest in these ate compositions are the synthetically important diisopropylamide (DA), 2,2,6,6-tetramethylpiperidide (TMP) and 1,1,1,3,3,3-hexamethyldisilazide (HMDS) (section 1.4, [Figure 1.27](#)), the homometallic lithium compounds of which have long been utility reagents in organic synthesis.

Focusing on zincates, [(THF)·Li(μ-TMP)(μ-<sup>t</sup>Bu)Zn(<sup>t</sup>Bu)],<sup>[90]</sup> **35**, [(TMEDA)·Na(μ-TMP)(μ-<sup>t</sup>Bu)Zn(<sup>t</sup>Bu)],<sup>[111]</sup> **38**, [(TMEDA)·Li(μ-TMP)(μ-<sup>n</sup>Bu)Zn(<sup>n</sup>Bu)],<sup>[124]</sup> **40** and [LiZn(TMP)<sub>3</sub>],<sup>[91a-c]</sup> **60**, have been shown to efficiently zincate (and sometimes even regioselectively multi-zincate) several key aromatic substrates such as benzene,<sup>[111, 187]</sup> toluene,<sup>[116]</sup> naphthalene,<sup>[112]</sup> aryl amides,<sup>[90b]</sup> nitriles,<sup>[188]</sup> anilines<sup>[114]</sup> and metallocenes.<sup>[124]</sup> As discussed in section 1.5, [(TMEDA)·Na(μ-TMP)(μ-CH<sub>2</sub>SiMe<sub>3</sub>)Zn(CH<sub>2</sub>SiMe<sub>3</sub>)], **39**, was successful in trapping and directly zincating the sensitive cyclic ether THF at the α-position at ambient temperature.<sup>[119]</sup> On changing the alkali metal from sodium to potassium and the donor ligand from TMEDA to PMDETA, the potassium zincate [(PMDETA)·K(μ-TMP)(μ-CH<sub>2</sub>SiMe<sub>3</sub>)Zn(CH<sub>2</sub>SiMe<sub>3</sub>)], **61**, was effective in metallating ethene, which is extraordinary as its metallation is exceedingly difficult due to its low acidity (pK<sub>a</sub> ~44).<sup>[119]</sup> In addition, [(TMEDA)·Li(μ-DA)(μ-<sup>t</sup>Bu)Zn(<sup>t</sup>Bu)], **62** and its sodium congener [(TMEDA)·Na(μ-DA)(μ-<sup>t</sup>Bu)Zn(<sup>t</sup>Bu)], **63**, have been shown to metallate alkynes.<sup>[125, 189]</sup> Complex **63** is also found to undergo a slow ligand reorganisation process to yield the bis(amido)alkyl zincate [(TMEDA)·Na(μ-DA)<sub>2</sub>Zn(<sup>t</sup>Bu)], **64** and the tris(alkyl) zincate [(TMEDA)·Na(μ-<sup>t</sup>Bu)<sub>2</sub>Zn(<sup>t</sup>Bu)], **65** (section 2.1.2, [Scheme 2.3](#)).<sup>[125]</sup>

Moving to the HMDS-containing lithium zincates, [(TMTA)·Li(μ-HMDS)Zn(CH<sub>2</sub>SiMe<sub>3</sub>)<sub>2</sub>],<sup>[190]</sup> **66** and [(PMDETA)·Li(μ-HMDS)Zn(Me)<sub>2</sub>],<sup>[191]</sup> **67**, (TMTA is 1,3,5-trimethyl-1,3,5-triazinane) have recently been prepared and characterised, and unusually the amido ligand in the latter occupies a terminal position in the solid-state. Recently, the first alkyl/amido zincates containing a primary amide (2,6-diisopropylphenylamide) have come to the fore.<sup>[192]</sup>

Turning to the magnesiates, several bimetallic alkyl/amido examples have been structurally characterised and utilised in synthesis.<sup>[38, 84, 86d, 87a, 87b, 88, 98, 100, 105-110, 115, 185c, 187, 193]</sup> Perhaps the most comprehensively studied is the sodium magnesiate [(TMEDA)·Na(μ-TMP)(μ-<sup>n</sup>Bu)Mg(TMP)],<sup>[106]</sup> **37**, which has recently been shown to selectively metallate benzene,<sup>[106]</sup> toluene<sup>[107]</sup> and metallocenes.<sup>[110]</sup> Remarkably, [(TMEDA)·Na(μ-TMP)(μ-CH<sub>2</sub>SiMe<sub>3</sub>)Mg(TMP)], **68**, was successful in deprotonating furan, producing a dodecasodium-hexamagnesium molecule [(TMEDA)<sub>3</sub>Na<sub>6</sub>Mg<sub>3</sub>-(CH<sub>2</sub>SiMe<sub>3</sub>)(2,5-C<sub>4</sub>H<sub>2</sub>O)<sub>3</sub>(2-C<sub>4</sub>H<sub>3</sub>O)<sub>5</sub>]<sub>2</sub>, **69**, in which ten furan ligands have been mono-deprotonated and six ligands have been di-deprotonated.<sup>[193p]</sup> Also, [LiMg(DA)<sub>3</sub>], **70** and its sodium congener [NaMg(DA)<sub>3</sub>], **71**, have been shown to smoothly magnesiate alkynes.<sup>[193o]</sup>

Work at Strathclyde is now focusing on chiral avenues in zincate/magnesiate chemistry.<sup>[162]</sup> One direction which we are pursuing is the incorporation of chiral amides within the mixed-

metal alkyl/amido metallate framework. In this study the metallate chemistry of achiral *cis*-2,6-dimethylpiperidide (*cis*-DMP) is explored (Figure 2.1). Due to the fact that this amine is much more accessible than either of its two chiral *trans*-isomers, we decided to focus on this isomer as a prelude to work with its chiral isomers. Surprisingly, little attention has been paid to *cis*-DMP despite its structural similarity to DA and TMP.

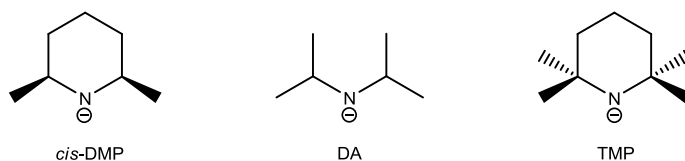


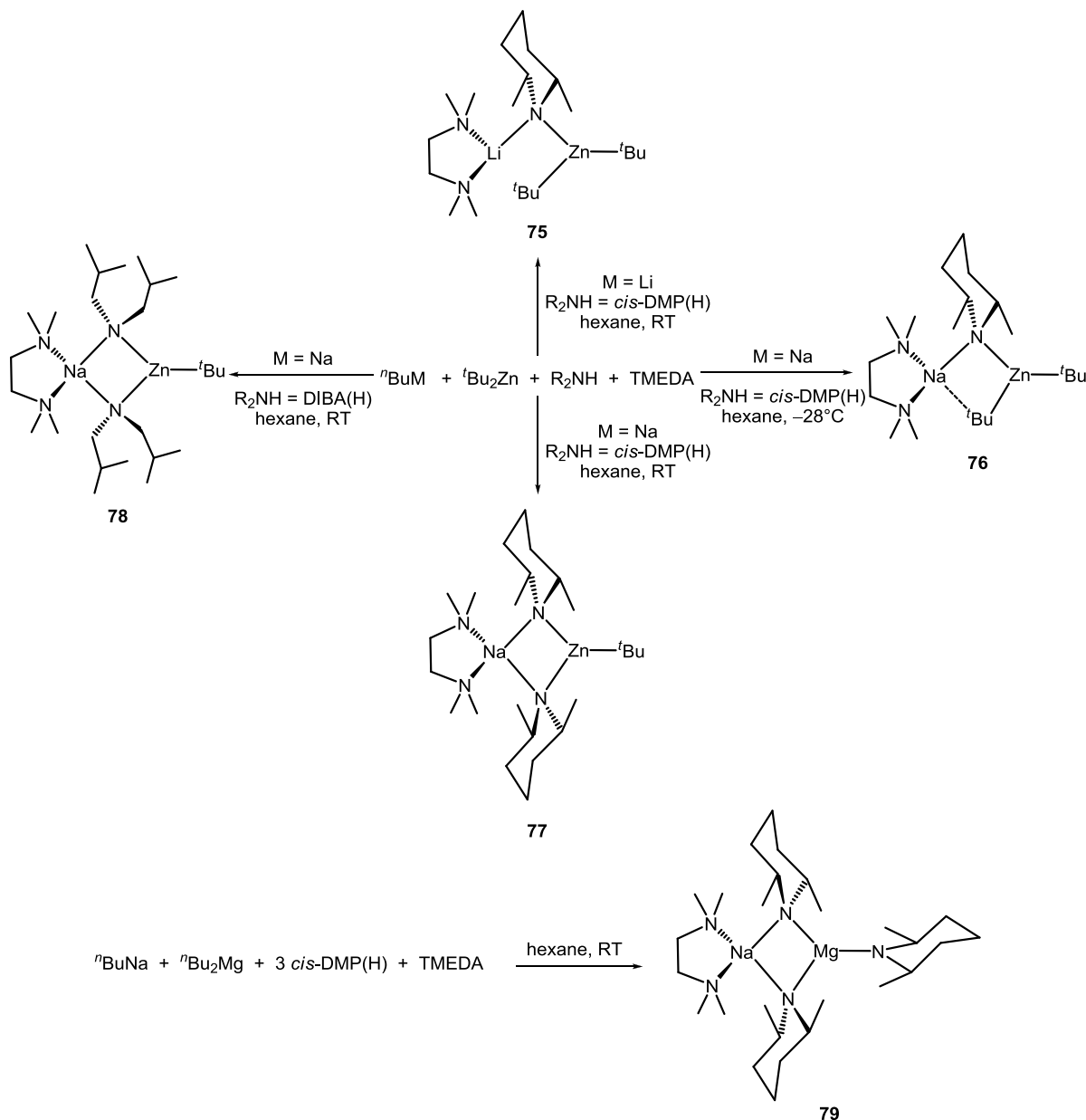
**Figure 2.1** Structural representation of *cis*-DMP with common utility amides.

To the best of our knowledge, only three metal amide species of this ligand are known: the polymeric TMEDA-solvated lithium amide [(TMEDA)Li(*cis*-DMP)]<sub>∞</sub>,<sup>[194]</sup> **72**, the dimeric amidoaluminium dihydride [(*cis*-DMP)Al(H<sub>2</sub>)<sub>2</sub>]<sub>2</sub>,<sup>[195]</sup> **73** and the tris(alkyl)amido potassium aluminate [(PMDETA)·K(μ-*cis*-DMP)(μ-<sup>*i*</sup>Bu)Al(<sup>*i*</sup>Bu)<sub>2</sub>],<sup>[196]</sup> **74**. Like DA, *cis*-DMP has two β-hydrogen atoms; and like TMP, *cis*-DMP is cyclic. Therefore *cis*-DMP can be regarded as a ‘tied-back’ variant of DA, or a less sterically demanding version of TMP which lacks two of the four CH<sub>3</sub> limbs (Figure 2.1). This begs the question: will *cis*-DMP function as a structural mimic of DA or TMP?

To begin to try and answer this question we attempted the synthesis and characterisation of lithium and sodium zincates, along with a sodium magnesiate which incorporate the *cis*-DMP anion, hoping to give some insight into the behaviour of *cis*-DMP in comparison to the much more comprehensively studied chemistry of DA and TMP.<sup>[181]</sup>

Four novel heterobimetallic ate complexes containing *cis*-DMP were prepared and characterised (Scheme 2.1). Two contain one *cis*-DMP ligand, namely the bis(alkyl)amido lithium and sodium zincates [(TMEDA)·Li(μ-*cis*-DMP)Zn(<sup>*t*</sup>Bu)<sub>2</sub>], **75** and [(TMEDA)·Na(μ-*cis*-DMP)(μ-<sup>*t*</sup>Bu)Zn(<sup>*t*</sup>Bu)], **76**. Both **75** and **76** were synthesised by co-complexation of the respective alkali metal amide with di-*tert*-butylzinc in the presence of a molar equivalent of TMEDA in a hydrocarbon medium. The third complex, containing two *cis*-DMP ligands, is the bis(amido)alkyl sodium zincate [(TMEDA)·Na(μ-*cis*-DMP)<sub>2</sub>Zn(<sup>*t*</sup>Bu)], **77**, which was prepared from **76** via a ligand reorganisation process where the by-product is [(TMEDA)·Na(μ-<sup>*t*</sup>Bu)<sub>2</sub>Zn(<sup>*t*</sup>Bu)], **65**. In a similar fashion, another bis(amido)alkyl sodium zincate, [(TMEDA)·Na(μ-DIBA)<sub>2</sub>Zn(<sup>*t*</sup>Bu)], **78**, was synthesised by utilising diisobutylamine [DIBA(H)], which emphasises the generality of the ligand reorganisation process (*i.e.*, the complex could not be prepared from utilising two molar equivalents of the amine). Complex

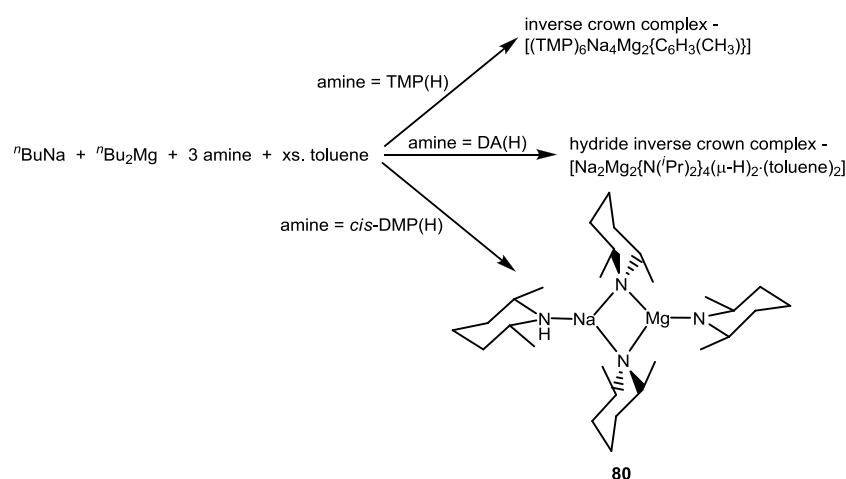
**79** contains three *cis*-DMP ligands and is a tris(amido) sodium magnesiumate [(TMEDA)·Na(μ-*cis*-DMP)<sub>2</sub>Mg(*cis*-DMP)], which is prepared by treating an equimolar mixture of *n*-butylsodium and di-*n*-butylmagnesium with three and one molar equivalents of *cis*-DMP and TMEDA respectively, in hydrocarbon solution. By comparison of **75-79** with appropriate complexes from the literature, it has been possible to experimentally determine that the steric bulk of *cis*-DMP closely resembles that of DA but is considerably less bulky than TMP.



**Scheme 2.1** Synthesis of complexes **75-79**.

To investigate the chemical reactivity of *cis*-DMP(H), the reaction shown in [Scheme 2.2](#) was carried out in a hydrocarbon medium and the resultant product (complex **80**) compared with the products obtained from the same reaction utilising TMP(H) or DA(H), which had previously been studied by Mulvey *et al.*<sup>[104a, 105]</sup> Changing the amine from TMP(H) to

DA(H) to *cis*-DMP(H) dramatically influences the type of product obtained. When TMP(H) is utilised in the reaction, an inverse crown structure is isolated, where a molecule of di-deprotonated toluene (2,5-positions) has been encapsulated [see chapter 1, section 1.5, [Figure 1.30](#) for representative structural motif (1,4-di-deprotonated benzene example)];<sup>[105]</sup> when DA(H) is utilised, the sole isolable organometallic species isolated was that of a hydride inverse crown structure, where a molecule of toluene solvates each of the alkali metal centres [see chapter 1, section 1.4, [Scheme 1.19](#) for representative structural motif (where M = Na and both sodium atoms are solvated by a molecule of toluene)];<sup>[104a]</sup> and finally on investigating the chemical reactivity of *cis*-DMP(H), no reaction with toluene was observed, and instead, a tris(amido) complex [ $\{cis\text{-DMP(H)}\}\cdot\text{Na}(\mu\text{-}cis\text{-DMP})_2\text{Mg}(cis\text{-DMP})$ ], **80**, was obtained, where the sodium atom is solvated by *cis*-DMP(H) ([Scheme 2.2](#)).



**Scheme 2.2** Synthesis of complex **80** utilising *cis*-DMP(H) and products obtained from the same reaction utilising TMP(H) or DA(H).

### 2.1.1 [(TMEDA)·Li(μ-*cis*-DMP)Zn(<sup>*t*</sup>Bu)<sub>2</sub>], **75**

Complex **75** was prepared by reacting *n*-butyllithium with an equimolar quantity of *cis*-DMP(H) and then one molar equivalent of di-*tert*-butylzinc in a hexane medium (introduced *via* cannula). One molar equivalent of TMEDA was required to produce a homogeneous solution. X-ray quality crystals of **75**, a bis(alkyl)amido lithium zincate, precipitated from the hydrocarbon solution at ambient temperature. It can be seen from [Scheme 2.1](#) that the synthetic approach and ultimate composition (that is an amido : alkyl ratio of 1 : 2) of **75** resembles that of Westerhausen's HMDS-containing lithium zincate [(TMTA)·Li(μ-HMDS)Zn(CH<sub>2</sub>SiMe<sub>3</sub>)<sub>2</sub>], **66**, reported in 1994.<sup>[190]</sup>

X-ray crystallographic analysis reveals that **75** crystallises in the monoclinic system, space group *P*2<sub>1</sub>. The structure of **75** ([Figure 2.2](#)) is composed of a lithium centre coordinated to a TMEDA ligand and a zinc centre coordinated to two <sup>*t*</sup>Bu anions, with a *cis*-DMP anion



bridging the two metal centres (each metal centre is three coordinate). Table 2.1 and Table 2.2 detail the key bond distances and bond angles respectively.

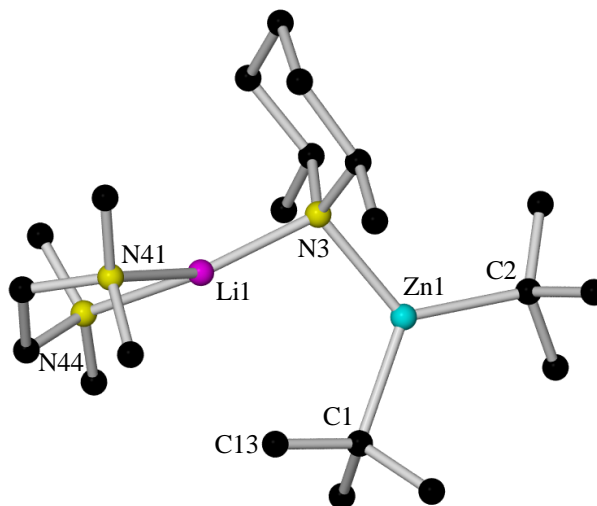


**Figure 2.2** Molecular structure of [(TMEDA)·Li(μ-*cis*-DMP)Zn(*t*Bu)<sub>2</sub>], **75**. H atoms are omitted for clarity.

Selected Bond	Bond Distance (Å) in [(TMEDA)·Li(μ- <i>cis</i> -DMP)Zn( <i>t</i> Bu) <sub>2</sub> ], <b>75</b>
Li1–N3	2.027(3)
Li1–N41	2.211(3)
Li1–N44	2.198(3)
Zn1–N3	2.062(1)
Zn1–C1	2.048(2)
Zn1–C2	2.051(2)

**Table 2.1** Key bond distances within [(TMEDA)·Li(μ-*cis*-DMP)Zn(*t*Bu)<sub>2</sub>], **75**.

Selected Angle	Bond Angle (°) in [(TMEDA)·Li(μ- <i>cis</i> -DMP)Zn( <i>t</i> Bu) <sub>2</sub> ], <b>75</b>
N3–Li1–N41	137.52(14)
N3–Li1–N44	133.22(14)
N41–Li1–N44	85.62(10)
N3–Zn1–C1	116.19(6)
N3–Zn1–C2	121.06(5)
C1–Zn1–C2	122.61(6)
Li1–N3–Zn1	106.16(9)

**Table 2.2** Key bond angles within [(TMEDA)·Li(μ-*cis*-DMP)Zn(*t*Bu)<sub>2</sub>], **75**.

Due to the acute TMEDA–Li bite angle (N41–Li1–N44) of 85.62(10)°, the Li geometry is best described as highly distorted trigonal planar (summed angles at Li, 356.36°), whereas that of Zn is almost perfectly trigonal planar [summed angles at Zn, 359.86°; range of angles, 116.19(6)-122.61(6)°]. The Li–N<sub>*cis*-DMP</sub> bond distance [2.027(3) Å] in **75** is slightly shorter than the corresponding bond in [(TMEDA)Li(*cis*-DMP)]<sub>∞</sub>,<sup>[194]</sup> **72** (mean distance, 2.044 Å); whilst the Li–N<sub>TMEDA</sub> bond distances are in turn longer (mean distance in **75** and **72** are 2.205 and 2.161 Å respectively). Zincate **75** has an open, curved Li–N3–Zn–C1 motif [Li1⋯C1 and Li1⋯C13 distances are 3.545(3) and 2.813(3) Å respectively]. A similar scenario was

encountered in the HMDS zincates [(TMTA)·Li(μ-HMDS)Zn(CH<sub>2</sub>SiMe<sub>3</sub>)<sub>2</sub>],<sup>[190]</sup> **66** and [(PMDETA)·Li(μ-HMDS)Zn(Me)<sub>2</sub>],<sup>[191]</sup> **67**. Presumably a ‘closed’ motif for **75** is not possible due to the combined steric bulk of a TMEDA ligand, the bridging amide and a <sup>t</sup>Bu group. In the latter HMDS zincate, a tridentate donor is utilised to sterically protect the Li centre; hence, reducing the need for an additional bridging ligand. In addition, the inclusion of PMDETA reverses the convention that an amide is a better bridging ligand than an alkyl group.

To aid the interpretation of the NMR data obtained in this project and in any future work, the <sup>1</sup>H, <sup>13</sup>C (Figure 2.3 and Figure 2.4 respectively), COSY and HSQC NMR spectra were obtained for the amine standard, *cis*-DMP(H), in C<sub>6</sub>D<sub>6</sub> solution. With the aid of the HSQC spectrum, the relevant chemical shifts from the <sup>13</sup>C NMR spectrum were assigned to their respective proton chemical shifts from the <sup>1</sup>H NMR spectrum and are shown in Table 2.3.

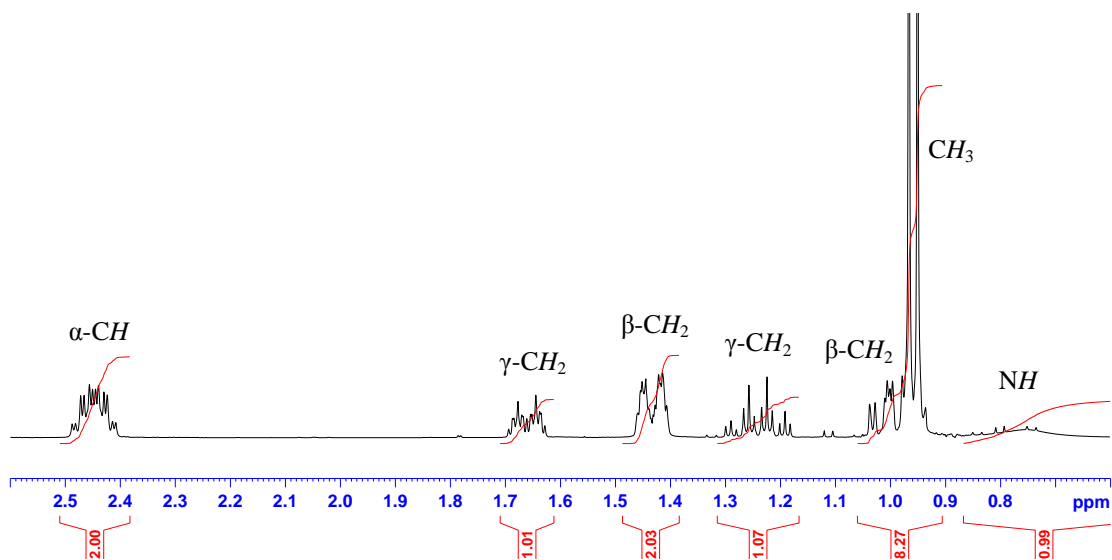


Figure 2.3 <sup>1</sup>H NMR spectrum of *cis*-DMP(H) in C<sub>6</sub>D<sub>6</sub>.

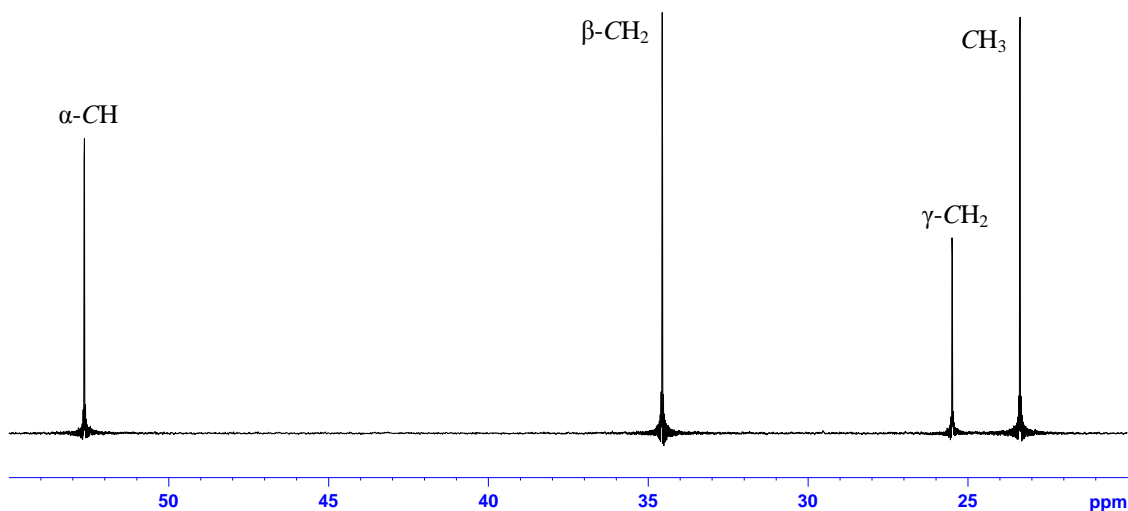


Figure 2.4 <sup>13</sup>C NMR spectrum of *cis*-DMP(H) in C<sub>6</sub>D<sub>6</sub>.

Due to the chair conformation adopted by *cis*-DMP(H) four resonances are observed for the four chemically distinct  $\beta$ - and  $\gamma$ -hydrogen atoms. There is a sextet of doublets at 2.45 ppm integrating to two protons, which corresponds to the two  $\alpha$ -hydrogens. The complex splitting pattern of this signal occurs due to coupling with the methyl group on the same  $\alpha$ -carbon and with the  $\beta$ -hydrogens. Further splitting, causing the doublets is due to coupling with the amino hydrogen atom. Two multiplets, each integrating to one proton, appear at 1.65 ppm (a doublet of quartets) and 1.24 ppm (a quartet of triplets) and correspond to the two  $\gamma$ -hydrogens. Also integrating to one proton is a broad signal at 0.75 ppm, which corresponds to the amino hydrogen (confirmed by COSY NMR spectroscopy). A large doublet at 0.96 ppm (which integrates to six protons) corresponds to the methyl groups, which are split due to coupling with the  $\alpha$ -hydrogens. Downfield of this doublet are signals at 1.43 and 1.00 ppm (both doublets of doublets), each integrating to two protons, corresponding to the  $\beta$ -hydrogens.

NMR chemical shifts of <i>cis</i> -DMP(H) in C <sub>6</sub> D <sub>6</sub>			
<sup>1</sup> H $\delta$ / ppm		<sup>13</sup> C $\delta$ / ppm	
$\alpha$ -CH	2.45	$\alpha$ -CH	52.6
$\beta$ -CH <sub>2</sub>	1.43	$\beta$ -CH <sub>2</sub>	34.6
	1.00		
$\gamma$ -CH <sub>2</sub>	1.65	$\gamma$ -CH <sub>2</sub>	25.5
	1.24		
CH <sub>3</sub>	0.96	CH <sub>3</sub>	23.4
NH	0.75	–	–

**Table 2.3** <sup>1</sup>H and <sup>13</sup>C NMR chemical shifts of *cis*-DMP(H) in C<sub>6</sub>D<sub>6</sub>.

In general, when deprotonated and incorporated within a bimetallic framework, the resonances associated with *cis*-DMP broaden and a systematic downfield shift of the  $\alpha$ -H, CH<sub>3</sub>, one  $\beta$ -H and one  $\gamma$ -H atom, and an upfield shift of the other  $\beta$ -H and  $\gamma$ -H atoms is observed. The corresponding <sup>13</sup>C NMR spectrum revealed that all *cis*-DMP chemical shifts are shifted downfield with respect to the uncoordinated amine.

Turning to the NMR spectroscopic analysis of **75**, the crystalline product was dissolved in C<sub>6</sub>D<sub>6</sub> solution and examined by <sup>7</sup>Li, <sup>1</sup>H, <sup>13</sup>C (Figures 2.5-2.7), COSY and HSQC NMR spectroscopy.

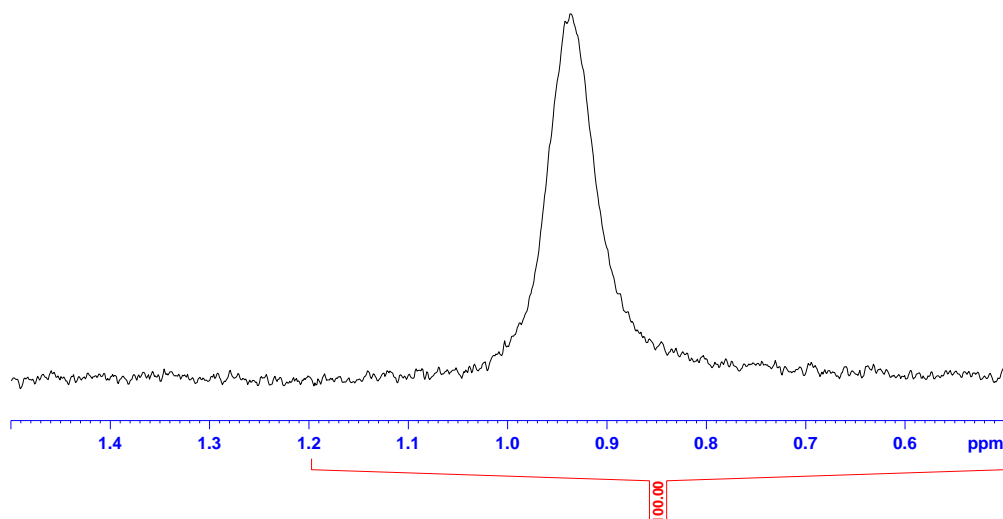


**Figure 2.5**  $^7\text{Li}$  NMR spectrum of  $[(\text{TMEDA})\cdot\text{Li}(\mu\text{-cis-DMP})\text{Zn}(\text{tBu})_2]$ , **75**, in  $\text{C}_6\text{D}_6$ .

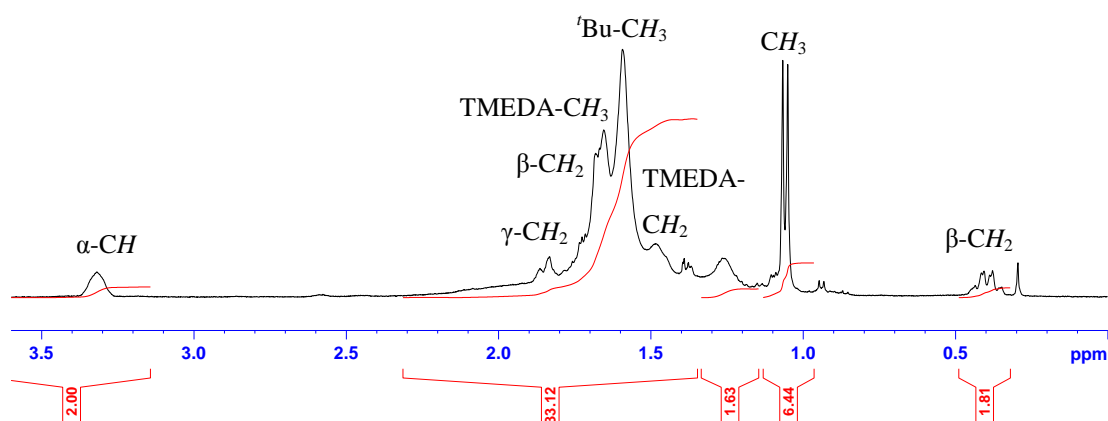


**Figure 2.6**  $^1\text{H}$  NMR spectrum of  $[(\text{TMEDA})\cdot\text{Li}(\mu\text{-cis-DMP})\text{Zn}(\text{tBu})_2]$ , **75**, in  $\text{C}_6\text{D}_6$ .

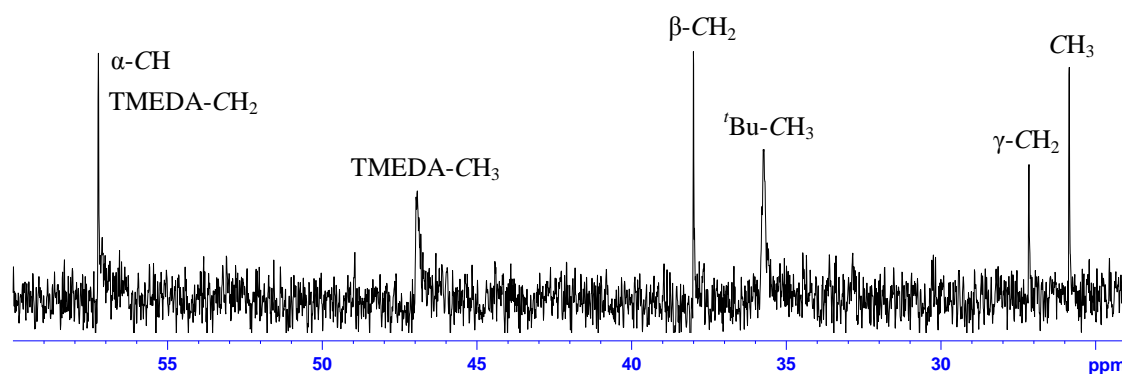


**Figure 2.7**  $^{13}\text{C}$  NMR spectrum of  $[(\text{TMEDA})\cdot\text{Li}(\mu\text{-cis-DMP})\text{Zn}(\text{tBu})_2]$ , **75**, in  $\text{C}_6\text{D}_6$ .

Assuming that there is free rotation about the Zn–N bond in **75**, the  $^1\text{H}$  NMR spectrum for a  $\text{C}_6\text{D}_6$  solution of **75** appears to indicate that the solid-state structure is maintained in solution. The resonances for the *cis*-DMP hydrogen atoms in **75** are significantly broader than those observed in the free amine and their chemical shifts are consistent with those reported for the  $d_8$ -THF solution of aforementioned  $[(\text{TMEDA})\text{Li}(\textit{cis}\text{-DMP})]_\infty$ , **72**.<sup>[194]</sup> The two  $^1\text{H}$  and two

$^{13}\text{C}$  resonances associated with the TMEDA ligand in **75** are different from those encountered in the free diamine, indicating that it remains coordinated to the alkali metal in arene solution. The resonance for the  $^t\text{Bu}$  quaternary *C* atom could not be located in the  $^{13}\text{C}$  NMR spectra for the solution of **75**.

With the aid of the HSQC spectrum, the relevant chemical shifts from the  $^{13}\text{C}$  NMR spectrum were assigned to their respective proton chemical shifts from the  $^1\text{H}$  NMR spectrum and are shown in Table 2.4.

NMR chemical shifts of [(TMEDA)·Li( $\mu$ - <i>cis</i> -DMP)Zn( $^t\text{Bu}$ ) <sub>2</sub> ], <b>75</b> , in C <sub>6</sub> D <sub>6</sub>			
$^1\text{H}$ $\delta$ / ppm		$^{13}\text{C}$ $\delta$ / ppm	
$\alpha$ -CH	3.32	$\alpha$ -CH	57.2
$\beta$ -CH <sub>2</sub>	1.67	$\beta$ -CH <sub>2</sub>	38.0
	0.39		
$\gamma$ -CH <sub>2</sub>	1.83	$\gamma$ -CH <sub>2</sub>	27.2
	1.72		
CH <sub>3</sub>	1.05	CH <sub>3</sub>	25.9
TMEDA (CH <sub>3</sub> )	1.66	TMEDA (CH <sub>3</sub> )	46.9
TMEDA (CH <sub>2</sub> )	1.48	TMEDA (CH <sub>2</sub> )	57.2
$^t\text{Bu}$ (CH <sub>3</sub> )	1.59	$^t\text{Bu}$ (CH <sub>3</sub> )	35.7
–	–	$^t\text{Bu}$ (C)	–

**Table 2.4**  $^1\text{H}$  and  $^{13}\text{C}$  NMR chemical shifts of [(TMEDA)·Li( $\mu$ -*cis*-DMP)Zn( $^t\text{Bu}$ )<sub>2</sub>], **75**, in C<sub>6</sub>D<sub>6</sub>.

### 2.1.2 [(TMEDA)·Na( $\mu$ -*cis*-DMP)( $\mu$ - $^t\text{Bu}$ )Zn( $^t\text{Bu}$ )], **76**

Complex **76**, a bis(alkyl)amido sodium zincate [(TMEDA)·Na( $\mu$ -*cis*-DMP)( $\mu$ - $^t\text{Bu}$ )Zn( $^t\text{Bu}$ )], is a *cis*-DMP analogue of [(TMEDA)·Na( $\mu$ -TMP)( $\mu$ - $^t\text{Bu}$ )Zn( $^t\text{Bu}$ )], **38**.<sup>[111]</sup> As mentioned previously, this latter complex has proven to be a useful utility base in the deprotonation of arenes<sup>[111, 187]</sup> and metallocenes<sup>[124]</sup> and indeed as a  $^t\text{Bu}$  nucleophile towards benzophenone.<sup>[197]</sup>

Following the same reaction methodology as that used to prepare **75** (using *n*-butylsodium in place of *n*-butyllithium) afforded X-ray quality crystals of **76** at  $-28^\circ\text{C}$  (Scheme 2.1).

X-ray crystallographic analysis reveals that **76** crystallises in the triclinic system, space group *P*1. Akin to its lithium congener **75**, the structure of **76** (Figure 2.8) is composed of the same basic building blocks – an alkali metal, a TMEDA ligand, a *cis*-DMP anion, a zinc centre and two  $^t\text{Bu}$  anions – the only difference being that one  $^t\text{Bu}$  anion bridges (*via* an agostic-type interaction) to the sodium atom rather than remaining terminally bound to the zinc atom (the sodium metal centre is four coordinate and the zinc metal centre three coordinate). Table 2.5 and Table 2.6 detail the key bond distances and bond angles respectively.

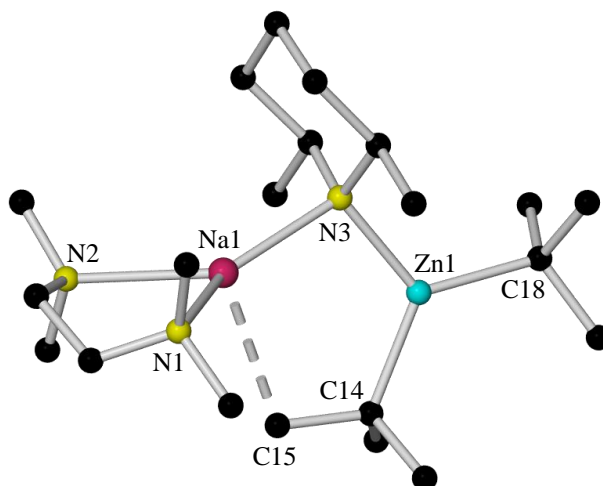


**Figure 2.8** Molecular structure of [(TMEDA)·Na(μ-*cis*-DMP)(μ-*t*Bu)Zn(*t*Bu)], **76**. H atoms are omitted for clarity.

Selected Bond	Bond Distance (Å) in [(TMEDA)·Na(μ- <i>cis</i> -DMP)(μ- <i>t</i> Bu)Zn( <i>t</i> Bu)], <b>76</b>
Na1–N1	2.452(5)
Na1–N2	2.462(6)
Na1–N3	2.342(5)
Na1···C15	2.845(10)
Zn1–N3	2.039(5)
Zn1–C14	2.048(5)
Zn1–C18	2.063(6)

**Table 2.5** Key bond distances within [(TMEDA)·Na(μ-*cis*-DMP)(μ-*t*Bu)Zn(*t*Bu)], **76**.

Selected Angle	Bond Angle (°) in [(TMEDA)·Na(μ- <i>cis</i> -DMP)(μ- <i>t</i> Bu)Zn( <i>t</i> Bu)], <b>76</b>
N1–Na1–N2	75.93(18)
N1–Na1–N3	137.69(19)
N2–Na1–N3	140.64(18)
N3–Zn1–C14	118.4(2)
N3–Zn1–C18	117.8(2)
C14–Zn1–C18	123.7(2)
Na1–N3–Zn1	103.3(2)

**Table 2.6** Key bond angles within [(TMEDA)·Na(μ-*cis*-DMP)(μ-*t*Bu)Zn(*t*Bu)], **76**.

The Zn centre in **76** has an almost identical coordination sphere [summed angles at Zn, 359.90°; range of angles, 117.8(2)-123.7(2)°] to that in **75**. The presence of the long Na1···C15 contact [2.845(10) Å] in **76** causes the coordination number of the alkali metal to increase from three (as in complex **75**) to four and the formation of a four-element, five-membered (NaNZnCC) ring system. Discounting this undoubtedly weak Na···C interaction, the total for the angles around the Na centre is 354.26°, suggesting that with respect to the N atoms, the metal's coordination sphere is much closer to planar (360°) than pyramidal (328.5°). Including the Na1···C15 interaction suggests that the geometry is therefore distorted

trigonal pyramidal rather than tetrahedral. In keeping with the larger size of the metal centre, the TMEDA bite-angle [75.93(18)°] is approximately 10° more acute in **76** than in **75**.

The bond distances within the respective five-membered bimetallic rings for **76** and the TMP analogue (complex **38**) differ significantly. For example, the shortest Na–C contact [2.845(7) Å] in **76** is longer (by 0.095 Å) than in complex **38** [2.750(10) Å]. This may be a consequence of the shorter Na–N<sub>amide</sub> and to a lesser extent the Zn–C<sub>bridging</sub> distances in **76** [Na–N<sub>amide</sub> and Zn–C<sub>bridging</sub> bond distances in complex **38** are 2.412(6) and 2.149(9) Å respectively].

Crystalline product **76** was dissolved in C<sub>6</sub>D<sub>6</sub> solution and examined by <sup>1</sup>H, <sup>13</sup>C (Figure 2.9 and Figure 2.10 respectively), COSY and HSQC NMR spectroscopy. The <sup>1</sup>H and <sup>13</sup>C NMR spectra essentially resemble that of **75**, except that the resonances associated with the two <sup>t</sup>Bu groups are extremely broad. This is possibly indicative of a significantly slower rotation about the Zn–N bond in **76** (when compared with **75**).

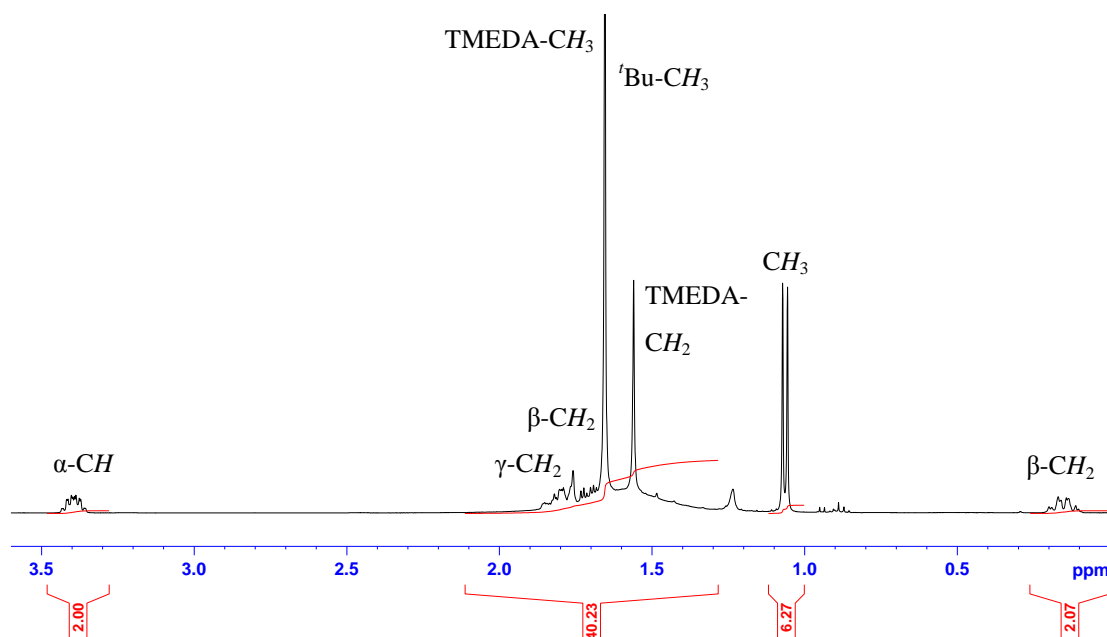


Figure 2.9 <sup>1</sup>H NMR spectrum of [(TMEDA)·Na(μ-*cis*-DMP)(μ-<sup>t</sup>Bu)Zn(<sup>t</sup>Bu)], **76**, in C<sub>6</sub>D<sub>6</sub>.

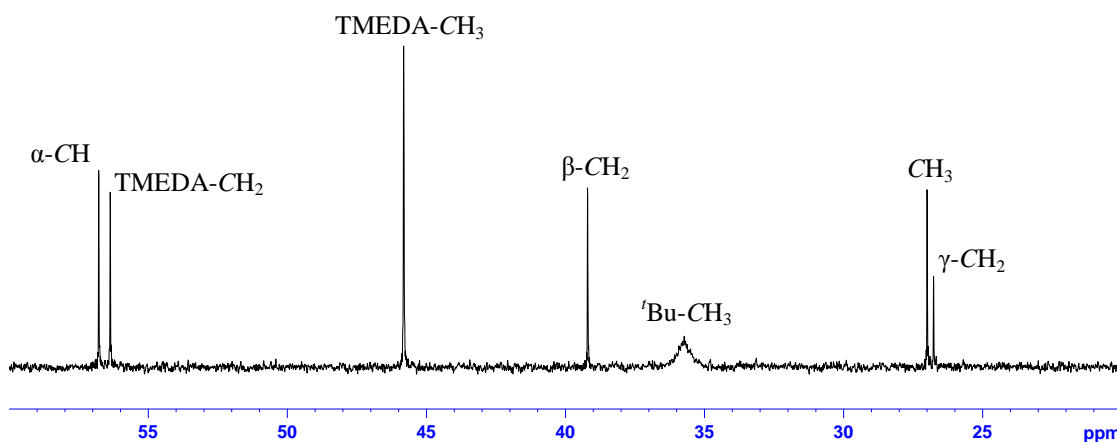


Figure 2.10 <sup>13</sup>C NMR spectrum of [(TMEDA)·Na(μ-*cis*-DMP)(μ-<sup>t</sup>Bu)Zn(<sup>t</sup>Bu)], **76**, in C<sub>6</sub>D<sub>6</sub>.

With the aid of the HSQC spectrum, the relevant chemical shifts from the  $^{13}\text{C}$  NMR spectrum were assigned to their respective proton chemical shifts from the  $^1\text{H}$  NMR spectrum and are shown in Table 2.7.

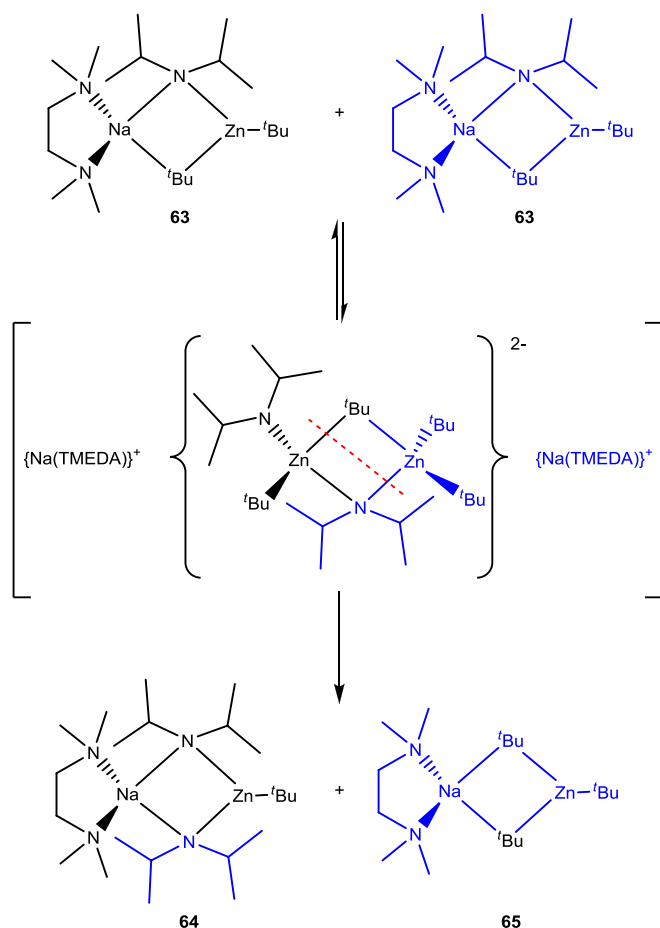
NMR chemical shifts of [(TMEDA)·Na(μ- <i>cis</i> -DMP)(μ- <sup>t</sup> Bu)Zn( <sup>t</sup> Bu)], <b>76</b> , in C <sub>6</sub> D <sub>6</sub>			
$^1\text{H}$ δ / ppm		$^{13}\text{C}$ δ / ppm	
α-CH	3.40	α-CH	56.4
β-CH <sub>2</sub>	1.70	β-CH <sub>2</sub>	39.2
	0.15		
γ-CH <sub>2</sub>	1.82	γ-CH <sub>2</sub>	26.8
	1.71		
CH <sub>3</sub>	1.07	CH <sub>3</sub>	27.0
TMEDA (CH <sub>3</sub> )	1.66	TMEDA (CH <sub>3</sub> )	45.8
TMEDA (CH <sub>2</sub> )	1.56	TMEDA (CH <sub>2</sub> )	56.8
<sup>t</sup> Bu (CH <sub>3</sub> )	1.61(br)	<sup>t</sup> Bu (CH <sub>3</sub> )	35.7
–	–	<sup>t</sup> Bu (C)	–

**Table 2.7**  $^1\text{H}$  and  $^{13}\text{C}$  NMR chemical shifts of [(TMEDA)·Na(μ-*cis*-DMP)(μ-<sup>t</sup>Bu)Zn(<sup>t</sup>Bu)], **76**, in C<sub>6</sub>D<sub>6</sub>.

For the sodium zincates, the reactivity for *cis*-DMP(H) is more in line with that of DA(H) than of TMP(H). For example, with TMP(H), only [(TMEDA)·Na(μ-TMP)(μ-<sup>t</sup>Bu)Zn(<sup>t</sup>Bu)],<sup>[111]</sup> **38**, is isolated and a bis(TMP) zincate has never been detected. With DA(H), the reaction is more complex than anticipated (Scheme 2.3). The aforementioned [(TMEDA)·Na(μ-DA)(μ-<sup>t</sup>Bu)Zn(<sup>t</sup>Bu)], **63**, is found to undergo a slow ligand reorganisation process (over 48 hours) to yield the bis(amido)alkyl zincate [(TMEDA)·Na(μ-DA)<sub>2</sub>Zn(<sup>t</sup>Bu)], **64** (*cf.*, complex **77**) and the tris(alkyl) zincate [(TMEDA)·Na(μ-<sup>t</sup>Bu)<sub>2</sub>Zn(<sup>t</sup>Bu)], **65**.<sup>[125]</sup>

Returning to **76**, this compound appears to exhibit identical behaviour to give **77** and [(TMEDA)·Na(μ-<sup>t</sup>Bu)<sub>2</sub>Zn(<sup>t</sup>Bu)], **65**, (observed by  $^1\text{H}$  NMR spectroscopic studies of the resultant filtrate) at ambient temperature over a period of approximately two weeks. To elaborate, the  $^1\text{H}$  NMR spectrum of the filtrate revealed a resonance at 1.41 ppm which was attributed to the C(CH<sub>3</sub>)<sub>3</sub> hydrogen atoms in [(TMEDA)·Na(μ-<sup>t</sup>Bu)<sub>2</sub>Zn(<sup>t</sup>Bu)], **65**. Also **76** does not appear to react with an additional equivalent of *cis*-DMP(H) to yield **77**.





**Scheme 2.3** Proposed pathway for the reorganisation of  $[(\text{TMEDA})\cdot\text{Na}(\mu\text{-DA})(\mu\text{-}^t\text{Bu})\text{Zn}(^t\text{Bu})]$ , **63**, to produce **64** and **65**.

### 2.1.3 $[(\text{TMEDA})\cdot\text{Na}(\mu\text{-}i\text{-cis-DMP})_2\text{Zn}(^t\text{Bu})]$ , **77**

Complex **77**, a bis(amido)alkyl sodium zincate  $[(\text{TMEDA})\cdot\text{Na}(\mu\text{-}i\text{-cis-DMP})_2\text{Zn}(^t\text{Bu})]$ , is only the second reported zincate which has a di(amido)alkyl constitution, the first being the DA zincate  $[(\text{TMEDA})\cdot\text{Na}(\mu\text{-DA})_2\text{Zn}(^t\text{Bu})]$ ,<sup>[125]</sup> **64**.

As mentioned previously, complex **77** is prepared from a solution used to make **76** via a ligand reorganisation process, which occurs over a period of approximately two weeks at ambient temperature, where the by-product is  $[(\text{TMEDA})\cdot\text{Na}(\mu\text{-}^t\text{Bu})_2\text{Zn}(^t\text{Bu})]$ , **65**.

Initial X-ray data suggests that **77** has the structure shown in Scheme 2.1, however, the data was of poor quality. Due to this, we decided to prepare another bis(amido)alkyl zincate so to prove further the generality of the ligand reorganisation process –  $[(\text{TMEDA})\cdot\text{Na}(\mu\text{-DIBA})_2\text{Zn}(^t\text{Bu})]$ ,<sup>[198]</sup> **78**, was prepared utilising diisobutylamine [DIBA(H)] (Scheme 2.1) (*i.e.*, the complex could not be prepared from utilising two molar equivalents of the amine).

The overall composition of complex **77** is confirmed by  $^1\text{H}$ ,  $^{13}\text{C}$  (Figure 2.11 and Figure 2.12 respectively), COSY and HSQC NMR spectroscopic studies conducted in  $\text{C}_6\text{D}_6$  solution. The  $^1\text{H}$  and  $^{13}\text{C}$  NMR spectra essentially resemble that of **75** and **76**, except that the resonances associated with the  $^t\text{Bu}$  groups are sharper, suggesting that this group does not undergo a dynamic exchange process to occupy a bridging position, presumably due to the retention of the strong Na–N bonding.

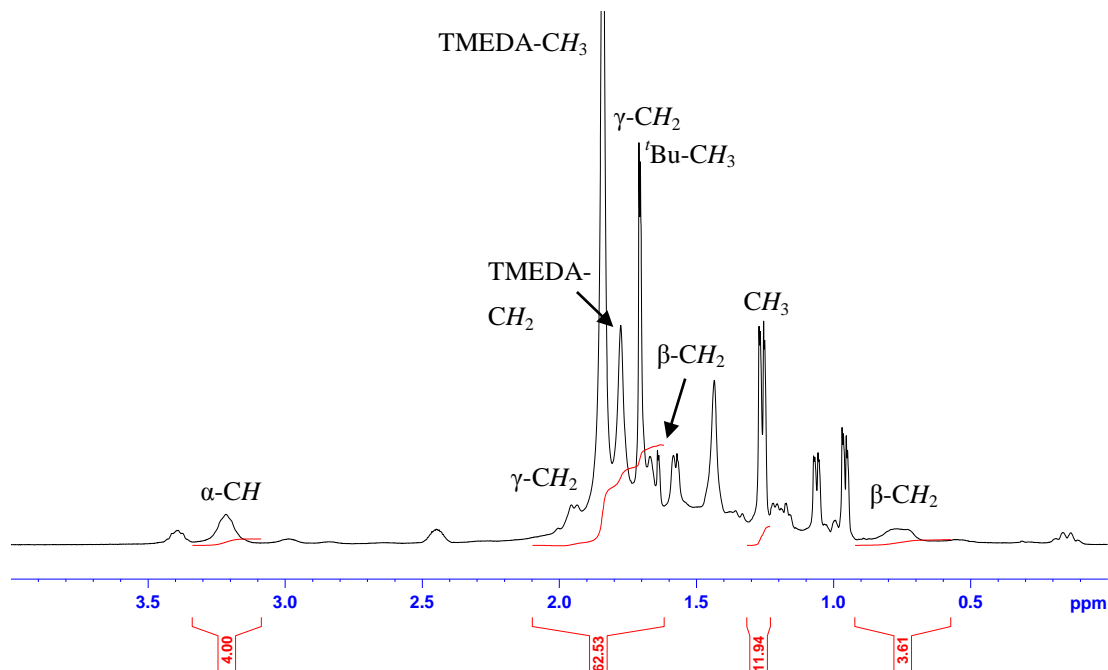


Figure 2.11  $^1\text{H}$  NMR spectrum of  $[(\text{TMEDA})\cdot\text{Na}(\mu\text{-cis-DMP})_2\text{Zn}(^t\text{Bu})]$ , **77**, in  $\text{C}_6\text{D}_6$ .

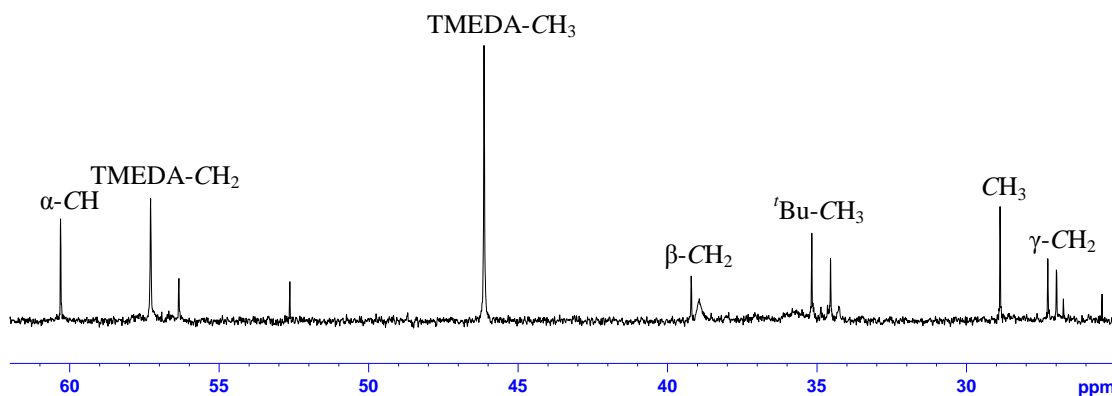


Figure 2.12  $^{13}\text{C}$  NMR spectrum of  $[(\text{TMEDA})\cdot\text{Na}(\mu\text{-cis-DMP})_2\text{Zn}(^t\text{Bu})]$ , **77**, in  $\text{C}_6\text{D}_6$ .

With the aid of the HSQC spectrum, the relevant chemical shifts from the  $^{13}\text{C}$  NMR spectrum were assigned to their respective proton chemical shifts from the  $^1\text{H}$  NMR spectrum and are shown in Table 2.8.

NMR chemical shifts of [(TMEDA)·Na(μ- <i>cis</i> -DMP) <sub>2</sub> Zn( <sup>t</sup> Bu)], <b>77</b> , in C <sub>6</sub> D <sub>6</sub>			
<sup>1</sup> H δ / ppm		<sup>13</sup> C δ / ppm	
α-CH	3.21	α-CH	60.3
β-CH <sub>2</sub>	1.68	β-CH <sub>2</sub>	38.9
	0.76		
γ-CH <sub>2</sub>	1.95	γ-CH <sub>2</sub>	27.3
	1.72		
CH <sub>3</sub>	1.26	CH <sub>3</sub>	28.9
TMEDA (CH <sub>3</sub> )	1.84	TMEDA (CH <sub>3</sub> )	46.3
TMEDA (CH <sub>2</sub> )	1.78	TMEDA (CH <sub>2</sub> )	57.3
<sup>t</sup> Bu (CH <sub>3</sub> )	1.71	<sup>t</sup> Bu (CH <sub>3</sub> )	35.2
–	–	<sup>t</sup> Bu (C)	–

**Table 2.8** <sup>1</sup>H and <sup>13</sup>C NMR chemical shifts of [(TMEDA)·Na(μ-*cis*-DMP)<sub>2</sub>Zn(<sup>t</sup>Bu)], **77**, in C<sub>6</sub>D<sub>6</sub>.

#### 2.1.4 [(TMEDA)·Na(μ-*cis*-DMP)<sub>2</sub>Mg(*cis*-DMP)], **79**

Magnesiates **79**, was prepared by a similar mixed-metallation approach which was adopted for the preparation of the previously prepared tris(DA) analogue [(TMEDA)·Na(μ-DA)<sub>2</sub>Mg(DA)],<sup>[193h]</sup> **81**. An equimolar mixture of *n*-butylsodium and di-*n*-butylmagnesium in hexane was treated with three molar equivalents of *cis*-DMP(H) and subsequently with one molar equivalent of TMEDA (Scheme 2.1). In contrast to the zincate scenario, this led to the complete conversion of all the alkyl substituents to gaseous alkane, resulting in the formation of the desired TMEDA-solvated heterobimetallic tris(amido) complex **79**. In keeping with the aforementioned zincate reactions (synthesis of **75-77**) the reactivity of *cis*-DMP(H) towards ate species appears to resemble that of DA(H) more than that of TMP(H), as like its DA analogue, **79** is homoleptic with respect to its anionic ligands. When TMP(H) is utilised in the corresponding reaction, full amination is not possible, and instead the bis(amide) species [(TMEDA)·Na(μ-TMP)(μ-<sup>n</sup>Bu)Mg(TMP)],<sup>[106]</sup> **37**, is formed.

X-ray crystallographic analysis reveals that **79** crystallises in the monoclinic system, space group *P*2<sub>1</sub>/*n*. The central feature of **79** (Figure 2.13) is a four-membered NaNMgN ring, where the coordination sphere of the sodium centre is completed by a molecule of the diamine TMEDA, and that of the magnesium centre by a *cis*-DMP anion (the sodium metal centre is four coordinate and the magnesium metal centre three coordinate). Table 2.9 and Table 2.10 detail the key bond distances and angles respectively.

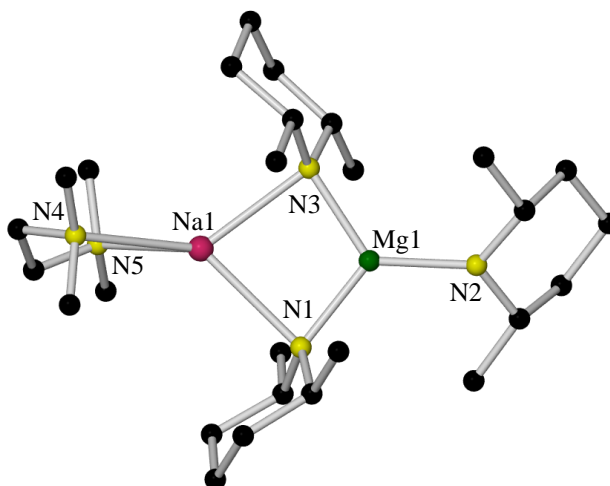


**Figure 2.13** Molecular structure of [(TMEDA)·Na(μ-*cis*-DMP)<sub>2</sub>Mg(*cis*-DMP)], **79**. H atoms are omitted for clarity.

Selected Bond	Bond Distance (Å) in [(TMEDA)·Na(μ- <i>cis</i> -DMP) <sub>2</sub> Mg( <i>cis</i> -DMP)], <b>79</b>
Na1–N1	2.626(1)
Na1–N3	2.498(1)
Na1–N4	2.612(1)
Na1–N5	2.641(1)
Mg1–N1	2.044(1)
Mg1–N2	1.984(1)
Mg1–N3	2.056(1)

**Table 2.9** Key bond distances within [(TMEDA)·Na(μ-*cis*-DMP)<sub>2</sub>Mg(*cis*-DMP)], **79**.

Selected Angle	Bond Angle (°) in [(TMEDA)·Na(μ- <i>cis</i> -DMP) <sub>2</sub> Mg( <i>cis</i> -DMP)], <b>79</b>
N1–Na1–N3	81.09(4)
N1–Na1–N4	129.20(4)
N1–Na1–N5	128.02(4)
N3–Na1–N4	125.90(4)
N3–Na1–N5	129.62(4)
N4–Na1–N5	71.13(4)
N1–Mg1–N2	125.83(5)
N1–Mg1–N3	108.74(5)
N2–Mg1–N3	125.43(5)
Na1–N1–Mg1	83.49(4)
Na1–N3–Mg1	86.59(4)

**Table 2.10** Key bond angles within [(TMEDA)·Na(μ-*cis*-DMP)<sub>2</sub>Mg(*cis*-DMP)], **79**.

Unlike the previously discussed zincate structures, the anions in magnesiate **79** are solely *cis*-DMP ligands (*i.e.*, full amination has occurred without retention of any alkyl groups). This is in line with magnesium's greater affinity for nitrogen anions. The metal-N core of the structure is a planar NaN<sub>amide</sub>MgN<sub>amide</sub> ring (sum of endocyclic angles, 359.91°). Three of the internal angles are acute and range from 81.09(4)-86.59(4)°. The remaining internal angle

(N1–Mg1–N3) is significantly wider [108.74(5)°], to accommodate the distorted trigonal planar geometry of the Mg centre. The Na atom is four coordinate (akin to those in **76** and **77**), bound only to N atoms (two belong to anions and two to the bidentate TMEDA ligand). The coordination environment around Na is best described as highly distorted tetrahedral (sum of angles, 665.14°). As expected, the majority of this distortion is caused by the tight TMEDA bite angle [71.13(4)°].

Turning to the bond distances, the Mg–N<sub>bridging</sub> bonds are longer (mean distance, 2.050 Å) than the Mg–N<sub>terminal</sub> one [bond distance, 1.984(1) Å] – this is in accordance with the coordination number difference between the bridging N1/N3 atoms (coordination number is four) and terminal N2 atom (coordination number is three). Perhaps counterintuitively, the two Na–N<sub>bridging</sub> bonds (Na1–N1 and Na1–N3) have very different lengths [2.626(1) and 2.498(1) Å respectively; hence,  $\Delta = 0.128$  Å]. Indeed, this former bond is essentially identical in length to the Na–N<sub>TMEDA</sub> dative bonds (mean distance, 2.627 Å). The mean Na–N bond distance in **79** (2.579 Å) is considerably longer (and by implication weaker) than that in **76** (mean Na–N bond distance, 2.419 Å), possibly indicating that this tris(amido) species is tending towards becoming a solvent-separated ion pair.

Complex **79** can be compared with the other structurally characterised sodium-magnesium tris(amide) complex [(TMEDA)·Na(μ-DA)<sub>2</sub>Mg(DA)],<sup>[193h]</sup> **81** and the bis(amide) complex [(TMEDA)·Na(μ-TMP)(μ-<sup>n</sup>Bu)Mg(TMP)],<sup>[106]</sup> **37** (*vide infra*). The key structural parameters are similar to those of **79**; however, there are two noticeable differences. Firstly, although the Na–N<sub>bridging</sub> bonds in the former complex are still asymmetric (difference in length, 0.065 Å), they are considerably more uniform than those in **79**, and secondly, the mean Na–N<sub>TMEDA</sub> distance in the DA complex (2.5505 Å) is shorter than that in **79** (2.627 Å). This second point possibly suggests that in **79** the chelating TMEDA ligand is more restricted in its approach to the Na centre, indicating that the steric demands of three *cis*-DMP ligands is actually greater than that of three DA anions.

The crystalline product **79** was dissolved in C<sub>6</sub>D<sub>6</sub> solution and examined by <sup>1</sup>H, <sup>13</sup>C (Figure 2.14 and Figure 2.15 respectively), COSY and HSQC NMR spectroscopy. With the aid of the HSQC spectrum, the relevant chemical shifts from the <sup>13</sup>C NMR spectrum were assigned to their respective proton chemical shifts from the <sup>1</sup>H NMR spectrum and are shown in Table 2.11. The two <sup>1</sup>H and two <sup>13</sup>C resonances associated with the TMEDA ligand are different from those encountered in the free diamine, indicating that it remains coordinated to the alkali metal in arene solution.

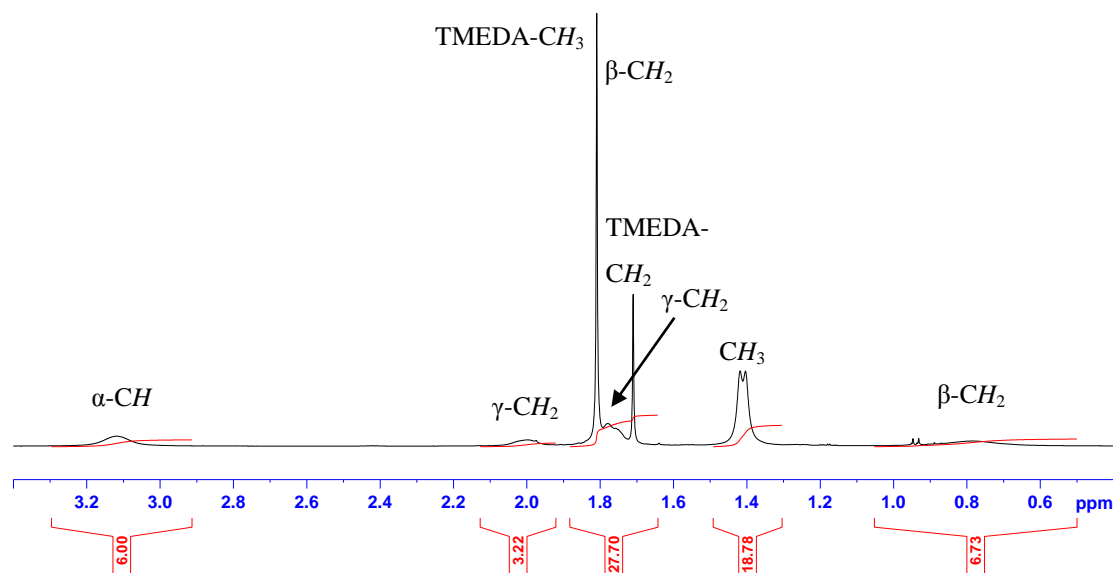


**Figure 2.14**  $^1\text{H}$  NMR spectrum of  $[(\text{TMEDA})\cdot\text{Na}(\mu\text{-cis-DMP})_2\text{Mg}(\text{cis-DMP})]$ , **79**, in  $\text{C}_6\text{D}_6$ .

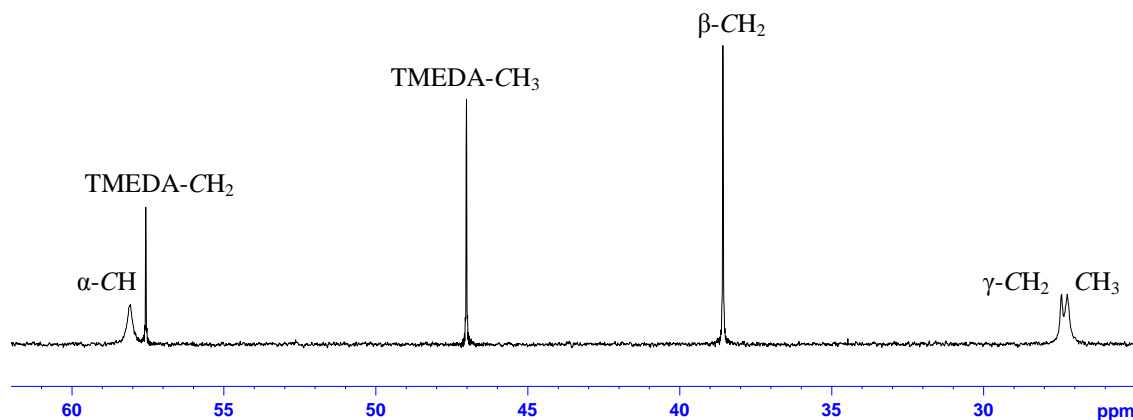


**Figure 2.15**  $^{13}\text{C}$  NMR spectrum of  $[(\text{TMEDA})\cdot\text{Na}(\mu\text{-cis-DMP})_2\text{Mg}(\text{cis-DMP})]$ , **79**, in  $\text{C}_6\text{D}_6$ .

$^1\text{H}$ $\delta$ / ppm		$^{13}\text{C}$ $\delta$ / ppm	
$\alpha\text{-CH}$	3.12	$\alpha\text{-CH}$	58.1
$\beta\text{-CH}_2$	1.76 0.79	$\beta\text{-CH}_2$	38.6
$\gamma\text{-CH}_2$	2.00 1.76	$\gamma\text{-CH}_2$	27.4
$\text{CH}_3$	1.41	$\text{CH}_3$	27.2
TMEDA ( $\text{CH}_3$ )	1.81	TMEDA ( $\text{CH}_3$ )	47.0
TMEDA ( $\text{CH}_2$ )	1.71	TMEDA ( $\text{CH}_2$ )	57.6

**Table 2.11**  $^1\text{H}$  and  $^{13}\text{C}$  NMR chemical shifts of  $[(\text{TMEDA})\cdot\text{Na}(\mu\text{-cis-DMP})_2\text{Mg}(\text{cis-DMP})]$ , **79**, in  $\text{C}_6\text{D}_6$ .

**Figure 2.14** shows that there is only one set of broad signals (in addition, the chemical shifts are not concentration dependent) present, suggesting that the solid-state structure of **79** may not be retained in solution (two distinct set of signals, due to the bridging and terminal amido ligands, would have been expected). This observation suggests that the chemically distinct

*cis*-DMP ligands in **79** undergo a dynamic fast exchange process in arene solution, or **79** forms a solvent-separated ion pair consisting of  $[\text{Na}\cdot(\text{arene})_x]^+$  and  $[\text{Mg}(\textit{cis}\text{-DMP})_3]^-$ .

To gain more insight into the solution behaviour of **79**, a variable temperature  $^1\text{H}$  NMR spectroscopic study of the magnesiate in  $d_8$ -toluene solution was conducted. The focus of our study was the resonance for the  $\alpha\text{-CH}$  atom (Figure 2.16). At 300 K, the resonance (3.05 ppm) was relatively broad. On cooling to 273 K, the resonance (3.03 ppm) broadened further without any sign of decoalescence. However, at 253 K, two distinct resonances (3.43 and 2.96 ppm) are present in a 1 : 2 ratio which can be attributed to terminal and bridging *cis*-DMP ligands respectively. This data suggests that in arene solution, **79** does indeed undergo a fast dynamic exchange at ambient temperature, which is sufficiently slowed on cooling to 253 K, to reveal the terminal and bridging amido ligands.

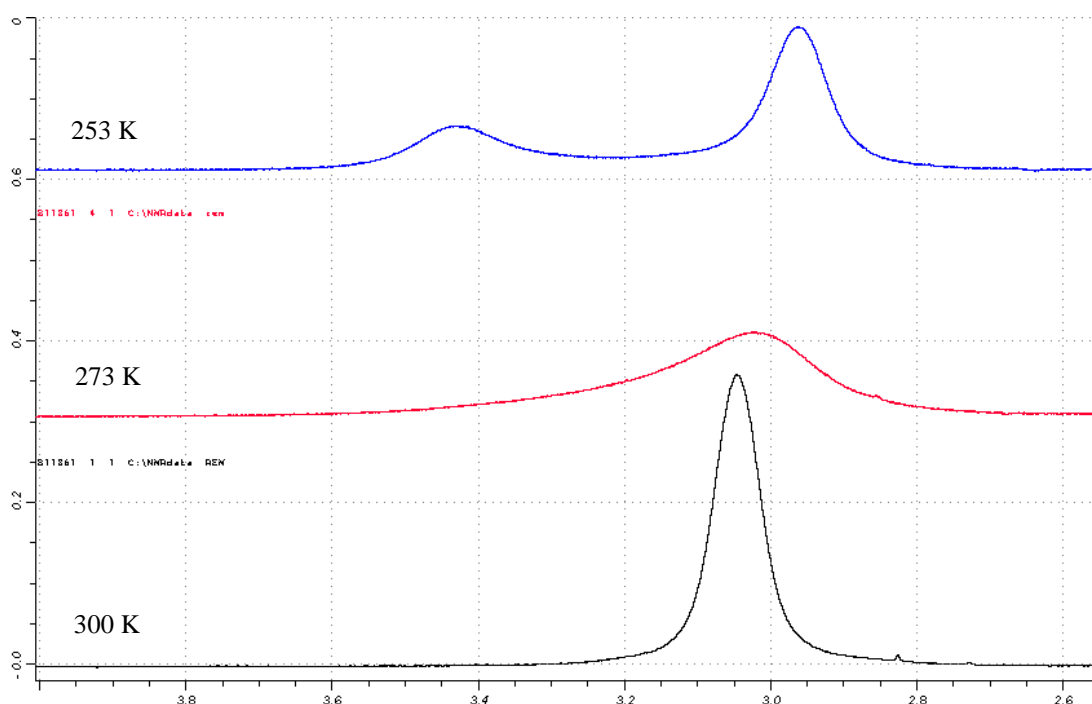


**Figure 2.16** Variable temperature  $^1\text{H}$  NMR spectra of **79** in  $\text{C}_6\text{D}_5\text{CD}_3$ , focusing on the resonance for the  $\alpha\text{-CH}$  atom of *cis*-DMP.

Like the DA complex  $[(\text{TMEDA})\cdot\text{Na}(\mu\text{-DA})_2\text{Mg}(\text{DA})]$ ,<sup>[193h]</sup> **81**, when *cis*-DMP(H) is utilised, a tris(amido) sodium magnesiate was forthcoming – potentially giving clues to the eventual reactivity of **79** and its TMEDA-free complex with certain organic substrates and metallocenes. As the reaction of “ $(\text{TMEDA})\cdot\text{NaMgBu}_3$ ” with excess TMP(H) only yielded bis(amido) magnesiate complex **37** (presumably due to steric-crowding around the metal centres),<sup>[106]</sup> it can be concluded that the steric bulk of the TMP ligand is far greater than that of the *cis*-DMP ligand which is similar to that of DA.

By comparing the solid-state structures of **75-79** along with some key examples from the literature, it is possible to determine experimentally the relative steric bulk of the amide ligands *cis*-DMP, TMP, DA and DIBA. Undoubtedly, and unsurprisingly, the most sterically demanding ligand of this set is TMP, as *contacted* tris(TMP) zincate or magnesiate complexes with this amide have not yet been detected, although a *solvent-separated* tris(TMP) sodium magnesiate has recently been reported.<sup>[108]</sup> Due to the similar reactivity of *cis*-DMP(H) and DA(H) [*i.e.*, to yield both mono- and bis(amido) zincates<sup>[125]</sup> and tris(amido) magnesiates<sup>[193h]</sup>] it can be concluded that they have similar steric properties. However, when **79** is compared with [(TMEDA)·Na(μ-DA)<sub>2</sub>Mg(DA)],<sup>[193h]</sup> **81**, from a steric perspective it appears that *cis*-DMP is more sterically encumbered than DA as the Na–N<sub>TMEDA</sub> interactions in **79** are longer than those found in the DA derivative. Finally, when [(TMEDA)·Na(μ-DA)<sub>2</sub>Zn(<sup>t</sup>Bu)],<sup>[125]</sup> **64** (mean Na–N<sub>TMEDA</sub> distance is 2.6195 Å) is compared with **78** (mean Na–N<sub>TMEDA</sub> distance is 2.5733 Å), it can be tentatively deduced that since the bidentate ligand makes a slightly closer approach to the metal in **78**, from a steric point of view, DA appears larger than DIBA. In summary, it can be concluded that the order of the amides, with decreasing steric bulk, is: TMP >> *cis*-DMP > DA > DIBA.

### 2.1.5 [{*cis*-DMP(H)}·Na(μ-*cis*-DMP)<sub>2</sub>Mg(*cis*-DMP)], **80**

By treating an equimolar mixture of *n*-butylsodium and di-*n*-butylmagnesium in hexane with three molar equivalents of *cis*-DMP(H) and excess toluene (Scheme 2.2), X-ray quality crystals of **80**, a *cis*-DMP(H)-solvated tris(amido) sodium magnesiate, precipitated from solution at ambient temperature.

Comparison of **80** with products obtained from the same reaction but utilising TMP(H) or DA(H), have previously been studied by Mulvey *et al.*<sup>[104a, 105]</sup> These revealed marked differences in the types of product obtained. When TMP(H) is utilised in the reaction, an inverse crown structure is isolated [where toluene has been di-deprotonated (2,5-positions), see chapter 1, section 1.5, Figure 1.30 for representative structural motif (1,4-di-deprotonated benzene example)],<sup>[105]</sup> and when DA(H) is utilised, deprotonation of toluene does not occur, and instead the generation of a hydride containing inverse crown structure transpires (presumably from the β-hydride elimination from a DA ligand) [see chapter 1, section 1.4, Scheme 1.19 for representative structural motif (where M = Na and both sodium atoms are solvated by a molecule of toluene)].<sup>[104a]</sup> In this case toluene simply acts as an η<sup>6</sup>-π-donor to the sodium atoms. When *cis*-DMP(H) is employed, neither of these scenarios is detected in solution. Instead, the sole isolable organometallic species isolated is the tris(amido) complex



$[\{cis\text{-DMP(H)}\} \cdot \text{Na}(\mu\text{-}cis\text{-DMP})_2\text{Mg}(cis\text{-DMP})]$ , **80**, where the sodium atom is solvated by *cis*-DMP(H) (Scheme 2.2).

X-ray crystallographic analysis revealed that **80** crystallises in the orthorhombic system, space group  $Pna2_1$ . Similar to its TMEDA congener **79**, the structure of **80** (Figure 2.17) is composed of a four-membered NaNMgN ring, where the coordination sphere of the magnesium centre is completed by a *cis*-DMP anion; however here, the coordination sphere of the sodium centre is completed by a molecule of *cis*-DMP(H) (both metal centres are three coordinate). Within the asymmetric unit of **80** there are two independent molecules of  $[\{cis\text{-DMP(H)}\} \cdot \text{Na}(\mu\text{-}cis\text{-DMP})_2\text{Mg}(cis\text{-DMP})]$ ; however, the differences in the dimensions of the two molecules are negligible, and thus Table 2.12 and Table 2.13 detail the key bond distances and angles respectively of only one of the independent molecules.

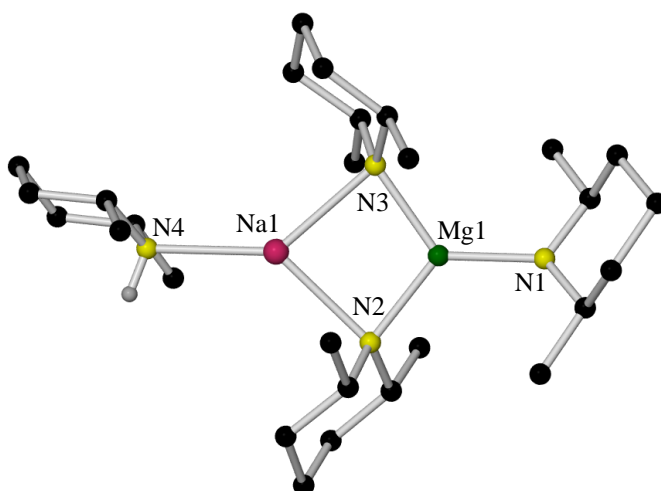


**Figure 2.17** Molecular structure of  $[\{cis\text{-DMP(H)}\} \cdot \text{Na}(\mu\text{-}cis\text{-DMP})_2\text{Mg}(cis\text{-DMP})]$ , **80**. H atoms omitted and only one of two similar molecules in the asymmetric unit shown for clarity.

Selected Bond	Bond Distance (Å) in $[\{cis\text{-DMP(H)}\} \cdot \text{Na}(\mu\text{-}cis\text{-DMP})_2\text{Mg}(cis\text{-DMP})]$ , <b>80</b>
Na1–N2	2.424(3)
Na1–N3	2.458(3)
Na1–N4	2.453(3)
Mg1–N1	1.966(3)
Mg1–N2	2.060(3)
Mg1–N3	2.041(3)

**Table 2.12** Key bond distances within  $[\{cis\text{-DMP(H)}\} \cdot \text{Na}(\mu\text{-}cis\text{-DMP})_2\text{Mg}(cis\text{-DMP})]$ , **80**.

Selected Angle	Bond Angle (°) in [ <i>cis</i> -DMP(H)]·Na( $\mu$ - <i>cis</i> -DMP) <sub>2</sub> Mg( <i>cis</i> -DMP), <b>80</b>
N2–Na1–N3	84.83(10)
N2–Na1–N4	136.29(12)
N3–Na1–N4	138.06(13)
N1–Mg1–N2	126.74(14)
N1–Mg1–N3	126.40(14)
N2–Mg1–N3	106.86(12)
Na1–N2–Mg1	84.39(11)
Na1–N3–Mg1	83.91(11)

**Table 2.13** Key bond angles within [*cis*-DMP(H)]·Na( $\mu$ -*cis*-DMP)<sub>2</sub>Mg(*cis*-DMP), **80**.

Unlike the previously discussed zincates and magnesiate, the alkali metal centre's coordination sphere in magnesiate **80** is completed by a molecule of *cis*-DMP(H) (rather than a TMEDA donor ligand), resulting in Na being three coordinate and adopting a slightly distorted trigonal planar environment (summed angles at Na, 359.18°). The core (NaNMgN) ring is planar (sum of endocyclic angles, 359.99°), and, as seen in complex **79**, three of the internal angles are acute [ranging from 83.91(11)-84.83(10)°, *cf.*, 81.09(4)-86.59(4)° for **79**] and the remaining internal angle (N2–Mg1–N3) is significantly wider [106.86(12)°, *cf.*, 108.74(5)° for **79**], to accommodate the distorted trigonal planar geometry of the Mg centre.

Turning to bond distances, a similar scenario to magnesiate **79** is observed, where the Mg–N<sub>bridging</sub> bonds are longer (mean distance, 2.051 Å, *cf.*, 2.050 Å for **79**) than the Mg–N<sub>terminal</sub> one [distance, 1.966(3) Å, *cf.*, 1.9840(11) Å for **79**] – in accordance with the difference in coordination number between the bridging N2/N3 atoms (coordination number is four) and terminal N1 atom (coordination number is three).

Notable differences on comparing complexes **79** and **80** are: i) the Na–N<sub>bridging</sub> bonds in **79** are longer (mean distance, 2.562 Å) and not as uniform (difference in length, 0.128 Å) than those in **80** (mean distance, 2.441 Å, and difference in length 0.034 Å); ii) the Na–N<sub>terminal</sub> bonds are also longer in **79** (mean distance, 2.6262 Å) than the Na–N<sub>amine</sub> bond distance [2.453(3) Å] – which can be attributed to the differences in coordination number of the Na centres (four coordinate in **79** and three coordinate in **80** respectively); iii) the Mg–N<sub>bridging</sub> bond distances are essentially identical in **79** and **80** (mean distance, 2.051 and 2.050 Å respectively); however, the Mg–N<sub>terminal</sub> bond distance is slightly longer (by 0.2 Å) in **79**; vi) and finally, a combination of the longer Na–N<sub>bridging</sub> bonds and the internal angles in **79** not being as uniform as those in **80**, gives rise to a smaller, tighter core (NaNMgN) ring in **80**.

The crystalline product **80** was dissolved in C<sub>6</sub>D<sub>6</sub> and examined by <sup>1</sup>H, <sup>13</sup>C (Figure 2.18 and Figure 2.19 respectively), COSY and HSQC NMR spectroscopy.

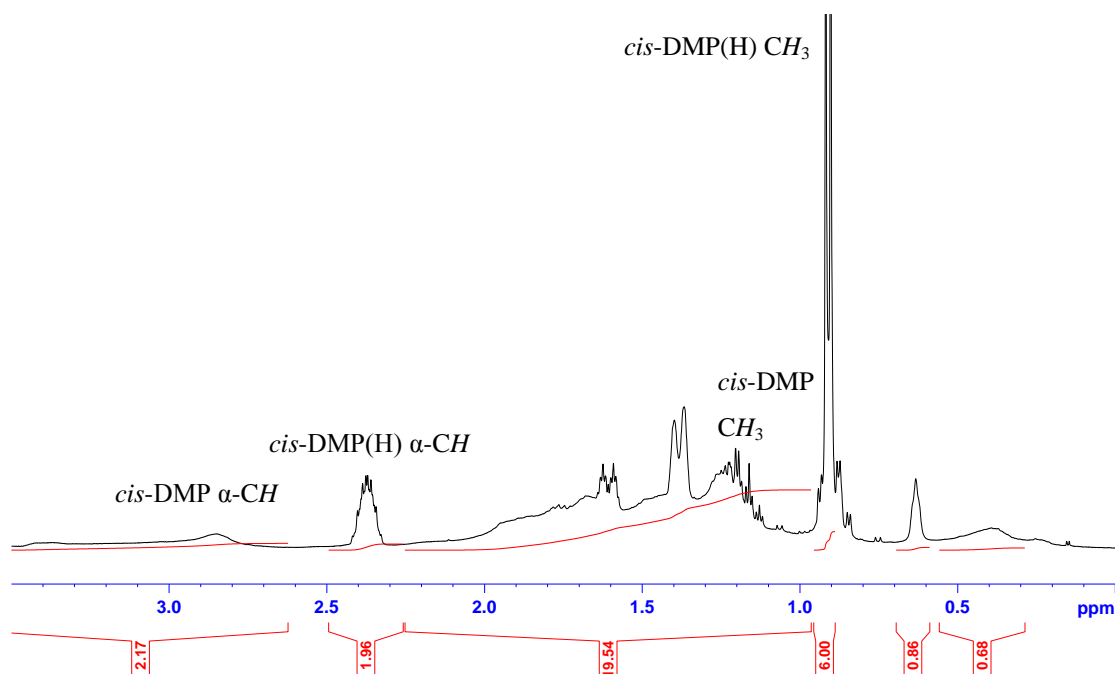


**Figure 2.18**  $^1\text{H}$  NMR spectrum of  $[\{\text{cis-DMP(H)}\}\cdot\text{Na}(\mu\text{-cis-DMP})_2\text{Mg}(\text{cis-DMP})]$ , **80**, in  $\text{C}_6\text{D}_6$  (for clarity, only distinguishable peaks have been labelled).

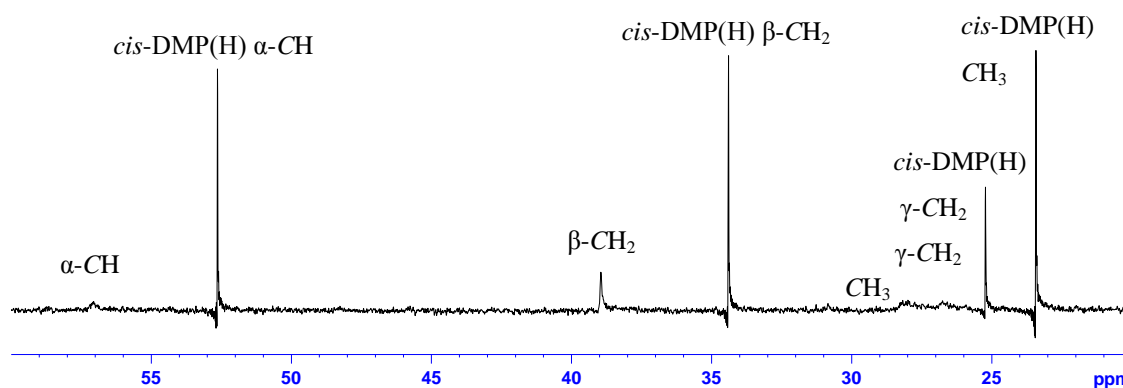


**Figure 2.19**  $^{13}\text{C}$  NMR spectrum of  $[\{\text{cis-DMP(H)}\}\cdot\text{Na}(\mu\text{-cis-DMP})_2\text{Mg}(\text{cis-DMP})]$ , **80**, in  $\text{C}_6\text{D}_6$ .

The  $^1\text{H}$  NMR spectrum (Figure 2.18) is complicated owing to the chair conformation adopted by *cis*-DMP, resulting in four resonances for the chemically distinct  $\beta$ - and  $\gamma$ -hydrogen atoms, and thus six resonances in total (1  $\times$   $\alpha$ , 2  $\times$   $\beta$ , 2  $\times$   $\gamma$  and 1  $\times$  methyl proton signals). The spectrum is further complicated by the presence of a molecule of solvating *cis*-DMP(H) (seven resonances in total, 1  $\times$   $\alpha$ , 2  $\times$   $\beta$ , 2  $\times$   $\gamma$ , 1  $\times$  methyl and 1  $\times$  amino proton signals), and the broadening of all resonances associated with the bridging and terminal amido ligands, suggesting that the chemically distinct *cis*-DMP ligands in **80** undergo a fast dynamic exchange process in arene solution, or **80** forms a solvent-separated ion pair consisting of  $[\text{Na}\cdot(\text{arene})_x]^+$  and  $[\text{Mg}(\text{cis-DMP})_3]^-$ . This results in a spectrum with poor base line resolution and thus the task of determining multiplicity and integration was difficult. However, integration of the signals associated with the  $\alpha$ -hydrogens (sextet of doublets at 2.38 ppm), the

methyl groups (doublet at 0.90 ppm), and the amino hydrogen atom (broad signal at 0.39 ppm) of the solvating *cis*-DMP(H) ligand was possible (integrating to two, six and one respectively). These chemical shifts are different from the chemical shifts of free *cis*-DMP(H) (section 2.1.1, Table 2.3), indicating that the amine remains coordinated to the alkali metal in arene solution.

The  $^{13}\text{C}$  NMR spectrum (Figure 2.19) is more informative, showing all expected resonances for the chemically distinct carbon environments in **80**, and with the aid of the HSQC spectrum, the relevant chemical shifts from the  $^{13}\text{C}$  NMR spectrum were assigned to their respective proton chemical shifts from the  $^1\text{H}$  NMR spectrum and are shown in Table 2.14.

NMR chemical shifts of [ <i>cis</i> -DMP(H)]·Na(μ- <i>cis</i> -DMP) <sub>2</sub> Mg( <i>cis</i> -DMP)], <b>80</b> , in C <sub>6</sub> D <sub>6</sub>			
$^1\text{H}$ δ / ppm		$^{13}\text{C}$ δ / ppm	
<i>cis</i> -DMP(H) α-CH	2.38	<i>cis</i> -DMP(H) α-CH	52.6
<i>cis</i> -DMP(H) β-CH <sub>2</sub>	1.38	<i>cis</i> -DMP(H) β-CH <sub>2</sub>	34.4
	0.89		
<i>cis</i> -DMP(H) γ-CH <sub>2</sub>	1.63	<i>cis</i> -DMP(H) γ-CH <sub>2</sub>	25.2
	1.18		
<i>cis</i> -DMP(H) CH <sub>3</sub>	0.91	<i>cis</i> -DMP(H) CH <sub>3</sub>	23.4
NH	0.39	–	–
α-CH	2.85	α-CH	57.1
β-CH <sub>2</sub>	1.68	β-CH <sub>2</sub>	39.0
	0.38		
γ-CH <sub>2</sub>	1.92	γ-CH <sub>2</sub>	26.7
	1.64		
CH <sub>3</sub>	1.23	CH <sub>3</sub>	28.1

**Table 2.14**  $^1\text{H}$  and  $^{13}\text{C}$  NMR chemical shifts of [*cis*-DMP(H)]·Na(μ-*cis*-DMP)<sub>2</sub>Mg(*cis*-DMP)], **80**, in C<sub>6</sub>D<sub>6</sub>.

To gain more insight into the solution behaviour of **80**, a variable temperature  $^1\text{H}$  NMR spectroscopic study of the magnesiate in d<sub>8</sub>-toluene solution was conducted. The focus of our study was the resonance for the α-CH atom of *cis*-DMP (Figure 2.20). At 300 K the resonance (range, 2.58-3.46 ppm) is extremely broad (Figure 2.20). On cooling to 273 K, two resonances (3.31 and 2.82 ppm) are present in a 1 : 2 ratio which can be attributed to terminal and bridging *cis*-DMP ligands respectively; however, the resonance at 3.31 ppm is still relatively broad with two shoulder peaks. A decrease in temperature to 243 K sharpens this resonance slightly, now at 3.38 ppm, (other resonance now at 2.87 ppm and resonances still present in a 1 : 2 ratio). On cooling further to 203 K, the resonances (now at 3.53 and 2.95 ppm) become more distinct. These data suggests that in arene solution, **80** does indeed undergo a fast dynamic exchange at ambient temperature, which is sufficiently slowed on cooling to 203 K, to reveal the terminal and bridging *cis*-DMP ligands.

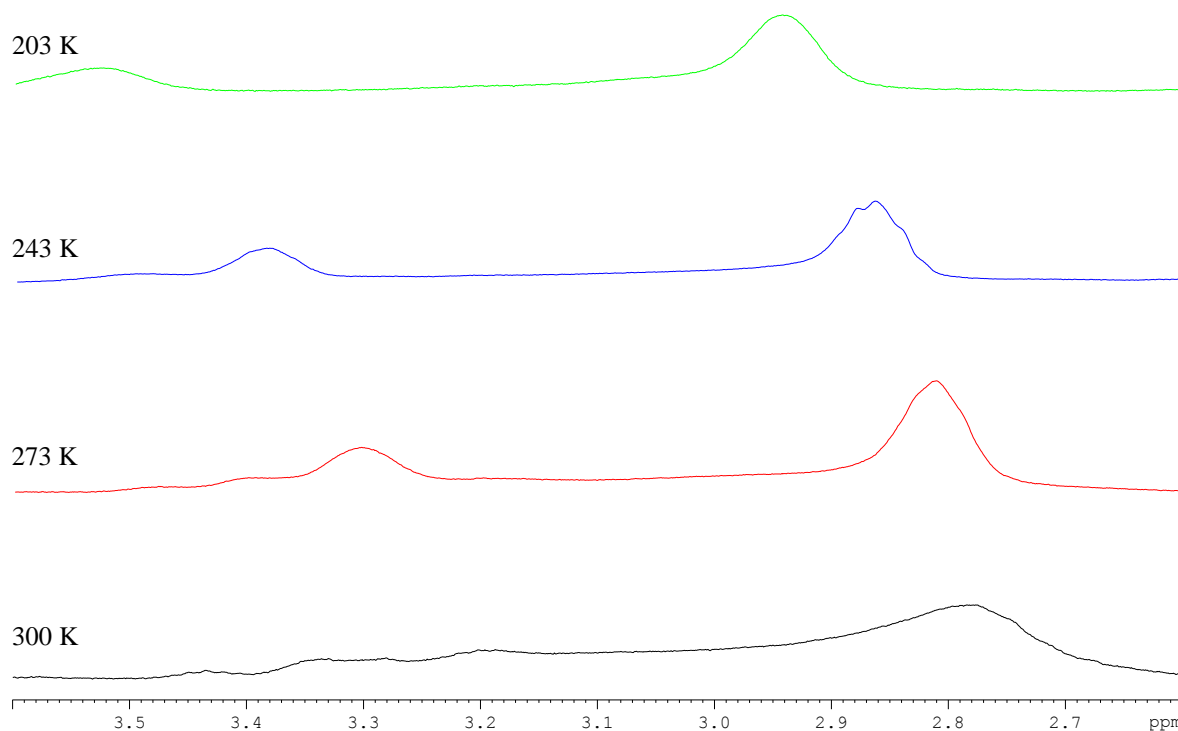


**Figure 2.20** Variable temperature  $^1\text{H}$  NMR spectra of **80** in  $\text{C}_6\text{D}_5\text{CD}_3$ , focusing on the resonance for the  $\alpha\text{-CH}$  atom of *cis*-DMP.

## 2.2 TMEDA-Solvated Alkali Metal Salts of HMDS

Since the birth of structural alkali metal amide chemistry with the characterisation of the lithium salt of 1,1,1,3,3,3-hexamethyldisilazide (LiHMDS),  $[\text{LiN}(\text{SiMe}_3)_2]_3$ ,<sup>[11a, 11b]</sup> **1** (chapter 1, section 1.1.3, Figure 1.3), the chemistry of the alkali metal amides and their solvates, in particular the metal salts of DA(H), TMP(H) and HMDS(H), has been growing at an exceptional rate.

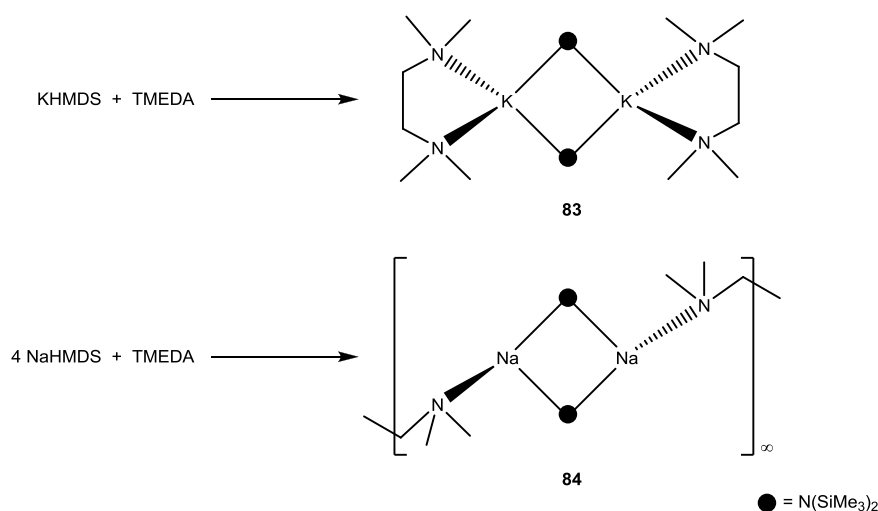
The area of research which has perhaps progressed the most is that of alkali metal HMDS complexes (both solvated and unsolvated), due to the lithium, sodium and potassium salts of HMDS(H) being commercially available at relatively low expense.<sup>[1]</sup> The solid- and solution-state structures of these amides are discussed in chapter 1, sections 1.1.3 and 1.1.5.

Focusing on crystallographically characterised solvated lithium, sodium and potassium bis(silyl)amides only, a search of the CCDC reveals 97 lithium, 19 sodium and 18 potassium bis(silyl)amide complexes (see appendix I for full tabulated lists of these amides).

A TMEDA solvate of LiHMDS has been crystallographically characterised, namely the monomer  $[\text{LiHMDS}\cdot\text{TMEDA}]$ ,<sup>[182]</sup> **82**. However, surprisingly no homometallic complexes of TMEDA-solvated NaHMDS or KHMDS have been structurally characterised to date (the only previously reported complexes which contain both NaHMDS or KHMDS and TMEDA

are a mixed aggregate of sodium ester enolate/sodium amide, reported by Williard,<sup>[199]</sup> and a solvent-separated potassium heteroleptic organochromate, reported by Mulvey).<sup>[200]</sup> Wishing to fill this gap in the literature and as a prelude to investigating mixed-metal systems, we report here the preparation and structural characterisation of two key monometallic building blocks: namely the TMEDA adducts of  $MN(\text{SiMe}_3)_2$  (where M is Na or K). This chemistry is being pursued as TMEDA has proved a useful co-ligand in reagents designed for *AMMM* applications.<sup>[84-85]</sup>

In this work, two novel homobimetallic complexes containing HMDS have been prepared and characterised; namely the TMEDA-solvated potassium and sodium bis(amido) complexes  $[\text{KHMDS}\cdot\text{TMEDA}]_2$ , **83** and  $[(\text{NaHMDS})_2\cdot\text{TMEDA}]_\infty$ , **84** (Scheme 2.4). Dimeric **83** is synthesised by treating one molar equivalent of KHMDS with an equimolar quantity of TMEDA in hexane solution. Polymeric **84** was initially synthesised by treating two molar equivalents of NaHMDS with one molar equivalent of di-*n*-butylmagnesium, followed by one molar equivalent of TMEDA in a hexane solution. Rational synthesis (NaHMDS : TMEDA in a 2 : 1 ratio) was not successful, although on varying the concentration of TMEDA in an attempt to further investigate the coordination chemistry of NaHMDS, a NaHMDS : TMEDA ratio of 4 : 1 provided polymer **84** in a quantitative yield.



**Scheme 2.4** Synthesis of complexes **83** and **84**.

### 2.2.1 $[\text{KHMDS}\cdot\text{TMEDA}]_2$ , **83**

Complex **83** was prepared by reacting KHMDS with an equimolar quantity of TMEDA in a hexane solution (Scheme 2.4). The resultant solution was heated and filtered through Celite and glass wool, affording crystals of **83** at  $-28^\circ\text{C}$ .

X-ray crystallographic analysis reveals that **83** (Figure 2.21) crystallises as a dimer in the monoclinic system, space group  $P2_1/c$ , and is composed of two potassium centres each coordinated to a TMEDA ligand, with two HMDS ligands bridging the two metal centres (*i.e.*, both metal centres are four coordinate). Unfortunately the X-ray data obtained was of poor quality, thus limiting the discussion of the structural parameters.

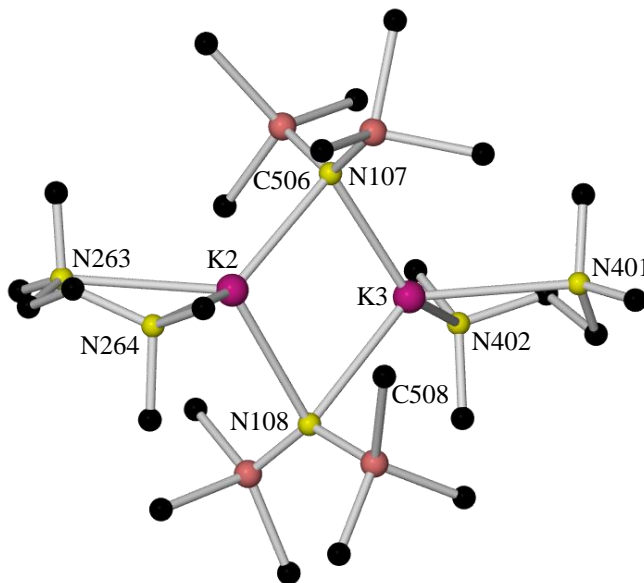


**Figure 2.21** Molecular structure of  $[\text{KHMS}\cdot\text{TMEDA}]_2$ , **83**. H atoms omitted and only one of six similar molecules in the asymmetric unit shown for clarity.

Although no other homometallic KHMS complexes solvated by TMEDA exist, complex **83** can be compared to the analogues TMEDA-solvated potassium-DA and -TMP dimers prepared and characterised by Clegg and Mulvey respectively.<sup>[43, 201]</sup>  $[\text{KN}^i\text{Pr}_2\cdot\text{TMEDA}]_2$ , **86**, is different from complex **83** in that it is centrosymmetric, hence the TMEDA ligands are crystallographically equivalent. The dimeric framework of  $[\text{KTMP}\cdot\text{TMEDA}]_2$ , **33**, is similar to that of complex **83**. Comparing **83** to the donor-free amide  $[\text{KN}(\text{SiMe}_3)_2]_\infty$ ,<sup>[27]</sup> **12**, the repeating core  $(\text{KN})_2$  asymmetric ring of polymeric **12** is nearly square. The bonding of the TMEDA ligands in **83** deaggregates the polymer, and causes the four-membered ring to deviate from a near perfect square by contracting and expanding at the K–N–K and N–K–N angles of the ring respectively.

The analogue (*R,R*)-TMCDA complex of **83**,  $[\text{KHMS}\cdot(\text{R,R})\text{-TMCDA}]_2$ , **85**, was also synthesised during this PhD study (full experimental details can be found in chapter 5, section 5.3.8 and full X-ray data can be found on the accompanying CD).

Moving to solution studies of **83** in  $\text{C}_6\text{D}_6$  solution, the two  $^1\text{H}$  and two  $^{13}\text{C}$  resonances associated with the TMEDA ligand are almost identical to those encountered in the free diamine, likewise the respective resonances associated with the HMDS ligand are almost

identical to those encountered in the free alkali metal amide, indicating that the solid-state structure of **83** does not appear to stay intact in solution, breaking down to its two component parts of TMEDA and KHMDS.

### 2.2.2 $[(\text{NaHMDS})_2 \cdot \text{TMEDA}]_\infty$ , **84**

X-ray crystallographic analysis reveals that **84** (Figure 2.22) crystallises as centrosymmetric dimeric units, which associate to form a linear polymeric arrangement (Figure 2.23), in the monoclinic system, space group  $P2_1/n$ .

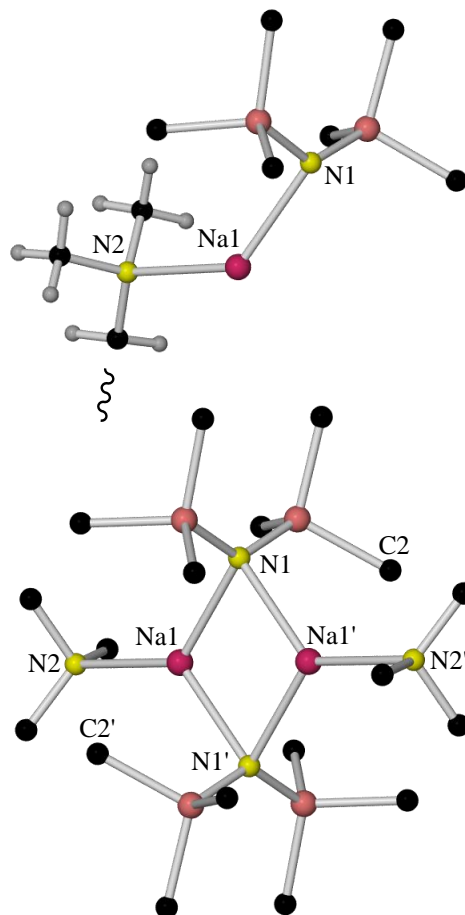


**Figure 2.22** Molecular structure of  $[(\text{NaHMDS})_2 \cdot \text{TMEDA}]_\infty$ , **84**, showing the asymmetric unit (top) and the dinuclear ring (bottom). H atoms for the HMDS ligands (both figures) and the TMEDA ligands (bottom figure) are omitted for clarity.



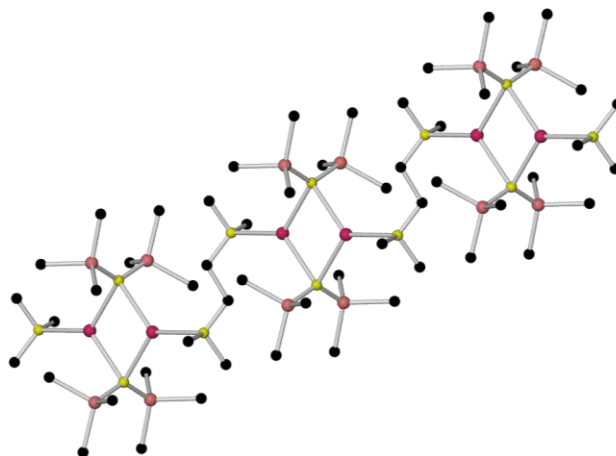


**Figure 2.23** Extended view of  $[(\text{NaHMDS})_2 \cdot \text{TMEDA}]_\infty$ , **84**. H atoms are omitted for clarity.

Each dimeric unit is composed of two sodium centres bridged by two HMDS anions, and to complete the coordination sphere of the metal centres, a TMEDA ligand coordinates to each metal centre in a monodentate fashion (both metal centres are three coordinate). It is through the appending TMEDA ligand that the polymeric complex is produced; hence, two sodium centres from two different dimeric units are connected by a TMEDA ligand bridging in a monodentate manner, and so the polymer continues to grow in a linear fashion. [Table 2.15](#) and [Table 2.16](#) detail the key bond distances and bond angles respectively.

Selected Bond	Bond Distance (Å) in $[(\text{NaHMDS})_2 \cdot \text{TMEDA}]_\infty$ , <b>84</b>
Na1–N1	2.451(1)
Na1–N2	2.567(1)
Na1–N1'	2.436(1)

**Table 2.15** Key bond distances within  $[(\text{NaHMDS})_2 \cdot \text{TMEDA}]_\infty$ , **84**.

Selected Angle	Bond Angle (°) in $[(\text{NaHMDS})_2 \cdot \text{TMEDA}]_\infty$ , <b>84</b>
N1–Na1–N2	130.73(3)
N1–Na1–N1'	99.58(3)
N2–Na1–N1'	129.70(3)
Na1–N1–Na1'	80.42(3)

**Table 2.16** Key bond angles within  $[(\text{NaHMDS})_2 \cdot \text{TMEDA}]_\infty$ , **84**.

The centrosymmetric dimeric units consist of a planar  $(\text{NaN})_2$  ring (sum of endocyclic angles,  $360.01^\circ$ ), where the bonding is asymmetric, with one edge  $0.015 \text{ \AA}$  shorter than the other [bond distances,  $2.436(1)$  and  $2.451(1) \text{ \AA}$  respectively; mean distance,  $2.444 \text{ \AA}$ ], and the internal angles at the Na atoms are  $19.16^\circ$  wider than the angles at the N atoms [bond angles,  $99.58(3)$  and  $80.42(3)^\circ$  at the Na and N atoms respectively]. The coordination spheres of the Na metal centres are completed by the binding of one N atom of a TMEDA ligand [bond distance,  $2.5665(10) \text{ \AA}$  for Na1–N2]. Supplementary stabilisation by  $\text{Na} \cdots \text{C}$  interactions

appears minimal [Na...C separation is 3.0415(12) Å for Na1–C2'], and the Na atoms are best described as being in a trigonal planar environment (summed angles at Na, 360.01°). Three coordinate sodium is rather unusual although not unique;<sup>[26, 125, 182, 202]</sup> generally, sodium is at least four coordinate.<sup>[117-118, 188, 193q, 203]</sup>

To the best of our knowledge, complex **84** represents the first example of a homometallic sodium complex in which a TMEDA ligand binds to the metal centre in a monodentate fashion. This mode of binding has previously been observed for lithium complexes,<sup>[204]</sup> including in the relevant crystal structure of TMEDA-solvated LDA, [(LDA)<sub>2</sub>·TMEDA]<sub>∞</sub>,<sup>[40]</sup> **27** (section 1.1.4, [Figure 1.20](#)), where, similar to complex **84**, the polymer is composed of an infinite array of dimers linked by bridging TMEDA ligands. The similar bidentate donor *N,N,N',N'*-tetramethylpropanediamine (TMPDA) has also been found to bind in a similar manner in the crystal structure of TMPDA-solvated NaHMDS, [(NaHMDS)<sub>2</sub>·TMPDA]<sub>∞</sub>,<sup>[182]</sup> **87**, which was the first example of a crystallographically characterised polymer of a sodium amide with bridging polyamine.

Comparing the geometric parameters of complex **84** to its TMPDA equivalent, complex **87**, there is little to discriminate between the two. Akin to **84**, the centrosymmetric dimeric units of **87** consist of a planar (NaN)<sub>2</sub> ring (sum of endocyclic angles, 359.39°), where the bonding is asymmetric and the bond lengths are identical within experimental error [bond distances, 2.425(4) and 2.430(4) Å respectively; mean distance, 2.428 Å]. The internal angles at the Na atoms are 23.1° wider than the angles at the N atoms [bond angles, 101.55(11) and 78.45(11)° at the Na and N atoms respectively], and these angles are slightly wider and tighter respectively compared to the angles in complex **84** (*vide supra*). The coordination sphere of the Na metal centres are completed by the binding of a TMPDA ligand in a monodentate manner [Na–N<sub>TMPDA</sub> bond distance, 2.541(4) Å], resulting in the Na centres each being three coordinate and in a trigonal planar environment. The Na–N<sub>TMPDA</sub> bond distance is 0.0255 Å shorter than the corresponding Na–N<sub>TMEDA</sub> bond distance in **84**. Presumably the contraction of this bond is possible due to the presence of an extra CH<sub>2</sub> unit in the alkyl backbone of the amine (in comparison to TMEDA) keeping the dimeric units further apart from one another. From a supramolecular perspective, a coordination polymer is constructed whereby the remaining TMPDA N atom intermolecularly binds to another Na atom.

Only two other donor complexes of NaHMDS have been crystallographically characterised, namely the polymeric dioxane<sup>[205]</sup> and ferrocene solvates ([Figure 2.24](#)).<sup>[193n]</sup> Both polymers are significantly different from complex **84**, with the Na metal centres in the dioxane complex being five coordinate and polymerising through 1,4-dioxane bridges; while in the ferrocene

complex the Na atoms are coordinated to two anionic N atoms and  $\eta^5$ -bind to one  $\pi$ -face of a ferrocene molecule. The ferrocene molecule acts as a ditopic linker, forming the one-dimensional polymer.

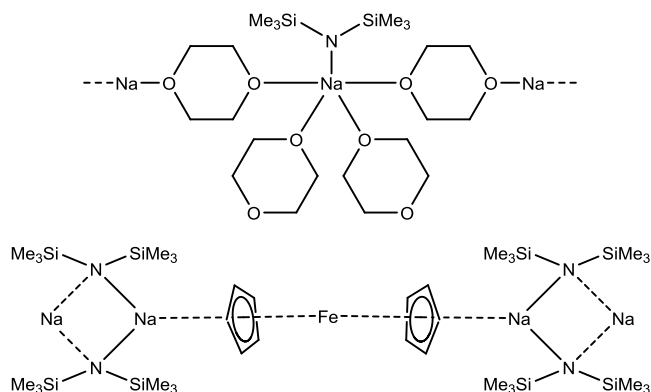


**Figure 2.24** Structural representations of solvated NaHMDS complexes crystallographically characterised prior to this work.

No other homometallic NaHMDS complexes solvated by TMEDA exist; however, as seen from the table of solvated sodium bis(silyl)amides in appendix I, other relevant crystallographically characterised complexes include the THF-<sup>[206]</sup> and TEMPO-solvated<sup>[193f]</sup> dimers of NaHMDS, as well as a TMEDA-solvated dimer of sodium-DA which has been crystallographically characterised by Andrews *et al.*<sup>[207]</sup>

Comparing **84** to the donor-free amide  $[\text{NaN}(\text{SiMe}_3)_2]_\infty$ ,<sup>[22]</sup> **7**, which crystallises as a polymer of trimeric units (polymorph of the same complex also known – a six-membered trimeric ring),<sup>[23]</sup> the addition of the donor TMEDA has, as expected, deaggregated the complex; however, the complex remains polymeric, now with dimeric repeating units.

Moving to solution studies of **84** in  $\text{C}_6\text{D}_6$  solution, the two  $^1\text{H}$  and two  $^{13}\text{C}$  resonances associated with the TMEDA ligand are different from those encountered in the free diamine, indicating that it remains coordinated to the alkali metal in arene solution. Likewise, the  $^1\text{H}$  and  $^{13}\text{C}$  resonances associated with the HMDS ligand are different from those encountered in the free amine and the free alkali metal amide, thus the solid-state structure of **84** appears to remain intact in solution; however, the formation of other oligomers cannot be ruled out.

Collectively comparing the structural motifs obtained on the addition of the donor TMEDA to LiHMDS, NaHMDS or KHMDS, it can be seen that the progression in the size of the alkali metals (and thus their bonding requirements) is reflected in the structural aggregates obtained as the homologous series is descended. Hence,  $[\text{LiHMDS}\cdot\text{TMEDA}]$ ,<sup>[182]</sup> **82**, is monomeric and the alkali metal is three coordinate. On progressing to  $[(\text{NaHMDS})_2\cdot\text{TMEDA}]_\infty$ , **84**, the alkali metal is again three coordinate, but, a polymeric complex is obtained, presumably so as

to satisfy the bonding requirements of the donor ligand, which binds in a monodentate fashion. Finally, in [KHMDS·TMEDA]<sub>2</sub>, **83**, a dimeric structure is obtained, most likely due to the necessity of the potassium to fill its substantially larger coordination sphere (four coordinate), in comparison to that of lithium or sodium.

The synthesis and characterisation of the homometallic complexes **83** and **84** laid down the foundations for the investigation into mixed-metal systems. The results from these studies will now follow.

## 2.3 Alkali Metal Tris(HMDS) Magnesiates Containing TMEDA Donor

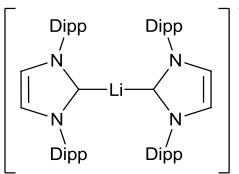
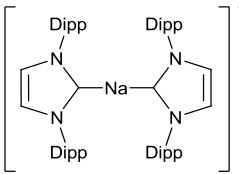
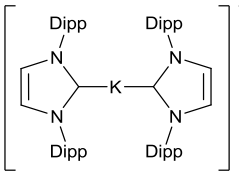
### Ligand

Having successfully synthesised homometallic alkali metal salts of HMDS solvated by TMEDA, our attention turned to the possibility of incorporating the alkaline earth metal magnesium into these systems to afford HMDS-containing alkali metal magnesiates.

A multitude of alkali metal alkyl/amido magnesiates have been structurally characterised and utilised in synthesis (*vide supra*),<sup>[38, 84, 86d, 87a, 87b, 88, 98, 100, 105-110, 115, 185c, 187, 193]</sup> including several containing the donor ligand TMEDA,<sup>[106-107, 110, 115, 187, 193b, 193h, 193o-r]</sup> however, of these TMEDA-solvated magnesiates, none contain the amide HMDS, the homometallic lithium compound of which has long been a utility reagent in organic synthesis.

Depending on the reaction stoichiometry employed in the preparation of these metall(ate) complexes and/or dynamic solution behaviour, various compositions of simple alkyl/amido containing magnesiates are possible including: solvated and unsolvated  $M^I M^{II}(R)_3$ ,  $M^I M^{II}(NR_2)(R)_2$ ,  $M^I M^{II}(NR_2)_2(R)$  and  $M^I M^{II}(NR_2)_3$  (where:  $M^I$  is an alkali metal;  $M^{II}$  is Mg; R is an alkyl group; and  $NR_2$  is an amido group). Predominantly, due to steric factors, ‘higher’ magnesiate formulations (where the Mg atom is coordinated to four anions) have also been isolated.<sup>[98, 193a-d]</sup> From a reactivity perspective, many of these complexes have been utilised as highly effective regioselective reagents which have high functional group tolerance at ambient temperatures.<sup>[84]</sup> Often their performance outshines that of their parent organo-alkali metal reagent (either alkyl or amide) or Grignard-type reagent.

Of the 18 HMDS-containing lithium, sodium and potassium magnesiates crystallographically characterised hitherto (Table 2.17) two are dimeric (*i.e.*, tetranuclear),<sup>[185c, 193g]</sup> six are polymeric,<sup>[110a, 193g, 193m, 193n]</sup> five are dinuclear species of the type  $[(S) \cdot M(\mu\text{-HMDS})_2 Mg(R)]$  (where S = solvent or vacant site and R = alkyl or amido group);<sup>[38, 100, 193m]</sup> and five adopt a solvent-separated ion pair composition.<sup>[193f, 193i, 193s]</sup>

HMDS-containing Lithium, Sodium and Potassium Magnesiate	Reference
$[\text{Li}(\mu\text{-HMDS})_2\text{Mg}(\text{HMDS})]$	[100]
$[\{\text{LiMg}(\text{TMP})\}\{\text{CH}_2\text{Si}(\text{Me})_2\text{N}(\text{SiMe}_3)\}]_2$	[185c]
$[\text{Li}_2(\mu\text{-HMDS})(\mu\text{-TEMPO})\cdot 2(\text{TEMPO})]^+[\text{Mg}(\text{HMDS})_3]^-$	[193f]
$[(\text{THF})\cdot\text{Li}(\mu\text{-HMDS})_2\text{Mg}(\text{HMDS})]$	[38]
$[(\text{Pyr})\cdot\text{Li}(\mu\text{-HMDS})_2\text{Mg}(\text{HMDS})]$	[38]
$[(\text{Pyr})\cdot\text{Li}(\mu\text{-HMDS})_2\text{Mg}(\text{Bu})]$	[38]
$[\text{Li}(\mu\text{-HMDS})_2\text{Mg}(\text{tBu})]_\infty$	[193m]
 $[\text{Mg}(\text{HMDS})_3]^-$	[193s]
$[(\text{Et}_2\text{O})\cdot\text{Na}(\mu\text{-HMDS})_2\text{Mg}(\text{tBu})]$	[193m]
 $[\text{Mg}(\text{HMDS})_3]^-$	[193s]
$[\{\text{K}(\text{benzene})_2\}^+\{\text{Mg}(\text{HMDS})_3\}^-]_\infty$	[193g]
$[\{\text{K}(\text{toluene})_2\}^+\{\text{Mg}(\text{HMDS})_3\}^-]_2$	[193g]
$[\{\text{K}(\text{toluene})_2\}^+\{\text{Mg}(\text{HMDS})_3\}^-]_\infty$	[193g]
$[\{\text{K}(p\text{-xylene})_2\}^+\{\text{Mg}(\text{HMDS})_3\}^-]_\infty$	[193g]
$[\text{K}(\eta^5\text{-ferrocene})_2(\eta^3\text{-toluene})_2]^+[\text{Mg}(\text{HMDS})_3]^-$	[193i]
$[\{\text{K}[(\text{C}_6\text{H}_6)_2\text{Cr}]_2\}^+\{\text{Mg}(\text{HMDS})_3\}^-]_\infty$	[110a]
$[\{\text{K}\{(\text{C}_6\text{H}_6)_2\text{Cr}\}_{1.5}\cdot(\text{Mes})\}^+\{\text{Mg}(\text{HMDS})_3\}^-]_\infty$	[193n]
 $[\text{Mg}(\text{HMDS})_3]^-$	[193s]

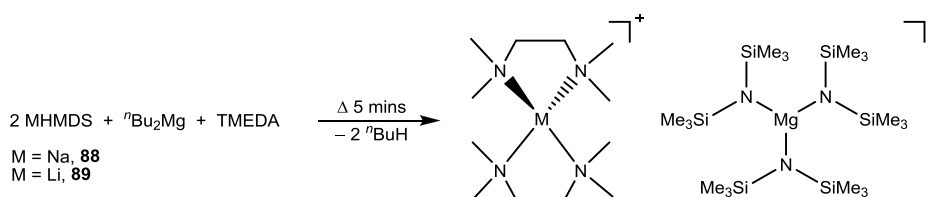
**Table 2.17** Crystallographically characterised HMDS-containing lithium, sodium and potassium magnesiate.

In the solvent-separated ion pair examples, unlike the dinuclear species in which the  $\text{Mg}(\text{HMDS})_3$  anion is tethered to an alkali metal, the alkali metal is sequestered by donor solvent molecules to leave a separate Mg containing anion. This discrete arrangement of  $\text{Mg}(\text{HMDS})_3$  was unprecedented prior to the characterisation of  $[\text{Li}_2(\mu\text{-HMDS})(\mu\text{-TEMPO})\cdot 2(\text{TEMPO})]^+[\text{Mg}(\text{HMDS})_3]^-$  in 2001,<sup>[193f]</sup> but is now common within magnesiate chemistry. Note, the presence of trace amounts of water or oxygen during the synthesis of

[Li( $\mu$ -HMDS)<sub>2</sub>Mg(HMDS)], afforded the inverse crown ether complex [Li<sub>2</sub>Mg<sub>2</sub>{N(SiMe<sub>3</sub>)<sub>2</sub>}<sub>4</sub>(O<sub>2</sub>)<sub>x</sub>(O)<sub>y</sub>], **36** (as detailed in chapter 1, section 1.4, Figure 1.28).<sup>[100]</sup>

Mulvey has been the forerunner in this area of exciting chemistry, showing that HMDS can be incorporated within heterobimetallic alkali metal/divalent metal ate complexes (all complexes detailed in Table 2.17 as well as the alkali metal zincates detailed in section 2.1) and utilised in *alkali metal mediated metallation* (AMMM);<sup>[85]</sup> however to date, none of these reagents contain the amide HMDS and the donor ligand TMEDA within the same complex. Wishing to fill this gap in knowledge, we herein report our attempts at the synthesis and characterisation of alkali metal magnesiates containing both HMDS and TMEDA. This was undertaken by carrying out the same reaction which initially produced complex **85** (*i.e.*, treating two molar equivalents of NaHMDS with one molar equivalent of di-*n*-butylmagnesium, followed by one molar equivalent of TMEDA in a hexane solution), but now heat was applied in each case. The reactions utilising LiHMDS or NaHMDS were successful in producing novel complexes; however, the reaction utilising KHMDS repeatedly yielded complex **83**.

Two new alkali metal tris(HMDS) magnesiate complexes, each containing the donor ligand TMEDA, have been prepared and characterised (Scheme 2.5). Both complexes have a solvent-separated ion pair composition of the form [M(TMEDA)<sub>2</sub>]<sup>+</sup>[Mg(HMDS)<sub>3</sub>]<sup>-</sup> (M = Na for **88**, Li for **89**). Although the cation – with the sodium or lithium sequestered by the diamine, and the anion – consisting of three HMDS ligands coordinated to a magnesium centre, have previously been reported, they have not been isolated within the same product.<sup>[208]</sup> Complexes **88** and **89** were synthesised by treating two molar equivalents of the respective alkali metal amide with one molar equivalent of di-*n*-butylmagnesium in the presence of a molar equivalent of TMEDA in a hydrocarbon medium. It is obvious from the very different quantities and constitution of ligands of the products that a dynamic reorganisation of the complexes has occurred. Rational synthesis *via* a mixed-metal approach (*i.e.*, treating an equimolar mixture of <sup>*n*</sup>BuNa and <sup>*n*</sup>Bu<sub>2</sub>Mg in hexane with three molar equivalents of HMDS and subsequently with two molar equivalents of TMEDA) revealed that co-complexation had not occurred. To elaborate, in both cases the chemical shifts in the <sup>1</sup>H NMR spectra resembled those of Mg(HMDS)<sub>2</sub>.<sup>[37c, 209]</sup>



Scheme 2.5 Serendipitous synthesis of complexes **88** and **89**.

2.3.1  $[\text{Na}(\text{TMEDA})_2]^+[\text{Mg}(\text{HMDS})_3]^-$ , **88**

Complex **88** was prepared by reacting two molar equivalents of NaHMDS with one molar equivalent of di-*n*-butylmagnesium, followed by one molar equivalent of TMEDA in a hexane solution (Scheme 2.5). The resultant solution was heated and filtered through Celite and glass wool, affording X-ray quality crystals of **88** at ambient temperature.

X-ray crystallographic analysis reveals that **88** crystallises as a solvent-separated ion pair complex in the triclinic system, space group  $P\bar{1}$ . The molecular structure of its cation (Figure 2.25) is composed of two TMEDA ligands which coordinate in their usual bidentate fashion to a sodium centre,<sup>[113, 116, 125, 210]</sup> whilst its anion (Figure 2.26) is composed of three HMDS ligands which coordinate to a magnesium centre (the sodium metal centre is four coordinate and the magnesium metal centre three coordinate). Within the asymmetric unit of **88** there are two independent molecules of the cation of  $[\text{Na}(\text{TMEDA})_2]^+[\text{Mg}(\text{HMDS})_3]^-$ , each of which sits on a centre of symmetry; however, the differences in the dimensions of the two cations are negligible, and thus Table 2.18 and Table 2.19 detail the key bond distances and angles respectively of only one of the independent cations.

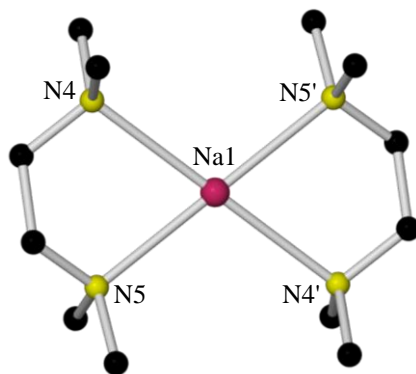


**Figure 2.25** Molecular structure of the cation of  $[\text{Na}(\text{TMEDA})_2]^+[\text{Mg}(\text{HMDS})_3]^-$ , **88**. H atoms omitted and only one of two similar molecules in the asymmetric unit shown for clarity.

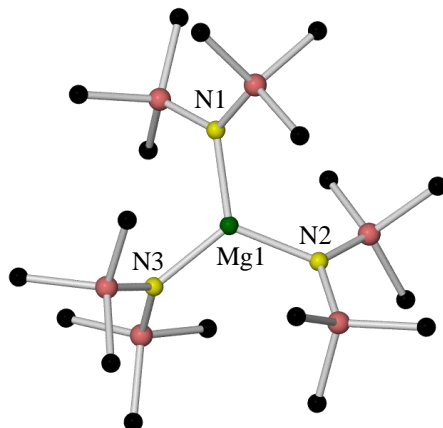


**Figure 2.26** Molecular structure of the anion of  $[\text{Na}(\text{TMEDA})_2]^+[\text{Mg}(\text{HMDS})_3]^-$ , **88**. H atoms are omitted for clarity.

Selected Bond	Bond Distance (Å) in [Na(TMEDA) <sub>2</sub> ] <sup>+</sup> [Mg(HMDS) <sub>3</sub> ] <sup>-</sup> , <b>88</b>
Na1–N4	2.562(1)
Na1–N5	2.472(2)
Mg1–N1	2.017(2)
Mg1–N2	2.024(2)
Mg1–N3	2.030(2)

**Table 2.18** Key bond distances within [Na(TMEDA)<sub>2</sub>]<sup>+</sup>[Mg(HMDS)<sub>3</sub>]<sup>-</sup>, **88**.

Selected Angle	Bond Angle (°) in [Na(TMEDA) <sub>2</sub> ] <sup>+</sup> [Mg(HMDS) <sub>3</sub> ] <sup>-</sup> , <b>88</b>
N4–Na1–N5	74.57(6)
N4–Na1–N4'	180.00(14)
N4–Na1–N5'	105.43(6)
N1–Mg1–N2	119.77(7)
N1–Mg1–N3	121.04(7)
N2–Mg1–N3	119.19(7)

**Table 2.19** Key bond angles within [Na(TMEDA)<sub>2</sub>]<sup>+</sup>[Mg(HMDS)<sub>3</sub>]<sup>-</sup>, **88**.

Due to the solvent-separated ion pair composition of complex **88**, the cationic and anionic moieties will be discussed independently. The molecular structure of its cation (Figure 2.25) is composed of a sodium metal centre sequestered by two bidentate TMEDA ligands, resulting in the sodium metal centre being four coordinate and in a distorted square planar geometry (summed angles at Na, 720°). This cation is known,<sup>[113, 116, 125, 210]</sup> having previously been incorporated within complexes such as [Na(TMEDA)<sub>2</sub>]<sup>+</sup>[HNi<sub>2</sub>(C<sub>2</sub>H)<sub>4</sub>]<sup>-</sup><sup>[210a]</sup> and [Na(TMEDA)<sub>2</sub>]<sup>+</sup>[I]<sup>-</sup>,<sup>[210c]</sup> for example; however, none of these complexes contain magnesium or HMDS. The mean Na–N bond distance within cation **88** (2.517 Å) and the mean N<sub>TMEDA</sub>–Na–N<sub>TMEDA</sub> bite angle (74.57°) lie in the range of the corresponding parameters observed for previously characterised complexes containing the same cation (range of mean bond distances and bite angles, 2.483–2.607 Å and 73.05–80.15° respectively).<sup>[113, 116, 125, 210]</sup>

Turning to the anion of **88** (Figure 2.26), it is composed of three HMDS ligands which coordinate to a magnesium metal centre, resulting in the magnesium metal centre being three coordinate and in a near ideal trigonal planar geometry (summed angles at Mg, 360°). This anion is known, having previously been incorporated within all but four of the 18 complexes listed in Table 2.17 (*vide supra*) and within the calcium magnesiate [(HMDS)·Ca(μ-HMDS)<sub>2</sub>Mg(HMDS)].<sup>[211]</sup> The mean Mg–N bond distance within anion **88** (2.024 Å) lies in the range of those complexes previously characterised containing the same anion (range of mean bond distances, 2.020–2.076 Å) and the N<sub>amide</sub>–Mg–N<sub>amide</sub> angles [119.77(7), 121.04(7) and 119.19(7)°] are unremarkable.<sup>[38, 100, 110a, 193f, 193g, 193i, 193n, 193s, 211]</sup>



Moving to solution studies of **88** in C<sub>6</sub>D<sub>6</sub> solution, the two <sup>1</sup>H and two <sup>13</sup>C resonances associated with the TMEDA ligand are different from those encountered in the free diamine, indicating that it remains coordinated to the alkali metal in arene solution. Likewise, the <sup>1</sup>H and <sup>13</sup>C resonances associated with the HMDS ligand are different from those encountered in the free amine, the free alkali metal amide, and the free alkaline earth metal bis(amide) (which undergoes monomer-dimer equilibrium in arene solution),<sup>[37c, 209]</sup> thus signifying that the coordination geometry seen in the solid-state structure of **88** appears to remain intact in solution.

### 2.3.2 [Li(TMEDA)<sub>2</sub>]<sup>+</sup>[Mg(HMDS)<sub>3</sub>]<sup>-</sup>, **89**

Following the same reaction methodology as that used to prepare **88** (using LiHMDS in place of NaHMDS) afforded X-ray quality crystals of **89** at ambient temperature (Scheme 2.5).

X-ray crystallographic analysis reveals that **89** crystallises in the monoclinic system, space group *P*2<sub>1</sub>/*c*. Akin to its sodium congener **88**, the structure of **89** is composed of the same basic building blocks – a cation (Figure 2.27) composed of an alkali metal centre and two TMEDA ligands, and an anion composed of a magnesium centre and three HMDS ligands – the only difference being that lithium replaces sodium as the alkali metal (the lithium metal centre is four coordinate and the magnesium metal centre three coordinate). Table 2.20 and Table 2.21 detail the key bond distances and bond angles respectively.

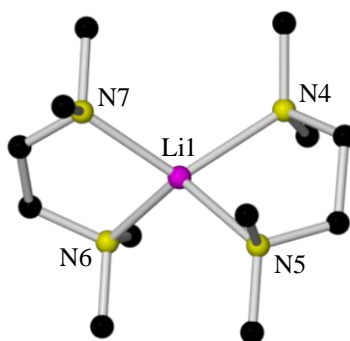


**Figure 2.27** Molecular structure of the cation of [Li(TMEDA)<sub>2</sub>]<sup>+</sup>[Mg(HMDS)<sub>3</sub>]<sup>-</sup>, **89**. H atoms are omitted for clarity.

Selected Bond	Bond Distance (Å) in [Li(TMEDA) <sub>2</sub> ] <sup>+</sup> [Mg(HMDS) <sub>3</sub> ] <sup>-</sup> , <b>89</b>
Li1–N4	2.170(7)
Li1–N5	2.147(8)
Li1–N6	2.093(7)
Li1–N7	2.057(8)
Mg1–N1	2.023(3)
Mg1–N2	2.021(3)
Mg1–N3	2.025(3)

**Table 2.20** Key bond distances within [Li(TMEDA)<sub>2</sub>]<sup>+</sup>[Mg(HMDS)<sub>3</sub>]<sup>-</sup>, **89**.

Selected Angle	Bond Angle (°) in [Li(TMEDA) <sub>2</sub> ] <sup>+</sup> [Mg(HMDS) <sub>3</sub> ] <sup>-</sup> , <b>89</b>
N4–Li1–N5	86.2(3)
N4–Li1–N6	125.5(3)
N4–Li1–N7	115.9(3)
N5–Li1–N6	116.1(3)
N5–Li1–N7	127.9(3)
N6–Li1–N7	89.6(3)
N1–Mg1–N2	119.96(12)
N1–Mg1–N3	120.17(13)
N2–Mg1–N3	119.86(13)

**Table 2.21** Key bond angles within [Li(TMEDA)<sub>2</sub>]<sup>+</sup>[Mg(HMDS)<sub>3</sub>]<sup>-</sup>, **89**.

The cation of **89** is similar to that of **88** in that it is composed of an alkali metal centre sequestered by two bidentate TMEDA ligands; however, on changing the alkali metal from sodium to lithium, the geometry at the metal centre changes from a square planar arrangement to a distorted tetrahedral arrangement (summed angles at Li, 661.20°). As expected, due to the different sizes of the metals, the mean M–N bond distance (2.116 Å) is 0.4014 Å shorter in **89** and the mean N<sub>TMEDA</sub>–M–N<sub>TMEDA</sub> bite angle (87.90°) is 13.33° wider than that of the corresponding parameters in **88**. Again, this cation is known, having previously been incorporated within at least 105 crystallographically characterised complexes such as [Li(TMEDA)<sub>2</sub>]<sup>+</sup>[MnMe<sub>6</sub>]<sup>-</sup>,<sup>[212]</sup> [Li(TMEDA)<sub>2</sub>]<sup>+</sup>[{N(SiMe<sub>3</sub>)<sub>2</sub>]<sub>2</sub>VMe<sub>2</sub>]<sup>-</sup><sup>[213]</sup> and [Li(TMEDA)<sub>2</sub>]<sup>+</sup>[AlH<sub>4</sub>]<sup>-</sup>,<sup>[214]</sup> to name but a few; however, only four such complexes contain [Li(TMEDA)<sub>2</sub>]<sup>+</sup> and HMDS,<sup>[213, 215]</sup> and none contain magnesium. The anion of **89** is essentially identical to that of **88** and warrants no further discussion.

Turning to solution studies of **89** in C<sub>6</sub>D<sub>6</sub> solution, the two <sup>1</sup>H and two <sup>13</sup>C resonances associated with the TMEDA ligand are different from those encountered in the free diamine, indicating that it remains coordinated to the alkali metal in arene solution. Likewise, the <sup>1</sup>H and <sup>13</sup>C resonances associated with the HMDS ligand are different from those encountered in the free amine, the free alkali metal amide, and the free alkaline earth metal bis(amide), thus signifying that the coordination structure seen in the solid-state of **89** appears to remain intact in solution.

In an effort to develop the chemistry of HMDS with the donor ligand TMEDA, we have prepared and characterised two new TMEDA-solvated homometallic alkali metal salts of HMDS and two new TMEDA-solvated heterobimetallic alkali metal tris(HMDS) magnesiates. Complexes **83** and **84** are the first structurally characterised homometallic complexes of TMEDA-solvated KHMDS or NaHMDS, and complexes **88** and **89** are rare

examples of the commonly synthesised alkali metal cation  $[M(\text{TMEDA})_2]^+$  and the magnesiate anion  $[\text{Mg}(\text{HMDS})_3]^-$  being present within the one complex.

As TMEDA has proved a useful co-ligand in reagents designed for *AMMM* applications,<sup>[84-85]</sup> and having successfully synthesised TMEDA adducts of HMDS, our attention turned to the possibility of introducing the amide diphenylamide into TMEDA systems. A description of the preparation and structural characterisation of three key monometallic TMEDA complexes of diphenylamide will now follow.

## 2.4 Diphenylamide TMEDA-Solvated Homobimetallic Complexes

As discussed previously, alkali metal amides and their solvates, in particular the metal salts of DA(H), TMP(H) and HMDS(H), are widely utilised within synthetic laboratories due to their strong Lowry-Brønsted basicity coupled with their relatively poor nucleophilicity.

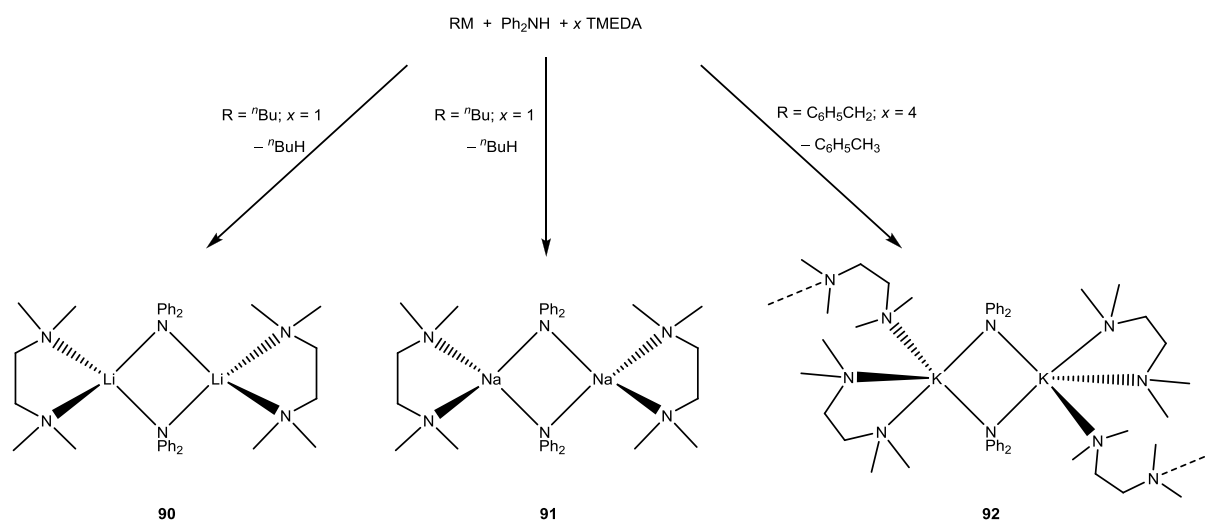
Another amido reagent, the highly thermally stable lithium diphenylamide,  $(\text{LiNPh}_2)$ , is particularly interesting and has shown promise in a range of synthetic transformations. As well as regioselective deprotonation reactions,<sup>[216]</sup> it has also been used in catalytic aldol reactions involving silyl enol ethers and aldehydes,<sup>[217]</sup> in elimination applications,<sup>[218]</sup> in metathesis reactions,<sup>[219]</sup> during the preparation of amino-containing carbenes<sup>[220]</sup> and as an indicator in the polymerisation of methyl methacrylate.<sup>[221]</sup>

Alkali metal diphenylamide complexes have been extensively studied in both the solid- and solution-state. The solution structures of  $\text{LiNPh}_2$  in THF (in the presence/absence of LiBr) have been comprehensively studied by Collum.<sup>[222]</sup> In the solid-state, the majority of the complexes reported to date take the form of solvent-separated alkali metal ate species, whereby the second metal is a transition metal,<sup>[223]</sup> lanthanide,<sup>[224]</sup> actinide<sup>[225]</sup> or a Group 13 element.<sup>[226]</sup> Contacted ate complexes are also prevalent, predominately with the heavier alkali metals (sodium and potassium) due to their need for further stabilisation *via* metal-arene  $\pi$ -interactions.<sup>[223c, 227]</sup>

Turning to homometallic species, lithium diphenylamide has been shown to form co-complexes with i) lithium chloride,<sup>[228]</sup> ii) *n*-butyllithium and mono *ortho*-metallated  $\text{LiNPh}_2$ ,<sup>[229]</sup> and iii) dilithium diphenylhydrazide.<sup>[11f]</sup> Several alkali metal diphenylamides stabilised by donor ligands (*e.g.*, various ethers<sup>[36b, 230]</sup> and pyridine<sup>[230b]</sup>) have also been reported. However, surprisingly no homometallic sodium diphenylamide complexes have been reported previous to this work.

As highlighted earlier, over the past few years Mulvey *et al.* have shown that DA, TMP and HMDS can be incorporated within heterobimetallic alkali metal/divalent metal ate complexes and utilised in *alkali metal mediated metallation* (AMMM).<sup>[85]</sup> Wishing to expand on this exciting, relatively new area of chemistry, we aim to introduce diphenylamide as a newcomer to AMMM, and as a prelude report here the preparation and structural characterisation of three key monometallic building blocks: namely TMEDA adducts of  $MNPh_2$  (where M is Li, Na or K).<sup>[85]</sup> This chemistry is being pursued as TMEDA has proved a useful co-ligand in reagents designed for AMMM applications.<sup>[84-85]</sup>

Three novel homobimetallic complexes containing diphenylamide ( $NPh_2$ ) have been prepared and characterised; namely the TMEDA-solvated lithium, sodium and potassium bis(amido) complexes (Scheme 2.6). Complexes **90** and **91**  $[(TMEDA)M(NPh_2)]_2$  (M = Li for **90**, Na for **91**) are synthesised by treating one molar equivalent of the parent amine with an equimolar quantity of  ${}^nBuM$  and TMEDA in hexane solution. The third complex  $[(TMEDA)_{3/2}K(NPh_2)]_2$ , **92**, is prepared in a similar way to **90** and **91** except that benzylpotassium is utilised as the metallating agent. In addition, an excess of TMEDA (at least four molar equivalents) is required to fully solubilise the heavy alkali metal amide mixture.



Scheme 2.6 Synthesis of **90-92**.

#### 2.4.1 $[(TMEDA)Li(NPh_2)]_2$ , **90**

Complex **90** was prepared by reacting *n*-butyllithium with an equimolar quantity of diphenylamine in a hexane solution. One molar equivalent of TMEDA in toluene was required to produce a homogeneous solution (Scheme 2.6). X-ray quality crystals of **90** precipitated from solution at ambient temperature.

X-ray crystallographic analysis reveals that **90** (Figure 2.28) crystallises as a dimer in the monoclinic system, space group  $P2_1/n$ , and is composed of two lithium centres each coordinated to a TMEDA ligand, with two diphenylamide ligands bridging the two metal centres (both metal centres are four coordinate). Table 2.22 and Table 2.23 detail the key bond distances and bond angles respectively.

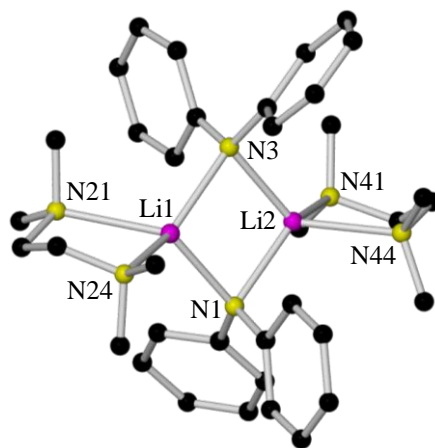


**Figure 2.28** Molecular structure of  $[(\text{TMEDA})\text{Li}(\text{NPh}_2)_2]_2$ , **90**. H atoms are omitted for clarity.

Selected Bond	Bond Distance (Å) in $[(\text{TMEDA})\text{Li}(\text{NPh}_2)_2]_2$ , <b>90</b>
Li1–N1	2.137(3)
Li1–N3	2.183(3)
Li1–N21	2.381(3)
Li1–N24	2.313(4)
Li2–N1	2.142(3)
Li2–N3	2.140(4)
Li2–N41	2.242(4)
Li2–N44	2.273(3)

**Table 2.22** Key bond distances within  $[(\text{TMEDA})\text{Li}(\text{NPh}_2)_2]_2$ , **90**.

Selected Angle	Bond Angle (°) in $[(\text{TMEDA})\text{Li}(\text{NPh}_2)_2]_2$ , <b>90</b>
N1–Li1–N3	97.82(14)
N1–Li1–N21	131.92(15)
N1–Li1–N24	108.66(15)
N3–Li1–N21	109.95(14)
N3–Li1–N24	134.21(15)
N21–Li1–N24	79.08(11)
N1–Li2–N3	99.01(14)
N1–Li2–N41	124.24(15)
N1–Li2–N44	114.13(16)
N3–Li2–N41	112.07(16)
N3–Li2–N44	125.18(15)
N41–Li2–N44	84.41(12)
Li1–N1–Li2	82.09(13)
Li1–N3–Li2	81.06(13)

**Table 2.23** Key bond angles within  $[(\text{TMEDA})\text{Li}(\text{NPh}_2)_2]_2$ , **90**.

The molecular framework of **90** consists of a planar (sum of endocyclic angles,  $359.98^\circ$ )  $(\text{LiN})_2$  ring, in which the *intra*-annular Li–N bond distances show only slight variation [range, 2.137(3)–2.183(3) Å; mean distance, 2.151 Å]. As mentioned earlier, the coordination spheres of the two crystallographically distinct Li centres are completed by binding to a TMEDA ligand, resulting in the metals adopting distorted tetrahedral geometries (sum of angles,  $661.64$  and  $659.04^\circ$  for Li1 and Li2 respectively). As expected, in both cases, the greatest cause of the distortion from ideal tetrahedral geometry is the acute  $\text{N}_{\text{TMEDA}}\text{--Li--N}_{\text{TMEDA}}$  bite angle [ $79.08(11)$  and  $84.41(12)^\circ$  for Li1 and Li2 respectively]. Presumably due to the steric constraints of the dimeric molecule, the Li– $\text{N}_{\text{TMEDA}}$  distances for each Li centre vary slightly; mean distance, 2.347 and 2.258 Å for Li1– $\text{N}_{\text{TMEDA}}$  and Li2– $\text{N}_{\text{TMEDA}}$  respectively.

There are several TMEDA adducts of lithium secondary amides known which adopt subtly different structural motifs (Figure 2.29). When less sterically demanding amides [*e.g.*,  $\text{N}(\text{Me})(\text{Ph})$ ]<sup>[35]</sup> are employed, ‘closed’ dimers (akin to **90**) are formed, where the Li centres are formally four coordinate. Using amides of an intermediate steric bulk (*e.g.*,  $\text{DA}$ <sup>[40]</sup> or *cis*- $\text{DMP}$ <sup>[194b]</sup>), similar  $(\text{LiN})_2$  four-membered rings are observed; however, in these instances the TMEDA ligand binds in a bridging, monodentate manner (hence Li is three coordinate), producing linear polymeric arrays. Using the most sterically demanding amides (*e.g.*,  $\text{TMP}$ )<sup>[39b]</sup> a closed dimer is not possible. Williard reported the ‘open’ dimeric complex, perhaps more correctly termed an open dinuclear complex (Figure 2.29), where one Li centre is formally three coordinate (bound to one amide and two TMEDA N atoms) and the other is two coordinate (bound only to two amide N atoms).<sup>[39b]</sup> When the silylamide HMDS is utilised, a monomeric TMEDA adduct is isolated.<sup>[182]</sup>

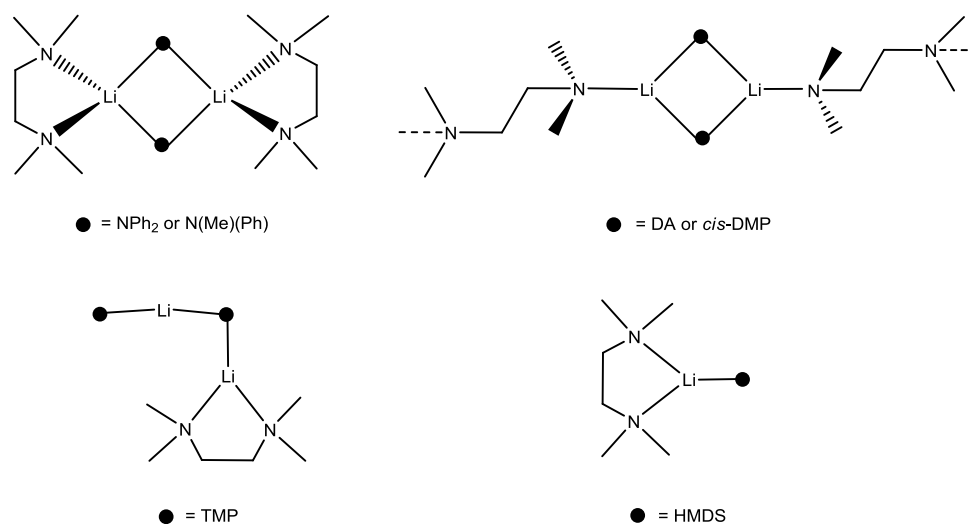


**Figure 2.29** Structural motifs of TMEDA solvates of synthetically important lithium amides.

To aid the interpretation of the NMR data obtained in this project and any future work, the  $^1\text{H}$ ,  $^{13}\text{C}$ , COSY and HSQC NMR spectra were obtained for the free amine standard,  $\text{Ph}_2\text{NH}$ , in both  $\text{C}_6\text{D}_6$  and  $\text{d}_8\text{-THF}$  solution. The  $^1\text{H}$  and  $^{13}\text{C}$  spectra of  $\text{Ph}_2\text{NH}$  in  $\text{C}_6\text{D}_6$  solution (Figure 2.30 and Figure 2.31) and  $\text{d}_8\text{-THF}$  solution (Figure 2.32 and Figure 2.33) are shown below.

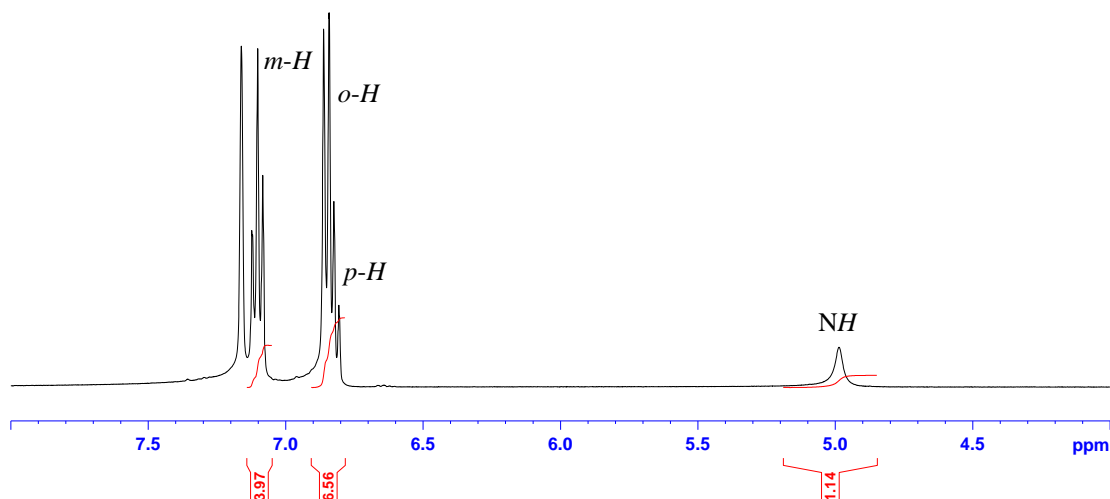


Figure 2.30  $^1\text{H}$  NMR spectrum of  $\text{Ph}_2\text{NH}$  in  $\text{C}_6\text{D}_6$ .

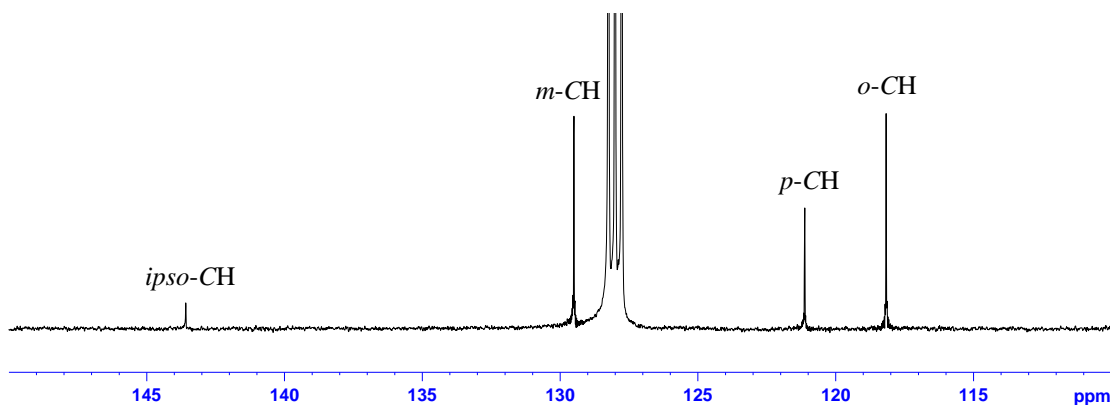


Figure 2.31  $^{13}\text{C}$  NMR spectrum of  $\text{Ph}_2\text{NH}$  in  $\text{C}_6\text{D}_6$ .

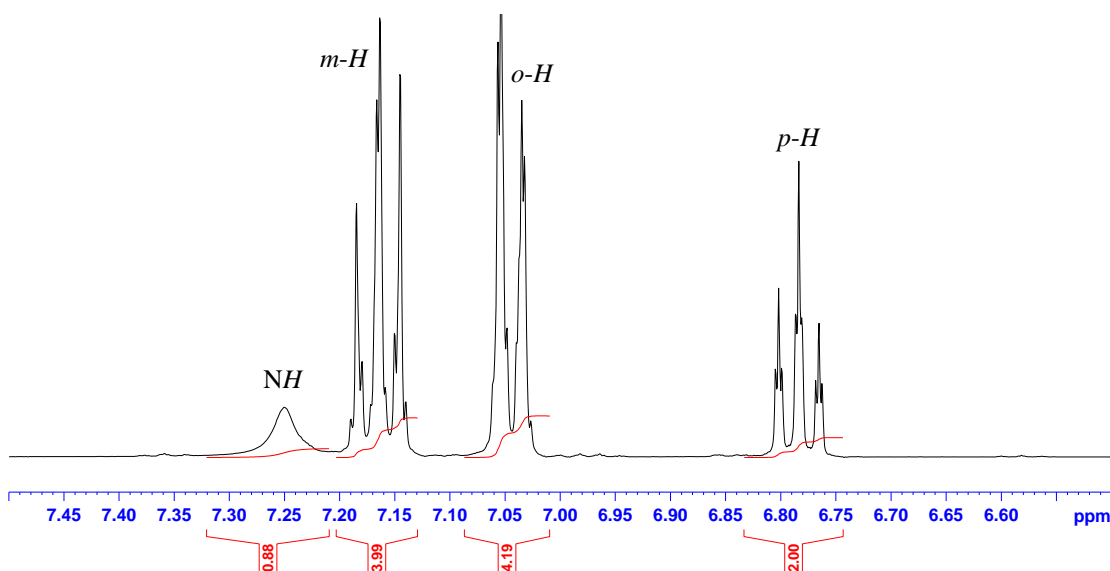
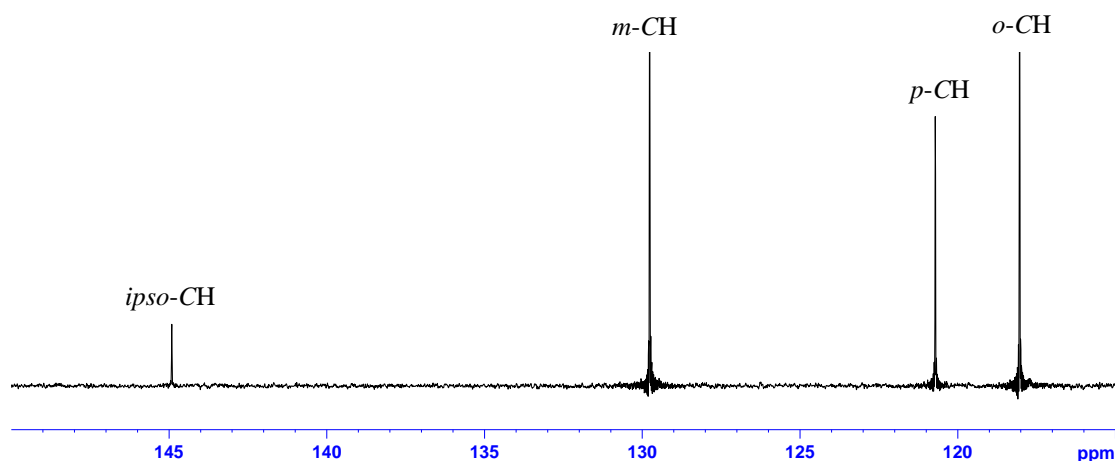


Figure 2.32  $^1\text{H}$  NMR spectrum of  $\text{Ph}_2\text{NH}$  in  $\text{d}_8\text{-THF}$ .



**Figure 2.33**  $^{13}\text{C}$  NMR spectrum of  $\text{Ph}_2\text{NH}$  in  $\text{d}_8\text{-THF}$ .

In the  $\text{C}_6\text{D}_6$  spectrum there are three resonances observed for the three chemically distinct *o*-, *m*- and *p*-hydrogen atoms. There is an apparent triplet at 7.10 ppm integrating to four protons, which corresponds to the four *m*-hydrogens. A doublet, integrating to four protons appears at 6.85 ppm, which corresponds to the four *o*-hydrogens and another doublet at 6.83 ppm integrating to two protons, corresponding to the *p*-hydrogens.

With the aid of the HSQC spectrum, the relevant chemical shifts from the  $^{13}\text{C}$  NMR spectrum were assigned to their respective proton chemical shifts from the  $^1\text{H}$  NMR spectrum and are shown in Table 2.24 and Table 2.25 respectively.

NMR chemical shifts of $\text{Ph}_2\text{NH}$ in $\text{C}_6\text{D}_6$			
$^1\text{H}$ $\delta$ / ppm		$^{13}\text{C}$ $\delta$ / ppm	
–	–	<i>ipso-CH</i>	143.6
<i>o-CH</i>	6.85	<i>o-CH</i>	118.2
<i>m-CH</i>	7.10	<i>m-CH</i>	129.5
<i>p-CH</i>	6.83	<i>p-CH</i>	121.1
NH	4.99	–	–

**Table 2.24**  $^1\text{H}$  and  $^{13}\text{C}$  NMR chemical shifts of  $\text{Ph}_2\text{NH}$  in  $\text{C}_6\text{D}_6$ .

NMR chemical shifts of $\text{Ph}_2\text{NH}$ in $\text{d}_8\text{-THF}$			
$^1\text{H}$ $\delta$ / ppm		$^{13}\text{C}$ $\delta$ / ppm	
–	–	<i>ipso-CH</i>	144.9
<i>o-CH</i>	7.04	<i>o-CH</i>	118.0
<i>m-CH</i>	7.16	<i>m-CH</i>	129.8
<i>p-CH</i>	6.78	<i>p-CH</i>	120.7
NH	7.25	–	–

**Table 2.25**  $^1\text{H}$  and  $^{13}\text{C}$  NMR chemical shifts of  $\text{Ph}_2\text{NH}$  in  $\text{d}_8\text{-THF}$ .

Turning to the NMR spectroscopic analysis of **90**, the crystalline product was dissolved in  $\text{C}_6\text{D}_6$  solution and examined by  $^7\text{Li}$ ,  $^1\text{H}$ ,  $^{13}\text{C}$  (Figures 2.34-2.36), COSY and HSQC NMR spectroscopy. With the aid of the HSQC spectrum, the relevant chemical shifts from the  $^{13}\text{C}$



NMR spectrum were assigned to their respective proton chemical shifts from the  $^1\text{H}$  NMR spectrum and are shown in Table 2.26.

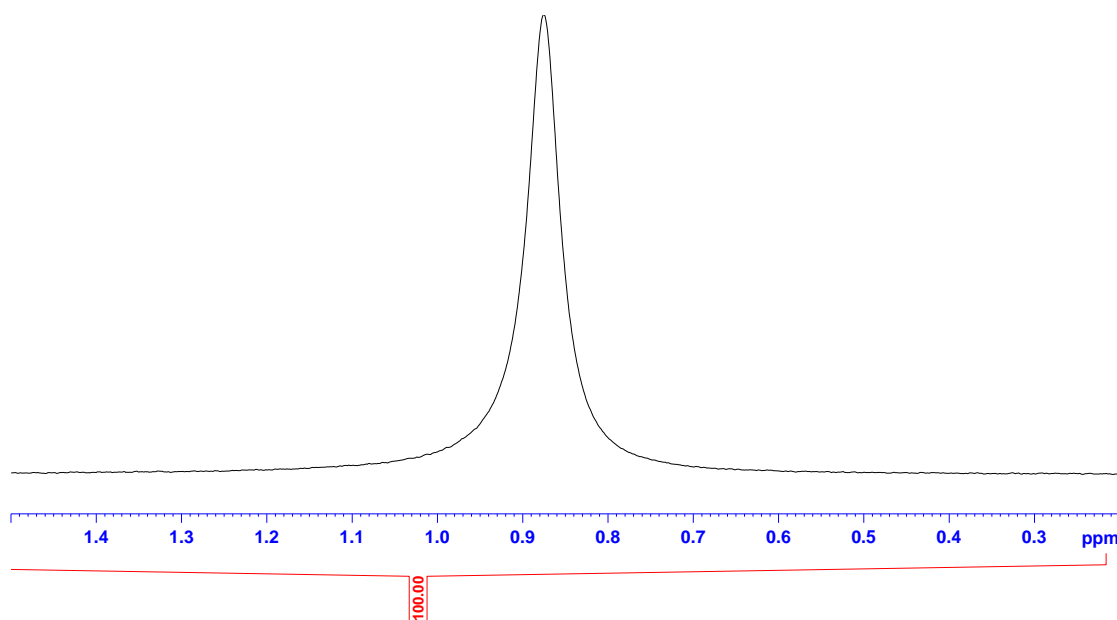


Figure 2.34  $^7\text{Li}$  NMR spectrum of  $[(\text{TMEDA})\text{Li}(\text{NPh}_2)_2]$ , **90**, in  $\text{C}_6\text{D}_6$ .

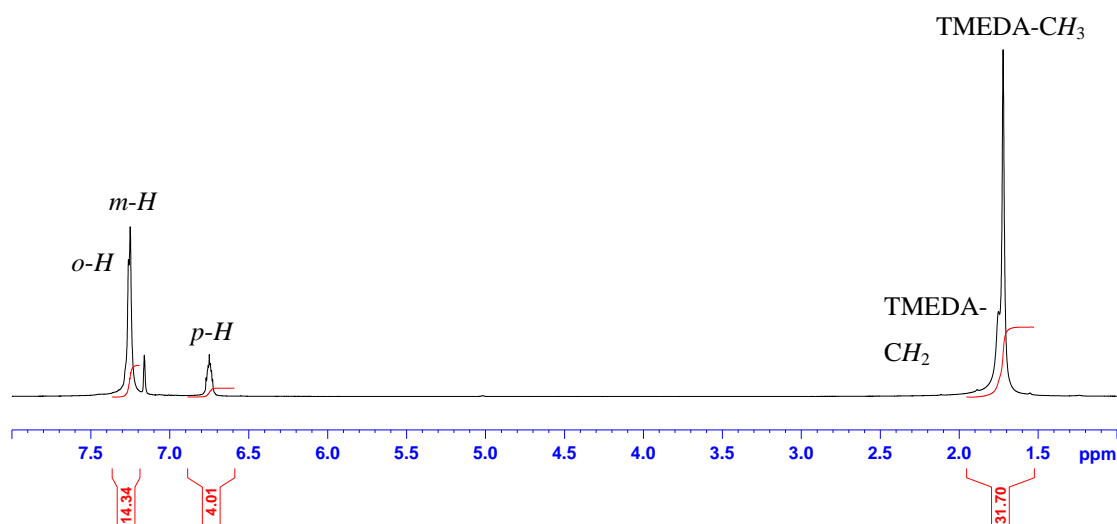


Figure 2.35  $^1\text{H}$  NMR spectrum of  $[(\text{TMEDA})\text{Li}(\text{NPh}_2)_2]$ , **90**, in  $\text{C}_6\text{D}_6$ .

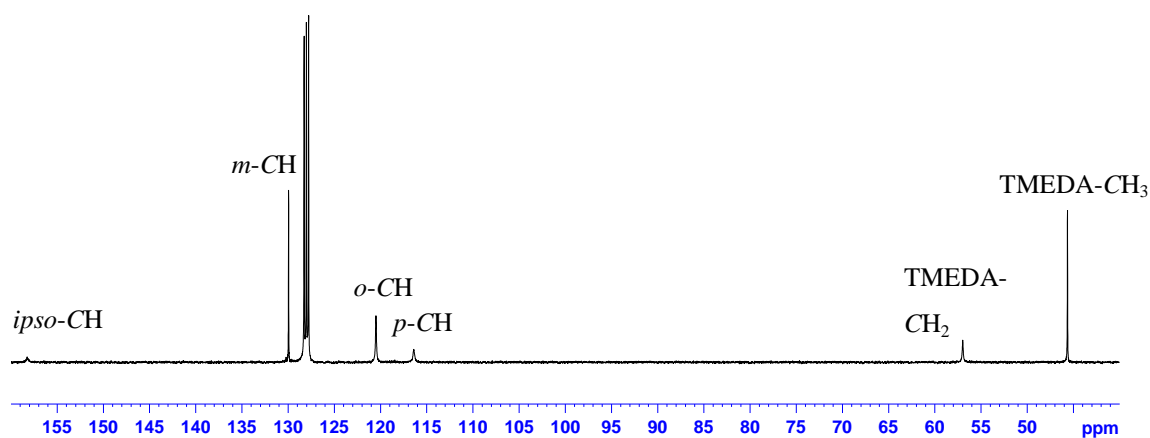


Figure 2.36  $^{13}\text{C}$  NMR spectrum of  $[(\text{TMEDA})\text{Li}(\text{NPh}_2)_2]$ , **90**, in  $\text{C}_6\text{D}_6$ .

The two  $^1\text{H}$  and two  $^{13}\text{C}$  resonances associated with the TMEDA ligand in **90** are different from those encountered in the free diamine, indicating that it remains coordinated to the alkali metal in arene solution. It appears that only one oligomer of solvated alkali metal amide [presumably the dimeric solid-state species (*vide infra*)] exists in solution,<sup>[222a]</sup> as only one set of diphenylamido resonances are observed, although there is a precedent for other *s*-block metal species to slowly convert to other oligomers over a long period of time.<sup>[231]</sup> The  $^7\text{Li}$  NMR spectrum also supports this conclusion as only one resonance (0.88 ppm) is observed. As mentioned previously, higher oligomeric forms (trimer,<sup>[11]</sup> tetramer,<sup>[12]</sup> hexamer,<sup>[13]</sup> octamer<sup>[14]</sup> and polymer<sup>[15]</sup>) of Li amides are known; however, they tend to exist only in the absence of donor solvents.

NMR chemical shifts of [(TMEDA)Li(NPh <sub>2</sub> ) <sub>2</sub> ] <sub>2</sub> , <b>90</b> , in C <sub>6</sub> D <sub>6</sub>			
$^1\text{H}$ $\delta$ / ppm		$^{13}\text{C}$ $\delta$ / ppm	
–	–	<i>ipso</i> -CH	158.1
<i>o</i> -CH	7.26	<i>o</i> -CH	120.5
<i>m</i> -CH	7.26	<i>m</i> -CH	130.1
<i>p</i> -CH	6.74	<i>p</i> -CH	116.5
TMEDA (CH <sub>3</sub> )	1.72	TMEDA (CH <sub>3</sub> )	45.7
TMEDA (CH <sub>2</sub> )	1.75	TMEDA (CH <sub>2</sub> )	57.1

**Table 2.26**  $^1\text{H}$  and  $^{13}\text{C}$  NMR chemical shifts of [(TMEDA)Li(NPh<sub>2</sub>)<sub>2</sub>]<sub>2</sub>, **90**, in C<sub>6</sub>D<sub>6</sub>.

#### 2.4.2 [(TMEDA)Na(NPh<sub>2</sub>)<sub>2</sub>]<sub>2</sub>, **91**

Following the same reaction methodology as that used to prepare **90** (using *n*-butylsodium in place of *n*-butyllithium) afforded X-ray quality crystals of **91** at ambient temperature (Scheme 2.6).

X-ray crystallographic analysis reveals that **91** crystallises as a dimer in the monoclinic system, space group  $P2_1/n$ . Similar to its lithium congener **90**, the structure of **91** (Figure 2.37) is composed of the same basic building blocks – two alkali metal centres, two TMEDA ligands and two diphenylamide ligands – the only difference being that sodium replaces lithium as the alkali metal (both metal centres are four coordinate). Table 2.27 and Table 2.28 detail the key bond distances and bond angles respectively.

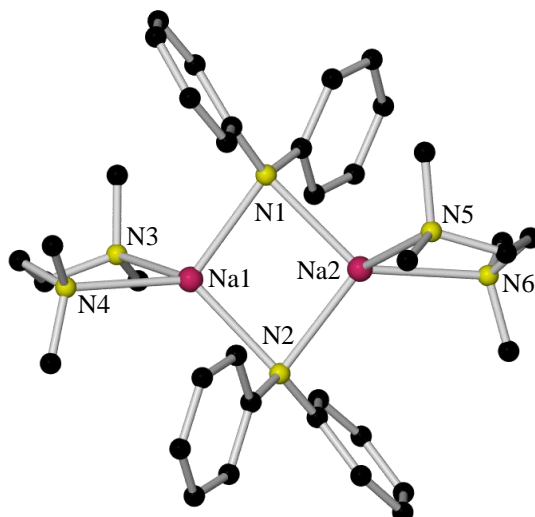


**Figure 2.37** Molecular structure of  $[(\text{TMEDA})\text{Na}(\text{NPh}_2)_2]$ , **91**. H atoms are omitted for clarity.

Selected Bond	Bond Distance (Å) in $[(\text{TMEDA})\text{Na}(\text{NPh}_2)_2]$ , <b>91</b>
Na1–N1	2.422(2)
Na1–N2	2.436(2)
Na1–N3	2.466(2)
Na1–N4	2.460(2)
Na2–N1	2.484(2)
Na2–N2	2.466(2)
Na2–N5	2.479(2)
Na2–N6	2.498(2)

**Table 2.27** Key bond distances within  $[(\text{TMEDA})\text{Na}(\text{NPh}_2)_2]$ , **91**.

Selected Angle	Bond Angle (°) in $[(\text{TMEDA})\text{Na}(\text{NPh}_2)_2]$ , <b>91</b>
N1–Na1–N2	99.43(8)
N1–Na1–N3	106.06(8)
N1–Na1–N4	123.92(8)
N2–Na1–N3	127.86(8)
N2–Na1–N4	124.35(8)
N3–Na1–N4	75.22(8)
N1–Na2–N2	96.96(7)
N1–Na2–N5	104.39(8)
N1–Na2–N6	133.17(8)
N2–Na2–N5	128.46(8)
N2–Na2–N6	120.95(8)
N5–Na2–N6	74.23(8)
Na1–N1–Na2	81.74(7)
Na1–N2–Na2	81.81(7)

**Table 2.28** Key bond angles within  $[(\text{TMEDA})\text{Na}(\text{NPh}_2)_2]$ , **91**.

The framework of **91** is essentially identical to that of **90**, containing a  $(\text{NaN})_2$  ring which is planar (sum of endocyclic angles,  $359.94^\circ$ ). The obtuse internal angles are at the Na atoms

and the acute angles are at the N atoms – a common feature in alkali metal amide ring systems. Akin to **90**, little discrimination exists between the distances of the Na–N<sub>amide</sub> bonds [range of distances, 2.422(2)–2.484(2) Å; mean distance, 2.457 Å]. As expected, these are slightly shorter than the dative Na–N<sub>TMEDA</sub> bonds [range of distances, 2.460(2)–2.498(2) Å; mean distance, 2.476 Å]. The mean N<sub>TMEDA</sub>–M–N<sub>TMEDA</sub> bite angle in **91** is 74.73°, which is approximately 7° more acute than the corresponding angle in lithium-containing **90**.

To the best of our knowledge, **91** was surprisingly the first homometallic sodium complex of diphenylamide to be crystallographically characterised, with Westerhausen subsequently reporting the solid-state structures of dimeric THF, dimeric PMDETA and polymeric dioxane solvates of sodium diphenylamide (Figure 2.38).<sup>[232]</sup>

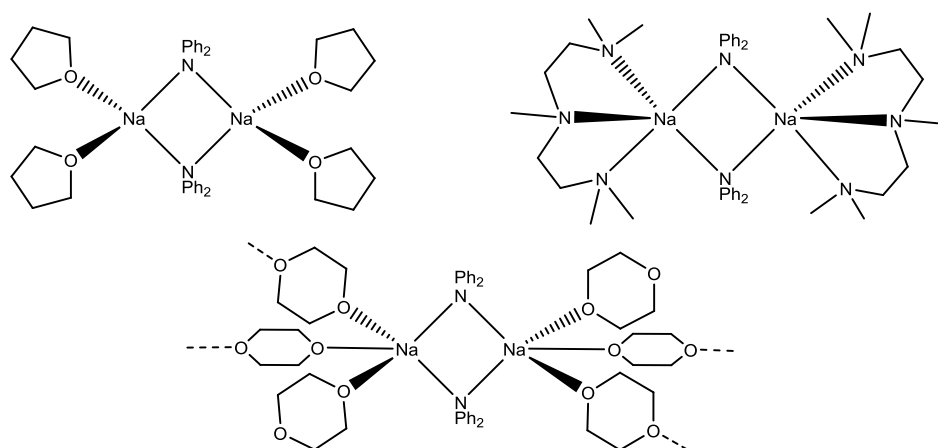


**Figure 2.38** Structural representations of solvated sodium diphenylamide complexes crystallographically characterised subsequent to this work.

Clear structural similarities exist between **91** and the aforementioned solvates. The THF solvate most resembles the sodium coordination environment in **91**. Indeed, the structural parameters are essentially identical within experimental error to those in **91** (mean Na–N bond distance and N–Na–N angle in THF solvate are 2.441 Å and 95.31° respectively).

The crystalline product **91** was dissolved in C<sub>6</sub>D<sub>6</sub> solution and examined by <sup>1</sup>H, <sup>13</sup>C (Figure 2.39 and Figure 2.40 respectively), COSY and HSQC NMR spectroscopy (Table 2.29). The two <sup>1</sup>H and two <sup>13</sup>C resonances associated with the TMEDA ligand in **91** are different from those encountered in the free diamine, indicating that it remains coordinated to the alkali metal in arene solution. Similar to its lithium congener **90**, it appears that only one oligomer of solvated alkali metal amide (presumably the dimeric solid-state species) exists in solution, as only one set of diphenylamido resonances are observed.

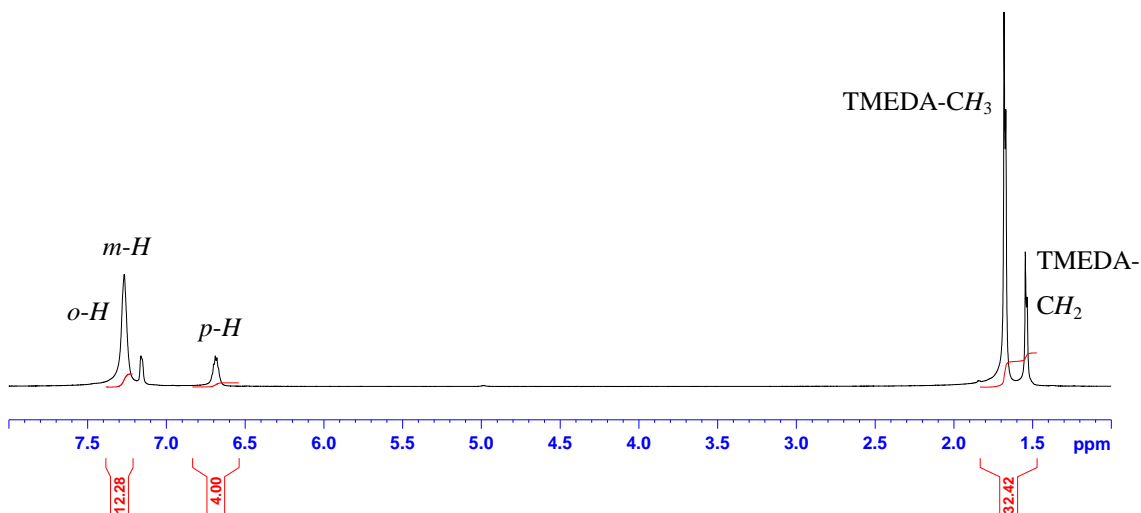


Figure 2.39  $^1\text{H}$  NMR spectrum of  $[(\text{TMEDA})\text{Na}(\text{NPh}_2)]_2$ , **91**, in  $\text{C}_6\text{D}_6$ .

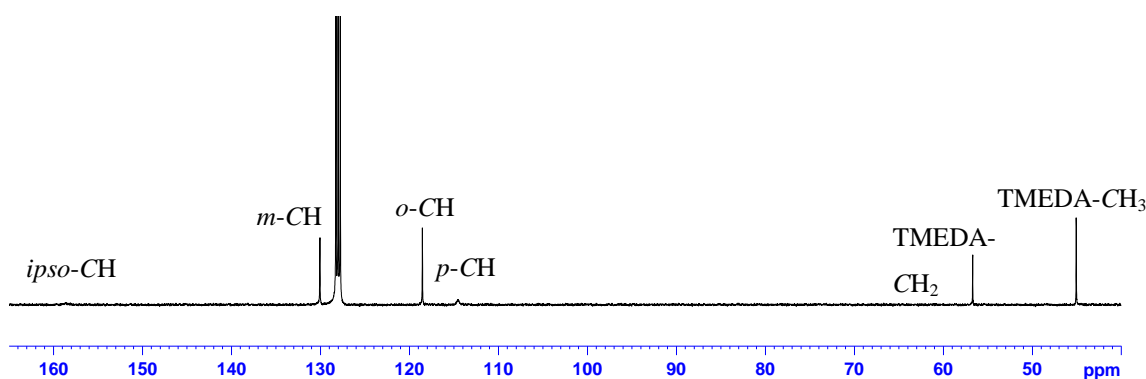


Figure 2.40  $^{13}\text{C}$  NMR spectrum of  $[(\text{TMEDA})\text{Na}(\text{NPh}_2)]_2$ , **91**, in  $\text{C}_6\text{D}_6$ .

NMR chemical shifts of $[(\text{TMEDA})\text{Na}(\text{NPh}_2)]_2$ , <b>91</b> , in $\text{C}_6\text{D}_6$			
$^1\text{H}$ $\delta$ / ppm		$^{13}\text{C}$ $\delta$ / ppm	
–	–	<i>ipso-CH</i>	158.8
<i>o-CH</i>	7.27	<i>o-CH</i>	118.7
<i>m-CH</i>	7.27	<i>m-CH</i>	130.2
<i>p-CH</i>	6.69	<i>p-CH</i>	114.7
TMEDA ( $\text{CH}_3$ )	1.68	TMEDA ( $\text{CH}_3$ )	45.1
TMEDA ( $\text{CH}_2$ )	1.54	TMEDA ( $\text{CH}_2$ )	56.8

Table 2.29  $^1\text{H}$  and  $^{13}\text{C}$  NMR chemical shifts of  $[(\text{TMEDA})\text{Na}(\text{NPh}_2)]_2$ , **91**, in  $\text{C}_6\text{D}_6$ .

### 2.4.3 $[(\text{TMEDA})_{3/2}\text{K}(\text{NPh}_2)]_2$ , **92**

Complex **92** is prepared in a similar way to **90** and **91** except benzylpotassium is utilised as the metallating agent. In addition, excess TMEDA (at least four equivalents) is required to fully solubilise the heavy alkali metal amide (a similar scenario was encountered in the preparation of the TMEDA adduct of KTMP).<sup>[43]</sup> In the solid-state **92** exists as a polymeric array of dinuclear K–N–K–N rings. Akin to **90** and **91**, the K atom is coordinated to a bidentate TMEDA molecule; however, each K is also bound to another TMEDA molecule which acts as a monodentate bridge, thus producing the coordination polymer. Complex **92** is

not soluble in  $C_6D_6$  solution, thus solution studies were performed in  $d_8$ -THF solution and these experiments revealed that **92** readily loses TMEDA during *in vacuo* isolation.

X-ray crystallographic analysis reveals that **92** crystallises in the triclinic system, space group  $P\bar{1}$  and, unlike its lithium and sodium analogues, **92** (Figure 2.41) adopts a linear polymeric arrangement of centrosymmetric dimeric units (Figure 2.42). The coordination of a TMEDA ligand to the metal centre in the usual bidentate fashion and a second TMEDA ligand bridging in a monodentate manner produces the coordination polymer (both metal centres are five coordinate). Table 2.30 and Table 2.31 detail the key bond distances and bond angles respectively.

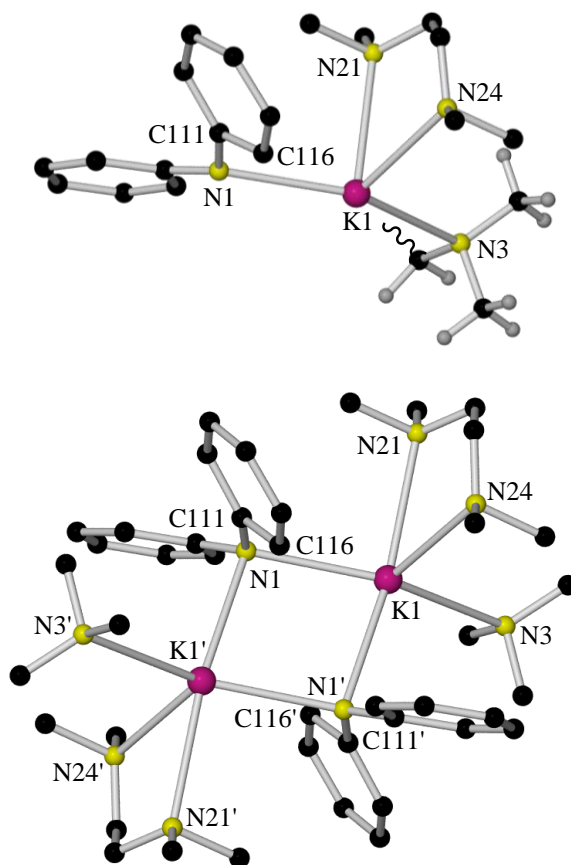


**Figure 2.41** Molecular structure of  $[(TMEDA)_{3/2}K(NPh_2)]_2$ , **92**, showing the asymmetric unit (top) and the dinuclear ring (bottom). H atoms for the  $NPh_2$  ligands (both figures) and the TMEDA ligands (bottom figure) are omitted for clarity.

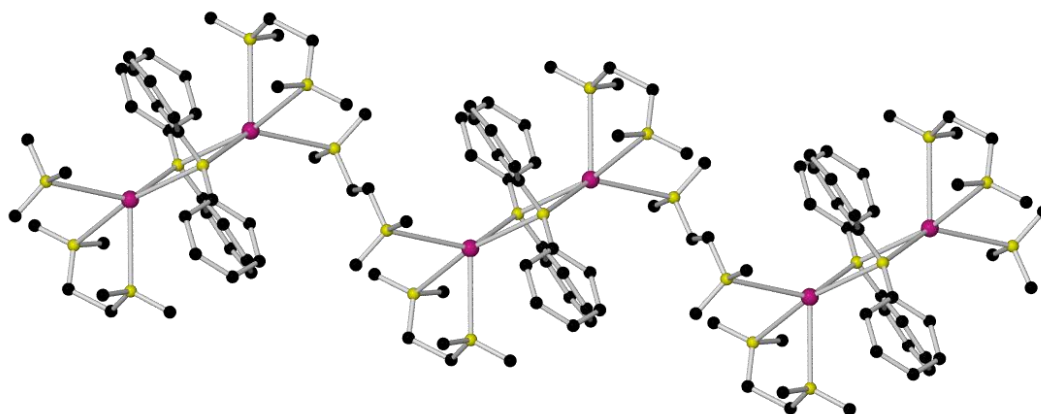


**Figure 2.42** Extended view of  $[(\text{TMEDA})_{3/2}\text{K}(\text{NPh}_2)]_2$ , **92**. H atoms are omitted for clarity.

Selected Bond	Bond Distance (Å) in $[(\text{TMEDA})_{3/2}\text{K}(\text{NPh}_2)]_2$ , <b>92</b>
K1–N1	2.810(1)
K1–N1'	2.922(1)
K1–N3	3.296(1)
K1–N21	2.947(5)
K1–N24	2.857(6)

**Table 2.30** Key bond distances within  $[(\text{TMEDA})_{3/2}\text{K}(\text{NPh}_2)]_2$ , **92**.

Selected Angle	Bond Angle (°) in $[(\text{TMEDA})_{3/2}\text{K}(\text{NPh}_2)]_2$ , <b>92</b>
N1–K1–N1'	80.55(3)
N1–K1–N3	142.93(3)
N1–K1–N21	91.32(10)
N1–K1–N24	114.04(9)
N1'–K1–N3	104.64(3)
N1'–K1–N21	165.81(10)
N1'–K1–N24	110.04(11)
N3–K1–N21	88.87(10)
N3–K1–N24	98.83(10)
N21–K1–N24	62.68(15)
K1–N1–K'	99.45(3)

**Table 2.31** Key bond angles within  $[(\text{TMEDA})_{3/2}\text{K}(\text{NPh}_2)]_2$ , **92**.

Although **92** adopts a linear polymeric arrangement, its centrosymmetric unit bears a close resemblance to those of **90** and **91**. It consists of a planar  $(\text{KN})_2$  ring (sum of endocyclic angles,  $360^\circ$ ); however, due to the larger size of potassium, its coordination sphere can accommodate an additional donor atom (hence each K atom is five-coordinate). Supplementary stabilisation by  $\text{K}\cdots\pi$ -arene interactions appears minimal [shortest  $\text{K}\cdots\text{C}$  separations are 3.194(1) and 3.241(1) Å for K1–C116' and K1–C111' respectively]. One TMEDA ligand binds to the metal centre in the usual bidentate fashion, whereas the second TMEDA molecule binds in a monodentate manner (K1–N3). The K–N bond distance in the

latter [3.296(1) Å] is considerably longer (and by implication weaker) than that of the bidentate-coordinated ligand (mean distance, 2.902 Å). From a supramolecular perspective, a coordination polymer is constructed whereby the remaining TMEDA N atom intermolecularly binds to another K atom (Figure 2.42). The K ions are in a distorted trigonal bipyramidal environment (Figure 2.41 and Scheme 2.6), where the anionic N and a N atom from the bidentate-coordinated TMEDA occupy the pseudo-axial positions [N1'–K1–N21, 165.81(10)°]. To the best of our knowledge, complex **92** represents the first example of a homometallic potassium complex in which a TMEDA ligand binds to the metal centre in a monodentate fashion.

Prior to this work, only three other donor complexes of potassium diphenylamide have been crystallographically characterised, namely the solvent-separated 18-crown-6,<sup>[233]</sup> dimeric THF<sup>[230d]</sup> and polymeric dioxane<sup>[230c]</sup> solvates (Figure 2.43). Clear structural similarities exist between **92** and the aforementioned THF and dioxane adducts. In each case, the K centres are five coordinate (the metals' coordination spheres being composed of two anionic N and three neutral donor centres). Despite the change from O- to N-based ligands, the K–N<sub>amide</sub> bond distance remains similar (mean distance; 2.826, 2.846 and 2.866 Å for the THF adduct, dioxane adduct and **92** respectively).

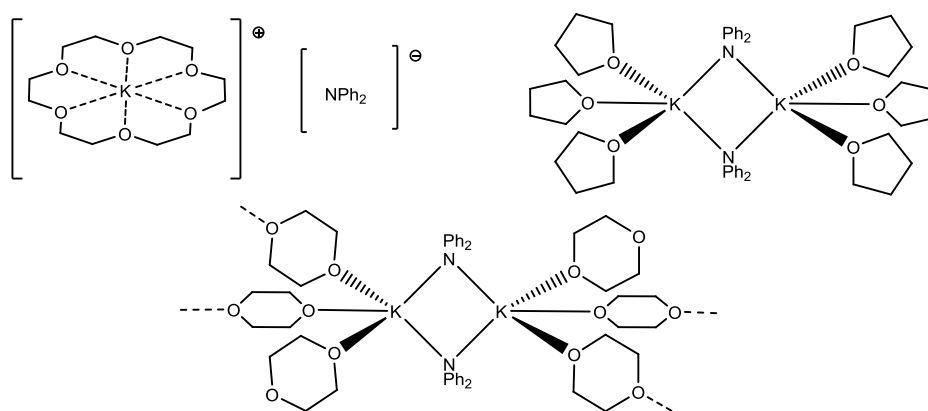


**Figure 2.43** Structural representations of solvated potassium diphenylamide complexes crystallographically characterised prior to this work.

Whilst writing this thesis, Westerhausen reported the solid-state structure of a dimeric PMDETA solvate of potassium diphenylamide, which adopts the same structural motif as that of its sodium congener (Figure 2.38).<sup>[232]</sup> Similar to **92**, its central (KN)<sub>2</sub> ring is planar (sum of endocyclic angles, 360°), with near equal K–N<sub>amide</sub> bond distances [2.821(2) and 2.837(3) Å for the PMDETA solvate and 2.810(1) and 2.922(1) Å for **92**]. Each of the K centres are completed by binding to a PMDETA ligand (due to the tridentate nature of the PMDETA ligand, each K metal centre is five coordinate, but polymerisation cannot occur as in **92**),



resulting in the metal centres adopting a geometry best described as a distorted trigonal bipyramid.

Our group recently published a rare example of a tris(amido) potassium magnesiate containing diphenylamide, namely  $[(\text{PMDETA})\cdot\text{K}(\mu\text{-NPh}_2)\text{Mg}(\text{THF})(\text{NPh}_2)_2]$ ,<sup>[234]</sup> **93** (Figure 2.44). This complex is unusual in that the coordination spheres of the metals differ significantly from that of the previously characterised potassium magnesiates (Figure 2.45),<sup>[181, 193h, 235]</sup> presumably due to the less sterically demanding nature and planar rotational flexibility of diphenylamide compared to the other well-studied amido ligands (DA and THF).

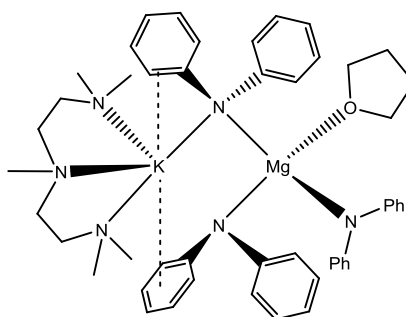


**Figure 2.44** Structural representation of  $[(\text{PMDETA})\cdot\text{K}(\mu\text{-NPh}_2)\text{Mg}(\text{THF})(\text{NPh}_2)_2]$ , **93**.

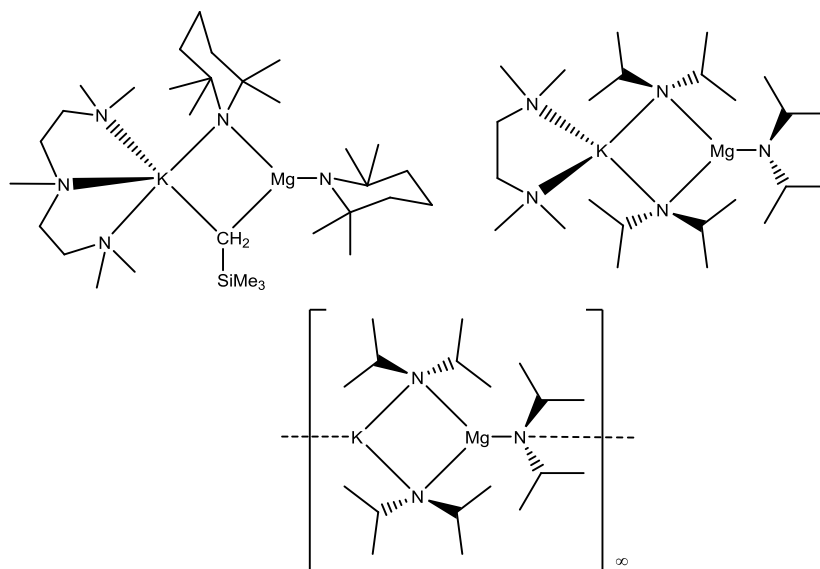


**Figure 2.45** Previously structurally characterised potassium amido-magnesiate complexes.

Here the Mg centre is in a four coordinate distorted tetrahedral geometry, binding to three diphenylamide ligands and one THF molecule. The Mg centres in other crystallographically characterised potassium amido magnesiates adopt trigonal planar geometries. Turning to the K centre, its coordination sphere is rather more complex due to a series of metal-arene  $\pi$ -interactions with the phenyl groups of the diphenylamide ligands (a scenario not encountered in previously crystallographically characterised potassium amido magnesiates). It is bound to three N atoms from the tridentate PMDETA ligand, one diphenylamide ligand, and its

coordination sphere is completed by a series of aryl- $\pi$  contacts (reflecting the soft nature of K).

On comparing **92** and **93**, there are no metal-arene  $\pi$ -interactions present in **92** presumably due to the symmetric nature of the molecule (in **93** the dative K–N interactions are 0.1–0.2 Å shorter than the K–N<sub>amide</sub> interactions, as if the alkali metal is pushing towards a solvent-separated ion pair composition), and the K metal centres' coordination spheres being sufficiently stabilised by coordinating to two anionic N atoms and three neutral donor centres. The K–N<sub>amide</sub> interaction in **93** is 0.2 Å longer than the mean K–N<sub>amide</sub> interaction in **92** (2.866 Å), in accordance with the molecule tending towards becoming a solvent-separated ion pair. Indeed, NMR spectroscopic studies conducted in arene solution were indicative of the presence of a solvent-separated species. The K–N<sub>donor</sub> bond distances are slightly shorter in **93** [range of distances, 2.830(3)–3.244(1) Å, *cf.*, 2.857(6)–3.296(1) Å for **92**; mean distance, 2.981 Å, *cf.*, 3.033 Å for **92**], again suggesting the ions desire to become solvent-separated.

Crystalline product **92** was insoluble in C<sub>6</sub>D<sub>6</sub> solution; hence, **92** was dissolved in d<sub>8</sub>-THF solution and examined by <sup>1</sup>H, <sup>13</sup>C (Figures 2.46–2.48), COSY and HSQC NMR spectroscopy (Table 2.32).

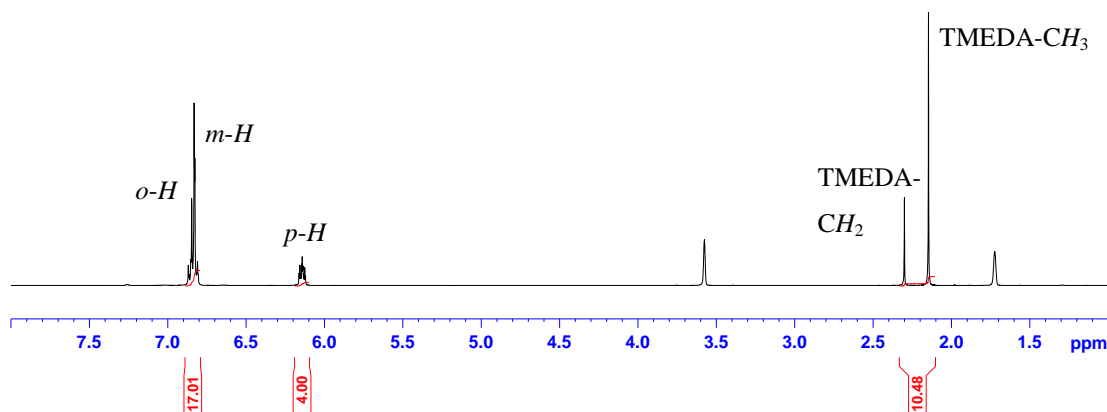


Figure 2.46 <sup>1</sup>H NMR spectrum of [(TMEDA)<sub>3/2</sub>K(NPh<sub>2</sub>)<sub>2</sub>], **92**, isolated in *vacuo* in d<sub>8</sub>-THF.

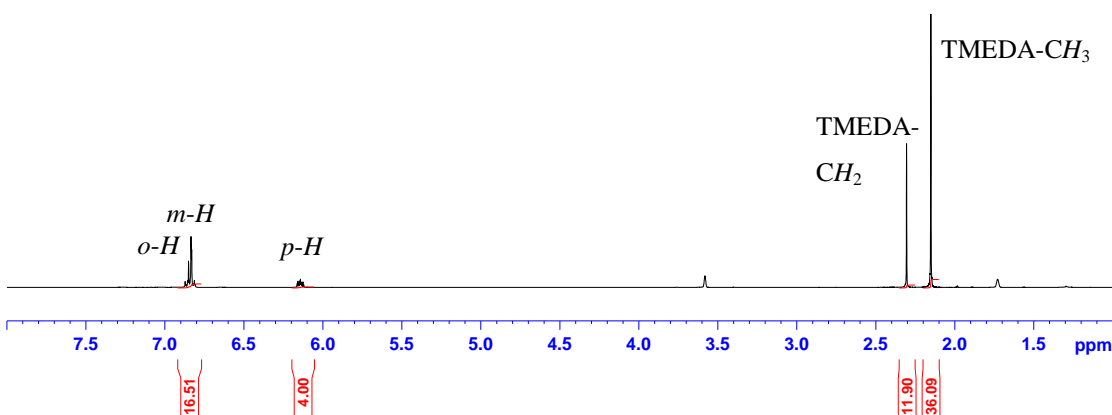
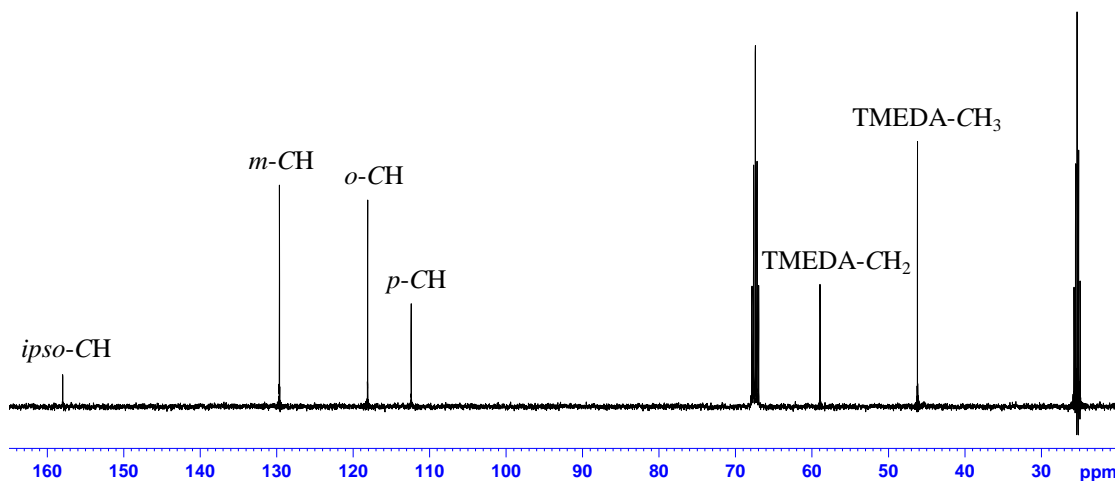


Figure 2.47 <sup>1</sup>H NMR spectrum of [(TMEDA)<sub>3/2</sub>K(NPh<sub>2</sub>)<sub>2</sub>], **92**, isolated without utilising vacuum techniques in d<sub>8</sub>-THF.



**Figure 2.48**  $^{13}\text{C}$  NMR spectrum of  $[(\text{TMEDA})_{3/2}\text{K}(\text{NPh}_2)]_2$ , **92**, isolated without utilising vacuum techniques in  $\text{d}_8$ -THF.

As alluded to earlier, isolation of **92** *in vacuo* resulted in loss of crystallinity of the sample. From the  $^1\text{H}$  NMR spectrum (Figure 2.46) of this powder, it can be seen that the amide : TMEDA ratio is approximately 2 : 0.66 (based on the solid-state molecular structure it should be 2 : 3). This data suggests that on isolation a significant quantity of TMEDA is removed, reflecting the weakness of its binding to the relatively soft potassium centre.

When **92** was isolated without utilising vacuum techniques the integration values of the  $^1\text{H}$  NMR spectrum (Figure 2.47) correspond well with the expected values from the solid-state structure. In both scenarios, the chemical shifts of the resonances associated with the  $\text{NPh}_2$  ligand were identical and the TMEDA resonances corresponded to the free TMEDA ligand; hence, suggesting the formation of a  $\text{d}_8$ -THF solvate.

NMR chemical shifts of $[(\text{TMEDA})_{3/2}\text{K}(\text{NPh}_2)]_2$ , <b>92</b> , in $\text{d}_8$ -THF			
$^1\text{H}$ $\delta$ / ppm		$^{13}\text{C}$ $\delta$ / ppm	
–	–	<i>ipso-CH</i>	158.1
<i>o-CH</i>	6.84	<i>o-CH</i>	118.2
<i>m-CH</i>	6.84	<i>m-CH</i>	129.7
<i>p-CH</i>	6.14	<i>p-CH</i>	112.6
TMEDA ( $\text{CH}_3$ )	2.15	TMEDA ( $\text{CH}_3$ )	46.3
TMEDA ( $\text{CH}_2$ )	2.30	TMEDA ( $\text{CH}_2$ )	59.3

**Table 2.32**  $^1\text{H}$  and  $^{13}\text{C}$  NMR chemical shifts of  $[(\text{TMEDA})_{3/2}\text{K}(\text{NPh}_2)]_2$ , **92**, in  $\text{d}_8$ -THF.

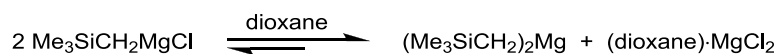
As well as focusing on the alkali metal building blocks of the heterobimetallic reagents, it was also deemed important to study the monometallic magnesium reagents. In the next section heteroleptic magnesium complexes containing TMP will be discussed.

## 2.5 Alkylmagnesium TMP Complexes

This section of work will focus on the magnesium monometallic building blocks [namely homoleptic magnesium bis(amide) and dialkylmagnesium, and heteroleptic alkylmagnesium amide complexes] which are key to the synthesis of heterobimetallic ate species.

Many of our group's studies over the past decade have relied upon  $\text{Mg}(\text{TMP})_2$  which is generally prepared by treating commercially available  ${}^n\text{Bu}_2\text{Mg}$ /heptane solution with two molar equivalents of  $\text{TMP}(\text{H})$  in hexane solution. To ensure complete bis(amination) of the dialkylmagnesium, the mixture is heated to reflux for at least 12 hours. Recently, the process used to prepare commercial  ${}^n\text{Bu}_2\text{Mg}$  has been altered, and the composition of the new solutions consist of approximately a 9 : 1 ratio of  ${}^n\text{Bu}_2\text{Mg} : \text{Et}_3\text{Al}$  in heptane (the aluminium additive is required to aid solubilisation of the magnesium reagent in the hydrocarbon medium). This additive was unexpectedly found to take part in and alter the course of reactions.<sup>[184]</sup>

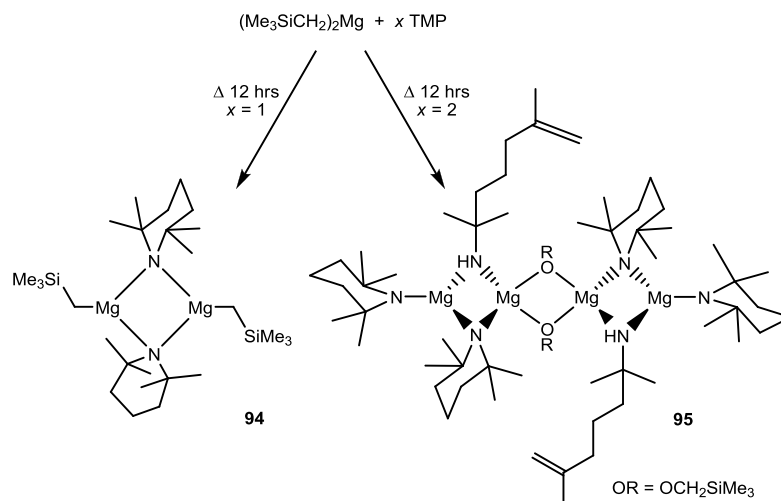
To overcome this complication, the group have introduced another magnesium reagent into their synthetic repertoire, namely  $(\text{Me}_3\text{SiCH}_2)_2\text{Mg}$ .<sup>[193p, 203b, 235-236]</sup> Prepared from the Grignard reagent  $(\text{Me}_3\text{SiCH}_2)\text{MgCl}$  by manipulation of the dioxane-driven Schlenk equilibrium (Scheme 2.7), the resultant off-white solid can be isolated and purified by sublimation in good yields. Shifting from  ${}^n\text{Bu}_2\text{Mg}$  to  $(\text{Me}_3\text{SiCH}_2)_2\text{Mg}$  can have a dramatic influence on the regioselectivity of specific reactions. For example, when toluene is reacted with “ $\text{NaMg}(\text{TMP})_2{}^n\text{Bu}$ ” a regioselective 2,5-dimetallation (dimagnesiumation) of toluene occurs;<sup>[105]</sup> however, when “ $\text{NaMg}(\text{TMP})_2\text{CH}_2\text{SiMe}_3$ ” is employed, regioselective dimagnesiumation also takes place, but this time at the 3- and 5-positions.<sup>[236a]</sup> In both cases, the dimagnesiumated toluene is manifested in inverse crown complexes.



**Scheme 2.7** Synthesis of the bis(alkyl)magnesium reagent  $(\text{Me}_3\text{SiCH}_2)_2\text{Mg}$ .

Using  $(\text{Me}_3\text{SiCH}_2)_2\text{Mg}$  to prepare new TMP complexes of magnesium, we attempted to prepare some fundamental monometallic building blocks which are crucial in building up a greater understanding of the role neutral magnesium reagents play in magnesiate systems,<sup>[84-85]</sup> and also in the chemistry of macrocyclic inverse crown complexes.<sup>[98]</sup>

Two novel monometallic complexes were prepared and characterised by treating one molar equivalent of  $(\text{Me}_3\text{SiCH}_2)_2\text{Mg}$  with one and two molar equivalents of  $\text{TMP}(\text{H})$  respectively in hydrocarbon solution (Scheme 2.8).



**Scheme 2.8** Synthesis of complexes **94** and **95**. Note the different conformations of the TMP ligands in complex **94** – one TMP ligand is in a chair conformation (top TMP ligand in complex **94**), whilst the other is in a boat conformation (bottom TMP ligand in complex **94**).

The complex formed on utilising one molar equivalent of TMP(H) in the reaction was that of the dimeric alkylmagnesium amide  $[(\text{Me}_3\text{SiCH}_2)\text{Mg}(\mu\text{-TMP})]_2$ , **94**. On utilising two molar equivalents of TMP(H) in order to try and prepare the parent bis(amide)  $\text{Mg}(\text{TMP})_2$  (the solid-state structure of which has remained elusive despite its wide use in synthesis), X-ray crystallographic analysis revealed that the crystalline material deposited was not representative of the simple formulation  $\text{Mg}(\text{TMP})_2$ ; but was the tetranuclear triheteroanionic amide-alkoxide-amidoalkene  $[(\text{TMP})\text{Mg}(\mu\text{-TMP})\{\mu\text{-N}(\text{H})\text{C}(\text{Me})_2(\text{CH}_2)_3\text{C}(\text{Me})=\text{CH}_2\}\text{Mg}(\mu\text{-OCH}_2\text{SiMe}_3)]_2$ , **95**.

### 2.5.1 $[(\text{Me}_3\text{SiCH}_2)\text{Mg}(\mu\text{-TMP})]_2$ , **94**

Complex **94** was prepared by treating one molar equivalent of  $(\text{Me}_3\text{SiCH}_2)_2\text{Mg}$  with an equimolar quantity of TMP(H) in a hexane solution and heating this solution to reflux for 16 hours (Scheme 2.8). X-ray quality crystals of **94** precipitated from the hydrocarbon medium at  $-28^\circ\text{C}$ .

X-ray crystallographic analysis reveals that **94** (Figure 2.49) crystallises as a dimer in the monoclinic system, space group  $P2_1/c$ , and is composed of two magnesium centres each coordinated to a  $\text{CH}_2\text{SiMe}_3$  group, with two TMP ligands bridging the two metal centres, rendering both metal centres three coordinate. Within the asymmetric unit of **94** there are two independent molecules of  $[(\text{Me}_3\text{SiCH}_2)\text{Mg}(\mu\text{-TMP})]_2$ ; however, the differences in the dimensions of these molecules are negligible, and thus Table 2.33 and Table 2.34 detail the key bond distances and bond angles respectively of only one of the independent molecules.

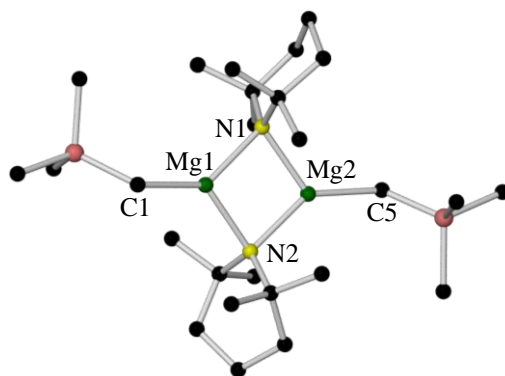


**Figure 2.49** Molecular structure of  $[(\text{Me}_3\text{SiCH}_2)\text{Mg}(\mu\text{-TMP})]_2$ , **94**. H atoms omitted and only one of two similar molecules in the asymmetric unit shown for clarity.

Selected Bond	Bond Distance (Å) in $[(\text{Me}_3\text{SiCH}_2)\text{Mg}(\mu\text{-TMP})]_2$ , <b>94</b>
Mg1–N1	2.144(2)
Mg1–N2	2.129(2)
Mg1–C1	2.108(3)
Mg2–N1	2.121(2)
Mg2–N2	2.125(2)
Mg1–C5	2.113(3)

**Table 2.33** Key bond distances within  $[(\text{Me}_3\text{SiCH}_2)\text{Mg}(\mu\text{-TMP})]_2$ , **94**.

Selected Angle	Bond Angle (°) in $[(\text{Me}_3\text{SiCH}_2)\text{Mg}(\mu\text{-TMP})]_2$ , <b>94</b>
N1–Mg1–N2	95.36(8)
N1–Mg1–C1	135.57(10)
N2–Mg1–C1	127.82(10)
N1–Mg2–N2	96.13(8)
N1–Mg2–C5	124.37(11)
N2–Mg2–C5	138.85(11)
Mg1–N1–Mg2	84.00(8)
Mg1–N2–Mg2	84.27(8)

**Table 2.34** Key bond angles within  $[(\text{Me}_3\text{SiCH}_2)\text{Mg}(\mu\text{-TMP})]_2$ , **94**.

While four-membered dimeric rings are common in *s*-block amide chemistry,<sup>[9c, 237]</sup> that of **94** is interesting for displaying two distinctly different TMP bridging conformations,<sup>[238]</sup> which renders the structure non-centrosymmetric. One ligand prefers the common chair conformation (N1 ligand in Figure 2.49), which is adopted in the vast majority of *s*-block homo- and heterometallic complexes;<sup>[102d, 105-106, 185]</sup> while the second TMP ligand adopts a rarer, less thermodynamically preferred twisted boat conformation<sup>[186]</sup> (N2 ligand in Figure 2.49). This is perhaps indicative of the steric strain which this latter ligand is under in **94**'s sterically congested architecture as this conformation has only previously been observed in other systems which encompass ligands of high steric demand [*e.g.*, in  $[\text{tBuMg}(\text{TMP})]_2$  both TMP ligands adopt boat forms].<sup>[186]</sup> The two crystallographically distinct Mg centres in **94**

adopt severely distorted trigonal planar environments [range of angles around Mg, 95.36(8)-138.85(11)°], where the narrowest angles belong to the Mg–N due to the constraints of forming the central four-membered (MgN)<sub>2</sub> ring. There is little discrimination between the four Mg–N bond distances [2.121(2)-2.144(2) Å] and between the two Mg–C bond distances in **94** [2.108(3) and 2.113(3) Å respectively].

The crystalline product **94** was dissolved in C<sub>6</sub>D<sub>6</sub> solution and examined by <sup>1</sup>H, <sup>13</sup>C (Figure 2.50 and Figure 2.51 respectively), COSY and HSQC NMR spectroscopy (Table 2.35). Only one set of TMP resonances is observed despite there being two chemically distinct TMP ligands in its solid-state structure. This is not too surprising as Collum has shown that the TMP anion is ‘conformationally mobile’ in solution.<sup>[56a]</sup> The three <sup>1</sup>H and four <sup>13</sup>C resonances associated with the TMP ligand in **94** are different from those encountered in the free amine, indicating that the ligands remain coordinated to the magnesium centres in arene solution.

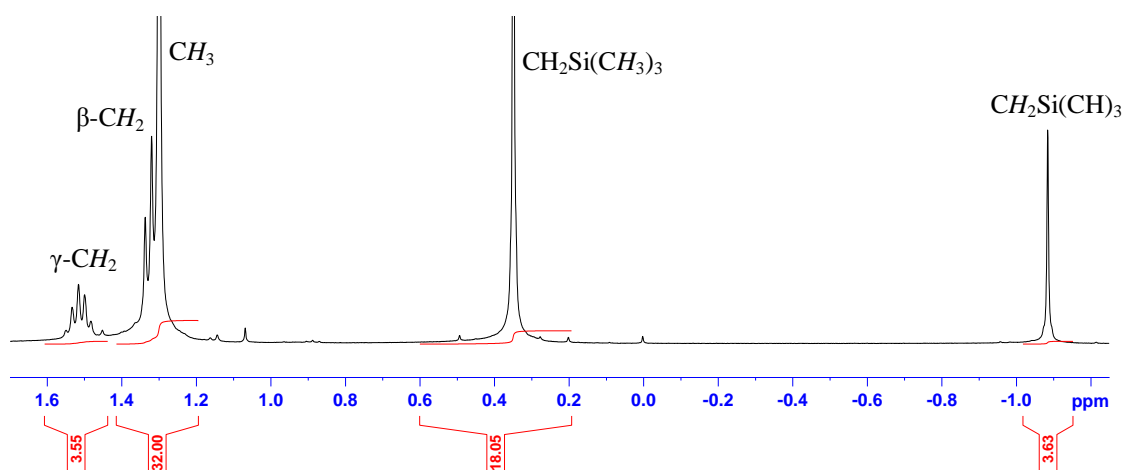


Figure 2.50 <sup>1</sup>H NMR spectrum of [(Me<sub>3</sub>SiCH<sub>2</sub>)Mg( $\mu$ -TMP)]<sub>2</sub>, **94**, in C<sub>6</sub>D<sub>6</sub>.

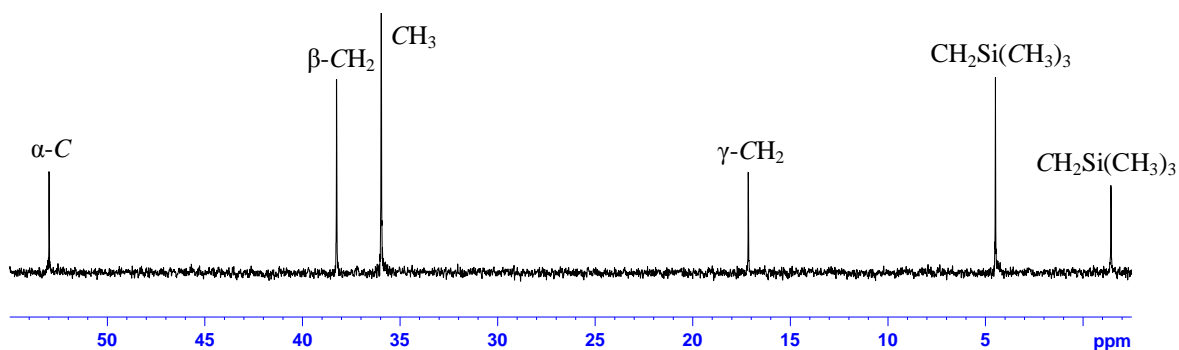
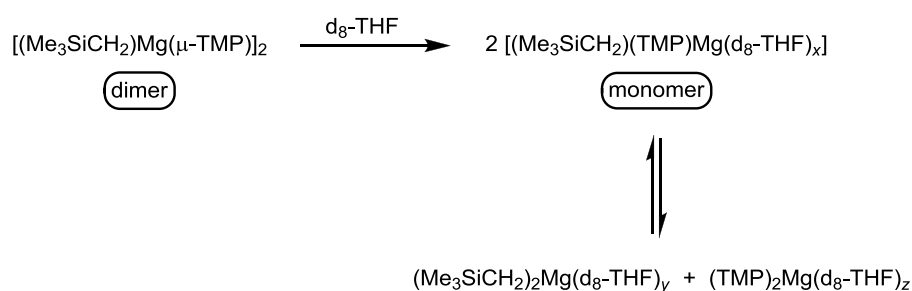


Figure 2.51 <sup>13</sup>C NMR spectrum of [(Me<sub>3</sub>SiCH<sub>2</sub>)Mg( $\mu$ -TMP)]<sub>2</sub>, **94**, in C<sub>6</sub>D<sub>6</sub>.

NMR chemical shifts of $[(\text{Me}_3\text{SiCH}_2)\text{Mg}(\mu\text{-TMP})]_2$ , <b>94</b> , in $\text{C}_6\text{D}_6$			
$^1\text{H}$ $\delta$ / ppm		$^{13}\text{C}$ $\delta$ / ppm	
–	–	$\alpha\text{-C}$	53.0
$\gamma\text{-CH}_2$	1.52	$\gamma\text{-CH}_2$	17.2
$\beta\text{-CH}_2$	1.33	$\beta\text{-CH}_2$	38.3
$\text{CH}_3$	1.30	$\text{CH}_3$	36.0
$\text{CH}_2\text{Si}(\text{CH}_3)_3$	0.35	$\text{CH}_2\text{Si}(\text{CH}_3)_3$	4.5
$\text{CH}_2\text{Si}(\text{CH}_3)_3$	-1.09	$\text{CH}_2\text{Si}(\text{CH}_3)_3$	-1.4

**Table 2.35**  $^1\text{H}$  and  $^{13}\text{C}$  NMR chemical shifts of  $[(\text{Me}_3\text{SiCH}_2)\text{Mg}(\mu\text{-TMP})]_2$ , **94**, in  $\text{C}_6\text{D}_6$ .

Examining a  $d_8$ -THF solution of **94** by  $^1\text{H}$ ,  $^{13}\text{C}$ , COSY and HSQC NMR spectroscopy revealed the solution behaviour of **94** to be rather more complex in this instance. The logical scenario when a donor solvent is utilised is that dimeric **94** is broken down to donor-solvated monomers. This was indeed observed and corroborated by DOSY NMR studies,<sup>[44]</sup> which give a predicted molecular weight ( $\text{MW}_{\text{DOSY}}$ ) of  $335 \text{ g mol}^{-1}$  which is intermediate between the expected values of an unsolvated ( $252 \text{ g mol}^{-1}$ ) and bis-THF solvated monomer ( $396 \text{ g mol}^{-1}$ ), perhaps suggesting the formation of a mono-THF monomer ( $324 \text{ g mol}^{-1}$ ). The predicted  $\text{MW}_{\text{DOSY}}$  is far removed from the dimeric species characterised in the solid-state ( $504 \text{ g mol}^{-1}$ ). In addition, a Schlenk-type equilibrium (Scheme 2.9) must also be operative as significant (equimolar) quantities of  $\text{Mg}(\text{CH}_2\text{SiMe}_3)_2$  and  $\text{Mg}(\text{TMP})_2$  were also observed (Figures 2.53 and 2.54). The ratio of these homoleptic products to ‘monomeric-**94**’ can be altered depending on the concentration of the  $d_8$ -THF solution (NMR data not detailed here can be found in chapter 5, section 5.3.14).



**Scheme 2.9** Monomerisation of **94** in  $d_8$ -THF and subsequent Schlenk equilibrium to produce homoanionic magnesium reagents.



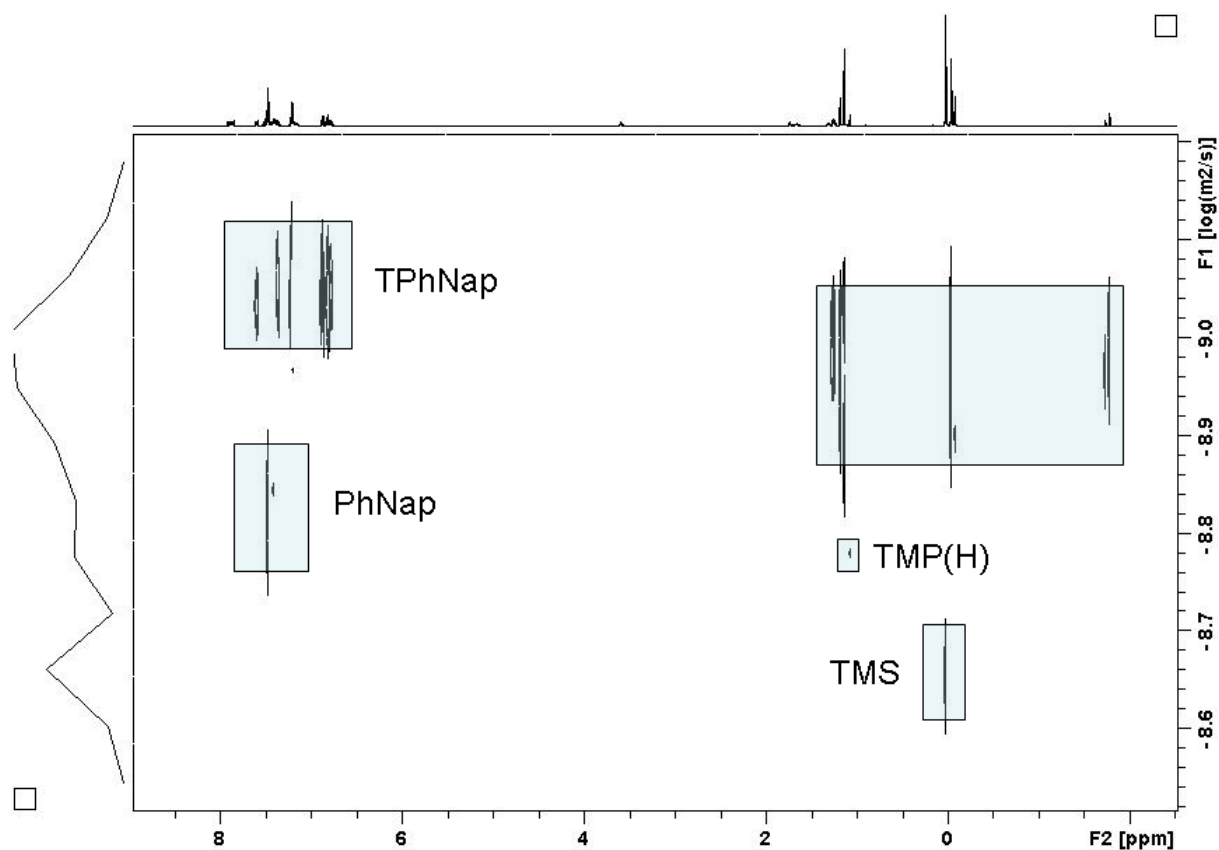


**Figure 2.52**  $^1\text{H}$  DOSY NMR spectrum of  $(\text{Me}_3\text{SiCH}_2)\text{Mg}(\text{TMP})$  in  $d_8$ -THF in the presence of the inert standards tetraphenylnaphthalene (TPhNap), phenylnaphthalene (PhNap) and tetramethylsilane (TMS).

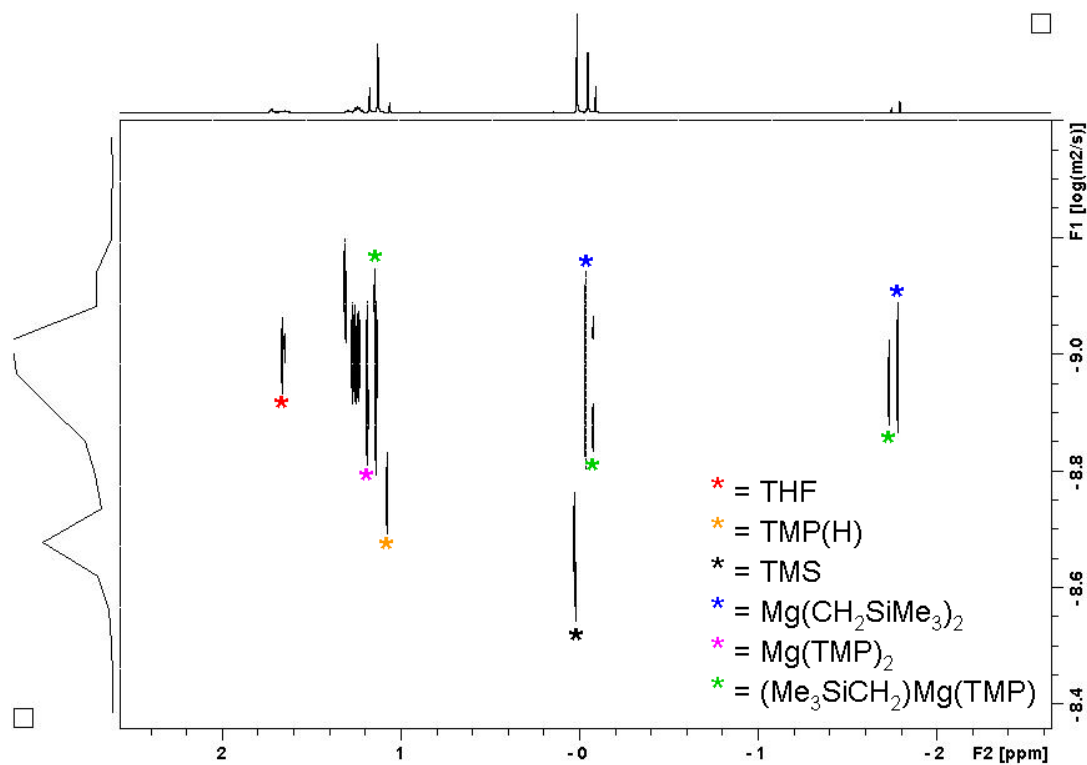


**Figure 2.53** Enlargement of  $^1\text{H}$  DOSY NMR spectrum of  $(\text{Me}_3\text{SiCH}_2)\text{Mg}(\text{TMP})$  in  $d_8$ -THF in the presence of the inert standards tetraphenylnaphthalene (TPhNap), phenylnaphthalene (PhNap) and tetramethylsilane (TMS), indicating the species present within solution.

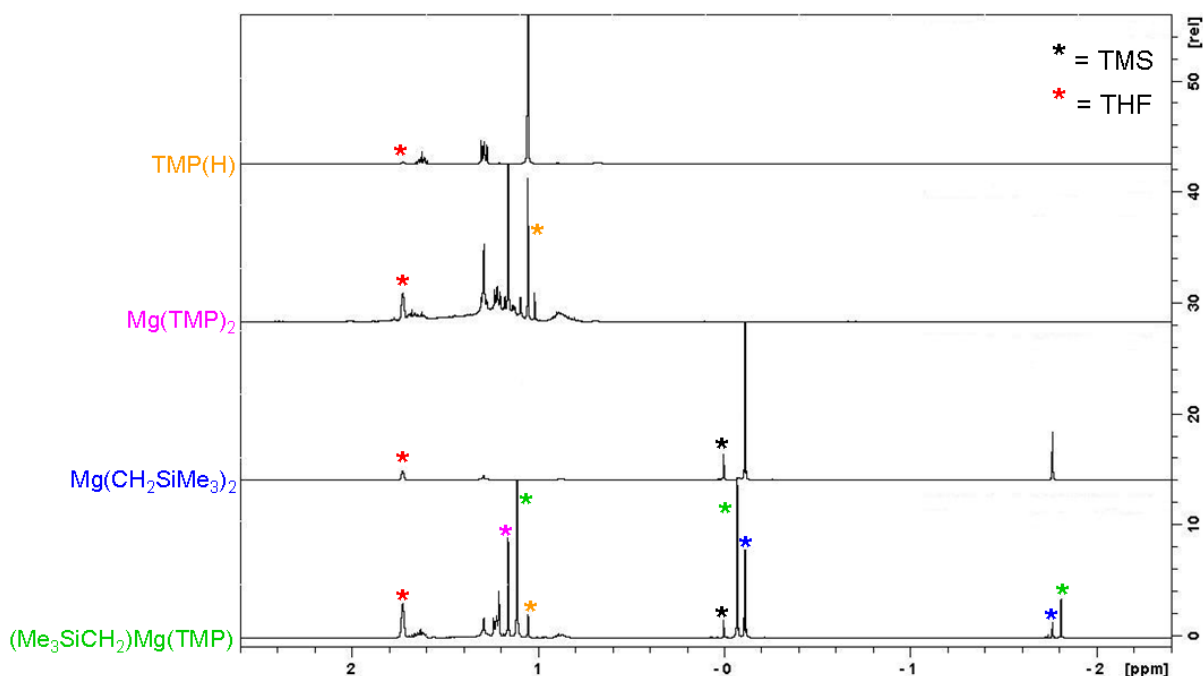


**Figure 2.54** Enlargement of the aliphatic region of  $^1\text{H}$  NMR spectra of TMP(H),  $\text{Mg}(\text{TMP})_2$ ,  $\text{Mg}(\text{CH}_2\text{SiMe}_3)_2$  and complex **94** in  $d_8$ -THF.

### 2.5.2 $[(\text{TMP})\text{Mg}(\mu\text{-TMP})\{\mu\text{-N}(\text{H})\text{C}(\text{Me})_2(\text{CH}_2)_3\text{C}(\text{Me})=\text{CH}_2\}\text{Mg}(\mu\text{-OCH}_2\text{SiMe}_3)]_2$ , **95**

Following the same reaction methodology as that used to prepare **94**, but using two equivalents of TMP(H), afforded X-ray quality crystals of **95** after approximately two weeks at  $-28^\circ\text{C}$  (Scheme 2.8).

X-ray crystallographic analysis reveals that **95** crystallises as a centrosymmetric tetranuclear dimer in the monoclinic system, space group  $P2_1/n$ . The structure of **95** (Figure 2.55) is composed of four magnesium metal centres, four TMP ligands, two alkoxide ligands and two amidoalkene ligands which form an inorganic  $[\text{Mg}(\mu\text{-N})\{\mu\text{-N}(\text{H})\}\text{Mg}(\mu\text{-O})_2\text{Mg}(\mu\text{-N})\{\mu\text{-N}(\text{H})\}\text{Mg}]$  chain terminated by two of the TMP ligands (where the outer magnesium metal centres are three coordinate and the inner magnesium metal centres four coordinate). Table 2.36 and Table 2.37 detail the key bond distances and bond angles respectively.

Two of the three anions present within this tetranuclear monometallic complex are unusual and unexpected: the alkoxide, produced *via* oxygen insertion into a Mg–C bond; and the primary amidoalkene, produced *via* ring-opening of a TMP anion. Thus, complex **95** is best described as a tetranuclear monometallic triheteroanionic amide-alkoxide-amidoalkene complex.

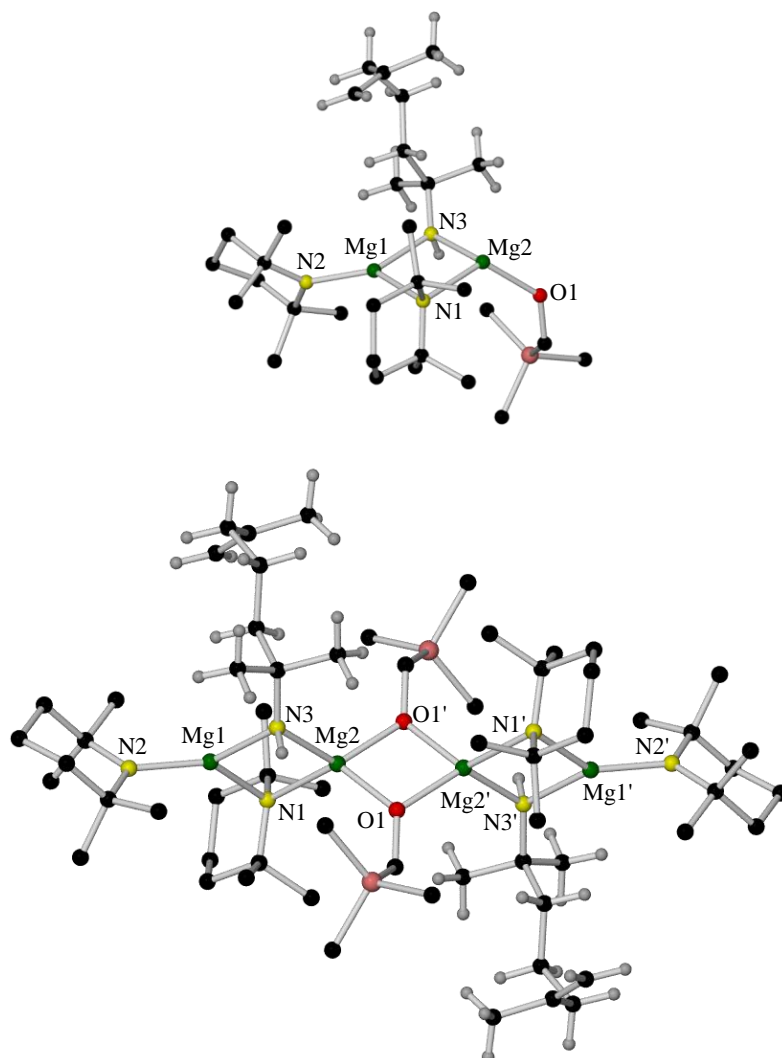


**Figure 2.55** Molecular structure of  $[(\text{TMP})\text{Mg}(\mu\text{-TMP})\{\mu\text{-N}(\text{H})\text{C}(\text{Me})_2(\text{CH}_2)_3\text{C}(\text{Me})=\text{CH}_2\}\text{Mg}(\mu\text{-OCH}_2\text{SiMe}_3)_2]$ , **95**, showing the asymmetric unit (top) and the dimeric tetranuclear chain (bottom). H atoms for the TMEDA-, TMP- and alkoxide ligands (both figures) are omitted for clarity.

Selected Bond	Bond Distance (Å) in $[(\text{TMP})\text{Mg}(\mu\text{-TMP})\{\mu\text{-N}(\text{H})\text{C}(\text{Me})_2(\text{CH}_2)_3\text{C}(\text{Me})=\text{CH}_2\}\text{Mg}(\mu\text{-OCH}_2\text{SiMe}_3)_2]$ , <b>95</b>
Mg1–N1	2.150(2)
Mg1–N2	1.980(2)
Mg1–N3	2.066(2)
Mg2–N1	2.197(2)
Mg2–N3	2.102(2)
Mg2–O1	1.998(1)
Mg2–O1'	1.991(2)

**Table 2.36** Key bond distances within  $[(\text{TMP})\text{Mg}(\mu\text{-TMP})\{\mu\text{-N}(\text{H})\text{C}(\text{Me})_2(\text{CH}_2)_3\text{C}(\text{Me})=\text{CH}_2\}\text{Mg}(\mu\text{-OCH}_2\text{SiMe}_3)_2]$ , **95**.

Selected Angle	Bond Angle (°) in [(TMP)Mg( $\mu$ -TMP){ $\mu$ - N(H)C(Me) <sub>2</sub> (CH <sub>2</sub> ) <sub>3</sub> C(Me)=CH <sub>2</sub> }Mg( $\mu$ -OCH <sub>2</sub> SiMe <sub>3</sub> ) <sub>2</sub> ], <b>95</b>
N1–Mg1–N2	137.56(7)
N1–Mg1–N3	91.41(7)
N2–Mg1–N3	129.45(8)
N1–Mg2–N3	89.16(7)
N1–Mg2–O1	126.04(7)
N1–Mg2–O1'	124.07(7)
N3–Mg2–O1	123.57(7)
N3–Mg2–O1'	114.08(7)
O1–Mg2–O1'	83.49(6)
Mg1–N1–Mg2	87.30(6)
Mg1–N3–Mg2	92.12(7)
Mg2–O1–Mg2'	96.51(6)

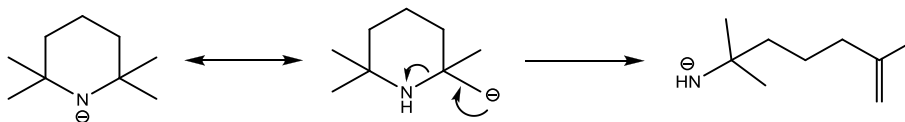
**Table 2.37** Key bond angles within [(TMP)Mg( $\mu$ -TMP){ $\mu$ -N(H)C(Me)<sub>2</sub>(CH<sub>2</sub>)<sub>3</sub>C(Me)=CH<sub>2</sub>}Mg( $\mu$ -OCH<sub>2</sub>SiMe<sub>3</sub>)<sub>2</sub>], **95**.

Homometallic, centrosymmetric **95** contains three orthogonal four-membered rings, two outer [Mg( $\mu$ -N){ $\mu$ -N(H)}Mg] diheteroanionic rings, which are connected through a central monoheteroanionic [Mg( $\mu$ -O)<sub>2</sub>Mg] ring. The Mg $\cdots$ Mg $\cdots$ Mg $\cdots$ Mg backbone is almost linear, as shown by the Mg2–Mg2'–Mg1'/Mg2'–Mg2–Mg1 angles, which, because the complex is centrosymmetric, are both 171.67(4)°. The three four-membered rings are planar, as evidenced by the sum of the internal angles, which are 359.99, 360.00 and 359.99° respectively. This kind of arrangement of linked orthogonal M<sub>2</sub>Hetero<sub>2</sub> rings has previously been found in other magnesium compounds such as the enolate [Mg<sub>4</sub>{ $\mu$ -OC(=CH<sub>2</sub>)Mes}<sub>6</sub>{OC(=CH<sub>2</sub>)Mes}<sub>2</sub>{OC(CH<sub>3</sub>)Mes}(toluene)<sub>2</sub>],<sup>[239]</sup> and the alkoxide compounds [Mg<sub>3</sub>( $\mu$ -ODipp)<sub>4</sub>(ODipp)<sub>2</sub>]<sup>[240]</sup> and [Mg<sub>3</sub>( $\mu$ -OSiPh<sub>3</sub>)<sub>4</sub>(OSiPh<sub>3</sub>)<sub>2</sub>].<sup>[241]</sup> There are also several examples of heterobimetallic compounds containing magnesium such as [{(O<sup>t</sup>Bu)SnMg( $\mu$ -O<sup>t</sup>Bu)<sub>3</sub>}]<sub>2</sub>,<sup>[242]</sup> [(Me)<sub>2</sub>AlMg( $\mu$ -N<sup>i</sup>Pr)<sub>2</sub>( $\mu$ -OMe)]<sub>2</sub>,<sup>[243]</sup> [(Me)<sub>2</sub>AlMg( $\mu$ -O<sup>t</sup>Bu)<sub>3</sub>}]<sub>2</sub>,<sup>[244]</sup> [(Me)<sub>2</sub>AlMg( $\mu$ -N<sup>i</sup>Pr)<sub>3</sub>}]<sub>2</sub>,<sup>[244]</sup> [(TMEDA)NaMg{( $\mu$ -OC(=CH<sub>2</sub>)Mes)<sub>3</sub>}]<sub>2</sub><sup>[245]</sup> and [(H)<sub>2</sub>GaMg( $\mu$ -O<sup>t</sup>Bu)<sub>3</sub>}]<sub>2</sub>,<sup>[246]</sup> which also possess a similar structural motif.

The outer Mg centres (Mg1 and Mg1') are coordinated to three N atoms – two from the TMP ligands and one from the amidoalkene, formed on ring-opening of a TMP anion – in a highly distorted trigonal planar geometry (summed angles at Mg1/Mg1', 358.42°). The inner Mg centres (Mg2 and Mg2') are coordinated to two N atoms – one from the TMP ligand and one from the amidoalkene – as well as to two O atoms from the alkoxide ligands, formed *via* oxygen insertion into a Mg–C bond – resulting in the metal centres adopting a highly distorted tetrahedral geometry (summed angles at Mg2/Mg2', 660.41°).

Turning to bond distances, the Mg–N bond distances within the two outer [Mg( $\mu$ -N){ $\mu$ -N(H)}Mg] diheteroanionic rings range from 2.066(2)-2.197(2) Å, with the two shortest distances being observed for the Mg–N<sub>amidoalkene</sub> bonds [2.066(2) and 2.102(2) Å for Mg1–N3/Mg1'–N3' and Mg2–N3/Mg2'–N3' respectively]. The terminal Mg–N<sub>amide</sub> bond distance [1.980(2) Å] is 0.194 Å shorter than the mean bridging Mg–N<sub>amide</sub> bond distance (2.174 Å), indicative of the steric constraints within the outer rings. The Mg–O bond distances [1.998(1) and 1.991(2) Å for Mg2–O1/Mg2'–O1 and Mg2–O1'/Mg2'–O1' respectively] lie in a range similar to the ones found in other Mg-alkoxide compounds.<sup>[240-241]</sup>

With complex **95** containing only one intact TMP ligand per Mg centre when two were expected, the reaction had clearly taken an unexpected course in generating two surprising anions. The first is a primary amidoalkene, which could be explained by a ring-opening of a TMP anion. To the best of our knowledge, this represents the first time that a ring-opened derivative of TMP has been captured within an organometallic product. Berg and Cowling reported that when TMP(H) is reacted with carbonyl dichloride or acetic anhydride, a mixture of isomeric isocyanates (6-isocyanato-2,6-dimethylhept-1-ene and 6-isocyanato-2,6-dimethylhept-2-ene) and a mixture of isomeric acetamides [*N*-(2,6-dimethylhept-6-en-2-yl)acetamide and *N*-(2,6-dimethylhept-5-en-2-yl)acetamide] respectively is produced; hence, providing indirect evidence of ring-fissure of TMP(H).<sup>[247]</sup> Ring-opening in our case is probably sterically driven by the congestion about the Mg centres and is induced thermally. Inevitably when TMP is contained within a Mg compound, the metal adopts a three coordinate, trigonal planar arrangement (akin to the outer Mg1 and Mg1' atoms in **95**). However, due to the fortuitous inclusion of oxygen in **95**, the second unexpected anion to form, the alkoxide imparts less steric hindrance (and electronically provides an excellent bridge) at the inner Mg sites (Mg2 and Mg2'), allowing coordination expansion (to four coordinate, distorted tetrahedral geometry) at these Mg centres. If ring-opening did not occur then it is envisaged that the outer Mg centres (Mg1 and Mg1') would be surrounded by three sterically demanding cyclic TMP anions. This situation has only been observed once before [in the solvent-separated mononuclear *tris*(TMP) anion, Mg(TMP)<sub>3</sub><sup>-</sup>]<sup>[108]</sup> and is not likely to reoccur with the geometric constraints which are applied in a neutral polynuclear complex; hence, to release steric strain, one could envisage that a H-shift from a CH<sub>3</sub> group to the amido N occurs followed by ring-opening to form the less sterically demanding, unsaturated, linear, primary amide ligand (Scheme 2.10).



**Scheme 2.10** Possible pathway for the generation of the acyclic amidoalkene ligand from its isomeric cyclic TMP anion.

The synthesis of an oxide-free analogue of **95** was attempted by treating two molar equivalents of  $(\text{Me}_3\text{SiCH}_2)_2\text{Mg}$  with three molar equivalents of TMP(H) in hexane. However, the only isolable product obtained from this reaction was the previously discussed alkylmagnesium amide dimer **94**. Despite our best efforts, it has proven difficult to reproduce **95** in significant yields. We have attempted to prepare **95** rationally by systematically studying a number of routes including: combining genuine, pre-prepared samples of  $\text{Mg}(\text{TMP})_2$  and  $(\text{Me}_3\text{SiCH}_2\text{O})\text{Mg}(\text{TMP})$ ; reacting 2 : 3 mixtures of  $(\text{Me}_3\text{SiCH}_2)_2\text{Mg}$  and TMP(H) with dried air; and oxygen-free **94** with  $\text{Mg}(\text{TMP})_2$  in the presence of dried air, but none of these has been successful thus far. Returning to the solid-state structure of **94**, the presence of a TMP ligand adopting a less thermodynamically stable boat conformation may have a role to play in the generation of a ring-opened form of the TMP anion.

This dramatic result of ring-opening the TMP anion and capturing it within **95** has demonstrated one possible decomposition pathway when metal TMP solutions are heated strongly. Thermal decompositions of this type may be synthetically useful provided refined, reproducible ways of generating primary amidoalkenes can be found.

## Chapter 3: Chiral Ligand Incorporation in Magnesiate and Zincate Chemistry

One of the objectives of this research programme was to try and incorporate chiral amides into mixed-metal compounds. Previously, the research group had successfully prepared a chiral bis(alkyl)amido sodium zincate (*R,R*)-[(TMEDA)·Na{μ-N(CH<sub>2</sub>Ph)(CH(CH<sub>3</sub>)Ph)}(μ-<sup>t</sup>Bu)Zn(<sup>t</sup>Bu)],<sup>[125]</sup> **41** (chapter 1, section 6, Figure 1.36), by carrying out a transamination reaction of [(TMEDA)·Na(μ-TMP)(μ-<sup>t</sup>Bu)Zn(<sup>t</sup>Bu)],<sup>[111]</sup> **38** (chapter 1, section 5, Figure 1.33) with the chiral amine (*R*)-*N*-benzyl- $\alpha$ -methylbenzylamine; and a chiral bis(amido)alkyl sodium magnesiate [{(-)-sparteine}·Na(μ-TMP)(μ-<sup>n</sup>Bu)Mg(TMP)],<sup>[162]</sup> **52** (chapter 1, section 1.6.1, Figure 1.39), by ligating (-)-sparteine to “[Na(μ-TMP)(μ-<sup>n</sup>Bu)Mg(TMP)]” as a chiral substitute for achiral TMEDA. Inspired by these initial results we looked at developing this area of organometallic chemistry through the design of new, potentially enantioselective, bases by incorporating the chiral diamines (-)-sparteine and (*R,R*)-TMCDA into the molecular framework of alkali metal, and mixed alkali metal-magnesium/zinc amide complexes.

Focusing on sodium TMP zincates initially, one complex containing the chiral diamine (-)-sparteine and two complexes containing the chiral diamine (*R,R*)-TMCDA, were prepared and characterised. All three complexes represent the first examples of (-)-sparteine or (*R,R*)-TMCDA being successfully incorporated within the molecular framework of an alkali metal/zinc synergic system [or indeed any alkali metal/divalent metal synergic system for (*R,R*)-TMCDA], and perhaps most significantly, one of the (*R,R*)-TMCDA bis(alkyl)amido sodium zincates formed is a chiral variant of a synthetically important utility ate base.

Moving to magnesiate chemistry, we successfully synthesised and structurally characterised a series of HMDS alkali metal magnesiates featuring the chiral diamines (-)-sparteine or (*R,R*)-TMCDA as supporting ligands.<sup>[248]</sup> Four of the complexes have a solvent-separated ion pair composition of the form [M(chiral diamine)<sub>2</sub>]<sup>+</sup>[Mg(HMDS)<sub>3</sub>]<sup>-</sup> [where M = Li or Na and chiral diamine = (-)-sparteine or (*R,R*)-TMCDA], and two have a contacted ion pair composition of the form [{K·chiral diamine}<sup>+</sup>{Mg(HMDS)<sub>3</sub>}]<sub>∞</sub><sup>-</sup> [where chiral diamine = (-)-sparteine or (*R,R*)-TMCDA]. Prior to this work, no (-)-sparteine or (*R,R*)-TMCDA adducts of potassium had been reported, and in addition, these potassium polymers appear to be the only structurally characterised complexes in which the chiral diamines (-)-sparteine or (*R,R*)-TMCDA have been incorporated within a polymeric framework.

Having investigated heterobimetallic systems containing the chiral diamines (–)-sparteine or (*R,R*)-TMEDA, it was also deemed important to study the alkali metal monometallic building blocks of such reagents, specifically chiral diamine adducts of the synthetically important lithium and sodium bis(trimethylsilyl)amides. ‘Conventional’ (–)-sparteine adducts of lithium and sodium HMDS were prepared and characterised, along with an unexpected and ‘unconventional’ hydroxyl-incorporated solvent-separated hexanuclear sodium sodiate – the anion of which is the first inverse crown ether anion to be reported.<sup>[249]</sup> Following this unusual result, a similar complex containing the chiral diamine (*R,R*)-TMEDA was prepared and characterised, namely a hydroxyl-incorporated solvent-separated pentanuclear sodium sodiate. Finally, revisiting chiral zincate chemistry, we looked at expanding the area of the (*R,R*)-TMEDA ate species to include magnesiates, specifically sodium HMDS-containing magnesiates. However, the reaction undertaken to produce such a species did not produce the expected contacted ion pair motif (as seen in previously synthesised ate complexes), but instead a polymeric complex – which represents the first example of a (*R,R*)-TMEDA-containing ‘inverse magnesiate’ complex.

### 3.1 Sodium TMP Zincates Containing Chiral Diamine Donor Ligands

Motivated by our success in synthesising and characterising *cis*-2,6-dimethylpiperidide zincate and magnesiate complexes (chapter 2, section 2.1), along with being encouraged by the successful preparation and isolation of the first chiral amidozincate (*R,R*)-[(TMEDA)·Na{μ-N(CH<sub>2</sub>Ph)(CH(CH<sub>3</sub>)Ph)}(μ-<sup>*t*</sup>Bu)Zn(<sup>*t*</sup>Bu)],<sup>[125]</sup> **41**, and having successfully ligated (–)-sparteine to “[Na(μ-TMP)(μ-<sup>*n*</sup>Bu)Mg(TMP)]” to form the first chiral amidomagnesiate [{"(–)-sparteine}·Na(μ-TMP)(μ-<sup>*n*</sup>Bu)Mg(TMP)],<sup>[162]</sup> **52**, we looked at developing this area of organometallic chemistry by incorporating the chiral diamines (–)-sparteine and (*R,R*)-TMEDA into the molecular framework of mixed sodium-zinc amide complexes, and investigating the solid-state and solution structures of the bases obtained.

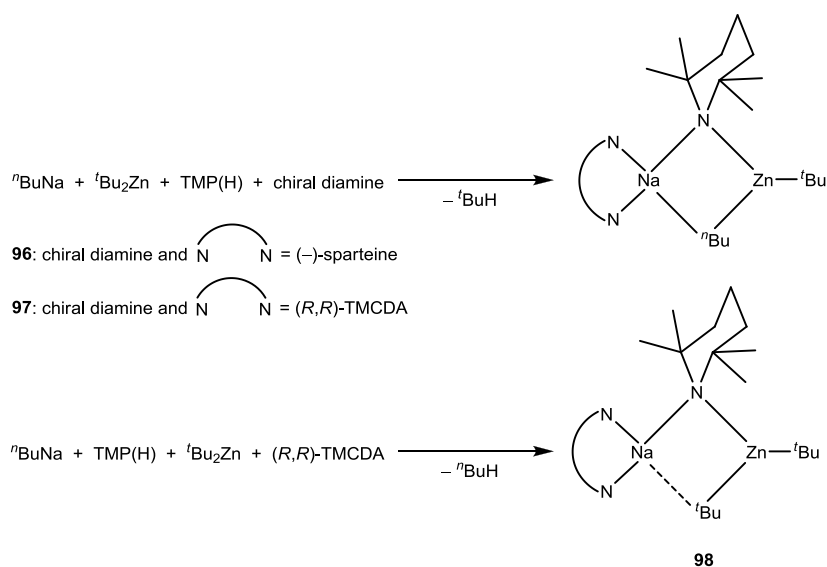
As detailed in chapter 2, section 2.1, several alkali metal alkyl/amido zincates have been structurally characterised with achiral donor ligands such as THF,<sup>[90, 192]</sup> TMEDA,<sup>[111, 119, 124-125, 189, 192]</sup> TMTA<sup>[190]</sup> and PMDETA,<sup>[119, 191-192, 250]</sup> with perhaps the most comprehensively studied sodium zincate being the aforementioned [(TMEDA)·Na(μ-TMP)(μ-<sup>*t*</sup>Bu)Zn(<sup>*t*</sup>Bu)],<sup>[111]</sup> **38**, which has proved to be a highly selective base towards naphthalene<sup>[112]</sup>, trifluoromethyl benzene,<sup>[113]</sup> dimethylanilines,<sup>[114]</sup> *N*-heterocyclic aromatics,<sup>[115]</sup> toluene,<sup>[116]</sup> benzylmethylether,<sup>[117]</sup> phenyl *O*-carbamate and benzamides.<sup>[118]</sup> Surprisingly, no such similar



zincate complexes have been prepared or characterised to date in which chiral donor ligands have been utilised.

Addressing this deficiency and wishing to expand on the synthetic and structural chemistry of chiral diamine complexes of alkali metal amides, an area which has thus far been largely neglected, we herein report the synthesis and structural characterisation of a series of TMP sodium zincates featuring the chiral diamines (–)-sparteine or (*R,R*)-TMCDA.

Three novel mixed alkyl/amido sodium zincates containing the chiral diamine donor ligands (–)-sparteine or (*R,R*)-TMCDA have been prepared and characterised (Scheme 3.1). Two of the complexes, with the general formula [ $\{\text{chiral diamine}\} \cdot \text{Na}(\mu\text{-TMP})(\mu\text{-}^n\text{Bu})\text{Zn}(\text{}^t\text{Bu})$ ] [chiral diamine = (–)-sparteine for **96**, (*R,R*)-TMCDA for **97**], were synthesised by a mixed-metal approach, reacting an equimolar mixture of *n*-butylsodium and di-*tert*-butylzinc in hexane with a molar equivalent of TMP(H), followed by one molar equivalent of (–)-sparteine (for **96**) or (*R,R*)-TMCDA (for **97**). The third complex [ $\{(R,R)\text{-TMCDA}\} \cdot \text{Na}(\mu\text{-TMP})(\mu\text{-}^t\text{Bu})\text{Zn}(\text{}^t\text{Bu})$ ], **98**, was synthesised by co-complexation of the alkali metal amide with di-*tert*-butylzinc in the presence of a molar equivalent of (*R,R*)-TMCDA in a hydrocarbon medium.



Scheme 3.1 Synthesis of complexes **96-98**.

As noted above, (–)-sparteine has already successfully been incorporated within the molecular framework of an alkali metal/magnesium synergic system (complex **52**),<sup>[162]</sup> but complex **96** represents the first example of (–)-sparteine being incorporated within the molecular framework of an alkali metal/zinc synergic system. Similarly, complexes **97** and **98** represent the first complexes in which (*R,R*)-TMCDA has successfully been incorporated within the molecular framework of an alkali metal/zinc synergic system (or indeed any alkali

metal/divalent metal synergic system). All three complexes are rare examples of sodium adducts of (–)-sparteine or (R,R)-TMEDA.

### 3.1.1 [ $\{(-)\text{-sparteine}\} \cdot \text{Na}(\mu\text{-TMP})(\mu\text{-}^n\text{Bu})\text{Zn}(^t\text{Bu})$ ], **96**

Complex **96** was prepared by reacting an equimolar mixture of *n*-butylsodium and di-*tert*-butylzinc in hexane with a molar equivalent of TMP(H), followed by one molar equivalent of (–)-sparteine. X-ray quality crystals of **96**, a chiral bis(alkyl)amido sodium zincate, precipitated from the hydrocarbon solution at  $-28^\circ\text{C}$  (Scheme 3.1).

X-ray crystallographic analysis reveals that **96** crystallises in the orthorhombic system, space group  $P2_12_12_1$ . The structure of **96** (Figure 3.1) is composed of a sodium centre coordinated to a (–)-sparteine ligand and a zinc centre coordinated to a  $^t\text{Bu}$  anion, with a TMP anion and a  $^n\text{Bu}$  anion bridging the two metal centres (the sodium metal centre is four coordinate and the zinc metal centre three coordinate). Table 3.1 and Table 3.2 detail the key bond distances and bond angles respectively.

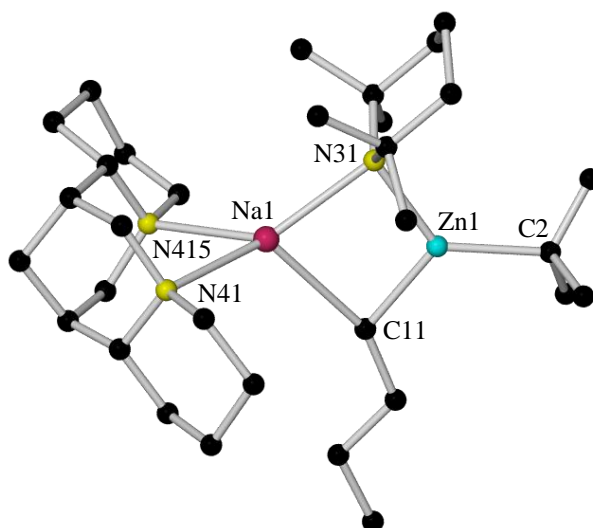


**Figure 3.1** Molecular structure of [ $\{(-)\text{-sparteine}\} \cdot \text{Na}(\mu\text{-TMP})(\mu\text{-}^n\text{Bu})\text{Zn}(^t\text{Bu})$ ], **96**. H atoms are omitted for clarity.

Selected Bond	Bond Distance (Å) in [ $\{(-)\text{-sparteine}\} \cdot \text{Na}(\mu\text{-TMP})(\mu\text{-}^n\text{Bu})\text{Zn}(^t\text{Bu})$ ], <b>96</b>
Na1–N31	2.435(5)
Na1–N41	2.535(5)
Na1–N415	2.467(4)
Na1–C11	2.686(5)
Zn1–N31	2.082(4)
Zn1–C2	2.073(5)
Zn1–C11	2.063(4)

**Table 3.1** Key bond distances within [ $\{(-)\text{-sparteine}\} \cdot \text{Na}(\mu\text{-TMP})(\mu\text{-}^n\text{Bu})\text{Zn}(^t\text{Bu})$ ], **96**.

Selected Angle	Bond Angle (°) in [(-)-sparteine]·Na(μ-TMP)(μ- <sup>n</sup> Bu)Zn( <sup>t</sup> Bu), <b>96</b>
N31–Na1–N41	139.00(14)
N31–Na1–N415	131.66(15)
N31–Na1–C11	80.94(14)
N41–Na1–N415	72.69(13)
N41–Na1–C11	120.73(15)
N415–Na1–C11	116.91(15)
N31–Zn1–C2	128.9(2)
N31–Zn1–C11	106.84(17)
C2–Zn1–C11	124.3(2)
Na1–N31–Zn1	88.96(15)
Na1–C11–Zn1	82.79(16)

**Table 3.2** Key bond angles within [(-)-sparteine]·Na(μ-TMP)(μ-<sup>n</sup>Bu)Zn(<sup>t</sup>Bu), **96**.

In keeping with the previously discussed zincates **75-77** (chapter 2, section 2.1), **96** is an ion-contacted zincate containing a four-atom ring; however, in this case it is a planar (NaNZnC) ring (sum of endocyclic angles, 359.53°), whereby the two metals are linked *via* a TMP and a <sup>n</sup>Bu bridge. Three of the internal angles are acute and range from 80.94(14)-88.96(15)°. The remaining internal angle (N31–Zn1–C11) is significantly wider [106.84(17)°], to accommodate the distorted trigonal planar geometry of the Zn centre. Due to the acute (-)-sparteine–Na bite angle (N41–Na1–N415) of 72.69(13)°, the Na geometry is best described as highly distorted tetrahedral [summed angles at Na, 661.93°; range of angles, 72.69(13)-139.00(14)°], whereas that of Zn is distorted trigonal planar [summed angles at Zn, 360.04°; range of angles, 106.84(17)-128.9(2)°]. The bonds which make up the perimeter of the tetra-element ring vary considerably [range of bond distances, 2.063(4)-2.686(5) Å], with the two longest bonds being Na1–N31 [2.435(5) Å] and Na1–C11 [2.686(5) Å], presumably due to the combined steric bulk of the TMP and <sup>n</sup>Bu anions, along with the (-)-sparteine ligand at the Na centre. A similar scenario was encountered in the previously reported (-)-sparteine ate complex (*vide supra*) – the chiral bis(amido)alkyl sodium magnesiate [[(-)-sparteine]·Na(μ-TMP)(μ-<sup>n</sup>Bu)Mg(TMP)],<sup>[162]</sup> **52** – and due to the structural motifs being almost identical to one another, there is little discrimination in the structural parameters corresponding to the Na centre in complexes **52** and **96** (Table 3.3).

Selected Structural Parameter	<b>52</b>	<b>96</b>
summed angles at Na (°)	661.43	661.93
range of angles around Na (°)	72.59(5)-138.35(6)	72.69(13)-139.00(14)
Na–N <sub>(-)-sparteine</sub> bite angle (°)	72.59(5)	72.69(13)
Na–N bond distance (Å)	2.527(2)	2.435(5)
Na–C bond distance (Å)	2.772(2)	2.686(5)
mean Na–N <sub>(-)-sparteine</sub> bond distance (Å)	2.499	2.501

**Table 3.3** Comparison of selected structural parameters within complexes **52** and **96**.

The bridging <sup>n</sup>Bu anion in complex **96** is unusual, having only been previously reported in magnesiate **52** and its TMEDA analogue [(TMEDA)·Na(μ-TMP)(μ-<sup>n</sup>Bu)Mg(TMP)],<sup>[106]</sup> **37**, along with two zincates, [(TMEDA)·Li(μ-TMP)(μ-<sup>n</sup>Bu)Zn(<sup>n</sup>Bu)],<sup>[124]</sup> **40** and [(PMDTA)·K(μ-TMP)(μ-<sup>n</sup>Bu)Zn(<sup>n</sup>Bu)],<sup>[250b]</sup> **99**. As discovered on comparing complex **52** to complex **96**, the majority of the structural parameters corresponding to the Na centre in the TMEDA magnesiate analogue of **52** (complex **37**) are almost identical within experimental error to those encountered in **96** (Table 3.4); however there are a few exceptions – the angle corresponding to the N41–Na1–C11 angle in **96** [120.73(15)°] is some 20.06° more acute in **37** [100.67(7)°], presumably due to the less steric demanding nature of TMEDA when compared to (–)-sparteine. The majority of the other angles are within 5° of the corresponding angle. As a consequence of these subtle changes, the geometry of the Na centre in **37** is distorted trigonal pyramidal – whereas as mentioned earlier – it is distorted tetrahedral in **96**. As expected, the Na–N<sub>diamine</sub> bite angle is wider (by 3.47°) in complex **37** [76.16(6)°] compared to the corresponding parameter in **96** [72.69(13)°], presumably due to the less steric demanding nature of TMEDA *versus* (–)-sparteine.

Selected Bond Distance (Å) and angle (°)	<b>37</b> (TMEDA)	<b>96</b> [(–)-sparteine]
Na1–N31	2.452(2)	2.435(2)
Na1–C11	2.669(2)	2.686(5)
Na1–N41	2.509(2)	2.535(5)
Na1–N415	2.474(2)	2.467(4)
N31–Na1–N41	140.01(7)	139.00(14)
N31–Na1–N415	135.78(6)	131.66(15)
N31–Na1–C11	85.34(7)	80.94(14)
N41–Na1–N415	76.16(6)	72.69(13)
N41–Na1–C11	100.67(7)	120.73(15)
N415–Na1–C11	117.31(7)	116.91(15)

**Table 3.4** Selected bond distances and angles within complexes **37** and **96**.

As noted above, (–)-sparteine has already successfully been incorporated within the molecular framework of an alkali metal/magnesium synergic system (complex **52**);<sup>[162]</sup> however, complex **96** represents the first example of (–)-sparteine being incorporated within the molecular framework of an alkali metal/zinc synergic system. In addition, complex **96** is a rare (–)-sparteine adduct of sodium.

To aid the interpretation of the NMR data obtained in this project and in any future work, the <sup>1</sup>H and <sup>13</sup>C NMR spectra were obtained for the diamine standard, (–)-sparteine, in C<sub>6</sub>D<sub>6</sub> (Figure 3.2 and Figure 3.3 respectively) and d<sub>8</sub>-THF solution (details given in the accompanying NMR Data Starting Materials handout). The <sup>1</sup>H and <sup>13</sup>C NMR spectra of (–)-sparteine are highly complicated, with the <sup>1</sup>H NMR spectrum having a large number of signals which fall within an area of approximately 2.0 ppm of the spectrum. This makes the

peaks difficult to assign and the multiplicity difficult to determine. There is also a large area from around 1.3-1.7 ppm, in which the peaks overlap with each other, thus making it extremely difficult to define the peaks in this region. Due to this series of problems, integration and distinction of peaks is increasingly difficult (a similar scenario is encountered in  $d_8$ -THF solution, where the peaks are extensively broader).

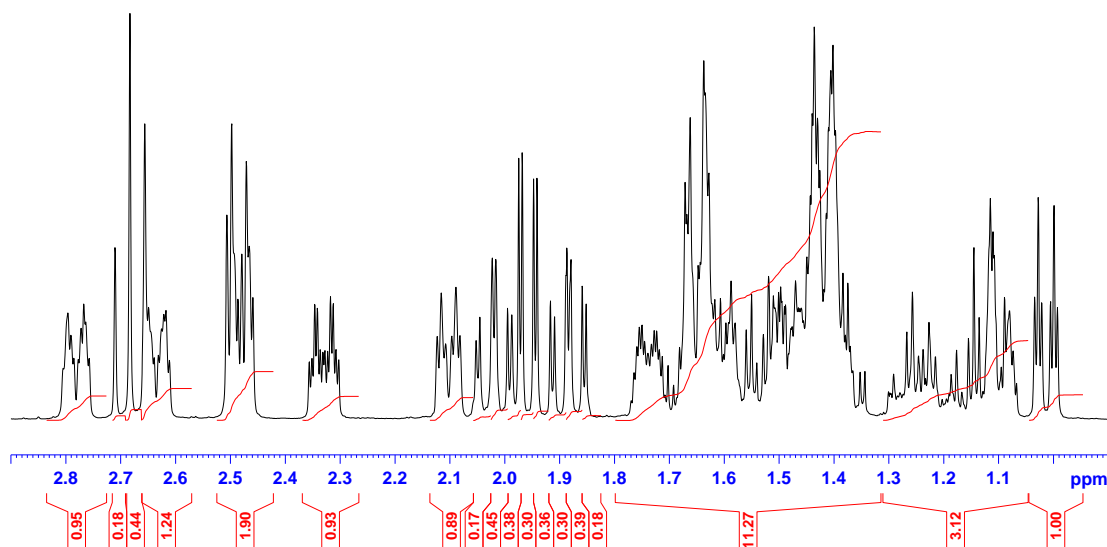


**Figure 3.2**  $^1\text{H}$  NMR spectrum of (-)-sparteine in  $\text{C}_6\text{D}_6$ .

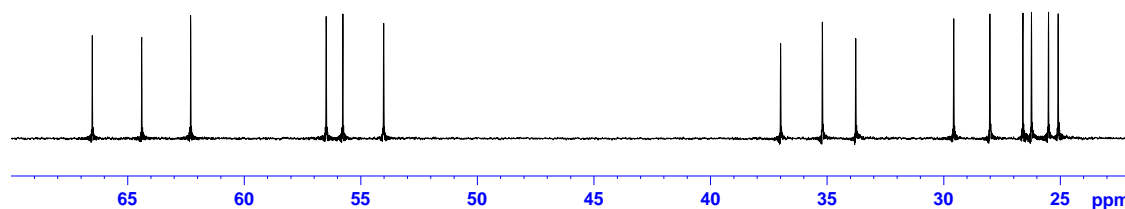


**Figure 3.3**  $^{13}\text{C}$  NMR spectrum of (-)-sparteine in  $\text{C}_6\text{D}_6$ .

If we consider how closely packed, and overlapping the peaks of the  $^1\text{H}$  NMR spectra of free (-)-sparteine are, it is clear that instead of trying to assign them, a more definitive method of analysis would be to compare the peaks of free (-)-sparteine with those of the products obtained throughout this project, and look for any subtle differences. Upon investigation, it became apparent that this was a useful technique when examining any potential metal·(-)-sparteine coordinated complexes. When a comparison was made between free (-)-sparteine and some of the novel (-)-sparteine complexes produced within the group, it could clearly be seen that there was a dramatic shift in the outermost (-)-sparteine signals when the (-)-sparteine molecule had successfully been coordinated to a metal centre (Figure 3.4).

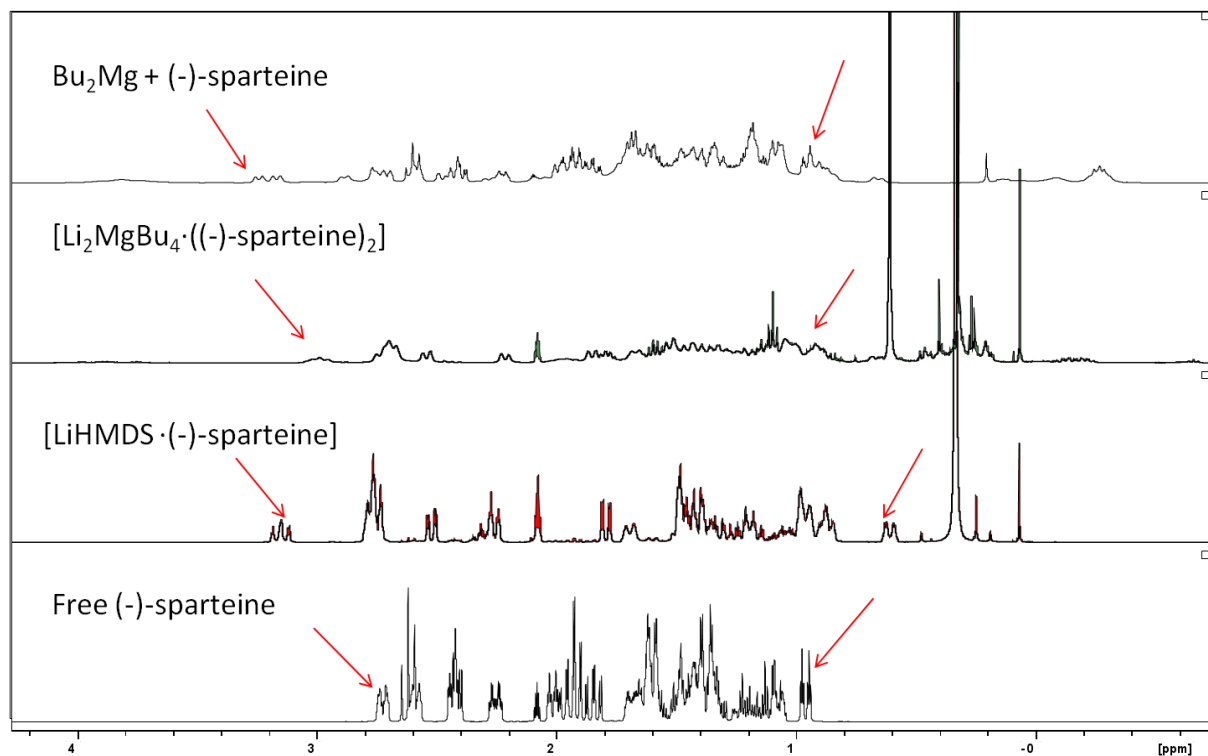


**Figure 3.4** Comparison of the  $^1\text{H}$  NMR spectra of free  $(-)$ -sparteine in  $\text{C}_6\text{D}_6$  with some novel  $(-)$ -sparteine complexes produced within the group.

Initial  $^1\text{H}$  NMR data obtained for complex **96** was highly complex due to the multitude of chemically distinct aliphatic H and C atoms – not only present in  $(-)$ -sparteine, but also in the remainder of the complex. Due to time constraints the NMR data was not fully characterised and hence future work will concentrate on rectifying this (detailed in chapter 6, section 6.2.1).

As stated in chapter 1,  $(-)$ -sparteine was withdrawn from sale by most chemical suppliers during the course of this research project. Following the diminishing supply and encouraged by our success in preparing various *s*-block homo- and heterobimetallic  $(-)$ -sparteine complexes (*vide infra*), our attention turned to utilising the readily synthesised  $(R,R)$ -TMCD $^{\text{[166c]}}$  chiral diamine ligand.

### 3.1.2 [ $(R,R)$ -TMCD $\cdot\text{Na}(\mu\text{-TMP})(\mu\text{-}^n\text{Bu})\text{Zn}(^t\text{Bu})$ ], **97**

Following the same reaction methodology as that used to prepare **96** [using  $(R,R)$ -TMCD $\cdot\text{Na}$  in place of  $(-)$ -sparteine] afforded X-ray quality crystals of **97** at  $-28^\circ\text{C}$  (Scheme 3.1).

X-ray crystallographic analysis reveals that **97** crystallises in the monoclinic system, space group  $P2_1$ . Akin to its  $(-)$ -sparteine congener **96**, the structure of **97** (Figure 3.5) is composed of the same basic building blocks – a sodium centre, a chiral donor ligand, a  $^n\text{Bu}$  anion, a zinc centre, a  $^t\text{Bu}$  anion and a TMP anion – the only difference being that  $(R,R)$ -TMCD $\cdot\text{Na}$  replaces

(-)-sparteine as the chiral donor ligand (the sodium metal centre is four coordinate and the zinc metal centre three coordinate). Within the asymmetric unit of **97** there are two independent molecules of  $[(R,R)\text{-TMCD A}]\cdot\text{Na}(\mu\text{-TMP})(\mu\text{-}^n\text{Bu})\text{Zn}(^t\text{Bu})$ ; however, one of the molecules is disordered, and thus Table 3.5 and Table 3.6 detail the key bond distances and angles respectively of only the non-disordered molecule of the two independent molecules.

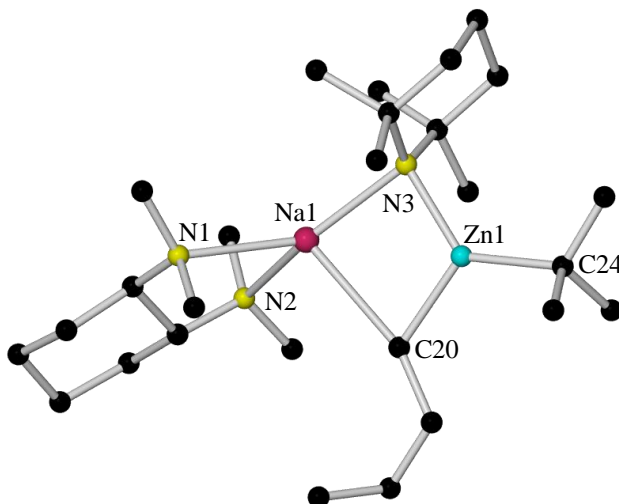


**Figure 3.5** Molecular structure of  $[(R,R)\text{-TMCD A}]\cdot\text{Na}(\mu\text{-TMP})(\mu\text{-}^n\text{Bu})\text{Zn}(^t\text{Bu})$ , **97**. H atoms omitted and only one of two molecules in the asymmetric unit shown for clarity.

Selected Bond	Bond Distance (Å) in $[(R,R)\text{-TMCD A}]\cdot\text{Na}(\mu\text{-TMP})(\mu\text{-}^n\text{Bu})\text{Zn}(^t\text{Bu})$ , <b>97</b>
Na1–N1	2.444(3)
Na1–N2	2.455(3)
Na1–N3	2.371(3)
Na1–C20	2.729(4)
Zn1–N3	2.050(3)
Zn1–C20	2.060(4)
Zn1–C24	2.044(4)

**Table 3.5** Key bond distances within  $[(R,R)\text{-TMCD A}]\cdot\text{Na}(\mu\text{-TMP})(\mu\text{-}^n\text{Bu})\text{Zn}(^t\text{Bu})$ , **97**.

Selected Angle	Bond Angle (°) in $[(R,R)\text{-TMCD A}]\cdot\text{Na}(\mu\text{-TMP})(\mu\text{-}^n\text{Bu})\text{Zn}(^t\text{Bu})$ , <b>97</b>
N1–Na1–N2	73.08(12)
N1–Na1–N3	137.55(13)
N1–Na1–C20	115.64(13)
N2–Na1–N3	144.21(12)
N2–Na1–C20	101.82(12)
N3–Na1–C20	82.04(12)
N3–Zn1–C20	109.59(13)
N3–Zn1–C24	130.00(15)
C20–Zn1–C24	120.41(16)
Na1–N3–Zn1	88.84(12)
Na1–C20–Zn1	79.44(12)

**Table 3.6** Key bond angles within  $[(R,R)\text{-TMCD A}]\cdot\text{Na}(\mu\text{-TMP})(\mu\text{-}^n\text{Bu})\text{Zn}(^t\text{Bu})$ , **97**.

The framework of **97** is essentially identical to that of **96**, containing a four-element (NaNZnC) ring which is planar (sum of endocyclic angles, 359.91°). On comparing complex **97** to its (-)-sparteine congener **96**, there is little discrimination in the majority of the structural parameters corresponding to the Na centre in the two complexes; however there are a few exceptions – the angles corresponding to the N2–Na1–C20 angle and the N2–Na1–N3 angle in **97** [101.82(12) and 144.21(12)° respectively] are 15.09° wider and 12.55° narrower respectively in **96** [116.91(15) and 131.66(15)° respectively], presumably due to the less steric demanding nature of (*R,R*)-TMCDa when compared to (-)-sparteine. The majority of the other angles are within 6° of the corresponding angle. As a consequence of these subtle changes, the geometry of the Na centre in **97** is distorted trigonal pyramidal [summed angles at Na, 654.34°; range of angles, 73.08(12)-144.21(12)°] – whereas as mentioned earlier – it is distorted tetrahedral in **96**. In keeping with the less steric demanding nature of (*R,R*)-TMCDa *versus* (-)-sparteine – the mean Na–N<sub>diamine</sub> bond distance (2.450 Å) and the Na–N<sub>diamine</sub> bite angle [73.08(12)°] in complex **97** are 0.051 Å shorter and 0.39° wider respectively than the corresponding parameters in (-)-sparteine-containing **96** [mean Na–N<sub>diamine</sub> bond distance and Na–N<sub>diamine</sub> bite angle, 2.501 Å and 72.69(13)° respectively]. A similar scenario is encountered on comparing complex **97** to that of the previously reported (-)-sparteine ate complex (*vide supra*) – the chiral bis(amido)alkyl sodium magnesiato [((-)-sparteine)·Na(μ-TMP)(μ-<sup>n</sup>Bu)Mg(TMP)],<sup>[162]</sup> **52** – here, the angles corresponding to the N2–Na1–C20 angle and the N2–Na1–N3 angle in **97** (*vide supra*) are 12.66° wider and 5.86° narrower respectively in **52** [114.48(6) and 138.35(6)° respectively], and the majority of the other angles are within 5° of the corresponding angle. Again these subtle changes are reflected in the geometry of the Na centres – distorted trigonal pyramidal in complex **97** and distorted tetrahedral in complex **52**.

Returning to complexes **96** and **97**, the steric demands of the chiral diamine donor ligands are also felt at the Zn metal centre – with the N–Zn–C(<sup>n</sup>Bu) and the N–Zn–C(<sup>t</sup>Bu) angles being slightly more obtuse, and the remaining C(<sup>n</sup>Bu)–Zn–C(<sup>t</sup>Bu) angle being slightly more acute in **97** [109.59(13), 130.00(15) and 120.41(16)° respectively] compared to **96** [106.84(17), 128.90(2) and 124.30(2)° respectively]. Presumably the less steric demanding nature of (*R,R*)-TMCDa *versus* (-)-sparteine allows the bulky TMP anion to lean closer to the Na centre in **97**, consequently increasing the N–Zn–C(<sup>n</sup>Bu) and the N–Zn–C(<sup>t</sup>Bu) angles and decreasing the C(<sup>n</sup>Bu)–Zn–C(<sup>t</sup>Bu) angle, while concurrently decreasing and increasing the Na–N and Na–C bond distances compared to **96** [2.371(3) *vs.* 2.435(5) Å and 2.729(4) *vs.* 2.686(5) Å respectively] to counterbalance such changes in the angles.



As expected, on comparing complex **97** to the TMEDA magnesiate analogue of **52** (*vide supra*) – [(TMEDA)·Na(μ-TMP)(μ-<sup>n</sup>Bu)Mg(TMP)],<sup>[106]</sup> **37**, only slight variation in the structural parameters corresponding to the Na centre are observed; with the Na–N<sub>diamine</sub> bite angle (N1–Na1–N2) being 3.08° wider in **37** [76.16(6)]° compared to that in **97** [73.08(12)]°, due to the slightly less steric demanding nature of TMEDA *versus* (*R,R*)-TMCDA; and the angles corresponding to the N3–Na1–C20 angle and the N2–Na1–N3 angle in **97** [82.04(12) and 144.21(12)]° respectively] are 3.3° wider and 4.2° narrower respectively in **37** [85.34(7) and 140.01(7)]° respectively], with the majority of the other angles being within 2° of the corresponding angle.

Complex **97** constitutes the first example of (*R,R*)-TMCDA being successfully incorporated within the molecular framework of an alkali metal/zinc synergic system (or indeed any alkali metal/divalent metal synergic system), and is a rare (*R,R*)-TMCDA adduct of sodium.

To aid the interpretation of the NMR data obtained in this project and any future work, the <sup>1</sup>H, <sup>13</sup>C, COSY and HSQC NMR spectra were obtained for the diamine standard, (*R,R*)-TMCDA, in both C<sub>6</sub>D<sub>6</sub> and d<sub>8</sub>-THF solution. The <sup>1</sup>H and <sup>13</sup>C spectra of (*R,R*)-TMCDA in C<sub>6</sub>D<sub>6</sub> solution (Figure 3.6 and Figure 3.7) and d<sub>8</sub>-THF solution (Figure 3.8 and Figure 3.9) are shown below.

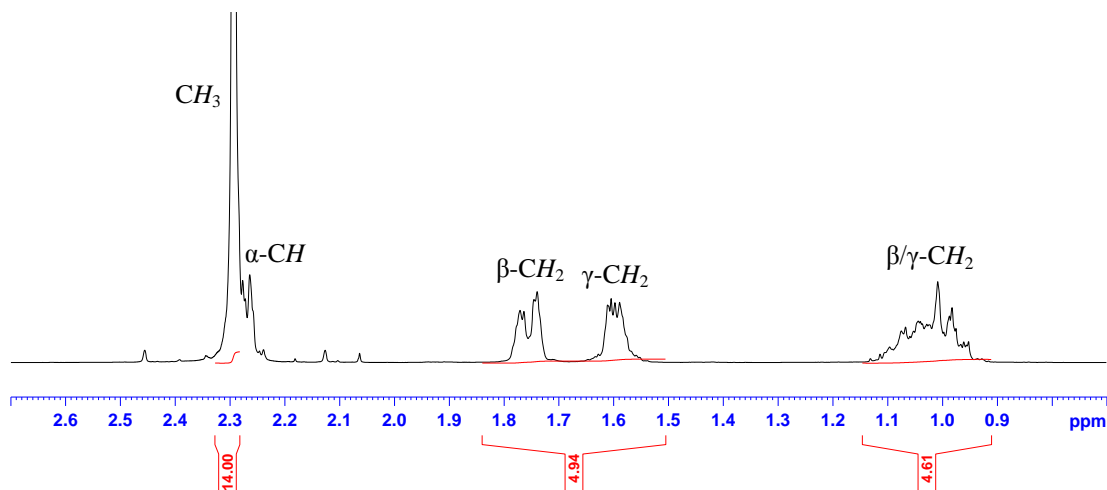


Figure 3.6 <sup>1</sup>H NMR spectrum of (*R,R*)-TMCDA in C<sub>6</sub>D<sub>6</sub>.

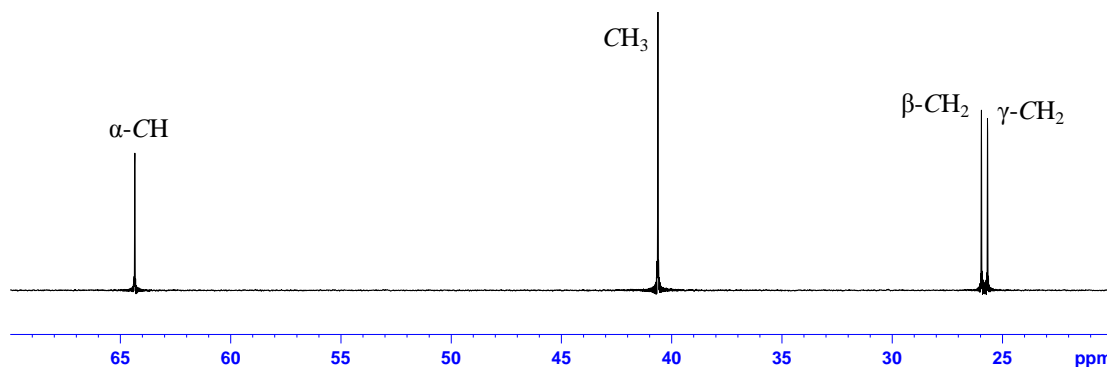
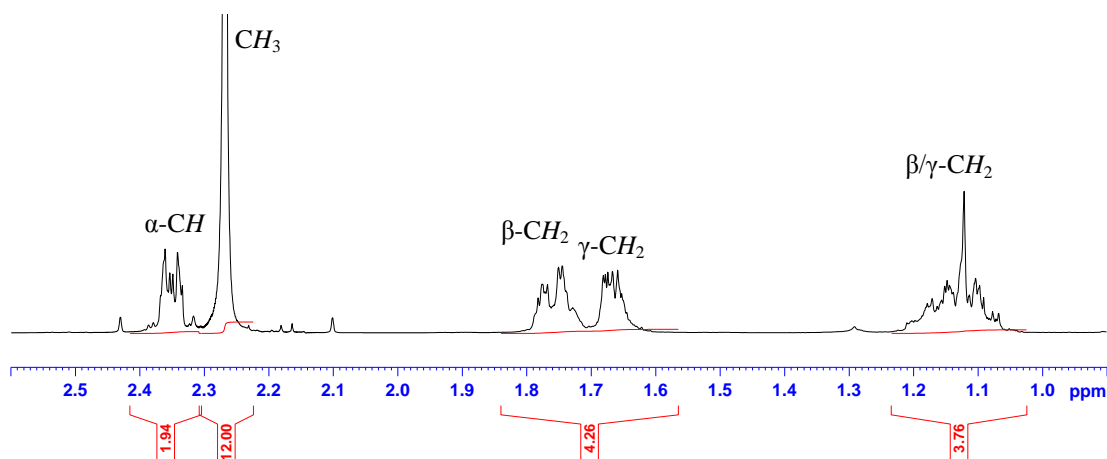
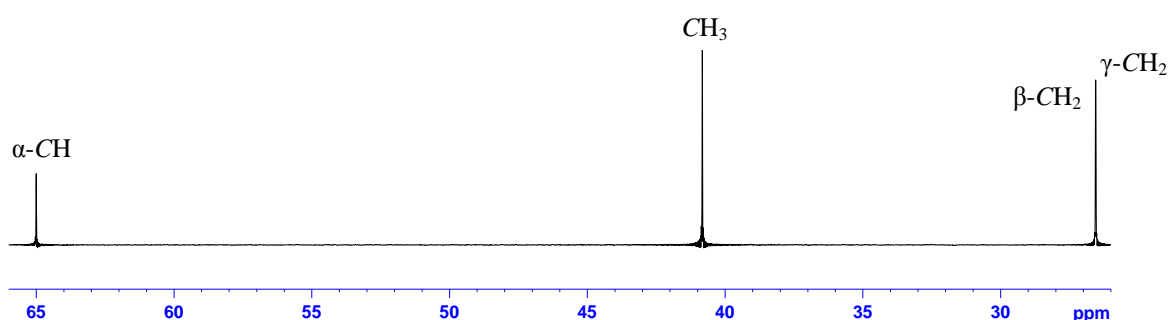


Figure 3.7 <sup>13</sup>C NMR spectrum of (*R,R*)-TMCDA in C<sub>6</sub>D<sub>6</sub>.



**Figure 3.8**  $^1\text{H}$  NMR spectrum of (*R,R*)-TMCDA in  $d_8$ -THF.



**Figure 3.9**  $^{13}\text{C}$  NMR spectrum of (*R,R*)-TMCDA in  $d_8$ -THF.

Due to the chair conformation adopted by (*R,R*)-TMCDA four resonances are observed for the four chemically distinct  $\beta$ - and  $\gamma$ -hydrogen atoms. In the  $\text{C}_6\text{D}_6$  spectrum there is a singlet at 2.29 ppm integrating to 12 protons, which corresponds to the methyl groups. A multiplet integrating to two protons appears at 2.26 ppm, which corresponds to the two  $\alpha$ -hydrogens. Two multiplets, each integrating to two protons, at 1.76 and 1.60 ppm correspond to two  $\beta$ -hydrogens and two  $\gamma$ -hydrogens respectively. The remaining signals for the  $\beta$ - and  $\gamma$ -hydrogen atoms overlap, forming a broad multiplet at 1.01 ppm which integrates to four protons.

With the aid of the HSQC spectrum, the relevant chemical shifts from the  $^{13}\text{C}$  NMR spectrum were assigned to their respective proton chemical shifts from the  $^1\text{H}$  NMR spectrum and are shown in [Table 3.7](#) and [Table 3.8](#) respectively.

NMR chemical shifts of ( <i>R,R</i> )-TMCDA in $\text{C}_6\text{D}_6$			
$^1\text{H}$ $\delta$ / ppm		$^{13}\text{C}$ $\delta$ / ppm	
$\alpha$ -CH	2.26	$\alpha$ -CH	64.3
$\beta$ -CH <sub>2</sub>	1.75	$\beta$ -CH <sub>2</sub>	26.0
	1.01		
$\gamma$ -CH <sub>2</sub>	1.60	$\gamma$ -CH <sub>2</sub>	25.7
	1.01		
CH <sub>3</sub>	2.29	CH <sub>3</sub>	40.6

**Table 3.7**  $^1\text{H}$  and  $^{13}\text{C}$  NMR chemical shifts of (*R,R*)-TMCDA in  $\text{C}_6\text{D}_6$ .

NMR chemical shifts of ( <i>R,R</i> )-TMCDA in d <sub>8</sub> -THF			
<sup>1</sup> H δ / ppm		<sup>13</sup> C δ / ppm	
α-CH	2.35	α-CH	65.0
β-CH <sub>2</sub>	1.76	β-CH <sub>2</sub>	26.5
	1.12		
γ-CH <sub>2</sub>	1.69	γ-CH <sub>2</sub>	26.5
	1.12		
CH <sub>3</sub>	2.27	CH <sub>3</sub>	40.8

**Table 3.8** <sup>1</sup>H and <sup>13</sup>C NMR chemical shifts of (*R,R*)-TMCDA in d<sub>8</sub>-THF.

As found with the initial <sup>1</sup>H NMR spectrum of **96**, the data obtained for complex **97** (and subsequently complex **98**) was complicated, even though the simpler (in terms of the number of chemically distinct aliphatic H and C atoms) (*R,R*)-TMCDA ligand is present within this structure. Again, due to time constraints the NMR data was not fully characterised and hence future work will concentrate on rectifying this (detailed in chapter 6, section 6.2.1).

### 3.1.3 [{(*R,R*)-TMCDA}·Na(μ-TMP)(μ-<sup>t</sup>Bu)Zn(<sup>t</sup>Bu)], **98**

Complex **98** was prepared by reacting *n*-butylsodium with an equimolar quantity of TMP(H) and then one molar equivalent of di-*tert*-butylzinc in a hexane medium (introduced *via* cannula). One molar equivalent of (*R,R*)-TMCDA was required to produce a homogeneous solution. X-ray quality crystals of **98**, a chiral bis(alkyl)amido sodium zincate, precipitated from the hydrocarbon solution at -28°C. It can be seen from [Scheme 3.1](#) that the synthetic approach and ultimate composition of **98** resembles that of Mulvey's sodium bis(alkyl)amido zincate [(TMEDA)·Na(μ-TMP)(μ-<sup>t</sup>Bu)Zn(<sup>t</sup>Bu)], **38** (chapter 1, section 5, [Figure 1.33](#)), reported in 2005,<sup>[111]</sup> which contains (*R,R*)-TMCDA's achiral relative TMEDA as the donor ligand. As detailed in section 3.1, complex **38** has proved to be a highly selective base towards various substrates;<sup>[112-118]</sup> hence, complex **98** is a chiral variant of an important utility ate base.

X-ray crystallographic analysis reveals that **98** crystallises in the monoclinic system, space group *P2*<sub>1</sub>. Similar to its TMEDA congener **38**, the structure of **98** ([Figure 3.10](#)) is composed of a sodium centre coordinated to a donor ligand [the chiral diamine (*R,R*)-TMCDA in this case] and a zinc centre coordinated to a <sup>t</sup>Bu anion, with a TMP anion and a <sup>t</sup>Bu anion bridging the two metal centres. The latter bridges asymmetrically to zinc through the quaternary C atom and to sodium *via* an agostic-type interaction through a methyl C atom (the sodium metal centre is four coordinate and the zinc metal centre three coordinate). Within the asymmetric unit of **98** there are two independent molecules of [{(*R,R*)-TMCDA}·Na(μ-TMP)(μ-<sup>t</sup>Bu)Zn(<sup>t</sup>Bu)]; however, the differences in the dimensions of these molecules are

negligible, and thus Table 3.9 and Table 3.10 detail the key bond distances and angles respectively of only one of the independent molecules.

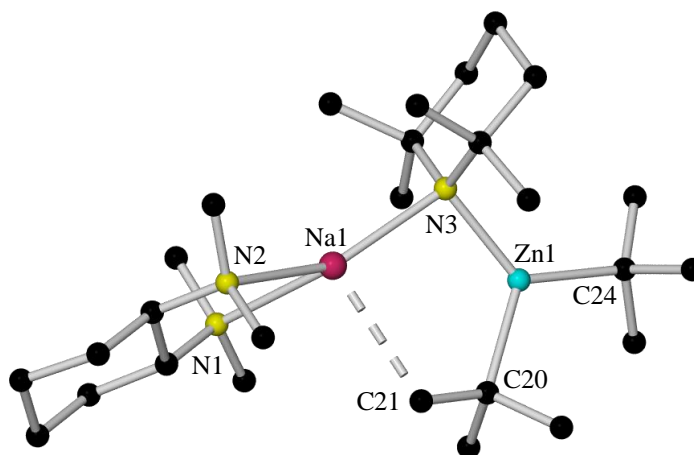


**Figure 3.10** Molecular structure of  $[(R,R)\text{-TMCDA}]\cdot\text{Na}(\mu\text{-TMP})(\mu\text{-}^t\text{Bu})\text{Zn}(^t\text{Bu})$ , **98**. H atoms omitted and only one of two similar molecules in the asymmetric unit shown for clarity.

Selected Bond	Bond Distance (Å) in $[(R,R)\text{-TMCDA}]\cdot\text{Na}(\mu\text{-TMP})(\mu\text{-}^t\text{Bu})\text{Zn}(^t\text{Bu})$ , <b>98</b>
Na1–N1	2.506(2)
Na1–N2	2.452(2)
Na1–N3	2.388(2)
Na1···C21	2.798(2)
Zn1–N3	2.055(2)
Zn1–C20	2.104(2)
Zn1–C24	2.078(3)

**Table 3.9** Key bond distances within  $[(R,R)\text{-TMCDA}]\cdot\text{Na}(\mu\text{-TMP})(\mu\text{-}^t\text{Bu})\text{Zn}(^t\text{Bu})$ , **98**.

Selected Angle	Bond Angle (°) in $[(R,R)\text{-TMCDA}]\cdot\text{Na}(\mu\text{-TMP})(\mu\text{-}^t\text{Bu})\text{Zn}(^t\text{Bu})$ , <b>98</b>
N1–Na1–N2	72.49(7)
N1–Na1–N3	136.76(8)
N2–Na1–N3	144.51(8)
N3–Zn1–C20	116.31(11)
N3–Zn1–C24	125.74(8)
C20–Zn1–C24	117.78(12)
Na1–N3–Zn1	97.87(8)

**Table 3.10** Key bond angles within  $[(R,R)\text{-TMCDA}]\cdot\text{Na}(\mu\text{-TMP})(\mu\text{-}^t\text{Bu})\text{Zn}(^t\text{Bu})$ , **98**.

The presence of the long Na1···C21 contact [2.798(2) Å] in **98** causes the formation of a four-element, five-membered (NaNZnCC) ring system. Discounting this undoubtedly weak Na···C interaction, the total for the angles around the Na centre is 353.76°, suggesting that with respect to the N atoms, the metal's coordination sphere is much closer to planar (360°) than pyramidal (328.5°). Including the Na1···C21 interaction suggests that the geometry is therefore distorted trigonal pyramidal rather than tetrahedral. The Zn centre is in a near ideal trigonal planar geometry, with the greatest distortion arising from the N3–Zn1–C20 angle

[116.31(11)°], which has to narrow to allow the Na1...C21 agostic interaction [summed angles at Zn, 359.83°; range, 116.31(11)-125.74(8)°].

The bond distances within the respective five-membered bimetallic rings for **98** and the TMEDA analogue **38** are essentially identical within experimental error; however significant differences are observed in the angles surrounding the Na centre – the N1–Na1–N2, N1–Na1–N3 and N2–Na1–N3 angles in **98** are 72.49(7), 136.78(8) and 144.51(8)° respectively, whereas the corresponding angles in **38** are 76.4(2), 138.5(2) and 137.8(2)° respectively – as expected, the Na–N<sub>diamine</sub> bite angle (N1–Na1–N2) is wider (by 3.91°) in **38** due to the slightly less steric demanding nature of TMEDA *versus* (*R,R*)-TMCDA; of the other two angles detailed, the greatest difference is observed for the N2–Na1–N3 angle, which is 6.71° more obtuse in **98**.

Complex **98** constitutes only the second example of (*R,R*)-TMCDA being successfully incorporated within the molecular framework of an alkali metal/zinc synergic system (or indeed any alkali metal/divalent metal synergic system). In addition, it is a rare (*R,R*)-TMCDA adduct of sodium, and perhaps most significantly, it is a chiral variant of an important utility ate base.

The synthesis and characterisation of the (–)-sparteine and (*R,R*)-TMCDA alkali metal zincates laid down the foundations for the investigation into incorporating these chiral diamines into alkali metal magnesiate systems. The results from these studies will now follow.

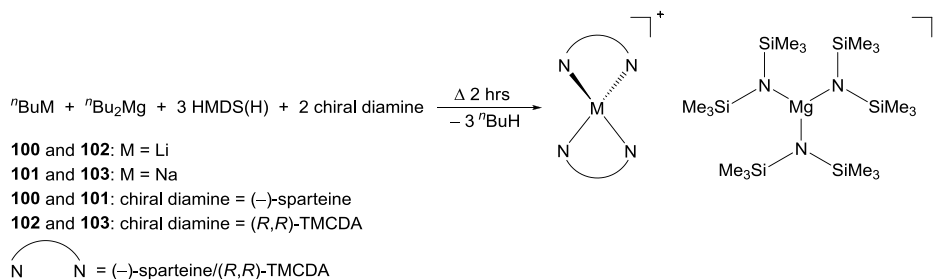
## 3.2 Alkali Metal Tris(HMDS) Magnesiates Containing Chiral Diamine

### Donor Ligands

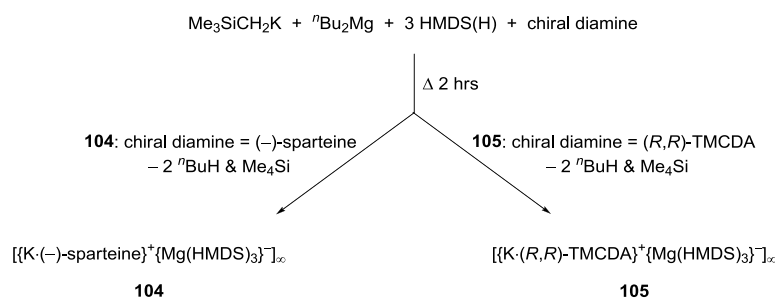
Striving to develop a new chiral avenue in the area of alkali metal magnesiate chemistry we herein report the synthesis and structural characterisation of a series of HMDS alkali metal magnesiates featuring the chiral diamines (–)-sparteine or (*R,R*)-TMCDA as supporting ligands.<sup>[248]</sup>

Six alkali metal tris(HMDS) magnesiate complexes containing the chiral diamine ligands have been prepared and characterised in both the solid- and solution-state. Four of the complexes have a solvent-separated ion pair composition of the form [M(chiral diamine)<sub>2</sub>]<sup>+</sup>[Mg(HMDS)<sub>3</sub>]<sup>–</sup> [M = Li for **100** and **102**, Na for **101** and **103**; chiral diamine = (–)-sparteine for **100** and **101**, (*R,R*)-TMCDA for **102** and **103**] (Scheme 3.2), and two have a

contacted ion pair composition of the form  $[\{K \cdot \text{chiral diamine}\}^+ \{\text{Mg}(\text{HMDS})_3\}^-]_\infty$  [chiral diamine = (-)-sparteine for **104**, (*R,R*)-TMCDA for **105**] (Scheme 3.3).



Scheme 3.2 Synthesis of complexes **100-103**.



Scheme 3.3 Synthesis of complexes **104** and **105**.

In the solid-state, the coordination geometry seen for complexes **100-103** is essentially identical, with the lithium or sodium cation sequestered by the respective chiral diamine and the previously reported anion consisting of three HMDS ligands coordinated to a magnesium centre. As such, complexes **100-103** are the first structurally characterised complexes in which the alkali metal is sequestered by two molecules of either of the chiral diamines (-)-sparteine (**100** and **101**) or (*R,R*)-TMCDA (**102** and **103**). In addition, complex **103** is a rare (*R,R*)-TMCDA adduct of sodium. In the solid-state, complexes **104** and **105** exist as polymeric arrays of  $[\{K \cdot \text{chiral diamine}\}^+ \{\text{Mg}(\text{HMDS})_3\}^-]_2$  dimeric subunits, with **104** adopting a two-dimensional net arrangement and **105** a linear arrangement. As such, complexes **104** and **105** appear to be the only structurally characterised complexes in which the chiral diamines (-)-sparteine (**104**) or (*R,R*)-TMCDA (**105**) have been incorporated within a polymeric framework. In addition, prior to this work, no (-)-sparteine or (*R,R*)-TMCDA adducts of potassium had been reported.

### 3.2.1 Complexes **100-103**

The synthetic routes to **100-103** are summarised in Scheme 3.2. *n*-Butyllithium (for **100** and **102**) or *n*-butylsodium (for **101** and **103**) was mixed with one molar equivalent of di-*n*-butylmagnesium in hexane solution, and reacted with three molar equivalents of HMDS(H). To ensure complete amination of the *s*-block organometallics, these mixtures were heated to

reflux for two hours before two molar equivalents of (–)-sparteine (for **100** and **101**) or of (*R,R*)-TMCDA (for **102** and **103**) were added, causing the precipitation of a white solid from solution. For **100**, **102** and **103**, the addition of toluene was necessary to produce a homogeneous solution and for **101**, a neat toluene solution was required to achieve homogeneity. Colourless crystals of the product grew from the solution at ambient temperature for **100** and by slowly cooling the Schlenk tube to ambient temperature from a hot water-filled Dewar flask for **101-103**.

Owing to the generality of the anion in this series of complexes, and having previously been reported within other alkali metal magnesiate complexes (detailed in chapter 2, section 2.3), only the solid-state structures of the cations of complexes **100-103** will be discussed.

X-ray crystallographic analysis reveals that **100** crystallises in the orthorhombic system, space group  $P2_12_12_1$ . The molecular structure of its cation (Figure 3.11) is composed of two (–)-sparteine molecules which coordinate in their usual bidentate fashion<sup>[141, 148-150, 152, 154-156]</sup> to the lithium centre (*i.e.*, the lithium metal centre is four coordinate). To the best of our knowledge, no (–)-sparteine adducts of alkali metals have been prepared thus far in which the metal centre is sequestered by two (–)-sparteine molecules; hence the cation of **100** as well as that of **101** are unique in this respect. Table 3.11 and Table 3.12 detail the key bond distances and bond angles respectively.

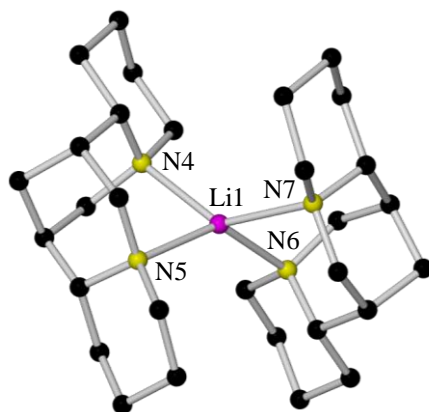


**Figure 3.11** Molecular structure of the cation of  $[\text{Li}\{(-)\text{-sparteine}\}_2]^+[\text{Mg}(\text{HMDS})_3]^-$ , **100**. H atoms are omitted for clarity.

Selected Bond	Bond Distance (Å) in $[\text{Li}\{(-)\text{-sparteine}\}_2]^+[\text{Mg}(\text{HMDS})_3]^-$ , <b>100</b>
Li1–N4	2.206(4)
Li1–N5	2.205(4)
Li1–N6	2.211(4)
Li1–N7	2.271(4)

**Table 3.11** Key bond distances within the cation of  $[\text{Li}\{(-)\text{-sparteine}\}_2]^+[\text{Mg}(\text{HMDS})_3]^-$ , **100**.

Selected Angle	Bond Angle (°) in [Li{(-)-sparteine} <sub>2</sub> ] <sup>+</sup> [Mg(HMDS) <sub>3</sub> ] <sup>-</sup> , <b>100</b>
N4–Li1–N5	84.65(13)
N4–Li1–N6	113.04(16)
N4–Li1–N7	135.15(17)
N5–Li1–N6	135.92(17)
N5–Li1–N7	112.50(16)
N6–Li1–N7	83.79(12)

**Table 3.12** Key bond angles within the cation of [Li{(-)-sparteine}<sub>2</sub>]<sup>+</sup>[Mg(HMDS)<sub>3</sub>]<sup>-</sup>, **100**.

As detailed in chapter 1, section 1.6.1, complexes in which one (-)-sparteine molecule coordinates to a lithium centre have recently been reported by Strohmman *et al.*, including the first monomeric butyllithium complex [tBuLi·(-)-sparteine],<sup>[149]</sup> **42**, and by Stalke *et al.* who, on forming the dimeric structure [Me<sub>3</sub>SiCH<sub>2</sub>Li·(-)-sparteine]<sub>2</sub>,<sup>[156]</sup> **51**, were able to deaggregate the hexameric aggregate of trimethylsilylmethylithium.<sup>[251]</sup>

The mean Li–N bond distance within cation **100** (2.223 Å) lies in the range of those complexes where the Li centre is only coordinated to one (-)-sparteine molecule (range of mean Li–N bond distances, 2.006–2.234 Å),<sup>[141, 148–150, 152, 154–156]</sup> and, as expected the greatest distortion from an ideal tetrahedral geometry for the Li centre [sum of angles, 665.05°; range of angles, 83.79(12)–135.92(17)°] arises due to the (-)-sparteine–Li bite angles (mean angle, 84.23°). This is in agreement with the mean bite angles (range, 82.22–87.74°) of the aforementioned complexes independently characterised by Strohmman and Stalke, which also have distorted tetrahedral environments for their Li centres.<sup>[141, 148–150, 152, 154–156]</sup> A toluene solvated phase of **100** was also isolated and characterised by single-crystal diffraction. No significant structural differences were observed between the molecular geometries of the two phases and thus selected crystallographic and refinement parameters for the solvated phase are included only in the experimental section (chapter 5, section 5.3.19).

X-ray crystallographic studies reveal that **101** crystallises in the orthorhombic system, space group *P*2<sub>1</sub>2<sub>1</sub>2<sub>1</sub>. The molecular structure of its cation (Figure 3.12) bears a close resemblance to that of its lithium congener **100**, despite the difference in size between the alkali metals. Within the asymmetric unit of **101** there are two independent sets of [Na{(-)-sparteine}<sub>2</sub>]<sup>+</sup>[Mg(HMDS)<sub>3</sub>]<sup>-</sup> ions; however, the differences in the dimensions of the two sets of ions are negligible, and thus Table 3.13 and Table 3.14 detail the key bond distances and angles respectively of only one of the independent cations.



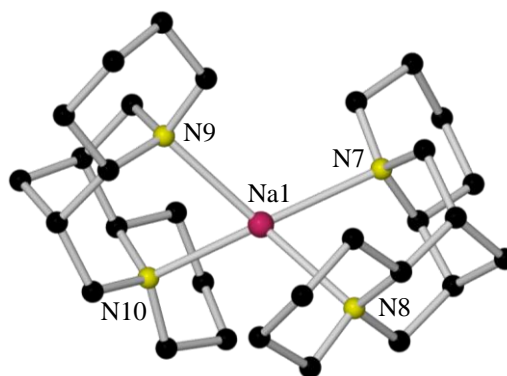


**Figure 3.12** Molecular structure of the cation of  $[\text{Na}\{(-)\text{-sparteine}\}_2]^+[\text{Mg}(\text{HMDS})_3]^-$ , **101**. H atoms and solvent of crystallisation (toluene) are omitted and only one of two similar molecules in the asymmetric unit shown for clarity.

Selected Bond	Bond Distance (Å) in $[\text{Na}\{(-)\text{-sparteine}\}_2]^+[\text{Mg}(\text{HMDS})_3]^-$ , <b>101</b>
Na1–N7	2.478(4)
Na1–N8	2.460(4)
Na1–N9	2.452(4)
Na1–N10	2.455(4)

**Table 3.13** Key bond distances within the cation of  $[\text{Na}\{(-)\text{-sparteine}\}_2]^+[\text{Mg}(\text{HMDS})_3]^-$ , **101**.

Selected Angle	Bond Angle (°) in $[\text{Na}\{(-)\text{-sparteine}\}_2]^+[\text{Mg}(\text{HMDS})_3]^-$ , <b>101</b>
N7–Na1–N8	74.60(12)
N7–Na1–N9	114.96(13)
N7–Na1–N10	143.49(15)
N8–Na1–N9	143.46(15)
N8–Na1–N10	118.65(14)
N9–Na1–N10	75.84(13)

**Table 3.14** Key bond angles within the cation of  $[\text{Na}\{(-)\text{-sparteine}\}_2]^+[\text{Mg}(\text{HMDS})_3]^-$ , **101**.

Cation **101** is only the third complex to be reported thus far which incorporates both sodium and (-)-sparteine, the preceding two complexes being  $[\{(-)\text{-sparteine}\} \cdot \text{Na}(\mu\text{-TMP})(\mu\text{-}^n\text{Bu})\text{Mg}(\text{TMP})]$ ,<sup>[162]</sup> **52** and the previously presented (section 3.1.1) zincate analogue of **52**,  $[\{(-)\text{-sparteine}\} \cdot \text{Na}(\mu\text{-TMP})(\mu\text{-}^n\text{Bu})\text{Zn}(^t\text{Bu})]$ , **96** [where in each complex the Na centre is only coordinated to one (-)-sparteine molecule]. The mean Na–N<sub>(-)-sparteine</sub> bond distance in the cation of **101** (2.461 Å) is in agreement with that in **52** (2.499 Å), and as is the case for the sodium magnesiate, the Na centre adopts a distorted tetrahedral environment here [summed angles at Na, 671.00°; range of angles, 74.60(12)–143.49(15)°]. As expected, this is also the case on comparing the cation of **101** with **96** (mean Na–N<sub>(-)-sparteine</sub> bond distance, 2.501 Å). Due to the (-)-sparteine molecule being slightly further away from the Na centres in complexes **52** and **96** compared to the cation of **101**, the (-)-sparteine–Na bite angle is

slightly more acute in **52** [72.59(6)°] and **96** [72.69(13)°] than in **101** [mean (–)-sparteine–Na bite angle, 75.22°].

The mean M–N bond distance of cation **101** is greater than that of its lithium analogue **100** (mean bond distance, 2.223 Å), due to the larger size of the metal centre, and as expected, the greatest distortion from an ideal tetrahedral geometry for the Na centre arises due to the (–)-sparteine–alkali metal bite angles, which in keeping with the larger size of the metal centre, are 9° more acute in **101** than in **100** (mean angles, 75.22 and 84.23° respectively).

X-ray crystallographic analysis reveals that **102** crystallises in the monoclinic system, space group  $P2_1$ . The molecular structure of its cation (Figure 3.13) is composed of two (*R,R*)-TMCDA molecules which chelate in a terminal fashion to a lithium centre (*i.e.*, the lithium metal centre is four coordinate), similar to the arrangement often observed in alkali metal complexes of its achiral relative TMEDA.<sup>[113, 116, 125, 210, 212-215]</sup> As for **101**, within the asymmetric unit of **102** there are two independent sets of  $[\text{Li}\{(R,R)\text{-TMCDA}\}_2]^+[\text{Mg}(\text{HMDS})_3]^-$  ions. Again as the differences in the dimensions of the two sets of ions are negligible, Table 3.15 and Table 3.16 detail the key bond distances and angles respectively of only one of the independent cations.

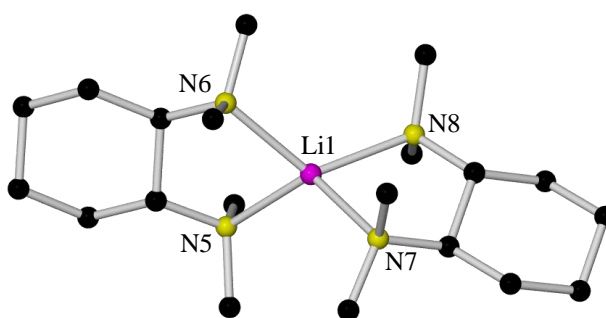


**Figure 3.13** Molecular structure of the cation of  $[\text{Li}\{(R,R)\text{-TMCDA}\}_2]^+[\text{Mg}(\text{HMDS})_3]^-$ , **102**. H atoms and solvent of crystallisation (toluene) are omitted and only one of two similar molecules in the asymmetric unit shown for clarity.

Selected Bond	Bond Distance (Å) in $[\text{Li}\{(R,R)\text{-TMCDA}\}_2]^+[\text{Mg}(\text{HMDS})_3]^-$ , <b>102</b>
Li1–N5	2.153(5)
Li1–N6	2.129(6)
Li1–N7	2.133(6)
Li1–N8	2.152(6)

**Table 3.15** Key bond distances within the cation of  $[\text{Li}\{(R,R)\text{-TMCDA}\}_2]^+[\text{Mg}(\text{HMDS})_3]^-$ , **102**.

Selected Angle	Bond Angle (°) in [Li{(R,R)-TMCDA} <sub>2</sub> ] <sup>+</sup> [Mg(HMDS) <sub>3</sub> ] <sup>-</sup> , <b>102</b>
N5–Li1–N6	84.7(2)
N5–Li1–N7	119.3(3)
N5–Li1–N8	127.1(3)
N6–Li1–N7	125.2(3)
N6–Li1–N8	122.5(3)
N7–Li1–N8	83.4(2)

**Table 3.16** Key bond angles within the cation of [Li{(R,R)-TMCDA}<sub>2</sub>]<sup>+</sup>[Mg(HMDS)<sub>3</sub>]<sup>-</sup>, **102**.

On searching the CCDC we can find no precedent of a lithium centre (or indeed any alkali metal) binding simultaneously to two (R,R)-TMCDA ligands. As detailed in chapter 1, section 1.6.2, complexes in which one (R,R)-TMCDA molecule coordinates to a lithium centre have recently been reported by Strohmann *et al.*,<sup>[78, 148, 169-171, 173]</sup> including [tBuLi·(R,R)-TMCDA],<sup>[78]</sup> **53**, which was the second structurally characterised alkyllithium monomer bearing a saturated hydrocarbon [the first being [tBuLi·(-)-sparteine],<sup>[149]</sup> **42**]. Comparing the mean Li–N bond distance in this bis(chiral) ligated cation **102** (2.142 Å) with its mono-ligated variants (range, 2.055–2.256 Å)<sup>[78, 148, 169-171, 173]</sup> reveals no significant differences. As expected, the greatest distortion from an ideal tetrahedral geometry for the Li centre in **102** [sum of angles, 662.20°; range, 83.4(2)–127.1(3)°] arises due to the (R,R)-TMCDA–Li bite angles (mean angle, 84.05°).

In comparison to its (-)-sparteine analogue (cation **100**), the cation of **102** has a slightly shorter mean Li–N bond distance and a virtually identical diamine–Li bite angle (2.142 Å vs. 2.223 Å; 84.05° vs. 84.23° respectively). The difference in these parameters is perhaps due to the less sterically demanding nature of (R,R)-TMCDA when compared with (-)-sparteine.

Turning to **103**, it crystallises in the orthorhombic system, space group *P*2<sub>1</sub>2<sub>1</sub>2<sub>1</sub>. Akin to its lithium congener cation **102**, the cation of **103** (Figure 3.14) is composed of two (R,R)-TMCDA molecules which chelate terminally to the sodium centre. Table 3.17 and Table 3.18 detail the key bond distances and bond angles respectively.

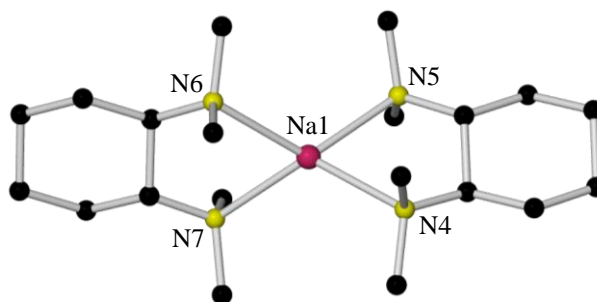


**Figure 3.14** Molecular structure of the cation of [Na{(R,R)-TMCDA}<sub>2</sub>]<sup>+</sup>[Mg(HMDS)<sub>3</sub>]<sup>-</sup>, **103**. H atoms and solvent of crystallisation (toluene) are omitted for clarity.

Selected Bond	Bond Distance (Å) in [Na{(R,R)-TMCDA} <sub>2</sub> ] <sup>+</sup> [Mg(HMDS) <sub>3</sub> ] <sup>-</sup> , <b>103</b>
Na1–N4	2.310(5)
Na1–N5	2.312(3)
Na1–N6	2.357(3)
Na1–N7	2.329(3)

**Table 3.17** Key bond distances within the cation of [Na{(R,R)-TMCDA}<sub>2</sub>]<sup>+</sup>[Mg(HMDS)<sub>3</sub>]<sup>-</sup>, **103**.

Selected Angle	Bond Angle (°) in [Na{(R,R)-TMCDA} <sub>2</sub> ] <sup>+</sup> [Mg(HMDS) <sub>3</sub> ] <sup>-</sup> , <b>103</b>
N4–Na1–N5	76.05(12)
N4–Na1–N6	133.06(14)
N4–Na1–N7	122.95(15)
N5–Na1–N6	121.84(10)
N5–Na1–N7	136.84(10)
N6–Na1–N7	75.85(9)

**Table 3.18** Key bond angles within the cation of [Na{(R,R)-TMCDA}<sub>2</sub>]<sup>+</sup>[Mg(HMDS)<sub>3</sub>]<sup>-</sup>, **103**.

Cation **103** is a rare (*R,R*)-TMCDA adduct of sodium, the previously presented (*R,R*)-TMCDA coordinated sodium zincates, [{(*R,R*)-TMCDA}·Na(μ-TMP)(μ-<sup>*n*</sup>Bu)Zn(<sup>*t*</sup>Bu)], **97** (section 3.1.2) and [{(*R,R*)-TMCDA}·Na(μ-TMP)(μ-<sup>*t*</sup>Bu)Zn(<sup>*t*</sup>Bu)], **98** (section 3.1.3) being the only other complexes to contain both (*R,R*)-TMCDA and sodium to date. The mean Na–N bond distance in the cation of **103** (2.327 Å) is in agreement with that in **97** and **98** (2.450 and 2.479 Å respectively), and as is the case for the sodium zincates, the Na centre adopts a distorted tetrahedral environment here [summed angles at Na, 666.59°; range, 75.85(9)-136.84(10)°]. Due to the (*R,R*)-TMCDA molecule being slightly further away from the Na centres in complexes **97** and **98** compared to the cation of **103**, the (*R,R*)-TMCDA–Na bite angle is slightly more acute in **97** [73.08(12)°] and **98** [72.49(7)°] than **103** [mean (*R,R*)-TMCDA–Na bite angle, 75.95°].

As expected, the mean M–N bond distance of cation **103** is greater than that of its lithium analogue **102** (mean bond distance, 2.142 Å) and as anticipated, the greatest distortion from an ideal tetrahedral geometry for the Na centre arises due to the (*R,R*)-TMCDA–Na bite angles, which in keeping with the larger size of the metal centre, are approximately 8° more acute in **103** than in **102** (mean angles, 75.95 and 84.05° respectively).

In comparison to its (–)-sparteine analogue (cation **101**), the cation of **103** has a shorter mean Na–N bond distance and a slightly more open diamine–Na bite angle (2.327 Å vs. 2.461 Å; 75.95° vs. 75.22° respectively), again emphasising the slightly reduced steric demands of (*R,R*)-TMCDA versus (–)-sparteine.

Comparing the cations of complexes **100-103** to those of their TMEDA analogues [complexes **88** and **89** (chapter 2, section 2.3)] reveals no significant differences, despite the variation in the steric demands of the three ligands [TMEDA, (*R,R*)-TMCDA and (–)-sparteine]; however, the structural parameters do reflect the change in moving from a lithium metal centre to a sodium metal centre. To elaborate, the mean Li–N bond distance in complexes **89**, **100** and **102** is 2.116, 2.223 and 2.142 Å respectively, and the mean bite angle of their respective ligands is 87.90, 84.23 and 84.05°. Moving to the Na complexes, the mean Na–N bond distance in complexes **88**, **101** and **103** is 2.517, 2.461 and 2.327 Å respectively, and the mean bite angle of their respective ligands is 74.57, 75.22 and 75.95°. Due to the larger size of the sodium metal centre in comparison to the lithium metal centre, the mean M–N bond distances are greater and the mean bite angles more acute in the sodium complexes.

Turning to solution studies, complexes **100-103** were dissolved in C<sub>6</sub>D<sub>6</sub>, d<sub>8</sub>-toluene and d<sub>8</sub>-THF solutions and examined by <sup>7</sup>Li (**100** and **102**), <sup>1</sup>H, <sup>13</sup>C, COSY and HSQC NMR spectroscopy. Focusing on the (–)-sparteine complexes, **100** and **101** in arene solution, the <sup>1</sup>H and <sup>13</sup>C NMR spectra obtained from the respective experiments were complex showing a forest of resonances due to the number of chemically distinct aliphatic hydrogen and carbon atoms present in the donor molecule (*vide supra*). The key features associated with the diamine ligand in both sets of these spectra are that the resonances are broader and differ slightly from those for the free ligand. Hence, (–)-sparteine appears to remain at least partially coordinated to the respective metal centres in arene solution. The HMDS region of these spectra is rather more complex than initially envisaged. If the solid-state structures were to be retained in solution, then a single resonance should be observed. This is indeed the scenario which is encountered when d<sub>8</sub>-THF solution is used. Although the spectra appear to indicate that a solvent-separated ion pair structure is forthcoming, it is obvious that the solid-state structures are not retained in THF solution as the resonances associated with the (–)-sparteine ligand exactly match those of free (–)-sparteine, indicating that the diamine has been displaced by d<sub>8</sub>-THF. This ligand displacement therefore implies that the chiral information associated with the alkali metal centres has been lost. As only one Si(CH<sub>3</sub>)<sub>3</sub> resonance is observed, the likely solution-state structures of these complexes are [M(d<sub>8</sub>-THF)<sub>x</sub>]<sup>+</sup>[Mg(HMDS)<sub>3</sub>]<sup>–</sup> (where M is Li or Na for **100** and **101** respectively). In d<sub>8</sub>-toluene solution (300 K) at least three chemically distinct Si(CH<sub>3</sub>)<sub>3</sub> resonances are observed, indicating much more complex solution dynamics. To shed light on these solution dynamics we undertook a variable temperature NMR spectroscopic study on a d<sub>8</sub>-toluene solution of **101** (Figure 3.15). At high temperature (353 K) one sharp, distinct resonance (0.26 ppm) was

observed. On decreasing the acquisition temperature, a broadening of this resonance and a gradual downfield shift was noted (*e.g.*, at 313 K, 0.44 ppm). As alluded to earlier, at 300 K, the first sign of decoalescence was noted [resonances at 0.49, 0.54 (br) and 0.64 ppm]. On cooling the solution further (253 K), these signals sharpened (0.75, 0.72 and 0.64 ppm). We believe these data may correspond to an equilibrium occurring between a solvent-separated and a contacted ion pair species. This will be discussed in more detail during the discussion of the solution structures of **102** and **103**.

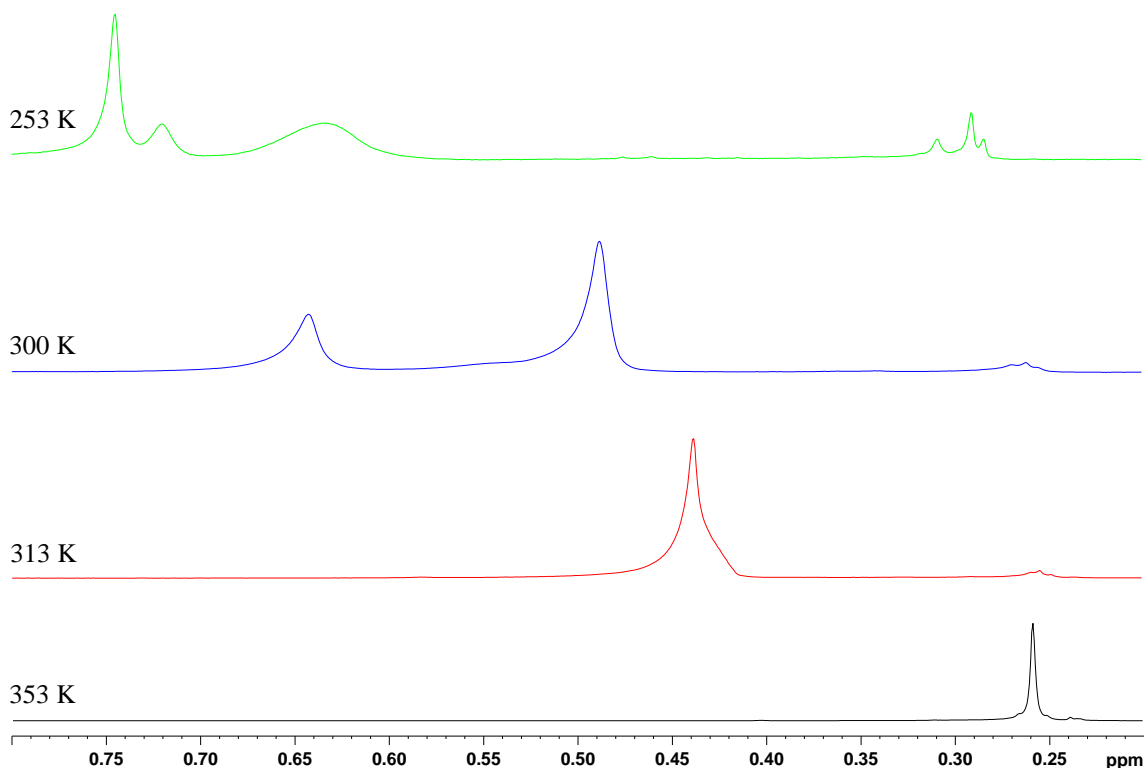
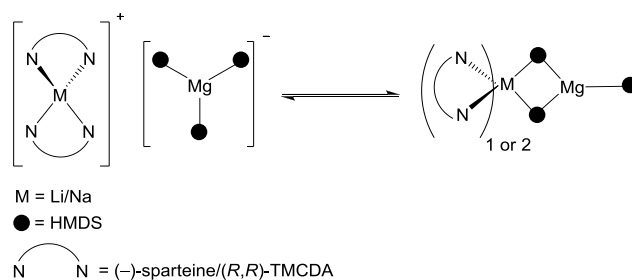


**Figure 3.15** Variable temperature  $^1\text{H}$  NMR spectra of **101** in  $\text{C}_6\text{D}_5\text{CD}_3$ .

The solutions of (*R,R*)-TMCDA-containing complexes **102** and **103**, behave similarly to their (–)-sparteine analogues. To emphasise, in  $d_8$ -toluene solution, the  $^1\text{H}$  NMR spectra reveal three unique  $\text{Si}(\text{CH}_3)_3$  resonances at 0.65, 0.39, 0.34 and 0.64, 0.39, 0.44 ppm for **102** and **103** respectively, and the diamine resonances are shifted from those of the free diamine. By comparing the  $^1\text{H}$  NMR spectra with a series of standards [*e.g.*, HMDS(H), LiHMDS, NaHMDS and  $\text{Mg}(\text{HMDS})_2$ ] we can exclude the formation of any of these compounds in our systems. The  $^7\text{Li}$  NMR spectra ( $d_8$ -toluene) of **100** and **102** show that there are two Li species in solution (1.34 and 1.08 and 1.48 and  $-0.62$  ppm for **100** and **102** respectively). This fact, coupled with the presence of three  $\text{Si}(\text{CH}_3)_3$  resonances in its corresponding  $^1\text{H}$  NMR spectrum, leads us to believe that a dynamic process is occurring in solution. Like **100** and **101**, the  $^1\text{H}$  NMR spectra for arene solutions of **102** and **103** showed that the (*R,R*)-TMCDA resonances were broad. In addition, due to the simpler structure of the diamine, it was clear

that only one type of (*R,R*)-TMCDA ligand was present. It is likely that on dissociation in  $d_8$ -toluene solution, the solvent-separated species (**100-103**) exist in equilibrium with their respective contacted ion pair, namely  $[(\text{diamine})_x \cdot \text{M}(\mu\text{-HMDS})_2\text{Mg}(\text{HMDS})]$  (Scheme 3.4).



**Scheme 3.4** Possible equilibrium between solvent-separated ion pair (akin to structures of **100-103**) and contacted ion pair structures in  $d_8$ -toluene solution.

The three different HMDS environments can be accounted for by one resonance corresponding to the three HMDS ligands present in the respective solvent-separated ion pair species, and the other two signals (which are in a 2 : 1 ratio) corresponding to the distinct bridging and terminal HMDS ligands present in the particular contacted ion pair structure. The most downfield resonance (0.65 for **102** and 0.64 for **103** respectively) can be attributed to the solvent-separated ion-pair structure. The ratio of the ‘solvent-separated’ resonance to the other two resonances alters depending on the concentration of the solution. Interestingly and surprisingly, for **102** this contacted ion pair structure appears to form solely in  $\text{C}_6\text{D}_6$  solution [*i.e.*, only two  $\text{Si}(\text{CH}_3)_3$  resonances observed], with the seeming absence of the ‘solid-state’ solvent-separated species. This is corroborated by the  $^7\text{Li}$  NMR spectrum of **102** which reveals a single Li environment (1.45 ppm).

Turning to  $d_8$ -THF solutions of **102** and **103**, the  $^1\text{H}$  NMR spectra reveal a similar scenario to that encountered for their (-)-sparteine analogues; that is a solvent-separated structure is present, with the cation being coordinated to  $d_8$ -THF molecules rather than the diamine ligands. Full NMR details for complexes **100-103** can be found in chapter 5, sections 5.3.19-5.3.22.

### 3.2.2 Complexes **104** and **105**

**Scheme 3.3** summarises the synthetic routes to **104** and **105**. An equimolar mixture of (trimethylsilylmethyl)potassium and di-*n*-butylmagnesium was reacted with three molar equivalents of HMDS(H) in hexane solution. These mixtures were heated to reflux for two hours before one molar equivalent of (-)-sparteine (for **104**) or of (*R,R*)-TMCDA (for **105**) was added, precipitating a white solid from solution. The precipitate dissolved on heating for **105**; however for **104**, the addition of toluene was required to produce a homogeneous

solution. In both cases (**104** and **105**), colourless crystals grew from the solution by slowly cooling the Schlenk tube to ambient temperature from a hot water-filled Dewar flask.

X-ray crystallographic analysis reveals that **104** crystallises in the monoclinic system, space group  $P2_1$ . In marked contrast to the previously discussed complexes, complex **104** is a *contacted* ion pair alkali metal magnesiate (Figure 3.16).

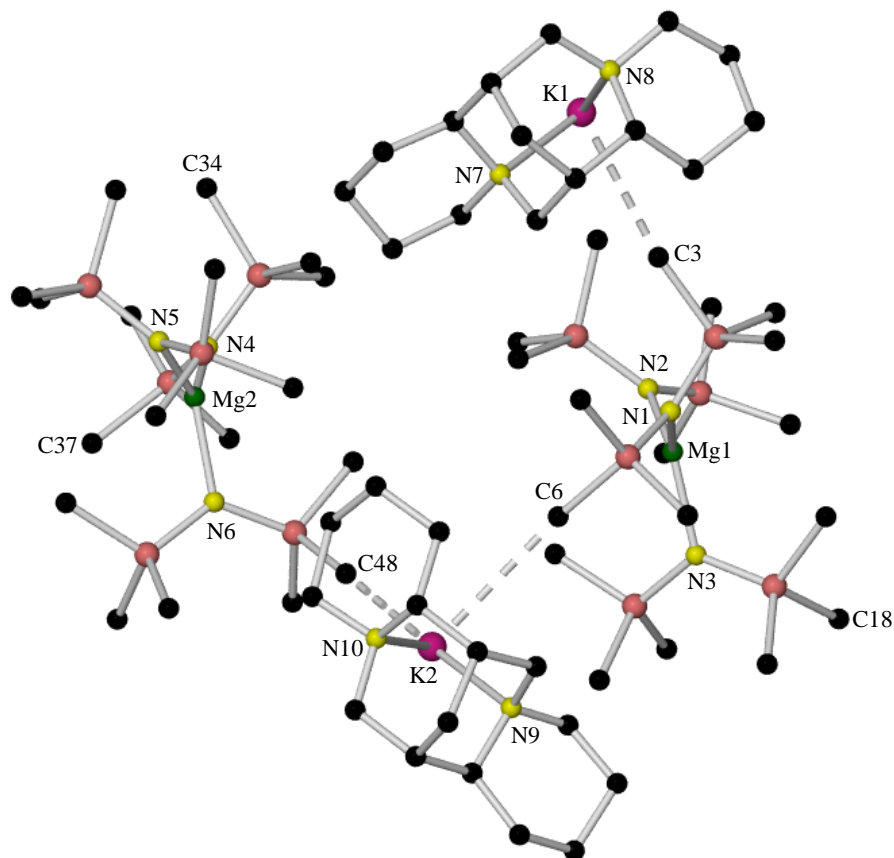


**Figure 3.16** Asymmetric unit of  $[\{K\cdot(-)\text{-sparteine}\}^+\{Mg(HMDS)_3\}^-]_\infty$ , **104**, which polymerises through  $K1\cdots C18$ ,  $K1\cdots C37$  and  $K2\cdots C34$ . These interactions and H atoms are omitted for clarity.

Its asymmetric unit contains two  $[\{K\cdot(-)\text{-sparteine}\}^+\{Mg(HMDS)_3\}^-]_2$  ion pairs linked by an agostic-type interaction ( $K2\cdots C6$ ) involving a  $\text{Me}(\text{SiMe}_2)\text{N}$  unit. Both  $Mg(HMDS)_3$  anions interact with the two potassium centres (again through  $K\cdots\text{CH}_3$  agostic interactions) within the asymmetric unit and a third neighbouring potassium centre (*i.e.*, the anions act as  $\mu_3$ -bridges), thus promoting the formation of a polymeric array (Figure 3.17). Table 3.19 and Table 3.20 detail the key bond distances and bond angles respectively.



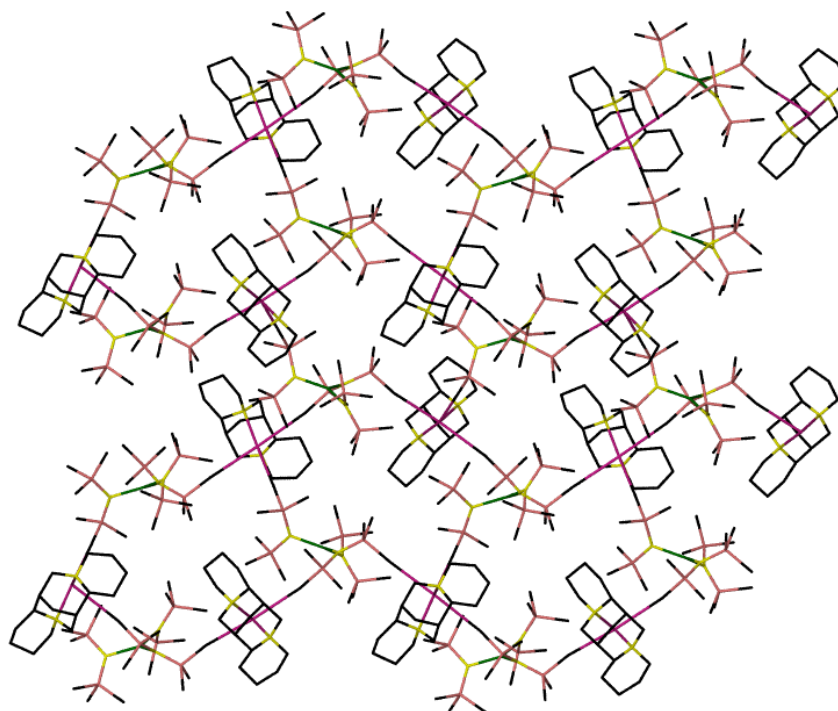


**Figure 3.17** Extended view of  $[\{K \cdot (-)\text{-sparteine}\}^+ \{Mg(HMDS)_3\}^-]_\infty$ , **104**, showing its two-dimensional net arrangement, with each 'hole' in the net consisting of 22 atoms and incorporating three  $[\{K \cdot (-)\text{-sparteine}\}^+ \{Mg(HMDS)_3\}^-]$  units. H atoms are omitted for clarity.

Selected Bond	Bond Distance (Å) in $[\{K \cdot (-)\text{-sparteine}\}^+ \{Mg(HMDS)_3\}^-]_\infty$ , <b>104</b>
K1–N7	2.789(2)
K1–N8	2.877(2)
K1...C3	3.222(3)
K1...C18	3.407(3)
K1...C37	3.297(3)
K2–N9	2.768(2)
K2–N10	2.813(2)
K2...C6	3.448(3)
K2...C34	3.248(3)
K2...C48	3.255(3)
Mg1–N1	2.038(2)
Mg1–N2	2.019(2)
Mg1–N3	2.032(2)
Mg2–N4	2.027(2)
Mg2–N5	2.011(2)
Mg2–N6	2.037(2)

**Table 3.19** Key bond distances within  $[\{K \cdot (-)\text{-sparteine}\}^+ \{Mg(HMDS)_3\}^-]_\infty$ , **104**.

Selected Angle	Bond Angle (°) in [ $\{K\cdot(-)\text{-sparteine}\}^+\{Mg(HMDS)_3\}^-]_\infty$ , <b>104</b>
N7–K1–N8	62.75(6)
N7–K1–C3	93.85(6)
N8–K1–C3	112.71(7)
N9–K2–N10	63.41(6)
N9–K2–C6	87.35(7)
N9–K2–C48	177.33(7)
N10–K2–C6	105.00(7)
N10–K2–C48	118.99(6)
C6–K2–C48	90.79(7)
N1–Mg1–N2	118.80(9)
N1–Mg1–N3	119.59(9)
N2–Mg1–N3	121.57(9)
N4–Mg2–N5	118.55(10)
N4–Mg2–N6	119.25(9)
N5–Mg2–N6	122.15(9)

**Table 3.20** Key bond angles within [ $\{K\cdot(-)\text{-sparteine}\}^+\{Mg(HMDS)_3\}^-]_\infty$ , **104**.

In this polymer, each K atom is five coordinate and bound to two (–)-sparteine N atoms (mean K–N distance, 2.812 Å), and three CH<sub>3</sub> groups [range of K–C distances, 3.222(3)–3.448(3) Å]. Interestingly, there are no K–N<sub>amide</sub> interactions. Figure 3.17 shows the extended structure, which exists as a two-dimensional net. Each ring of the net consists of 22 atoms and incorporates three [ $\{K\cdot(-)\text{-sparteine}\}^+\{Mg(HMDS)_3\}^-]_\infty$  units. To the best of our knowledge, no complexes (alkali metal or indeed any metal) have been prepared thus far in which the chiral diamine (–)-sparteine has been incorporated within a polymeric framework, and in addition, no (–)-sparteine adducts of potassium have been reported thus far; hence **104** is unique in both of these respects. Both solvent-separated and contacted ion pair potassium magnesiate have been previously reported by Mulvey *et al.*. These include, arene- or metallo-arene incorporated contacted ion pair complexes such as [ $\{K(\text{benzene})_2\}^+\{Mg(HMDS)_3\}^-]_\infty$ <sup>[193g]</sup> and [ $\{K[(C_6H_6)_2Cr]_2\}^+\{Mg(HMDS)_3\}^-]_\infty$ <sup>[110a]</sup> and the ferrocene-containing solvent-separated system [ $K(\eta^5\text{-ferrocene})_2(\eta^3\text{-toluene})_2]^+ [Mg(HMDS)_3]^-$ <sup>[193i]</sup>. More recently, Hill has reported the isolation and characterisation of an N-heterocyclic carbene-containing solvent-separated potassium magnesiate, namely [ $K(\text{IPr})_2]^+ [Mg(HMDS)_3]^-$ <sup>[193s]</sup> (where IPr is 1,3-bis(2,6-diisopropylphenyl)-imidazol-2-ylidene). Despite the Mg(HMDS)<sub>3</sub> anion being part of the contacted ion pair structure of **104** the range of N–Mg–N angles [118.6(1)–122.15(9)°] is essentially identical to that found in the solvent-separated structure of **100**.

X-ray crystallographic studies reveal that **105** crystallises in the triclinic system, chiral space group *P*1. As is the case with **104**, complex **105** is a contacted ion pair potassium magnesiate and also akin to **104**, its asymmetric unit contains two crystallographically unique anion-cation pairs, this time of the composition  $[\{K \cdot (R,R)\text{-TMCD A}\}^+ \{Mg(\text{HMDS})_3\}^-]$ . Four  $K \cdots \text{CH}_3$  agostic interactions ( $K1 \cdots C5$ ,  $K1 \cdots C29$ ,  $K2 \cdots C1$  and  $K2 \cdots C32$ ) result in the asymmetric unit adopting a 12-membered  $K_2C_4N_2Si_4$  ring motif (Figure 3.18). Both  $Mg(\text{HMDS})_3$  anions interact with the two potassium centres (via  $K \cdots \text{CH}_3$  agostic interactions) within the asymmetric unit and a third neighbouring potassium centre (*i.e.*, the anions act as  $\mu_3$ -bridges), thus promoting polymerisation (Figure 3.19). Table 3.21 and Table 3.22 detail the key bond distances and bond angles respectively.

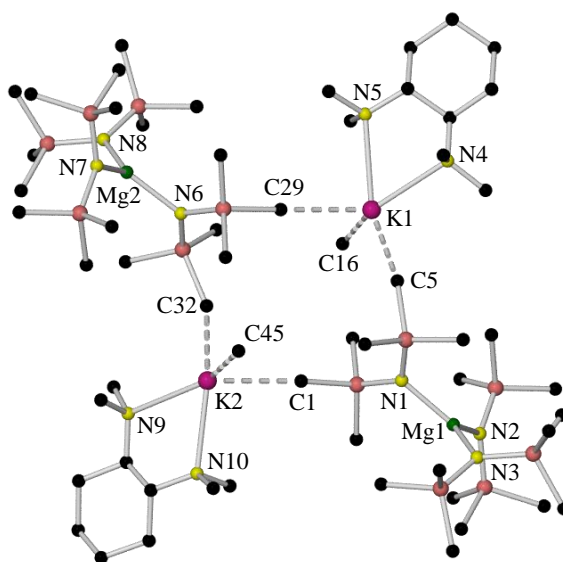


**Figure 3.18** Asymmetric unit of  $[\{K \cdot (R,R)\text{-TMCD A}\}^+ \{Mg(\text{HMDS})_3\}^-]_\infty$ , **105**, which polymerises through  $K1 \cdots C16$  and  $K2 \cdots C45$ . H atoms are omitted for clarity.

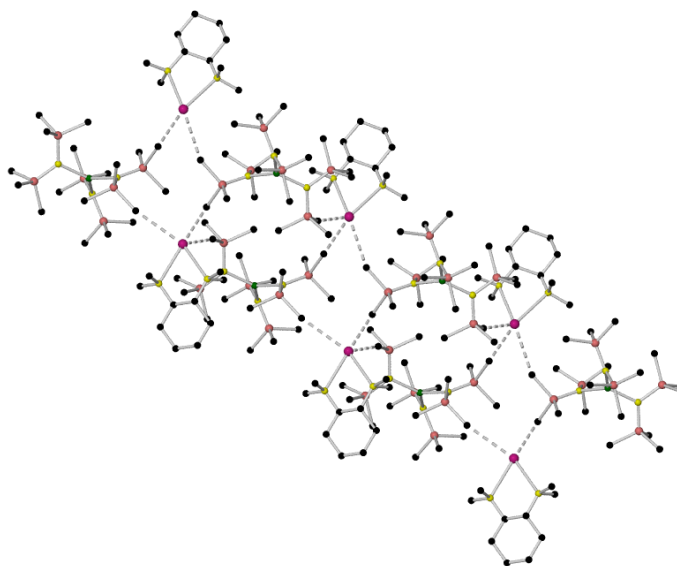


**Figure 3.19** Extended view of  $[\{K \cdot (R,R)\text{-TMCD A}\}^+ \{Mg(\text{HMDS})_3\}^-]_\infty$ , **105**, showing the linear arrangement of three asymmetric units, with alternating large and small rings. H atoms are omitted for clarity.

Selected Bond	Bond Distance (Å) in [ $\{K \cdot (R,R)\text{-TMCDA}\}^+ \{Mg(\text{HMDS})_3\}^- \]_{\infty}$ , <b>105</b>
K1–N4	2.727(2)
K1–N5	2.849(2)
K1...C5	3.368(2)
K1...C16	3.257(4)
K1...C29	3.075(2)
K2–N9	2.767(2)
K2–N10	2.771(2)
K2...C1	3.112(2)
K2...C32	3.684(4)
K2...C45	3.202(4)
Mg1–N1	2.028(2)
Mg1–N2	2.024(2)
Mg1–N3	2.036(2)
Mg2–N6	2.032(2)
Mg2–N7	2.026(2)
Mg2–N8	2.008(2)

**Table 3.21** Key bond distances within [ $\{K \cdot (R,R)\text{-TMCDA}\}^+ \{Mg(\text{HMDS})_3\}^- \]_{\infty}$ , **105**.

Selected Angle	Bond Angle (°) in [ $\{K \cdot (R,R)\text{-TMCDA}\}^+ \{Mg(\text{HMDS})_3\}^- \]_{\infty}$ , <b>105</b>
N4–K1–N5	62.35(5)
N4–K1–C5	90.83(6)
N4–K1–C29	130.01(6)
N5–K1–C5	136.16(6)
N5–K1–C29	88.11(6)
C5–K1–C29	81.14(7)
N9–K2–N10	63.44(5)
N9–K2–C1	126.09(6)
N9–K2–C32	84.14(7)
N10–K2–C1	95.49(6)
N10–K2–C32	126.60(7)
C1–K2–C32	69.70(7)
N1–Mg1–N2	118.83(8)
N1–Mg1–N3	118.84(9)
N2–Mg1–N3	122.32(8)
N6–Mg2–N7	119.91(9)
N6–Mg2–N8	118.69(9)
N7–Mg2–N8	121.38(9)

**Table 3.22** Key bond angles within [ $\{K \cdot (R,R)\text{-TMCDA}\}^+ \{Mg(\text{HMDS})_3\}^- \]_{\infty}$ , **105**.

In this polymer, each K centre is five coordinate and bound to two (*R,R*)-TMCDA N atoms [mean K–N distance, 2.779 Å, which is slightly shorter than the mean K–N distance in **104**, (2.812 Å), perhaps due to the less sterically demanding nature of (*R,R*)-TMCDA when compared with (–)-sparteine], and three CH<sub>3</sub> groups [range of K–C distances, 3.112(2)–3.684(4) Å]. Mirroring the situation in **104**, there are no K–N<sub>amide</sub> interactions. [Figure 3.19](#)

shows the extended structure, which exists as a linear polymeric framework, consisting of alternating ‘small’ 12-atom ( $K_2C_4N_2Si_4$ ) and ‘large’ 16-atom ( $K_2Mg_2C_4N_4Si_4$ ) fused rings. Complex **105** is the first (*R,R*)-TMCDA adduct of potassium and it also appears to represent the only example of a coordination polymer involving this chiral diamine.

Moving to solution studies, complexes **104** and **105** were dissolved in  $d_8$ -THF solution and examined by  $^1H$ ,  $^{13}C$ , COSY and HSQC NMR spectroscopy. In both instances, the polymeric structures are not retained in solution, evidenced by the chemical shifts of the resonances associated with the chiral diamine ligands [(–)-sparteine for **104** and (*R,R*)-TMCDA for **105**], corresponding almost identically to those encountered in the respective free ligands; hence, indicating the formation of a  $d_8$ -THF solvate. Full NMR details can be found in chapter 5, sections 5.3.23-5.3.24.

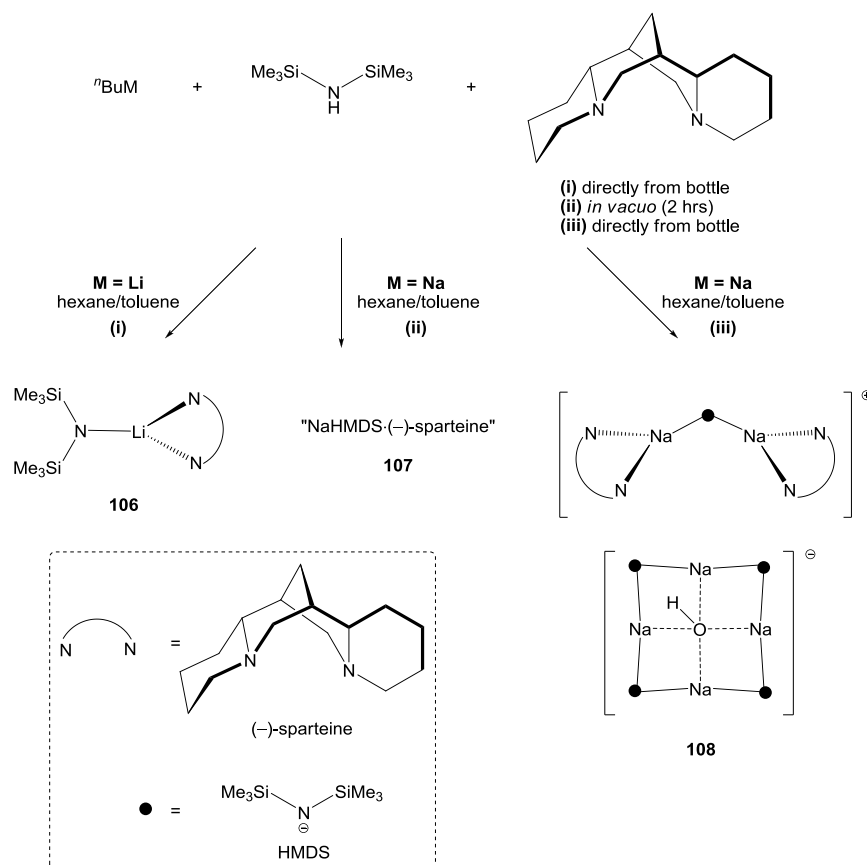
Collectively, the structural data presented for the complexes reported herein, indicate that only one molecule of the diamine [(–)-sparteine or (*R,R*)-TMCDA] is necessary to saturate the K centre (complexes **104** and **105**). This is counterintuitive as the larger size of a K metal centre with respect to a Li and/or Na metal centre would seem to suggest that a K centre should require two or more molecules of the diamine to fill its substantially larger coordination sphere and not only one. However, due to the softer nature of K (*cf.*, Li and Na), more competition from agostic interactions arises, rendering additional K–N interactions unnecessary. Furthermore, the utility of either of the diamines (–)-sparteine or (*R,R*)-TMCDA for complexes **100-103**, in which the metal centre is either Li or Na, does not produce connectivity differences for their corresponding alkali metal magnesiates; however, when K is the alkali metal (in complexes **104** and **105**), changing the diamine dramatically alters the final arrangement of the complex from a supramolecular point of view. Possibly the more sterically demanding nature of (–)-sparteine hinders the closure of the  $K_2C_4N_2Si_4$  ring observed for **105** (Figure 3.18) and therefore gives the final more open polymeric arrangement seen for **104** (Figure 3.17).

Having investigated heterobimetallic systems containing the chiral diamines (–)-sparteine or (*R,R*)-TMCDA, it was also deemed important to study the alkali metal monometallic building blocks of such reagents, specifically chiral diamine adducts of the synthetically important lithium and sodium bis(trimethylsilyl)amides. The results obtained during these studies will now follow.

### 3.3 Reactions of Chiral Diamine Donor Ligands with Alkali Metal HMDS Complexes: Conventional Meets the Unconventional

This section will focus on the ‘conventional’ and ‘unconventional’ complexes obtained on reacting the chiral diamine (–)-sparteine with the synthetically important lithium and sodium bis(trimethylsilyl)amides,<sup>[249]</sup> followed by the discussion of an ‘unconventional’ (*R,R*)-TMCDAs complex obtained in a similar manner, and finally, a (*R,R*)-TMCDAs-containing ‘inverse magnesiato’ complex will be presented.

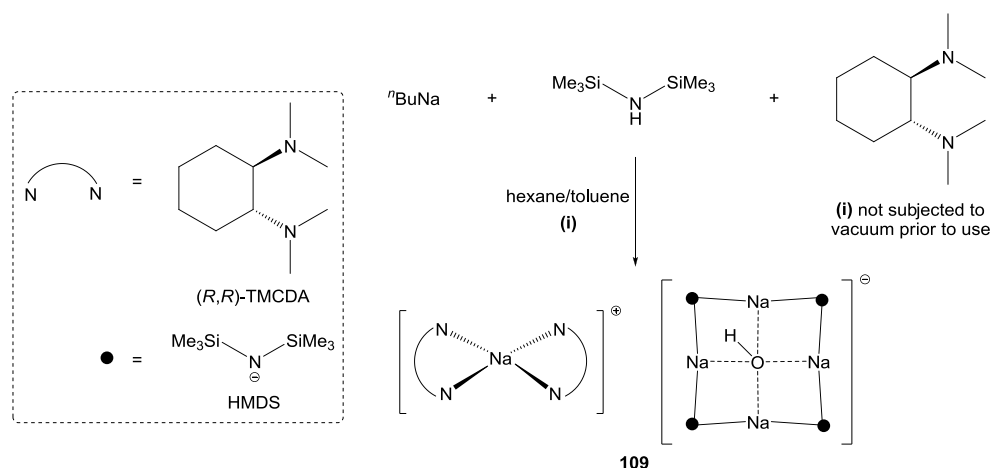
‘Conventional’ (–)-sparteine adducts of lithium and sodium HMDS have been prepared and characterised, [MHMDS·(–)-sparteine] (M = Li for **106**, Na for **107**), along with an unexpected and ‘unconventional’ hydroxyl-incorporated solvent-separated hexanuclear sodium sodiate, [(–)-sparteine·Na(μ-HMDS)Na·(–)-sparteine]<sup>+</sup>[Na<sub>4</sub>(μ-HMDS)<sub>4</sub>(μ<sub>4</sub>-OH)]<sup>–</sup>, **108** – the anion of which is the first inverse crown ether anion to be reported (Scheme 3.5).



Scheme 3.5 Synthesis of complexes **106-108**.

Following this unusual result, a similar complex containing the chiral diamine (*R,R*)-TMCDAs was prepared and characterised, namely the hydroxyl-incorporated solvent-separated pentanuclear sodium sodiate [Na{(*R,R*)-TMCDAs}<sub>2</sub>]<sup>+</sup>[Na<sub>4</sub>(μ-HMDS)<sub>4</sub>(μ<sub>4</sub>-OH)]<sup>–</sup>, **109** – the

anion of which is the same as that in **108**, and thus represents the second inverse crown ether anion to be reported (Scheme 3.6).



Scheme 3.6 Synthesis of complex **109**.

### 3.3.1 (–)-Sparteine Complexes **106-108**

(–)-Sparteine-coordinated **106** was prepared by reacting *n*-butyllithium with an equimolar quantity of HMDS(H) in hexane solution. This mixture was left to stir for 30 minutes, before one molar equivalent of (–)-sparteine was introduced. The addition of toluene was required to produce a homogeneous solution (Scheme 3.5). X-ray quality crystals of **106** precipitated from the hydrocarbon medium at  $-28^\circ\text{C}$ .

In an attempt to prepare a sodium analogue of **106**, *n*-butylsodium was utilised. After stirring the (–)-sparteine and metal amide solution for 30 minutes, a crop of crystals precipitated at ambient temperature within one hour. To our surprise, X-ray crystallographic studies revealed that these crystals were not simple (–)-sparteine adducts of NaHMDS, but an unusual hydroxyl-incorporated sodium sodiate, [(–)-sparteine·Na( $\mu$ -HMDS)Na·(–)-sparteine]<sup>+</sup>[Na<sub>4</sub>( $\mu$ -HMDS)<sub>4</sub>( $\mu_4$ -OH)]<sup>–</sup>, **108**, despite the apparent strict use of an inert atmosphere and Schlenk techniques (Scheme 3.5).

This synthesis was deemed reproducible by checking the unit cell of several batches of the crystalline material. It was assumed that the hydroxide contaminant arose from the reaction of the metal amide mixture with adventitious water which was present in the (–)-sparteine. When (–)-sparteine was subjected to vacuum for two hours prior to use – in an attempt to remove volatiles such as entrained H<sub>2</sub>O – crystals of **108** were not forthcoming. Instead a microcrystalline material (**107**) precipitated from solution at  $-28^\circ\text{C}$  (Scheme 3.5). Unfortunately, this material was not suitable for X-ray crystallographic analysis. However, by <sup>1</sup>H NMR analysis of **107** in C<sub>6</sub>D<sub>6</sub> solution, it was evident that the HMDS : (–)-sparteine ratio

was 1 : 1 (akin to **106**); different from the ratio for crystalline **108** in  $C_6D_6$  which was 5 : 2 (Figure 3.25 and Figure 3.23 respectively). A lithium analogue of **108** could not be obtained.

X-ray crystallographic analysis reveals that **106** crystallises in the triclinic system, chiral space group  $P1$ , and is monomeric in the solid-state (Figure 3.20). Table 3.23 and Table 3.24 detail the key bond distances and bond angles respectively.

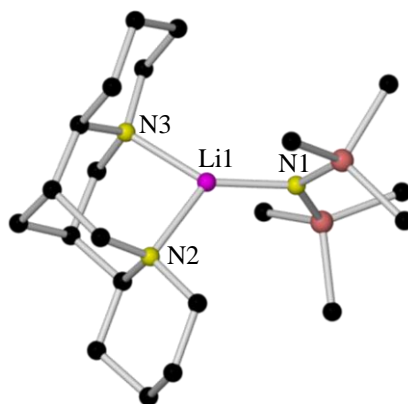


**Figure 3.20** Molecular structure of [LiHMDS·(-)-sparteine], **106**. H atoms are omitted for clarity.

Selected Bond	Bond Distance (Å) in [LiHMDS·(-)-sparteine], <b>106</b>
Li1–N1	1.910(5)
Li1–N2	2.048(5)
Li1–N3	2.047(5)

**Table 3.23** Key bond distances within [LiHMDS·(-)-sparteine], **106**.

Selected Angle	Bond Angle (°) in [LiHMDS·(-)-sparteine], <b>106</b>
N1–Li1–N2	127.2(3)
N1–Li1–N3	139.1(3)
N2–Li1–N3	89.9(2)

**Table 3.24** Key bond angles within [LiHMDS·(-)-sparteine], **106**.

The Li centre is three coordinate, adopting a distorted trigonal planar environment (summed angles at Li,  $356.2^\circ$ ). As expected, the greatest distortion from an ideal trigonal planar geometry occurs at the (-)-sparteine–Li bite angle [ $89.9(2)^\circ$ ]. To the best of our knowledge, only four monomeric LiHMDS complexes have been reported previously. These are a 12-crown-4,<sup>[36a]</sup> a  $Me_6$ -TREN<sup>[252]</sup> [tris{2-(dimethylamino)ethyl}amine], a PMDETA<sup>[182]</sup> and – perhaps most pertinent to this study – a bidentate TMEDA<sup>[182]</sup> complex. The Li–N<sub>HMDS</sub> bond distance in **106** [1.910(5) Å] is consistent with that in the TMEDA complex [1.893(3) Å]. In **106**, the (-)-sparteine coordinates to the Li centre symmetrically and the mean Li–N<sub>(-)-sparteine</sub> bond distance is 2.0475 Å, which is slightly shorter than the mean Li–N<sub>TMEDA</sub> bond distance (2.0805 Å) in the TMEDA adduct. The N<sub>TMEDA</sub>–Li–N<sub>TMEDA</sub> bite angle in this complex



[87.6(1) Å] is similar to the corresponding angle in **106** despite the much greater steric demands of the (–)-sparteine ligand.<sup>[182]</sup>

Collum has meticulously studied the solution chemistry of LiHMDS in the presence of more than 100 synthetically useful and commonly employed ligands.<sup>[253]</sup> Focusing on (–)-sparteine, his studies have shown that in hydrocarbon solution with a low concentration of the diamine present, the chelated monomer exists, with the exclusion of the solvated dimer or highly solvated monomer,<sup>[54, 253]</sup> an observation which is in line with the solid-state structure of **106**. Full NMR details for complex **106** in *d*<sub>8</sub>-toluene solution can be found in chapter 5, section 5.3.25. The key features in the <sup>1</sup>H spectrum obtained are that the HMDS : (–)-sparteine ratio is 1 : 1, and the resonances due to the diamine ligand are broader and differ slightly from those associated with the free diamine; hence, (–)-sparteine appears to remain at least partially coordinated to the lithium metal centre in arene solution.

X-ray crystallographic analysis reveals that **108** crystallises in the monoclinic system, chiral space group *C*2, as a solvent-separated ion pair, and as such, the cationic and anionic moieties of **108** will be discussed independently. The molecular structure of its cation (Figure 3.21) is composed of two (–)-sparteine molecules which coordinate in their usual chelating fashion<sup>[141, 148-150, 152, 154-156]</sup> to two sodium centres, with a HMDS anion bridging the two metal centres (both metal centres are three coordinate). Table 3.25 and Table 3.26 detail the key bond distances and bond angles respectively.

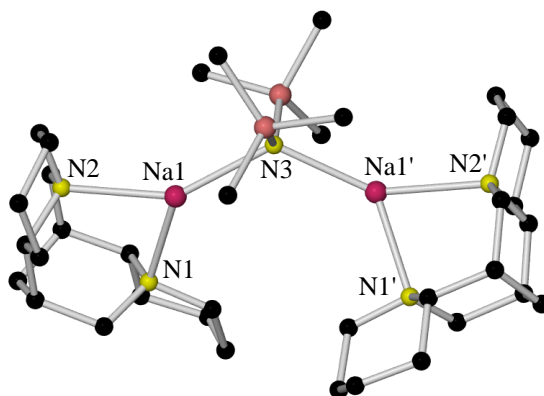


**Figure 3.21** Molecular structure of the cation of [(–)-sparteine·Na(μ-HMDS)Na·(–)-sparteine]<sup>+</sup>[Na<sub>4</sub>(μ-HMDS)<sub>4</sub>(μ<sub>4</sub>-OH)]<sup>–</sup>, **108**. H atoms are omitted for clarity.

Selected Bond	Bond Distance (Å) in [(–)-sparteine·Na(μ-HMDS)Na·(–)-sparteine] <sup>+</sup> [Na <sub>4</sub> (μ-HMDS) <sub>4</sub> (μ <sub>4</sub> -OH)] <sup>–</sup> , <b>108</b>
Na1–N1	2.393(4)
Na1–N2	2.458(4)
Na1–N3	2.399(2)

**Table 3.25** Key bond distances within the cation of [(–)-sparteine·Na(μ-HMDS)Na·(–)-sparteine]<sup>+</sup>[Na<sub>4</sub>(μ-HMDS)<sub>4</sub>(μ<sub>4</sub>-OH)]<sup>–</sup>, **108**.

Selected Angle	Bond Angle (°) in [(-)-sparteine·Na(μ-HMDS)Na·(-)- sparteine] <sup>+</sup> [Na <sub>4</sub> (μ-HMDS) <sub>4</sub> (μ <sub>4</sub> -OH)] <sup>-</sup> , <b>108</b>
N1–Na1–N2	74.86(12)
N1–Na1–N3	130.86(13)
N2–Na1–N3	148.38(14)

**Table 3.26** Key bond angles within the cation of [(-)-sparteine·Na(μ-HMDS)Na·(-)-sparteine]<sup>+</sup>[Na<sub>4</sub>(μ-HMDS)<sub>4</sub>(μ<sub>4</sub>-OH)]<sup>-</sup>, **108**.

Cation **108** appears to represent only the second crystallographically characterised solvent-separated cation which takes the form ‘donor-alkali metal-amide-alkali metal-donor’, the first being a lithium sodiate, [{TMTCY}·Li{μ-N(H)CH<sub>3</sub>}Li·(TMTCY)]<sup>+</sup>(Na<sup>-</sup>) (where TMTCY is 1,4,7-trimethyl-1,4,7-triazacyclonane).<sup>[254]</sup> It is also only the third complex to be reported thus far which incorporates both sodium and (-)-sparteine, the preceding two complexes, [(-)-sparteine}·Na(μ-TMP)(μ-<sup>n</sup>Bu)Mg(TMP)],<sup>[162]</sup> **52** and [Na{(-)-sparteine}<sub>2</sub>]<sup>+</sup>[Mg(HMDS)<sub>3</sub>]<sup>-</sup>,<sup>[248]</sup> **101** (section 3.2.1) being reported by our group. The Na centres in **108** adopt distorted trigonal planar arrangements here (sum of angles around Na1, 354.1°), whereas in complexes **52** and **101**, both Na centres are in distorted tetrahedral environments, as a consequence the mean Na–N<sub>(-)-sparteine</sub> bond distance in **108** (2.426 Å) is slightly shorter than that found in complexes **52** and **101** (mean Na–N<sub>(-)-sparteine</sub> bond distance, 2.499 and 2.461 Å for complexes **52** and **101** respectively). This decrease in coordination number (from four to three) accompanies a slight widening of the diamine bite angle when compared to complex **52** [from 72.59(5)° to 74.86(12)° in **108**]; but, when compared to complex **101**, which has a mean bite angle of 75.22°, the angles are almost identical. As expected, a similar scenario is encountered on comparing the cation of **108** to the previously discussed (section 3.1.1) zincate analogue of **52**, the (-)-sparteine coordinated sodium zincate [(-)-sparteine}·Na(μ-TMP)(μ-<sup>n</sup>Bu)Zn(<sup>t</sup>Bu)], **96** [mean Na–N<sub>(-)-sparteine</sub> bond distance and diamine bite angle, 2.501 Å and 72.69(13)° respectively].

When compared to the cation of the previously discussed TMEDA complex, [Na(TMEDA)<sub>2</sub>]<sup>+</sup>[Mg(HMDS)<sub>3</sub>]<sup>-</sup>, **88** (chapter 2, section 2.3.1), as expected, the mean Na–N<sub>diamine</sub> bond distance in **108** (2.426 Å) is slightly shorter than that found in **88** (2.517 Å), and due to the decrease in coordination number (from four to three), a slightly wider diamine bite angle is observed (74.57° vs. 74.86°).

The anionic moiety of **108** (Figure 3.22) is composed of four sodium centres and four HMDS ligands arranged in an almost perfectly planar eight-membered (NaN)<sub>4</sub> ring [N4–N5–N6–N5' torsion angle is 0°; Na2–Na3–Na3'–Na2' is 1.88(11)°] which acts as a tetranuclear host

towards a hydroxyl anion guest. This guest is disordered over two sites in the centre of the metal-amido ring [one above and one below the plane of the (NaN)<sub>4</sub> ring, occupancy 50 : 50].

Table 3.27 and Table 3.28 detail the key bond distances and bond angles respectively.

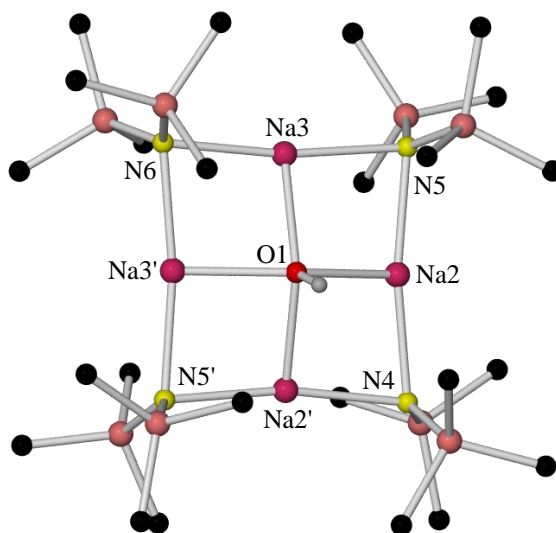


**Figure 3.22** Molecular structure of the anion of  $[(-)\text{-sparteine}\cdot\text{Na}(\mu\text{-HMDS})\text{Na}\cdot(-)\text{-sparteine}]^+[\text{Na}_4(\mu\text{-HMDS})_4(\mu_4\text{-OH})]^-$ , **108**. H atoms [except OH (the H atom of which was both found and refined crystallographically)] and disorder component are omitted for clarity.

Selected Bond	Bond Distance (Å) in $[(-)\text{-sparteine}\cdot\text{Na}(\mu\text{-HMDS})\text{Na}\cdot(-)\text{-sparteine}]^+[\text{Na}_4(\mu\text{-HMDS})_4(\mu_4\text{-OH})]^-$ , <b>108</b>
Na2–N4	2.393(4)
Na2–N5	2.393(3)
Na2–O1	2.324(5)
Na2'–O1	2.345(5)
Na3–N5	2.412(3)
Na3–N6	2.394(3)
Na3–O1	2.310(5)
Na3'–O1	2.365(5)

**Table 3.27** Key bond distances within the anion of  $[(-)\text{-sparteine}\cdot\text{Na}(\mu\text{-HMDS})\text{Na}\cdot(-)\text{-sparteine}]^+[\text{Na}_4(\mu\text{-HMDS})_4(\mu_4\text{-OH})]^-$ , **108**.

Selected Angle	Bond Angle (°) in $[(-)\text{-sparteine}\cdot\text{Na}(\mu\text{-HMDS})\text{Na}\cdot(-)\text{-sparteine}]^+[\text{Na}_4(\mu\text{-HMDS})_4(\mu_4\text{-OH})]^-$ , <b>108</b>
N4–Na2–N5	170.01(11)
N4–Na2'–N5'	170.01(11)
N5–Na3–N6	171.91(11)
N5'–Na3'–N6	171.91(11)
Na2–N5–Na3	81.66(8)
Na2–N4–Na2'	79.88(14)
Na3–N6–Na3'	81.04(14)
Na2'–N5'–Na3'	81.66(8)

**Table 3.28** Key bond angles within the anion of  $[(-)\text{-sparteine}\cdot\text{Na}(\mu\text{-HMDS})\text{Na}\cdot(-)\text{-sparteine}]^+[\text{Na}_4(\mu\text{-HMDS})_4(\mu_4\text{-OH})]^-$ , **108**.

The mean Na–O bond distance is 2.336 Å. In addition to the Na–O bonding within the structure, each Na centre is bound to two amido-N atoms. The mean ‘corner’ Na–N–Na and ‘side’ N–Na–N angles of the eight-membered ring are 81.06 and 170.96° respectively.

The structures of two other discrete (NaN)<sub>4</sub> eight-membered rings have been published previously. Veith *et al.* reported the pair of solvent-free sodium amides [ $\{\text{RNSiMe}_2\text{OSiMe}_2\text{NR}\}_2\text{Na}_4$ ]<sup>[255]</sup> (where R is *t*Bu or SiMe<sub>3</sub>), although their structures are fundamentally different from that of the anion of **108**. The rings in Veith’s complexes deviate significantly from planarity, the Na centres are stabilised by internal chelation, and of course, these complexes are electronically neutral.

As alluded to in chapter 1, donor-free NaHMDS has been isolated in the solid-state as polymeric<sup>[22]</sup> and cyclic trimeric<sup>[23]</sup> polymorphs. Despite the incorporation of OH<sup>−</sup> in the anion of **108**, the mean Na–N bond distance (2.398 Å) only experiences a modest elongation in comparison to the polymeric<sup>[22]</sup> and cyclic<sup>[23]</sup> NaHMDS polymorphs (2.352 and 2.380 Å respectively); the mean Na–N–Na and N–Na–N angles (101.99 and 150.22° respectively for the polymeric polymorph, and 100.02 and 139.71° respectively for the cyclic polymorphs) are approximately 20° wider and 20 and 30° narrower than their respective counterparts in the anion of **108**.

Turning to the NMR spectroscopic analysis of **108**, the crystalline product was dissolved in C<sub>6</sub>D<sub>6</sub> solution and examined by <sup>1</sup>H and <sup>13</sup>C NMR spectroscopy (Figure 3.23 and Figure 3.24 respectively). Unfortunately, a high quality <sup>13</sup>C NMR spectrum could not be obtained, despite repeated attempts at the preparation of concentrated samples and long acquisition times.

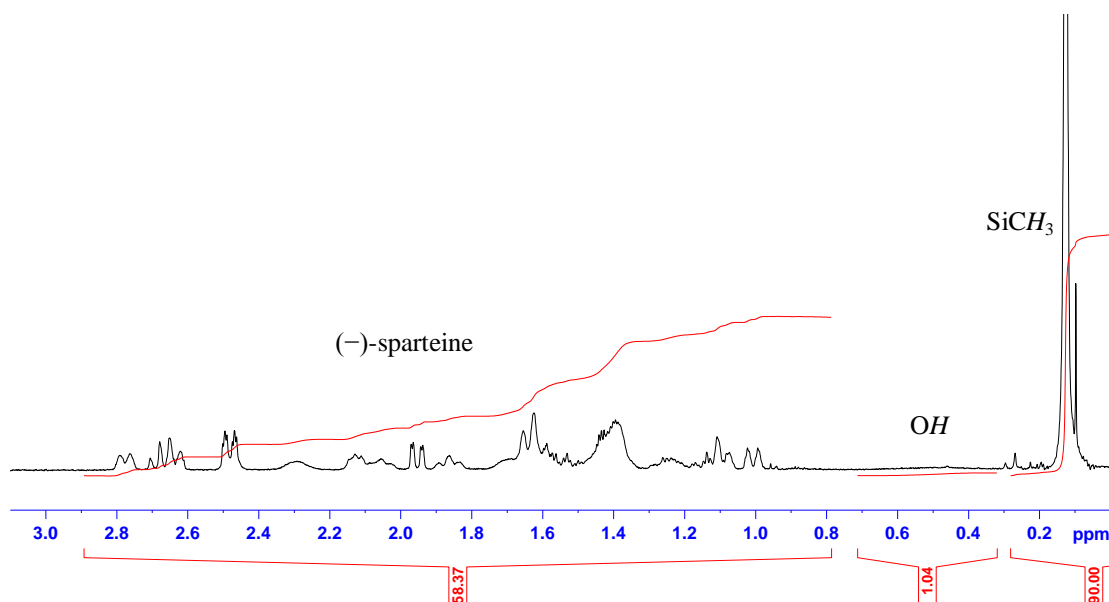


**Figure 3.23** <sup>1</sup>H NMR spectrum of  $[(-)\text{-sparteine}\cdot\text{Na}(\mu\text{-HMDS})\text{Na}\cdot(-)\text{-sparteine}]^+[\text{Na}_4(\mu\text{-HMDS})_4(\mu_4\text{-OH})]^-$ , **108**, in C<sub>6</sub>D<sub>6</sub>.

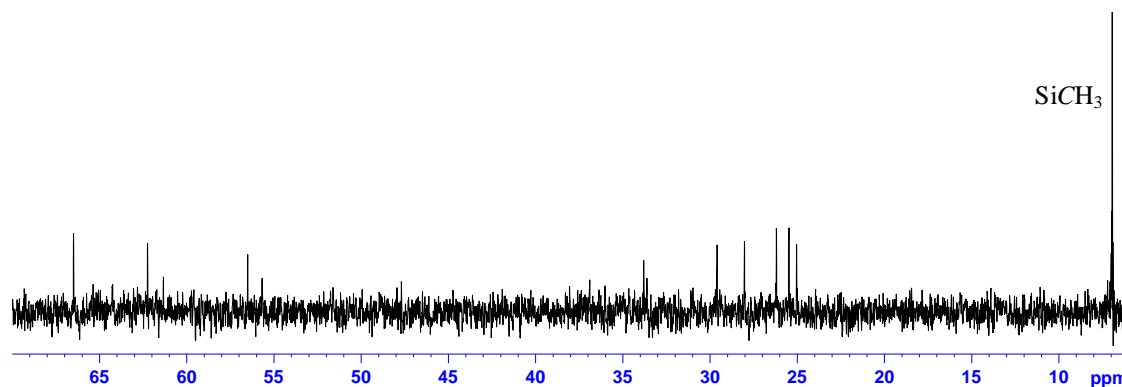


**Figure 3.24**  $^{13}\text{C}$  NMR spectrum of  $[(-)\text{-sparteine}\cdot\text{Na}(\mu\text{-HMDS})\text{Na}\cdot(-)\text{-sparteine}]^+[\text{Na}_4(\mu\text{-HMDS})_4(\mu_4\text{-OH})]^-$ , **108**, in  $\text{C}_6\text{D}_6$ .

Due to the large number of chemically distinct aliphatic H and C atoms in  $(-)$ -sparteine (section 3.1.1, [Figure 3.2](#) and [Figure 3.3](#)), the  $^1\text{H}$  and  $^{13}\text{C}$  NMR spectra are extremely complex. The  $(-)$ -sparteine region of the  $^1\text{H}$  spectrum is broad (0.9-2.9 ppm), and although the defined area integrates to a slightly higher value (58) than that required to satisfy two molecules of  $(-)$ -sparteine being present (52), it can be seen from [Figure 3.23](#) that this excess may be accounted for as many of the peaks do not touch the baseline. There is also a peak at 0.48 ppm integrating to one proton, which has tentatively been assigned as the OH group within the anion of the complex.

Finally, there is a peak at 0.13 ppm which corresponds to the 90 protons of the five HMDS ligands within the complex. It may be expected that there would be two resonances observed for the HMDS groups as there are two chemically distinct ligands in the solid-state structure (one for HMDS ligand in the cation and one for the four HMDS ligands in the anion), then again, it may not be too surprising that there is only one resonance observed given the local coordination environment of the different HMDS groups (in both the cation and anion HMDS bridges in a  $\mu_2$ -fashion to two Na atoms). Low temperature NMR spectroscopic studies proved futile in resolving the two distinct HMDS resonances.

[Figure 3.25](#) shows the  $^1\text{H}$  NMR spectrum of **107** in  $\text{C}_6\text{D}_6$  solution, which illustrates the HMDS :  $(-)$ -sparteine ratio is 1 : 1 (akin to **106**); different from the ratio for crystalline **108** in  $\text{C}_6\text{D}_6$  which is 5 : 2, as previously discussed.

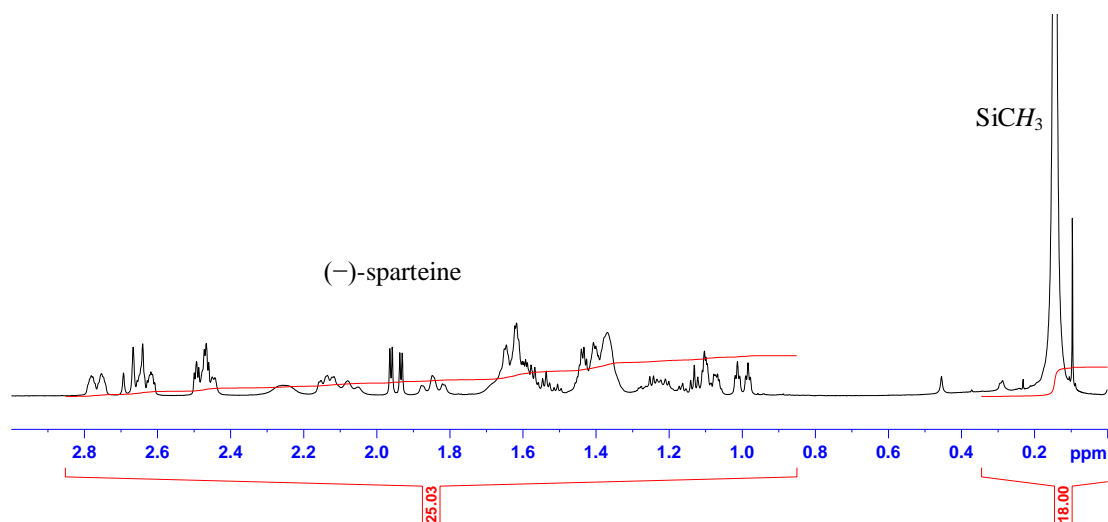


**Figure 3.25**  $^1\text{H}$  NMR spectrum of “[NaHMDS·(-)-sparteine]”, **107**, in  $\text{C}_6\text{D}_6$ .

Comparison of the  $^1\text{H}$  NMR ‘(-)-sparteine’ region of **107** and **108** with the spectral data of the free diamine reveals broadness of the resonances for **107** and **108** and movement of resonances particularly at approximately 2.3, 2.1 and 1.6 ppm with respect to free (-)-sparteine and to one another (Figure 3.26).

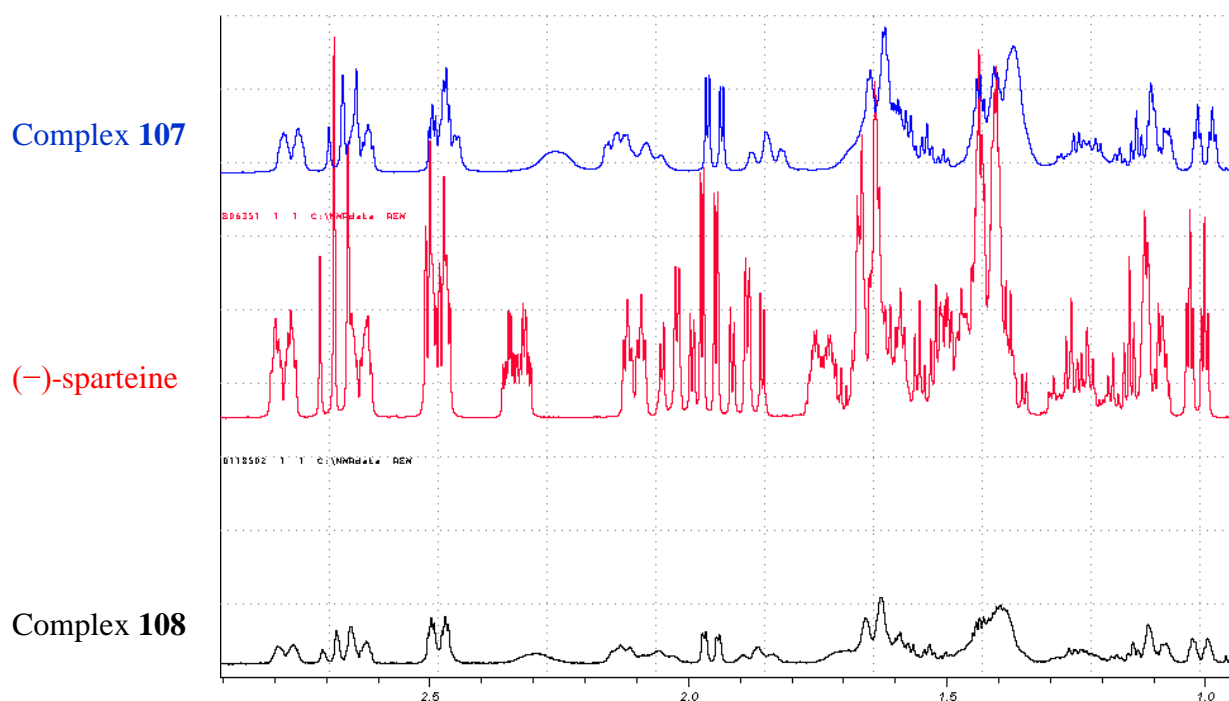


**Figure 3.26** Comparison of the  $^1\text{H}$  NMR spectra of the (-)-sparteine region in **107** (top), (-)-sparteine (middle) and **108** (bottom) in  $\text{C}_6\text{D}_6$ . Note the broadness of the resonances in **107** and **108**, and the movement of resonances, particularly at approximately 2.3, 2.1 and 1.6 ppm.

This provides evidence that the diamine appears to remain at least partially coordinated to the respective metal centres in arene solution for both novel complexes and that they are indeed different from one another. Further evidence to support this is shown in Figure 3.27, where it

can be seen that the HMDS resonances for complexes **107** and **108** are different from one another (at approximately 0.15 and 0.13 ppm respectively), indicating again that they are indeed different complexes. The small resonance at 0.09 ppm is due to HMDS(H).

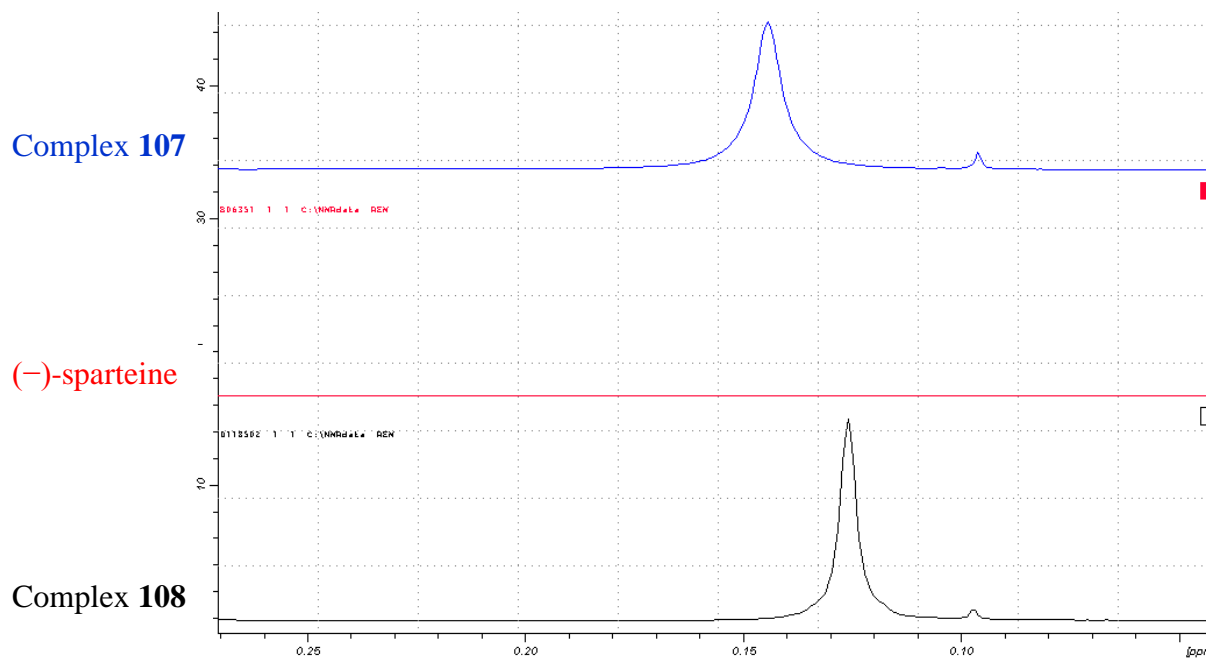


**Figure 3.27** Comparison of the  $^1\text{H}$  NMR spectra of the HMDS region in **107** (top),  $(-)$ -sparteine (middle) and **108** (bottom) in  $\text{C}_6\text{D}_6$ . The small resonance at 0.09 ppm is due to HMDS(H).

Crudely the reaction pathway to produce  $[(-)\text{-sparteine}\cdot\text{Na}(\mu\text{-HMDS})\text{Na}\cdot(-)\text{-sparteine}]^+[\text{Na}_4(\mu\text{-HMDS})_4(\mu_4\text{-OH})]^-$ , **108**, shows that if one molar equivalent of  $\text{H}_2\text{O}$  is present, then it consumes *six* molar equivalents of NaHMDS to form **108** – possibly indicating why  $(-)$ -sparteine solvates of alkali metal amides (in particular NaHMDS) have not yet been employed to any significant degree in asymmetric synthesis.

The anion of **108** is interesting and can be directly compared to a cationic crown ether complex. Whereas a neutral crown ether molecule encapsulates a metal cation to become a cationic species, here the ‘NaHMDS tetramer’ encapsulates a hydroxyl ligand forming the anion of **108**. In keeping with the chemistry and terminology developed by Mulvey *et al.*,<sup>[84-85]</sup> this anion can be considered as the first anionic inverse crown ether, the isolation of this is presumably possible due to the large steric bulk of  $(-)$ -sparteine which sufficiently stabilises the cation of **108**.

### 3.3.2 $[\text{Na}\{(R,R)\text{-TMCDA}\}_2]^+[\text{Na}_4(\mu\text{-HMDS})_4(\mu_4\text{-OH})]^-$ , **109**

Having obtained the unexpected and ‘unconventional’ product **108**, our attention turned to the possibility of preparing a similar complex utilising freshly synthesised  $(R,R)$ -TMCDA which had been pre-dried with molecular sieves only, in the hope of deliberately preparing another

complex which contains an inverse crown ether anion. Thus, *n*-butylsodium was reacted with an equimolar quantity of HMDS(H) in hexane solution, and this mixture was left to stir for 30 minutes, before one molar equivalent of (*R,R*)-TMCDA was introduced. The addition of toluene was required to produce a homogeneous solution (Scheme 3.6). X-ray quality crystals of **109** precipitated from the hydrocarbon medium by slowly cooling the Schlenk tube to ambient temperature from a hot water-filled Dewar flask.

X-ray crystallographic analysis reveals that **109** crystallises in the monoclinic system, space group  $P2_1$ . Akin to **108**, complex **109** is a hydroxyl-incorporated solvent-separated sodium sodiate, where the anion (Figure 3.29) of the complex is the same as that in **108** (hydroxyl group not disordered in this case) and thus represents the second inverse crown ether anion to be reported. However, the cation of the complex is different from that encountered in complex **108** – here the cation (Figure 3.28) is composed of two (*R,R*)-TMCDA molecules which chelate terminally to a sodium centre (*i.e.*, the sodium metal centre is four coordinate), similar to the arrangement often observed in alkali metal complexes of its achiral relative TMEDA,<sup>[113, 116, 125, 210, 212-215]</sup> and having previously been observed in complex **103** (section 3.2.1). Due to the solvent-separated composition of this pentanuclear sodium sodiate, the cationic and anionic moieties of **109** will now be discussed independently. Table 3.29 and Table 3.30 detail the key bond distances and bond angles respectively within the cation of **109**.

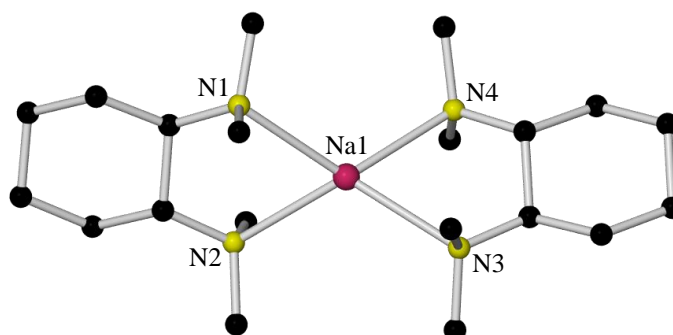


**Figure 3.28** Molecular structure of the cation of  $[\text{Na}\{(R,R)\text{-TMCDA}\}_2]^+[\text{Na}_4(\mu\text{-HMDS})_4(\mu_4\text{-OH})]^-$ , **109**. H atoms are omitted for clarity.

Selected Bond	Bond Distance (Å) in $[\text{Na}\{(R,R)\text{-TMCDA}\}_2]^+[\text{Na}_4(\mu\text{-HMDS})_4(\mu_4\text{-OH})]^-$ , <b>109</b>
Na1–N1	2.430(2)
Na1–N2	2.424(2)
Na1–N3	2.441(2)
Na1–N4	2.431(2)

**Table 3.29** Key bond distances within the cation of  $[\text{Na}\{(R,R)\text{-TMCDA}\}_2]^+[\text{Na}_4(\mu\text{-HMDS})_4(\mu_4\text{-OH})]^-$ , **109**.



Selected Angle	Bond Angle (°) in [Na{(R,R)-TMCDA} <sub>2</sub> ] <sup>+</sup> [Na <sub>4</sub> (μ-HMDS) <sub>4</sub> (μ <sub>4</sub> -OH)] <sup>-</sup> , <b>109</b>
N1–Na1–N2	73.23(5)
N1–Na1–N3	144.57(6)
N1–Na1–N4	119.40(6)
N2–Na1–N3	120.39(6)
N2–Na1–N4	139.78(6)
N3–Na1–N4	73.14(5)

**Table 3.30** Key bond angles within the cation of [Na{(R,R)-TMCDA}<sub>2</sub>]<sup>+</sup>[Na<sub>4</sub>(μ-HMDS)<sub>4</sub>(μ<sub>4</sub>-OH)]<sup>-</sup>, **109**.

The Na centre adopts a distorted tetrahedral environment (summed angles at Na, 669.51°) and as expected, the greatest distortion from an ideal tetrahedral geometry for the Na centre arises due to the (R,R)-TMCDA–Na bite angles (mean angle, 73.19°). This cation has been observed before within the previously discussed complex [Na{(R,R)-TMCDA}<sub>2</sub>]<sup>+</sup>[Mg(HMDS)<sub>3</sub>]<sup>-</sup>,<sup>[248]</sup> **103** (section 3.2.1, Figure 3.14). Comparing the cation of **109** to that of **103** reveals only slight differences – the mean Na–N bond distance of cation **109** (2.432 Å) is 0.105 Å greater than the corresponding distance within cation **103** (2.327 Å) and consequently the mean (R,R)-TMCDA–Na bite angle is approximately 3° more acute in **109** (*vide supra*) than in **103** (mean angle, 75.95°).

Similar to the anion of **108**, the anionic moiety of **109** (Figure 3.29) is composed of four sodium centres and four HMDS ligands arranged in an almost perfectly planar eight-membered (NaN)<sub>4</sub> ring [N5–N6–N7–N8 torsion angle is 0°; Na2–Na3–Na4–Na5 is 0.88(3)°] which acts as a tetranuclear host towards a hydroxyl anion guest, which sits 0.7 Å above the plane of the metal-amido ring. Table 3.31 and Table 3.32 detail the key bond distances and bond angles respectively.

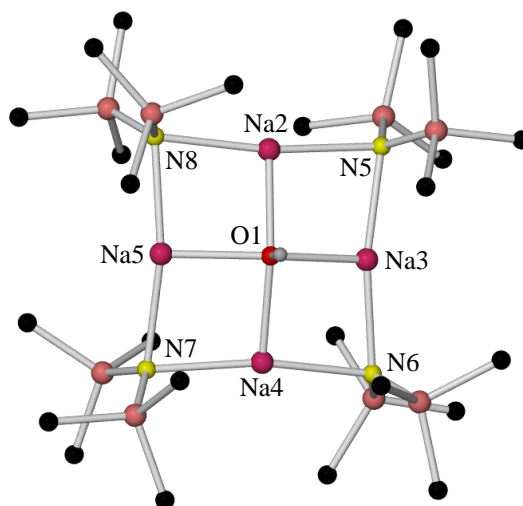


**Figure 3.29** Molecular structure of the anion of [Na{(R,R)-TMCDA}<sub>2</sub>]<sup>+</sup>[Na<sub>4</sub>(μ-HMDS)<sub>4</sub>(μ<sub>4</sub>-OH)]<sup>-</sup>, **109**. H atoms [except OH (the H atom of which was both found and refined crystallographically)] are omitted for clarity.

Selected Bond	Bond Distance (Å) in [Na{(R,R)-TMCDA} <sub>2</sub> ] <sup>+</sup> [Na <sub>4</sub> (μ-HMDS) <sub>4</sub> (μ <sub>4</sub> -OH)] <sup>-</sup> , <b>109</b>
Na2–N5	2.429(2)
Na2–N8	2.428(2)
Na2–O1	2.293(1)
Na3–N5	2.379(1)
Na3–N6	2.380(2)
Na3–O1	2.292(1)
Na4–N6	2.417(2)
Na4–N7	2.408(2)
Na4–O1	2.286(1)
Na5–N7	2.444(2)
Na5–N8	2.440(2)
Na5–O1	2.273(1)

**Table 3.31** Key bond distances within the anion of [Na{(R,R)-TMCDA}<sub>2</sub>]<sup>+</sup>[Na<sub>4</sub>(μ-HMDS)<sub>4</sub>(μ<sub>4</sub>-OH)]<sup>-</sup>, **109**.

Selected Angle	Bond Angle (°) in [Na{(R,R)-TMCDA} <sub>2</sub> ] <sup>+</sup> [Na <sub>4</sub> (μ-HMDS) <sub>4</sub> (μ <sub>4</sub> -OH)] <sup>-</sup> , <b>109</b>
N5–Na2–N8	170.40(5)
N5–Na3–N6	166.30(6)
N6–Na4–N7	163.35(5)
N7–Na5–N8	163.82(6)
Na2–N5–Na3	79.98(5)
Na3–N6–Na4	80.20(5)
Na4–N7–Na5	80.17(5)
Na2–N8–Na5	81.31(5)

**Table 3.32** Key bond angles within the anion of [Na{(R,R)-TMCDA}<sub>2</sub>]<sup>+</sup>[Na<sub>4</sub>(μ-HMDS)<sub>4</sub>(μ<sub>4</sub>-OH)]<sup>-</sup>, **109**.

The mean Na–O bond distance is 2.286 Å. In addition to the Na–O bonding within the structure, each Na centre is bound to two amido-N atoms. The mean ‘corner’ Na–N–Na and ‘side’ N–Na–N angles of the eight-membered ring are 80.42 and 165.97° respectively.

Comparing the anion of complex **109** to that of **108** the (NaN)<sub>4</sub> ring is slightly puckered at the Na centres for **109** – the mean Na–O bond distance (2.286 Å) is slightly shorter than that in the anion of **108** (2.336 Å); and consequently the mean N–Na–N angle is approximately 5° more acute in **109** (165.97°) compared to **108** (170.95°). The mean ‘corner’ Na–N–Na angle of the eight-membered ring does not change dramatically in reflection of this puckering; a narrowing of 0.64° is observed (mean Na–N–Na angle, 81.06 and 80.42° for **108** and **109** respectively).

In comparison to donor-free NaHMDS, the mean Na–N bond distance (2.416 Å) is slightly greater than that encountered in the polymeric<sup>[22]</sup> and cyclic<sup>[23]</sup> NaHMDS polymorphs (2.352 and 2.380 Å respectively); the mean Na–N–Na and N–Na–N angles (101.99 and 150.22° respectively for the polymeric polymorph, and 100.02 and 139.71° respectively for the cyclic

polymorphs) are approximately 20° wider and 15 and 25° narrower than their respective counterparts in the anion of **109**.

Turning to the NMR spectroscopic analysis of **109**, the crystalline product was dissolved in C<sub>6</sub>D<sub>6</sub> solution and examined by <sup>1</sup>H and <sup>13</sup>C NMR spectroscopy. Unfortunately, a high quality <sup>13</sup>C NMR spectrum could not be obtained, despite repeated attempts at the preparation of concentrated samples and long acquisition times. Full NMR details can be found in chapter 5, section 5.3.28. The key features in the <sup>1</sup>H spectrum obtained are that the HMDS : (*R,R*)-TMCDAs ratio is 2 : 4, and the resonances due to the diamine ligand are broader and differ slightly from those associated with the free diamine; hence, (*R,R*)-TMCDAs appears to remain at least partially coordinated to the sodium metal centre in arene solution. Similar to **108**, there is also a peak observed at 0.48 ppm integrating to one proton, which was previously assigned as the OH group within the anion of complex **108**. Its appearance here seems to verify that this peak was assigned correctly.

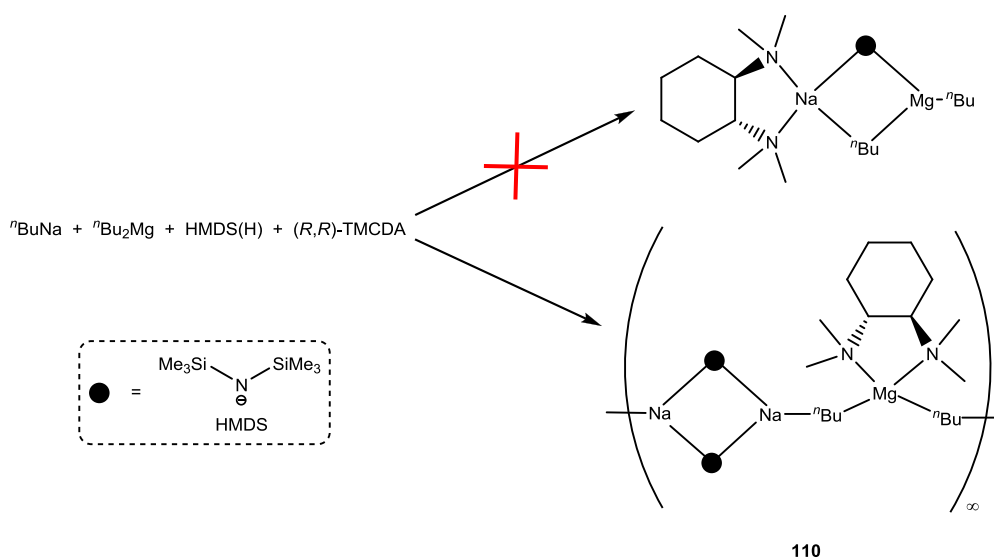
Although closely related to known inverse crown ether complexes,<sup>[98, 100, 102-103]</sup> complexes **108** and **109** possess important differences. They are monometallic anionic, solvent-separated ion pairs, unlike inverse crown ethers, which are heterobimetallic neutral entities. With these differences in mind, the preparation and isolation of complexes **108** and **109**, has paved the way for the development of a new Group 1 macrocyclic/supramolecular chemistry, which will be discussed in the following chapter.

Revisiting the chiral zincate chemistry explored in section 3.1, we looked at expanding the area of the (*R,R*)-TMCDAs ate species to include magnesiates, specifically sodium HMDS-containing magnesiates. However, the reaction undertaken to produce such a species did not produce the expected contacted ion pair motif (as seen in previously synthesised ate complexes), but instead a polymeric complex – which can be termed an ‘inverse magnesiate’ – with (*R,R*)-TMCDAs bound to magnesium, where unexpectedly [<sup>n</sup>Bu<sub>2</sub>Mg·{(*R,R*)-TMCDAs}] functions as a η<sup>1</sup>, μ ligand to dimeric (NaHMDS)<sub>2</sub> molecules to afford a zig-zag chain polymer. This result will now be discussed in greater detail.

### 3.3.3 [(NaHMDS)<sub>2</sub>{<sup>n</sup>Bu<sub>2</sub>Mg·(*R,R*)-TMCDAs}]<sub>∞</sub>, **110**

In an attempt to prepare the chiral bis(alkyl)amido sodium magnesiate [(*R,R*)-TMCDAs·Na(μ-HMDS)(μ-<sup>n</sup>Bu)Mg(<sup>n</sup>Bu)], by reacting together an equimolar mixture of *n*-butylsodium, di-*n*-butylmagnesium and HMDS(H) in hexane solution, followed by the addition of a molar equivalent of (*R,R*)-TMCDAs (Scheme 3.7), X-ray crystallographic studies identified the colourless crystals deposited at –28°C as [(NaHMDS)<sub>2</sub>{<sup>n</sup>Bu<sub>2</sub>Mg·(*R,R*)-TMCDAs}]<sub>∞</sub>, **110**,

which represents an example of a mixed sodium-magnesium but ‘non-magnesiate’ (in the conventional sense) compound.



**Scheme 3.7** Synthesis of complex **110**, showing the expected product from the reaction (top) and the actual product obtained (bottom).

Complex **110** crystallises in the tetragonal system, space group  $P4_22_12$ , and can be envisaged as an adduct of two neutral molecules, dimeric  $(\text{NaHMDS})_2$  and monomeric  $[\text{}^n\text{Bu}_2\text{Mg}\cdot(\text{R,R})\text{-TMCDA}]$  (Figure 3.30), where the formally coordinatively saturated donor molecule (magnesium metal centre four coordinate) links the sodium centres (which are three coordinate) to each other through a  $\text{Na}^n\text{BuMg}^n\text{BuNa}$  arrangement to propagate a polymeric chain (Figure 3.31). Table 3.33 and Table 3.34 detail the key bond distances and bond angles respectively.

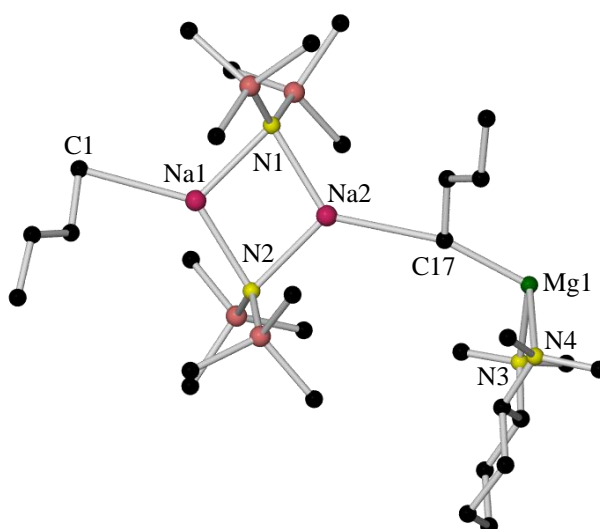


**Figure 3.30** Molecular structure of the asymmetric unit of  $[(\text{NaHMDS})_2\{\text{}^n\text{Bu}_2\text{Mg}\cdot(\text{R,R})\text{-TMCDA}\}]_\infty$ , **110**. H atoms are omitted for clarity.

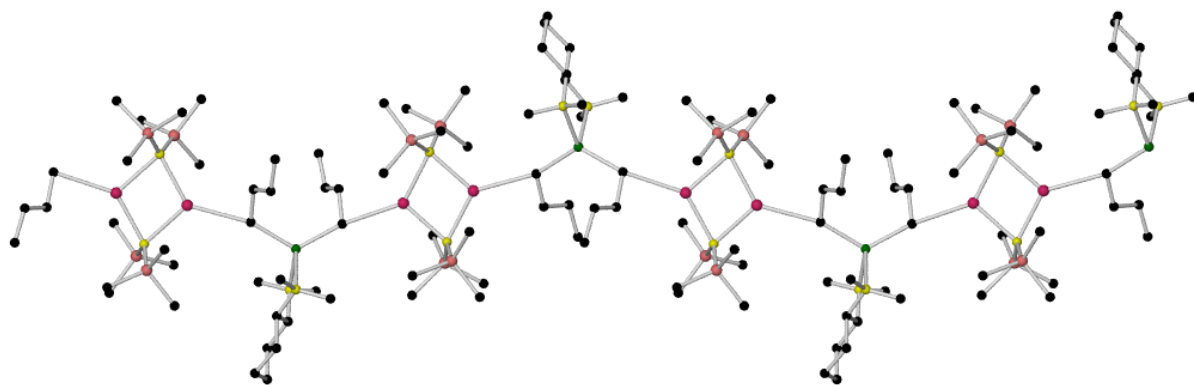


**Figure 3.31** Extended view of  $[(\text{NaHMDS})_2\{^n\text{Bu}_2\text{Mg}\cdot(\text{R},\text{R})\text{-TMCDA}\}]_\infty$ , **110**. H atoms are omitted for clarity.

Selected Bond	Bond Distance (Å) in $[(\text{NaHMDS})_2\{^n\text{Bu}_2\text{Mg}\cdot(\text{R},\text{R})\text{-TMCDA}\}]_\infty$ , <b>110</b>
Na1–N1	2.405(1)
Na1–N2	2.388(2)
Na2–N1	2.377(2)
Na2–N2	2.403(2)
Na1–C1	2.710(2)
Na2–C17	2.707(2)
Mg1–C1	2.159(2)
Mg1–C17	2.162(2)
Mg1–N3	2.215(2)
Mg1–N4	2.179(2)

**Table 3.33** Key bond distances within  $[(\text{NaHMDS})_2\{^n\text{Bu}_2\text{Mg}\cdot(\text{R},\text{R})\text{-TMCDA}\}]_\infty$ , **110**.

Selected Angle	Bond Angle (°) in $[(\text{NaHMDS})_2\{^n\text{Bu}_2\text{Mg}\cdot(\text{R},\text{R})\text{-TMCDA}\}]_\infty$ , <b>110</b>
N1–Na1–N2	103.10(5)
N1–Na1–C1	120.17(6)
N2–Na1–C1	136.68(6)
N1–Na2–N2	103.48(5)
N1–Na2–C17	133.00(6)
N2–Na2–C17	123.50(6)
Na1–N1–Na2	76.69(4)
Na1–N2–Na2	76.53(5)
N3–Mg1–N4	81.13(6)
N3–Mg1–C1	116.68(7)
N3–Mg1–C17	109.88(6)
N4–Mg1–C1	111.96(6)
N4–Mg1–C17	109.14(7)
C1–Mg1–C17	120.96(7)
Na1–C1–Mg1	163.69(9)
Na2–C17–Mg1	161.12(8)

**Table 3.34** Key bond angles within  $[(\text{NaHMDS})_2\{^n\text{Bu}_2\text{Mg}\cdot(\text{R},\text{R})\text{-TMCDA}\}]_\infty$ , **110**.

The zig-zag shape of the polymeric chain is imposed by the C–Mg–C angle [120.96(7)°], while the Na–C–Mg and C–Na···Na units are slightly distorted from linearity (average Na–

C–Mg angle,  $162.41^\circ$ , average C–Na $\cdots$ Na angle,  $173.06^\circ$ ). The Na centres assume trigonal planar geometries (sum of angles,  $359.95$  and  $359.98^\circ$  for Na1 and Na2 respectively), being bound to two (*R,R*)-TMCDA N atoms and a <sup>n</sup>Bu C atom. The mean Na–C bond distance is  $2.709 \text{ \AA}$ , whilst the mean Na–N bond distance ( $2.381 \text{ \AA}$ ) is slightly shorter than the range of those found in other dimeric (NaHMDS)<sub>2</sub> structures with different monodentate ligands such as TMPDA,<sup>[182]</sup> THF<sup>[206]</sup> and TEMPO,<sup>[193f]</sup> to name but a few (range of mean Na–N bond distances,  $2.391$ – $2.428 \text{ \AA}$ ).<sup>[26, 182, 193f, 202a, 206, 256]</sup> The mean Na–N bond distance of **110** is also shorter than the corresponding mean distance ( $2.444 \text{ \AA}$ ) in the previously discussed polymer, [(NaHMDS)<sub>2</sub>·TMEDA]<sub>∞</sub>, **84** (chapter 2, section 2.2.2). Turning to the bond angles within the (NaN)<sub>2</sub> ring, the mean N–Na–N angle ( $103.29^\circ$ ) and the mean Na–N–Na angle ( $76.61^\circ$ ) are slightly wider and narrower respectively compared to the corresponding parameters within the other dimeric (NaHMDS)<sub>2</sub> structures with different monodentate ligands (range of mean N–Na–N and Na–N–Na angles,  $100.23$ – $101.67$  and  $78.33$ – $79.77^\circ$  respectively).<sup>[26, 182, 193f, 202a, 206, 256]</sup> This is also the case when compared to **84** (mean N–Na–N and Na–N–Na angles,  $99.58$  and  $80.42^\circ$  respectively).

Comparing **110** to the donor-free amide [NaN(SiMe<sub>3</sub>)<sub>2</sub>]<sub>∞</sub>,<sup>[22]</sup> **7**, which crystallises as a polymer of trimeric units (polymorph of the same complex also known – a six-membered trimeric ring),<sup>[23]</sup> the addition of the donor in **110** has, as expected, deaggregated the complex; however, the complex remains polymeric, now with dimeric repeating units.

Turning to the coordination sphere of the Mg centre, it adopts a distorted tetrahedral geometry (summed angles at Mg,  $649.75^\circ$ ), binding to two <sup>n</sup>Bu C atoms and two (*R,R*)-TMCDA N atoms. As expected, the greatest distortion from a perfect tetrahedral geometry for the Mg centre arises due to the (*R,R*)-TMCDA–Mg bite angle [ $81.13(6)$ ]. The mean Mg–N bond distance is  $2.197 \text{ \AA}$ , whilst the mean Mg–C bond distance ( $2.161 \text{ \AA}$ ) is slightly shorter than the range of those found in other complexes containing a <sup>n</sup>Bu<sub>2</sub>Mg fragment where the Mg centre is four coordinate (range of mean Mg–C bond distances,  $2.200$ – $2.273 \text{ \AA}$ ).<sup>[184, 257]</sup>

Complex **110** is unusual in three respects: firstly, the <sup>n</sup>Bu<sub>2</sub>Mg fragment is extremely uncommon, especially within bimetallic complexes of this type, having only previously been incorporated within six other crystallographically characterised complexes,<sup>[184, 257]</sup> none of which are polymeric and only two of which are mixed-metal species; secondly, no complexes in which a (*R,R*)-TMCDA ligand is bound to a magnesium metal centre have been reported to date; and finally complex **110** is a rare example of a mixed-metal sodium-magnesium complex which is a ‘non-magnesiate’.

To elaborate, in general terms an ate species can be described as a bimetallic system in which one metal (the alkali metal) exhibits a greater Lewis acidity than the other metal (the divalent metal) and so is able to accept more anionic (Lewis basic) ligands. In complex **110** however, these Lewis acid/base roles are reversed, with  ${}^n\text{Bu}_2\text{Mg}$  acting as a Lewis base through the  ${}^n\text{Bu}$  groups that bond to the Na centres, while  $(\text{NaHMDS})_2$  acts as the Lewis acid counterpart (Scheme 3.7). Thus, in coordination terms **110** can be described as a ‘sodiate’ or an ‘inverse magnesiate’, where each sodium centre is bound to three anionic ligands, carrying then a partial negative charge, while the magnesium centres are solely bonded to two *n*-butyl groups and the neutral Lewis base (*R,R*)-TMCDA (Figures 3.30 and 3.31).

In constructing **110**, the presence of (*R,R*)-TMCDA on the Mg must activate the butyl groups, increasing their nucleophilicity such that the magnesium compound can behave as a bidentate donor through these butyl groups, with each of them bound to a sodium centre. This scenario has been encountered before, albeit within a mixed lithium-zinc ‘inverse zincate’,<sup>[258]</sup> which akin to **110**, possesses a zig-zag polymeric arrangement composed of dimeric  $(\text{LiHMDS})_2$  and  $[\text{Me}_2\text{Zn}\cdot\text{TMEDA}]$  [*i.e.*, here,  $\text{Me}_2\text{Zn}$  acts as the Lewis base and  $(\text{LiHMDS})_2$  as the Lewis acid].

On searching the CCDC for mixed-metal structures in which (*R,R*)-TMCDA’s achiral relative TMEDA is bound to a magnesium centre, only four such structures were found: a lithium and a sodium alkynyl magnesiate,  $\text{Li}_2[(\text{PhC}\equiv\text{C})_3\text{Mg}(\text{TMEDA})]_2$ ,<sup>[193c]</sup> **111** and  $\text{Na}_2[({}^t\text{BuC}\equiv\text{C})_3\text{Mg}(\text{TMEDA})]_2$ ,<sup>[259]</sup> **112**; a disodium dimagnesium hexafuryl tri(thf) complex,  $[\{\text{Na}_2(\text{THF})_3\}\{\text{Mg}_2(\text{TMEDA})\}(2\text{-C}_4\text{H}_3\text{O})_6]_\infty$ ,<sup>[108]</sup> **113**; and a sodium magnesiate,  $[(\text{TMEDA})\cdot\text{Na}(\mu\text{-C}_4\text{H}_3\text{S})_3\text{Mg}(\text{TMEDA})]$ ,<sup>[193r]</sup> **114**. Comparing these complexes to complex **110**, the magnesium centres are not solely solvated in preference to the alkali metal centres as is the case within **110**; hence, complex **110** is unique in this respect.

Turning to solution studies of complex **110** in  $\text{C}_6\text{D}_6$  solution, the  ${}^1\text{H}$  NMR spectrum is rather more complicated than envisaged. Two singlets, each integrating to six protons, appear at 1.97 and 1.75 ppm and correspond to the methyl groups of a (*R,R*)-TMCDA ligand, indicating that (*R,R*)-TMCDA remains coordinated to a metal centre in arene solution. More specifically, these solution studies suggest that the (*R,R*)-TMCDA ligand is actually coordinated to a Na cation as the resonances associated with the HMDS ligands are essentially identical to those found in a genuine sample of donor-free  $\text{Mg}(\text{HMDS})_2$ .<sup>[37c, 209]</sup> This indicates that **110** undergoes reorganisation in solution to yield  $[({}^n\text{BuNa})_2\cdot\{(\text{R,R})\text{-TMCDA}\}_x]$  and  $\text{Mg}(\text{HMDS})_2$ .

Returning to complexes **108** and **109**, given that both of these diamine-NaHMDS systems have formally captured monomeric NaOH, we envisaged that similar systems could encapture substoichiometric quantities of other salts, particularly the Lewis amphoteric metal halides, and in doing so, develop a new Group 1 macrocyclic/supramolecular family of complexes. The results from these studies will be discussed in the following chapter.



## Chapter 4: New Developments in Lithium and Sodium Amide Chemistry; Capturing Halides to Form Metal Anionic Crowns

As detailed in chapter 1, alkali metal halide salts (particularly those of lithium) can produce substantial positive or negative effects on the reactivity and/or selectivity of organic transformations.<sup>[176]</sup> In many circumstances, the metal halide salt formed *in situ* in a metathesis reaction is dismissed as an innocent by-product. Recent publications (discussed in greater detail in chapter 1, section 1.7) have shown how lithium halides can affect organometallic reactions in a profound way. For instance, Knochel has excelled in exploiting this effect, adding stoichiometric LiCl to conventional Grignard reagents to induce an enhanced reactivity with respect to that of monometallic magnesium reagents.<sup>[86k]</sup> Collum has shown that LiCl catalysis in organic reactions is detectable with even miniscule concentrations (<1.0 mol% LiCl) and that ‘striking accelerations’ (70 fold) are customary.<sup>[178n, 178v]</sup> Despite this, firm structural evidence of the crucial halide-incorporated species which may be involved in these reactions is rare.<sup>[177e, 177h, 178w]</sup>

In this chapter we start to deconvolute the complex chemistry at work when synthetically important alkali metal bis(trimethylsilyl)amides come into contact with a halide source, and in doing so, a new Group 1 macrocyclic/supramolecular family of complexes has emerged.<sup>[260]</sup> Pertinent to this work was the synthesis and characterisation of the first inverse crown ether anion complexes within the group – the previously discussed hydroxyl-incorporated sodium sodiates  $[(-)\text{-sparteine}\cdot\text{Na}(\mu\text{-HMDS})\text{Na}\cdot(-)\text{-sparteine}]^+[\text{Na}_4(\mu\text{-HMDS})_4(\mu_4\text{-OH})]^-$ ,<sup>[249]</sup> **108** (chapter 3, section 3.3, [Scheme 3.5](#)) and  $[\text{Na}\{(R,R)\text{-TMCDA}\}_2]^+[\text{Na}_4(\mu\text{-HMDS})_4(\mu_4\text{-OH})]^-$ , **109** (chapter 3, section 3.3, [Scheme 3.6](#)). Given that both of these diamine-NaHMDS systems have formally captured monomeric NaOH, we envisaged that similar systems could capture substoichiometric quantities of other salts, particularly the Lewis amphoteric metal halides, which appear far more important than metal hydroxides for metal salt-enhanced reactions.

Our research focused on growing crystals suitable for X-ray analysis that could provide insight into species potentially present in alkali metal bis(trimethylsilyl)amide-halide-containing solutions used in organic transformations. Initially concentrating on LiHMDS systems and investigating several approaches in reaching this goal (detailed in section 4.1), we successfully isolated four solvent-separated ion pair complexes; two of the form  $[\text{Li}\cdot\{(R,R)\text{-TMCDA}\}_2]^+[\text{Li}_5(\mu\text{-HMDS})_5(\mu_5\text{-X})]^-$  (where X = Cl or Br); and two of the form  $[\text{Me}_6\text{-TREN}\cdot\text{Li}(\mu\text{-X})\text{Li}\cdot\text{Me}_6\text{-TREN}]^+[\text{Li}_5(\mu\text{-HMDS})_5(\mu_5\text{-X})]^-$  [where Me<sub>6</sub>-TREN = tris[2-

(dimethylamino)ethyl]amine and X = Cl or Br]. Similar to complexes **108** and **109**, in which NaOH has been captured within their respective molecular frameworks, the former two complexes have captured one LiX unit and the latter two complexes two LiX units (bearing parallels with **108** where an additional monomeric NaHMDS unit has been trapped). The anions of these complexes – ten-membered (LiN)<sub>5</sub> rings (which host halide guests) – are unprecedented. In addition, the Li–X–Li bond angle in the latter two complexes is found to be linear, which is unique with regards to a Li–Br–Li cation and extremely rare for a Li–Cl–Li cation.<sup>[261]</sup>

The four complexes obtained here can be considered as belonging to a new class of complexes called *metal anionic crowns* (MAC). Closely related to known inverse crown complexes,<sup>[84-85]</sup> this type of complex has two important differences. Firstly, the MAC complexes are monometallic (specifically alkali metals to date), and secondly, they are ionic, solvent-separated ion pairs, unlike inverse crowns, which are heterobimetallic neutral entities. Therefore, the novel complexes boast a perfect inverse topological relationship to conventional crown ether complexes, which have the general formula [M(crown)]<sup>+</sup>[anion]<sup>-</sup>.<sup>[101]</sup>

Whilst initially trying to prepare the lithium bromide Me<sub>6</sub>-TREN MAC complex an unusual hydroxyl-incorporated species was isolated. Unlike complexes **108** and **109** which are sodium sodiates, the hydroxyl-incorporated solvent-separated system isolated here is a lithium lithiate.

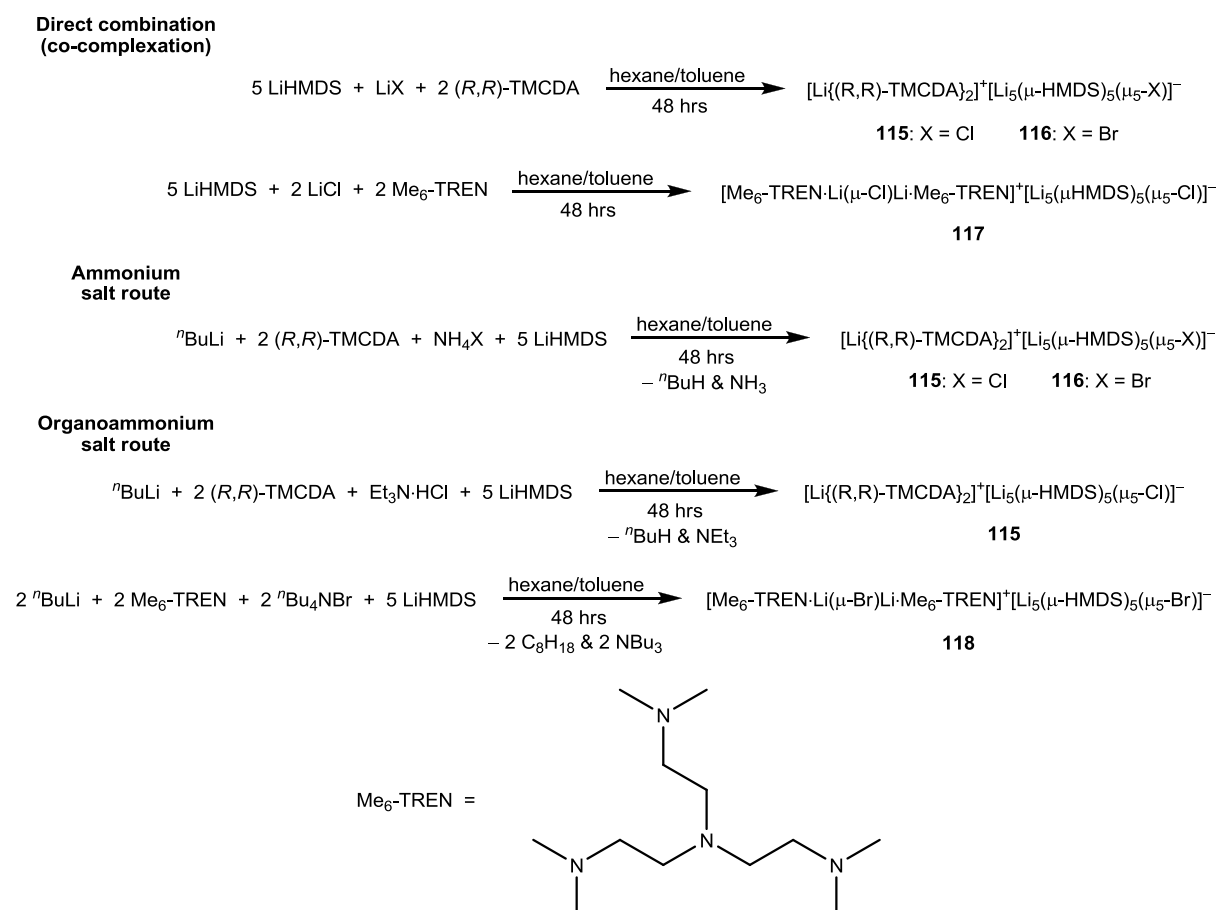
Having successfully prepared lithium MAC complexes, our attention turned to extending these complexes to include sodium MAC complexes. Sodium chloride-containing MAC complexes were not forthcoming; however, sodium bromide- and sodium iodide-containing MAC complexes of the form [Me<sub>6</sub>-TREN·Na(μ-X)Na·Me<sub>6</sub>-TREN]<sup>+</sup>[Na<sub>5</sub>(μ-HMDS)<sub>5</sub>(μ<sub>5</sub>-X)]<sup>-</sup> (where X = Br or I), were successfully synthesised. Ten-membered (NaN)<sub>5</sub> rings are unique and the bromide complex represents the first example of a Na–Br–Na cation.

Finally, during our investigations into the design and synthesis of novel MAC complexes, other non-MAC mixed alkali metal amide-alkali metal halide complexes were found to be forthcoming at times. Six non-MAC complexes were isolated in total.

## 4.1 Mixed Lithium Amide-Lithium Halide Compounds: Unusual Halide-Deficient Amido Metal Anionic Crowns

Here we report some of our recent efforts in uncovering the complex chemistry at work when synthetically important lithium amides come into contact with a halide source, including the isolation and characterisation of the first members of a new class of macrocyclic complexes.<sup>[260]</sup>

Our research focused on growing crystals suitable for X-ray analysis that could provide insight into species potentially present in lithium amide-halide-containing solutions used in organic transformations. We have investigated several approaches in reaching this goal. Firstly, by attempting direct combination (co-complexation) of LiHMDS and an amine with sub-stoichiometric LiX (where X = Cl or Br); secondly, by combining <sup>n</sup>BuLi with an amine and then introducing NH<sub>4</sub>X (ammonium salt route),<sup>[262]</sup> followed by super-stoichiometric LiHMDS; and thirdly, by treating Et<sub>3</sub>N·HCl/<sup>n</sup>Bu<sub>4</sub>NBr (organoammonium salt route) in a similar manner to the previous approach (Scheme 4.1).



Scheme 4.1 Various synthetic routes to complexes 115-118.

Gratifyingly, these reactions provide us with enhanced structural insight into the coordination of LiX with LiHMDS. For brevity, only the co-complexation route (for **115-117**) and the organoammonium salt route (for **118**) are discussed herein, although full details of the other routes possible to these complexes are given in chapter 5, sections 5.3.30-5.3.33.

#### 4.1.1 Complexes **115** and **116**

The first reaction combined LiHMDS, LiCl and the chiral diamine (*R,R*)-TMCDA, initially in a 1 : 1 : 1 stoichiometric ratio in hexane solution. A small crop of X-ray quality crystalline material was afforded from this mixture after 24 hours. X-ray crystallographic analysis revealed that despite the equimolar ratio of LiHMDS and LiCl in the reaction, crystallisation of the chloride-incorporated solvent-separated hexanuclear lithium lithiate  $[\text{Li}\{(R,R)\text{-TMCDA}\}_2]^+[\text{Li}_5(\mu\text{-HMDS})_5(\mu_5\text{-Cl})]^-$ , **115**, resulted (Figure 4.1). Complex **115** can also be prepared by utilising a rational stoichiometry, that is, a ratio of LiHMDS : LiCl : (*R,R*)-TMCDA of 5 : 1 : 2, as well as by utilisation of the higher yielding ammonium salt and organoammonium salt routes (Scheme 4.1).

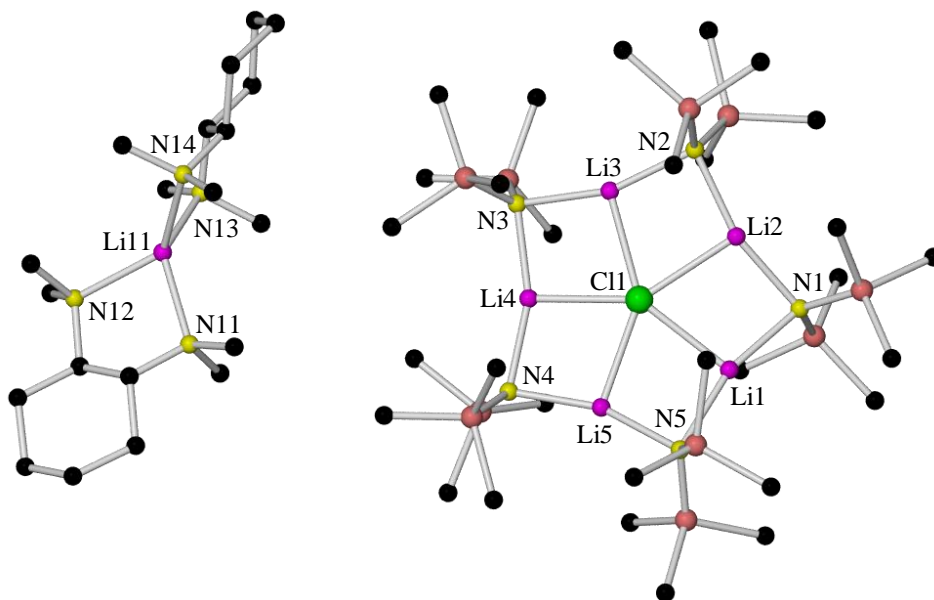


**Figure 4.1** Molecular structure of  $[\text{Li}\{(R,R)\text{-TMCDA}\}_2]^+[\text{Li}_5(\mu\text{-HMDS})_5(\mu_5\text{-Cl})]^-$ , **115**. Left: cation, right: anion. H atoms omitted and only one of two independent sets of ions in the asymmetric unit shown for clarity.

Complex **115** crystallises in the monoclinic system, space group  $P2_1$ , and exists as a solvent-separated ion pair. The cation of **115** has been observed before within the previously discussed complex  $[\text{Li}\{(R,R)\text{-TMCDA}\}_2]^+[\text{Mg}(\text{HMDS})_3]^-$ ,<sup>[248]</sup> **102** (chapter 3, section 3.2.1, Figure 3.13). The differences in the structural parameters of these two cations are minor, and thus the cation of **115** warrants no further discussion. The anion of **115** is a ten-membered  $(\text{LiN})_5$  ring of alternating metal and nitrogen atoms that hosts a chloride anion. Within the

asymmetric unit of **115** there are two independent sets of  $[\text{Li}\{(R,R)\text{-TMCD A}\}_2]^+[\text{Li}_5(\mu\text{-HMDS})_5(\mu_5\text{-Cl})]^-$  ions; however, the differences in the dimensions of the two sets of ions are negligible, and thus Table 4.1 and Table 4.2 detail the key bond distances and angles respectively of only one of the independent anions.

Selected Bond	Bond Distance (Å) in $[\text{Li}\{(R,R)\text{-TMCD A}\}_2]^+[\text{Li}_5(\mu\text{-HMDS})_5(\mu_5\text{-Cl})]^-$ , <b>115</b>
Li1–N1	2.065(9)
Li1–N5	2.090(9)
Li1–Cl1	2.451(6)
Li2–N1	2.065(8)
Li2–N2	2.053(8)
Li2–Cl1	2.468(8)
Li3–N2	2.038(8)
Li3–N3	2.053(8)
Li3–Cl1	2.426(7)
Li4–N3	2.054(8)
Li4–N4	2.033(9)
Li4–Cl1	2.414(7)
Li5–N4	2.051(8)
Li5–N5	2.064(7)
Li5–Cl1	2.435(8)

**Table 4.1** Key bond distances within the anion of  $[\text{Li}\{(R,R)\text{-TMCD A}\}_2]^+[\text{Li}_5(\mu\text{-HMDS})_5(\mu_5\text{-Cl})]^-$ , **115**.

Selected Angle	Bond Angle (°) in $[\text{Li}\{(R,R)\text{-TMCD A}\}_2]^+[\text{Li}_5(\mu\text{-HMDS})_5(\mu_5\text{-Cl})]^-$ , <b>115</b>
N1–Li1–N5	163.3(3)
N1–Li2–N2	161.4(4)
N2–Li3–N3	161.8(4)
N3–Li4–N4	160.8(4)
N4–Li5–N5	160.0(5)
Li1–N1–Li2	87.5(3)
Li2–N2–Li3	89.9(3)
Li3–N3–Li4	89.0(3)
Li4–N4–Li5	88.9(3)
Li1–N5–Li5	86.7(3)

**Table 4.2** Key bond angles within the anion of  $[\text{Li}\{(R,R)\text{-TMCD A}\}_2]^+[\text{Li}_5(\mu\text{-HMDS})_5(\mu_5\text{-Cl})]^-$ , **115**.

This unexpected entity must be considered in the context of the well-developed structural chemistry of LiHMDS species. As alluded to in chapter 1, donor-free LiHMDS exists as a trimer in the solid-state,<sup>[11a, 11b]</sup> whilst solution studies by Collum reveal that an equilibrium exists between a dimeric and a tetrameric species.<sup>[253]</sup> To the best of our knowledge, a discrete ten-atom (LiN)<sub>5</sub> ring (or indeed of any lithium anion combination) has not been reported to date. Indeed, pentanuclear Li<sub>5</sub> species of any compound class or architecture are exceptionally rare.<sup>[263]</sup>

Returning to the theme of halide entrapment, the lithium amidinate  $[\text{Li}\{(\text{}^n\text{Bu})\text{C}(\text{N}^t\text{Bu})_2\}]$  can capture halide salts to form ladders which dimerise to form complexes such as  $[\{\text{Li}(\text{}^n\text{Bu})\text{C}(\text{N}^t\text{Bu})_2\}_2\cdot\text{LiX}\cdot\text{THF}]_2$  (where  $\text{X} = \text{Cl}$  or  $\text{Br}$ ) or, due to solvation, trinuclear ladders such as  $[\{\text{THF}\cdot\text{Li}(\text{}^n\text{Bu})\text{C}(\text{N}^t\text{Bu})_2\}_2\cdot\text{LiI}]$  can form, the latter could be considered as adopting a *hemi-MAC* motif.<sup>[264]</sup> Other structures which adopt this motif include the trilithium amido reagents  $[(\text{DAME}\cdot\text{LiHMDS})_2\cdot\text{LiCl}]$ ,<sup>[177h]</sup> **119** [where DAME is 2-(*N,N*-dimethylamino)ethyl methyl ether],  $[(\text{TMEDA}\cdot\text{LiHMDS})_2\cdot\text{LiCl}]$ ,<sup>[177h]</sup> **120**,  $[(\text{TMEDA}\cdot\text{LiN}^i\text{Pr}_2)_2\cdot\text{LiCl}]$ ,<sup>[177e]</sup> **121** and  $[\{\text{THF}\cdot\text{Li}(\text{N}(\text{Ad})(\text{SiMe}_3))\}_2\cdot\text{LiI}]$ ,<sup>[10i]</sup> **122**, which is formed serendipitously by the reaction of  $[\text{Li}\{\text{N}(\text{Ad})(\text{SiMe}_3)\}]$  and  $\text{CaI}_2$  in THF solution (Figure 4.2).

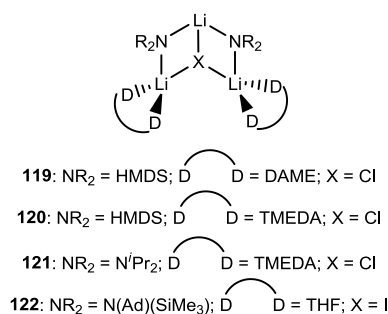


**Figure 4.2** Examples of amide-containing *hemi-MAC* complexes.

It is perhaps surprising that during our studies we did not encounter any structures which embraced this *hemi-MAC* motif (especially when higher amide : halide ratios were utilised) underlining the complexity of the chemistry which is involved in these seemingly so simple systems.

Returning to the anion of **115**, its mean Li–Cl bond distance is 2.439 Å, which is longer than those in the aforementioned *hemi-MAC* complexes (range of mean Li–Cl bond distances, 2.342–2.361 Å),<sup>[177e, 177h]</sup> which is most likely due to the higher  $\mu_5$ -coordination of the chlorine atom in **115**. In addition to the Li–Cl bonding within the star-shaped ring of the anion, each Li centre is bound to two amido N atoms (mean Li–N bond distance, 2.057 Å). The mean ‘point’ Li–N–Li and ‘side’ N–Li–N angles for the ten-membered ring are 88.40 and 161.46° respectively. The ring is puckered at the N1 atom (Figure 4.3), and the remaining nine annular atoms are essentially planar [N1 is situated 0.895(5) Å out of this plane], with the chloride ion co-planar with the lithium cations. Initially, this data suggested that the cavity formed by a planar  $(\text{LiN})_5$  ring would be too large to adequately sequester the chloride anion, and this thought prompted the investigation of bromide capture (*vide infra*); however, in subsequent  $(\text{LiN})_5$  anions of this type [isolated by ourselves and subsequently by Layfield<sup>[265]</sup> (*vide*

*infra*], the  $(\text{LiN})_5$  rings were found to be planar, indicating that the puckered nature of the anion in **115** was perhaps due to an artefact of crystal packing.

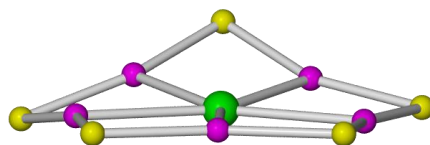


**Figure 4.3** Alternative view of the anion of **115** showing the puckered nature of the  $(\text{LiN})_5$  ring. Amide atoms are omitted for clarity.

Following the direct combination route, utilising a ratio of LiHMDS : LiBr :  $(R,R)$ -TMCD A of 5 : 1 : 2 (Scheme 4.1), afforded the bromide-containing MAC  $[\text{Li}\{(R,R)\text{-TMCD A}\}_2]^+[\text{Li}_5(\mu\text{-HMDS})_5(\mu_5\text{-Br})]^-$ , **116**. Unfortunately, the X-ray data obtained was of poor quality, thus precluding any discussion of structural parameters; however, atom connectivity was unambiguous. The ammonium salt route was also undertaken to improve the yield of the compound and to hopefully obtain better X-ray data; however, such data was not forthcoming.

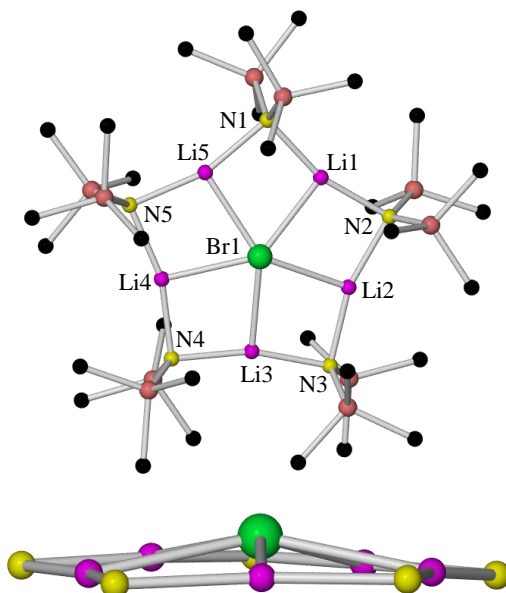


**Figure 4.4** Molecular structure of the anion of  $[\text{Li}\{(R,R)\text{-TMCD A}\}_2]^+[\text{Li}_5(\mu\text{-HMDS})_5(\mu_5\text{-Br})]^-$ , **116** (top), and an alternative view showing the relatively planar nature of the  $(\text{LiN})_5$  ring (bottom). Only one of two independent anions in the asymmetric unit shown for clarity. H atoms, amide atoms (bottom) solvent of crystallisation (toluene) and disorder component are also omitted for clarity.

The most striking features of the anion of **116** (Figure 4.4) with respect to **115** is that the entire  $(\text{LiN})_5$  ring is planar, and the bromine atom, rather than occupying a position in the plane of the ring, is situated approximately 0.5 Å above or below the plane (as it is disordered over both sites, occupancy 50 : 50).

MAC formation seems to be largely insensitive towards the sequestering amine as (*R,R*)-TMCDA, TMEDA and the potentially tetradentate donor Me<sub>6</sub>-TREN all give rise to this unusual anion (*vide infra*). The structures of the products obtained using TMEDA were essentially isostructural to their (*R,R*)-TMCDA analogues;<sup>[266]</sup> however, the X-ray data obtained was of poor quality. When Me<sub>6</sub>-TREN was utilised, a different cation to that observed in **115** and **116** was obtained (*vide infra*).

Turning to solution studies, complexes **115** and **116** were dissolved in C<sub>6</sub>D<sub>6</sub> solution and examined by <sup>7</sup>Li, <sup>1</sup>H, <sup>13</sup>C, COSY and HSQC NMR spectroscopy (full NMR details can be found in chapter 5, section 5.3.30 and 5.3.31 respectively). In both cases, <sup>7</sup>Li spectra revealed two different environments, in keeping with the solid-state structures. The expected diamine to HMDS ratio in the respective <sup>1</sup>H NMR spectra was observed and the resonances associated with the diamine and the HMDS ligand were different from those encountered in the free diamine and both the free amine and the free alkali metal amide respectively, indicating that the solid-state structures of **115** and **116** appear to remain intact in solution.

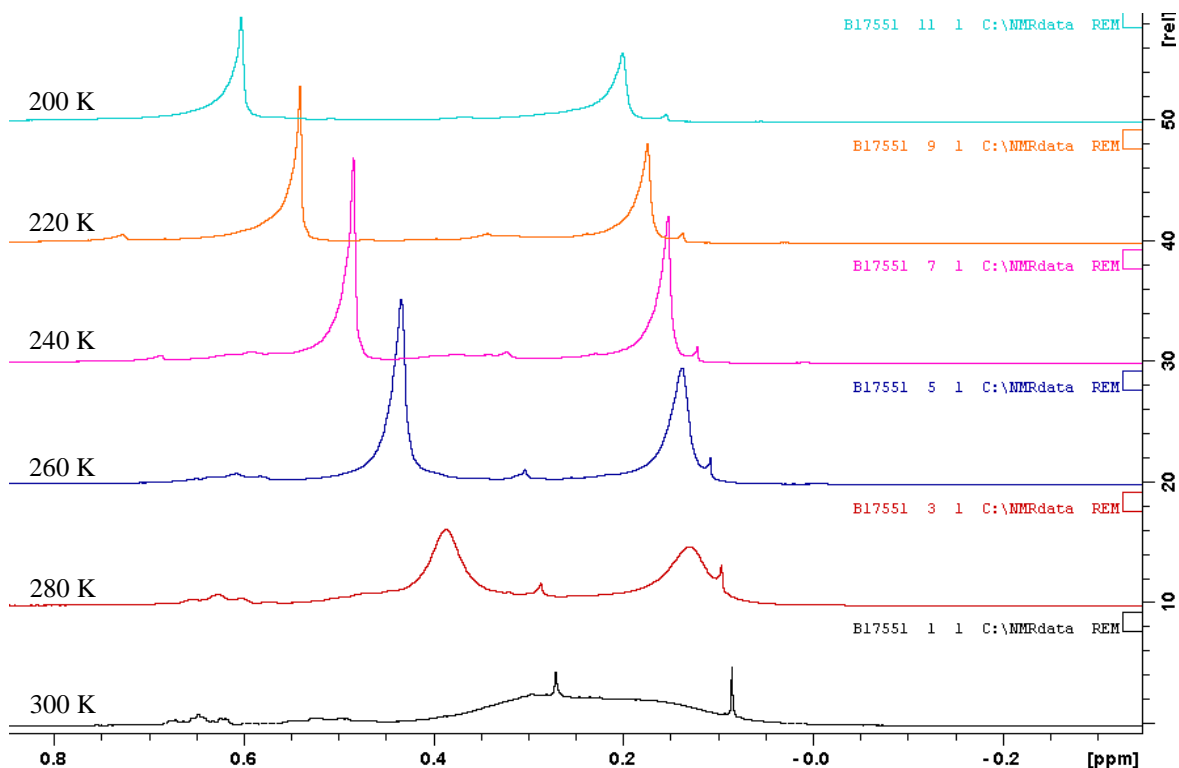


Figure 4.5 Variable temperature <sup>1</sup>H NMR spectra of **116** in C<sub>6</sub>D<sub>5</sub>CD<sub>3</sub>.

An interesting feature was observed in the <sup>1</sup>H NMR spectrum of **116**. Two extremely broad SiCH<sub>3</sub> resonances were observed, which is most likely due to conformational fluctuations of the (LiN)<sub>5</sub> ring and the fact that the bromide ion sits out of the ring plane, giving rise to inequivalence in the tetrahedrally-orientated TMS groups. A low temperature NMR



spectroscopic study of the complex in  $d_8$ -toluene solution proved effective in deconvoluting the two HMDS resonances into two distinct sharp peaks (Figure 4.5).

#### 4.1.2 Complexes 117 and 118

The versatile ( $\kappa^3$ <sup>[252, 267]</sup> or  $\kappa^4$ <sup>[268]</sup>) dentate, readily synthesised,  $\text{Me}_6\text{-TREN}$ <sup>[269]</sup> donor ligand was investigated as a possible sequestering amine in the preparation of similar complexes to that of **115** and **116**, due to its recent application in Group 1 metal chemistry within our group<sup>[270]</sup> and outwith in the wider research community.<sup>[252]</sup> Combining LiHMDS, LiCl and  $\text{Me}_6\text{-TREN}$  in a 1 : 1 : 1 stoichiometric ratio in hydrocarbon solution afforded a small crop of X-ray quality crystals after two hours. X-ray crystallographic analysis revealed that despite the equimolar ratio of LiHMDS and LiCl in the reaction, crystallisation of the chloride-incorporated solvent-separated septanuclear lithium lithiate  $[\text{Me}_6\text{-TREN}\cdot\text{Li}(\mu\text{-Cl})\text{Li}\cdot\text{Me}_6\text{-TREN}]^+[\text{Li}_5(\mu\text{-HMDS})_5(\mu_5\text{-Cl})]^-$ , **117**, resulted. Complex **117** can also be prepared by utilising a rational stoichiometry, that is, a ratio of LiHMDS : LiCl :  $\text{Me}_6\text{-TREN}$  of 5 : 2 : 2 (Scheme 4.1).

Complex **117** crystallises in the monoclinic system, space group  $C2/c$ , and exists as a solvent-separated ion pair, which in terms of composition, possesses an identical anion to **115** but a different cation (Figure 4.6). Now an additional LiCl unit has been captured, thus bearing parallels with the previously presented  $[(-)\text{-sparteine}\cdot\text{Na}(\mu\text{-HMDS})\text{Na}\cdot(-)\text{-sparteine}]^+[\text{Na}_4(\mu\text{-HMDS})_4(\mu_4\text{-OH})]^-$ ,<sup>[249]</sup> **108** (chapter 3, section 3.3, Scheme 3.5), where an additional monomeric NaHMDS unit has been trapped. All four nitrogen donor atoms of the  $\text{Me}_6\text{-TREN}$  ligand coordinate to one lithium centre, whose coordination sphere is completed by a chlorine atom locked in a linear Li–Cl–Li chain [Li–Cl–Li angle,  $180.00(15)^\circ$ ]. Table 4.3 details the key bond distances within the cation of **117** (full X-ray data can be found on the accompanying CD).

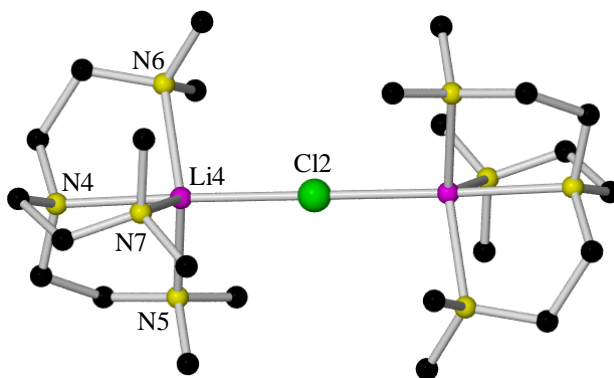


**Figure 4.6** Molecular structure of the cation of  $[\text{Me}_6\text{-TREN}\cdot\text{Li}(\mu\text{-Cl})\text{Li}\cdot\text{Me}_6\text{-TREN}]^+[\text{Li}_5(\mu\text{-HMDS})_5(\mu_5\text{-Cl})]^-$ , **117**. H atoms and solvent of crystallisation (toluene) are omitted for clarity.

Selected Bond	Bond Distance (Å) in [Me <sub>6</sub> -TREN·Li(μ-Cl)Li·Me <sub>6</sub> -TREN] <sup>+</sup> [Li <sub>5</sub> (μ-HMDS) <sub>5</sub> (μ <sub>5</sub> -Cl)] <sup>-</sup> , <b>117</b>
Li4–N4	2.254(3)
Li4–N5	2.257(3)
Li4–N6	2.217(3)
Li4–N7	2.186(3)
Li4–Cl2	2.401(3)

**Table 4.3** Key bond distances within the cation of [Me<sub>6</sub>-TREN·Li(μ-Cl)Li·Me<sub>6</sub>-TREN]<sup>+</sup>[Li<sub>5</sub>(μ-HMDS)<sub>5</sub>(μ<sub>5</sub>-Cl)]<sup>-</sup>, **117**.

The κ<sup>4</sup> coordination of Me<sub>6</sub>-TREN here represents merely the second example of such Me<sub>6</sub>-TREN–Li bonding, having only been observed hitherto in the monomeric complex [Me<sub>6</sub>-TREN·LiCH<sub>2</sub>Ph],<sup>[270]</sup> **123**. In addition, the centrosymmetric cation of **117** is a rare example of a linear Li–Cl–Li cation, the only two previous examples being [PMDETA·Li(μ-Cl)Li·PMDETA]<sup>+</sup>,<sup>[261a]</sup> **124** and [(THF)<sub>3</sub>·Li(μ-Cl)Li·(THF)<sub>3</sub>]<sup>+</sup>,<sup>[261b]</sup> **125** (which possess Li- and Zr-containing counter-anions respectively). The Me<sub>6</sub>-TREN ligands in **117** are staggered perfectly with respect to one another so as to minimise repulsion (Figure 4.7), and the Li–Cl bond distance [2.401(3) Å] is 0.231 Å greater than the corresponding bond distance in **124** [2.170(3) Å], despite the coordination number of the Li centres in **117** being only one greater than that of the Li centres in **124** (from four coordinate to five coordinate due to the κ<sup>4</sup> coordination of Me<sub>6</sub>-TREN *vs.* the κ<sup>3</sup> coordination of PMDETA). The unusual five coordinate Li centres in **117** are in trigonal bipyramidal environments (where N4 and Cl2 adopt the pseudo-axial positions, whilst the three NMe<sub>2</sub> groups of the Me<sub>6</sub>-TREN ligand occupy the pseudo-equatorial positions) and the mean Li–N bond distance (2.229 Å) is slightly shorter (by 0.021 Å) than that found in the aforementioned Me<sub>6</sub>-TREN monomer complex **123** (mean Li–N bond distance, 2.250 Å).

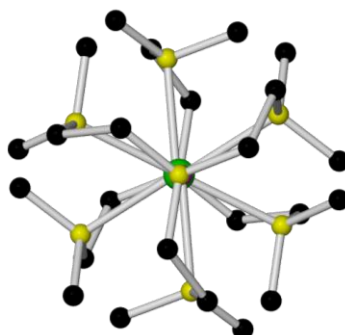


**Figure 4.7** Alternative view of of the cation of [Me<sub>6</sub>-TREN·Li(μ-Cl)Li·Me<sub>6</sub>-TREN]<sup>+</sup>[Li<sub>5</sub>(μ-HMDS)<sub>5</sub>(μ<sub>5</sub>-Cl)]<sup>-</sup>, **117**, showing the staggered arrangement of the Me<sub>6</sub>-TREN ligands. H atoms and solvent of crystallisation (toluene) are omitted for clarity.

Subsequent to the publication of complexes **115** and **117**, Layfield reported the serendipitous isolation of the (LiN)<sub>5</sub> anion whilst preparing cationic guanidinate-bridged bimetallic cubes, by reacting the heteroleptic lithium amide [Li<sub>3</sub>(μ-HMDS)<sub>2</sub>(μ,μ-HPP)] (where HPP is hexahydropyrimidopyrimidine) with MnCl<sub>2</sub> or CoCl<sub>2</sub> respectively.<sup>[265]</sup> In these anions, the (LiN)<sub>5</sub> ring is planar with a mirror plane present along one of the Li–Cl bonds. This was also found to be the case in **117**; however, as discussed previously, the (LiN)<sub>5</sub> ring in **115** was found to be puckered at one of the N atoms. As a planar (LiN)<sub>5</sub> ring can adequately sequester a chloride anion, the puckered nature of the ring in **115** was attributed to crystal packing effects. As expected, there is little discrimination in the structural parameters of the four (LiN)<sub>5</sub> rings (Table 4.4).

Selected Mean Bond Distance (Å) and Angle (°)	<b>115</b>	<b>117</b>	Layfield's anion (Mn cation)	Layfield's anion (Co cation)
Li–N	2.057	2.055	2.059	2.058
Li–Cl	2.439	2.447	2.438	2.449
N–Li–N	161.46	161.03	160.24	160.72
Li–N–Li	88.40	88.89	88.24	88.74

**Table 4.4** Selected bond distances and angles for the anion within complexes **115**, **117** and Layfield's Mn and Co complexes.

As the replacement of (*R,R*)-TMCDA [and TMEDA (*vide supra*)] with Me<sub>6</sub>-TREN in the reaction utilised to prepare chloride-containing complex **115** yielded the same anion, but a different cation to that in **115** (*vide supra*), the analogues Me<sub>6</sub>-TREN bromide reaction was attempted. Firstly, to hopefully obtain better X-ray data (to that of bromide-containing complex **116**), so as to compare the structural parameters of the anticipated bromide encapsulated anion with that of its chloride analogues (**115** and **117**, and subsequently Layfield's anions). Secondly, to compare the structural parameters of the anticipated LiBr captured cation with that of its LiCl analogue (**117**).

As we had found the ammonium salt route to be higher yielding in the synthesis of complexes **115** and **116**, we by-passed the direct combination route and concentrated on utilising the more soluble tetrabutylammonium bromide reagent in the organoammonium route (Scheme 4.1) in attempts to prepare a bromide analogue of **117**. This route proved successful, and the bromide-containing MAC [Me<sub>6</sub>-TREN·Li(μ-Br)Li·Me<sub>6</sub>-TREN]<sup>+</sup>[Li<sub>5</sub>(μ-HMDS)<sub>5</sub>(μ<sub>5</sub>-Br)]<sup>-</sup>, **118**, was obtained in moderate yield.

Bromide-containing complex **118** crystallises in the monoclinic system, space group *C2/c*, and akin to its chloride analogue **117**, the structure of **118** is composed of a Me<sub>6</sub>-TREN sequestered linear Li–X–Li cation and a ten-membered planar (LiN)<sub>5</sub> ring which hosts a halide anion; however here, as encountered in the anion of **116**, the bromine atom in the anion

of **118** is disordered over two sites in the centre of the planar metal-amido ring due to its larger size compared to chlorine. The anion of **118** is also isostructural to the chloride containing anions of **115**, **117** and Layfield's Mn and Co complexes. As the isostructural component parts of complex **118** have previously been shown (cation: [Figure 4.6](#); anion: [Figure 4.4](#)), the molecular structure of **118** will not be shown, nor will the key bond distances and angles be tabulated (full X-ray data can be found on the accompanying CD).

Similar to the cation of **117**, the Me<sub>6</sub>-TREN ligands (staggered with respect to one another so as to minimise repulsion) are  $\kappa^4$  coordinated to the Li centres in the centrosymmetric anion of **118**, and thus **118** represents merely the third example of such Me<sub>6</sub>-TREN–Li bonding (the other complex being the aforementioned monomeric complex [Me<sub>6</sub>-TREN·LiCH<sub>2</sub>Ph],<sup>[270]</sup> **123**). In addition, the centrosymmetric cation of **118** is an unprecedented example of a linear Li–Br–Li cation [Li–Br–Li angle, 180.0(3)°]. The only previous cations of this form are non-linear [(THF)<sub>3</sub>·Li(μ-Br)Li·(THF)<sub>3</sub>]<sup>+</sup> cations found within gallium cluster chemistry.<sup>[271]</sup> As expected, due to the larger size of a bromine atom in comparison to a chlorine atom, the Li–X bond distance is greater in bromine-containing **118** [(2.579(4) Å)] than in chlorine-containing **117** [2.401(3) Å]. The mean Li–N bond distance in **118** (2.213 Å) is shorter than that found in **117** (2.229 Å) and **123** (2.250 Å).

The anion of **118** is isostructural to the previously discussed chloride anions of **115**, **117** and Layfield's Mn and Co complexes; however here (as encountered in the anion of **116**), the bromine atom, rather than occupying a position in the plane of the (LiN)<sub>5</sub> ring (as is the case for the chlorine atom in **115**, **117** and Layfield's Mn and Co complexes), is situated approximately 0.5 Å above or below the plane (as it is disordered over both sites). In keeping with the larger encapsulated halide ion, the structural parameters of the anion of **118** (mean Li–N and Li–X bond distance, 2.067 and 2.557 Å respectively; mean Li–N–Li and N–Li–N angle, 91.59 and 163.70° respectively) are greater than that of **115**, **117** and Layfield's Mn and Co complexes (*vide supra*).

Williard unexpectedly formed a tetranuclear ladder complex ([Figure 4.8](#)), which can also be regarded as adopting a *hemi-MAC* motif (*vide supra*), during his investigations into the use of lithium halide additives in enolisation and addition reactions.<sup>[272]</sup> The mean Li–Br bond distance of this complex (2.609 Å) is 0.052 Å greater than the corresponding distance in the anion of **118** (2.557 Å), presumably due to the greater steric demands of the surrounding ligands here.

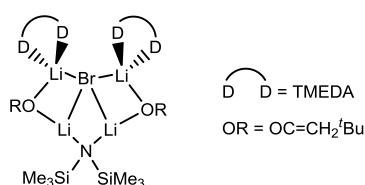


**Figure 4.8** Structural representation of Williard's *hemi*-MAC complex.

In hindsight, it is unusual that during our studies we did not isolate any complexes with a *hemi*-MAC motif; however, after our first successful synthesis of a MAC complex, our reaction systems were 'designed' to obtain MAC motifs, whereas the *hemi*-MAC motifs were obtained serendipitously. Presumably the isolation of a MAC complex first time round was due to a combination of subtle steric effects.

Whilst initially trying to prepare complex **118**, crystals were obtained utilising the ammonium salt route. X-ray crystallographic studies revealed that these crystals were not the expected product, but another unusual hydroxyl-incorporated species [prior hydroxyl-incorporated species being complexes **108** and **109** discussed previously (chapter 3, section 3.3)]. Unlike complexes **108** and **109** which are sodium sodiates, the hydroxyl-incorporated solvent-separated system which was isolated here is a lithium lithiate,  $[\text{Me}_6\text{-TREN}\cdot\text{Li}(\mu\text{-Br})\text{Li}\cdot\text{Me}_6\text{-TREN}]^+[\text{Li}_4(\mu\text{-HMDS})_4(\mu_4\text{-OH})]^-$ , **126** (full experimental details can be found in chapter 5, section 5.3.34). Hexanuclear complex **126** crystallises in the monoclinic system, space group *C*2, and possesses the same cation as that of **118** (and is the bromide analogue of the cation of **117**) and its anion is the lithium analogue of the anions of **108** and **109**, and thus its anion represents the third inverse crown ether anion to be reported. As the isostructural component parts of complex **126** have previously been shown (cation: [Figure 4.6](#); anion: [Figure 3.22](#)), the molecular structure of **126** will not be shown, nor will the key bond distances and angles be tabulated (full X-ray data can be found on the accompanying CD). In addition, as the cation of **126** is essentially identical to that of **118**, it warrants no further discussion.

Akin to its sodium anion analogues **108** and **109**, the anion of **126** consists of a perfectly planar eight-membered (MN)<sub>4</sub> ring which acts as a tetranuclear host towards a hydroxyl guest which is disordered over two sites in the centre of the metal-amido ring [one above and one below the plane of the (LiN)<sub>4</sub> ring]. As expected, due to the smaller size of the lithium metal centres, the mean M–N bond distance in **126** (2.083 Å) is shorter than the corresponding bond distance in **108** (2.398 Å) and **109** (2.416 Å), and consequently the mean M–O bond distance is also shorter in **126** (1.969, 2.336 and 2.286 Å for **126**, **108** and **109** respectively).

Veith *et al.* published discrete  $(\text{NaN})_4$  eight-membered rings in the pair of solvent-free sodium amides  $[\{\text{RNSiMe}_2\text{OSiMe}_2\text{NR}\}_2\text{Na}_4]^{[255]}$  (where R is  $t\text{Bu}$  or  $\text{SiMe}_3$ ). Similarly, he has reported three isostructural  $(\text{LiN})_4$  eight-membered rings (where R is  $t\text{Bu}$ ,  $\text{SiMe}_3$  or  $\text{SiMe}_2t\text{Bu}$ ); however (as discussed previously in regard to the sodium complexes), their structures are fundamentally different from that of the anion of **126**, as the rings in Veith's complexes deviate significantly from planarity, the Li centres are stabilised by internal chelation, and of course, these complexes are electronically neutral.

To the best of our knowledge, in addition to Veith's complexes, only another three discrete  $(\text{LiN})_4$  eight-membered rings have been previously reported. These are a tetralithium solvated tetrakis(1-naphthylimido)silicate tetraanion complex<sup>[273]</sup> and, perhaps most pertinent to this work, the tetrameric lithium amides,  $[\text{Li}(\text{TMP})]_4^{[12a]}$  and  $[\text{LiN}(\text{cyclohexyl})_2]_4^{[12b]}$ . Similar to **126**, the  $(\text{LiN})_4$  rings of the tetrameric lithium amides are planar. The mean Li–N bond distance in **126** (2.08 Å) is almost identical to that in the tetrameric amides (2.00 and 1.96 Å respectively), as is the mean 'side' N–Li–N angle of the eight-membered ring (mean N–Li–N angle, 167.5, 168.5 and 165.5° for **126** and the tetrameric amides respectively); however, the mean 'corner' Li–N–Li differs significantly from 77.5° in **126** to 101.5 and 105.5° in the tetrameric amides respectively, presumably due to the less steric demanding nature of the amide in **126** (HMDS) *versus* the amides (TMP and dicyclohexylamide respectively) in the tetrameric amides.

As alluded to in chapter 1, donor-free LiHMDS has been isolated in the solid-state as a trimer, forming a six-membered  $(\text{LiN})_3$  planar ring.<sup>[11a, 11b]</sup> Despite the incorporation of  $\text{OH}^-$  in the anion of **126**, the mean Na–N bond distance (2.08 Å) is essentially identical to that in trimeric LiHMDS (2.00 Å); the mean Li–N–Li and N–Li–N angles (92 and 148° respectively) are approximately 14° wider and 20° narrower than their respective counterparts in the anion of **126**.

To aid the interpretation of the NMR data obtained in this project and any future work, the  $^1\text{H}$ ,  $^{13}\text{C}$ , COSY and HSQC NMR spectra were obtained for the free amine standard,  $\text{Me}_6\text{-TREN}$ , in both  $\text{C}_6\text{D}_6$  and  $d_8\text{-THF}$  solution. The  $^1\text{H}$  and  $^{13}\text{C}$  spectra of  $\text{Me}_6\text{-TREN}$  in  $\text{C}_6\text{D}_6$  solution (Figure 4.9 and Figure 4.10) and  $d_8\text{-THF}$  solution (Figure 4.11 and Figure 4.12) are shown overleaf.

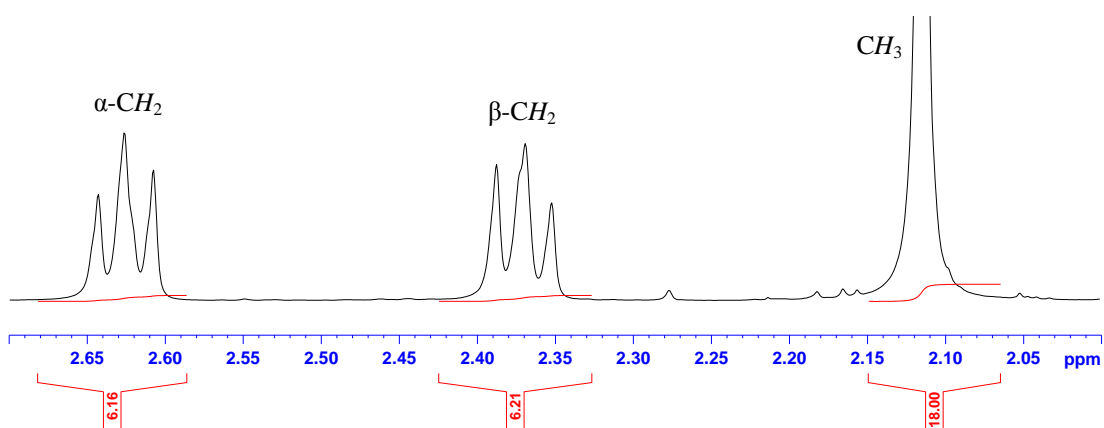


Figure 4.9 <sup>1</sup>H NMR spectrum of Me<sub>6</sub>-TREN in C<sub>6</sub>D<sub>6</sub>.

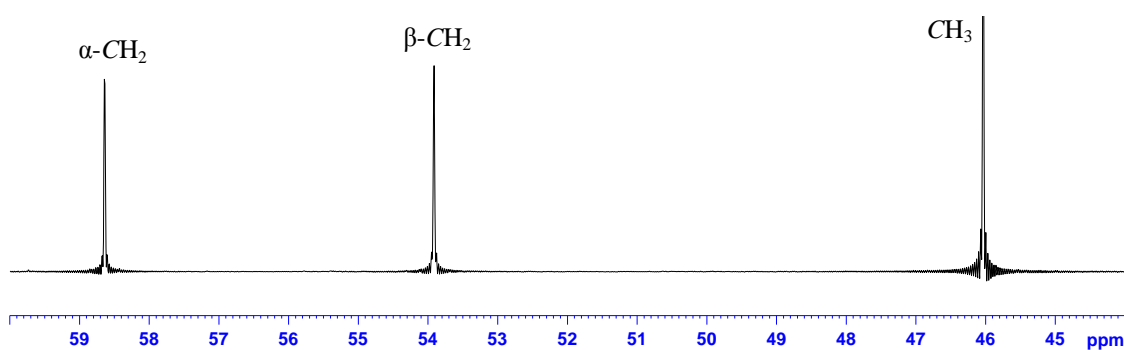


Figure 4.10 <sup>13</sup>C NMR spectrum of Me<sub>6</sub>-TREN in C<sub>6</sub>D<sub>6</sub>.

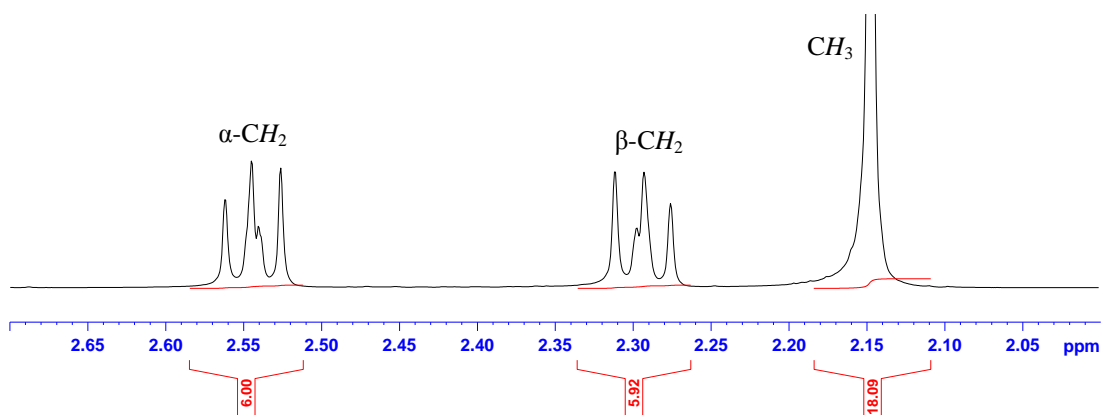


Figure 4.11 <sup>1</sup>H NMR spectrum of Me<sub>6</sub>-TREN in d<sub>8</sub>-THF.

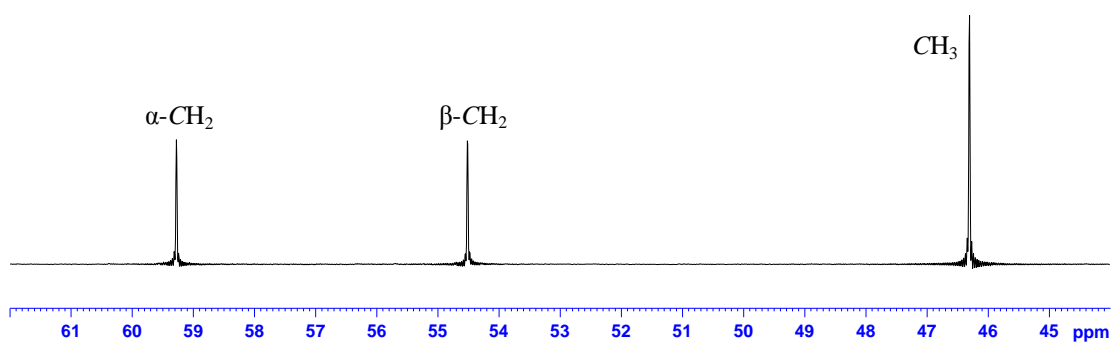


Figure 4.12 <sup>13</sup>C NMR spectrum of Me<sub>6</sub>-TREN in d<sub>8</sub>-THF.

In the  $C_6D_6$  spectrum there are three resonances observed for the three chemically distinct  $\alpha$ -,  $\beta$ - and methyl-hydrogen atoms. Two triplets, each integrating to six protons, appear at 2.63 and 2.37 ppm and correspond to the six  $\alpha$ - and six  $\beta$ -hydrogens respectively. Upfield from these triplets, a singlet, integrating to 12 protons appears at 2.12 ppm, which corresponds to the methyl hydrogens.

With the aid of the HSQC spectrum, the relevant chemical shifts from the  $^{13}C$  NMR spectrum were assigned to their respective proton chemical shifts from the  $^1H$  NMR spectrum and are shown in Table 4.5 and Table 4.6 respectively.

NMR chemical shifts of Me <sub>6</sub> -TREN in C <sub>6</sub> D <sub>6</sub>			
$^1H$ $\delta$ / ppm		$^{13}C$ $\delta$ / ppm	
$\alpha$ -CH <sub>2</sub>	2.63	$\alpha$ -CH <sub>2</sub>	58.6
$\beta$ -CH <sub>2</sub>	2.37	$\beta$ -CH <sub>2</sub>	53.9
CH <sub>3</sub>	2.12	CH <sub>3</sub>	46.0

Table 4.5  $^1H$  and  $^{13}C$  NMR chemical shifts of Me<sub>6</sub>-TREN in C<sub>6</sub>D<sub>6</sub>.

NMR chemical shifts of Me <sub>6</sub> -TREN in d <sub>8</sub> -THF			
$^1H$ $\delta$ / ppm		$^{13}C$ $\delta$ / ppm	
$\alpha$ -CH <sub>2</sub>	2.55	$\alpha$ -CH <sub>2</sub>	59.3
$\beta$ -CH <sub>2</sub>	2.29	$\beta$ -CH <sub>2</sub>	54.5
CH <sub>3</sub>	2.15	CH <sub>3</sub>	46.3

Table 4.6  $^1H$  and  $^{13}C$  NMR chemical shifts of Me<sub>6</sub>-TREN in d<sub>8</sub>-THF.

Turning to the NMR spectroscopic analysis of complexes **117** and **118**, the crystalline products were dissolved in  $C_6D_6$  solution and examined by  $^7Li$ ,  $^1H$ ,  $^{13}C$ , COSY and HSQC NMR spectroscopy (full NMR details can be found in chapter 5, section 5.3.32 and 5.3.33 respectively). The spectra obtained essentially mirror those acquired for complexes **115** and **116**, with the  $^7Li$  spectra revealing two different environments. The expected Me<sub>6</sub>-TREN to HMDS (two singlets observed in  $^1H$  spectrum of **118** corresponding to the inequivalent SiCH<sub>3</sub> groups) ratio in the respective  $^1H$  NMR spectra is observed, and the resonances associated with these ligands are different from those encountered in the free donor and both the free amine and the free alkali metal amide respectively, indicating that the solid-state structures of **117** and **118** appear to remain intact in solution.

The synthesis and characterisation of complexes **115-118** has stripped back another layer of the structural complexity covering simple lithium amide-lithium halide systems, and in doing so, the beginnings of a new family of Group 1 macrocyclic complexes has emerged – MAC complexes. Efforts to extend this chemistry to sodium amide-sodium halide systems will now follow.



## 4.2 Unusual Halide-Deficient Amido Metal Anionic Crowns: Extensions to Mixed Sodium Amide-Sodium Halide Compounds

Following our success in the preparation of lithium MAC complexes, our attention turned to extending these complexes to include sodium MAC complexes, by replacing the lithium components of our ‘designed’ reaction systems (Scheme 4.1) with their sodium counterparts (*i.e.*, replacing LiHMDS with NaHMDS, LiX with NaX, and <sup>*n*</sup>BuLi with <sup>*n*</sup>BuNa). Sodium chloride-containing MAC complexes were not forthcoming, presumably due to moving to a larger alkali metal (*i.e.*, the cavity formed by a planar (NaN)<sub>5</sub> ring would be too large to adequately sequester a chloride anion); however, a sodium bromide-containing MAC complex was successfully synthesised, [Me<sub>6</sub>-TREN·Na(μ-Br)Na·Me<sub>6</sub>-TREN]<sup>+</sup>[Na<sub>5</sub>(μ-HMDS)<sub>5</sub>(μ<sub>5</sub>-Br)]<sup>-</sup>, **127**, utilising the organoammonium route (full experimental details can be found in chapter 5, section 5.3.35).

### 4.2.1 [Me<sub>6</sub>-TREN·Na(μ-Br)Na·Me<sub>6</sub>-TREN]<sup>+</sup>[Na<sub>5</sub>(μ-HMDS)<sub>5</sub>(μ<sub>5</sub>-Br)]<sup>-</sup>, **127**

Complex **127** crystallises in the monoclinic system, space group *P*2<sub>1</sub>/*n*, and akin to its lithium analogue **118**, the structure of **127** is composed of a Me<sub>6</sub>-TREN sequestered M–Br–M cation and a ten-membered planar (MN)<sub>5</sub> ring which hosts a bromide anion. The bromine atom is not disordered in the anion – as observed in the anion of **118** – but is disordered in the cation, which causes the M–Br–M angle in the cation to deviate from linearity (mean Na–Br–Na angle, 148.82°) – in comparison to the linear cation of **118**. Due to the solvent-separated composition of this MAC complex, the cationic and anionic moieties of **127** will now be discussed independently. Figure 4.13 shows the molecular structure of the cation of **127** and Table 4.7 details its key bond distances (full X-ray data can be found on the accompanying CD).

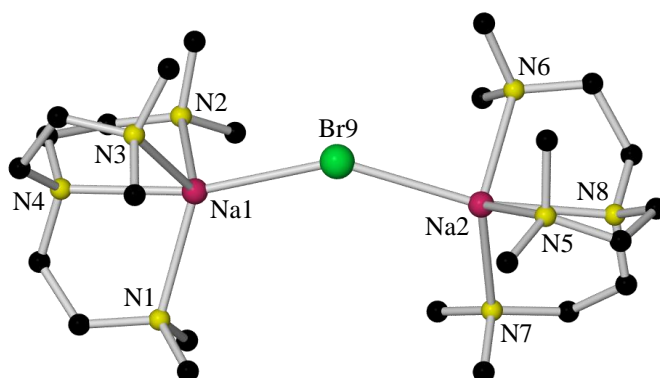


**Figure 4.13** Molecular structure of the cation of [Me<sub>6</sub>-TREN·Na(μ-Br)Na·Me<sub>6</sub>-TREN]<sup>+</sup>[Na<sub>5</sub>(μ-HMDS)<sub>5</sub>(μ<sub>5</sub>-Br)]<sup>-</sup>, **127**. H atoms, disorder component (Br1 in Table 4.7) and solvent of crystallisation (toluene) are omitted for clarity.

Selected Bond	Bond Distance (Å) in [Me <sub>6</sub> -TREN·Na(μ-Br)Na·Me <sub>6</sub> -TREN] <sup>+</sup> [Na <sub>5</sub> (μ-HMDS) <sub>5</sub> (μ <sub>5</sub> -Br)] <sup>-</sup> , <b>127</b>
Na1–N1	2.467(4)
Na1–N2	2.468(4)
Na1–N3	2.460(4)
Na1–N4	2.496(4)
Na1–Br1	2.7304(17)
Na1–Br9	2.704(4)
Na2–N5	2.461(4)
Na2–N6	2.427(4)
Na2–N7	2.441(5)
Na2–N8	2.500(4)
Na2–Br1	2.7149(16)
Na2–Br9	2.734(4)

**Table 4.7** Key bond distances within the cation of [Me<sub>6</sub>-TREN·Na(μ-Br)Na·Me<sub>6</sub>-TREN]<sup>+</sup>[Na<sub>5</sub>(μ-HMDS)<sub>5</sub>(μ<sub>5</sub>-Br)]<sup>-</sup>, **127**.

The κ<sup>4</sup> coordination of Me<sub>6</sub>-TREN here in the cation of **127** represents the fourth example of such Me<sub>6</sub>-TREN–Na bonding, the preceding three complexes being the Na variant of complex **123**<sup>[270]</sup> (*vide supra*) and monomeric complexes containing the phenol ligands 2,4,6-trimethylphenol and 2,6-di-*tert*-butyl-4-methylphenol respectively.<sup>[252]</sup> In addition, this represents the first example of a Na–Br–Na cation. As expected, due to the larger sodium metal centre, the mean M–X and M–N bond distances are greater in the cation of **127** (2.721 and 2.465 Å respectively) compared to the corresponding distances in the lithium cations of **118** and **126** (mean M–X and M–N bond distances, 2.579 and 2.213 Å for **118** and 2.580 and 2.205 Å for **126** respectively). The mean Na–N bond distance is shorter than the corresponding distance in the three previously reported Me<sub>6</sub>-TREN–Na monomer complexes (mean Na–N bond distance for preceding three complexes, 2.496, 2.533 and 2.656 Å respectively).

Figure 4.14 shows the molecular structure of the anion of **127** and Table 4.8 and Table 4.9 detail the key bond distances and angles respectively.

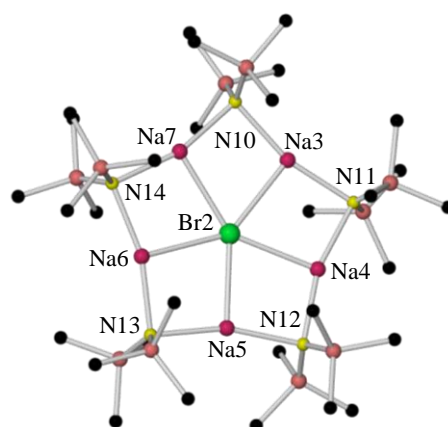


**Figure 4.14** Molecular structure of the anion of  $[\text{Me}_6\text{-TREN}\cdot\text{Na}(\mu\text{-Br})\text{Na}\cdot\text{Me}_6\text{-TREN}]^+[\text{Na}_5(\mu\text{-HMDS})_5(\mu_5\text{-Br})]^-$ , **127**. H atoms and solvent of crystallisation (toluene) are omitted for clarity.

Selected Bond	Bond Distance (Å) in $[\text{Me}_6\text{-TREN}\cdot\text{Na}(\mu\text{-Br})\text{Na}\cdot\text{Me}_6\text{-TREN}]^+[\text{Na}_5(\mu\text{-HMDS})_5(\mu_5\text{-Br})]^-$ , <b>127</b>
Na3–N10	2.365(4)
Na3–N11	2.371(4)
Na3–Br2	2.9179(16)
Na4–N11	2.374(4)
Na4–N12	2.364(4)
Na4–Br2	2.8805(17)
Na5–N12	2.377(4)
Na5–N13	2.362(4)
Na5–Br2	2.8827(18)
Na6–N13	2.374(4)
Na6–N14	2.363(4)
Na6–Br2	2.8957(17)
Na7–N10	2.365(4)
Na7–N14	2.381(4)
Na7–Br2	2.8955(18)

**Table 4.8** Key bond distances within the anion of  $[\text{Me}_6\text{-TREN}\cdot\text{Na}(\mu\text{-Br})\text{Na}\cdot\text{Me}_6\text{-TREN}]^+[\text{Na}_5(\mu\text{-HMDS})_5(\mu_5\text{-Br})]^-$ , **127**.

Selected Angle	Bond Angle (°) in $[\text{Me}_6\text{-TREN}\cdot\text{Na}(\mu\text{-Br})\text{Na}\cdot\text{Me}_6\text{-TREN}]^+[\text{Na}_5(\mu\text{-HMDS})_5(\mu_5\text{-Br})]^-$ , <b>127</b>
N10–Na3–N11	164.63(14)
N11–Na4–N12	163.32(14)
N12–Na5–N13	162.62(14)
N13–Na6–N14	163.74(13)
N10–Na7–N14	164.24(14)
Na3–N10–Na7	91.85(13)
Na3–N11–Na4	92.11(13)
Na4–N12–Na5	91.40(13)
Na5–N13–Na6	90.52(12)
Na6–N14–Na7	92.57(12)

**Table 4.9** Key bond angles within the anion of  $[\text{Me}_6\text{-TREN}\cdot\text{Na}(\mu\text{-Br})\text{Na}\cdot\text{Me}_6\text{-TREN}]^+[\text{Na}_5(\mu\text{-HMDS})_5(\mu_5\text{-Br})]^-$ , **127**.

To the best of our knowledge, a discrete ten-atom (NaN)<sub>5</sub> ring (or indeed of any sodium anion combination) has not been reported to date. Indeed, no pentanuclear Na<sub>5</sub> species of any compound class or architecture has been previously reported, with the exception of the previously discussed hydroxyl-incorporated sodium sodiate [Na{(R,R)-TMCDA}<sub>2</sub>]<sup>+</sup>[Na<sub>4</sub>(μ-HMDS)<sub>4</sub>(μ<sub>4</sub>-OH)]<sup>-</sup>, **109** (chapter 3, section 3.3.2).

By moving from lithium to sodium, the size of the (MN)<sub>5</sub> ring increases – as evidenced by the mean M–N bond distances of the anion of **118** and **127** (2.067 and 2.370 Å respectively) – and so the bromine atom in the anion of **127** essentially sits in the plane of the (NaN)<sub>5</sub> ring (0.1 Å out of the plane of the ring), whereas it sits 0.5 Å above or below the plane in its lithium congener **118**. Consequently the mean M–Br bond distance increases from 2.557 Å in **118** to 2.912 Å in **127**. The mean ‘point’ M–N–M and ‘side’ N–M–N angles for the ten-membered rings are essentially unaffected by these changes in bond distances (mean M–N–M and N–M–N angles, 91.59 and 163.70° for **118** and 91.69 and 163.71° for **127** respectively).

Crystalline product **127** was dissolved in C<sub>6</sub>D<sub>6</sub> solution and examined by <sup>1</sup>H, COSY and HSQC NMR spectroscopy (full NMR details can be found in chapter 5, sections 5.3.35). The <sup>1</sup>H and <sup>13</sup>C NMR spectra essentially resemble that of **118**, with the expected Me<sub>6</sub>-TREN to HMDS ratio being observed. The resonances associated with these ligands are different from those encountered in the free donor and both the free amine and the free alkali metal amide respectively, indicating that the solid-state structure of **127** appears to remain intact in solution. In the HMDS region of the <sup>1</sup>H spectra only one singlet (compared to two in **118**) is observed due to the bromine atom now sitting in the plane of the (MN)<sub>5</sub> ring (*i.e.*, tetrahedrally-orientated TMS groups are now equivalent).

As the sodium anion of **127** was able to capture a bromide anion in the plane of its (NaN)<sub>5</sub> ring, we were intrigued to discover what would happen if we moved to trying to encapsulate an iodide anion within this system – would an iodide anion be successfully encapsulated and would it sit in the plane of the ring, or more likely, be disordered and sit above and below the plane of the ring?

#### 4.2.2 [Me<sub>6</sub>-TREN·Na(μ-I)Na·Me<sub>6</sub>-TREN]<sup>+</sup>[Na<sub>5</sub>(μ-HMDS)<sub>5</sub>(μ<sub>5</sub>-I)]<sup>-</sup>, **128**

Following the organoammonium route (Scheme 4.1), replacing the lithium components of the reaction with their sodium counterparts and utilising tetrabutylammonium iodide in place of tetrabutylammonium bromide, afforded the iodide-containing MAC [Me<sub>6</sub>-TREN·Na(μ-I)Na·Me<sub>6</sub>-TREN]<sup>+</sup>[Na<sub>5</sub>(μ-HMDS)<sub>5</sub>(μ<sub>5</sub>-I)]<sup>-</sup>, **128** (full experimental details can be found in

chapter 5, section 5.3.36). Unfortunately, the X-ray data obtained was of poor quality, thus precluding any discussion of structural parameters; however, atom connectivity was unambiguous. The iodide anion is indeed disordered and sits above and below the plane of the ring.

Efforts to capture fluoride and hydride anions within both the lithium and sodium amide systems were also undertaken, but to no avail. Reactions designed to hopefully produce MAC complexes did however sometimes produce unexpected products. These complexes will now be discussed in greater detail.

### 4.3 Non-MAC Mixed Alkali Metal Amide-Alkali Metal Halide Complexes

During our investigations into the design and synthesis of novel MAC complexes, other non-MAC mixed alkali metal amide-alkali metal halide complexes were found to be forthcoming at times. Six non-MAC complexes were isolated in total: the first three were obtained from reactions designed to produce lithium/sodium iodide-containing MAC complexes; the fourth, whilst trying to encapsulate pseudo-halides within our systems; and finally, the last two complexes were obtained from efforts to extend the MAC chemistry to potassium amide-potassium halide systems and to crown-solvated MAC complexes.

#### 4.3.1 $[\{(R,R)\text{-TMCD}\cdot\text{LiI}\}_2(\text{LiHMDS})_2]_\infty$ , **129**

The first reaction, combining  $n\text{BuLi}$ ,  $(R,R)\text{-TMCD}$ ,  $\text{NH}_4\text{I}$  and  $\text{LiHMDS}$  in a 1 : 2 : 1 : 7 stoichiometric ratio, was undertaken following the synthesis of complexes **115** and **116**, in an effort to try and expand the ring size of the anionic host and hopefully to obtain an iodide-containing MAC. However a MAC complex was not obtained, and instead, crystals of polymeric species  $[\{(R,R)\text{-TMCD}\cdot\text{LiI}\}_2(\text{LiHMDS})_2]_\infty$ , **129**, were isolated (Figure 4.15).

Complex **129** crystallises in the orthorhombic system, space group  $P2_12_12_1$ , and is composed of alternate  $(\text{LiI})_2$  and  $(\text{LiHMDS})_2$  units (that is, a 1 : 1 I/HMDS complex), which are linked together *via* intermolecular  $\text{Li}\cdots\text{I}$  contacts (mean distance, 2.814 Å), forming a linear polymeric arrangement. The iodide anions are thus bound to three lithium centres (mean intramolecular  $\text{Li}\text{-I}$  bond distance, 2.743 Å), and in distorted trigonal planar environments. In essence, the  $(\text{LiI})_2$  units act as pseudo-donors towards the  $\text{LiHMDS}$  dimers akin to conventional donors, such as THF.<sup>[37c, 37d]</sup> The lithium centres bound to two  $\text{N}_{\text{HMDS}}$  atoms (mean  $\text{Li}\text{-N}_{\text{HMDS}}$  bond distance, 2.026 Å) are in distorted trigonal planar geometries, while those attached to two iodine atoms are in distorted tetrahedral arrangements owing to

additional coordination by bidentate (*R,R*)-TMCDA [mean Li–N<sub>(*R,R*)-TMCDA</sub> bond distance, 2.052 Å]. Full X-ray data for complex **129** can be found on the accompanying CD.

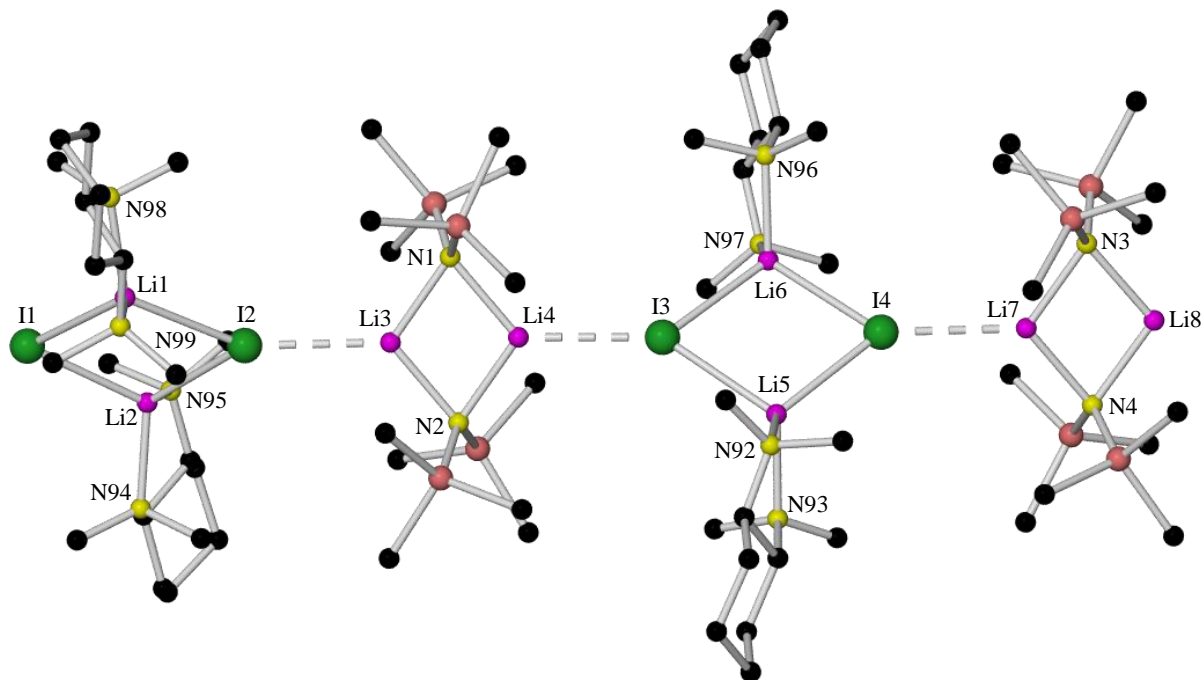


**Figure 4.15** Asymmetric unit of  $[\{(R,R)\text{-TMCDA}\cdot\text{LiI}\}_2(\text{LiHMDS})_2]_\infty$ , **129**, which polymerises through Li8...I1, 2.860(11) Å. This interaction and H atoms are omitted for clarity.

In comparison to donor-free LiHMDS, the mean Li–N bond distance of the (LiHMDS)<sub>2</sub> units (2.026 Å) is slightly shorter than that encountered in trimeric LiHMDS (2.080 Å);<sup>[11a, 11b]</sup> and the mean Li–N–Li and N–Li–N angles (92 and 148° respectively) are approximately 17 and 43° wider than their respective counterparts in **129** (75.05 and 104.95° respectively).

Crystalline product **129** was dissolved in C<sub>6</sub>D<sub>6</sub> solution and examined by <sup>7</sup>Li, <sup>1</sup>H, COSY and HSQC NMR spectroscopy (full NMR details can be found in chapter 5, sections 5.3.37). The <sup>7</sup>Li spectrum revealed two different environments, in keeping with the solid-state structure. The expected diamine to HMDS ratio in the <sup>1</sup>H NMR spectrum was observed, and the resonances associated with the diamine and the HMDS ligand were different from those encountered in the free diamine and both the free amine and the free alkali metal amide respectively, thus the coordination structure seen in the solid-state of **129** appears to remain intact in solution; however, the formation of other oligomers cannot be ruled out.

As the reaction designed to produce a lithium iodide-containing MAC complex [where the counter cation would hopefully contain (*R,R*)-TMCDA ligands] produced polymeric **129**, we were intrigued to discover what would happen if we moved to trying to encapsulate an iodide anion within the similar Me<sub>6</sub>-TREN system – would an iodide anion be successfully

encapsulated, or more likely, would a polymeric or even a lower aggregate state complex be obtained?

### 4.3.2 [Me<sub>6</sub>-TREN·LiI], **130**

Following the synthesis of complexes **117** and **118**, <sup>n</sup>BuLi, Me<sub>6</sub>-TREN, NH<sub>4</sub>I and LiHMDS were reacted together in a 2 : 2 : 2 : 6 stoichiometric ratio, in an effort to try and expand the ring size of the anionic host and to hopefully obtain an iodide-containing MAC. However a MAC complex was not obtained, and instead, crystals of the monomeric species [Me<sub>6</sub>-TREN·LiI], **130**, were isolated (Figure 4.16).

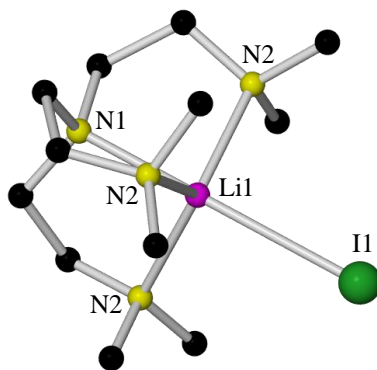


**Figure 4.16** Molecular structure of [Me<sub>6</sub>-TREN·LiI], **130**. H atoms are omitted for clarity.

All four nitrogen donor atoms of the Me<sub>6</sub>-TREN ligand coordinate to the lithium centre, whose coordination sphere is completed by a iodine atom, where the lithium centre is locked in a linear N–Li–I chain. Table 4.10 details the key bond distances (full X-ray data can be found on the accompanying CD).

Selected Bond	Bond Distance (Å) in [Me <sub>6</sub> -TREN·LiI], <b>130</b>
Li1–N1	2.180(2)
Li1–N2	2.215(3)
Li1–I1	2.983(10)

**Table 4.10** Key bond distances within [Me<sub>6</sub>-TREN·LiI], **130**.

Complex **130** crystallises in the hexagonal system, space group *P*6<sub>3</sub>, and represents only the second example of a monomeric complex in which the Me<sub>6</sub>-TREN ligand is κ<sup>4</sup> coordinated to a lithium centre, the previous complex being the aforementioned [Me<sub>6</sub>-TREN·LiCH<sub>2</sub>Ph],<sup>[270]</sup> **123**. The mean Li–N bond distance in **130** (2.206 Å) is slightly shorter than the corresponding distance in **123** (2.250 Å), presumably due to the lack of steric bulk at the anionic moiety of **130**.

To the best of our knowledge, only three Lewis base monomeric LiI complexes have been published previously. These are a DME<sup>[274]</sup> (1,2-dimethoxyethane), a THF<sup>[275]</sup> and – perhaps most pertinent to this work – a tridentate PMDETA<sup>[276]</sup> complex. As expected, due to the  $\kappa^4$  coordination of Me<sub>6</sub>-TREN vs. the  $\kappa^3$  coordination of PMDETA, the mean Li–N and Li–I bond distances are greater in complex **130** (mean Li–N and Li–I bond distances, 2.206 and 2.983 Å for **130** and 2.102 and 2.710 Å for PMDETA complex respectively).

In comparison to the product obtained whilst trying to prepare an iodide-containing MAC complex utilising (*R,R*)-TMCDA (polymeric complex **129**, Figure 4.15), a monomeric complex is presumably formed here due to the greater sterically demanding nature of Me<sub>6</sub>-TREN when compared with (*R,R*)-TMCDA. Subsequent work has shown that the isostructural chlorine and bromine monomers can also be obtained.<sup>[277]</sup>

Crystalline product **130** was dissolved in C<sub>6</sub>D<sub>6</sub> solution and examined by <sup>7</sup>Li, <sup>1</sup>H, COSY and HSQC NMR spectroscopy (full NMR details can be found in chapter 5, sections 5.3.38). The <sup>7</sup>Li spectrum revealed one signal, in keeping with the solid-state structure. The resonances associated with the amine in the <sup>1</sup>H spectrum were different from those encountered in the free amine, thus indicating that coordination geometry seen in the solid-state structure of **130** appears to remain intact in solution; however, the formation of other oligomers cannot be ruled out.

The isolation of complexes **129** and **130** from reactions designed to produce lithium iodide-containing MAC complexes suggested that the cavity formed by a planar ten-membered (LiN)<sub>5</sub> ring would be too small to adequately sequester an iodide anion. Therefore, we moved to utilising the larger alkali metal sodium within our systems in the anticipation that the larger cavity formed by a planar (NaN)<sub>5</sub> ring would successfully encapsulate an iodide anion. This approach proved effective (*vide supra* – complex **128**); however, an attempt to remake this complex produced a non-MAC mixed sodium amide-sodium iodide complex.

#### 4.3.3 [Me<sub>6</sub>-TREN·Na(μ-I)Na(μ-HMDS)<sub>2</sub>Na(μ-I)Na·Me<sub>6</sub>-TREN], **131**

Repeating the reaction utilised to form the sodium iodide-containing MAC complex **128**, but this time employing the less soluble ammonium iodide reagent in place of tetrabutylammonium iodide (full experimental details can be found in chapter 5, section 5.3.39), did not afford crystals of **128**, but instead crystals of dimeric species [Me<sub>6</sub>-TREN·Na(μ-I)Na(μ-HMDS)<sub>2</sub>Na(μ-I)Na·Me<sub>6</sub>-TREN], **131**, resulted (Figure 4.17).



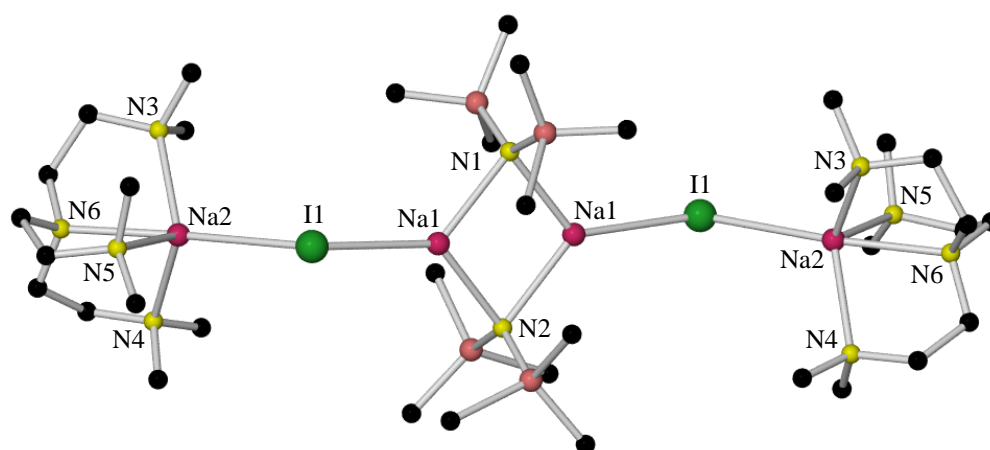


**Figure 4.17** Molecular structure of  $[\text{Me}_6\text{-TREN}\cdot\text{Na}(\mu\text{-I})\text{Na}(\mu\text{-HMDS})_2\text{Na}(\mu\text{-I})\text{Na}\cdot\text{Me}_6\text{-TREN}]$ , **131**. H atoms are omitted for clarity.

Unfortunately, the X-ray data obtained was of poor quality, thus precluding any discussion of structural parameters; however, atom connectivity was unambiguous. Interestingly, with respect to the previously discussed polymer  $[\{(R,R)\text{-TMCDA}\cdot\text{LiI}\}_2(\text{LiHMDS})_2]_\infty$ , **129** (section 4.3.1, Figure 4.15), in which  $(R,R)\text{-TMCDA}\cdot\text{LiI}$  dimers act as pseudo-donors towards LiHMDS dimers, here,  $\text{Me}_6\text{-TREN}\cdot\text{NaI}$  monomers act as pseudo-donors towards NaHMDS dimers, thus ensuring the formation of a dimeric complex. This scenario presumably occurs due to the greater denticity and steric bulk of  $\text{Me}_6\text{-TREN}$  *versus*  $(R,R)\text{-TMCDA}$ . To the best of our knowledge, a  $\kappa^4$  coordinated  $\text{Me}_6\text{-TREN}\text{-Na}$  dimer (or indeed a  $\kappa^4$  coordinated  $\text{Me}_6\text{-TREN}$  dimer of any alkali metal) has not been reported to date.

Crystalline product **131** was dissolved in  $\text{C}_6\text{D}_6$  solution and examined by  $^1\text{H}$ , COSY and HSQC NMR spectroscopy (full NMR details can be found in chapter 5, sections 5.3.39). The key features in the  $^1\text{H}$  spectrum obtained are that the HMDS :  $\text{Me}_6\text{-TREN}$  ratio is 2 : 2, and the resonances associated with these ligands are different from those encountered in the free donor and both the free amine and the free alkali metal amide respectively, thus the solid-state structure of **131** appears to remain intact in solution.

Returning to the MAC complexes, the successful incorporation of ‘conventional’ halides within these systems prompted the investigation of ‘pseudo’ halide capture.

#### 4.3.4 $[\{(R,R)\text{-TMCDA}\cdot\text{Li}(\text{SCN})\}_2(\text{LiHMDS})_2]_\infty$ , **132**

Having successfully encapsulated ‘conventional’ halides within our MAC complexes, our attention turned to the possibility of capturing ‘pseudo’ halides within these systems. Thus, focusing on the LiHMDS/ $(R,R)\text{-TMCDA}$  systems initially, various ammonium salts (Figure

4.18) were employed in the ammonium salt route reaction (Scheme 4.1) in an attempt to obtain more novel MAC complexes. Of the 15 reactions undertaken, X-ray quality crystals were only deposited from the one reaction – that which utilised the thiocyanate anion (highlighted in green in Figure 4.18). X-ray crystallographic studies revealed that these crystals were not representative of a MAC complex, but a thiocyanate polymeric species,  $[\{(R,R)\text{-TMCDA}\cdot\text{Li}(\text{SCN})\}_2(\text{LiHMDS})_2]_\infty$ , **132** (Figure 4.19).

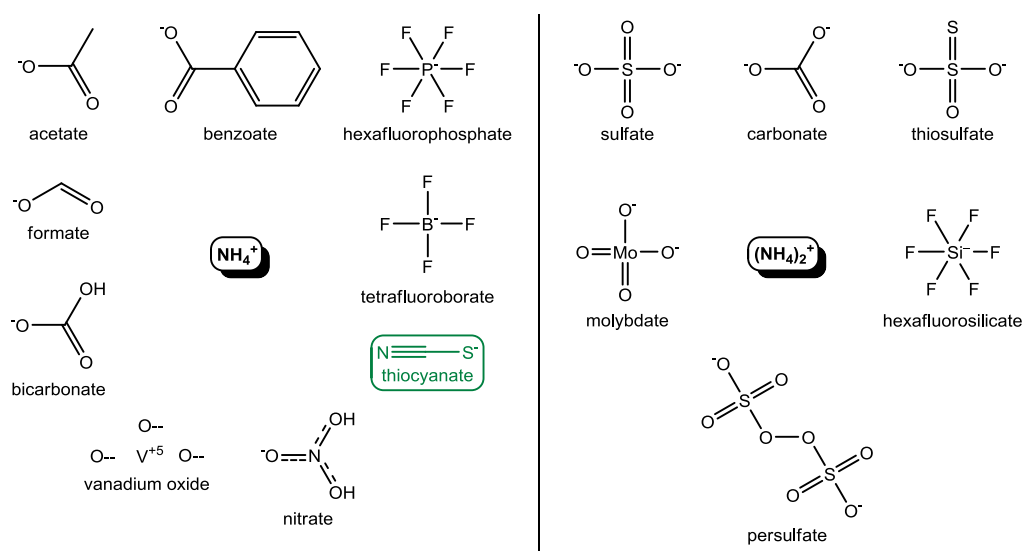


**Figure 4.18** ChemDraw<sup>®</sup> representation of the various ammonium salts employed in ammonium salt route reactions undertaken in an attempt to obtain MAC complexes. X-ray quality crystals were isolated solely from the reaction utilising the thiocyanate anion (highlighted in green).

Complex **132** crystallises in the hexagonal system, space group  $P6_1$ , and is composed of alternating  $[\text{Li}(\text{SCN})]_2$  and  $(\text{LiHMDS})_2$  units (that is, a 1 : 1 SCN/HMDS complex), which are linked together *via* intra- and intermolecular  $\text{Li}\cdots\text{S}$  contacts [ $\text{Li}\cdots\text{S}2$  bond distance, 2.594(6) Å;  $\text{Li}3\cdots\text{S}$  distance, 2.566(6) Å], forming a linear polymer. This arrangement is isostructural to that observed in the previously discussed polymeric species  $[\{(R,R)\text{-TMCDA}\cdot\text{LiI}\}_2(\text{LiHMDS})_2]_\infty$ , **129**, where, akin to the  $(\text{LiI})_2$  units in **129**, the  $[\text{Li}(\text{SCN})]_2$  units in **132** act as pseudo-donors towards the LiHMDS dimers. The lithium centres bound to two  $\text{N}_{\text{HMDS}}$  atoms (mean  $\text{Li}\text{-}\text{N}_{\text{HMDS}}$  bond distance, 2.017 Å) are in distorted trigonal planer geometries, while those attached to two thiocyanate anions are in distorted tetrahedral arrangements owing to additional coordination by bidentate  $(R,R)\text{-TMCDA}$  (mean  $\text{Li}\text{-}\text{N}_{(R,R)\text{-TMCDA}}$  bond distance, 2.033 Å). The mean  $\text{Li}\text{-}\text{N}$  bond distances are shorter in **132** compared to those in **129** (2.026 and 2.052 Å respectively), presumably due to the lithium atoms in **132** bonding to smaller atoms (N or S *vs.* I). Full X-ray data for complex **132** can be found on the accompanying CD.

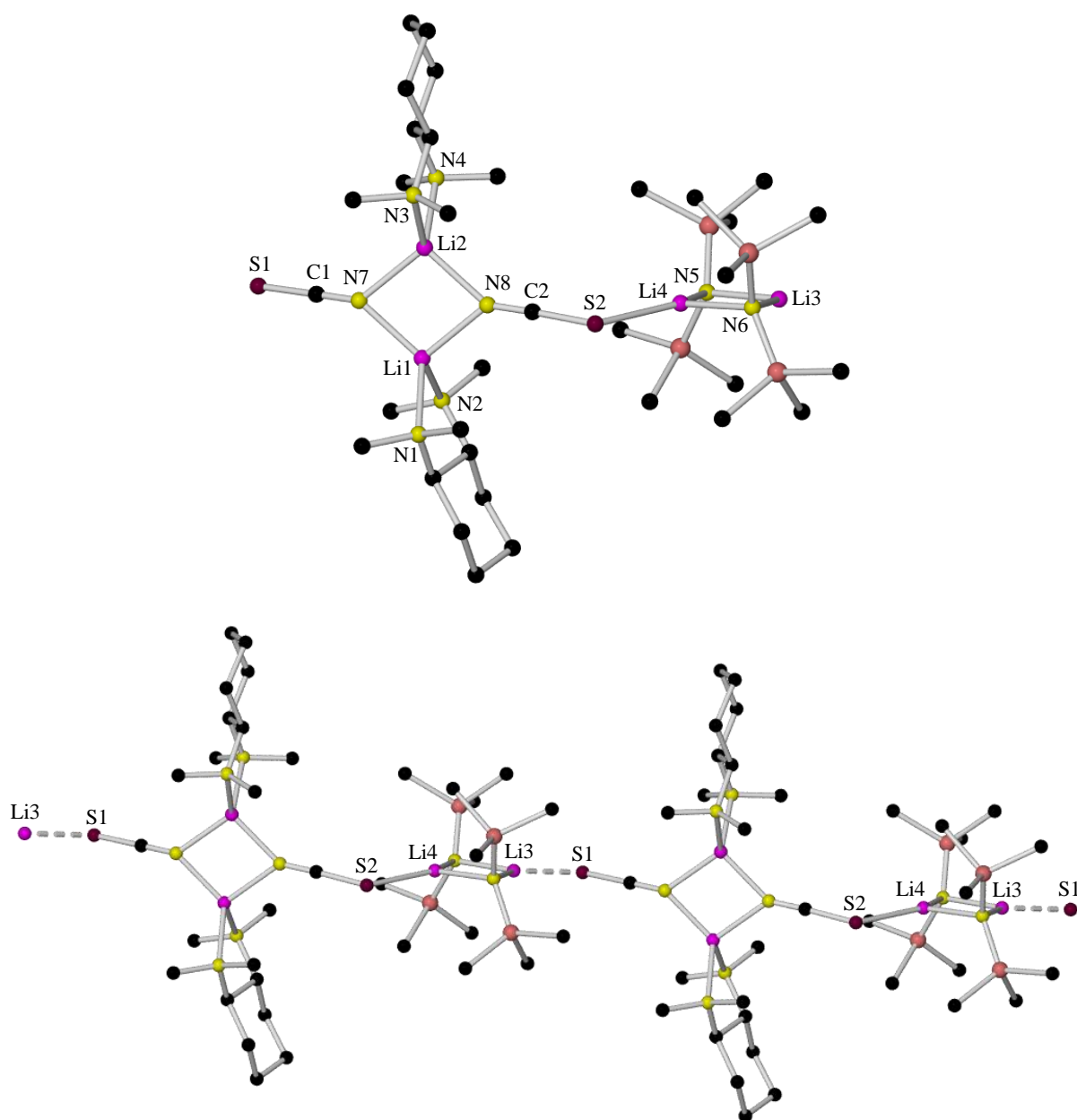


**Figure 4.19** Molecular structure of  $[(R,R)\text{-TMCD A} \cdot \text{Li}(\text{SCN})_2(\text{LiHMDS})_2]_\infty$ , **132**, showing the asymmetric unit (top) and a section of the polymer (bottom) which polymerises through  $\text{Li3} \cdots \text{S1}$ , 2.566(6) Å. H atoms and solvent of crystallisation (toluene) are omitted for clarity.

Complex **132** represents only the second example of the bifunctional thiocyanate ligand being incorporated within an alkali metal compound, having only been observed hitherto in the polymeric complex  $[\text{Li}(\text{SCN}) \cdot \text{TMEDA}]_\infty$ ,<sup>[278]</sup> **133**. However, in this complex, each lithium centre is bound to the S atom of one thiocyanate ligand and to the N atom of another, whereas in **132** each lithium centre is solely bound to the one thiocyanate ligand (be it to the S or N atom).

In comparison to donor-free LiHMDS, the mean Li–N bond distance of the (LiHMDS)<sub>2</sub> units (2.017 Å) is slightly shorter than that encountered in trimeric LiHMDS (2.080 Å);<sup>[11a, 11b]</sup> and the mean Li–N–Li and N–Li–N angles (92 and 148° respectively) are approximately 17 and 43° wider than their respective counterparts in **132** (75.45 and 104.55° respectively).

Crystalline product **132** was dissolved in C<sub>6</sub>D<sub>6</sub> solution and examined by <sup>7</sup>Li, <sup>1</sup>H, COSY and HSQC NMR spectroscopy (full NMR details can be found in chapter 5, sections 5.3.40). The <sup>7</sup>Li spectrum revealed two different environments, in keeping with the solid-state structure. The expected diamine to HMDS ratio in the <sup>1</sup>H NMR spectrum was observed, and the resonances associated with the diamine and the HMDS ligand were different from those encountered in the free diamine and both the free amine and the free alkali metal amide respectively, thus the solid-state structure of **132** appears to remain intact in solution; however, the formation of other oligomers cannot be ruled out.

Running in parallel with the reactions designed to capture ‘pseudo’ halides, we investigated the possibility of extending the chemistry of the MAC complexes to potassium amide-potassium halide systems.

#### 4.3.5 [Me<sub>6</sub>-TREN·K(μ-HMDS)K(μ-HMDS)<sub>2</sub>K(μ-HMDS)K·Me<sub>6</sub>-TREN], **134**

Following our success in the preparation of lithium and sodium MAC complexes, our attention turned to extending these complexes to include potassium MAC complexes, by replacing the lithium/sodium components of our ‘designed’ reaction systems (Scheme 4.1) with their potassium counterparts. Of the multiple reactions undertaken in an attempt to achieve this goal, X-ray quality crystals were only deposited from the one reaction – that which combined PhCH<sub>2</sub>K, Me<sub>6</sub>-TREN, <sup>n</sup>Bu<sub>4</sub>NBr and KHMDS in a 2 : 2 : 2 : 5 stoichiometric ratio. X-ray crystallographic studies revealed that these crystals were not representative of a potassium bromide-containing MAC complex, but a dimeric species, [Me<sub>6</sub>-TREN·K(μ-HMDS)K(μ-HMDS)<sub>2</sub>K(μ-HMDS)K·Me<sub>6</sub>-TREN], **134** (Figure 4.20).

Complex **134** crystallises as a centrosymmetric tetranuclear dimer in the triclinic system, space group *P* $\bar{1}$ , and is composed of four potassium metal centres, four HMDS ligands, and two Me<sub>6</sub>-TREN ligands which form an inorganic [K(μ-N)K(μ-N)<sub>2</sub>K(μ-N)K] chain terminated by the Me<sub>6</sub>-TREN ligands (where the outer potassium metal centres are five coordinate and the inner potassium metal centres three coordinate). Table 4.11 details the key bond distances (full X-ray data can be found on the accompanying CD).

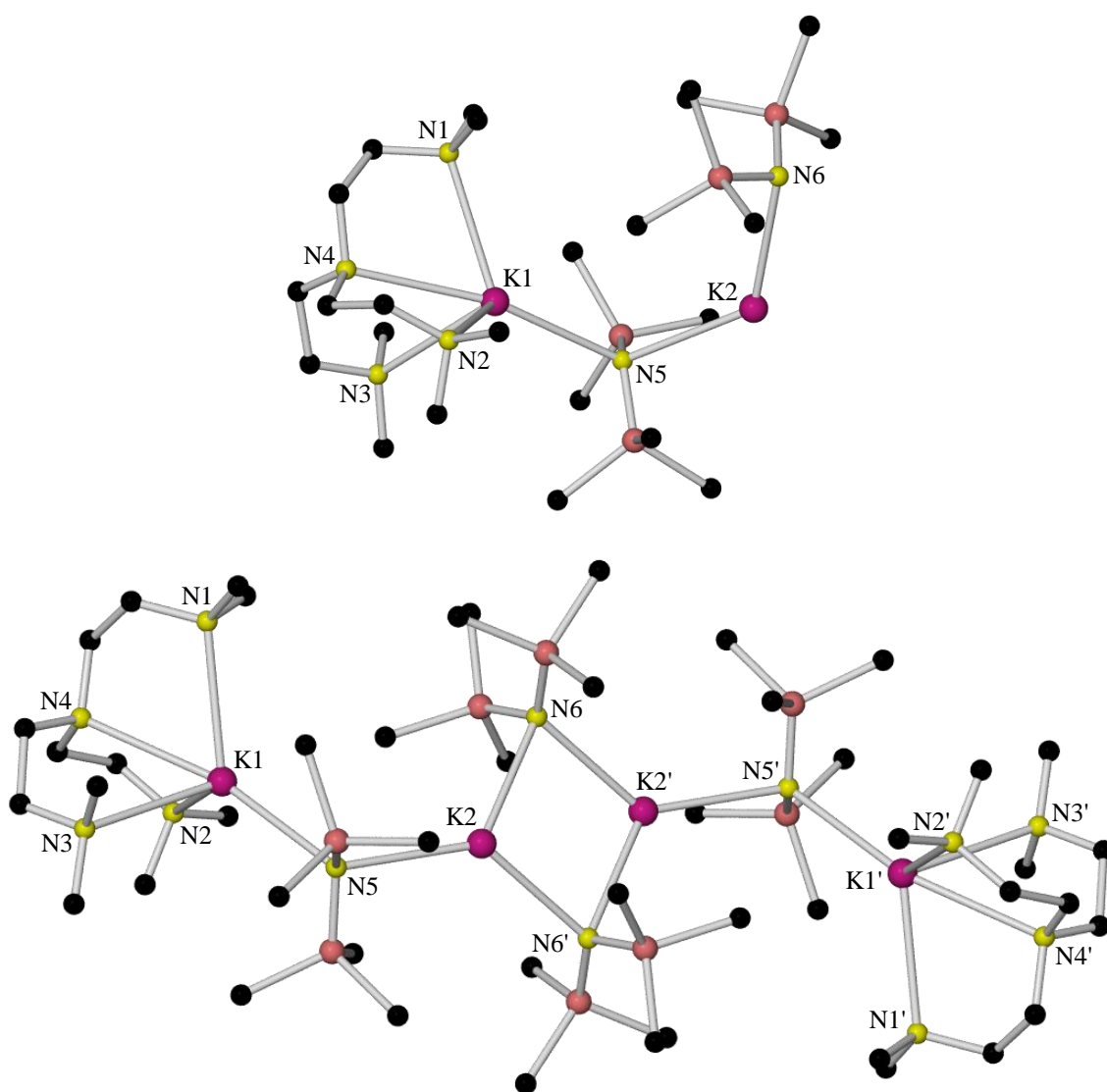


**Figure 4.20** Molecular structure of  $[\text{Me}_6\text{-TREN}\cdot\text{K}(\mu\text{-HMDS})\text{K}(\mu\text{-HMDS})_2\text{K}(\mu\text{-HMDS})\text{K}\cdot\text{Me}_6\text{-TREN}]$ , **134**, showing the asymmetric unit (top) and the tetranuclear dimer (bottom). H atoms and solvent of crystallisation (toluene) are omitted for clarity.

Selected Bond	Bond Distance (Å) in $[\text{Me}_6\text{-TREN}\cdot\text{K}(\mu\text{-HMDS})\text{K}(\mu\text{-HMDS})_2\text{K}(\mu\text{-HMDS})\text{K}\cdot\text{Me}_6\text{-TREN}]$ , <b>134</b>
K1–N1	3.003(3)
K1–N2	2.919(2)
K1–N3	3.048(2)
K1–N4	3.018(2)
K1–N5	2.913(2)
K2–N5	2.906(2)
K2–N6	2.848(2)
K2–N6'	2.846(2)

**Table 4.11** Key bond distances within  $[\text{Me}_6\text{-TREN}\cdot\text{K}(\mu\text{-HMDS})\text{K}(\mu\text{-HMDS})_2\text{K}(\mu\text{-HMDS})\text{K}\cdot\text{Me}_6\text{-TREN}]$ , **134**. Centrosymmetric **134** contains two  $\text{Me}_6\text{-TREN}$  coordinated KHMDS units, which are connected through a central  $(\text{KHMDS})_2$  ring. As alluded to in chapter 1, donor-free KHMDS

has been isolated in the solid-state as a polymer of dimeric units.<sup>[27]</sup> In **134** this polymer has been opened up – hence, complex **134** can be considered as a Me<sub>6</sub>-TREN entrapped open dimer of KHMDS or, as this unit dimerises, it can also be thought of as a dimer of a dinuclear fragment. In addition, the  $\kappa^4$  coordination of Me<sub>6</sub>-TREN here represents merely the second example of such Me<sub>6</sub>-TREN–K bonding, the preceding complex being the K variant of complex **123**<sup>[270]</sup> (*vide supra*).

Turning to the structural parameters within complex **134**, the inner potassium centres (K2 and K2'), bound symmetrically by two bridging N<sub>HMDS</sub> atoms (mean K–N bond distance, 2.857 Å) and exocyclically by another N<sub>HMDS</sub> atom [K2–N5 bond distance, 2.905(2) Å], are in distorted trigonal planar geometries, while the outer potassium centres (K1 and K1'), bound to a  $\kappa^4$  coordinated Me<sub>6</sub>-TREN ligand (mean K1/K1'–N<sub>donor</sub> bond distance, 2.997 Å) and to the latter N<sub>HMDS</sub> atom [K1/K1'–N5 bond distance, 2.913(2) Å], are in trigonal bipyramidal arrangements. The mean K–N<sub>donor</sub> bond distance of **134** is slightly greater than the mean K–N<sub>donor</sub> bond distance of the preceding Me<sub>6</sub>-TREN coordinated potassium complex (K variant of complex **123**; mean K–N<sub>donor</sub> bond distance, 2.849 Å).<sup>[270]</sup> As expected, the mean K–N bond distance (2.857 Å) and the bond angle at the K atoms [96.58(6)°] of the central (KHMDS)<sub>2</sub> ring of **134** are greater and wider respectively than those observed in donor-free KHMDS<sup>[27]</sup> [mean K–N bond distance and bond angle at the K atoms for KHMDS and the toluene solvated phase of KHMDS, 2.787 and 2.773 Å and 94.47(9) and 94.20(1)° respectively], whilst the angle at the N atoms [83.42(6)°] is narrower [bond angle at the N atoms for KHMDS and the toluene solvated phase of KHMDS, 85.53(9) and 85.80(1)° respectively].

A search of the CCDC reveals only one potassium complex which has a similar motif to that of **134**, the potassium alkyl/amido tetranuclear dimer [PMDETA·K{ $\mu$ -CH(SiMe<sub>3</sub>)<sub>2</sub>}K{ $\mu$ -CH(SiMe<sub>3</sub>)<sub>2</sub>}<sub>2</sub>K{ $\mu$ -CH(SiMe<sub>3</sub>)<sub>2</sub>}K·PMDETA],<sup>[279]</sup> **135**, reported by Lappert – where in place of Me<sub>6</sub>-TREN we have PMDETA, and in place of HMDS we have the isoelectronic CH(SiMe<sub>3</sub>)<sub>2</sub> unit. As expected, due to the  $\kappa^4$  coordination of Me<sub>6</sub>-TREN *vs.* the  $\kappa^3$  coordination of PMDETA, the mean K–N<sub>donor</sub> bond distance is greater in **134** (2.997 Å *vs.* 2.871 Å). Note, the structural motif of **134** is very similar to that of the previously discussed sodium tetranuclear dimer [Me<sub>6</sub>-TREN·Na( $\mu$ -I)Na( $\mu$ -HMDS)<sub>2</sub>Na( $\mu$ -I)Na·Me<sub>6</sub>-TREN], **131** (section 4.3.3, Figure 4.17), where, in contrast to **134**, the halide anion utilised in the reaction has been incorporated within the structure.

Crystalline product **134** was dissolved in C<sub>6</sub>D<sub>6</sub> solution and examined by <sup>1</sup>H, COSY and HSQC NMR spectroscopy (full NMR details can be found in chapter 5, section 5.3.41). The key features in the <sup>1</sup>H spectrum obtained are that the HMDS : Me<sub>6</sub>-TREN ratio is 4 : 2, and the resonances associated with Me<sub>6</sub>-TREN and the HMDS ligand are different from those encountered in the free donor and both the free amine and the free alkali metal amide respectively, thus the solid-state structure of **131** appears to remain intact in solution.

Revisiting MAC complexes – with respect to potential donor ligands – we investigated the possibility of combining conventional crown ethers with these inverse crown anions in anticipation of preparing crown-solvated metal anionic crowns.

#### 4.3.6 [KHMDS·12-crown-4]<sub>2</sub>, **136**

Wishing to combine conventional crown ethers with our novel metal anionic crowns – in the hope of preparing crown-solvated metal anionic crowns – 12-crown-4 was investigated as a possible donor ligand within our MAC systems, due to its ability to coordinate to alkali metals<sup>[101]</sup> and various halide salts thereof.<sup>[280]</sup> Following the direct combination route utilised to prepare complex **117** (Scheme 4.1), we anticipated that replacing the two equivalents of the sequestering amine Me<sub>6</sub>-TREN with two equivalents of crown ether would produce a similar complex in which the lithium centres in the cation of the complex would now be solvated by crown ether molecules, *i.e.*, formation of a crown-solvated metal anionic crown would have ensued. This however, proved not to be the case.

Combining LiHMDS, LiX (where X = Cl or Br) and 12-crown-4 in a 5 : 2 : 2 stoichiometric ratio in hydrocarbon solution, afforded a small crop of X-ray quality crystals after 48 hours. X-ray crystallographic analysis revealed that a crown-solvated MAC complex had not been isolated (despite the deficit of LiX to LiHMDS in the reaction), and instead, crystallisation of the previously published monomer [LiHMDS·12-crown-4],<sup>[36]</sup> **24** (chapter 1, section 1.1.4, Figure 1.18) had resulted. Repeating the reaction employing NaHMDS and NaX in place of LiHMDS and LiX gave rise to precipitation of a microcrystalline material from the reaction solution. Unfortunately, this material was not suitable for X-ray crystallographic analysis.

Moving to the utilisation of KHMDS and KX in the reaction afforded X-ray quality crystals after 24 hours. X-ray crystallographic analysis revealed that again a crown-solvated MAC complex had not been isolated, but instead, crystallisation of a dimeric species, [KHMDS·12-crown-4]<sub>2</sub>, **136**, had ensued (Figure 4.21). Complex **136** – a rare example of an alkali metal

amide 12-crown-4 dimer<sup>[281]</sup> – can also be prepared by utilising a rational stoichiometry, that is, a ratio of KHMDS : 12-crown-4 of 1 : 1.

Complex **136** crystallises as a centrosymmetric dimer in the monoclinic system, space group  $P2_1/c$ , and is composed of two potassium centres each coordinated to a 12-crown-4 molecule, with two HMDS ligands bridging the two metal centres (both metal centres are six coordinate). [Table 4.12](#) details the key bond distances (full X-ray data can be found on the accompanying CD).

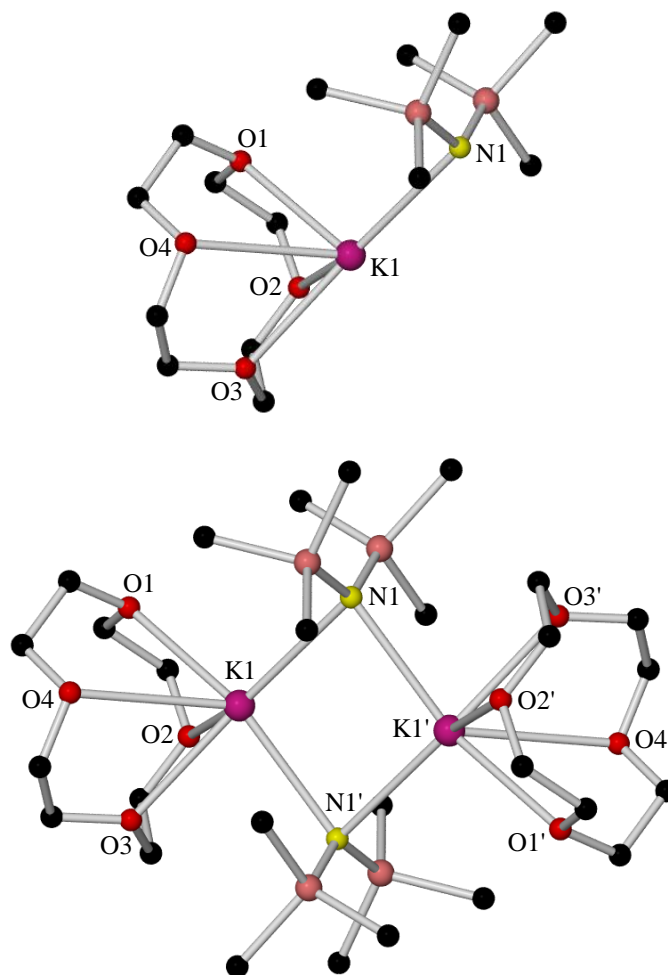


**Figure 4.21** Molecular structure of  $[\text{KHMDS}\cdot 12\text{-crown-4}]_2$ , **136**, showing the asymmetric unit (top) and the dimer (bottom). H atoms and solvent of crystallisation (toluene) are omitted for clarity.

Selected Bond	Bond Distance (Å) in $[\text{KHMDS}\cdot 12\text{-crown-4}]_2$ , <b>136</b>
K1–N1	3.073(2)
K1–N1'	2.913(2)
K1–O1	2.912(2)
K1–O2	2.773(2)
K1–O3	2.802(2)
K1–O4	3.121(2)

**Table 4.12** Key bond distances within  $[\text{KHMDS}\cdot 12\text{-crown-4}]_2$ , **136**.



The molecular framework of **136** consists of a planar (KN)<sub>2</sub> ring (sum of endocyclic angles, 360°); where the bonding is asymmetric, with one edge 0.16 Å shorter than the other [bond distances, 2.913(2) and 3.073(2) Å respectively; mean distance, 2.993 Å], and the internal angles at the K atoms are 13.84° wider than the angles at the N atoms [bond angles, 96.92(5) and 83.08(5)° at the K and N atoms respectively]. The coordination spheres of the K centres are completed by the binding of a 12-crown-4 molecule (mean K–O bond distance, 2.902 Å), resulting in six coordinate K centres. The 12-crown-4 molecules are distorted due to the proximity of the bulky trimethylsilyl groups of the bridging HMDS ligands. This results in three K–O bond distances that span the range 2.773(2)–2.912(2) Å, with a distinctly longer K1–O4 bond distance of 3.121(2) Å. Consequently, the K centres are located 2.1 Å above the mean oxygen plane of the crown molecules.

Complex **136** is a rare example of an alkali metal amide 12-crown-4 dimer, the only four previous examples being K, Rb and Cs (2-trimethylsilylamido)pyridine analogues<sup>[281a]</sup> and a potassium (2-phenylamido)pyridine analogue.<sup>[281b]</sup> However, in comparison to complex **136**, these complexes possess additional M–N bridging bonds due to the amide ligands coordinating through both the amido and pyridyl N atoms, resulting in eight coordinate metal centres. The bonding mode of the 12-crown-4 molecules in complex **136** (one long M–O bond and three shorter M–O bonds) is similar to that observed in the K, Rb and Cs (2-trimethylsilylamido)pyridine analogues, where, as expected, the M–O bond distances increase as the size of the alkali metal increases (*i.e.*, disruption of the host-guest relationship).<sup>[281a]</sup>

In comparison to donor-free KHMDS,<sup>[27]</sup> the mean K–N bond distance and the bond angle (2.993 Å) at the K atoms [96.92(5)°] of the central (KHMDS)<sub>2</sub> ring of **136** are greater and wider respectively [mean K–N bond distance and bond angle at the K atoms for KHMDS and the toluene solvated phase of KHMDS, 2.787 and 2.773 Å and 94.47(9) and 94.20(1)° respectively], whilst the angle at the N atoms [83.08(5)°] is narrower [bond angle at the N atoms for KHMDS and the toluene solvated phase of KHMDS, 85.53(9) and 85.80(1)° respectively].

Compared to monomeric [LiHMDS·12-crown-4],<sup>[36]</sup> **24**, a dimeric structure is presumably obtained when KHMDS is utilised, due to the necessity of the potassium to fill its substantially larger coordination sphere in comparison to that of lithium (five coordinate lithium *vs.* six coordinate potassium).

Crystalline product **136** was dissolved in C<sub>6</sub>D<sub>6</sub> solution and examined by <sup>1</sup>H, COSY and HSQC NMR spectroscopy (full NMR details can be found in chapter 5, sections 5.3.42). The

key features in the  $^1\text{H}$  NMR spectrum are that the HMDS : 12-crown-4 ratio is 2 : 2, and the resonances associated with these ligands are different from those encountered in the free donor and both the free amine and the free alkali metal amide respectively, thus the solid-state structure of **136** appears to remain intact in solution.

## **Chapter 5: Experimental**

This chapter contains the experimental procedures which have been undertaken during the course of this PhD study. As well as detailing each individual reaction, general experimental techniques which were employed will be summarised. The technical specifications of the analytical instruments are also included.

### **5.1 General Experimental Techniques**

Reactions undertaken throughout the course of this project involved reactants and isolated products which were air and moisture sensitive to some extent; hence, all compounds and reactions were manipulated under an inert atmosphere of argon. To achieve this, standard Schlenk techniques were employed, along with the use of a glove box, pre-dried solvents and liquid reagents, and oven-dried glassware.

#### **5.1.1 Schlenk Techniques**

All reactions performed in this research project were carried out using Schlenk apparatus connected to a Schlenk line. The Schlenk line is a glass manifold which consists of two independent pathways: one which is connected to a vacuum pump; and one which is connected to a supply of dry and oxygen-free argon. The Schlenk line which was utilised had five junctions which connected the line to the apparatus. At each of these junctions a lubricated two-way tap was in-place, which could be adjusted to subject the apparatus to either the vacuum or argon supply or indeed to be closed to both.

Air and moisture were removed from the Schlenk apparatus prior to their use by evacuating them (using a vacuum pump) and refilling them with argon; a procedure which was repeated three times as standard practice.

To ensure there was no build-up of pressure in the apparatus a release bubbler was employed. A trap (enclosed in a Dewar flask filled with liquid nitrogen) was incorporated before the vacuum pump to condense any volatile substances from the reaction media which are removed before they reach, and potentially damage, the vacuum pump.

#### **5.1.2 Glove Box Operation**

The storage and manipulation (such as the weight determination of reactant solids and product yields, as well as the preparation of samples for NMR spectroscopy) of all air and moisture

sensitive solid reactants and products was carried out in an argon filled MBraun MB10 glove box to prevent decomposition.

The integrity of the argon atmosphere in the box was maintained by a gas circulation system, in which the working gas was constantly circulated between the glove box and the H<sub>2</sub>O/O<sub>2</sub> gas purification system. Oxygen and moisture levels in ppm were monitored *via* an LCD control panel and the box was regenerated as often as necessary (usually every two to three months).

The transfer of materials in and out of the glove box was achieved using one of two ports. With the internal port door closed and the port under an argon atmosphere, the necessary items to be taken into the box were placed inside the port. The port was then sealed by the closure and tightening of the external port door and the port evacuated using a high vacuum pump for 20 minutes (ten minutes for the small port) before being refilled half-way with argon. To ensure the removal of all traces of oxygen and moisture, the evacuation and argon-fill procedure was repeated a further two times at ten minute intervals. The internal port door can then be opened and materials transferred into the box safe in the knowledge that no O<sub>2</sub> or H<sub>2</sub>O had inadvertently entered into the inert argon atmosphere. Items were removed from the glove box by placing them in the argon-filled, moisture-free port, closing the internal port door and removing them *via* the external port door.

### 5.1.3 Solvent and Liquid Reagent Purification

As mentioned previously, the presence of oxygen and/or water in our reactions is undesirable; therefore, all solvents and liquid reagents used in this project were distilled under nitrogen and degassed (where applicable) before use. This involved the solvents being distilled in the presence of sodium metal and benzophenone and the liquid reagents in the presence of calcium hydride.

Sodium and benzophenone react, forming an intensely blue ketyl radical, which is highly reactive towards water – producing colourless or yellow products, making it a useful self-indicating desiccant.<sup>[282]</sup> The presence of an intense blue colour indicates that the solvent is therefore dry. The dried solvent was then collected (under a nitrogen atmosphere) into an oven-dried round bottom flask containing 4 Å molecular sieves. The round bottom flask was then sealed using a Subaseal<sup>®</sup>; a rubber stopper that enables the easy removal of solvent from the flask, without ingress of any air or moisture into the system. The removal of the solvent was carried out by using a glass syringe and needle, which had been flushed with argon three times prior to use.

To prevent a negative pressure arising within the round bottom flask, a volume of argon (slightly greater than that of the solvent to be removed) was injected into the flask *via* the Subaseal<sup>®</sup> before withdrawal of the solvent. If a negative pressure was to develop, solvent removal would become increasingly difficult, and more importantly, the gradual ingress of atmospheric gases into the round bottom flask as the pressure gradient tries to re-equilibrate would result in contamination of the solvent.

The degassing of deuterated solvents and commercially available amines was carried out using the freeze-pump-thaw methodology to ensure the removal of any dissolved oxygen.<sup>[283]</sup> This involved freezing the solvent/amine in a liquid nitrogen bath prior to thawing to room temperature under vacuum, whereby they were then stored in oven-dried glassware containing 4 Å molecular sieves to prevent contamination by moisture.

#### 5.1.4 Preparation of Glassware

Schlenks were steeped in a basic solution of potassium hydroxide in propan-2-ol overnight prior to being re-used to ensure the removal of any silicon grease which may have built up in the tap. Sintered glass frits of filter sticks were cleaned using a mixture of nitric acid and propan-2-ol. All glassware was then cleaned using a commercial cleaner and rinsed with cold water and acetone, before being placed in an oven operating at approximately 130°C for at least two hours, preferably overnight, prior to use. After cooling, any moisture present was removed by heating the assembled apparatus with a hairdryer whilst under high vacuum.

#### 5.1.5 Reagents Used

The bulk of reagents employed during this research project were purchased from the Aldrich Chemical Company including *n*-butyllithium (1.6 M solution in hexanes), di-*n*-butylmagnesium (1 M solution in heptane), (–)-sparteine, all deuterated NMR solvents and lithium/sodium/potassium 1,1,1,3,3,3-hexamethyldisilazide, to name but a few. The alkoxides sodium *tert*-butoxide and potassium *tert*-butoxide were purchased from Alfa Aesar, as were the amines *cis*-2,6-dimethylpiperidine, diphenylamine and N,N,N',N'-tetramethylethylenediamine. The amine 2,2,6,6-tetramethylpiperidine was purchased from Merck Chemicals and the bases sodium hydroxide and potassium hydroxide from VWR. Unless otherwise stated, other reagents utilised throughout this project were bought from the Aldrich Chemical Company at the highest purity available.

### 5.1.6 Analytical Procedures

All  $^1\text{H}$  and  $^{13}\text{C}$  NMR spectroscopic experiments were performed on either a Bruker AV400 spectrometer or a Bruker DPX400 spectrometer, which operate at 400.03 MHz and 400.13 MHz for  $^1\text{H}$  experiments and 100.59 MHz and 100.61 MHz for  $^{13}\text{C}$  experiments respectively. The chemical shifts quoted are relative to trimethylsilyl at 0.00 ppm.

$^7\text{Li}$  NMR spectra were recorded on the AV400 spectrometer, operating at 155.47 MHz. The chemical shifts quoted are relative to external lithium chloride in deuterated water.

Standard abbreviations of NMR patterns are used within this thesis, which are as follows: s (singlet), d (doublet), t (triplet), q (quartet), m (multiplet), br (broad peak) and combinations thereof, *e.g.*, dd (doublet of doublets).

$^1\text{H}$  DOSY NMR experiments were performed on the Bruker AV400 spectrometer equipped with a BBFO-z-atm probe with actively shielded z-gradient coil capable of delivering a maximum gradient strength of 54 G/cm. Diffusion ordered NMR data was acquired using the Bruker pulse program *dsteqp3s* employing a double stimulated echo with three spoiling gradients. Sine-shaped gradient pulses were used with a duration of 3 ms together with a diffusion period of 100 ms. Gradient recovery delays of 200  $\mu\text{s}$  followed the application of each gradient pulse. Data was accumulated by linearly varying the diffusion encoding gradients over a range from 2% to 95% of maximum for 64 gradient increment values. DOSY plot was generated by use of the DOSY processing module of TopSpin. Parameters were optimized empirically to find the best quality of data for presentation purposes. Diffusion coefficients were calculated by fitting intensity data to the Stejskal-Tanner expression with estimates of errors taken from the variability in the calculated diffusion coefficients by consideration of different NMR responses for the same molecules of interest (except TMS).

All samples for NMR spectroscopic studies were prepared under an argon atmosphere either in the glove box or on the Schlenk line. Compounds were dissolved in deuterated solvents which had been pre-dried over 4 Å molecular sieves and the NMR tubes were made air-tight using a combination of caps and Parafilm<sup>®</sup>.

The X-ray structural data (single-crystal diffraction pattern) was obtained on Oxford Diffraction Gemini S or Oxford Diffraction Xcalibur E CCD instruments. Data was typically collected at 123 K using graphite monochromated Mo-K $\alpha$  or Cu-K $\alpha$  ( $\lambda = 0.71073$  or  $1.54180$  Å) radiation generated by sealed-tube sources. All structures were refined to convergence with SHELX-97.<sup>[284]</sup> Full details of structures are given on the accompanying CD.

## 5.2 Preparation of Starting Materials

Preparation of the common starting materials prepared numerous times throughout the course of this research project (due to their low thermodynamic stability and high pyrophoricity, only small batches were prepared at any one time) will be detailed in this section.

### 5.2.1 Preparation of $n$ BuNa

$n$ -Butylsodium was prepared according to the literature method reported by Schleyer.<sup>[285]</sup> Thus, sodium *tert*-butoxide (3.84 g, 40 mmol) was placed in an oven-dried Schlenk tube within the inert atmosphere of the glove box. On removal from the glove box, dried hexane (40 mL) was added under a flow of argon gas. This was placed in an ultrasonic bath for ten minutes, producing a fine suspension. The Schlenk tube was then cooled in an ice bath, before  $n$ -butyllithium (25 mL of a 1.6 M solution in hexanes, 40 mmol) was added dropwise. The resulting thick white suspension was left to stir at room temperature overnight.

The solid product was isolated using standard Schlenk filtration techniques, and washed with several aliquots of hexane in an effort to minimise the presence of any lithium by-product contaminant. The product was dried *in vacuo* for at least an hour, prior to being transferred to the glove box, where it could be used for subsequent reactions. Typical yield = 2.84 g (89%).

### 5.2.2 Preparation of PhCH<sub>2</sub>K

Benzylpotassium was prepared according to the literature method reported by Schleyer.<sup>[286]</sup> Thus, potassium *tert*-butoxide (2.80 g, 25 mmol) was placed in an oven-dried Schlenk tube within the inert atmosphere of the glove box. On removal from the glove box, dried toluene (40 mL) was added under a flow of argon gas. This was placed in an ultrasonic bath for ten minutes, producing a fine suspension. The Schlenk tube was then cooled in an ice bath, before  $n$ -butyllithium (16 mL of a 1.6 M solution in hexanes, 25 mmol) was added dropwise. The resulting thick red suspension was left to stir at room temperature overnight.

The solid product was isolated using standard Schlenk filtration techniques, and washed with several aliquots of hexane in an effort to minimise the presence of any lithium by-product contaminant. The product was dried *in vacuo* for at least an hour, prior to being transferred to the glove box, where it could be used for subsequent reactions. Typical yield = 3.12 g (96%).

### 5.2.3 Preparation of Me<sub>3</sub>SiCH<sub>2</sub>K

(Trimethylsilylmethyl)potassium was prepared according to the literature method reported by Mulvey.<sup>[250b]</sup> Thus, potassium *tert*-butoxide (2.80 g, 25 mmol) was placed in an oven-dried

Schlenk tube within the inert atmosphere of the glove box. On removal from the glove box, dried hexane (50 mL) was added under a flow of argon gas. This was placed in an ultrasonic bath for ten minutes, producing a fine suspension. The Schlenk tube was then cooled in an ice bath, before (trimethylsilylmethyl)lithium (25 mL of a 1 M solution in pentane, 25 mmol) was added dropwise. The resulting thick off-white suspension was left to stir at room temperature overnight.

The solid product was isolated using standard Schlenk filtration techniques, and washed with several aliquots of hexane. The product was then dried *in vacuo* for at least an hour, prior to being transferred to the glove box, where it could be used for subsequent reactions. Typical yield = 2.76 g (88%).

#### 5.2.4 Preparation of $(\text{Me}_3\text{SiCH}_2)_2\text{Mg}$

Magnesium turnings (4 g, 165 mmol) were added to a 500 mL round bottom flask equipped with a condenser and addition funnel and the system evacuated (using a vacuum pump) and refilled with argon three times, prior to the addition of dried diethylether (100 mL). A solution of chloromethyltrimethylsilane (19 mL, 136 mmol) in diethylether (50 mL) was added dropwise *via* the addition funnel. The reaction mixture was heated to reflux for two hours, after which dried dioxane (9 mL, 106 mmol) in diethylether (50 mL) was added *via* the addition funnel. The resulting thick grey suspension was left to stir at room temperature for two to three days.

Subsequently, the solution was filtered under gravity through Celite and glass wool and washed with diethylether (2 x 40 mL), producing a homogeneous solution. The solvent was removed slowly under vacuum, yielding a pale yellow solid. This was then subjected to heat, washed with more diethylether (2 mL) and the solvent removed once again, affording an off-white solid. This was then purified by sublimation (170°C) and the resulting white crystalline powder transferred to the glove box, where it could be used for subsequent reactions. Typical yield = 9.47 g (70%).

$^1\text{H}$  NMR (400.03 MHz, 300 K,  $d_8$ -THF):  $\delta$  -0.11 ( $\text{SiCH}_3$ , 18H, s), -1.77 ( $\text{CH}_2$ , 4H, s).  $^{13}\text{C}$  NMR (100.59 MHz, 300 K,  $d_8$ -THF):  $\delta$  4.6 ( $\text{SiCH}_3$ ), -7.6 ( $\text{CH}_2$ ).

#### 5.2.5 Preparation of $^t\text{Bu}_2\text{Zn}$

Di-*tert*-butylzinc was prepared according to the literature method reported by Mulvey.<sup>[111]</sup> Thus, anhydrous zinc chloride (5.45 g, 40 mmol) was placed in an oven-dried Schlenk tube within the inert atmosphere of the glove box. On removal from the glove box, dried



diethylether (10 mL) was added under a flow of argon gas. The solution was then cooled in an ice bath, before *tert*-butyllithium (42 mL of a 1.9 M solution in pentane, 80 mmol) was added dropwise, precipitating a white solid. The Schlenk was then surrounded with a black plastic bag to block out the light, and its contents stirred for three hours.

The white powder obtained was isolated using standard Schlenk filtration techniques through Celite and glass wool. The resulting transparent, colourless solution was then transferred by cannula to a sublimator and the solvent removed under vacuum. When it was judged that all solvent had been removed, but before any di-*tert*-butylzinc had sublimed, the cold finger was filled with an acetone/liquid nitrogen mixture ( $-78^{\circ}\text{C}$ ) and the di-*tert*-butylzinc allowed to sublime on the finger for approximately one hour.

The coolant was then removed and the sublimator placed in the glove box, where the di-*tert*-butylzinc was scraped from the cold finger and placed in Schlenk tubes in 2 mmol portions. On removal from the glove box, dried hexane (10 mL) was added to the Schlenk tubes. The di-*tert*-butylzinc solutions were then stored in a freezer operating at  $-28^{\circ}\text{C}$  for no longer than 24 hours before use. Typical yield = 5.75 g (80%).

### 5.2.6 Preparation of (*R,R*)-TMCDA

*N,N,N',N'*-(1*R*,2*R*)-Tetramethylcyclohexane-1,2-diamine was prepared according to the literature method reported by Alexakis.<sup>[166c]</sup> Thus, (*R,R*)-1,2-diammoniumcyclohexane mono-(+)-tartrate salt (25 g, 95 mmol) was placed in a 250 mL round bottom flask and dissolved in formic acid (36 mL of a 95 wt.% solution) with slight heating, followed by the slow addition of formaldehyde (44 mL of a 37 wt.% solution). The mixture was heated at reflux for two hours, where a colour change from peach to orange was observed. After cooling, the reaction mixture was made basic until pH 14 by the addition of sodium hydroxide pellets and subsequently extracted with diethylether. The combined organic layers were washed with brine, dried over anhydrous sodium sulphate, filtered and concentrated under reduced pressure. The product was distilled (bp =  $50^{\circ}\text{C}/0.1$  mmHg) to give a colourless liquid, which was stored in an oven-dried round bottom flask containing 4 Å molecular sieves. Typical yield = 11.78 g (73%).

$^1\text{H}$  NMR (400.03 MHz, 300 K,  $\text{C}_6\text{D}_6$ ):  $\delta$  2.29 ( $\text{CH}_3$ , 12H, s), 2.26 ( $\alpha\text{-CH}$ , 2H, s), 1.75 ( $\beta\text{-CH}_2$ , 2H, br m), 1.60 ( $\gamma\text{-CH}_2$ , 2H, br m), 1.01 ( $\beta\text{-CH}_2$ , 2H, br m), 1.01 ( $\gamma\text{-CH}_2$ , 2H, br m).  $^{13}\text{C}$  NMR (100.59 MHz, 300 K,  $\text{C}_6\text{D}_6$ ):  $\delta$  64.3 ( $\alpha\text{-CH}$ ), 40.6 ( $\text{CH}_3$ ), 26.0 ( $\beta\text{-CH}_2$ ), 25.7 ( $\gamma\text{-CH}_2$ ).

$^1\text{H}$  NMR (400.03 MHz, 300 K,  $d_8$ -THF):  $\delta$  2.35 ( $\alpha$ -CH, 2H, s), 2.27 ( $\text{CH}_3$ , 12H, s), 1.76 ( $\beta$ - $\text{CH}_2$ , 2H, br m), 1.69 ( $\gamma$ - $\text{CH}_2$ , 2H, br m), 1.12 ( $\beta$ - $\text{CH}_2$ , 2H, br m), 1.12 ( $\gamma$ - $\text{CH}_2$ , 2H, br m).  $^{13}\text{C}$  NMR (100.59 MHz, 300 K,  $d_8$ -THF):  $\delta$  65.0 ( $\alpha$ -CH), 40.8 ( $\text{CH}_3$ ), 26.5 ( $\beta$ - $\text{CH}_2$ ), 26.5 ( $\gamma$ - $\text{CH}_2$ ).

### 5.2.7 Preparation of $\text{Me}_6$ -TREN

Tris[2-(dimethylamino)ethyl]amine was prepared according to the literature method reported by Britovsek.<sup>[269]</sup> Thus, acetonitrile (600 mL), along with acetic acid (135 mL), tris(2-aminoethyl)amine (5 mL, 33 mmol) and formaldehyde (49 mL of a 37 wt.% solution) were placed in a 1 L round bottom flask and the mixture allowed to stir for one hour. Subsequently, the reaction mixture was cooled in an ice bath and sodium borohydride (10 g, 13 mmol) slowly added. After being stirred for 48 hours, all solvents were removed, the residue made strongly basic (pH 14) by the addition of sodium hydroxide pellets, and extracted several times with dichloromethane. The combined dichloromethane extracts were dried over magnesium sulphate, filtered and the solvent removed. The resulting residue was dissolved in pentane, filtered and the filtrate reduced to dryness to give a pale yellow oil, which was stored in an oven-dried sample vial containing 4 Å molecular sieves. Typical yield = 4.32 g (94%).

$^1\text{H}$  NMR (400.03 MHz, 300 K,  $\text{C}_6\text{D}_6$ ):  $\delta$  2.63 ( $\alpha$ - $\text{CH}_2$ , 6H, t), 2.37 ( $\beta$ - $\text{CH}_2$ , 6H, t), 2.12 ( $\text{CH}_3$ , 18H, s).  $^{13}\text{C}$  NMR (100.59 MHz, 300 K,  $\text{C}_6\text{D}_6$ ):  $\delta$  58.6 ( $\alpha$ - $\text{CH}_2$ ), 53.9 ( $\beta$ - $\text{CH}_2$ ), 46.0 ( $\text{CH}_3$ ).

$^1\text{H}$  NMR (400.03 MHz, 300 K,  $d_8$ -THF):  $\delta$  2.55 ( $\alpha$ - $\text{CH}_2$ , 6H, s), 2.29 ( $\beta$ - $\text{CH}_2$ , 6H, s), 2.15 ( $\text{CH}_3$ , 18H, s).  $^{13}\text{C}$  NMR (100.59 MHz, 300 K,  $d_8$ -THF):  $\delta$  59.3 ( $\alpha$ - $\text{CH}_2$ ), 54.5 ( $\beta$ - $\text{CH}_2$ ), 46.3 ( $\text{CH}_3$ ).

## 5.3 Synthesis of Products

### 5.3.1 Synthesis of [(TMEDA)·Li( $\mu$ -*cis*-DMP)Zn(*t*Bu)<sub>2</sub>], **75**

*n*-Butyllithium (0.63 mL of a 1.6 M solution in hexanes, 1 mmol) was suspended in dried hexane (2 mL) in an oven-dried Schlenk tube. *Cis*-2,6-dimethylpiperidine (0.14 mL, 1 mmol) was then introduced and the reaction mixture allowed to stir for 30 minutes. In a separate Schlenk tube, freshly prepared di-*tert*-butylzinc (0.18 g, 1 mmol) was dissolved in dried hexane (5 mL). This latter solution was transferred to the former *via* a cannula, which was followed by the addition of *N,N,N',N'*-tetramethylethylenediamine (0.15 mL, 1 mmol). This pale yellow solution was left to stand at ambient temperature and after 48 hours, small colourless X-ray quality crystals of **75** were deposited (0.32 g, 77%).

$^1\text{H}$  NMR (400.03 MHz, 300 K,  $\text{C}_6\text{D}_6$ ):  $\delta$  3.32 ( $\alpha\text{-CH}$ , 2H, m), 1.83 ( $\gamma\text{-CH}_2$ , 1H, m), 1.72 ( $\gamma\text{-CH}_2$ , 1H, m), 1.67 ( $\beta\text{-CH}_2$ , 2H, m), 1.66 (TMEDA  $\text{CH}_3$ , 12H, s), 1.59 ( $t\text{Bu CH}_3$ , 9H, s), 1.48 (TMEDA  $\text{CH}_2$ , 4H, s), 1.05 ( $\text{CH}_3$ , 6H, d), 0.39 ( $\beta\text{-CH}_2$ , 2H, m).  $^{13}\text{C}$  NMR (100.59 MHz, 300 K,  $\text{C}_6\text{D}_6$ ):  $\delta$  57.2 ( $\alpha\text{-C}$ ), 57.2 (TMEDA  $\text{CH}_2$ ), 46.9 (TMEDA  $\text{CH}_3$ ), 38.0 ( $\beta\text{-CH}_2$ ), 35.7 ( $t\text{Bu CH}_3$ ), 27.2 ( $\gamma\text{-CH}_2$ ), 25.9 ( $\text{CH}_3$ ).  $^7\text{Li}$  NMR (155.47 MHz, 300 K,  $\text{C}_6\text{D}_6$ ):  $\delta$  0.93.

Crystal data for **75**:  $\text{C}_{21}\text{H}_{48}\text{N}_3\text{LiZn}$ ,  $M_r = 414.93$ , monoclinic, space group  $P2_1$ ,  $a = 8.3990(3)$ ,  $b = 16.7308(4)$ ,  $c = 9.5282(4)$  Å,  $\beta = 108.761(4)^\circ$ ,  $V = 1267.78(10)$  Å<sup>3</sup>,  $Z = 2$ ,  $\lambda = 0.71073$  Å,  $\mu = 0.977$  mm<sup>-1</sup>,  $T = 123$  K; 12776 reflections, 6035 unique,  $R_{\text{int}} = 0.0204$ ; final refinement to convergence on  $F^2$  gave  $R = 0.0252$  ( $F$ , 5446 obs. data only) and  $R_w = 0.0512$  ( $F^2$ , all data), GOF = 0.975.

### 5.3.2 Synthesis of [(TMEDA)·Na( $\mu\text{-cis-DMP}$ )( $\mu\text{-}t\text{Bu}$ )Zn( $t\text{Bu}$ )], **76**

Freshly prepared *n*-butylsodium (0.08 g, 1 mmol) was suspended in dried hexane (5 mL) in an oven-dried Schlenk tube and placed in an ultrasonic bath for ten minutes. *Cis*-2,6-dimethylpiperidine (0.14 mL, 1 mmol) was then introduced and the reaction mixture allowed to stir for 30 minutes. In a separate Schlenk tube, freshly prepared di-*tert*-butylzinc (0.18 g, 1 mmol) was dissolved in dried hexane (5 mL). This latter solution was transferred to the former *via* a cannula, which was followed by the addition of *N,N,N',N'*-tetramethylethylenediamine (0.15 mL, 1 mmol). This pale yellow solution was immediately placed in a freezer operating at  $-28^\circ\text{C}$  and after 48 hours, small colourless X-ray quality crystals of **76** were deposited (0.10 g, 23%).

$^1\text{H}$  NMR (400.03 MHz, 300 K,  $\text{C}_6\text{D}_6$ ):  $\delta$  3.40 ( $\alpha\text{-CH}$ , 2H, m), 1.82 ( $\gamma\text{-CH}_2$ , 1H, m), 1.71 ( $\gamma\text{-CH}_2$ , 1H, m), 1.70 ( $\beta\text{-CH}_2$ , 2H, m), 1.66 (TMEDA  $\text{CH}_3$ , 12H, s), 1.61 ( $t\text{Bu CH}_3$ , 9H, br s), 1.56 (TMEDA  $\text{CH}_2$ , 4H, s), 1.07 ( $\text{CH}_3$ , 6H, d), 0.15 ( $\beta\text{-CH}_2$ , 2H, m).  $^{13}\text{C}$  NMR (100.59 MHz, 300 K,  $\text{C}_6\text{D}_6$ ):  $\delta$  56.8 (TMEDA  $\text{CH}_2$ ), 56.4 ( $\alpha\text{-C}$ ), 45.8 (TMEDA  $\text{CH}_3$ ), 39.2 ( $\beta\text{-CH}_2$ ), 35.7 ( $t\text{Bu CH}_3$ ), 27.0 ( $\text{CH}_3$ ), 26.8 ( $\gamma\text{-CH}_2$ ).

Crystal data for **76**:  $\text{C}_{21}\text{H}_{48}\text{N}_3\text{NaZn}$ ,  $M_r = 430.98$ , triclinic, space group  $P1$ ,  $a = 8.3370(4)$ ,  $b = 9.6409(5)$ ,  $c = 9.7024(4)$  Å,  $\alpha = 61.815(4)$ ,  $\beta = 78.623(4)$ ,  $\gamma = 73.435(5)^\circ$ ,  $V = 657.03(5)$  Å<sup>3</sup>,  $Z = 1$ ,  $\lambda = 1.54180$  Å,  $\mu = 1.502$  mm<sup>-1</sup>,  $T = 123$  K; 6022 reflections, 3312 unique,  $R_{\text{int}} = 0.0418$ ; final refinement to convergence on  $F^2$  gave  $R = 0.0658$  ( $F$ , 3302 obs. data only) and  $R_w = 0.1841$  ( $F^2$ , all data), GOF = 1.061.

### 5.3.3 Synthesis of [(TMEDA)·Na(μ-*cis*-DMP)<sub>2</sub>Zn(<sup>*t*</sup>Bu)], **77**

Freshly prepared *n*-butylsodium (0.08 g, 1 mmol) was suspended in dried hexane (5 mL) in an oven-dried Schlenk tube and placed in an ultrasonic bath for ten minutes. *Cis*-2,6-dimethylpiperidine (0.14 mL, 1 mmol) was then introduced and the reaction mixture allowed to stir for 30 minutes. In a separate Schlenk tube, freshly prepared di-*tert*-butylzinc (0.18 g, 1 mmol) was dissolved in dried hexane (5 mL). This latter solution was transferred to the former *via* a cannula, which was followed by the addition of *N,N,N',N'*-tetramethylethylenediamine (0.15 mL, 1 mmol). This pale yellow solution was left to stand at ambient temperature and after 48 hours, small colourless X-ray quality crystals of **77** were deposited (0.14 g, 29%).

<sup>1</sup>H NMR (400.03 MHz, 300 K, C<sub>6</sub>D<sub>6</sub>): δ 3.21 (α-CH, 4H, m), 1.95 (γ-CH<sub>2</sub>, 2H, m), 1.84 (TMEDA CH<sub>3</sub>, 12H, s), 1.78 (TMEDA CH<sub>2</sub>, 4H, s), 1.72 (γ-CH<sub>2</sub>, 2H, m), 1.71 (<sup>*t*</sup>Bu CH<sub>3</sub>, 9H, s), 1.68 (β-CH<sub>2</sub>, 4H, m), 1.26 (CH<sub>3</sub>, 12H, d), 0.76 (β-CH<sub>2</sub>, 4H, m). <sup>13</sup>C NMR (100.59 MHz, 300 K, C<sub>6</sub>D<sub>6</sub>): δ 60.3 (α-C), 57.3 (TMEDA CH<sub>2</sub>), 46.3 (TMEDA CH<sub>3</sub>), 38.9 (β-CH<sub>2</sub>), 35.2 (<sup>*t*</sup>Bu CH<sub>3</sub>), 28.9 (CH<sub>3</sub>), 27.3 (γ-CH<sub>2</sub>).

Crystal data for **77**: C<sub>24</sub>H<sub>53</sub>N<sub>4</sub>NaZn, *M<sub>r</sub>* = 486.06, orthorhombic, space group *P*2<sub>1</sub>2<sub>1</sub>2<sub>1</sub>, *a* = 10.4292(5), *b* = 14.0867(6), *c* = 19.4254(8) Å, *V* = 2853.9(4) Å<sup>3</sup>, *Z* = 4, λ = 0.71073 Å, μ = 0.892 mm<sup>-1</sup>, *T* = 123 K; 7681 reflections, 4500 unique, *R*<sub>int</sub> = 0.0467; final refinement to convergence on *F*<sup>2</sup> gave *R* = 0.0524 (*F*, 2612 obs. data only) and *R<sub>w</sub>* = 0.1022 (*F*<sup>2</sup>, all data), GOF = 0.881.

### 5.3.4 Synthesis of [(TMEDA)·Na(μ-*cis*-DMP)<sub>2</sub>Mg(*cis*-DMP)], **79**

Freshly prepared *n*-butylsodium (0.16 g, 2 mmol) was suspended in dried hexane (4 mL) in an oven-dried Schlenk tube and placed in an ultrasonic bath for ten minutes. Di-*n*-butylmagnesium (2 mL of a 1 M solution in heptane, 2 mmol) was then introduced, followed by three molar equivalents of *cis*-2,6-dimethylpiperidine (0.84 mL, 6 mmol) added dropwise, producing a cloudy yellow solution. The solution was vigorously stirred for one hour and then *N,N,N',N'*-tetramethylethylenediamine (0.3 mL, 2 mmol) was introduced dropwise, producing a transparent yellow solution. This solution was subsequently stirred for a further 30 minutes and left to stand at ambient temperature. After 48 hours, a crop of colourless X-ray quality needle-like crystals of **79** were deposited (0.55 g, 55%).

<sup>1</sup>H NMR (400.03 MHz, 300 K, C<sub>6</sub>D<sub>6</sub>): δ 3.12 (α-CH, 6H, m), 2.00 (γ-CH<sub>2</sub>, 3H, m), 1.81 (TMEDA CH<sub>3</sub>, 12H, s), 1.76 (γ-CH<sub>2</sub>, 3H, m), 1.76 (β-CH<sub>2</sub>, 6H, m), 1.71 (TMEDA CH<sub>2</sub>, 4H,

s), 1.41 ( $CH_3$ , 12H, d), 0.79 ( $\beta$ - $CH_2$ , 6H, m).  $^{13}C$  NMR (100.59 MHz, 300 K,  $C_6D_6$ ):  $\delta$  58.1 ( $\alpha$ -C), 57.6 (TMEDA  $CH_2$ ), 47.0 (TMEDA  $CH_3$ ), 38.6 ( $\beta$ - $CH_2$ ), 27.4 ( $\gamma$ - $CH_2$ ), 27.2 ( $CH_3$ ).

Crystal data for **79**:  $C_{27}H_{58}N_5NaMg$ ,  $M_r = 500.08$ , monoclinic, space group  $P2_1/n$ ,  $a = 14.1862(4)$ ,  $b = 15.1005(5)$ ,  $c = 14.6621(4)$  Å,  $\beta = 97.090(3)^\circ$ ,  $V = 3116.88(16)$  Å<sup>3</sup>,  $Z = 4$ ,  $\lambda = 0.71073$  Å,  $\mu = 0.093$  mm<sup>-1</sup>,  $T = 123$  K; 25234 reflections, 8635 unique,  $R_{int} = 0.0370$ ; final refinement to convergence on  $F^2$  gave  $R = 0.0475$  ( $F$ , 5421 obs. data only) and  $R_w = 0.1045$  ( $F^2$ , all data), GOF = 0.949.

### 5.3.5 Synthesis of [ $\{cis\text{-DMP(H)}\} \cdot Na(\mu\text{-}cis\text{-DMP})_2Mg(cis\text{-DMP})$ ], **80**

Freshly prepared *n*-butylsodium (0.16 g, 2 mmol) was suspended in dried hexane (5 mL) in an oven-dried Schlenk tube and placed in an ultrasonic bath for ten minutes. Di-*n*-butylmagnesium (2 mL of a 1 M solution in heptane, 2 mmol) was then introduced, followed by three molar equivalents of *cis*-2,6-dimethylpiperidine (0.84 mL, 6 mmol) added dropwise, producing a cloudy yellow solution. The solution was vigorously stirred for one hour and then dried toluene (1 mL) introduced dropwise, producing a slightly less cloudy yellow solution. After two hours, the solution was heated to reflux for 15 minutes and left to stand at ambient temperature. After 48 hours the solution was concentrated by removal of some solvent *in vacuo*, heated and left to stand at ambient temperature. Seven days later, a crop of orange X-ray quality crystals of **80** were deposited [0.26 g, 26% (with respect to <sup>n</sup>BuNa)].

$^1H$  NMR (400.03 MHz, 300 K,  $C_6D_6$ ):  $\delta$  2.85 ( $\alpha$ - $CH$ , 6H, m), 2.38 [*cis*-DMP(H)  $\alpha$ - $CH$ , 2H, m], 1.92 ( $\gamma$ - $CH_2$ , 3H, m), 1.68 ( $\beta$ - $CH_2$ , 6H, m), 1.64 ( $\gamma$ - $CH_2$ , 3H, m), 1.63 [*cis*-DMP(H)  $\gamma$ - $CH_2$ , 1H, m], 1.38 [*cis*-DMP(H)  $\beta$ - $CH_2$ , 2H, m], 1.23 ( $CH_3$ , 18H, d), 1.18 [*cis*-DMP(H)  $\gamma$ - $CH_2$ , 1H, m], 0.91 [*cis*-DMP(H)  $CH_3$ , 6H, d], 0.89 [*cis*-DMP(H)  $\beta$ - $CH_2$ , 2H, m], 0.39 (NH, 1H, br s), 0.38 ( $\beta$ - $CH_2$ , 6H, m).  $^{13}C$  NMR (100.59 MHz, 300 K,  $C_6D_6$ ):  $\delta$  57.1 ( $\alpha$ -C), 52.6 [*cis*-DMP(H)  $\alpha$ -C], 39.0 ( $\beta$ - $CH_2$ ), 34.4 [*cis*-DMP(H)  $\beta$ - $CH_2$ ], 28.1 ( $CH_3$ ), 26.7 ( $\gamma$ - $CH_2$ ), 25.2 [*cis*-DMP(H)  $\gamma$ - $CH_2$ ], 23.4 [*cis*-DMP(H)  $CH_3$ ].

Crystal data for **80**:  $C_{28}H_{57}N_4NaMg$ ,  $M_r = 497.08$ , orthorhombic, space group  $Pna2_1$ ,  $a = 19.8056(6)$ ,  $b = 11.6235(4)$ ,  $c = 27.1270(8)$  Å,  $V = 6244.9(3)$  Å<sup>3</sup>,  $Z = 8$ ,  $\lambda = 0.71073$  Å,  $\mu = 0.092$  mm<sup>-1</sup>,  $T = 123$  K; 24717 reflections, 10545 unique,  $R_{int} = 0.0621$ ; final refinement to convergence on  $F^2$  gave  $R = 0.0508$  ( $F$ , 5046 obs. data only) and  $R_w = 0.0807$  ( $F^2$ , all data), GOF = 0.782.

### 5.3.6 Synthesis of [KHMDS·TMEDA]<sub>2</sub>, **83**

Potassium 1,1,1,3,3,3-hexamethyldisilazide (0.40 g, 2 mmol) was suspended in dried hexane (8 mL) in an oven-dried Schlenk tube and allowed to stir for ten minutes, producing a white suspension. *N,N,N',N'*-Tetramethylethylenediamine (0.30 mL, 2 mmol) was then introduced, producing a slightly cloudy solution. This solution was stirred for 20 minutes, heated and filtered through Celite and glass wool. Once cooled, the resultant clear solution was immediately placed in a freezer operating at  $-28^{\circ}\text{C}$ . After 48 hours, X-ray quality needle-like crystals of **83** were deposited (0.33 g, 55%).

$^1\text{H}$  NMR (400.03 MHz, 300 K,  $\text{C}_6\text{D}_6$ ):  $\delta$  2.31 (TMEDA  $\text{CH}_2$ , 8H, s), 2.12 (TMEDA  $\text{CH}_3$ , 24H, s), 0.16 (Si $\text{CH}_3$ , 36H, s).  $^{13}\text{C}$  NMR (100.59 MHz, 300 K,  $\text{C}_6\text{D}_6$ ):  $\delta$  58.3 (TMEDA  $\text{CH}_2$ ), 45.9 (TMEDA  $\text{CH}_3$ ), 7.2 (Si $\text{CH}_3$ ).

Crystal data for **83**:  $\text{C}_{47}\text{H}_{87.83}\text{N}_{11.67}\text{Si}_8\text{K}_4$ ,  $M_r = 1197.58$ , monoclinic, space group  $P2_1/c$ ,  $a = 25.0098(4)$ ,  $b = 41.6744(7)$ ,  $c = 11.7634(16)$  Å,  $\beta = 91.6063(13)^{\circ}$ ,  $V = 12255.8(17)$  Å<sup>3</sup>,  $Z = 12$ ,  $\lambda = 0.71073$  Å,  $\mu = 0.735$  mm<sup>-1</sup>,  $T = 123$  K; 70895 reflections, 28587 unique,  $R_{\text{int}} = 0.0252$ ; final refinement to convergence on  $F^2$  gave  $R = 0.0816$  ( $F$ , 17031 obs. data only) and  $R_w = 0.2846$  ( $F^2$ , all data), GOF = 1.042.

### 5.3.7 Synthesis of $[(\text{NaHMDS})_2\cdot\text{TMEDA}]_{\infty}$ , **84**

Sodium 1,1,1,3,3,3-hexamethyldisilazide (0.73 g, 4 mmol) was suspended in dried hexane (10 mL) in an oven-dried Schlenk tube and placed in an ultrasonic bath for ten minutes, producing a white suspension. *N,N,N',N'*-Tetramethylethylenediamine (0.15 mL, 1 mmol) was then introduced, along with dried toluene (7.5 mL), yielding a clear pale yellow solution. This solution was allowed to stir for three hours, heated, and once cooled, placed in a freezer operating at  $-28^{\circ}\text{C}$ . After 5 days, a small mass of crystalline material was observed. Solvent was removed *in vacuo* and dried toluene (8 mL) added, producing a clear yellow solution. The solution was heated and left to stand at ambient temperature. After approximately 45 minutes, a crop of colourless X-ray quality crystals of **84** were deposited [0.81 g, 84% (with respect to NaHMDS)].

$^1\text{H}$  NMR (400.03 MHz, 300 K,  $\text{C}_6\text{D}_6$ ):  $\delta$  1.99 (TMEDA  $\text{CH}_2$ , 4H, s), 1.97 (TMEDA  $\text{CH}_3$ , 12H, s), 0.19 (Si $\text{CH}_3$ , 36H, s).  $^{13}\text{C}$  NMR (100.59 MHz, 300 K,  $\text{C}_6\text{D}_6$ ):  $\delta$  57.6 (TMEDA  $\text{CH}_2$ ), 45.8 (TMEDA  $\text{CH}_3$ ), 7.0 (Si $\text{CH}_3$ ).

Crystal data for **84**:  $\text{C}_9\text{H}_{26}\text{N}_2\text{Si}_2\text{Na}$ ,  $M_r = 241.49$ , monoclinic, space group  $P2_1/n$ ,  $a = 9.9761(12)$ ,  $b = 13.8292(12)$ ,  $c = 11.7983(14)$  Å,  $\beta = 113.523(14)^{\circ}$ ,  $V = 1492.4(3)$  Å<sup>3</sup>,  $Z = 4$ ,  $\lambda$

$\lambda = 0.71073 \text{ \AA}$ ,  $\mu = 0.240 \text{ mm}^{-1}$ ,  $T = 123 \text{ K}$ ; 8332 reflections, 3436 unique,  $R_{\text{int}} = 0.0123$ ; final refinement to convergence on  $F^2$  gave  $R = 0.0227$  ( $F$ , 3064 obs. data only) and  $R_w = 0.0674$  ( $F^2$ , all data), GOF = 1.073.

### 5.3.8 Synthesis of $[\text{KHMDs} \cdot (R,R)\text{-TMCDa}]_2$ , **85**

Potassium 1,1,1,3,3,3-hexamethyldisilazide (0.40 g, 2 mmol) was suspended in dried hexane (10 mL) in an oven-dried Schlenk tube and allowed to stir for ten minutes, producing a white suspension. *N,N,N',N'*-(1*R*,2*R*)-Tetramethylcyclohexane-1,2-diamine (0.38 mL, 2 mmol) was then introduced, producing a clear pale yellow solution. The solution was immediately placed in a freezer operating at  $-28^\circ\text{C}$  and after 48 hours, small X-ray quality crystals of **85** were deposited (0.50 g, 68%).

$^1\text{H}$  NMR (400.03 MHz, 300 K,  $d_8$ -THF):  $\delta$  2.35 ( $\alpha$ -CH, 4H, m), 2.27 ( $\text{CH}_3$ , 24H, s), 1.77 ( $\beta$ - $\text{CH}_2$ , 4H, m), 1.67 ( $\gamma$ - $\text{CH}_2$ , 4H, m), 1.12 ( $\beta$ - $\text{CH}_2$ , 4H, m), 1.12 ( $\gamma$ - $\text{CH}_2$ , 4H, m),  $-0.21$  ( $\text{SiCH}_3$ , 36H, s).  $^{13}\text{C}$  NMR (100.59 MHz, 300 K,  $d_8$ -THF):  $\delta$  67.4 ( $\alpha$ -CH), 40.8 ( $\text{CH}_3$ ), 26.5 ( $\beta$ - $\text{CH}_2$ ), 26.5 ( $\gamma$ - $\text{CH}_2$ ), 6.8 ( $\text{SiCH}_3$ ).

Crystal data for **85**:  $\text{C}_{16}\text{H}_{40}\text{N}_3\text{Si}_2\text{K}$ ,  $M_r = 369.79$ , orthorhombic, space group  $P2_12_12_1$ ,  $a = 11.7946(4)$ ,  $b = 11.9020(3)$ ,  $c = 32.6416(8) \text{ \AA}$ ,  $V = 4582.2(2) \text{ \AA}^3$ ,  $Z = 8$ ,  $\lambda = 0.71073 \text{ \AA}$ ,  $\mu = 0.338 \text{ mm}^{-1}$ ,  $T = 123 \text{ K}$ ; 18855 reflections, 7506 unique,  $R_{\text{int}} = 0.0769$ ; final refinement to convergence on  $F^2$  gave  $R = 0.0659$  ( $F$ , 6740 obs. data only) and  $R_w = 0.1663$  ( $F^2$ , all data), GOF = 1.108.

### 5.3.9 Synthesis of $[\text{Na}(\text{TMEDA})_2]^+[\text{Mg}(\text{HMDS})_3]^-$ , **88**

Sodium 1,1,1,3,3,3-hexamethyldisilazide (0.73 g, 4 mmol) was suspended in dried hexane (10 mL) in an oven-dried Schlenk tube and placed in an ultrasonic bath for ten minutes, producing a white suspension. Di-*n*-butylmagnesium (2 mL of a 1 M solution in heptane, 2 mmol) was then introduced, yielding a peach coloured suspension. On the addition of *N,N,N',N'*-tetramethylethylenediamine (0.30 mL, 2 mmol), a peach to pale pink colour change was observed. This solution was allowed to stir for one hour, before being heated and immediately placed in a hot water-filled Dewar flask. After 24 hours, a white non-crystalline precipitate was observed in a pale pink coloured cloudy solution. The solution was filtered through Celite and glass wool and the resultant clear pale yellow solution heated and left to stand at ambient temperature. After 48 hours, a crop of colourless X-ray quality needle-like crystals of **88** were deposited (0.14 g).

$^1\text{H}$  NMR (400.03 MHz, 300 K,  $\text{C}_6\text{D}_6$ ):  $\delta$  1.97 (TMEDA  $\text{CH}_3$ , 8H, s), 1.96 (TMEDA  $\text{CH}_2$ , 24H, s), 0.20 (Si $\text{CH}_3$ , 54H, s).  $^{13}\text{C}$  NMR (100.59 MHz, 300 K,  $\text{C}_6\text{D}_6$ ):  $\delta$  57.5 (TMEDA  $\text{CH}_2$ ), 45.8 (TMEDA  $\text{CH}_3$ ), 7.0 (Si $\text{CH}_3$ ).

Crystal data for **88**:  $\text{C}_{30}\text{H}_{83}\text{N}_7\text{Si}_6\text{NaMg}$ ,  $M_r = 757.87$ , triclinic, space group  $P\bar{1}$ ,  $a = 11.8176(10)$ ,  $b = 11.9680(11)$ ,  $c = 18.4164(16)$  Å,  $\alpha = 94.913(7)$ ,  $\beta = 99.478(7)$ ,  $\gamma = 103.922(8)^\circ$ ,  $V = 2472.2(4)$  Å<sup>3</sup>,  $Z = 2$ ,  $\lambda = 0.71073$  Å,  $\mu = 0.216$  mm<sup>-1</sup>,  $T = 123$  K; 24497 reflections, 13120 unique,  $R_{\text{int}} = 0.0438$ ; final refinement to convergence on  $F^2$  gave  $R = 0.0467$  ( $F$ , 7499 obs. data only) and  $R_w = 0.1015$  ( $F^2$ , all data), GOF = 0.864.

### 5.3.10 Synthesis of $[\text{Li}(\text{TMEDA})_2]^+[\text{Mg}(\text{HMDS})_3]^-$ , **89**

Lithium 1,1,1,3,3,3-hexamethyldisilazide (0.67 g, 4 mmol) was suspended in dried hexane (10 mL) in an oven-dried Schlenk tube and stirred for ten minutes. Di-*n*-butylmagnesium (2 mL of a 1 M solution in heptane, 2 mmol) was then introduced, followed by the addition of *N,N,N',N'*-tetramethylethylenediamine (0.30 mL, 2 mmol), yielding a slightly cloudy solution. This solution was heated and left to stand at ambient temperature and after 48 hours, a crop of colourless X-ray quality cubic-like crystals of **89** were deposited (0.03 g).

$^1\text{H}$  NMR (400.03 MHz, 300 K,  $\text{C}_6\text{D}_6$ ):  $\delta$  1.74 (TMEDA  $\text{CH}_3$ , 8H, s), 1.48 (TMEDA  $\text{CH}_2$ , 24H, s), 0.40 (Si $\text{CH}_3$ , 54H, s).  $^{13}\text{C}$  NMR (100.59 MHz, 300 K,  $\text{C}_6\text{D}_6$ ):  $\delta$  58.2 (TMEDA  $\text{CH}_2$ ), 46.3 (TMEDA  $\text{CH}_3$ ), 6.6 (Si $\text{CH}_3$ ).  $^7\text{Li}$  NMR (155.47 MHz, 300 K,  $\text{C}_6\text{D}_6$ ):  $\delta$  1.42.

Crystal data for **89**:  $\text{C}_{30}\text{H}_{86}\text{N}_7\text{Si}_6\text{LiMg}$ ,  $M_r = 744.85$ , monoclinic, space group  $P2_1/c$ ,  $a = 17.8377(10)$ ,  $b = 18.5503(6)$ ,  $c = 16.6290(9)$  Å,  $\beta = 115.934(7)^\circ$ ,  $V = 4948.3(4)$  Å<sup>3</sup>,  $Z = 4$ ,  $\lambda = 0.71073$  Å,  $\mu = 0.207$  mm<sup>-1</sup>,  $T = 123$  K; 47102 reflections, 11912 unique,  $R_{\text{int}} = 0.0550$ ; final refinement to convergence on  $F^2$  gave  $R = 0.0792$  ( $F$ , 7588 obs. data only) and  $R_w = 0.2281$  ( $F^2$ , all data), GOF = 1.076.

### 5.3.11 Synthesis of $[(\text{TMEDA})\text{Li}(\text{NPh}_2)]_2$ , **90**

*n*-Butyllithium (1.56 mL of a 1.6 M solution in hexanes, 2.5 mmol) was suspended in dried hexane (2 mL) in an oven-dried Schlenk tube. Diphenylamine (0.423 g, 2.5 mmol) was then introduced, *via* a solid addition tube, yielding a cloudy solution. The reaction mixture was sonicated for five minutes, before *N,N,N',N'*-tetramethylethylenediamine (0.38 mL, 2.5 mmol) was added, producing a peach coloured suspension. On standing, a white non-crystalline precipitate was observed in a peach coloured clear solution. The reaction mixture was allowed to stir again and heat applied. Dried toluene (1 mL required) was gradually added to the hot solution until the solution became clear. This pale yellow/peach solution was allowed to stand



at ambient temperature and after 24 hours, small colourless X-ray quality crystals of **90** were deposited [0.35 g, 48% (not optimised)].

$^1\text{H}$  NMR (400.03 MHz, 300 K,  $\text{C}_6\text{D}_6$ ):  $\delta$  7.26 (*o*- and *m*-CH, 16H, m), 6.74 (*p*-CH, 4H, m), 1.75 ( $\text{CH}_2$ , 8H, s), 1.72 ( $\text{CH}_3$ , 24H, s).  $^{13}\text{C}$  NMR (100.59 MHz, 300 K,  $\text{C}_6\text{D}_6$ ):  $\delta$  158.1 (*ipso*-C), 130.1 (*m*-C), 120.5 (*o*-C), 116.5 (*p*-C), 57.1 ( $\text{CH}_2$ ), 45.7 ( $\text{CH}_3$ ).  $^7\text{Li}$  NMR (155.47 MHz, 300 K,  $\text{C}_6\text{D}_6$ ):  $\delta$  0.88.

Crystal data for **90**:  $\text{C}_{36}\text{H}_{52}\text{N}_6\text{Li}_2$ ,  $M_r = 582.72$ , monoclinic, space group  $P2_1/n$ ,  $a = 10.894(3)$ ,  $b = 18.465(4)$ ,  $c = 17.264(4)$  Å,  $\alpha = 90.038(18)$ ,  $\beta = 91.174(19)$ ,  $\gamma = 89.95(2)^\circ$ ,  $V = 3472(1)$  Å<sup>3</sup>,  $Z = 4$ ,  $\lambda = 0.71073$  Å,  $\mu = 0.066$  mm<sup>-1</sup>,  $T = 123$  K; 21818 reflections, 7551 unique,  $R_{\text{int}} = 0.0968$ ; final refinement to convergence on  $F^2$  gave  $R = 0.0600$  ( $F$ , 4889 obs. data only) and  $R_w = 0.1815$  ( $F^2$ , all data), GOF = 1.035.

### 5.3.12 Synthesis of [(TMEDA)Na(NPh<sub>2</sub>)<sub>2</sub>], **91**

Freshly prepared *n*-butylsodium (0.20 g, 2.5 mmol) was suspended in dried hexane (5 mL) in an oven-dried Schlenk tube and placed in an ultrasonic bath for ten minutes. Diphenylamine (0.423 g, 2.5 mmol) was then introduced, *via* a solid addition tube, yielding a pale green suspension. The reaction mixture was sonicated again for five minutes, before *N,N,N',N'*-tetramethylethylenediamine (0.38 mL, 2.5 mmol) was added and the reaction mixture allowed to stir for 30 minutes. On standing, an off white/pale green non-crystalline precipitate in a pale yellow solution was observed. The reaction mixture was allowed to stir again and heat applied, turning the solution more yellow in colour. Dried toluene (3 mL required) was gradually added to the hot solution until the solution became clear. After 30 minutes, X-ray quality crystals of **91** deposited at ambient temperature [0.25 g, 32% (not optimised)].

$^1\text{H}$  NMR (400.03 MHz, 300 K,  $\text{C}_6\text{D}_6$ ):  $\delta$  7.27 (*o*- and *m*-CH, 16H, m), 6.69 (*p*-CH, 4H, m), 1.68 ( $\text{CH}_3$ , 24H, s), 1.54 ( $\text{CH}_2$ , 8H, s).  $^{13}\text{C}$  NMR (100.59 MHz, 300 K,  $\text{C}_6\text{D}_6$ ):  $\delta$  158.8 (*ipso*-C), 130.2 (*m*-C), 118.7 (*o*-C), 114.7 (*p*-C), 56.8 ( $\text{CH}_2$ ), 45.1 ( $\text{CH}_3$ ).

Crystal data for **91**:  $\text{C}_{36}\text{H}_{52}\text{N}_6\text{Na}_2$ ,  $M_r = 614.82$ , monoclinic, space group  $P2_1/n$ ,  $a = 9.4833(2)$ ,  $b = 19.8108(5)$ ,  $c = 19.6247(6)$  Å,  $\beta = 103.849(1)^\circ$ ,  $V = 3579.75(16)$  Å<sup>3</sup>,  $Z = 4$ ,  $\lambda = 0.71073$  Å,  $\mu = 0.089$  mm<sup>-1</sup>,  $T = 123$  K; 31758 reflections, 5555 unique,  $R_{\text{int}} = 0.105$ ; final refinement to convergence on  $F^2$  gave  $R = 0.0538$  ( $F$ , 3637 obs. data only) and  $R_w = 0.1144$  ( $F^2$ , all data), GOF = 1.051.

### 5.3.13 Synthesis of [(TMEDA)<sub>3/2</sub>K(NPh<sub>2</sub>)<sub>2</sub>], **92**

Freshly prepared benzylpotassium (0.33 g, 2.5 mmol) was suspended in dried hexane (8 mL) in an oven-dried Schlenk tube and placed in an ultrasonic bath for ten minutes. Diphenylamine (0.423 g, 2.5 mmol) was introduced, *via* a solid addition tube, yielding a pink suspension. This was dissolved by the addition of four molar equivalents of *N,N,N',N'*-tetramethylethylenediamine (1.51 mL, 10 mmol). The resultant slightly cloudy pale yellow solution was heated gently to ensure complete dissolution. At ambient temperature, a small mass of white powder was observed in solution. The reaction mixture was heated again and filtered through Celite and glass wool. Once cooled, the transparent yellow solution was placed in a freezer operating at  $-28^{\circ}\text{C}$  and after 24 hours, small yellow X-ray quality crystals of **92** were deposited [0.35 g, 46% (not optimised)].

This reaction was repeated using (trimethylsilylmethyl)potassium instead of benzylpotassium as the source of potassium, yielding the same product.

$^1\text{H}$  NMR (400.03 MHz, 300 K,  $d_8$ -THF):  $\delta$  6.84 (*o*- and *m*-CH, 16H, m), 6.14 (*p*-CH, 4H, m), 2.30 ( $\text{CH}_2$ , 12H, s), 2.15 ( $\text{CH}_3$ , 36H, s).  $^{13}\text{C}$  NMR (100.59 MHz, 300 K,  $d_8$ -THF):  $\delta$  158.1 (*ipso*-C), 129.7 (*m*-C), 118.2 (*o*-C), 112.6 (*p*-C), 59.3 ( $\text{CH}_2$ ), 46.3 ( $\text{CH}_3$ ).

Crystal data for **92**:  $\text{C}_{42}\text{H}_{68}\text{N}_8\text{K}_2$ ,  $M_r = 763.24$ , triclinic, space group  $P \bar{1}$ ,  $a = 10.9581(11)$ ,  $b = 11.2224(9)$ ,  $c = 11.7229(13)$  Å,  $\alpha = 63.275(9)$ ,  $\beta = 66.062(11)$ ,  $\gamma = 62.674(9)^{\circ}$ ,  $V = 1107.28(17)$  Å<sup>3</sup>,  $Z = 1$ ,  $\lambda = 0.71073$  Å,  $\mu = 0.251$  mm<sup>-1</sup>,  $T = 123$  K; 16157 reflections, 5330 unique,  $R_{\text{int}} = 0.0245$ ; final refinement to convergence on  $F^2$  gave  $R = 0.0351$  ( $F$ , 4476 obs. data only) and  $R_w = 0.0932$  ( $F^2$ , all data), GOF = 1.105.

### 5.3.14 Synthesis of [(Me<sub>3</sub>SiCH<sub>2</sub>)Mg( $\mu$ -TMP)]<sub>2</sub>, **94**

Freshly prepared bis(trimethylsilylmethyl)magnesium (0.4 g, 2 mmol) was suspended in dried hexane (8 mL) in an oven-dried Schlenk tube and placed in an ultrasonic bath for 15 minutes. 2,2,6,6-Tetramethylpiperidine (0.34 mL, 2 mmol) was then introduced and the solution heated to reflux for 16 hours. The pale yellow solution was allowed to cool to ambient temperature, before being placed in a freezer operating at  $-28^{\circ}\text{C}$ . After approximately 72 hours, small colourless X-ray quality needle-like crystals of **94** were deposited (0.47 g, 93%).

$^1\text{H}$  NMR (400.03 MHz, 300 K,  $\text{C}_6\text{D}_6$ ):  $\delta$  1.52 (TMP  $\gamma$ -CH<sub>2</sub>, 4H, m), 1.33 (TMP  $\beta$ -CH<sub>2</sub>, 8H, m), 1.30 (TMP CH<sub>3</sub>, 24H, s), 0.35 [ $\text{CH}_2\text{Si}(\text{CH}_3)_3$ , 18H, s], -1.09 [ $\text{CH}_2\text{Si}(\text{CH}_3)_3$ , 4H, s].  $^{13}\text{C}$  NMR (100.59 MHz, 300 K,  $\text{C}_6\text{D}_6$ ):  $\delta$  53.0 (TMP  $\alpha$ -C), 38.3 (TMP  $\beta$ -CH<sub>2</sub>), 36.0 (TMP CH<sub>3</sub>), 17.2 (TMP  $\gamma$ -CH<sub>2</sub>), 4.5 [ $\text{CH}_2\text{Si}(\text{CH}_3)_3$ ], -1.4 [ $\text{CH}_2\text{Si}(\text{CH}_3)_3$ ].

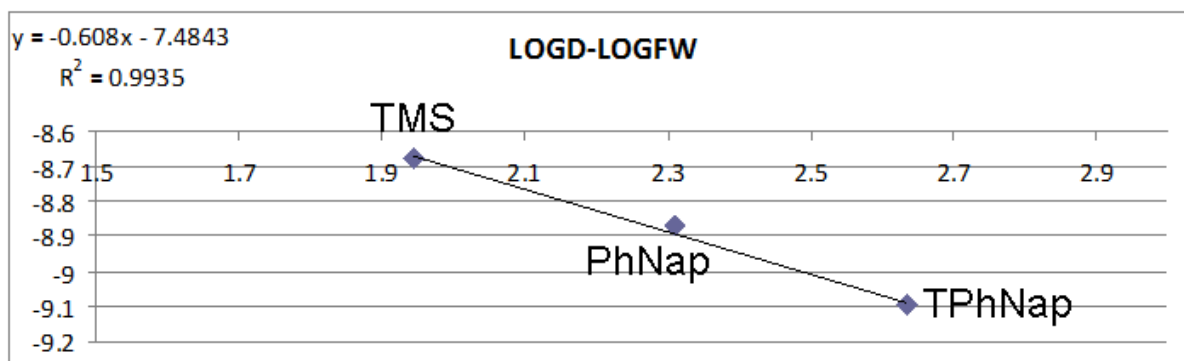
$^1\text{H}$  NMR (400.03 MHz, 300 K,  $d_8$ -THF):  $\delta$  1.63 [TMP(H)  $\gamma$ - $\text{CH}_2$ , 2H, m], 1.29 [TMP(H)  $\beta$ - $\text{CH}_2$ , 4H, m], 1.22 [ $\text{Mg}(\text{TMP})_2$   $\beta$ - $\text{CH}_2$ , 8H, m], 1.16 [ $\text{Mg}(\text{TMP})_2$   $\text{CH}_3$ , 24H, s], 1.11 [{" $(\text{CH}_3)_3\text{SiCH}_2$ "} $\text{Mg}(\text{TMP})$  - TMP  $\text{CH}_3$ , 12H, s], 1.06 [TMP(H)  $\text{CH}_3$ , 12H, s], -0.07 [{" $(\text{CH}_3)_3\text{SiCH}_2$ "} $\text{Mg}(\text{TMP})$ , 9H, s], -0.11 [ $\text{Mg}\{\text{CH}_2\text{Si}(\text{CH}_3)_3\}_2$ , 18H, s], -1.77 [ $\text{Mg}\{\text{CH}_2\text{Si}(\text{CH}_3)_3\}_2$ , 4H, s], -1.81 [{" $(\text{CH}_3)_3\text{SiCH}_2$ "} $\text{Mg}(\text{TMP})$ , 2H, s].  $^{13}\text{C}$  NMR (100.59 MHz, 300 K,  $D_8$ THF):  $\delta$  52.3 [TMP(H)  $\alpha$ -C], 42.5 [ $\text{Mg}(\text{TMP})_2$   $\beta$ - $\text{CH}_2$ ], 41.5 [TMP(H)  $\gamma$ - $\text{CH}_2$ ], 35.9 [ $\text{Mg}(\text{TMP})_2$   $\text{CH}_3$ ], 35.8 [{" $(\text{CH}_3)_3\text{SiCH}_2$ "} $\text{Mg}(\text{TMP})$  - TMP  $\text{CH}_3$ ], 32.16 [TMP(H)  $\text{CH}_3$ ], 4.9 [{" $(\text{CH}_3)_3\text{SiCH}_2$ "} $\text{Mg}(\text{TMP})$ ], 4.6 [ $\text{Mg}\{\text{CH}_2\text{Si}(\text{CH}_3)_3\}_2$ ], -4.7 [{" $(\text{CH}_3)_3\text{SiCH}_2$ "} $\text{Mg}(\text{TMP})$ ], -7.6 [ $\text{Mg}\{\text{CH}_2\text{Si}(\text{CH}_3)_3\}_2$ ].

Crystal data for **94**:  $\text{C}_{26}\text{H}_{58}\text{N}_2\text{Si}_2\text{Mg}_2$ ,  $M_r = 503.54$ , monoclinic, space group  $P2_1/c$ ,  $a = 19.9838(14)$ ,  $b = 13.0725(10)$ ,  $c = 24.1832(11)$  Å,  $\beta = 94.452(5)^\circ$ ,  $V = 6298.5(7)$  Å<sup>3</sup>,  $Z = 8$ ,  $\lambda = 0.71073$  Å,  $\mu = 0.168$  mm<sup>-1</sup>,  $T = 123$  K; 32469 reflections, 13737 unique,  $R_{\text{int}} = 0.0635$ ; final refinement to convergence on  $F^2$  gave  $R = 0.0690$  ( $F$ , 9145 obs. data only) and  $R_w = 0.1366$  ( $F^2$ , all data), GOF = 1.076.

Diffusion study of **94**:  $^1\text{H}$  DOSY NMR experiment of recrystallised ( $\text{Me}_3\text{SiCH}_2$ ) $\text{Mg}(\text{TMP})$  with internal references present (tetraphenylphthalene TPhNap, phenylphthalene PhNap and tetramethylsilane TMS) was recorded at 27°C in  $d_8$ -THF. All the different components of the mixture separate clearly in the diffusion dimension with a relative size sequence of TPhNap > " $\text{Mg}(\text{CH}_2\text{SiMe}_3)_2$ "  $\approx$  " $\text{Mg}(\text{TMP})_2$ "  $\approx$  " $(\text{Me}_3\text{SiCH}_2)\text{Mg}(\text{TMP})$ "  $\gg$  PhNap > TMP(H) > TMS (chapter 2, section 2.5.1, Figure 2.52), according to their increasing D values:  $D(\text{TPhNap}) = 7.99 \times 10^{-10} \text{ m}^2 \text{ s}^{-1} < D\text{"Mg}(\text{CH}_2\text{SiMe}_3)_2\text{"} = 9.56 \times 10^{-10} \text{ m}^2 \text{ s}^{-1} \approx D\text{"Mg}(\text{TMP})_2\text{"} = 9.82 \times 10^{-10} \text{ m}^2 \text{ s}^{-1} \approx D\text{"(Me}_3\text{SiCH}_2)\text{Mg}(\text{TMP})\text{"} = 1.03 \times 10^{-9} \text{ m}^2 \text{ s}^{-1} \ll D(\text{PhNap}) = 1.35 \times 10^{-9} \text{ m}^2 \text{ s}^{-1} < D[\text{TMP(H)}] = 1.63 \times 10^{-9} \text{ m}^2 \text{ s}^{-1} \ll D(\text{TMS}) = 2.11 \times 10^{-9} \text{ m}^2 \text{ s}^{-1}$  (Table 5.1).

Compound	$10^{-10} D(\text{m}^2/\text{s})$	Calculated MW
TPhNap	7.99	–
PhNap	13.52	–
TMS	21.07	–
( $\text{Me}_3\text{SiCH}_2$ ) $\text{Mg}(\text{TMP})$	9.56	335
$\text{Mg}(\text{TMP})_2$	9.82	321
$\text{Mg}(\text{CH}_2\text{SiMe}_3)_2$	10.26	298
TMP(H)	16.31	139

**Table 5.1** Diffusion coefficients obtained from  $^1\text{H}$  DOSY NMR experiment.



**Graph 5.1** log  $D$  – log FW representation from the  $^1\text{H}$  DOSY NMR data obtained for  $(\text{Me}_3\text{SiCH}_2)\text{Mg}(\text{TMP})$ , and the standards TPhNap, PhNap and TMS at  $27^\circ\text{C}$  in  $d_8$ -THF.

### 5.3.15 Synthesis of $[(\text{TMP})\text{Mg}(\mu\text{-TMP})\{\mu\text{-N}(\text{H})\text{C}(\text{Me})_2(\text{CH}_2)_3\text{C}(\text{Me})=\text{CH}_2\}\text{Mg}(\mu\text{-OCH}_2\text{SiMe}_3)]_2$ , **95**

Freshly prepared bis(trimethylsilylmethyl)magnesium (0.2 g, 1 mmol) was suspended in dried hexane (5 mL) in an oven-dried Schlenk tube and placed in an ultrasonic bath for 15 minutes. 2,2,6,6-Tetramethylpiperidine (0.34 mL, 2 mmol) was then introduced and the solution heated to reflux for 16 hours. The pale yellow solution was allowed to cool to ambient temperature, before being placed in a freezer operating at  $-28^\circ\text{C}$ . After approximately two weeks, a small crop of colourless X-ray quality crystals of **95** were deposited (less than 0.05 g).

Crystal data for **95**:  $\text{C}_{62}\text{H}_{130}\text{N}_6\text{O}_2\text{Si}_2\text{Mg}_4$ ,  $M_r = 1145.14$ , monoclinic, space group  $P2_1/n$ ,  $a = 11.6060(6)$ ,  $b = 23.3204(10)$ ,  $c = 13.5540(6)$  Å,  $\beta = 107.695(5)^\circ$ ,  $V = 3494.9(3)$  Å<sup>3</sup>,  $Z = 2$ ,  $\lambda = 0.71073$  Å,  $\mu = 0.129$  mm<sup>-1</sup>,  $T = 123$  K; 34462 reflections, 8338 unique,  $R_{\text{int}} = 0.0599$ ; final refinement to convergence on  $F^2$  gave  $R = 0.0595$  ( $F$ , 5614 obs. data only) and  $R_w = 0.1386$  ( $F^2$ , all data), GOF = 1.040.

### 5.3.16 Synthesis of $[(\text{-})\text{-sparteine}] \cdot \text{Na}(\mu\text{-TMP})(\mu\text{-}^n\text{Bu})\text{Zn}(^t\text{Bu})$ , **96**

Freshly prepared di-*tert*-butylzinc (0.18 g, 1 mmol) dissolved in dried hexane (5 mL) was transferred *via* cannula to an oven-dried Schlenk tube containing freshly prepared *n*-butylsodium (0.08 g, 1 mmol), which was then placed in an ultrasonic bath for ten minutes. 2,2,6,6-Tetramethylpiperidine (0.17 mL, 1 mmol) was then introduced and the reaction mixture allowed to stir for ten minutes, followed by the addition of (–)-sparteine (0.23 mL, 1 mmol). This slightly cloudy yellow solution was stirred for a further 15 minutes, heated slightly, and once cooled, placed in a freezer operating at  $-28^\circ\text{C}$ . After 48 hours, small colourless X-ray quality crystals of **96** were deposited [0.14 g, 24% (first batch)].

Crystal data for **96**:  $C_{32}H_{62}N_3NaZn$ ,  $M_r = 577.21$ , orthorhombic, space group  $P2_12_12_1$ ,  $a = 8.4785(3)$ ,  $b = 19.6591(12)$ ,  $c = 19.6684(9)$  Å,  $V = 3278.3(3)$  Å<sup>3</sup>,  $Z = 4$ ,  $\lambda = 1.54180$  Å,  $\mu = 1.326$  mm<sup>-1</sup>,  $T = 123$  K; 10724 reflections, 5125 unique,  $R_{int} = 0.0608$ ; final refinement to convergence on  $F^2$  gave  $R = 0.0505$  ( $F$ , 3605 obs. data only) and  $R_w = 0.1136$  ( $F^2$ , all data), GOF = 0.893. Absolute configuration confirmed by refinement of Flack parameter to  $-0.02(4)$ .

### 5.3.17 Synthesis of $\{[(R,R)\text{-TMCDA}]\cdot\text{Na}(\mu\text{-TMP})(\mu\text{-}^n\text{Bu})\text{Zn}(^t\text{Bu})\}$ , **97**

Freshly prepared di-*tert*-butylzinc (0.18 g, 1 mmol) dissolved in dried hexane (5 mL) was transferred *via* cannula to an oven-dried Schlenk tube containing freshly prepared *n*-butylsodium (0.08 g, 1 mmol), which was then placed in an ultrasonic bath for ten minutes. 2,2,6,6-Tetramethylpiperidine (0.17 mL, 1 mmol) was then introduced and the reaction mixture allowed to stir for ten minutes, followed by the addition of *N,N,N',N'*-(1*R*,2*R*)-tetramethylcyclohexane-1,2-diamine (0.19 mL, 1 mmol). This clear peach solution was stirred for a further 15 minutes, heated slightly, and once cooled, placed in a freezer operating at  $-28^\circ\text{C}$ . After 48 hours, a crop of colourless X-ray quality cubic-like crystals of **97** were deposited (0.12 g, 23%).

Crystal data for **97**:  $C_{54}H_{114}N_6Na_2Zn_2$ ,  $M_r = 1024.24$ , monoclinic, space group  $P2_1$ ,  $a = 10.2757(3)$ ,  $b = 11.3237(4)$ ,  $c = 26.2560(8)$  Å,  $\beta = 92.692(2)^\circ$ ,  $V = 3051.75(17)$  Å<sup>3</sup>,  $Z = 2$ ,  $\lambda = 0.71073$  Å,  $\mu = 0.836$  mm<sup>-1</sup>,  $T = 123$  K; 17294 reflections, 10708 unique,  $R_{int} = 0.0270$ ; final refinement to convergence on  $F^2$  gave  $R = 0.0490$  ( $F$ , 7489 obs. data only) and  $R_w = 0.1129$  ( $F^2$ , all data), GOF = 0.940. Absolute configuration confirmed by refinement of Flack parameter to 0.024(11).

### 5.3.18 Synthesis of $\{[(R,R)\text{-TMCDA}]\cdot\text{Na}(\mu\text{-TMP})(\mu\text{-}^t\text{Bu})\text{Zn}(^t\text{Bu})\}$ , **98**

Freshly prepared *n*-butylsodium (0.08 g, 1 mmol) was suspended in dried hexane (5 mL) in an oven-dried Schlenk tube and placed in an ultrasonic bath for ten minutes. 2,2,6,6-Tetramethylpiperidine (0.17 mL, 1 mmol) was then introduced and the reaction mixture allowed to stir for 30 minutes. In a separate Schlenk tube, freshly prepared di-*tert*-butylzinc (0.18 g, 1 mmol) was dissolved in dried hexane (5 mL). This latter solution was transferred to the former *via* a cannula, which was followed by the addition of *N,N,N',N'*-(1*R*,2*R*)-tetramethylcyclohexane-1,2-diamine (0.19 mL, 1 mmol). After stirring for 15 minutes, this clear yellow solution was placed in a freezer operating at  $-28^\circ\text{C}$  and after 48 hours, yellow X-ray quality cubic-like crystals of **98** were deposited [0.23 g, 45% (first batch)].

Crystal data for **98**:  $C_{27}H_{58}N_3NaZn$ ,  $M_r = 513.12$ , monoclinic, space group  $P2_1$ ,  $a = 13.2674(7)$ ,  $b = 11.3877(5)$ ,  $c = 20.2430(10)$  Å,  $\beta = 90.518(2)^\circ$ ,  $V = 3058.3(3)$  Å<sup>3</sup>,  $Z = 4$ ,  $\lambda = 0.71073$  Å,  $\mu = 0.835$  mm<sup>-1</sup>,  $T = 123$  K; 38196 reflections, 15558 unique,  $R_{int} = 0.0446$ ; final refinement to convergence on  $F^2$  gave  $R = 0.0344$  ( $F$ , 9856 obs. data only) and  $R_w = 0.0569$  ( $F^2$ , all data), GOF = 0.809. Absolute configuration confirmed by refinement of Flack parameter to 0.001(5).

### 5.3.19 Synthesis of $[Li\{(-)\text{-sparteine}\}_2]^+[Mg(HMDS)_3]^-$ , **100**

*n*-Butyllithium (1.25 mL of a 1.6 M solution in hexanes, 2 mmol) was suspended in dried hexane (5 mL) in an oven-dried Schlenk tube. Di-*n*-butylmagnesium (2 mL of a 1 M solution in heptane, 2 mmol) was then introduced, followed by the addition of three molar equivalents of 1,1,1,3,3,3-hexamethyldisilane (1.26 mL, 6 mmol), yielding a clear solution. This solution was heated to reflux for two hours and whilst still warm, two molar equivalents of (-)-sparteine (0.92 mL, 4 mmol) were added, precipitating a white solid. Dried toluene (11 mL) was added, along with heating, to form a homogeneous pale yellow solution. After 24 hours at ambient temperature, a crop of colourless X-ray quality crystals of **100** were deposited [1.57 g, 80% (with respect to <sup>n</sup>BuLi)].

<sup>1</sup>H NMR (400.03 MHz, 300 K, d<sub>8</sub>-THF):  $\delta$  2.70, 2.67, 2.59, 2.57, 2.49, 2.11, 1.97, 1.90, 1.78, 1.68, 1.50, 1.45, 1.39, 1.29, 1.23, 0.98, 0.88, 0.06 (SiCH<sub>3</sub>, 54 H, s). <sup>13</sup>C NMR (100.59 MHz, 300 K, d<sub>8</sub>-THF):  $\delta$  67.3, 65.0, 62.8, 57.0, 56.3, 54.5, 37.7, 35.7, 34.5, 30.1, 28.4, 27.1, 26.8, 26.0, 25.9, 25.6, 6.9 (SiCH<sub>3</sub>). <sup>7</sup>Li NMR (155.47 MHz, 300 K, d<sub>8</sub>-THF):  $\delta$  -2.29.

Crystal data for **100**:  $C_{48}H_{106}N_7Si_6LiMg$ ,  $M_r = 981.19$ , orthorhombic, space group  $P2_12_12_1$ ,  $a = 16.5576(2)$ ,  $b = 18.5861(3)$ ,  $c = 19.5813(3)$  Å,  $V = 6025.97(15)$  Å<sup>3</sup>,  $Z = 4$ ,  $\lambda = 0.71073$  Å,  $\mu = 0.185$  mm<sup>-1</sup>,  $T = 123$  K; 35383 reflections, 11806 unique,  $R_{int} = 0.0472$ ; final refinement to convergence on  $F^2$  gave  $R = 0.0358$  ( $F$ , 8728 obs. data only) and  $R_w = 0.0587$  ( $F^2$ , all data), GOF = 0.872. Absolute configuration confirmed by refinement of Flack parameter to 0.01(6).

Crystal data for toluene solvated phase of **100**:  $C_{55}H_{113}N_7Si_6LiMg$ ,  $M_r = 1072.31$ , monoclinic, space group  $P2_1$ ,  $a = 17.2800(5)$ ,  $b = 17.3017(5)$ ,  $c = 22.0598(6)$  Å,  $\beta = 90.512(5)^\circ$ ,  $V = 6595.0(3)$  Å<sup>3</sup>,  $Z = 4$ ,  $\lambda = 1.54180$  Å,  $\mu = 1.557$  mm<sup>-1</sup>,  $T = 123$  K; 67242 reflections, 22172 unique,  $R_{int} = 0.0604$ ; final refinement to convergence on  $F^2$  gave  $R = 0.0554$  ( $F$ , 11224 obs. data only) and  $R_w = 0.1262$  ( $F^2$ , all data), GOF = 0.831. Absolute configuration confirmed by refinement of Flack parameter to -0.003(19).

**5.3.20 Synthesis of  $[\text{Na}\{(-)\text{-sparteine}\}_2]^+[\text{Mg}(\text{HMDS})_3]^-$ , **101****

Freshly prepared *n*-butylsodium (0.16 g, 2 mmol) was suspended in dried hexane (5 mL) in an oven-dried Schlenk tube and placed in an ultrasonic bath for ten minutes. Di-*n*-butylmagnesium (2 mL of a 1 M solution in heptane, 2 mmol) was then introduced, producing a brown congealed mass. On the addition of three molar equivalents of 1,1,1,3,3,3-hexamethyldisilane (1.26 mL, 6 mmol) the solution became cloudy white and some precipitate was observed. The solution was heated to reflux for two hours and whilst still warm, two molar equivalents of (-)-sparteine (0.92 mL, 4 mmol) were added. A cloudy white to pale yellow colour change was observed, along with the precipitation of a large quantity of white solid. Solvent was removed *in vacuo* and dried toluene (5 mL) was added, along with heating, to form a homogeneous solution. The pale yellow solution was immediately placed in a hot water-filled Dewar flask and after 48 hours, a crop of colourless X-ray quality crystals of **101** were deposited [1.08 g, 57% (with respect to *n*BuNa)].

$^1\text{H}$  NMR (400.03 MHz, 300 K,  $d_8$ -THF):  $\delta$  7.10-7.19 (toluene *CHo/m/p*, 0.49H, m), 2.70, 2.66, 2.62, 2.59, 2.56, 2.51, 2.48, 2.34, 2.11, 1.99, 1.90, 1.78, 1.68, 1.51, 1.39, 1.32, 1.29, 1.26, 1.23, 1.20, 1.00, 0.98, 0.06 (SiCH<sub>3</sub>, 54 H, s).  $^{13}\text{C}$  NMR (100.59 MHz, 300 K,  $d_8$ -THF):  $\delta$  67.3, 65.0, 62.8, 57.0, 56.3, 54.5, 37.7, 35.7, 34.5, 30.1, 28.4, 27.1, 26.8, 26.0, 25.9, 25.6, 6.9 (SiCH<sub>3</sub>).

From the X-ray crystallography data it is expected that two molecules of toluene should be present per complex. NMR data has revealed that only 0.049 molecules of toluene per complex are incorporated. Therefore, for yield purposes the  $M_r$  of the complex has been adjusted from 1133.93 g to 954.44 g.

Crystal data for **101**: C<sub>58.50</sub>H<sub>116.50</sub>N<sub>7</sub>Si<sub>6</sub>NaMg,  $M_r = 1133.93$ , orthorhombic, space group  $P2_12_12_1$ ,  $a = 17.5291(5)$ ,  $b = 23.5696(6)$ ,  $c = 33.9026(9)$  Å,  $V = 14007.0(7)$  Å<sup>3</sup>,  $Z = 8$ ,  $\lambda = 0.71073$  Å,  $\mu = 0.173$  mm<sup>-1</sup>,  $T = 123$  K; 48737 reflections, 25549 unique,  $R_{\text{int}} = 0.0735$ ; final refinement to convergence on  $F^2$  gave  $R = 0.0614$  ( $F$ , 12053 obs. data only) and  $R_w = 0.1032$  ( $F^2$ , all data), GOF = 0.811. Absolute configuration confirmed by refinement of Flack parameter to 0.13(8).

**5.3.21 Synthesis of  $[\text{Li}\{(R,R)\text{-TMCDA}\}_2]^+[\text{Mg}(\text{HMDS})_3]^-$ , **102****

*n*-Butyllithium (0.63 mL of a 1.6 M solution in hexanes, 1 mmol) was suspended in dried hexane (10 mL) in an oven-dried Schlenk tube. Di-*n*-butylmagnesium (1 mL of a 1 M solution in heptane, 1 mmol) was then introduced, followed by the addition of three molar

equivalents of 1,1,1,3,3,3-hexamethyldisilane (0.63 mL, 3 mmol), yielding a clear solution. This solution was heated to reflux for two hours and whilst still warm, two molar equivalents of *N,N,N',N'*-(1*R*,2*R*)-tetramethylcyclohexane-1,2-diamine (0.38 mL, 2 mmol) were added, precipitating a white solid. Dried toluene (30 mL) was added, along with heating, to form a homogeneous pale yellow solution. The solution was immediately placed in a hot water-filled Dewar flask and after 48 hours, a crop of colourless X-ray quality crystals of **102** were deposited [0.26 g, 28% (with respect to <sup>n</sup>BuLi)].

<sup>1</sup>H NMR (400.03 MHz, 300 K, d<sub>8</sub>-THF): δ 7.11-7.18 (toluene *CHo/m/p*, m), 2.35 (α-*CH*, 4H, m), 2.30 (toluene *CH*<sub>3</sub>, 6.96H, s), 2.27 (*CH*<sub>3</sub>, 24H, s), 1.78 (β-*CH*<sub>2</sub>, 4H, m), 1.67 (γ-*CH*<sub>2</sub>, 4H, m), 1.13 (β-*CH*<sub>2</sub>, 4H, m), 1.13 (γ-*CH*<sub>2</sub>, 4H, m), 0.06 (Si*CH*<sub>3</sub>, 54H, s). <sup>13</sup>C NMR (100.59 MHz, 300 K, d<sub>8</sub>-THF): δ 65.0 (α-*CH*), 40.8 (*CH*<sub>3</sub>), 26.5 (β-*CH*<sub>2</sub>), 26.5 (γ-*CH*<sub>2</sub>), 6.9 (Si*CH*<sub>3</sub>). <sup>7</sup>Li NMR (155.47 MHz, 300 K, d<sub>8</sub>-THF): δ -0.50.

Crystal data for **102**: C<sub>45</sub>H<sub>106</sub>N<sub>7</sub>Si<sub>6</sub>LiMg, *M*<sub>r</sub> = 945.16, monoclinic, space group *P*2<sub>1</sub>, *a* = 11.7763(3), *b* = 35.6239(8), *c* = 14.4655(3) Å, β = 96.227(2)°, *V* = 6032.7(2) Å<sup>3</sup>, *Z* = 4, λ = 0.71073 Å, μ = 0.182 mm<sup>-1</sup>, *T* = 123 K; 29468 reflections, 21184 unique, *R*<sub>int</sub> = 0.0316; final refinement to convergence on *F*<sup>2</sup> gave *R* = 0.0418 (*F*, 14010 obs. data only) and *R*<sub>w</sub> = 0.0638 (*F*<sup>2</sup>, all data), GOF = 0.801. Absolute configuration confirmed by refinement of Flack parameter to -0.03(5).

### 5.3.22 Synthesis of [Na{(*R,R*)-TMCDA}<sub>2</sub>]<sup>+</sup>[Mg(HMDS)<sub>3</sub>]<sup>-</sup>, **103**

Freshly prepared *n*-butylsodium (0.08 g, 1 mmol) was suspended in dried hexane (20 mL) in an oven-dried Schlenk tube and placed in an ultrasonic bath for ten minutes. Di-*n*-butylmagnesium (1 mL of a 1 M solution in heptane, 1 mmol) was then introduced, producing a brown congealed mass. On the addition of three molar equivalents of 1,1,1,3,3,3-hexamethyldisilane (0.63 mL, 3 mmol) the solution became cloudy white with precipitate observed. The solution was heated to reflux for two hours and whilst still warm, two molar equivalents of *N,N,N',N'*-(1*R*,2*R*)-tetramethylcyclohexane-1,2-diamine (0.38 mL, 2 mmol) were added, precipitating a white solid. Dried toluene (15 mL) was added, along with heating, to form a homogeneous pale yellow solution. The solution was immediately placed in a hot water-filled Dewar flask and after 48 hours, a crop of colourless X-ray quality crystals of **103** were deposited [0.35 g, 42% (with respect to <sup>n</sup>BuNa)].

<sup>1</sup>H NMR (400.03 MHz, 300 K, d<sub>8</sub>-THF): δ 7.10-7.18 (toluene *CHo/m/p*, m), 2.35 (α-*CH*, 4H, m), 2.30 (toluene *CH*<sub>3</sub>, 7.02H, s), 2.27 (*CH*<sub>3</sub>, 24H, s), 1.78 (β-*CH*<sub>2</sub>, 4H, m), 1.67 (γ-*CH*<sub>2</sub>, 4H, m), 1.12 (β-*CH*<sub>2</sub>, 4H, m), 1.12 (γ-*CH*<sub>2</sub>, 4H, m), 0.06 (Si*CH*<sub>3</sub>, 54H, s). <sup>13</sup>C NMR (100.59 MHz,



300 K,  $d_8$ -THF):  $\delta$  129.7 (toluene), 128.9 (toluene), 65.0 ( $\alpha$ -CH), 40.8 ( $\text{CH}_3$ ), 26.5 ( $\beta$ - $\text{CH}_2$ ), 26.5 ( $\gamma$ - $\text{CH}_2$ ), 6.9 ( $\text{SiCH}_3$ ).

From the X-ray crystallography data it is expected that two molecules of toluene should be present per complex. NMR data has revealed that only 0.59 molecules of toluene per complex are incorporated. Therefore, for yield purposes the  $M_r$  of the complex has been adjusted from 961.21 g to 831.49 g.

Crystal data for **103**:  $\text{C}_{45}\text{H}_{106}\text{N}_7\text{Si}_6\text{NaMg}$ ,  $M_r = 961.21$ , orthorhombic, space group  $P2_12_12_1$ ,  $a = 16.3363(4)$ ,  $b = 17.3342(4)$ ,  $c = 21.8477(5)$  Å,  $V = 6186.8(3)$  Å<sup>3</sup>,  $Z = 4$ ,  $\lambda = 0.71073$  Å,  $\mu = 0.185$  mm<sup>-1</sup>,  $T = 123$  K; 25964 reflections, 15834 unique,  $R_{\text{int}} = 0.0298$ ; final refinement to convergence on  $F^2$  gave  $R = 0.0549$  ( $F$ , 10128 obs. data only) and  $R_w = 0.1246$  ( $F^2$ , all data), GOF = 0.927. Absolute configuration confirmed by refinement of Flack parameter to  $-0.06(9)$ .

### 5.3.23 Synthesis of $[\{\text{K}\cdot(-)\text{-sparteine}\}^+\{\text{Mg}(\text{HMDS})_3\}^-]_{\infty}$ , **104**

Freshly prepared (trimethylsilylmethyl)potassium (0.32 g, 2.5 mmol) was suspended in dried hexane (5 mL) in an oven-dried Schlenk tube and placed in an ultrasonic bath for ten minutes. Di-*n*-butylmagnesium (2.5 mL of a 1 M solution in heptane, 2.5 mmol) was then introduced, producing a brown congealed mass. The solution remained the same on the addition of three molar equivalents of 1,1,1,3,3,3-hexamethyldisilane (1.58 mL, 7.5 mmol). The solution was placed in an ultrasonic bath for 15 minutes, producing a cloudy creamy solution with precipitate observed. The solution was heated to reflux for two hours and whilst still warm, one molar equivalent of (-)-sparteine (0.58 mL, 2.5 mmol) was added. A cloudy white to yellow colour change was observed, along with the precipitation of a large quantity of white solid. Dried toluene (5 mL) was added, along with heating, to form a homogeneous solution. The yellow solution was immediately placed in a hot water-filled Dewar flask and after 48 hours, a crop of colourless X-ray quality crystals of **104** were deposited [1.65 g, 85% (with respect to  $\text{Me}_3\text{SiCH}_2\text{K}$ )].

<sup>1</sup>H NMR (400.03 MHz, 300 K,  $d_8$ -THF):  $\delta$  2.70, 2.67, 2.61, 2.59, 2.56, 2.51, 2.48, 2.31, 2.11, 1.99, 1.96, 1.90, 1.78, 1.69, 1.50, 1.45, 1.39, 1.29, 1.23, 1.00, 0.97, 0.06 ( $\text{SiCH}_3$ , 54H, s). <sup>13</sup>C NMR (100.59 MHz, 300 K,  $d_8$ -THF):  $\delta$  67.32, 65.01, 62.83, 57.04, 56.26, 54.52, 37.68, 35.71, 34.45, 30.14, 28.38, 27.13, 26.78, 26.00, 25.85, 6.93 ( $\text{SiCH}_3$ ).

Crystal data for **104**:  $\text{C}_{33}\text{H}_{80}\text{N}_5\text{Si}_6\text{KMg}$ ,  $M_r = 778.97$ , monoclinic, space group  $P2_1$ ,  $a = 12.2778(3)$ ,  $b = 20.7952(6)$ ,  $c = 18.5454(6)$  Å,  $\beta = 91.334(3)^\circ$ ,  $V = 4733.7(2)$  Å<sup>3</sup>,  $Z = 4$ ,  $\lambda = 0.71073$  Å,  $\mu = 0.304$  mm<sup>-1</sup>,  $T = 123$  K; 45075 reflections, 19412 unique,  $R_{\text{int}} = 0.0520$ ; final

refinement to convergence on  $F^2$  gave  $R = 0.0421$  ( $F$ , 13133 obs. data only) and  $R_w = 0.0587$  ( $F^2$ , all data), GOF = 0.798. Absolute configuration confirmed by refinement of Flack parameter to  $-0.04(3)$ .

### 5.3.24 Synthesis of $[\{K \cdot (R,R)\text{-TMCDA}\}^+ \{Mg(\text{HMDS})_3\}^-]_\infty$ , **105**

Freshly prepared (trimethylsilylmethyl)potassium (0.13 g, 1 mmol) was suspended in dried hexane (10 mL) in an oven-dried Schlenk tube and placed in an ultrasonic bath for ten minutes. Di-*n*-butylmagnesium (1 mL of a 1 M solution in heptane, 1 mmol) was then introduced, producing a brown congealed mass. Upon the addition of three molar equivalents of 1,1,1,3,3,3-hexamethyldisilane (0.63 mL, 3 mmol) the solution became cloudy with white precipitate observed. The solution was heated to reflux for two hours and whilst still warm, one molar equivalent of *N,N,N',N'*-(1*R*,2*R*)-tetramethylcyclohexane-1,2-diamine (0.19 mL, 1 mmol) was added. A cloudy white to pale yellow colour change was observed, along with the precipitation of a large quantity of white solid. The precipitate dissolved on heating, forming a homogeneous solution. The pale yellow solution was immediately placed in a hot water-filled Dewar flask and after 48 hours, a crop of colourless X-ray quality crystals of **105** were deposited [0.32 g, 45% (with respect to  $\text{Me}_3\text{SiCH}_2\text{K}$ )].

$^1\text{H}$  NMR (400.03 MHz, 300 K,  $\text{d}_8\text{-THF}$ ):  $\delta$  2.35 ( $\alpha\text{-CH}$ , 2H, m), 2.27 ( $\text{CH}_3$ , 12H, s), 1.78 ( $\beta\text{-CH}_2$ , 2H, m), 1.67 ( $\gamma\text{-CH}_2$ , 2H, m), 1.12 ( $\beta\text{-CH}_2$ , 2H, m), 1.12 ( $\gamma\text{-CH}_2$ , 2H, m), 0.06 ( $\text{SiCH}_3$ , 54H, s).  $^{13}\text{C}$  NMR (100.59 MHz, 300 K,  $\text{d}_8\text{-THF}$ ):  $\delta$  65.0 ( $\alpha\text{-CH}$ ), 40.8 ( $\text{CH}_3$ ), 26.5 ( $\beta\text{-CH}_2$ ), 26.5 ( $\gamma\text{-CH}_2$ ), 6.9 ( $\text{SiCH}_3$ ).

Crystal data for **105**:  $\text{C}_{28}\text{H}_{76}\text{N}_5\text{Si}_6\text{KMg}$ ,  $M_r = 714.89$ , triclinic, chiral space group  $P1$ ,  $a = 11.7004(3)$ ,  $b = 12.1366(3)$ ,  $c = 16.3796(5)$  Å,  $\alpha = 103.209(2)$ ,  $\beta = 90.700(2)$ ,  $\gamma = 92.796(2)^\circ$ ,  $V = 2261.07(11)$  Å<sup>3</sup>,  $Z = 2$ ,  $\lambda = 0.71073$  Å,  $\mu = 0.313$  mm<sup>-1</sup>,  $T = 123$  K; 27798 reflections, 20958 unique,  $R_{\text{int}} = 0.0205$ ; final refinement to convergence on  $F^2$  gave  $R = 0.0346$  ( $F$ , 15659 obs. data only) and  $R_w = 0.0699$  ( $F^2$ , all data), GOF = 0.889. Absolute configuration confirmed by refinement of Flack parameter to 0.01(3).

### 5.3.25 Synthesis of $[\text{LiHMDS} \cdot (-)\text{-sparteine}]$ , **106**

*n*-Butyllithium (1.25 mL of a 1.6 M solution in hexanes, 2 mmol) was suspended in dried hexane (5 mL) in an oven-dried Schlenk tube. 1,1,1,3,3,3-Hexamethyldisilane (0.42 mL, 2 mmol) was then introduced and the reaction mixture allowed to stir for 30 minutes, after which  $(-)$ -sparteine (0.46 mL, 2 mmol) and dried toluene (1 mL) were added. The colourless solution was reduced in volume by approximately 50% and placed in a freezer operating at

$-28^{\circ}\text{C}$ . After 48 hours, small colourless X-ray quality crystals of **106** were deposited (0.51 g, 64%).

$^1\text{H}$  NMR (400.03 MHz, 300 K,  $\text{C}_6\text{D}_5\text{CD}_3$ ):  $\delta$  3.16, 2.78, 2.53, 2.33, 2.28, 1.81, 1.71, 1.50, 1.44, 1.32, 1.22, 1.03, 0.89, 0.62, 0.35 ( $\text{SiCH}_3$ , 18H, s).  $^{13}\text{C}$  NMR (100.59 MHz, 300 K,  $\text{C}_6\text{D}_5\text{CD}_3$ ):  $\delta$  67.6, 61.8, 60.3, 58.3, 54.4, 46.5, 35.8, 35.6, 30.4, 29.0, 25.6, 25.2, 24.9, 24.7, 18.6, 7.5 ( $\text{SiCH}_3$ ).  $^7\text{Li}$  NMR (155.47 MHz, 300 K,  $\text{C}_6\text{D}_5\text{CD}_3$ ):  $\delta$  1.50.

Crystal data for **106**:  $\text{C}_{21}\text{H}_{44}\text{N}_3\text{Si}_2\text{Li}$ ,  $M_r = 401.71$ , triclinic, space group  $P1$ ,  $a = 7.6371(3)$ ,  $b = 9.1030(3)$ ,  $c = 10.5163(4)$  Å,  $\alpha = 111.657(2)$ ,  $\beta = 106.120(2)$ ,  $\gamma = 97.915(2)^{\circ}$ ,  $V = 628.71(4)$  Å<sup>3</sup>,  $Z = 1$ ,  $\lambda = 0.71073$  Å,  $\mu = 0.151$  mm<sup>-1</sup>,  $T = 123$  K; 15393 reflections, 5224 unique,  $R_{\text{int}} = 0.050$ ; final refinement to convergence on  $F^2$  gave  $R = 0.0504$  ( $F$ , 4570 obs. data only) and  $R_w = 0.1416$  ( $F^2$ , all data), GOF = 1.091. Absolute configuration confirmed by refinement of Flack parameter to  $-0.08(12)$ .

### 5.3.26 Synthesis of “[NaHMDS·(-)-sparteine]”, **107**

Freshly prepared *n*-butylsodium (0.16 g, 2 mmol) was suspended in dried hexane (5 mL) in an oven-dried Schlenk tube and placed in an ultrasonic bath for ten minutes. 1,1,1,3,3,3-Hexamethyldisilane (0.42 mL, 2 mmol) was then introduced and the reaction mixture allowed to stir for 30 minutes, after which (-)-sparteine (0.46 mL, 2 mmol), which had been subjected to vacuum for two hours, and dried toluene (1 mL) were added. The colourless solution was immediately placed in a freezer operating at  $-28^{\circ}\text{C}$  and after 24 hours, a colourless microcrystalline material (**107**) deposited [0.22 g, 26% (MW of **107** = 417.76 g)].

$^1\text{H}$  NMR (400.03 MHz, 300 K,  $\text{C}_6\text{D}_6$ ):  $\delta$  2.77, 2.66, 2.47, 2.26, 2.14, 2.08, 1.95, 1.85, 1.62, 1.54, 1.41, 1.37, 1.23, 1.10, 1.00, 0.15 ( $\text{SiCH}_3$ , 18H, s).

### 5.3.27 Synthesis of $[(-)\text{-sparteine}\cdot\text{Na}(\mu\text{-HMDS})\text{Na}\cdot(-)\text{-sparteine}]^+[\text{Na}_4(\mu\text{-HMDS})_4(\mu_4\text{-OH})]^-$ , **108**

Freshly prepared *n*-butylsodium (0.16 g, 2 mmol) was suspended in dried hexane (5 mL) in an oven-dried Schlenk tube and placed in an ultrasonic bath for ten minutes. 1,1,1,3,3,3-Hexamethyldisilane (0.42 mL, 2 mmol) was then introduced and the reaction mixture allowed to stir for 30 minutes, after which ‘non-dried’ (-)-sparteine (0.46 mL, 2 mmol) and dried toluene (1 mL) were added. After stirring for one hour, X-ray quality crystals of **108** deposited at ambient temperature [0.12 g, 25% (first batch)].

$^1\text{H}$  NMR (400.03 MHz, 300 K,  $\text{C}_6\text{D}_6$ ):  $\delta$  2.77, 2.66, 2.48, 2.30, 2.13, 2.06, 1.95, 1.86, 1.69, 1.53, 1.42, 1.39, 1.25, 1.14, 1.11, 1.01, 0.48 (OH), 0.13 ( $\text{SiCH}_3$ , 90H, s).

Crystal data for **108**:  $C_{60}H_{143}N_9OSi_{10}Na_6$ ,  $M_r = 1425.67$ , monoclinic, space group  $C2$ ,  $a = 18.2491(4)$ ,  $b = 16.2717(3)$ ,  $c = 14.9831(3)$  Å,  $\beta = 90.450(2)^\circ$ ,  $V = 4449.00(16)$  Å<sup>3</sup>,  $Z = 2$ ,  $\lambda = 1.54184$  Å,  $\mu = 1.973$  mm<sup>-1</sup>,  $T = 123$  K; 13781 reflections, 6757 unique,  $R_{int} = 0.0212$ ; final refinement to convergence on  $F^2$  gave  $R = 0.0435$  ( $F$ , 5176 obs. data only) and  $R_w = 0.1083$  ( $F^2$ , all data), GOF = 0.926. Absolute configuration confirmed by refinement of Flack parameter to  $-0.03(3)$ . The OH group is modelled as disordered over two sites, occupancy 50 : 50.

### 5.3.28 Synthesis of $[Na\{(R,R)\text{-TMCDA}\}_2]^+[Na_4(\mu\text{-HMDS})_4(\mu_4\text{-OH})]^-$ , **109**

Freshly prepared *n*-butylsodium (0.16 g, 2 mmol) was suspended in dried hexane (10 mL) in an oven-dried Schlenk tube and placed in an ultrasonic bath for ten minutes. 1,1,1,3,3,3-Hexamethyldisilane (0.42 mL, 2 mmol) was then introduced and the reaction mixture allowed to stir for 30 minutes, after which *N,N,N',N'*-(1*R*,2*R*)-tetramethylcyclohexane-1,2-diamine (0.38 mL, 2 mmol) was added, precipitating a white solid. Dried toluene (3 mL) was added, along with heating, to form a homogeneous pale yellow solution. The solution was immediately placed in a hot water-filled Dewar flask and after 48 hours, a crop of colourless X-ray quality crystals of **109** were deposited [0.11 g, 25% (first batch)].

<sup>1</sup>H NMR (400.03 MHz, 300 K, C<sub>6</sub>D<sub>6</sub>):  $\delta$  2.16 (CH<sub>3</sub>, 24H, s), 2.10 ( $\alpha$ -CH, 4H, m), 1.61 ( $\beta$ -CH<sub>2</sub>, 4H, m), 1.53 ( $\gamma$ -CH<sub>2</sub>, 4H, m), 1.13 ( $\beta$ -CH<sub>2</sub>, 4H, m), 1.13 ( $\gamma$ -CH<sub>2</sub>, 4H, m), 0.48 (OH), 0.31 (SiCH<sub>3</sub>, 72H, s).

Crystal data for **109**:  $C_{44}H_{117}N_8OSi_8Na_5$ ,  $M_r = 1114.13$ , monoclinic, space group  $P2_1$ ,  $a = 11.8262(3)$ ,  $b = 24.8172(6)$ ,  $c = 12.5684(4)$  Å,  $\beta = 103.838(3)^\circ$ ,  $V = 3581.68(17)$  Å<sup>3</sup>,  $Z = 2$ ,  $\lambda = 0.71073$  Å,  $\mu = 0.214$  mm<sup>-1</sup>,  $T = 123$  K; 31310 reflections, 16622 unique,  $R_{int} = 0.0244$ ; final refinement to convergence on  $F^2$  gave  $R = 0.0315$  ( $F$ , 13020 obs. data only) and  $R_w = 0.0586$  ( $F^2$ , all data), GOF = 0.881. Absolute configuration confirmed by refinement of Flack parameter to  $-0.01(4)$ .

### 5.3.29 Synthesis of $[(NaHMDS)_2\{^nBu_2Mg \cdot (R,R)\text{-TMCDA}\}]_\infty$ , **110**

Freshly prepared *n*-butylsodium (0.08 g, 1 mmol) was suspended in dried hexane (10 mL) in an oven-dried Schlenk tube and placed in an ultrasonic bath for ten minutes. Di-*n*-butylmagnesium (1 mL of a 1 M solution in heptane, 1 mmol) was then introduced, producing a brown congealed mass. On the addition of 1,1,1,3,3,3-hexamethyldisilane (0.21 mL, 1 mmol) a white precipitate was observed. *N,N,N',N'*-(1*R*,2*R*)-Tetramethylcyclohexane-1,2-diamine (0.19 mL, 1 mmol) was then added, producing a clear solution. The pale yellow

solution was immediately placed in a freezer operating at  $-28^{\circ}\text{C}$  and after 48 hours, a crop of colourless X-ray quality crystals of **110** were deposited [0.17 g, 25% (with respect to  ${}^n\text{Bu}_2\text{Mg}$ )].

${}^1\text{H}$  NMR (400.03 MHz, 300 K,  $\text{C}_6\text{D}_6$ ):  $\delta$  2.14, 1.97, 1.93, 1.85, 1.75, 1.35, 0.39, 0.37, 0.16,  $-0.13$ .

Crystal data for **110**:  $\text{C}_{30}\text{H}_{76}\text{N}_4\text{Si}_4\text{Na}_2\text{Mg}$ ,  $M_r = 675.60$ , tetragonal, space group  $P4_22_12$ ,  $a = 23.56120(10)$ ,  $b = 23.56120(10)$ ,  $c = 15.9472(2)$  Å,  $V = 8852.77(12)$  Å<sup>3</sup>,  $Z = 8$ ,  $\lambda = 0.71073$  Å,  $\mu = 0.190$  mm<sup>-1</sup>,  $T = 123$  K; 88604 reflections, 13539 unique,  $R_{\text{int}} = 0.0487$ ; final refinement to convergence on  $F^2$  gave  $R = 0.445$  ( $F$ , 10226 obs. data only) and  $R_w = 0.0978$  ( $F^2$ , all data), GOF = 0.960. Absolute configuration confirmed by refinement of Flack parameter to 0.03(8).

### 5.3.30 Synthesis of $[\text{Li}\{(R,R)\text{-TMCDA}\}_2]^+[\text{Li}_5(\mu\text{-HMDS})_5(\mu_5\text{-Cl})]^-$ , **115**

Direct combination route: Lithium 1,1,1,3,3,3-hexamethyldisilazide (0.837 g, 5 mmol) was suspended in dried hexane (7.5 mL) in an oven-dried Schlenk tube and stirred for 30 minutes. Lithium chloride (0.042 g, 1 mmol) was then introduced and the mixture allowed to stir for a further 30 minutes, after which two molar equivalents of  $N,N,N',N'$ -(1*R*,2*R*)-tetramethylcyclohexane-1,2-diamine (0.38 mL, 2 mmol) were added and a clear to pale yellow colour change was observed. This suspension was heated slightly and allowed to vigorously stir at ambient temperature for 72 hours to ensure the majority of the lithium chloride salt had dissolved. The now cloudy white solution was heated and filtered through Celite and glass wool and the resultant clear solution immediately placed in a freezer operating at  $-28^{\circ}\text{C}$ . After 48 hours, a crop of colourless X-ray quality needle-like crystals of **115** were deposited (0.10 g, 8%).

Ammonium salt route: An oven-dried Schlenk tube was charged with *n*-butyllithium (0.63 mL of 1.6 M solution in hexanes, 1 mmol) and the hexane removed *in vacuo* and replaced with dried toluene (5 mL). Two molar equivalents of  $N,N,N',N'$ -(1*R*,2*R*)-tetramethylcyclohexane-1,2-diamine (0.38 mL, 2 mmol) were then added, yielding a bright fluorescent red/orange solution which was allowed to stir for 30 minutes. On the addition of one molar equivalent of ammonium chloride (0.053 g, 1 mmol) this bright fluorescent red/orange colour slowly dissipated on stirring to yield a pale yellow solution. The mixture was heated to reflux for one hour and the clear solution allowed to stir whilst cooling for 30 minutes. Five molar equivalents of lithium 1,1,1,3,3,3-hexamethyldisilazide (0.837 g, 5 mmol) were then introduced and the resultant pale yellow solution heated slightly and allowed to stir at ambient temperature for 48 hours, before being placed in a freezer operating

at  $-72^{\circ}\text{C}$ . Precipitation of a non-crystalline solid (0.94 g, 77%) was observed, which by NMR analysis was identical to the crystalline material.

Organoammonium salt route: An oven-dried Schlenk tube was charged with *n*-butyllithium (0.63 mL of 1.6 M solution in hexanes, 1 mmol) and the hexane removed *in vacuo* and replaced with dried toluene (5 mL). Two molar equivalents of *N,N,N',N'*-(1*R*,2*R*)-tetramethylcyclohexane-1,2-diamine (0.38 mL, 2 mmol) were then added, yielding a bright fluorescent red/orange solution which was allowed to stir for 30 minutes. On the addition of one molar equivalent of triethylamine hydrochloride (0.14 g, 1mmol) this bright fluorescent red/orange colour slowly dissipated on stirring to yield a pale yellow/peach solution. The mixture was heated to reflux for one hour and the clear yellow solution allowed to stir whilst cooling for 30 minutes. Five molar equivalents of lithium 1,1,1,3,3,3-hexamethyldisilazide (0.84 g, 5 mmol) were then introduced affording a more intense yellow colour to the solution. The mixture was heated slightly and allowed to stir at ambient temperature for 48 hours. Dried toluene (5 mL) was then added to the now slightly cloudy yellow suspension and the solution heated and filtered through Celite and glass wool. The resultant clear yellow solution was concentrated by removal of some solvent *in vacuo* and immediately placed in a freezer operating at  $-72^{\circ}\text{C}$ . After 48 hours, a crop of colourless X-ray quality needle-like crystals of **115** were deposited (0.58 g 48%).

$^1\text{H}$  NMR (400.03 MHz, 300 K,  $\text{C}_6\text{D}_6$ ):  $\delta$  1.97 ( $\text{CH}_3$ , 12H, s), 1.68 ( $\text{CH}_3$ , 12H, s), 1.65 ( $\alpha\text{-CH}$ , 4H, s), 1.33 ( $\beta\text{-CH}_2$ , 2H, m), 1.33 ( $\gamma\text{-CH}_2$ , 2H, m), 1.22 ( $\beta\text{-CH}_2$ , 2H, m), 1.22 ( $\gamma\text{-CH}_2$ , 2H, m), 0.57 ( $\beta\text{-CH}_2$ , 4H, m), 0.57 ( $\gamma\text{-CH}_2$ , 4H, m), 0.44 ( $\text{SiCH}_3$ , 90H, s).  $^{13}\text{C}$  NMR (100.59 MHz, 300 K,  $\text{C}_6\text{D}_6$ ):  $\delta$  63.8 ( $\alpha\text{-CH}$ ), 44.2 ( $\text{CH}_3$ ), 35.8 ( $\text{CH}_3$ ), 24.9 ( $\beta\text{-CH}_2$ ), 24.9 ( $\gamma\text{-CH}_2$ ), 21.4 ( $\beta\text{-CH}_2$ ), 21.4 ( $\gamma\text{-CH}_2$ ), 6.8 ( $\text{SiCH}_3$ ).  $^7\text{Li}$  NMR (155.47 MHz, 300 K,  $\text{C}_6\text{D}_6$ ):  $\delta$  1.45, 0.67.

Crystal data for **115**:  $\text{C}_{50}\text{H}_{134}\text{N}_9\text{ClSi}_{10}\text{Li}_6$ ,  $M_r = 1219.65$ , monoclinic, space group  $P2_1$ ,  $a = 15.3460(4)$ ,  $b = 27.91338(7)$ ,  $c = 19.0059(5)$  Å,  $\beta = 102.300(2)^{\circ}$ ,  $V = 7960.3(4)$  Å<sup>3</sup>,  $Z = 4$ ,  $\lambda = 0.71073$  Å,  $\mu = 0.232$  mm<sup>-1</sup>,  $T = 123$  K; 42579 reflections, 27286 unique,  $R_{\text{int}} = 0.0317$ ; final refinement to convergence on  $F^2$  gave  $R = 0.0390$  ( $F$ , 16036 obs. data only) and  $R_w = 0.0683$  ( $F^2$ , all data), GOF = 0.786. Absolute configuration confirmed by refinement of Flack parameter to  $-0.08(5)$ .

### 5.3.31 Synthesis of $[\text{Li}\{(\text{R,R})\text{-TMCDA}\}_2]^+[\text{Li}_5(\mu\text{-HMDS})_5(\mu_5\text{-Br})]^-$ , **116**

Direct combination route: Lithium 1,1,1,3,3,3-hexamethyldisilazide (0.837 g, 5 mmol) was suspended in dried hexane (7.5 mL) in an oven-dried Schlenk tube and stirred for 30 minutes. Lithium bromide (0.087 g, 1 mmol) was then introduced and the mixture allowed to stir for a

further 30 minutes, after which two molar equivalents of *N,N,N',N'*-(1*R*,2*R*)-tetramethylcyclohexane-1,2-diamine (0.38 mL, 2 mmol) were added and a clear to pale yellow colour change was observed. This suspension was heated slightly and allowed to vigorously stir at ambient temperature for 72 hours to ensure the majority of the lithium bromide salt had dissolved. The hexane was removed *in vacuo* and dried toluene (7 mL) introduced, yielding a cloudy pale yellow solution. The solution was then heated and filtered through Celite and glass wool and the resultant clear yellow solution immediately placed in a freezer operating at  $-28^{\circ}\text{C}$ . After 48 hours, a crop of colourless X-ray quality needle-like crystals of **116** were deposited (0.14 g 12%).

Ammonium salt route: An oven-dried Schlenk tube was charged with *n*-butyllithium (0.63 mL of 1.6 M solution in hexanes, 1 mmol) and the hexane removed *in vacuo* and replaced with dried toluene (5 mL). Two molar equivalents of *N,N,N',N'*-(1*R*,2*R*)-tetramethylcyclohexane-1,2-diamine (0.38 mL, 2 mmol) were then added, yielding a bright fluorescent red/orange solution which was allowed to stir for 30 minutes. On the addition of one molar equivalent of ammonium bromide (0.098 g, 1 mmol) this bright fluorescent red/orange colour slowly dissipated on stirring to yield a pale pink/peach solution. The mixture was heated to reflux for one hour and the clear solution allowed to stir whilst cooling for 30 minutes. Five molar equivalents of lithium 1,1,1,3,3,3-hexamethyldisilazide (0.837 g, 5 mmol) were then introduced and the resultant slightly cloudy pale yellow solution heated slightly and allowed to stir at ambient temperature for 24 hours. Additional toluene (5 mL) was then introduced and the solution allowed to stir at ambient temperature for a further 12 hours, before being placed in a freezer operating at  $-28^{\circ}\text{C}$ . After 48 hours, a crop of colourless X-ray quality needle-like crystals of **116** were deposited (0.50 g 44%).

$^1\text{H}$  NMR (400.03 MHz, 300 K,  $\text{C}_6\text{D}_6$ ):  $\delta$  7.09-6.96 (toluene *CHo/m/p*, m), 2.11 (toluene  $\text{CH}_3$ , 1.08H, s), 1.97 ( $\text{CH}_3$ , 12H, s), 1.69 ( $\text{CH}_3$ , 12H, s), 1.65 ( $\alpha\text{-CH}$ , 4H, s), 1.33 ( $\beta\text{-CH}_2$ , 2H, m), 1.33 ( $\gamma\text{-CH}_2$ , 2H, m), 1.22 ( $\beta\text{-CH}_2$ , 2H, m), 1.22 ( $\gamma\text{-CH}_2$ , 2H, m), 0.58 ( $\beta\text{-CH}_2$ , 2H, m), 0.58 ( $\gamma\text{-CH}_2$ , 2H, m), 0.43 ( $\beta\text{-CH}_2$ , 2H, m), 0.43 ( $\gamma\text{-CH}_2$ , 2H, m), 0.43 ( $\text{SiCH}_3$ , 45H, br s), 0.17 ( $\text{SiCH}_3$ , 45H, br s).  $^{13}\text{C}$  NMR (100.59 MHz, 300 K,  $\text{C}_6\text{D}_6$ ):  $\delta$  63.8 ( $\alpha\text{-CH}$ ), 44.1 ( $\text{CH}_3$ ), 35.8 ( $\text{CH}_3$ ), 24.9 ( $\beta\text{-CH}_2$ ), 24.9 ( $\gamma\text{-CH}_2$ ), 21.4 ( $\beta\text{-CH}_2$ ), 21.4 ( $\gamma\text{-CH}_2$ ), 6.7 ( $\text{SiCH}_3$ ).  $^7\text{Li}$  NMR (155.47 MHz, 300 K,  $\text{C}_6\text{D}_6$ ):  $\delta$  1.44, 1.14.

From the X-ray crystallography data it is expected that four molecules of toluene should be present per complex. NMR data has revealed that only 0.09 molecules of toluene per complex are incorporated. Therefore, for yield purposes the  $M_r$  of the complex has been adjusted from

1126.43 g ( $M_r$  of one complex – two complexes present in asymmetric unit and eight molecules of toluene) to 1134.71 g.

Crystal data for **116**:  $C_{135}H_{308}N_{18}Br_2Si_{20}Li_{12}$ ,  $M_r = 2988.86$ , triclinic, space group  $P1$ ,  $a = 12.3602(3)$ ,  $b = 19.5652(5)$ ,  $c = 20.4985(4)$  Å,  $\alpha = 79.344(2)$ ,  $\beta = 76.458(2)$ ,  $\gamma = 87.979(2)^\circ$ ,  $V = 4736.06(19)$  Å<sup>3</sup>,  $Z = 1$ ,  $\lambda = 0.71073$  Å,  $\mu = 0.598$  mm<sup>-1</sup>,  $T = 123$  K; 59223 reflections, 35427 unique,  $R_{int} = 0.0359$ ; final refinement to convergence on  $F^2$  gave  $R = 0.0696$  ( $F$ , 24610 obs. data only) and  $R_w = 0.2050$  ( $F^2$ , all data), GOF = 1.009. Absolute configuration confirmed by refinement of Flack parameter to 0.102(7).

### 5.3.32 Synthesis of $[Me_6\text{-TREN}\cdot Li(\mu\text{-Cl})Li\cdot Me_6\text{-TREN}]^+[Li_5(\mu\text{-HMDS})_5(\mu_5\text{-Cl})]^-$ ,

#### 117

Lithium 1,1,1,3,3,3-hexamethyldisilazide (0.837 g, 5 mmol) was suspended in dried hexane (7.5 mL) in an oven-dried Schlenk tube and stirred for 30 minutes. Lithium chloride (0.085 g, 2 mmol) was then introduced and the mixture allowed to stir for a further 30 minutes, after which two molar equivalents of tris[2-(dimethylamino)ethyl]amine (0.52 mL, 2 mmol) were added. A colour change from clear to milky pale yellow to clear yellow was observed, along with a yellow/orange oily precipitate. This emulsion was heated slightly and allowed to vigorously stir at ambient temperature for 72 hours to ensure the majority of the lithium chloride salt had dissolved. The solvent was removed *in vacuo* and dried toluene (10 mL) introduced, yielding a slightly cloudy yellow/orange solution, which on standing deposited a slightly oily precipitate. The solution was heated and filtered through Celite and glass wool and after two hours at ambient temperature, a crop of colourless X-ray quality needle-like crystals of **117** were deposited (0.13 g, 9%).

<sup>1</sup>H NMR (400.03 MHz, 300 K, C<sub>6</sub>D<sub>6</sub>):  $\delta$  7.09-6.96 (toluene  $CH_o/m/p$ , m), 2.11 (toluene  $CH_3$ , 22H, s), 2.04 ( $CH_3$ , 36H, s), 1.66 ( $\alpha\text{-CH}_2$ , 12H, s), 1.66 ( $\beta\text{-CH}_2$ , 12H, s), 0.57 (Si $CH_3$ , 90H, s). <sup>13</sup>C NMR (100.59 MHz, 300 K, C<sub>6</sub>D<sub>6</sub>):  $\delta$  56.1 ( $\alpha\text{-CH}_2$ ), 49.7 ( $\beta\text{-CH}_2$ ), 45.3 ( $CH_3$ ), 6.1 (Si $CH_3$ ). <sup>7</sup>Li NMR (155.47 MHz, 300 K, C<sub>6</sub>D<sub>6</sub>):  $\delta$  1.84, -0.07.

Crystal data for **117**:  $C_{61}H_{158}N_{13}Cl_2Si_{10}Li_7$ ,  $M_r = 1474.38$ , monoclinic, space group  $C2/c$ ,  $a = 17.8926(4)$ ,  $b = 19.5064(4)$ ,  $c = 27.4603(7)$  Å,  $\beta = 94.934(2)^\circ$ ,  $V = 9548.7(4)$  Å<sup>3</sup>,  $Z = 4$ ,  $\lambda = 0.71073$  Å,  $\mu = 0.232$  mm<sup>-1</sup>,  $T = 123$  K; 28913 reflections, 11885 unique,  $R_{int} = 0.0292$ ; final refinement to convergence on  $F^2$  gave  $R = 0.0425$  ( $F$ , 8859 obs. data only) and  $R_w = 0.1067$  ( $F^2$ , all data), GOF = 1.022.



**5.3.33** Synthesis of  $[\text{Me}_6\text{-TREN}\cdot\text{Li}(\mu\text{-Br})\text{Li}\cdot\text{Me}_6\text{-TREN}]^+[\text{Li}_5(\mu\text{-HMDS})_5(\mu_5\text{-Br})]^-$ ,**118**

An oven-dried Schlenk tube was charged with *n*-butyllithium (1.25 mL of 1.6 M solution in hexanes, 2 mmol) and the hexane removed *in vacuo* and replaced with dried toluene (5 mL). Two molar equivalents of tris[2-(dimethylamino)ethyl]amine (0.52 mL, 2 mmol) were then added, yielding a bright fluorescent red/orange solution which was allowed to stir for 30 minutes. On the addition of an equimolar quantity of tetrabutylammonium bromide (0.65 g, 2 mmol) this bright fluorescent red/orange colour slowly dissipated on stirring to yield a raspberry/pink solution. The mixture was heated to reflux for one hour and the clear pale yellow solution allowed to stir whilst cooling for 30 minutes. Five molar equivalents of lithium 1,1,1,3,3,3-hexamethyldisilazide (0.84 g, 5 mmol) were then introduced affording a cloudy yellow solution. The mixture was heated slightly and allowed to stir at ambient temperature for 48 hours. On standing, a slightly oily precipitate was deposited from the now clear brown solution. The solution was then heated and dried toluene (5 mL) added. After two hours at ambient temperature, a crop of colourless X-ray quality needle-like crystals of **118** were deposited (0.89 g, 61%).

$^1\text{H}$  NMR (400.03 MHz, 300 K,  $\text{C}_6\text{D}_6$ ):  $\delta$  2.03 ( $\text{CH}_3$ , 36H, s), 1.62 ( $\alpha\text{-CH}_2$ , 12H, s), 1.62 ( $\beta\text{-CH}_2$ , 12H, s), 0.68 ( $\text{SiCH}_3$ , 45H, s), 0.51 ( $\text{SiCH}_3$ , 45H, s).  $^{13}\text{C}$  NMR (100.59 MHz, 300 K,  $\text{C}_6\text{D}_6$ ):  $\delta$  56.3 ( $\alpha\text{-CH}_2$ ), 49.7 ( $\beta\text{-CH}_2$ ), 45.6 ( $\text{CH}_3$ ), 7.8 ( $\text{SiCH}_3$ ), 6.1 ( $\text{SiCH}_3$ ).  $^7\text{Li}$  NMR (155.47 MHz, 300 K,  $\text{C}_6\text{D}_6$ ):  $\delta$  1.84, 0.14.

Crystal data for **118**:  $\text{C}_{54}\text{H}_{150}\text{N}_{13}\text{Br}_2\text{Si}_{10}\text{Li}_7$ ,  $M_r = 1471.17$ , monoclinic, space group  $C2/c$ ,  $a = 17.8919(7)$ ,  $b = 19.5508(9)$ ,  $c = 27.5458(13)$  Å,  $\beta = 94.219(4)^\circ$ ,  $V = 9609.4(7)$  Å<sup>3</sup>,  $Z = 4$ ,  $\lambda = 0.71073$  Å,  $\mu = 1.003$  mm<sup>-1</sup>,  $T = 123$  K; 23380 reflections, 11577 unique,  $R_{\text{int}} = 0.0396$ ; final refinement to convergence on  $F^2$  gave  $R = 0.0578$  ( $F$ , 7738 obs. data only) and  $R_w = 0.1352$  ( $F^2$ , all data), GOF = 1.035.

**5.3.34** Synthesis of  $[\text{Me}_6\text{-TREN}\cdot\text{Li}(\mu\text{-Br})\text{Li}\cdot\text{Me}_6\text{-TREN}]^+[\text{Li}_4(\mu\text{-HMDS})_4(\mu_4\text{-OH})]^-$ ,**126**

An oven-dried Schlenk tube was charged with *n*-butyllithium (1.25 mL of 1.6 M solution in hexanes, 2 mmol) and the hexane removed *in vacuo* and replaced with dried toluene (5 mL). Two molar equivalents of tris[2-(dimethylamino)ethyl]amine (0.52 mL, 2 mmol) were then added, yielding a bright fluorescent red/orange solution which was allowed to stir for 30 minutes. On the addition of an equimolar quantity of ammonium bromide (0.20 g, 2 mmol) this bright fluorescent red/orange colour slowly dissipated on stirring to yield a raspberry/pink

solution. The mixture was heated to reflux for one hour and the clear pale yellow solution allowed to stir whilst cooling for 30 minutes. Five molar equivalents of lithium 1,1,1,3,3,3-hexamethyldisilazide (0.84 g, 5 mmol) were then introduced affording a clear yellow/brown solution. The mixture was heated slightly and allowed to stir at ambient temperature for 48 hours, before being placed in a freezer operating at  $-28^{\circ}\text{C}$ . After 48 hours, a crop of colourless X-ray quality crystals of **126** were deposited (0.13 g).

The reaction was also carried out rationally (*i.e.*, utilising a 2 : 2 : 1 : 4 ratio of reagents), which afforded crystals of a higher symmetry polymorph of **126**; unfortunately however, the crystals decomposed, before a yield could be obtained or NMR spectroscopic analysis carried out.

$^1\text{H}$  NMR (400.03 MHz, 300 K,  $\text{C}_6\text{D}_6$ ):  $\delta$  2.06 ( $\text{CH}_3$ , 36H, s), 1.66 ( $\alpha\text{-CH}_2$ , 12H, s), 1.66 ( $\beta\text{-CH}_2$ , 12H, s), 0.92 (OH), 0.62 ( $\text{SiCH}_3$ , 72H, s).  $^{13}\text{C}$  NMR (100.59 MHz, 300 K,  $\text{C}_6\text{D}_6$ ):  $\delta$  56.3 ( $\alpha\text{-CH}_2$ ), 49.8 ( $\beta\text{-CH}_2$ ), 45.6 ( $\text{CH}_3$ ), 6.3 ( $\text{SiCH}_3$ ).  $^7\text{Li}$  NMR (155.47 MHz, 300 K,  $\text{C}_6\text{D}_6$ ):  $\delta$  1.93, 0.18.

Crystal data for **126**:  $\text{C}_{55}\text{H}_{141}\text{N}_{12}\text{BrOSi}_3\text{Li}_6$ ,  $M_r = 1333.07$ , monoclinic, space group  $C2$ ,  $a = 15.7435(6)$ ,  $b = 17.3227(7)$ ,  $c = 17.2023(8)$  Å,  $\beta = 103.413(5)^{\circ}$ ,  $V = 4563.4(3)$  Å<sup>3</sup>,  $Z = 2$ ,  $\lambda = 0.71073$  Å,  $\mu = 0.591$  mm<sup>-1</sup>,  $T = 123$  K; 13544 reflections, 13544 unique,  $R_{\text{int}} = 0.0000$ ; final refinement to convergence on  $F^2$  gave  $R = 0.0783$  ( $F$ , 9096 obs. data only) and  $R_w = 0.2143$  ( $F^2$ , all data), GOF = 1.044.

### 5.3.35 Synthesis of $[\text{Me}_6\text{-TREN}\cdot\text{Na}(\mu\text{-Br})\text{Na}\cdot\text{Me}_6\text{-TREN}]^+[\text{Na}_5(\mu\text{-HMDS})_5(\mu_5\text{-Br})]^-$ , **127**

Freshly prepared *n*-butylsodium (0.16 g, 2 mmol) was suspended in dried toluene (5 mL) in an oven-dried Schlenk tube and placed in an ultrasonic bath for ten minutes. Two molar equivalents of tris[2-(dimethylamino)ethyl]amine (0.52 mL, 2 mmol) were then added to this bright yellow/orange suspension, yielding a deep red solution which was allowed to stir for 30 minutes. On the addition of an equimolar quantity of tetrabutylammonium bromide (0.65 g, 2 mmol) the solution turned cloudy pink. The mixture was heated to reflux for one hour and the now cloudy yellow solution allowed to stir whilst cooling for 30 minutes. Five molar equivalents of sodium 1,1,1,3,3,3-hexamethyldisilazide (0.92 g, 5 mmol) were then introduced and the mixture heated slightly and allowed to stir at ambient temperature for 48 hours. Dried toluene (3 mL) was added to the now cloudy brown suspension and the solution heated and filtered through Celite and glass wool. The resultant slightly cloudy orange/brown solution was concentrated by removal of some solvent *in vacuo* and immediately placed in a

freezer operating at  $-28^{\circ}\text{C}$ . After 48 hours, a crop of colourless X-ray quality needle-like crystals of **127** were deposited (0.50 g, 32%).

$^1\text{H}$  NMR (400.03 MHz, 300 K,  $\text{C}_6\text{D}_6$ ):  $\delta$  7.09-6.96 (toluene  $\text{CHo}/m/p$ , m), 2.11 (toluene  $\text{CH}_3$ , 0.75H, s), 1.95 ( $\text{CH}_3$ , 36H, s), 1.86 ( $\alpha\text{-CH}_2$ , 12H, s), 1.86 ( $\beta\text{-CH}_2$ , 12H, s), 0.53 ( $\text{SiCH}_3$ , 90H, s).  $^{13}\text{C}$  NMR (100.59 MHz, 300 K,  $\text{C}_6\text{D}_6$ ):  $\delta$  56.6 ( $\alpha\text{-CH}_2$ ), 50.7 ( $\beta\text{-CH}_2$ ), 45.2 ( $\text{CH}_3$ ), 7.3 ( $\text{SiCH}_3$ ).

From the X-ray crystallography data it is expected that one molecule of toluene should be present per complex. NMR data has revealed that only 0.25 molecules of toluene per complex are incorporated. Therefore, for yield purposes the  $M_r$  of the complex has been adjusted from 1629.59 g to 1606.59 g.

Crystal data for **127**:  $\text{C}_{57.50}\text{H}_{154}\text{N}_{13}\text{Br}_2\text{Si}_{10}\text{Na}_7$ ,  $M_r = 1629.59$ , monoclinic, space group  $P2_1/n$ ,  $a = 13.5400(16)$ ,  $b = 18.521(2)$ ,  $c = 40.888(4)$  Å,  $\beta = 95.932(11)^{\circ}$ ,  $V = 10198.8(19)$  Å<sup>3</sup>,  $Z = 4$ ,  $\lambda = 0.71073$  Å,  $\mu = 0.978$  mm<sup>-1</sup>,  $T = 123$  K; 70847 reflections, 20010 unique,  $R_{\text{int}} = 0.0789$ ; final refinement to convergence on  $F^2$  gave  $R = 0.0760$  ( $F$ , 13367 obs. data only) and  $R_w = 0.1743$  ( $F^2$ , all data), GOF = 1.046.

### 5.3.36 Synthesis of $[\text{Me}_6\text{-TREN}\cdot\text{Na}(\mu\text{-I})\text{Na}\cdot\text{Me}_6\text{-TREN}]^+[\text{Na}_5(\mu\text{-HMDS})_5(\mu_5\text{-I})]^-$ , **128**

Freshly prepared *n*-butylsodium (0.16 g, 2 mmol) was suspended in dried toluene (5 mL) in an oven-dried Schlenk tube and placed in an ultrasonic bath for ten minutes. Two molar equivalents of tris[2-(dimethylamino)ethyl]amine (0.52 mL, 2 mmol) were then added to this bright yellow/orange suspension, yielding a deep red solution which was allowed to stir for 30 minutes. On the addition of an equimolar quantity of tetrabutylammonium iodide (0.74 g, 2 mmol) the solution turned pink. The mixture was heated to reflux for one hour and the now cloudy peach/orange solution allowed to stir whilst cooling for 30 minutes. Five molar equivalents of sodium 1,1,1,3,3,3-hexamethyldisilazide (0.92 g, 5 mmol) were then introduced and the mixture heated slightly, yielding a clear orange solution. The Schlenk tube was covered with a black plastic bag (iodide reagents are light sensitive) and allowed to stir at ambient temperature for 48 hours, before being placed in a freezer operating at  $-28^{\circ}\text{C}$ . After 24 hours, a crop of colourless needle-like crystals of **128** were deposited [1.42 g, 85% (MW of **128** = 1675.80 g)].

$^1\text{H}$  NMR (400.03 MHz, 300 K,  $\text{C}_6\text{D}_6$ ):  $\delta$  1.99 ( $\text{CH}_3$ , 36H, s), 1.78 ( $\alpha\text{-CH}_2$ , 12H, s), 1.78 ( $\beta\text{-CH}_2$ , 12H, s), 0.52 ( $\text{SiCH}_3$ , 90H, s).  $^{13}\text{C}$  NMR (100.59 MHz, 300 K,  $\text{C}_6\text{D}_6$ ):  $\delta$  56.5 ( $\alpha\text{-CH}_2$ ), 50.5 ( $\beta\text{-CH}_2$ ), 45.2 ( $\text{CH}_3$ ), 7.5 ( $\text{SiCH}_3$ ).

**5.3.37** Synthesis of  $[\{(R,R)\text{-TMCDA}\cdot\text{LiI}\}_2(\text{LiHMDS})_2]_\infty$ , **129**

An oven-dried Schlenk tube was charged with *n*-butyllithium (0.63 mL of 1.6 M solution in hexanes, 1 mmol) and the hexane removed *in vacuo* and replaced with dried toluene (5 mL). Two molar equivalents of *N,N,N',N'*-(1*R*,2*R*)-tetramethylcyclohexane-1,2-diamine (0.38 mL, 2 mmol) were then added, yielding a bright fluorescent red/orange solution which was allowed to stir for 30 minutes. On the addition of one molar equivalent of ammonium iodide (0.15 g, 1 mmol) this bright fluorescent red/orange colour slowly dissipated with slight heating and stirring to yield a pale pink/peach solution. The mixture was heated to reflux for one hour and the resultant clear pale yellow solution allowed to stir whilst cooling for 30 minutes. Seven molar equivalents of lithium 1,1,1,3,3,3-hexamethyldisilazide (1.17 g, 7 mmol) were then introduced and the resultant slightly cloudy pale yellow solution heated slightly. The Schlenk tube was covered with a black plastic bag (iodide reagents are light sensitive) and the mixture allowed to stir at ambient temperature for 48 hours. Additional toluene (2.5 mL) was then introduced, along with heating and the solution immediately placed in a hot water-filled Dewar flask. After 24 hours, a crop of colourless X-ray quality crystals of **129** were deposited [0.40 g, 85% (with respect to NH<sub>4</sub>I)].

<sup>1</sup>H NMR (400.03 MHz, 300 K, C<sub>6</sub>D<sub>6</sub>): δ 2.33 (CH<sub>3</sub>, 12H, s), 2.12 (CH<sub>3</sub>, 12H, s), 2.04 (α-CH, 4H, s), 1.35 (β-CH<sub>2</sub>, 4H, m), 1.35 (γ-CH<sub>2</sub>, 4H, m), 0.64 (β-CH<sub>2</sub>, 4H, m), 0.64 (γ-CH<sub>2</sub>, 4H, m), 0.57 (β-CH<sub>2</sub>, 4H, m), 0.57 (γ-CH<sub>2</sub>, 4H, m), 0.36 (SiCH<sub>3</sub>, 36H, s). <sup>13</sup>C NMR (100.59 MHz, 300 K, C<sub>6</sub>D<sub>6</sub>): δ 63.9 (α-CH), 45.9 (CH<sub>3</sub>), 38.5 (CH<sub>3</sub>), 24.9 (β-CH<sub>2</sub>), 24.9 (γ-CH<sub>2</sub>), 21.7 (β-CH<sub>2</sub>), 21.7 (γ-CH<sub>2</sub>), 5.9 (SiCH<sub>3</sub>). <sup>7</sup>Li NMR (155.47 MHz, 300 K, C<sub>6</sub>D<sub>6</sub>): δ 2.16, 1.54.

Crystal data for **129**: C<sub>64</sub>H<sub>160</sub>N<sub>12</sub>I<sub>4</sub>Si<sub>8</sub>Li<sub>8</sub>, *M<sub>r</sub>* = 1885.88, orthorhombic, space group *P*2<sub>1</sub>2<sub>1</sub>2<sub>1</sub>, *a* = 14.2443(3), *b* = 19.9051(4), *c* = 35.7460(8) Å, *V* = 10135.2(4) Å<sup>3</sup>, *Z* = 4, λ = 0.71073 Å, μ = 1.361 mm<sup>-1</sup>, *T* = 123 K; 36095 reflections, 19991 unique, *R*<sub>int</sub> = 0.0436; final refinement to convergence on *F*<sup>2</sup> gave *R* = 0.0656 (*F*, 15351 obs. data only) and *R<sub>w</sub>* = 0.1235 (*F*<sup>2</sup>, all data), GOF = 1.082. Absolute configuration confirmed by refinement of Flack parameter to 0.000(17).

**5.3.38** Synthesis of [Me<sub>6</sub>-TREN·LiI], **130**

An oven-dried Schlenk tube was charged with *n*-butyllithium (1.25 mL of 1.6 M solution in hexanes, 2 mmol) and the hexane removed *in vacuo* and replaced with dried toluene (5 mL). Two molar equivalents of tris[2-(dimethylamino)ethyl]amine (0.52 mL, 2 mmol) were then added, yielding a bright fluorescent red/orange solution which was allowed to stir for 30 minutes. No colour change was observed on the addition of an equimolar quantity of

ammonium iodide (0.28 g, 2 mmol). The mixture was heated to reflux for one hour and the now clear pale brown solution allowed to stir whilst cooling for 30 minutes. Six molar equivalents of lithium 1,1,1,3,3,3-hexamethyldisilazide (1.00 g, 6 mmol) were then introduced and the solution heated slightly. The Schlenk tube was covered with a black plastic bag (iodide reagents are light sensitive) and the mixture allowed to stir at ambient temperature for 48 hours. The now dark brown solution was heated and filtered through Celite and glass wool, and the resultant pale brown solution immediately placed in a freezer operating at  $-28^{\circ}\text{C}$ . After 24 hours, a crop of colourless X-ray quality cubic-like crystals of **130** were deposited [0.68 g, 93% (with respect to  ${}^n\text{BuLi}$ )].

${}^1\text{H}$  NMR (400.03 MHz, 300 K,  $\text{C}_6\text{D}_6$ ):  $\delta$  2.17 ( $\text{CH}_3$ , 18H, s), 1.66 ( $\alpha\text{-CH}_2$ , 6H, s), 1.66 ( $\beta\text{-CH}_2$ , 6H, s).  ${}^{13}\text{C}$  NMR (100.59 MHz, 300 K,  $\text{C}_6\text{D}_6$ ):  $\delta$  56.3 ( $\alpha\text{-CH}_2$ ), 49.8 ( $\beta\text{-CH}_2$ ), 46.0 ( $\text{CH}_3$ ).  ${}^7\text{Li}$  NMR (155.47 MHz, 300 K,  $\text{C}_6\text{D}_6$ ):  $\delta$  0.81.

Crystal data for **130**:  $\text{C}_{12}\text{H}_{30}\text{N}_4\text{ILi}$ ,  $M_r = 364.24$ , hexagonal, space group  $P6_3$ ,  $a = 9.91540(10)$ ,  $b = 9.91540(10)$ ,  $c = 10.3711(2)$  Å,  $\gamma = 120.00^{\circ}$ ,  $V = 883.03(2)$  Å<sup>3</sup>,  $Z = 2$ ,  $\lambda = 0.71073$  Å,  $\mu = 1.805$  mm<sup>-1</sup>,  $T = 123$  K; 3232 reflections, 1332 unique,  $R_{\text{int}} = 0.0135$ ; final refinement to convergence on  $F^2$  gave  $R = 0.0253$  ( $F$ , 1265 obs. data only) and  $R_w = 0.0621$  ( $F^2$ , all data), GOF = 1.101.

### 5.3.39 Synthesis of $[\text{Me}_6\text{-TREN}\cdot\text{Na}(\mu\text{-I})\text{Na}(\mu\text{-HMDS})_2\text{Na}(\mu\text{-I})\text{Na}\cdot\text{Me}_6\text{-TREN}]$ , **131**

Freshly prepared *n*-butylsodium (0.16 g, 2 mmol) was suspended in dried toluene (5 mL) in an oven-dried Schlenk tube and placed in an ultrasonic bath for ten minutes. Two molar equivalents of tris[2-(dimethylamino)ethyl]amine (0.52 mL, 2 mmol) were then added to this bright yellow/orange suspension, yielding a deep red solution which was allowed to stir for 30 minutes. On the addition of an equimolar quantity of ammonium iodide (0.28 g, 2 mmol) the solution darkened in colour. The mixture was heated to reflux for one hour and the now cloudy brown solution allowed to stir whilst cooling for 30 minutes. Five molar equivalents of sodium 1,1,1,3,3,3-hexamethyldisilazide (0.92 g, 5 mmol) were then introduced and the mixture heated slightly, yielding a dark brown solution. The Schlenk tube was covered with a black plastic bag (iodide reagents are light sensitive) and allowed to stir at ambient temperature for 48 hours. Additional toluene (2.5 mL) was then introduced and the solution heated and filtered through Celite and glass wool, before being placed in a freezer operating at  $-28^{\circ}\text{C}$ . After 48 hours, a crop of colourless X-ray quality needle-like crystals of **131** were deposited [0.20 g, 18% (with respect to  ${}^n\text{BuNa}$ )].

$^1\text{H}$  NMR (400.03 MHz, 300 K,  $\text{C}_6\text{D}_6$ ):  $\delta$  2.03 ( $\text{CH}_3$ , 36H, s), 1.72 ( $\alpha\text{-CH}_2$ , 12H, s), 1.72 ( $\beta\text{-CH}_2$ , 12H, s), 0.51 ( $\text{SiCH}_3$ , 36H, s).  $^{13}\text{C}$  NMR (100.59 MHz, 300 K,  $\text{C}_6\text{D}_6$ ):  $\delta$  56.5 ( $\alpha\text{-CH}_2$ ), 50.6 ( $\beta\text{-CH}_2$ ), 45.2 ( $\text{CH}_3$ ), 7.4 ( $\text{SiCH}_3$ ).

Crystal data for **131**:  $\text{C}_{36}\text{H}_{96}\text{N}_{10}\text{I}_2\text{Si}_4\text{Na}_4$ ,  $M_r = 1127.35$  orthorhombic, space group  $Pbcn$ ,  $a = 16.0429(3)$ ,  $b = 16.1993(7)$ ,  $c = 23.8631(4)$  Å,  $V = 6201.6(3)$  Å<sup>3</sup>,  $Z = 4$ ,  $\lambda = 0.71073$  Å,  $\mu = 1.150$  mm<sup>-1</sup>,  $T = 123$  K; 23026 reflections, 6690 unique,  $R_{\text{int}} = 0.1195$ ; final refinement to convergence on  $F^2$  gave  $R = 0.0853$  ( $F$ , 2722 obs. data only) and  $R_w = 0.2387$  ( $F^2$ , all data), GOF = 0.993.

### 5.3.40 Synthesis of $[\{(R,R)\text{-TMCDA}\cdot\text{Li}(\text{SCN})\}_2(\text{LiHMDS})_2]_{\infty}$ , **132**

An oven-dried Schlenk tube was charged with *n*-butyllithium (0.63 mL of 1.6 M solution in hexanes, 1 mmol) and the hexane removed *in vacuo* and replaced with dried toluene (5 mL). Two molar equivalents of *N,N,N',N'*-(1*R*,2*R*)-tetramethylcyclohexane-1,2-diamine (0.38 mL, 2 mmol) were then added, yielding a bright fluorescent red/orange solution which was allowed to stir for 30 minutes. On the addition of one molar equivalent of ammonium thiocyanate (0.076 g, 1 mmol) this bright fluorescent red/orange colour slowly dissipated on stirring to yield a clear solution. The mixture was heated to reflux for one hour and the clear solution allowed to stir whilst cooling for 30 minutes. Five molar equivalents of lithium 1,1,1,3,3,3-hexamethyldisilazide (0.837 g, 5 mmol) were then introduced and the resultant slightly cloudy pale yellow solution heated slightly and allowed to stir at ambient temperature for 48 hours, before being placed in a freezer operating at  $-28^\circ\text{C}$ . After 24 hours, a crop of colourless X-ray quality needle-like crystals of **132** were deposited [0.39 g, 87% (with respect to  $\text{NH}_4\text{SCN}$ )].

$^1\text{H}$  NMR (400.03 MHz, 300 K,  $\text{C}_6\text{D}_6$ ):  $\delta$  7.09-6.96 (toluene  $\text{CH}_o/m/p$ , m), 2.17 ( $\text{CH}_3$ , 12H, s), 2.11 (toluene  $\text{CH}_3$ , 3H, s), 1.92 ( $\text{CH}_3$ , 12H, s), 1.92 ( $\alpha\text{-CH}$ , 4H, s), 1.36 ( $\beta\text{-CH}_2$ , 4H, m), 1.36 ( $\gamma\text{-CH}_2$ , 4H, m), 0.62 ( $\beta\text{-CH}_2$ , 4H, m), 0.62 ( $\gamma\text{-CH}_2$ , 4H, m), 0.32 ( $\text{SiCH}_3$ , 36H, s).  $^{13}\text{C}$  NMR (100.59 MHz, 300 K,  $\text{C}_6\text{D}_6$ ):  $\delta$  63.8 ( $\alpha\text{-CH}$ ), 44.4 ( $\text{CH}_3$ ), 36.0 ( $\text{CH}_3$ ), 24.9 ( $\beta\text{-CH}_2$ ), 24.9 ( $\gamma\text{-CH}_2$ ), 21.6 ( $\beta\text{-CH}_2$ ), 21.6 ( $\gamma\text{-CH}_2$ ), 5.9 ( $\text{SiCH}_3$ ).  $^7\text{Li}$  NMR (155.47 MHz, 300 K,  $\text{C}_6\text{D}_6$ ):  $\delta$  1.30, 0.72.

Crystal data for **132**:  $\text{C}_{41}\text{H}_{88}\text{N}_8\text{S}_2\text{Si}_4\text{Li}_4$ ,  $M_r = 897.43$ , hexagonal, space group  $P6_1$ ,  $a = 14.2443(3)$ ,  $b = 19.9051(4)$ ,  $c = 35.7460(8)$  Å,  $\gamma = 120.00^\circ$ ,  $V = 8519.2(19)$  Å<sup>3</sup>,  $Z = 6$ ,  $\lambda = 0.71073$  Å,  $\mu = 0.211$  mm<sup>-1</sup>,  $T = 123$  K; 77864 reflections, 12915 unique,  $R_{\text{int}} = 0.0793$ ; final refinement to convergence on  $F^2$  gave  $R = 0.0571$  ( $F$ , 10070 obs. data only) and  $R_w = 0.1308$

( $F^2$ , all data), GOF = 1.061. Absolute configuration confirmed by refinement of Flack parameter to 0.03(8).

### 5.3.41 Synthesis of [Me<sub>6</sub>-TREN·K(μ-HMDS)K(μ-HMDS)<sub>2</sub>K(μ-HMDS)K·Me<sub>6</sub>-TREN], **134**

Freshly prepared benzylpotassium (0.264 g, 2 mmol) was suspended in dried toluene (5 mL) in an oven-dried Schlenk tube and placed in an ultrasonic bath for ten minutes. Two molar equivalents of tris[2-(dimethylamino)ethyl]amine (0.52 mL, 2 mmol) were then added to this red suspension, yielding a bright fluorescent deep red solution which was allowed to stir for 30 minutes. On the addition of an equimolar quantity of tetrabutylammonium bromide (0.65 g, 2 mmol) the solution darkened in colour. The mixture was heated to reflux for one hour and the now cloudy green/grey solution allowed to stir whilst cooling for 30 minutes. Five molar equivalents of potassium 1,1,1,3,3,3-hexamethyldisilazide (1.00 g, 5 mmol) were then introduced and the mixture heated slightly and allowed to stir at ambient temperature for 48 hours. Dried toluene (3 mL) was added to the now cloudy red/pink suspension and the solution heated and filtered through Celite and glass wool. The resultant clear orange solution was concentrated by removal of some solvent *in vacuo* and immediately placed in a freezer operating at -28°C. After 48 hours, a crop of colourless X-ray quality cubic-like crystals of **134** were deposited [0.09 g, 17% (maximum yield 50% with respect to tris[2-(dimethylamino)ethyl]amine)].

This reaction was repeated using (trimethylsilylmethyl)potassium instead of benzylpotassium as the source of potassium, yielding the same product.

<sup>1</sup>H NMR (400.03 MHz, 300 K, C<sub>6</sub>D<sub>6</sub>): δ 2.26 (β-CH<sub>2</sub>, 12H, t), 2.13 (α-CH<sub>2</sub>, 12H, t), 2.04 (CH<sub>3</sub>, 36H, s), 0.27 (SiCH<sub>3</sub>, 72H, s). <sup>13</sup>C NMR (100.59 MHz, 300 K, C<sub>6</sub>D<sub>6</sub>): δ 58.2 (α-CH<sub>2</sub>), 53.3 (β-CH<sub>2</sub>), 45.8 (CH<sub>3</sub>), 7.4 (SiCH<sub>3</sub>).

From the X-ray crystallography data it is expected that four molecules of toluene should be present per complex. NMR data has revealed that all four molecules of toluene have been removed *in vacuo*. Therefore, for yield purposes the  $M_r$  of the complex has been adjusted from 1406.19 g to 1038.19 g.

Crystal data for **134**: C<sub>59.20</sub>H<sub>144.80</sub>N<sub>12</sub>Si<sub>8</sub>K<sub>4</sub>,  $M_r = 1406.19$ , triclinic, space group  $P \bar{1}$ ,  $a = 12.2066(4)$ ,  $b = 12.8113(4)$ ,  $c = 15.0375(4)$  Å,  $\alpha = 79.045(3)$ ,  $\beta = 81.833(2)$ ,  $\gamma = 79.141(3)^\circ$ ,  $V = 2253.60(12)$  Å<sup>3</sup>,  $Z = 1$ ,  $\lambda = 0.71073$  Å,  $\mu = 0.341$  mm<sup>-1</sup>,  $T = 123$  K; 22235 reflections, 10995

unique,  $R_{\text{int}} = 0.0245$ ; final refinement to convergence on  $F^2$  gave  $R = 0.0609$  ( $F$ , 8648 obs. data only) and  $R_w = 0.1711$  ( $F^2$ , all data), GOF = 1.050.

### 5.3.42 Synthesis of [KHMDS·12-crown-4]<sub>2</sub>, **136**

Potassium 1,1,1,3,3,3-hexamethyldisilazide (0.20 g, 1 mmol) was suspended in dried toluene (5 mL) in an oven-dried Schlenk tube and allowed to stir for ten minutes, producing a pale yellow suspension. 12-Crown-4 (0.16 mL, 1 mmol) was then introduced, yielding a bright yellow solution. The mixture was heated slightly and allowed to stir at ambient temperature for 48 hours, before being placed in a freezer operating at  $-28^\circ\text{C}$ . After 24 hours, a crop of colourless X-ray quality crystals of **136** were deposited (0.38 g, 95%).

$^1\text{H}$  NMR (400.03 MHz, 300 K,  $\text{C}_6\text{D}_6$ ):  $\delta$  7.09-6.96 (toluene  $\text{CHo}/m/p$ , m), 3.06 ( $\text{CH}_2$ , 32H, s), 2.11 (toluene  $\text{CH}_3$ , 2.79H, s), 0.43 ( $\text{SiCH}_3$ , 36H, s).  $^{13}\text{C}$  NMR (100.59 MHz, 300 K,  $\text{C}_6\text{D}_6$ ):  $\delta$  67.0 ( $\text{CH}_2$ ), 7.4 ( $\text{SiCH}_3$ ).

From the X-ray crystallography data it is expected that two molecules of toluene should be present per complex. NMR data has revealed that only 0.47 molecules of toluene per complex are incorporated. Therefore, for yield purposes the  $M_r$  of the complex has been adjusted from 843.54 g to 800.30 g.

Crystal data for **136**:  $\text{C}_{35}\text{H}_{76}\text{N}_2\text{O}_8\text{Si}_4\text{K}_2$ ,  $M_r = 843.54$ , monoclinic, space group  $P2_1/c$ ,  $a = 12.4604(4)$ ,  $b = 12.4931(3)$ ,  $c = 16.0780(5)$  Å,  $\beta = 107.587(3)^\circ$ ,  $V = 2385.86(12)$  Å<sup>3</sup>,  $Z = 2$ ,  $\lambda = 0.71073$  Å,  $\mu = 0.343$  mm<sup>-1</sup>,  $T = 123$  K; 17250 reflections, 5630 unique,  $R_{\text{int}} = 0.0298$ ; final refinement to convergence on  $F^2$  gave  $R = 0.0522$  ( $F$ , 4539 obs. data only) and  $R_w = 0.1182$  ( $F^2$ , all data), GOF = 1.215.



## Chapter 6: Future Work

The work undertaken during the course of this PhD study has kick-started several new lines of research, and as such, there is scope for extending the chemistry of the various areas of research detailed within. To aid the reader, this chapter will be broken down into three primary sections outlining further extensions to the various areas of research embarked on according to the chapter into which they principally fall.

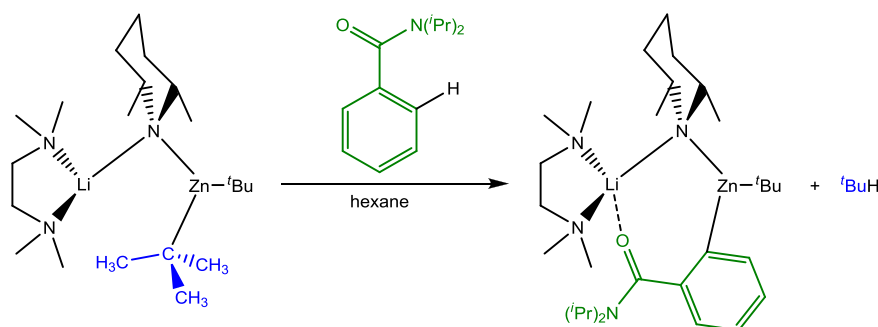
### 6.1 Further Extensions to the Work Contained Within Chapter 2

Chapter 2 looked at enhancing the scope of *s*-block homo- and heterobimetallic amide chemistry through the synthesis and characterisation of various complexes containing the amides *cis*-DMP, HMDS, diphenylamide and TMP.

#### 6.1.1 *cis*-DMP

Reactivity studies are now underway within the group to ascertain whether the structural patterns observed here profoundly affect reactivities. Initial studies have focused on the reactivity of [(TMEDA)·Li(μ-*cis*-DMP)Zn(*t*Bu)<sub>2</sub>], **75**, with the aromatic substrate *N,N*-diisopropylbenzamide, which has previously been successfully *ortho*-metallated<sup>[89a]</sup> with the more commonly utilised TMP base [(THF)·Li(μ-TMP)(μ-*t*Bu)Zn(*t*Bu)],<sup>[90]</sup> **35**. Akin to complex **35**, complex **75** was effective in *ortho*-metallating *N,N*-diisopropylbenzamide (confirmed by structural elucidation and iodine quenching studies), with concomitant loss of *t*BuH as the co-product of the reaction (Scheme 6.1). Complex **35** is a THF and TMP analogue of **75**. The *in situ* generated TMEDA and TMP analogue of **75**, “[TMEDA)·Li(μ-TMP)(μ-*t*Bu)Zn(*t*Bu)]”, has previously been shown to selectively *ortho*-metallate two molecules of *N,N*-diisopropylbenzamide (even when the stoichiometry of base : amide is 1 : 1), forming the bis(amide) [(TMEDA)·Li{2-(1-C(O)N<sup>*i*</sup>Pr<sub>2</sub>)C<sub>6</sub>H<sub>4</sub>}<sub>2</sub>Zn(*t*Bu)],<sup>[90b]</sup> **137**. Nonetheless, this preliminary result is highly encouraging, as the successful replacement of TMP(H) (£59.90 per 25 g)<sup>[1]</sup> with *cis*-DMP(H) (£14.20 per 100 g)<sup>[1]</sup> within synergic bases would significantly reduce the cost of goods barrier to the exploitation of multicomponent metallators for the manufacture of drug substances for the pharmaceutical industry. Future work will centre on the reactions of **75** and the other novel *cis*-DMP zincates and magnesiates with a multitude of aromatic and heterocyclic substrates (such as arenes, naphthalenes, pyridines, pyrimidines, quinolines, quinoxalines, indoles, furans, thiophenes and benzofurans), and comparing their reactivity to that of their DA and TMP analogues – with

the ultimate aim of providing metallation access to *meta*-, *para*- and other challenging to access C–H bonds within these compounds. In addition, we hope to synthesis the THF analogue of **75** along with THF analogues of the other novel *cis*-DMP zincates and magnesiates and explore their reactivity. Full characterisation and optimised yields of the organic products obtained after performing electrophilic interceptions will also be required.



**Scheme 6.1** Selective *ortho*-deprotonation of *N,N*-diisopropylbenzamide with the lithium *cis*-DMP zincate [(TMEDA)·Li( $\mu$ -*cis*-DMP)Zn(<sup>t</sup>Bu)<sub>2</sub>], **75**.

Running parallel to work examining **75** and its reactivity, the synthesis of analogues in which the alkyl groups on the zinc atom, as well as the donor ligand on the lithium atom are varied has also been researched. Following the same reaction methodology as that used to prepare **75**, but utilising the commercially available zinc reagent Et<sub>2</sub>Zn in place of <sup>t</sup>Bu<sub>2</sub>Zn, yielded the formation of a new bis(alkyl)amido lithium zincate [(TMEDA)·Li( $\mu$ -*cis*-DMP)( $\mu$ -Et)Zn(Et)], **138**. Crystals obtained using Me<sub>2</sub>Zn in an analogues reaction are awaiting analysis by X-ray crystallography. These systems may show even greater potential in an industrial setting due to the commercial availability of the zinc reagents. Also awaiting analysis are crystals obtained utilising the tridentate donor PMDETA in place of the didentate donor TMEDA. Recently the aggressive <sup>t</sup>Bu<sup>−</sup> anions in **75** have also been replaced with gentler trimethylsilyl (Me<sub>3</sub>SiCH<sub>2</sub><sup>−</sup>) ligands, yielding [(TMEDA)·Li( $\mu$ -*cis*-DMP)( $\mu$ -CH<sub>2</sub>SiMe<sub>3</sub>)Zn(CH<sub>2</sub>SiMe<sub>3</sub>)], **139**. This work will be extended utilising the other novel *cis*-DMP zincates and magnesiates, with future work concentrating on the synthesis of similar systems by altering the metal cations, amido-, alkyl- and donor ligands, with the ultimate aim of taking these novel systems through to reactivity studies. In addition, the introduction of the chiral *trans*-isomer of DMP(H) into these systems [or the chiral diamines (−)-sparteine (when commercially available again), (*R,R*)-TMCDA and other various chiral amides (*vide infra* – [Scheme 6.2](#))] could lead to the formation of a vast array of new synthetic reagents which may have a high regio- and stereoselective potential.

### 6.1.2 HMDS

Regarding the work carried out on the TMEDA-solvated alkali metal salts of HMDS, better X-ray quality crystals of  $[\text{KHMDS}\cdot\text{TMEDA}]_2$ , **83**, are required, along with the rational preparation of  $[(\text{NaHMDS})_2\cdot\text{TMEDA}]_\infty$ , **84**. This could possibly be achieved by allowing the reaction mixture to cool more slowly for **83**, by immediately placing the Schlenk tube in a hot water-filled Dewar flask once the solution had been heated to reflux; and by further probing of the systematic manipulation of the reactions conditions (stoichiometry of reagents, reaction solvents, reaction time and temperature, crystallisation techniques *etc.*) for **84**. Extending this chemistry to Rb and Cs should also be attempted prior to considering this work for possible submission to publication.

Turning to the alkali metal tris(HMDS) magnesiate containing TMEDA donor ligand, the rational synthesis of these products (complexes **88** and **89**) is paramount, together with attempts to prepare contacted ion pair HMDS-containing alkali metal magnesiate which contain TMEDA donor ligand. Initial efforts to achieve the latter have been undertaken by combining  ${}^n\text{BuM}$ ,  ${}^n\text{Bu}_2\text{Mg}$ , HMDS(H) and TMEDA in a 1 : 1 : 3 : 1 stoichiometric ratio and heating the solution to reflux in an attempt to prepare a TMEDA-solvated lithium/sodium tris(HMDS) magnesiate. Microcrystalline material was deposited from these solutions; however, each batch was not suitable for X-ray crystallographic analysis. Hence, manipulation of the crystallisation conditions is required to try and obtain X-ray quality crystals – for example, by slowly cooling the Schlenk tubes using the aforementioned technique or by diluting the solutions *via* the addition of more solvent. Attempts to prepare bis(amido) and bis(alkyl) magnesiate of similar form should also be investigated, along with the possibility of extending this chemistry to Rb and Cs. Efforts to obtain complexes **88** and **89** rationally have thus far been unsuccessful.

### 6.1.3 Diphenylamide

Future studies will focus on the preparation of mixed alkali metal-magnesium/zinc diphenylamides (hopefully extending the chemistry to Rb and Cs) with the ultimate aim of performing alkali metal mediated metallations using these bases. Synthesis of the PMDETA, dioxane and THF adducts synthesised by Westerhausen will be undertaken,<sup>[230c, 230d, 232]</sup> along with attempts to synthesise (–)-sparteine and (*R,R*)-TMCDA adducts, in the anticipation of also utilising these homometallic reagents in the field of alkali metal magnesiate and zincate chemistry – will the expected lower basicity of diphenylamide (*cf.*, DA or TMP) be reversed

by synergic mixed-metal effects and will the chiral systems be efficient in enantioselective reactions?

### 6.1.4 TMP

Reproducibility of the fortuitous ring-opening product of the TMP anion and subsequent spectroscopic analysis is first and foremost. A general route to obtain the ring-opening product amidoalkene should also be sought for the rational generation of amidoalkenes from the thermal decomposition of similar cyclic structures. One possible method would be to react  $\text{Mg}(\text{TMP})_2$  with a stronger base (RLi) to see whether it facilitates ring-opening of TMP at higher temperatures.

Future work is needed to provide greater insight into the mechanism. The ring-opening reaction is somewhat reminiscent of cleavages of cyclic ethers producing enolates and Hofmann-elimination reactions, and as alluded to previously, may be the first step in the thermal degradation of  $\text{Mg}(\text{TMP})$  complexes. Consideration of the ring-opening process occurring *via* a di-metallated TMP species instead of a H-shift, by means of a  $\beta$ -elimination pathway at high temperatures, must also be investigated. The role of oxygen in this reaction is also unclear. It does not necessarily play a role in the ring-opening, but could enter the vessel to slowly oxidise the carbanions to alkoxides, which then drives the formation of crystals. Synthesis of the oxygen-containing adduct of the synthesised dimeric alkylmagnesium amide species may provide a greater understanding of the role oxygen plays in these  $\text{Mg}(\text{TMP})$  reactions.

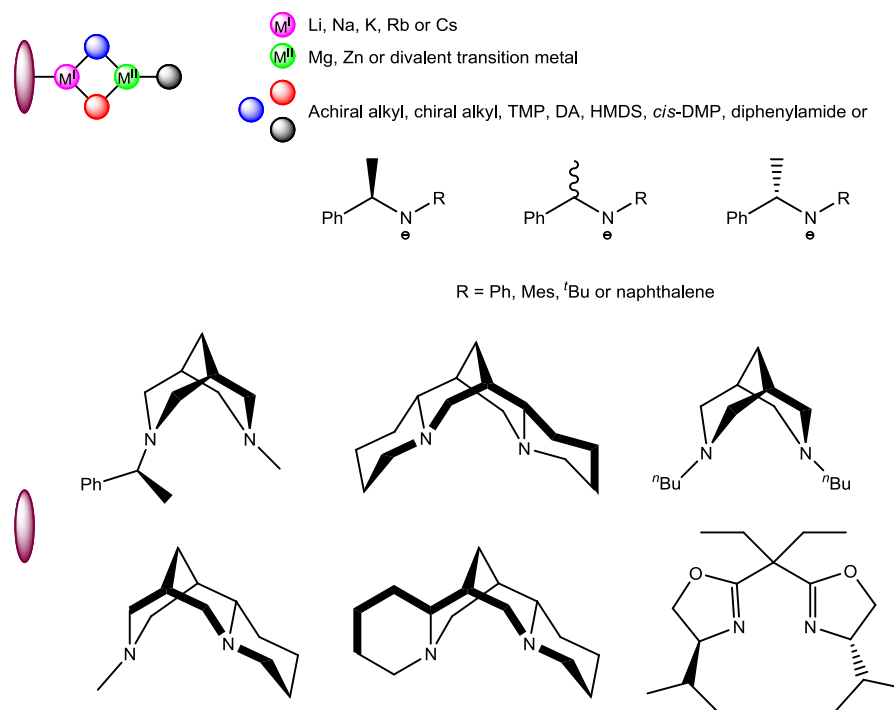
## 6.2 Further Extensions to the Work Contained Within Chapter 3

Chapter 3 looked at chiral ligand incorporation in magnesiate and zincate chemistry through the design of new, potentially enantioselective, bases by incorporating the chiral diamines (–)-sparteine and (*R,R*)-TMCDA into the molecular framework of alkali metal, and mixed alkali metal-magnesium/zinc amide complexes.

### 6.2.1 (–)-Sparteine- and (*R,R*)-TMCDA-containing Sodium TMP Zincates

Future work will concentrate on solution studies of these complexes, including the utilisation of multinuclear NMR and DOSY to fully explain their solution-state chemistry. Synthetically, the (–)-sparteine analogue of  $[\{(R,R)\text{-TMCDA}\}\cdot\text{Na}(\mu\text{-TMP})(\mu\text{-}^t\text{Bu})\text{Zn}(^t\text{Bu})]$ , **98**, will be prepared, as this too would represent a chiral variant of the important utility ate base  $[(\text{TMEDA})\cdot\text{Na}(\mu\text{-TMP})(\mu\text{-}^t\text{Bu})\text{Zn}(^t\text{Bu})]$ ,<sup>[111]</sup> **38**.<sup>[112-118]</sup> Endeavours will also be made to build

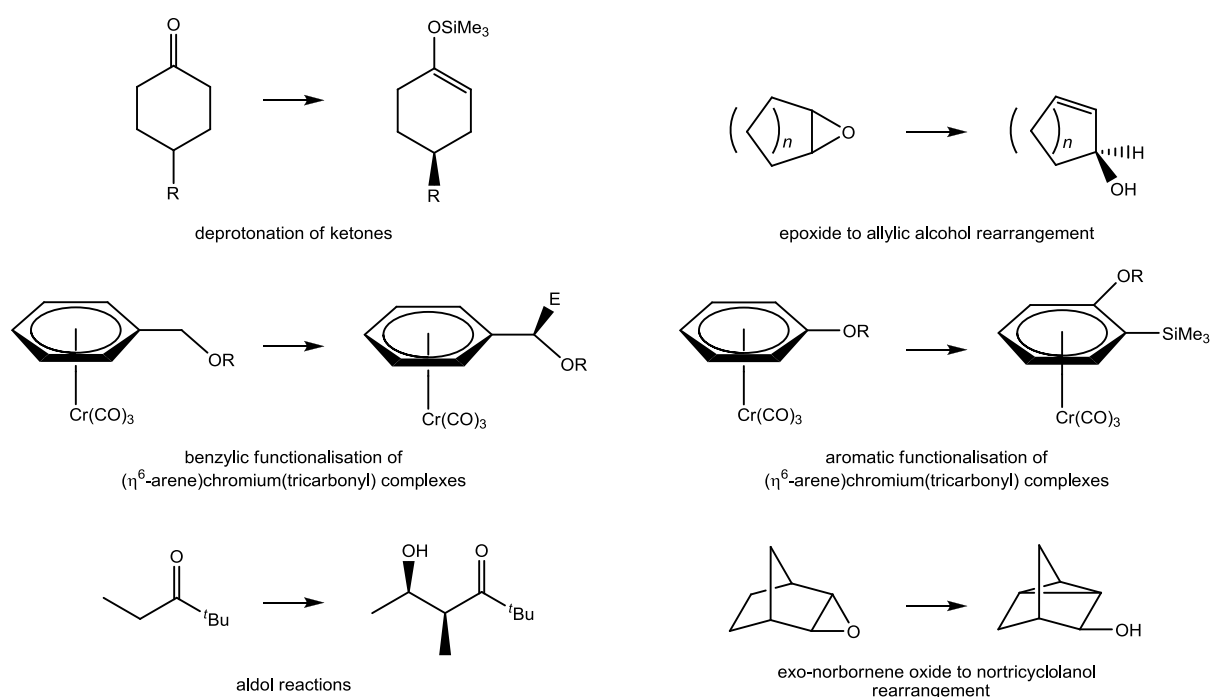
up a library of these chiral complexes by varying the metal cations, amido-, alkyl- and chiral ligands (Scheme 6.2). Prime candidates for the amido- and alkyl-components of these systems – in addition to TMP, <sup>n</sup>Bu and <sup>t</sup>Bu – include DA, HMDS, *cis*-DMP, diphenylamide, <sup>s</sup>Bu, <sup>i</sup>Pr, Np and silylamides [*i.e.*, Me<sub>3</sub>SiCH<sub>2</sub> and (Me<sub>3</sub>Si)<sub>2</sub>CH]. A wide variety of chiral donor ligands can be substituted in place of (–)-sparteine and (*R,R*)-TMCDA, or another approach to forming chiral bimetallics is by utilising neutral donor ligands but incorporating chiral amine ligands – a selection of chiral donor ligands and chiral anions are highlighted in Scheme 6.2.



**Scheme 6.2** Possible permutations which can be studied systematically to produce a range of new chiral heterobimetallic reagents.

Scheme 6.2 shows that there is almost a limitless number of possible permutations which can be attempted during a systematic study. We have found previously, that even when some reactions do not follow the desired course, interesting and exploitable chemistry can still emerge. For example, when dealing with reactive organometallic complexes,  $\beta$ -hydride elimination can sometimes be an undesired complication. Some of the ligands outlined above do contain  $\beta$ -hydrogen atoms; however, it has previously been shown that similar bimetallic environments can inhibit complete degradation of the reactants to form ‘intermediate’ hydrido inverse crown structures [*e.g.*,  $[M_2Mg_2(DA)_4(\mu-H)_2 \cdot (toluene)_2]$ ,<sup>[104]</sup> where M = Na or K (chapter 1, section 1.4, Scheme 1.19)]. Indeed, it may be possible to utilise the  $\beta$ -hydride elimination ‘side-reaction’ to prepare the first ever inverse crown complex containing chiral ligands.

Thus far, the use of mixed-metal chiral systems in asymmetric synthesis has been in the main neglected. Independently, Hilmersson *et al.*<sup>[287]</sup> and Johansson and Davidsson<sup>[288]</sup> discovered that the rate of metallation of cyclohexene oxide was enhanced by mixed lithium/sodium chiral amides (in comparison with the individual metal amides); however, the stereoselectivity was diminished. The key difference between these systems and those introduced here are that in the former the organic substrate is formally alkali metallated; whereas in the latter it should be magnesiated or zincated (hence, kinetically and conformationally more stable). This should have the effect of enhancing the stereoselectivity of the reaction. Therefore, the complexes prepared during this project (and those subsequently prepared) will be taken forward to be screened to ascertain whether they can be used to deprotonate or carry out further synthetic transformations on carefully selected organic substrates (Scheme 6.3) in a regioselective and enantioselective manner.



**Scheme 6.3** A selection of organic transformations which currently employ chiral lithium amides.

Scheme 6.3 outlines some of the transformations which currently employ chiral lithium amides to achieve enantioselectivity.<sup>[70e, 129c]</sup> For simplicity, no reaction conditions or addition reagents have been detailed. One may ponder the need to use alternative chemistry when it seems that the current systems work to an adequate degree; however, as the synergic systems described herein (chapter 1, sections 1.3-1.5) have already shown, an unexpected, high impact and unique chemistry is often obtainable. Two other important advantages that these new reagents possess over most lithium bases is that they are soluble in non-polar hydrocarbon solvents, and the synthetic chemistry can be carried out at ambient temperature rather than at

cryogenic temperatures. This former point is a major must-have synthetic feature for enantioselective synthesis since previously it has been shown that a loss of enantioselection is possible in ethereal solvents.<sup>[129c]</sup> It is our aim to use the aforementioned heterobimetallic bases in place of the more conventional lithium reagents. This will allow us to compare our bimetallic results directly with those of monometallic lithium (or magnesium) amides and to determine strengths, limitations and potential improvements to our methodology. As well as traditional synthetic screening of the new synergic reagents, the isolation and characterisation of the intermediate metal-containing species will be attempted – possibly giving an insight into the mechanistic details of the reaction and why enantioselection is (or indeed is not) achieved.

In the future more elaborate syntheses will be undertaken, including the enantioselective metallation of biaryls at ambient temperatures, as part of the synthesis of ligands with axial chirality (*e.g.*, BINAP) for asymmetric synthesis. In addition, we hope to prepare chiral variants of Knochel's 'turbo-Grignard' reagents using the chiral diamines mentioned earlier. These will be systematically screened in terms of their reactivity towards prochiral organic and metallocene substrates, utilising chiral gas chromatography to determine enantiomeric excess values.

### 6.2.2 (–)-Sparteine- and (*R,R*)-TMCDA-containing Alkali Metal Tris(HMDS)

#### Magnesiates

NMR studies conducted in  $d_8$ -THF solutions of the four lithium and sodium solvent-separated complexes (complexes **100-103**) and the two potassium contacted ion pair polymers (complexes **104** and **105**) revealed that the chiral diamines had been displaced by  $d_8$ -THF. This ligand displacement therefore implies that the chiral information associated with the alkali metal centres has been lost; this however would need to be proved or disproved by assessing their ability in certain enantioselective reactions (*e.g.*, deprotonation of prochiral ketones). The synthesis of contacted ion pair HMDS-containing lithium/sodium magnesiates which contain chiral donor ligands (as detailed previously) should also be attempted and their reactivity compared with their zincate analogues. In addition, the reactions which produced the polymeric motifs could be extended to Rb and Cs.

### 6.2.3 Conventional and Unconventional (–)-Sparteine- and (R,R)-TMCDA-containing Alkali Metal HMDS Complexes

Regarding the (–)-sparteine adducts of the synthetically important lithium and sodium bis(trimethylsilyl)amides, this chemistry will be extended to include (R,R)-TMCDA and other chiral diamines (as detailed previously), before chiral donor adducts of other alkali metal amides (such as TMP, DA, *cis*-DMP, diphenylamide *etc.*) will be explored.

The beginnings of the family of inverse crown ether anions could possibly be built upon by extending the chemistry to other alkali metal amides and donor ligands, perhaps even to mixed alkali metal systems; however, these complexes have been put on the back burner in favour of the investigation into the MAC complexes which stemmed from these studies (*vide infra*).

The reproducibility and rational synthesis of  $[(\text{NaHMDS})_2\{\text{}^n\text{Bu}_2\text{Mg}\cdot(\text{R,R})\text{-TMCDA}\}]_\infty$ , **110**, is vital, as the chiral component of the complex is coordinated to the magnesium centre and not the alkali metal centre; hence, we have an ideal complex to be put forward for enantioselective transformation reactions – the substrate to be metallated would be formally magnesiated. Subsequently, the lithium analogue could be prepared, and other chiral ligands utilised to form similar complexes in which the chirality of the complex is associated with the magnesium centre and their reactivity in asymmetric reactions explored.

During the writing of this thesis, Gros developed chiral organomagnesiates of the form “ $\text{LBuMgLi}$ ” [where L = (R,R)-TADDOL] and “ $\text{LBu}_2\text{MgLi}_2$ ” [where L = (R,R)-TADDOL or (R)-BIPHEN H2], which have been shown to be effective in promoting the bromine-magnesium exchange of 2-bromopyridine at room temperature, and the formed hetaryl magnesiates to be enantioselectively reactive towards various aldehydes, leading to the formation of chiral  $\alpha$ -substituted 2-pyridylcarbinols.<sup>[289]</sup> This work builds upon the works of Noyori and co-workers on the asymmetric alkylation of carbonyl derivatives utilising BINOL dilithium dialkylmagnesiates, reported back in 1988,<sup>[290]</sup> and represents the first example of an organomagnesiate-induced asymmetric exchange-addition sequence to be reported. However, the trapping of the aldehyde in these reactions has to be carried out at subambient temperatures (as low as  $-100^\circ\text{C}$  to achieve good enantioselectivity); hence, of great synthetic advantage is the possibility that complex **110** or others similar (particularly its lithium analogue) could be utilised in comparable reactions at higher temperatures.

In probing the formation of complex **110**, multinuclear NMR spectroscopic characterisation of the solid precipitate deposited from the reaction mixture, prior to the addition of the



diamine, may prove useful. To explain, if these studies established the formation of the unsolvated magnesiate “ $\text{NaMg}(\text{HMDS})^n\text{Bu}_2$ ” (utilising NaHMDS in the reaction mixture, thus alleviating the need to use  $^n\text{BuNa}$  as the sodium source), the formation of the inverse magnesiate could possibly be attributed to the cleavage of this mixed-metal complex, when the diamine is introduced, into its homometallic components,  $(\text{NaHMDS})_2$  and  $[^n\text{Bu}_2\text{Mg}\cdot(\text{R,R})\text{-TMCDA}]$ , which must recombine to form **110**. Utilisation of more basic amides in the reaction system, such as NaTMP for example, would presumably give rise to contacted ion pair motifs – *i.e.*, formation of stronger Mg–N bonds, which would be resilient to cleavage in the presence of (R,R)-TMCDA.

### 6.3 Further Extensions to the Work Contained Within Chapter 4

Chapter 4 looked at new developments in lithium and sodium amide chemistry; capturing halides to form *metal anionic crowns* (MAC complexes). A series of these complexes were prepared and characterised, forming the beginnings of an exciting new Group 1 macrocyclic/supramolecular family of complexes.<sup>[260]</sup> The novel complexes represent the perfect inverse of conventional crown ether complexes having a metal-anion, host-guest pair within an anionic environment.

This unexpected new development in inverse crown chemistry will be of high interest to coordination and macrocyclic chemists and also, due to the importance of alkali metal amides in fine chemical and pharmaceutical manufacture, to synthetic chemists. The new area of metal anionic crowns can be pushed forward and developed in several ways: by investigating the solid- and solution-structural chemistry of these systems; the synthetic chemistry of the new complexes; and their utilisation in anion coordination and recognition chemistry.

#### 6.3.1 Solid- and Solution-Structural Chemistry of MAC Complexes

Due to the unequivocal and inextricable relationship between structure and reactivity, it is important to systematically study the solid- and solution-structural chemistry of these new systems. X-ray crystallography and multinuclear NMR spectroscopy have already been utilised effectively in contributing to the achievement of this goal; however, DFT calculations and DOSY studies are required to further assist in the transformation of this novel, unusual chemistry into a predictable, well understood class of compounds. In addition, if  $^6\text{LiCl}$  were to be used instead of  $^7\text{LiCl}$  within our reaction systems (designed to produce lithium chloride-containing MAC complexes) and a  $^6\text{Li}$  NMR spectrum obtained, would the chemical shift obtained correspond to one of the signals observed in the  $^7\text{Li}$  spectrum? Hence, allowing the

identification of the position of the lithium metal associated with the LiCl unit (*i.e.*, would it be present in the cation or in the anion of the complex?).

Moving to the possible synthetic routes utilised to achieve these complexes, the ammonium salt route, and to a greater extent the organoammonium salt route, should be explored for each particular system (if not already done so), as thus far these approaches have been the most effective and high-yielding. With regard to the vast array of variables within these reactions, a multitude of possible combinations of alkali metal amide, alkali metal halide and donor ligand is feasible.

Thus far, we have mainly concentrated on lithium and sodium bis(trimethylsilyl)amide systems, successfully forming ten-membered (MN)<sub>5</sub> rings which play host to anionic guests. Future work includes: the repeat of  $[\text{Li}\{(R,R)\text{-TMCD}\}_2]^+[\text{Li}_5(\mu\text{-HMDS})_5(\mu_5\text{-Br})]^-$ , **116** and  $[\text{Me}_6\text{-TREN}\cdot\text{Na}(\mu\text{-I})\text{Na}\cdot\text{Me}_6\text{-TREN}]^+[\text{Na}_5(\mu\text{-HMDS})_5(\mu_5\text{-I})]^-$ , **128**, to obtain better X-ray quality crystals; carrying out more reactions utilising KHMDS and KX to try and obtain potassium MAC complexes and investigating the trends in the ring sizes of the complexes obtained, and the position of the halide anion (with respect to the ring) captured therein; altering the stoichiometries of the reactions, for example, to try and obtain a sodium chloride-containing MAC complex, the quantity of NaHMDS added to the reaction could be systematically studied (*i.e.*, in the hope of forming a smaller NaN ring which would adequately sequester a chloride anion); trying different donor ligands of various denticities, atom compositions and steric properties to see what effects they may induce in the compositions of the cations of the MAC complexes; and further probing into the capture of fluoride and hydride anions within both the lithium and sodium amide systems.

If these initial steps forward could be achieved, the possibility of extending the chemistry to Rb and Cs should be explored, with the aim of producing larger host ring systems allowing the capture of larger anions [perhaps even organic in nature – the ‘pseudo’ halides already employed in the reactions utilised ideally to have produced lithium MAC complexes (section 4.3.4, [Figure 4.18](#)) are ideal candidates here] or more than one anion. In addition, two or more different anions could be utilised to try and prepare mixed-halide MAC complexes.

Thus far the complexes which have been obtained are homometallic in nature. By systematically combining different ratios of amides and halides of two different alkali metals, it may be possible to produce heterobimetallic rings, crucially again changing the ring dimensions and hence anion capture properties. There is also precedent for the +2 oxidation state metal systems to be investigated, as Hernández and Grévy recently reported the isolation

of two new inverse crown ether structures of the form  $[M_4(\text{Me}_3\text{SiNPPh}_2\text{CH}_2)_4(\mu_4\text{-O})(\mu_2\text{-Cl})_2]$  (where  $M = \text{Mg/Zn}$ ), in which one  $\text{O}^{2-}$  and two  $\text{Cl}^-$  ions have been encapsulated by polar organometallic complexes in a tetrameric arrangement.<sup>[291]</sup> These novel complexes were prepared by the reaction of  $[\text{Me}_3\text{SiNPPh}_2\text{CH}_3]$  with  $(\text{CH}_3)\text{CHMgCl}$  or  $^t\text{BuLi/ZnCl}_2$  respectively, and akin to the synthesis of previously reported inverse crown ethers (and the novel inverse crown ether anions reported herein), the chalcogen source in these complexes was attributed to either air contamination ( $\text{O}_2$  or  $\text{H}_2\text{O}$ ) of the reaction medium or to the presence of traces of metal oxide or hydroxide in the metallic starting material.

Another potentially exciting change is to alter the amide itself. Until now our work has been restricted to HMDS. The solid-state structures of the alkali metal complexes of this amide have been known for many years,<sup>[11a, 11b, 22, 27, 32]</sup> and the solution chemistry of  $\text{LiHMDS}$  has been studied extensively by Collum.<sup>[253]</sup> Intriguingly, despite the years of high quality research which have focused on this complex, a  $\text{Li}_5\text{HMDS}_5$  ring, to the best of our knowledge, has never been isolated or detected or even postulated to exist. Turning to other important utility amides will hopefully deliver further exciting chemistry. For instance, undoubtedly the most widely employed utility metal amide, LDA, is a prime target for our studies. Unsolvated LDA (crystallised from hexane) is polymeric in nature (chapter 1, section 1.1.3, [Figure 1.9](#)).<sup>[15]</sup> It is envisaged that using our systems, the polymer will behave as a molecular rope and lasso anions of various shapes and sizes resulting in the self-assembly of the inverse crown metallates. Thus, the systematic study of the complexation of LDA [and other amides such as TMP, diphenylamide, *cis*-DMP and various chiral amides ([Scheme 6.2](#))] with the range of anions alluded to earlier and the determination of the anion capture strengths and limitations of each system will also be undertaken in the near future.

As demonstrated by the excellent seminal review by Beer and Gale,<sup>[292]</sup> and the recent Chemical Society Reviews special issue (*Supramolecular chemistry of anionic species*)<sup>[293]</sup> anion capture and recognition continues to attract high quality research and considerable funding due to the field's importance in biological and environmental applications. Our new MAC systems represent a novel addition to this high interest and important field which will be fully studied.

### 6.3.2 Synthetic Chemistry of MAC Complexes

It has been highlighted that alkali metal halide salts play a pivotal role in enhancing the reactivity of Grignard reagents to 'turbo' status (reagents developed by Knochel<sup>[86k]</sup> – chapter 1, section 1.7 and chapter 4, introduction). In addition, it is widely regarded that ate

complexes have a higher reactivity than their neutral counterparts. Here, we have characterised complexes of alkali metal amides and alkali metal halides. This begs an intriguing series of questions. Will the synthetic chemistry of our new well-defined MAC complexes differ from that of the neutral amide LiHMDS (or NaHMDS)? Will the addition of the halide salt initiate a ‘turbo’-effect, akin to that of Knochel’s reagents? Or, will it tranquilise the reactivity of the amide, hence allowing syntheses to be conducted at more ambient temperatures than current technologies?

As detailed in chapter 1, alkali metal halide salts (particularly those of lithium) can produce substantial positive effects on the reactivity and/or selectivity of organic transformations.<sup>[176]</sup> Intriguingly, only small quantities of the additive are generally needed to achieve such effects.<sup>[178n, 178v]</sup> Could this sub-stoichiometric requirement be due to MAC formation? Hence, the investigation into any potential effects the lithium systems may impart on conventional lithium amide deprotonation reactions and other synthetically indispensable organic transformations such as enolisations, additions *etc.* will be pursued.

### 6.3.3 Non-MAC Mixed Alkali Metal Amide-Alkali Metal Halide Complexes

Future studies will focus on the preparation of each complex rationally (if not already done so) and the synthesis of similar systems by altering the alkali metal amide, alkali metal halide (or organic halide) and donor ligand employed in the reactions. A systematic approach is required to cover all possible combinations of these reagents. For example, would a similar structural motif to that observed for  $[\{(R,R)\text{-TMCDA}\cdot\text{LiI}\}_2(\text{LiHMDS})_2]_\infty$ , **129**, be obtained if NaHMDS/KHMDS were to be utilised in place of LiHMDS?

If the fluoride analogue of **130** could be obtained, this would complete the series of Me<sub>6</sub>-TREN-solvated lithium halide monomers (however, due to the high lattice energy of lithium fluoride this may prove considerably difficult). The synthesis of sodium and potassium analogues should be attempted, along with the systematic study of the complexation of metal halides to other amides (*vide supra*). (*R,R*)-TMCDA has already been investigated in this capacity, forming dimeric species of the form  $[(R,R)\text{-TMCDA}\cdot\text{LiX}]_2$  (where X = Cl, Br or I). Again, the synthesis of sodium and potassium variants should be attempted, along with fluoride analogues.

Further investigation is required into the reaction which produced  $[\text{Me}_6\text{-TREN}\cdot\text{Na}(\mu\text{-I})\text{Na}(\mu\text{-HMDS})_2\text{Na}(\mu\text{-I})\text{Na}\cdot\text{Me}_6\text{-TREN}]$ , **131**, as essentially the same reaction produced the MAC complex  $[\text{Me}_6\text{-TREN}\cdot\text{Na}(\mu\text{-I})\text{Na}\cdot\text{Me}_6\text{-TREN}]^+[\text{Na}_5(\mu\text{-HMDS})_5(\mu_5\text{-I})]^-$ , **128**. The ‘pseudo’ halide reactions concentrated solely on LiHMDS/(*R,R*)-TMCDA systems; thus these reactions

---

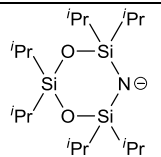
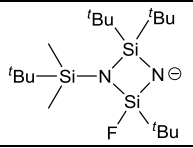
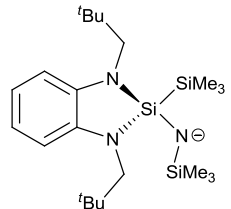
can be extended to NaHMDS and KHMDS systems and to the incorporation of Me<sub>6</sub>-TREN in place of (*R,R*)-TMCDA.

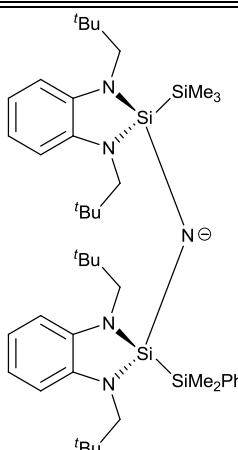
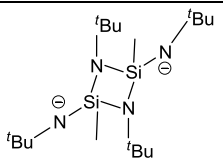
Regarding [Me<sub>6</sub>-TREN·K(μ-HMDS)K(μ-HMDS)<sub>2</sub>K(μ-HMDS)K·Me<sub>6</sub>-TREN], **134**, as this complex has formally opened up the dimer of donor-free KHMDS through the coordination of Me<sub>6</sub>-TREN, could a similar scenario occur with the entrapment of donor-free LiHMDS/NaHMDS by Me<sub>6</sub>-TREN? (*i.e.*, would the trimeric units be opened up?).

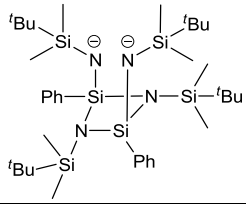
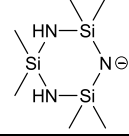
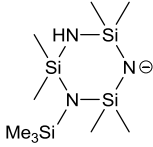
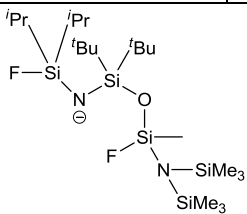
As reactions utilising LiHMDS and 12-crown-4 repeatedly produced the previously published monomer [LiHMDS·12-crown-4],<sup>[36]</sup> **24**, and those which utilised KHMDS and 12-crown-4 produced the dimer [KHMDS·12-crown-4]<sub>2</sub>, **136**, revisiting the NaHMDS-12-crown-4 reaction is imperative. Manipulation of the reaction conditions (for example, slowing down the cooling process of the reaction mixture by immediately placing the Schlenk tube in a hot water-filled Dewar flask once the solution had been heated to reflux) should hopefully produce X-ray quality crystals from the solution, as microcrystalline material was deposited from the initial reaction undertaken. If this were to be achieved, it would complete a homologues series of 12-crown-4-solvated alkali metal HMDS complexes. It will be interesting to note what type of motif the 12-crown-4 adduct of NaHMDS adopts; will a similar scenario to that observed for the homologues series of TMEDA-solvated alkali metal HMDS complexes (chapter 2, section 2.2) be witnessed here? 15-Crown-5 and 18-crown-6 should also be utilised within these reaction systems to build up a series of complexes, thus allowing investigation into the effect of the ring size of the crown ethers on the structural motifs obtained.

Finally, extending the chemistry of the non-MAC complexes to Rb and Cs should be explored.

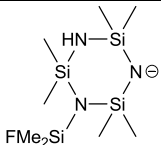
## Appendix I

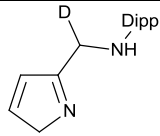
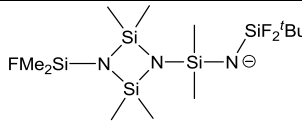
Crystallographically Characterised Solvated Lithium Bis(silyl)amides			
NR <sub>2</sub>	Donor Ligand	Aggregation State	Reference
N(SiMe <sub>3</sub> ) <sub>2</sub>	12-crown-4	monomer	[36a]
N(SiPh <sub>2</sub> Me) <sub>2</sub>	2 THF	monomer	[294]
N(SiPh <sub>3</sub> ) <sub>2</sub>	2 THF	monomer	[294]
N(SiPh <sub>2</sub> Me) <sub>2</sub>	12-crown-4	monomer	[294]
N(Si <sup>t</sup> Bu <sub>2</sub> F) <sub>2</sub>	2 THF	monomer	[295]
N(Si <sup>t</sup> Bu <sub>2</sub> F){SiO(SiMe <sub>3</sub> )(Mes) <sub>2</sub> }		monomer	[296]
N(Si <sup>t</sup> Bu <sub>2</sub> Cl)(Si <sup>i</sup> Pr <sub>2</sub> O <sup>t</sup> Bu)	2 THF	monomer	[296]
N(Si <sup>t</sup> Bu <sub>2</sub> Me){SiF <sub>2</sub> N(SiMe <sub>3</sub> )}(Si <sup>t</sup> Bu <sub>2</sub> Me)	2 THF	monomer	[12c]
N(SiMe <sub>3</sub> ) <sub>2</sub>	TMEDA	monomer	[182]
N(SiMe <sub>3</sub> ) <sub>2</sub>	PMDETA	monomer	[182]
N(Si <sup>t</sup> Bu <sub>2</sub> Me)(Si <sup>t</sup> Bu <sub>2</sub> F)	NEt <sub>3</sub>	monomer	[297]
N(Si <sup>t</sup> Bu <sub>2</sub> F)(Si <sup>t</sup> Bu <sub>2</sub> H)	2 THF	monomer	[298]
N{Si <sup>i</sup> Pr <sub>2</sub> O(SiMe <sub>3</sub> ) <sub>2</sub> }	TMEDA	monomer	[299]
	TMEDA	monomer	[299]
N(Si <sup>t</sup> Bu <sub>2</sub> F){Si <sup>t</sup> Bu <sub>2</sub> (2-furyl)}	2 THF	monomer	[300]
	TMEDA	monomer	[301]
	TMEDA	monomer	[302]

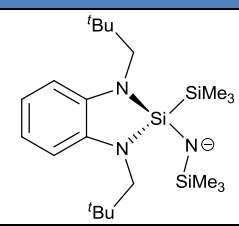
	THF	monomer	[302]
$N(\text{SiPh}_2^t\text{Bu})(\text{SiMe}_3)$	2 THF	monomer	[10i]
$N(\text{SiPh}_2^t\text{Bu})(\text{SiMe}_3)$	2 pyridine	monomer	[10i]
$N(\text{SiPh}_2^t\text{Bu})(\text{SiMe}_3)$	2 HMPA	monomer	[10i]
$N(\text{SiPh}_3)(\text{SiMe}_3)$	2 pyridine	monomer	[10i]
$N\{\text{Si}(\text{SiMe}_3)_3\}(\text{SiMe}_3)$	2 pyridine	monomer	[10i]
$N(\text{Si}^t\text{Bu}_2\text{Me})_2$	THF	monomer	[303]
$N(\text{SiMe}_3)_2$	Me <sub>6</sub> -TREN	monomer	[252]
$N(^t\text{Bu})\text{SiMe}(\mu\text{-N}^t\text{Bu})_2\text{SiMe}(^t\text{Bu})\text{N}$		dinuclear monomer	[304]
	2 Et <sub>2</sub> O	dinuclear monomer	[304]
$[\text{Me}^t\text{Bu}_2\text{Si-N-SiF}_2\text{-N-Si}^t\text{Bu}_2\text{Me}]$	THF	dinuclear monomer	[305]
$[\text{N}(\text{SiMe}_3)\{\text{SiN}(\text{H})\text{SiMe}_3\}\text{N}(\text{SiMe}_3)]_2$	2 THF	dinuclear monomer	[21f]
$\text{cyc-}\{\text{N}(\text{SiMe}_2)\text{CH}_2\text{P}(\text{Ph})\text{CH}_2(\text{SiMe}_2)\}_2$	2 THF	dinuclear monomer	[306]
$\text{cyc-}\{\text{N}(\text{SiMe}_2)\text{CH}_2\text{P}(\text{Ph})\text{CH}_2(\text{SiMe}_2)\}_2$	THF	dinuclear monomer	[306]
$N(^t\text{Bu})\text{SiMe}(\mu\text{-N}^t\text{Bu})_2\text{SiMe}(^t\text{Bu})\text{N}$	2 THF	dinuclear monomer	[307]
$\text{cyc-}\{\text{N}(\text{SiMe}_2)\text{CH}_2\text{P}(\text{cy-hexyl})\text{CH}_2(\text{SiMe}_2)\}_2$		dinuclear monomer	[308]
$[\text{N}(\text{SiMe}_3)\{\text{SiMe}_2\text{N}(\text{SiMe}_3)\text{CH}_2\}]_2$	2 THF	dinuclear monomer	[21x]
$[\text{N}(\text{SiMe}_3)\{\text{SiMe}_2\text{N}(\text{SiMe}_3)\text{CH}_2\}]_2$	2 TMEDA	dinuclear monomer	[21x]
$[\text{N}(\text{SiMe}_3)\{\text{SiMe}_2\text{N}(\text{SiMe}_3)\}]_2$	2 THF	dinuclear monomer	[309]
$\{\text{N}(\text{SiMe}_3)(\text{SiMe}_2)\text{N}(\text{SiMe}_3)\}_2$		dinuclear monomer	[309]
$\text{cyc-}\{\text{N}(\text{SiMe}_2\text{O})(\text{SiMe}_2)(\text{SiMe}_2\text{O})\}_2$		dinuclear monomer	[310]

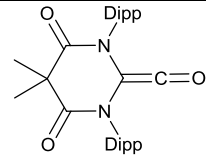
$N(\text{Si}^t\text{Bu}_2\text{Me})(\text{Si}^t\text{Bu}_2)N(\text{Si}^t\text{Bu}_2\text{Me})$	2 12-crown-4 and THF	dinuclear monomer (solvent-separated)	[305]
	4 THF	dinuclear monomer (solvent-separated)	[311]
$N(\text{SiMe}_3)_2$	2 12-crown-4	dinuclear monomer (solvent-separated)	[312]
$\{N(\text{SiMe}_3)(\text{SiMe}_2\text{O})\}_3\text{Si}^t\text{Bu}$		trinuclear monomer	[313]
$\{N(\text{SiMe}_2^t\text{Bu})\}_3\text{SiPh}$	3 THF	trinuclear monomer	[314]
$N(\text{SiMe}_3)_2$	fluorobenzene	mono-solvated dimer	[315]
$N(\text{SiMe}_3)_2$	1,2-difluorobenzene	mono-solvated dimer	[315]
$N(\text{SiMe}_3)\text{Si}(\text{H})\{N(\text{H})\text{SiMe}_3\}_2$	THF	mono-solvated dimer	[21f]
$N\{\text{SiMe}_2(5\text{-SiMe}_3\text{-2-furyl})\}_2$	THF	mono-solvated dimer	[316]
$N(\text{SiMe}_3)_2$	$\text{Et}_2\text{O}$	dimer	[12a, 37a]
	THF	dimer	[317]
$N(\text{SiMe}_3)_2$	THF	dimer	[37c, 37d]
	THF	dimer	[318]
		dimer	[319]
$N(\text{SiMe}_3)_2$	$\text{O}=\text{CO}^t\text{Bu}^i\text{Pr}$	dimer	[320]
$N(\text{SiMe}_3)_2$	$\text{O}=\text{CO}^t\text{Bu}_2$	dimer	[320]
$N(\text{Si}^t\text{Bu}_2\text{F})\{\text{Si}^i\text{Pr}_2\text{O}(\text{SiMe}_3)\}$		dimer	[321]

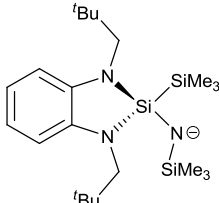
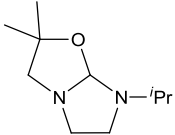
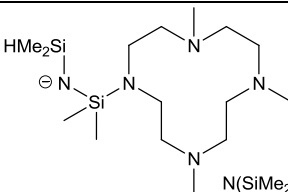


$N(SiMe_3)_2$	$N\equiv C-tBu$	dimer	[322]
$N\{SiMe_3Si(NMe_2)_3\}$		dimer	[323]
$N\{Si(NMe_2)_3\}_2$		dimer	[323]
$N(Si^tBu_2Me)(Si^tBu_2F)$		dimer	[324]
$N(SiMe_2O^tBu)_2$		dimer	[325]
$N(SiMe_3)_2$	$O=PPh_2Me$	dimer	[326]
$N(SiMe_2CH_2NMe_2)_2$		dimer	[327]
$N(SiMe_3)_2$	$NMe_2CH_2Ph$	dimer	[182]
$N(SiMe_3)_2$	$OMe(CH_2)_2OMe$	dimer	[182]
$N(SiMe_3)_2$	dioxane	dimer	[182]
$N(SiMe_3)_2$	$C\equiv N-Ph$	dimer	[328]
$N(SiMe_2NMe_2)_2$		dimer	[10e]
$N(SiMe_2NEt_2)_2$		dimer	[10e]
$N\{SiMe_2N(H)^iPr\}_2$		dimer	[10e]
$N(SiMe_2OPh)_2$		dimer	[10e]
$N\{SiMe_2O(SiMe_3)\}_2$		dimer	[10e]
$N\{SiMe_2(2-furyl)\}_2$		dimer	[10e]
$N(SiMe_3)_2$	$NH_2CH_2CMe_2CH_2NMe_2$	dimer	[329]
$N(SiMe_3)_2$	$NH_2(CH_2)_3NH_2$	dimer	[329]
$N(Si^tBu_2F)\{Si^tBu_2(2-furyl)\}$		dimer	[300]
$N(SiMe_3)_2$	TEMPO	dimer	[193f]
$N(SiMe_3)_2$	pyridine	dimer	[38]
	THF	dimer	[330]
$N\{Si^tBu_2O(SiMe_3)\}\{SiF_2N(SiMe_3)_2\}$		dimer	[331]
$N\{Si^tBu_2O(SiMe_3)\}\{SiF_2(2,4,6-tBuC_6H_2)\}$		dimer	[331]
$N(SiMe_3)_2$	$Et_2O$	dimer	[332]
$N(SiMe_3)_2$	$N\equiv C-Ad$	dimer	[26]
$N(SiMe_3)\{SiMe_2N(H)SiMe_3\}$	THF	dimer	[11j]
$N\{SiMe_2(5-Me-2-furyl)\}_2$		dimer	[316]
$N(SiMe_3)_2$	2-ethylbenzotrile	dimer	[333]
$N\{SiMe_2(CH_2)_2SiMe_2\}$	THF	dimer	[334]
<i>cyc</i> - $\{N(SiMe_2)N(H)(SiMe_2)\}_2$	THF	tetranuclear dimer	[335]
<i>cyc</i> - $\{N(SiMe_2)N(H)(SiMe_2)\}_2$	TMEDA	tetranuclear dimer	[336]
$N(SiMe_3)\{Si(H)N(SiMe_3)_2\}N(SiMe_3)$		tetranuclear	[21g]

		dimer	
$N(\text{SiMe}_2^t\text{Bu})(\text{SiMe}_2)N(\text{SiMe}_2^t\text{Bu})$		tetranuclear dimer	[337]
$N(\text{SiMe}_2^t\text{Bu})(\text{Si}^i\text{Pr}_2)N(\text{SiMe}_2^t\text{Bu})$		tetranuclear dimer	[337]
$N(\text{SiMe}_3)_2$	$\text{NHCH}_2\text{CMe}_2\text{CH}_2\text{NMe}_2$	tetranuclear dimer	[329]
$N(\text{SiMe}_2^t\text{Bu})\{\text{Si}^i\text{Pr}(\text{CH}_2)_2\text{CHCH}_2\}N(\text{SiMe}_2^t\text{Bu})$		tetranuclear dimer	[338]
$N(\text{SiMe}_3)_2$		tetranuclear dimer	[339]
$N(\text{SiMe}_3)_2$	1,4-difluorobenzene	polymer	[315]
		polymer	[340]
$N(\text{SiMe}_3)_2$	dioxane	polymer	[182]

Crystallographically Characterised Solvated Sodium Bis(silyl)amides			
$\text{NR}_2$	Donor Ligand	Aggregation State	Reference
	3 THF	monomer	[302]
$N\{\text{SiH}(\text{Mes})_2\}_2$	$\text{Et}_2\text{O}$	monomer	[341]
$N(\text{SiMe}_2\text{O}^t\text{Bu})(\text{SiMe}_3)$	bipyridyl	mono-solvated dimer	[342]
$N(\text{SiMe}_2\text{Ph})(\text{SiMe}_3)$	TMEDA	mono-solvated dimer	[10g]
$N(\text{SiMe}_3)_2$	THF	mono-solvated dimer	[343]
$N(\text{SiMe}_2\text{O}^t\text{Bu})(\text{SiMe}_3)$		dimer	[344]
$N(\text{SiMe}_2\text{O}^t\text{Bu})(\text{SiMe}_3)$	pyridine	dimer	[342]
$N(\text{SiMe}_3)_2$	THF	dimer	[206]
$N(\text{SiMe}_3)_2$	TEMPO	dimer	[193f]
$N(\text{SiMe}_3)_2$	$\text{N}\equiv\text{C}-^t\text{Bu}$	dimer	[26, 202a]
$N(\text{SiMe}_2\text{Ph})(\text{SiMe}_3)$	$\text{N}\equiv\text{C}-^t\text{Bu}$	dimer	[26]
$N(\text{SiMe}_3)_2$	$\text{N}\equiv\text{C}-\text{Ad}$	dimer	[26]
$N(\text{SiMe}_2\text{Ph})(\text{SiMe}_3)$	$\text{N}\equiv\text{C}-\text{Ad}$	dimer	[26]
$N(\text{SiMe}_2\text{Ph})_2$	THF	dimer	[345]

$N(\text{SiMe}_3)_2$		dimer	[256]
$\text{cyc-}\{N(\text{SiMe}_2)N(\text{H})(\text{SiMe}_2)\}_2$	THF	tetranuclear dimer	[336]
$N(\text{SiMe}_3)_2$	dioxane	polymer	[205]
$N(\text{SiMe}_3)_2$	TMPDA	polymer	[182]
$N(\text{SiMe}_3)_2$	ferrocene	polymer	[193n]

Crystallographically Characterised Solvated Potassium Bis(silyl)amides			
$\text{NR}_2$	Donor Ligand	Aggregation State	Reference
$N(\text{SiMe}_3)_2$	2 dioxane	monomer	[346]
$N(\text{SiMe}_3)_2$	18-crown-6	monomer	[345]
	3 THF	monomer	[302]
$N(\text{SiMe}_2\text{Ph})_2$	18-crown-6	monomer	[345]
$N(\text{SiPh}_2\text{Me})_2$	PMDETA	monomer	[29]
$N(\text{Si}^i\text{Bu}_2\text{H})(\text{SiMe}_3)$	THF	mono-solvated dimer	[347]
$N(\text{SiMe}_2\text{O}^i\text{Bu})(\text{SiMe}_3)$		dimer	[344]
$N(\text{SiMe}_2\text{O}^i\text{Bu})(\text{SiMe}_3)$	bipyridyl	dimer	[342]
$N(\text{SiMe}_3)_2$	$:\text{C}(\text{N}^i\text{Pr})_2(\text{CH}_2)_3$	dimer	[348]
$N(\text{SiMe}_2\text{Ph})_2$	toluene	dimer	[345]
$N\{\text{SiMe}_2(2\text{-furyl})\}_2$	toluene	dimer	[316]
$N\{\text{SiMe}_2(5\text{-Me-2-furyl})\}_2$	toluene	dimer	[316]
$N(\text{SiMe}_3)_2$		dimer	[349]
$N(\text{SiMe}_3)_2$	$:\text{C}(\text{NDipp})_2(\text{CH}_2)_2$	dimer	[193s]
		dimer	[350]
$N(\text{SiMe}_3)_2$	ferrocene	polymer	[193n]
$N(\text{SiPh}_2\text{Me})_2$	THF	polymer	[29]
$N(\text{SiPh}_2\text{Me})_2$	18-crown-6	polymer	[29]

1	[LiN(SiMe <sub>3</sub> ) <sub>2</sub> ] <sub>3</sub>	27	[(LDA) <sub>2</sub> ·TMEDA] <sub>∞</sub>	52	[{(-)-sparteine}·Na(μ-TMP)(μ- <sup>n</sup> Bu)Mg(TMP)]
2	[Li(TMP)] <sub>4</sub>	28	[{LiNH(PhCH <sub>2</sub> ) <sub>2</sub> ·THF] <sub>∞</sub>	53	[ <sup>t</sup> BuLi·(R,R)-TMCDA]
3	[LiNH(Si <sup>t</sup> Bu <sub>2</sub> Me)] <sub>4</sub>	29	[Li <sub>2</sub> {cyc-N(CH <sub>2</sub> ) <sub>3</sub> CH <sub>2</sub> ] <sub>2</sub> ·TMEDA] <sub>2</sub>	54	[MeLi·(R,R)-TMCDA] <sub>2</sub>
4	[Li{cyc-N(CH <sub>2</sub> ) <sub>5</sub> CH <sub>2</sub> }] <sub>6</sub>	30	[Li <sub>3</sub> {cyc-N(CH <sub>2</sub> ) <sub>3</sub> CH <sub>2</sub> ] <sub>3</sub> ·PMDETA] <sub>2</sub>	55	[ <sup>s</sup> BuLi·(R,R)-TMCDA]
5	[LiNH( <sup>t</sup> Bu)] <sub>8</sub>	31	[NaTMP·THF] <sub>2</sub>	56	[ <sup>i</sup> PrLi·(R,R)-TMCDA] <sub>2</sub>
6	[LiN <sup>i</sup> Pr <sub>2</sub> ] <sub>∞</sub>	32	[{Na(NMe <sub>2</sub> ) <sub>2</sub> ] <sub>12</sub> ·(TMEDA) <sub>4</sub> ]	57	[ <sup>n</sup> BuLi·(R,R)-TMCDA] <sub>2</sub>
7	[NaN(SiMe <sub>3</sub> ) <sub>2</sub> ] <sub>∞</sub>	33	[KTMP·TMEDA] <sub>2</sub>	58	[( <sup>n</sup> BuLi) <sub>2</sub> ·(R,R)-TMCDA] <sub>2</sub>
8	[NaN(SiMe <sub>2</sub> H) <sub>2</sub> ] <sub>∞</sub>	34	<i>trans</i> -[{KN( <sup>t</sup> Bu)(SiMe <sub>3</sub> ) <sub>4</sub> (η <sup>6</sup> -C <sub>6</sub> H <sub>6</sub> ) <sub>2</sub> ]	59	[ <sup>t</sup> BuLi·(R,R)-TMCDA-Li] <sub>2</sub>
9	<i>trans</i> -[NaN(SiMe <sub>2</sub> Ph)(SiMe <sub>3</sub> )] <sub>∞</sub>	35	[(THF)·Li(μ-TMP)(μ- <sup>t</sup> Bu)Zn( <sup>t</sup> Bu)]	60	[LiZn(TMP) <sub>3</sub> ]
10	[Na(TMP)] <sub>3</sub>	36	[Li <sub>2</sub> Mg <sub>2</sub> {N(SiMe <sub>3</sub> ) <sub>2</sub> ] <sub>4</sub> (O <sub>2</sub> ) <sub>x</sub> (O) <sub>y</sub> ]	61	[(PMDETA)·K(μ-TMP)(μ-CH <sub>2</sub> SiMe <sub>3</sub> )Zn(CH <sub>2</sub> SiMe <sub>3</sub> )]
11	[NaN( <sup>t</sup> Bu)(SiMe <sub>3</sub> )] <sub>3</sub>	37	[(TMEDA)·Na(μ-TMP)(μ- <sup>n</sup> Bu)Mg(TMP)]	62	[(TMEDA)·Li(μ-DA)(μ- <sup>t</sup> Bu)Zn( <sup>t</sup> Bu)]
12	[KN(SiMe <sub>3</sub> ) <sub>2</sub> ] <sub>∞</sub>	38	[(TMEDA)·Na(μ-TMP)(μ- <sup>t</sup> Bu)Zn( <sup>t</sup> Bu)]	63	[(TMEDA)·Na(μ-DA)(μ- <sup>t</sup> Bu)Zn( <sup>t</sup> Bu)]
13	[KN(SiMe <sub>2</sub> H) <sub>2</sub> ] <sub>∞</sub>	39	[(TMEDA)·Na(μ-TMP)(μ-CH <sub>2</sub> SiMe <sub>3</sub> )Zn(CH <sub>2</sub> SiMe <sub>3</sub> )]	64	[(TMEDA)·Na(μ-DA) <sub>2</sub> Zn( <sup>t</sup> Bu)]
14	[KN(SiPh <sub>2</sub> Me) <sub>2</sub> ] <sub>∞</sub>	40	[(TMEDA)·Li(μ-TMP)(μ- <sup>n</sup> Bu)Zn( <sup>n</sup> Bu)]	65	[(TMEDA)·Na(μ- <sup>t</sup> Bu) <sub>2</sub> Zn( <sup>t</sup> Bu)]
15	[KN{SiMe <sub>3</sub> }{Si(SiMe <sub>3</sub> )(1,2-C <sub>6</sub> H <sub>4</sub> (Np) <sub>2</sub> )] <sub>∞</sub>	41	(R,R)-[(TMEDA)·Na{μ-N(CH <sub>2</sub> Ph)(CH(CH <sub>3</sub> )Ph)}(μ- <sup>t</sup> Bu)Zn( <sup>t</sup> Bu)]	66	[(TMTA)·Li(μ-HMDS)Zn(CH <sub>2</sub> SiMe <sub>3</sub> ) <sub>2</sub> ]
16	<i>trans</i> -[KN(SiMe <sub>2</sub> Ph)(SiMe <sub>3</sub> )] <sub>∞</sub>	42	[ <sup>t</sup> BuLi·(-)-sparteine]	67	[(PMDETA)·Li(μ-HMDS)Zn(Me) <sub>2</sub> ]
17	<i>trans</i> -[KN(SiMe <sub>2</sub> <sup>t</sup> Bu)(SiMe <sub>3</sub> )] <sub>∞</sub>	43	[ <sup>n</sup> BuLi·(-)-sparteine] <sub>2</sub>	68	[(TMEDA)·Na(μ-TMP)(μ-CH <sub>2</sub> SiMe <sub>3</sub> )Mg(TMP)]
18	[RbN(SiMe <sub>3</sub> ) <sub>2</sub> ] <sub>2</sub>	44	[Et <sub>2</sub> O·( <sup>i</sup> PrLi) <sub>2</sub> ·(-)-sparteine]	69	[(TMEDA) <sub>3</sub> Na <sub>6</sub> Mg <sub>3</sub> -(CH <sub>2</sub> SiMe <sub>3</sub> )(2,5-C <sub>4</sub> H <sub>2</sub> O) <sub>3</sub> (2-C <sub>4</sub> H <sub>3</sub> O) <sub>5</sub> ] <sub>2</sub>
19	[RbN(SiPh <sub>2</sub> Me) <sub>2</sub> ] <sub>∞</sub>	45	[MeLi·(-)-sparteine] <sub>2</sub>	70	[LiMg(DA) <sub>3</sub> ]
20	<i>trans</i> -[RbN(SiMe <sub>2</sub> Ph)(SiMe <sub>3</sub> )] <sub>∞</sub>	46	[Ph <sub>4</sub> Li <sub>4</sub> ·{(-)-sparteine} <sub>2</sub> ]	71	[NaMg(DA) <sub>3</sub> ]
21	[CsN(SiMe <sub>3</sub> ) <sub>2</sub> ] <sub>2</sub>	47	[PhMe <sub>2</sub> SiLi·(-)-sparteine·thf]	72	[(TMEDA)Li( <i>cis</i> -DMP)] <sub>∞</sub>
22	<i>trans</i> -[CsN(SiMe <sub>2</sub> Ph)(SiMe <sub>3</sub> )] <sub>∞</sub>	48	[Ph <sub>2</sub> (Et <sub>2</sub> N)SiLi·(-)-sparteine]	73	[( <i>cis</i> -DMP)Al(H <sub>2</sub> ) <sub>2</sub> ] <sub>2</sub>
23	[CsNH(SiMe <sub>3</sub> )] <sub>∞</sub>	49	[Ph <sub>2</sub> MeSiLi·(-)-sparteine·thf]	74	[(PMDETA)·K(μ- <i>cis</i> -DMP)(μ- <sup>t</sup> Bu)Al( <sup>t</sup> Bu) <sub>2</sub> ]
24	[LiHMDS·12-crown-4]	50	[Ph(Et <sub>2</sub> N) <sub>2</sub> SiLi·(-)-sparteine·thf]	75	[(TMEDA)·Li(μ- <i>cis</i> -DMP)Zn( <sup>t</sup> Bu) <sub>2</sub> ]
25	[LiN(PhCH <sub>2</sub> ) <sub>2</sub> ·HMPA] <sub>2</sub>	51	[Me <sub>3</sub> SiCH <sub>2</sub> Li·(-)-sparteine] <sub>2</sub>		
26	<i>trans</i> -[LiN(Me)Ph·TMEDA] <sub>2</sub>				

76	[(TMEDA)·Na(μ- <i>cis</i> -DMP)(μ- <sup>t</sup> Bu)Zn( <sup>t</sup> Bu)]	100	[Li{(-)-sparteine} <sub>2</sub> ] <sup>+</sup> [Mg(HMDS) <sub>3</sub> ] <sup>-</sup>	123	[Me <sub>6</sub> -TREN·LiCH <sub>2</sub> Ph]
77	[(TMEDA)·Na(μ- <i>cis</i> -DMP) <sub>2</sub> Zn( <sup>t</sup> Bu)]	101	[Na{(-)-sparteine} <sub>2</sub> ] <sup>+</sup> [Mg(HMDS) <sub>3</sub> ] <sup>-</sup>	124	[PMDETA·Li(μ-Cl)Li·PMDETA] <sup>+</sup>
78	[(TMEDA)·Na(μ-DIBA) <sub>2</sub> Zn( <sup>t</sup> Bu)]	102	[Li{(R,R)-TMCDA} <sub>2</sub> ] <sup>+</sup> [Mg(HMDS) <sub>3</sub> ] <sup>-</sup>	125	[(THF) <sub>3</sub> ·Li(μ-Cl)Li·(THF) <sub>3</sub> ] <sup>+</sup>
79	[(TMEDA)·Na(μ- <i>cis</i> -DMP) <sub>2</sub> Mg( <i>cis</i> -DMP)]	103	[Na{(R,R)-TMCDA} <sub>2</sub> ] <sup>+</sup> [Mg(HMDS) <sub>3</sub> ] <sup>-</sup>	126	[Me <sub>6</sub> -TREN·Li(μ-Br)Li·Me <sub>6</sub> -TREN] <sup>+</sup> [Li <sub>4</sub> (μ-HMDS) <sub>4</sub> (μ <sub>4</sub> -OH)] <sup>-</sup>
80	[{ <i>cis</i> -DMP(H)}·Na(μ- <i>cis</i> -DMP) <sub>2</sub> Mg( <i>cis</i> -DMP)]	104	[{K·(-)-sparteine} <sup>+</sup> {Mg(HMDS) <sub>3</sub> }] <sub>∞</sub> <sup>-</sup>	127	[Me <sub>6</sub> -TREN·Na(μ-Br)Na·Me <sub>6</sub> -TREN] <sup>+</sup> [Na <sub>5</sub> (μ-HMDS) <sub>5</sub> (μ <sub>5</sub> -Br)] <sup>-</sup>
81	[(TMEDA)·Na(μ-DA) <sub>2</sub> Mg(DA)]	105	[{K·(R,R)-TMCDA} <sup>+</sup> {Mg(HMDS) <sub>3</sub> }] <sub>∞</sub> <sup>-</sup>	128	[Me <sub>6</sub> -TREN·Na(μ-I)Na·Me <sub>6</sub> -TREN] <sup>+</sup> [Na <sub>5</sub> (μ-HMDS) <sub>5</sub> (μ <sub>5</sub> -I)] <sup>-</sup>
82	[LiHMDS·TMEDA]	106	[LiHMDS·(-)-sparteine]	129	[{(R,R)-TMCDA·LiI] <sub>2</sub> (LiHMDS) <sub>2</sub> ] <sub>∞</sub>
83	[KHMDS·TMEDA] <sub>2</sub>	107	“[NaHMDS·(-)-sparteine]”	130	[Me <sub>6</sub> -TREN·LiI]
84	[(NaHMDS) <sub>2</sub> ·TMEDA] <sub>∞</sub>	108	[(-)-sparteine·Na(μ-HMDS)Na·(-)-sparteine] <sup>+</sup> [Na <sub>4</sub> (μ-HMDS) <sub>4</sub> (μ <sub>4</sub> -OH)] <sup>-</sup>	131	[Me <sub>6</sub> -TREN·Na(μ-I)Na(μ-HMDS) <sub>2</sub> Na(μ-I)Na·Me <sub>6</sub> -TREN]
85	[KHMDS·(R,R)-TMCDA] <sub>2</sub>	109	[Na{(R,R)-TMCDA} <sub>2</sub> ] <sup>+</sup> [Na <sub>4</sub> (μ-HMDS) <sub>4</sub> (μ <sub>4</sub> -OH)] <sup>-</sup>	132	[{(R,R)-TMCDA·Li(SCN)} <sub>2</sub> (LiHMDS) <sub>2</sub> ] <sub>∞</sub>
86	[KN <sup>t</sup> Pr <sub>2</sub> ·TMEDA] <sub>2</sub>	110	[(NaHMDS) <sub>2</sub> { <sup>n</sup> Bu <sub>2</sub> Mg·(R,R)-TMCDA}]] <sub>∞</sub>	133	[Li(SCN)·TMEDA] <sub>∞</sub>
87	[(NaHMDS) <sub>2</sub> ·TMPDA] <sub>∞</sub>	111	Li <sub>2</sub> [(PhC≡C) <sub>3</sub> Mg(TMEDA)] <sub>2</sub>	134	[Me <sub>6</sub> -TREN·K(μ-HMDS)K(μ-HMDS) <sub>2</sub> K(μ-HMDS)K·Me <sub>6</sub> -TREN]
88	[Na(TMEDA) <sub>2</sub> ] <sup>+</sup> [Mg(HMDS) <sub>3</sub> ] <sup>-</sup>	112	Na <sub>2</sub> [( <sup>t</sup> BuC≡C) <sub>3</sub> Mg(TMEDA)] <sub>2</sub>	135	[PMDETA·K{μ-CH(SiMe <sub>3</sub> ) <sub>2</sub> }K{μ-CH(SiMe <sub>3</sub> ) <sub>2</sub> } <sub>2</sub> K{μ-CH(SiMe <sub>3</sub> ) <sub>2</sub> }K·PMDETA]
89	[Li(TMEDA) <sub>2</sub> ] <sup>+</sup> [Mg(HMDS) <sub>3</sub> ] <sup>-</sup>	113	[{Na <sub>2</sub> (THF) <sub>3</sub> }{Mg <sub>2</sub> (TMEDA)}(2-C <sub>4</sub> H <sub>3</sub> O) <sub>6</sub> ] <sub>∞</sub>	136	[KHMDS·12-crown-4] <sub>2</sub>
90	[(TMEDA)Li(NPh <sub>2</sub> ) <sub>2</sub> ]	114	[(TMEDA)·Na(μ-C <sub>4</sub> H <sub>3</sub> S) <sub>3</sub> Mg(TMEDA)]	137	[(TMEDA)·Li{2-(1-C(O)N <sup>t</sup> Pr <sub>2</sub> )C <sub>6</sub> H <sub>4</sub> ] <sub>2</sub> Zn( <sup>t</sup> Bu)]
91	[(TMEDA)Na(NPh <sub>2</sub> ) <sub>2</sub> ]	115	[Li{(R,R)-TMCDA} <sub>2</sub> ] <sup>+</sup> [Li <sub>5</sub> (μ-HMDS) <sub>5</sub> (μ <sub>5</sub> -Cl)] <sup>-</sup>	138	[(TMEDA)·Li(μ- <i>cis</i> -DMP)(μ-Et)Zn(Et)]
92	[(TMEDA) <sub>3/2</sub> K(NPh <sub>2</sub> ) <sub>2</sub> ]	116	[Li{(R,R)-TMCDA} <sub>2</sub> ] <sup>+</sup> [Li <sub>5</sub> (μ-HMDS) <sub>5</sub> (μ <sub>5</sub> -Br)] <sup>-</sup>	139	[(TMEDA)·Li(μ- <i>cis</i> -DMP)(μ-CH <sub>2</sub> SiMe <sub>3</sub> )Zn(CH <sub>2</sub> SiMe <sub>3</sub> )]
93	[(PMDETA)·K(μ-NPh <sub>2</sub> )Mg(THF)(NPh <sub>2</sub> ) <sub>2</sub> ]	117	[Me <sub>6</sub> -TREN·Li(μ-Cl)Li·Me <sub>6</sub> -TREN] <sup>+</sup> [Li <sub>5</sub> (μ-HMDS) <sub>5</sub> (μ <sub>5</sub> -Cl)] <sup>-</sup>		
94	[(Me <sub>3</sub> SiCH <sub>2</sub> )Mg(μ-TMP)] <sub>2</sub>	118	[Me <sub>6</sub> -TREN·Li(μ-Br)Li·Me <sub>6</sub> -TREN] <sup>+</sup> [Li <sub>5</sub> (μ-HMDS) <sub>5</sub> (μ <sub>5</sub> -Br)] <sup>-</sup>		
95	[(TMP)Mg(μ-TMP){μ-N(H)C(Me) <sub>2</sub> (CH <sub>2</sub> ) <sub>3</sub> C(Me)=CH <sub>2</sub> }Mg(μ-OCH <sub>2</sub> SiMe <sub>3</sub> ) <sub>2</sub> ]	119	[(DAME·LiHMDS) <sub>2</sub> ·LiCl]		
96	[{(-)-sparteine}·Na(μ-TMP)(μ- <sup>n</sup> Bu)Zn( <sup>t</sup> Bu)]	120	[(TMEDA·LiHMDS) <sub>2</sub> ·LiCl]		
97	[{(R,R)-TMCDA}·Na(μ-TMP)(μ- <sup>n</sup> Bu)Zn( <sup>t</sup> Bu)]	121	[(TMEDA·LiN <sup>t</sup> Pr <sub>2</sub> ) <sub>2</sub> ·LiCl]		
98	[{(R,R)-TMCDA}·Na(μ-TMP)(μ- <sup>t</sup> Bu)Zn( <sup>t</sup> Bu)]	122	[{THF·Li(N(Ad)(SiMe <sub>3</sub> )) <sub>2</sub> ·LiI]		
99	[(PMDETA)·K(μ-TMP)(μ- <sup>n</sup> Bu)Zn( <sup>n</sup> Bu)]				

NMR Chemical Shifts of Starting Materials in C <sub>6</sub> D <sub>6</sub>			
Starting Material	<sup>1</sup> H δ / ppm	<sup>13</sup> C δ / ppm	<sup>7</sup> Li δ / ppm
<i>cis</i> -DMP(H)	2.45 ( $\alpha$ -CH), 1.65 ( $\gamma$ -CH <sub>2</sub> ), 1.43 ( $\beta$ -CH <sub>2</sub> ), 1.24 ( $\gamma$ -CH <sub>2</sub> ), 1.00 ( $\beta$ -CH <sub>2</sub> ), 0.96 (CH <sub>3</sub> ), 0.75 (NH)	52.6 ( $\alpha$ -CH), 34.6 ( $\beta$ -CH <sub>2</sub> ), 25.5 ( $\gamma$ -CH <sub>2</sub> ), 23.4 (CH <sub>3</sub> )	–
TMEDA	2.36 (CH <sub>2</sub> ), 2.12 (CH <sub>3</sub> )	58.4 (CH <sub>2</sub> ), 46.0 (CH <sub>3</sub> )	–
HMDS(H)	0.09 (SiCH <sub>3</sub> )	2.6 (SiCH <sub>3</sub> )	–
LiHMDS	0.13 (SiCH <sub>3</sub> )	5.0 (SiCH <sub>3</sub> )	1.11
NaHMDS	0.12 (SiCH <sub>3</sub> )	6.9 (SiCH <sub>3</sub> )	–
KHMDS	0.13 (SiCH <sub>3</sub> )	7.1 (SiCH <sub>3</sub> )	–
Mg(HMDS) <sub>2</sub>	0.45 (SiCH <sub>3</sub> ), 0.37 (SiCH <sub>3</sub> ), 0.16 (SiCH <sub>3</sub> )	8.1 (SiCH <sub>3</sub> ), 7.1 (SiCH <sub>3</sub> ), 5.0 (SiCH <sub>3</sub> )	–
Ph <sub>2</sub> NH	7.10 ( <i>m</i> -CH), 6.85 ( <i>o</i> -CH), 6.83 ( <i>p</i> -CH), 4.99 (NH)	143.6 ( <i>ipso</i> -CH), 129.5 ( <i>m</i> -CH), 121.1 ( <i>p</i> -CH), 118.2 ( <i>o</i> -CH)	–
TMP(H)	1.54 ( $\gamma$ -CH <sub>2</sub> ), 1.25 ( $\beta$ -CH <sub>2</sub> ), 1.07 (CH <sub>3</sub> ), 0.31 (NH)	49.6 ( $\alpha$ -C), 38.6 ( $\beta$ -CH <sub>2</sub> ), 32.0 (CH <sub>3</sub> ), 18.8 ( $\gamma$ -CH <sub>2</sub> )	–
(–)-sparteine	2.78, 2.71, 2.68, 2.66, 2.63, 2.48, 2.33, 2.10, 2.05, 2.02, 1.99, 1.97, 1.94, 1.91, 1.88, 1.86, 1.74, 1.67, 1.64, 1.59, 1.55, 1.52, 1.50, 1.47, 1.44, 1.40, 1.38, 1.35, 1.26, 1.23, 1.18, 1.15, 1.11, 1.08, 1.01	66.5, 64.4, 62.3, 56.5, 55.8, 54.0, 37.0, 35.2, 33.8, 29.6, 28.0, 26.6, 26.2, 25.5, 25.1	–
( <i>R,R</i> )-TMCDA	2.29 (CH <sub>3</sub> ), 2.26 ( $\alpha$ -CH), 1.75 ( $\beta$ -CH <sub>2</sub> ), 1.60 ( $\gamma$ -CH <sub>2</sub> ), 1.01 ( $\beta$ -CH <sub>2</sub> ), 1.01 ( $\gamma$ -CH <sub>2</sub> )	64.3 ( $\alpha$ -CH), 40.6 (CH <sub>3</sub> ), 26.0 ( $\beta$ -CH <sub>2</sub> ), 25.7 ( $\gamma$ -CH <sub>2</sub> )	–
Me <sub>6</sub> -TREN	2.63 ( $\alpha$ -CH <sub>2</sub> ), 2.37 ( $\beta$ -CH <sub>2</sub> ), 2.12 (CH <sub>3</sub> )	58.6 ( $\alpha$ -CH <sub>2</sub> ), 53.9 ( $\beta$ -CH <sub>2</sub> ), 46.0 (CH <sub>3</sub> )	–
12-crown-4	3.49 (CH <sub>2</sub> )	71.2 (CH <sub>2</sub> )	–

NMR Chemical Shifts of Starting Materials in d <sub>8</sub> -THF			
Starting Material	<sup>1</sup> H δ / ppm	<sup>13</sup> C δ / ppm	<sup>7</sup> Li δ / ppm
HMDS(H)	0.04 (SiCH <sub>3</sub> )	2.7 (SiCH <sub>3</sub> )	–
LiHMDS	–0.16 (SiCH <sub>3</sub> )	6.1 (SiCH <sub>3</sub> )	–1.14
NaHMDS	–0.19 (SiCH <sub>3</sub> )	6.8 (SiCH <sub>3</sub> )	–
KHMDS	–0.21 (SiCH <sub>3</sub> )	6.8 (SiCH <sub>3</sub> )	–
Mg(HMDS) <sub>2</sub>	0.06 (SiCH <sub>3</sub> )		–
Ph <sub>2</sub> NH	7.25 (NH), 7.16 ( <i>m</i> -CH), 7.04 ( <i>o</i> -CH), 6.78 ( <i>p</i> -CH)	144.9 ( <i>ipso</i> -CH), 129.8 ( <i>m</i> -CH), 120.7 ( <i>p</i> -CH), 118.0 ( <i>o</i> -CH)	–
TMP(H)	1.63 (γ-CH <sub>2</sub> ), 1.29 (β-CH <sub>2</sub> ), 1.06 (CH <sub>3</sub> ), 0.68 (NH)	50.1 (α-C), 39.2 (β-CH <sub>2</sub> ), 32.3 (CH <sub>3</sub> ), 19.3 (γ-CH <sub>2</sub> )	–
Mg(CH <sub>2</sub> SiMe <sub>3</sub> ) <sub>2</sub>	–0.11 (SiCH <sub>3</sub> ), –1.77 (CH <sub>2</sub> )	4.6 (SiCH <sub>3</sub> ), –7.6 (CH <sub>2</sub> )	–
Mg(TMP) <sub>2</sub>	1.68 (γ-CH <sub>2</sub> ), 1.22 (β-CH <sub>2</sub> ), 1.16 (CH <sub>3</sub> ),		–
(–)-sparteine	2.69, 2.59, 2.50, 2.38, 2.11, 1.98, 1.90, 1.72, 1.68, 1.50, 1.38, 1.23, 0.98	67.3, 65.0, 62.8, 57.0, 56.3, 54.5, 37.7, 35.7, 34.5, 30.1, 28.4, 27.1, 26.8, 26.0, 25.7	–
( <i>R,R</i> )-TMCDA	2.35 (α-CH), 2.27 (CH <sub>3</sub> ), 1.76 (β-CH <sub>2</sub> ), 1.69 (γ-CH <sub>2</sub> ), 1.12 (β-CH <sub>2</sub> ), 1.12 (γ-CH <sub>2</sub> )	65.0 (α-CH), 40.8 (CH <sub>3</sub> ), 26.5 (β-CH <sub>2</sub> ), 26.5 (γ-CH <sub>2</sub> )	–
Me <sub>6</sub> -TREN	2.55 (α-CH <sub>2</sub> ), 2.29 (β-CH <sub>2</sub> ), 2.15 (CH <sub>3</sub> )	59.3 (α-CH <sub>2</sub> ), 54.5 (β-CH <sub>2</sub> ), 46.3 (CH <sub>3</sub> )	–

---

## References

- [1] *Aldrich Handbook of Fine Chemicals*, United Kingdom, **2009-2010**.
- [2] D. B. Collum, *Acc. Chem. Res.* **1993**, *26*, 227.
- [3] In a comprehensive study of approximately 500 natural product syntheses (compiled by H. J. Reich, unpublished), LDA was found to be the most commonly used reagent.
- [4] M. Hammel, R. Levine, *J. Org. Chem.* **1950**, *15*, 162.
- [5] a) G. Stork, L. Maldonado, *J. Am. Chem. Soc.* **1971**, *93*, 5286; b) J. Clayden, *Organolithiums: Selectivity for Synthesis, Tetrahedron Organic Chemistry Series, Vol. 23*, Elsevier Science Ltd., Oxford, **2002**.
- [6] a) D. Seebach, D. Enders, *Angew. Chem. Int. Ed. Engl.* **1972**, *11*, 301; b) D. Seebach, D. Enders, *Angew. Chem. Int. Ed. Engl.* **1975**, *14*, 15.
- [7] M. F. Lappert, P. P. Power, A. R. Sanger, R. C. Srivastava, *Metal and Metalloid Amides, Vol. 2*, Ellis Horwood Ltd., John Wiley & Sons, **1980**.
- [8] M. Schlosser, in *Organometallics in Synthesis*, 2nd ed., John Wiley & Sons Ltd., Chichester, **2002**.
- [9] a) W. Setzer, P. v. R. Schleyer, *Adv. Organomet. Chem.* **1985**, *24*, 353; b) K. Gregory, P. v. R. Schleyer, R. Snaith, *Adv. Inorg. Chem.* **1991**, *37*, 47; c) R. E. Mulvey, *Chem. Soc. Rev.* **1991**, *20*, 167.
- [10] a) D. K. Kennepohl, S. Brooker, G. M. Sheldrick, H. W. Roesky, *Chem. Ber.* **1991**, *124*, 2223; b) M. Westerhausen, W. Schwarz, *Z. Anorg. Allg. Chem.* **1993**, *619*, 1053; c) H. Witte-Abel, U. Klingebiel, M. Schafer, *Z. Anorg. Allg. Chem.* **1998**, *624*, 271; d) K. Junge, E. Popowski, R. Kempe, W. Baumann, *Z. Anorg. Allg. Chem.* **1998**, *624*, 1369; e) M. Veith, A. Koban, K. Fries, P. Spaniol, R. Elsasser, A. Rammo, V. Huch, U. Kleinstaubler, *Organometallics* **1998**, *17*, 2612; f) F. Antolini, P. B. Hitchcock, M. F. Lappert, P. Merle, *Chem. Commun.* **2000**, 1301; g) F. Antolini, P. B. Hitchcock, A. V. Khvostov, M. F. Lappert, *Eur. J. Inorg. Chem.* **2003**, 3391; h) U. Klingebiel, M. Noltemeyer, *Eur. J. Inorg. Chem.* **2001**, 1889; i) Y. Tang, L. N. Zakharov, A. L. Rheingold, R. A. Kemp, *Polyhedron* **2005**, *24*, 1739; j) L. Bourget-Merle, P. B. Hitchcock, M. F. Lappert, P. G. Merle, *Dalton Trans.* **2008**, 3493.
- [11] a) D. Mootz, A. Zinnius, B. Bottcher, *Angew. Chem. Int. Ed. Engl.* **1969**, *8*, 378; b) R. D. Rogers, J. L. Atwood, R. Grüning, *J. Organomet. Chem.* **1978**, *157*, 229; c) D. Barr, W. Clegg, R. E. Mulvey, R. Snaith, *J. Chem. Soc., Chem. Commun.* **1984**, 285; d) D. R. Armstrong, R. E. Mulvey, G. T. Walker, D. Barr, R. Snaith, W. Clegg, D. Reed, *J. Chem. Soc., Dalton Trans.* **1988**, 617; e) M. Rannenbergh, H.-D. Hausen, J. Weidlein, *J. Organomet. Chem.* **1989**, *376*, C27; f) B. Germünd, H. Nöth, H. Sachdev, M. Schmidt, *Chem. Ber.* **1996**, *129*, 1335; g) D. R. Armstrong, D. R. Baker, F. J. Craig, R. E. Mulvey, W. Clegg, L. Horsburgh, *Polyhedron* **1996**, *15*, 3533; h) B. Wrackmeyer, B. Schwarze, J. Weidinger, W. Millius, *Z. Naturforsch., B* **1997**, *52*, 431; i) D. R. Armstrong, K. W. Henderson, A. R. Kennedy, W. J. Kerr, F. S. Mair, J. H. Moir, P. H. Moran, R. Snaith, *J. Chem. Soc., Dalton Trans.* **1999**, 4063; j) C. Matthes, M. Noltemeyer, U. Klingebiel, S. Schmatz, *Organometallics* **2007**, *26*, 838.
- [12] a) M. F. Lappert, M. J. Slade, A. Singh, J. L. Atwood, R. D. Rogers, R. Shakir, *J. Am. Chem. Soc.* **1983**, *105*, 302; b) J. Jubb, P. Berno, S. K. Hao, S. Gambarotta, *Inorg. Chem.* **1995**, *34*, 3563; c) L. Ruwisch, U. Klingebiel, S. Rudolph, R. Herbstlrmr, M. Noltemeyer, *Chem. Ber.* **1996**, *129*, 823.
- [13] D. Barr, W. Clegg, S. M. Hodgson, G. R. Lamming, R. E. Mulvey, A. J. Scott, R. Snaith, D. S. Wright, *Angew. Chem. Int. Ed. Engl.* **1989**, *28*, 1241.
- [14] N. D. R. Barnett, W. Clegg, L. Horsburgh, D. M. Lindsay, Q.-Y. Liu, F. M. Mackenzie, R. E. Mulvey, P. G. Williard, *Chem. Commun.* **1996**, 2321.



- [15] N. D. R. Barnett, R. E. Mulvey, W. Clegg, P. A. O'Neil, *J. Am. Chem. Soc.* **1991**, *113*, 8187.
- [16] L. Pauling, *The Nature of the Chemical Bond*, 3rd ed., Cornell University Press, New York, **1960**.
- [17] a) D. R. Armstrong, D. Barr, W. Clegg, R. E. Mulvey, D. Reed, R. Snaith, K. Wade, *J. Chem. Soc., Chem. Commun.* **1986**, 869; b) D. R. Armstrong, D. Barr, W. Clegg, S. M. Hodgson, R. E. Mulvey, D. Reed, R. Snaith, D. S. Wright, *J. Am. Chem. Soc.* **1989**, *111*, 4719.
- [18] R. J. Wright, J. Steiner, S. Beaini, P. P. Power, *Inorg. Chim. Acta.* **2006**, *359*, 1939.
- [19] A. A. Skatova, I. L. Fedushkin, O. V. Maslova, M. Hummert, H. Schumann, *Russ. Chem. Bull. Int. Ed.* **2007**, *56*, 2284.
- [20] D. J. Brauer, H. Burger, G. R. Liewald, *J. Organomet. Chem.* **1986**, *308*, 119.
- [21] a) D. J. Brauer, H. Burger, G. R. Liewald, J. Wilke, *J. Organomet. Chem.* **1985**, 287, 305; b) H. Chen, R. A. Bartlett, H. V. R. Dias, M. M. Olmstead, P. P. Power, *Inorg. Chem.* **1991**, *30*, 2487; c) L. H. Gade, N. Mahr, *J. Chem. Soc., Dalton Trans.* **1993**, 489; d) L. H. Gade, C. Becker, J. W. Lauher, *Inorg. Chem.* **1993**, *32*, 2308; e) M. Veith, A. Spaniol, J. Pohlmann, F. Gross, V. Huch, *Chem. Ber.* **1993**, *126*, 2625; f) P. Kosse, E. Popowski, M. Veith, V. Huch, *Chem. Ber.* **1994**, *127*, 2103; g) M. Veith, M. Zimmer, P. Kosse, *Chem. Ber.* **1994**, *127*, 2099; h) M. Schubart, B. Findeis, L. H. Gade, W.-S. Li, M. McPartlin, *Chem. Ber.* **1995**, *128*, 329; i) M. G. Gardiner, C. L. Raston, *Inorg. Chem.* **1996**, *35*, 4162; j) H.-J. Rakebrandt, U. Klingebiel, M. Noltemeyer, *Z. Anorg. Allg. Chem.* **1997**, *623*, 288; k) K. W. Hellmann, A. Bergner, L. H. Gade, I. J. Scowen, M. McPartlin, *J. Organomet. Chem.* **1999**, *573*, 156; l) R. M. Gauvin, N. Kyritsakas, J. Fischer, J. Kress, *Chem. Commun.* **2000**, 965; m) J. Engering, E.-M. Peters, M. Jansen, *Z. Naturforsch., B: Chem. Sci.* **2001**, *56*, 90; n) P. Renner, C. H. Galka, L. H. Gade, M. McPartlin, *Inorg. Chem. Commun.* **2001**, *4*, 191; o) P. Renner, C. H. Galka, L. H. Gade, S. Radojevic, M. McPartlin, *J. Chem. Soc., Dalton Trans.* **2001**, 964; p) P. Renner, C. H. Galka, L. H. Gade, S. Radojevic, M. McPartlin, *Eur. J. Inorg. Chem.* **2001**, 1425; q) L. H. Gade, P. Renner, H. Memmler, F. Fecher, C. H. Galka, M. Laubender, S. Radojevic, M. McPartlin, J. W. Lauher, *Chem.–Eur. J.* **2001**, *7*, 2563; r) S. Daniele, C. Drost, B. Gehrhus, S. M. Hawkins, P. B. Hitchcock, M. F. Lappert, P. G. Merle, S. G. Bott, *J. Chem. Soc., Dalton Trans.* **2001**, 3179; s) J. Engering, E.-M. Peters, M. Jansen, *Z. Naturforsch., B: Chem. Sci.* **2002**, *57*, 976; t) J.-F. Li, L.-H. Weng, X.-H. Wei, D.-S. Liu, *J. Chem. Soc., Dalton Trans.* **2002**, 1401; u) M. S. Hill, P. B. Hitchcock, *Organometallics* **2002**, *21*, 3258; v) J. Engering, M. Jansen, *New. Cryst. Struct.* **2003**, *218*, 153; w) J. Hao, X. Wei, S. Huang, J. Guo, D. Liu, *Appl. Organomet. Chem.* **2005**, *19*, 1010; x) C. Matthes, U. Klingebiel, S. Deuerlein, H. Ott, D. Stalke, *Z. Anorg. Allg. Chem.* **2008**, *634*, 2402.
- [22] R. Grüning, J. L. Atwood, *J. Organomet. Chem.* **1997**, *137*, 101.
- [23] a) J. Knizek, I. Krossing, H. Nöth, H. Schwenk, T. Seifert, *Chem. Ber.* **1997**, *130*, 1053; b) M. Driess, H. Pritzkow, M. Skipinski, U. Winkler, *Organometallics* **1997**, *16*, 5108.
- [24] J. Eppinger, E. Herdtweck, R. Andwander, *Polyhedron* **1998**, *17*, 1195.
- [25] B. Gehrhus, P. B. Hitchcock, A. R. Kennedy, M. F. Lappert, R. E. Mulvey, P. J. A. Rodger, *J. Organomet. Chem.* **1999**, *587*, 88.
- [26] A. G. Avent, F. Antolini, P. B. Hitchcock, A. V. Khvostov, M. F. Lappert, A. V. Protchenko, *Dalton Trans.* **2006**, 919.
- [27] a) P. G. Williard, *Acta. Crystallogr. Sect. C* **1988**, *C44*, 270; b) K. F. Tesh, T. P. Hanusa, J. C. Huffman, *Inorg. Chem.* **1990**, *29*, 1584.
- [28] S. M. Mansell, B. Fernandez Perandones, P. L. Arnold, *J. Organomet. Chem.* **2010**, *695*, 2814.
- [29] A. Torvisco, K. Decker, F. Uhlig, K. Ruhlandt-Senge, *Inorg. Chem.* **2009**, *48*, 11459.

- [30] B. Gehrhus, P. B. Hitchcock, M. F. Lappert, J. C. Slootweg, *Chem. Commun.* **2000**, 1427.
- [31] Y. Tang, L. N. Zakharov, W. S. Kassel, A. L. Rheingold, R. A. Kemp, *Inorg. Chim. Acta.* **2005**, 358, 2014.
- [32] S. Neander, U. Behrens, *Z. Anorg. Allg. Chem.* **1999**, 625, 1429.
- [33] K. F. Tesh, B. D. Jones, T. P. Hanusa, J. C. Huffman, *J. Am. Chem. Soc.* **1992**, 114, 6590.
- [34] R. E. Marsh, D. A. Clemente, *Inorg. Chim. Acta.* **2007**, 360, 4017.
- [35] D. Barr, W. Clegg, R. E. Mulvey, R. Snaith, D. S. Wright, *J. Chem. Soc., Chem. Commun.* **1987**, 716.
- [36] a) P. P. Power, X. J. Xiaojie, *J. Chem. Soc., Chem. Commun.* **1984**, 358; b) R. A. Bartlett, H. V. R. Dias, H. Hope, B. D. Murray, M. M. Olmstead, P. P. Power, *J. Am. Chem. Soc.* **1986**, 108, 6921.
- [37] a) L. M. Engelhardt, A. S. May, C. L. Raston, A. H. White, *J. Chem. Soc., Dalton Trans.* **1983**, 1671; b) B. Cetinkaya, P. B. Hitchcock, M. F. Lappert, M. C. Misra, A. J. Thorne, *J. Chem. Soc., Chem. Commun.* **1984**, 148; c) L. M. Engelhardt, B. S. Jolly, P. C. Junk, C. L. Raston, B. W. Skelton, A. H. White, *Aust. J. Chem.* **1986**, 39, 1337; d) H. Mack, G. Frenzen, M. Bendikov, M. S. Eisen, *J. Organomet. Chem.* **1997**, 549, 39; e) P. G. Williard, J. M. Salvino, *J. Org. Chem.* **1993**, 58, 1; f) D. R. Armstrong, P. García-Álvarez, A. R. Kennedy, R. E. Mulvey, S. D. Robertson, *Chem.–Eur. J.* **2011**, 17, 6725.
- [38] G. C. Forbes, A. R. Kennedy, R. E. Mulvey, P. J. A. Rodger, R. B. Rowlings, *J. Chem. Soc., Dalton Trans.* **2001**, 1477.
- [39] a) G. Boche, M. Marsch, K. Harms, *Angew. Chem. Int. Ed. Engl.* **1986**, 98, 373; b) P. G. Williard, Q.-Y. Liu, *J. Am. Chem. Soc.* **1993**, 115, 3380.
- [40] M. P. Bernstein, F. E. Romesberg, D. J. Fuller, A. T. Harrison, D. B. Collum, Q.-Y. Liu, P. G. Williard, *J. Am. Chem. Soc.* **1992**, 114, 5100.
- [41] W. Clegg, S. T. Liddle, R. E. Mulvey, A. Robertson, *Chem. Commun.* **1999**, 511.
- [42] N. P. Lorenzen, J. Kopf, F. Olbrich, U. Schümann, E. Weiss, *Angew. Chem. Int. Ed. Engl.* **1990**, 29, 1441.
- [43] D. R. Armstrong, D. V. Graham, A. R. Kennedy, R. E. Mulvey, C. T. O'Hara, *Chem.–Eur. J.* **2008**, 14, 8025.
- [44] D. Li, I. Keresztes, R. Hopson, P. G. Williard, *Acc. Chem. Res.* **2009**, 42, 270.
- [45] D. B. Collum, A. J. McNeil, A. Ramirez, *Angew. Chem. Int. Ed.* **2007**, 46, 3002.
- [46] Y.-J. Kim, M. P. Bernstein, A. S. Galiano-Roth, F. E. Romesberg, P. G. Williard, D. J. Fuller, A. T. Harrison, D. B. Collum, *J. Org. Chem.* **1991**, 56, 4435.
- [47] A. S. Galiano-Roth, D. B. Collum, *J. Am. Chem. Soc.* **1989**, 111, 6772.
- [48] K. Bergander, R. He, N. Chandrakumar, O. Eppers, H. Günther, *Tetrahedron* **1994**, 50, 5861.
- [49] J. F. Remenar, B. L. Lucht, D. B. Collum, *J. Am. Chem. Soc.* **1997**, 119, 5567.
- [50] J. L. Rutherford, D. B. Collum, *J. Am. Chem. Soc.* **2001**, 123, 199.
- [51] F. E. Romesberg, J. H. Gilchrist, A. T. Harrison, D. J. Fuller, D. B. Collum, *J. Am. Chem. Soc.* **1991**, 113, 5751.
- [52] a) F. E. Romesberg, M. P. Bernstein, J. H. Gilchrist, A. T. Harrison, D. J. Fuller, D. B. Collum, *J. Am. Chem. Soc.* **1993**, 115, 3475; b) B. L. Lucht, D. B. Collum, *J. Am. Chem. Soc.* **1994**, 116, 6009; c) B. L. Lucht, D. B. Collum, *J. Am. Chem. Soc.* **1995**, 117, 9863.
- [53] B. L. Lucht, D. B. Collum, *J. Am. Chem. Soc.* **1996**, 118, 2217.
- [54] B. L. Lucht, M. P. Bernstein, J. F. Remenar, D. B. Collum, *J. Am. Chem. Soc.* **1996**, 118, 10707.
- [55] a) P. Renaud, M. A. Fox, *J. Am. Chem. Soc.* **1988**, 110, 5702; b) J. H. Gilchrist, D. B. Collum, *J. Am. Chem. Soc.* **1992**, 114, 794.

- [56] a) B. L. Lucht, D. B. Collum, *J. Am. Chem. Soc.* **1994**, *116*, 7949; b) J. F. Remenar, B. L. Lucht, D. Kruglyak, F. E. Romesberg, J. H. Gilchrist, D. B. Collum, *J. Org. Chem.* **1997**, *62*, 5748.
- [57] F. E. Romesberg, D. B. Collum, *J. Am. Chem. Soc.* **1992**, *114*, 2112.
- [58] a) R. P. C. Cousins, N. S. Simpkins, *Tetrahedron Lett.* **1989**, *30*, 7241; b) C. M. Cain, R. P. C. Cousins, G. Coumbarides, N. S. Simpkins, *Tetrahedron* **1990**, *46*, 523; c) N. S. Simpkins, *Chem. Soc. Rev.* **1990**, *19*, 335; d) P. J. Cox, N. S. Simpkins, *Tetrahedron: Asymmetry* **1991**, *2*, 1.
- [59] a) R. Shirai, M. Tanaka, K. Koga, *J. Am. Chem. Soc.* **1986**, *108*, 543; b) M. Murakata, M. Nakajima, K. Koga, *J. Chem. Soc., Chem. Commun.* **1990**, 1657.
- [60] a) E. J. Corey, A. W. Gross, *Tetrahedron Lett.* **1984**, *25*, 495; b) M. Sobukawa, M. Nakajima, K. Koga, *Tetrahedron: Asymmetry* **1990**, *1*, 295; c) P. J. Cox, N. S. Simpkins, *Synlett* **1991**, 321; d) D. Sato, H. Kawasaki, I. Shimada, Y. Arata, K. Okamura, T. Date, K. Koga, *J. Am. Chem. Soc.* **1992**, *114*, 761; e) B. J. Bunn, P. J. Cox, N. S. Simpkins, *Tetrahedron* **1993**, *49*, 207; f) M. Sobukawa, K. Koga, *Tetrahedron Lett.* **1993**, *34*, 5101; g) K. Aoki, H. Noguchi, K. Tomioka, K. Koga, *Tetrahedron Lett.* **1993**, *34*, 5105; h) K. Bambridge, B. P. Clark, N. S. Simpkins, *J. Chem. Soc., Perkin Trans. 1* **1995**, 2535; i) N. S. Simpkins, *Pure Appl. Chem.* **1996**, *68*, 691; j) H. Chatani, M. Nakajima, H. Kawasaki, K. Koga, *Heterocycles* **1997**, *46*, 53; k) M. Toriyama, K. Sugasawa, M. Shindo, N. Tokutake, K. Koga, *Tetrahedron Lett.* **1997**, *38*, 567; l) K. Aoki, K. Koga, *Tetrahedron Lett.* **1997**, *38*, 2505; m) R. Shirai, D. Sato, K. Aoki, M. Tanaka, H. Kawasaki, K. Koga, *Tetrahedron* **1997**, *53*, 5963; n) K. Aoki, K. Tomioka, H. Noguchi, K. Koga, *Tetrahedron* **1997**, *53*, 13641; o) M. Toriyama, K. Sugasawa, S. Motohashi, N. Tokutake, K. Koga, *Chem. Pharm. Bull.* **2001**, *49*, 468; p) B. Butler, T. Schultz, N. S. Simpkins, *Chem. Commun.* **2006**, 3634.
- [61] a) J. K. Whitesell, S. W. Felman, *J. Org. Chem.* **1980**, *45*, 755; b) D. Bhuniya, A. DattaGupta, V. K. Singh, *J. Org. Chem.* **1996**, *61*, 6108; c) D. M. Hodgson, A. R. Gibbs, G. P. Lee, *Tetrahedron* **1996**, *52*, 14361; d) J. P. Tierney, A. Alexakis, P. Mangeney, *Tetrahedron: Asymmetry* **1997**, *8*, 1019; e) P. Saravanan, V. K. Singh, *Tetrahedron Lett.* **1998**, *39*, 167; f) A. Z.-Q. Khan, R. W. de Groot, P. I. Arvidsson, Ö. Davidsson, *Tetrahedron: Asymmetry* **1998**, *9*, 1223; g) S. E. de Sousa, P. O'Brien, P. Poumellec, *J. Chem. Soc., Perkin Trans. 1* **1998**, 1483; h) P. O'Brien, P. Poumellec, *J. Chem. Soc., Perkin Trans. 1* **1998**, 2435; i) M. Asami, M. Ogawa, S. Inoue, *Tetrahedron Lett.* **1999**, *40*, 1563; j) S. E. de Sousa, P. O'Brien, H. C. Steffens, *Tetrahedron Lett.* **1999**, *40*, 8423.
- [62] a) D. A. Price, N. S. Simpkins, A. M. MacLeod, A. P. Watt, *J. Org. Chem.* **1994**, *59*, 1961; b) R. A. Ewin, A. M. MacLeod, D. A. Price, N. S. Simpkins, A. P. Watt, *J. Chem. Soc., Perkin Trans. 1* **1997**, 401; c) A. Ariffin, A. J. Blake, W. S. Li, N. S. Simpkins, *Synlett* **1997**, 1453; d) A. Ariffin, A. J. Blake, R. A. Ewin, N. S. Simpkins, *Tetrahedron: Asymmetry* **1998**, *9*, 2563; e) A. Ariffin, A. J. Blake, R. A. Ewin, W. S. Li, N. S. Simpkins, *J. Chem. Soc., Perkin Trans. 1* **1999**, 3177; f) R. E. J. Beckwith, N. Heron, N. S. Simpkins, *J. Organomet. Chem.* **2002**, *658*, 21.
- [63] a) T. Yasukata, K. Koga, *Tetrahedron: Asymmetry* **1993**, *4*, 35; b) Y. Hasegawa, H. Kawasaki, K. Koga, *Tetrahedron Lett.* **1993**, *34*, 1963; c) M. Murakata, T. Yasukata, T. Aoki, M. Nakajima, K. Koga, *Tetrahedron* **1998**, *54*, 2449.
- [64] a) Y. Landais, P. Ogay, *Tetrahedron: Asymmetry* **1994**, *5*, 541; b) M. Uragami, K. Tomioka, K. Koga, *Tetrahedron: Asymmetry* **1995**, *6*, 701.
- [65] V. K. Aggarwal, P. S. Humphries, A. Fenwick, *J. Chem. Soc., Perkin Trans. 1* **1999**, 2883.

- [66] a) E. L. M. Cowton, S. E. Gibson, M. J. Schneider, M. H. Smith, *Chem. Commun.* **1996**, 839; b) N. S. Simpkins, *Chimia* **2000**, *54*, 53; c) M. J. McGrath, C. Bolm, *Beilstein J. Org. Chem.* **2007**, *3*, 33.
- [67] a) H. Kubota, M. Nakajima, K. Koga, *Tetrahedron Lett.* **1993**, *34*, 8135; b) E. M. Brun, S. Gil, M. Parra, *Tetrahedron: Asymmetry* **2002**, *12*, 915; c) C. E. Stivala, A. Zakarian, *J. Am. Chem. Soc.* **2011**, *133*, 11936.
- [68] K. Takeda, Y. Ohnishi, T. Koizumi, *Org. Lett.* **1999**, *1*, 237.
- [69] a) M. B. Eleveld, H. Hogeveen, *Tetrahedron Lett.* **1984**, *25*, 5187; b) E. Juaristi, A. K. Beak, J. Hansen, T. Matt, T. Mukhopadhyay, M. Simson, D. Seebach, *Synthesis* **1993**, 1271; c) M. Nakajima, K. Tomioka, K. Koga, *Tetrahedron* **1993**, *49*, 9751; d) I. Inoue, M. Shindo, K. Koga, K. Tomioka, *Tetrahedron* **1994**, *50*, 4429; e) K. Yasuda, M. Shindo, K. Koga, *Tetrahedron Lett.* **1996**, *37*, 6343; f) A. Corruble, J.-Y. Valnot, J. Maddaluno, P. Duhamel, *Tetrahedron: Asymmetry* **1997**, *8*, 1519; g) K. Yasuda, M. Shindo, K. Koga, *Tetrahedron Lett.* **1997**, *38*, 3531; h) A. Corruble, J.-Y. Valnot, J. Maddaluno, P. Duhamel, *J. Org. Chem.* **1998**, *63*, 8266; i) P. I. Arvidsson, Ö. Davidsson, G. Hilmersson, *Tetrahedron: Asymmetry* **1999**, *10*, 527; j) J. G. Urones, N. M. Garrido, D. Diez, S. H. Dominguez, S. G. Davies, *Tetrahedron: Asymmetry* **1999**, *10*, 1637; k) R. Sott, J. Granander, G. Hilmersson, *Chem.–Eur. J.* **2002**, *8*, 2081; l) J. Granander, R. Sott, G. Hilmersson, *Tetrahedron: Asymmetry* **2003**, *14*, 439; m) A. Harrison-Marchand, J.-Y. Valnot, A. Corruble, N. Duguet, H. Oulyadi, S. Desjardins, C. Fressigné, J. Maddaluno, *Pure Appl. Chem.* **2006**, *78*, 321; n) S. G. Davies, N. M. Garrido, D. Kruchinin, O. Ishihara, L. J. Kotchie, P. D. Price, A. J. P. Mortimer, A. J. Russell, A. D. Smith, *Tetrahedron: Asymmetry* **2006**, *17*, 1793; o) J. Granander, J. Eriksson, G. Hilmersson, *Tetrahedron: Asymmetry* **2006**, *17*, 2021; p) N. Duguet, A. Harrison-Marchand, J. Maddaluno, *Org. Lett.* **2006**, *8*, 5745; q) N. Duguet, S. Petit, P. Marchand, A. Harrison-Marchand, J. Maddaluno, *J. Org. Chem.* **2008**, *73*, 5397.
- [70] a) P. Coggins, N. S. Simpkins, *Synlett* **1991**, 515; b) P. Coggins, N. S. Simpkins, *Synlett* **1992**, 313; c) K. Bambridge, N. S. Simpkins, B. P. Clark, *Tetrahedron Lett.* **1992**, *33*, 8141; d) A. D. Hughes, D. A. Price, O. Shishkin, N. S. Simpkins, *Tetrahedron Lett.* **1996**, *37*, 7607; e) V. Rodeschini, N. S. Simpkins, C. Wilson, *J. Org. Chem.* **2007**, *72*, 4265.
- [71] a) M. Imai, A. Hagihara, H. Kawasaki, K. Manabe, K. Koga, *J. Am. Chem. Soc.* **1994**, *116*, 8829; b) T. Yamashita, D. Sato, T. Kiyoto, A. Kumar, K. Koga, *Tetrahedron Lett.* **1996**, *37*, 8195; c) P. Riviere, K. Koga, *Tetrahedron Lett.* **1997**, *38*, 7589; d) T. Yamashita, D. Sato, T. Kiyoto, A. Kumar, K. Koga, *Tetrahedron* **1997**, *53*, 16987; e) M. Imai, A. Hagihara, H. Kawasaki, K. Manabe, K. Koga, *Tetrahedron* **2000**, *56*, 179; f) A. Seki, M. Asami, *Tetrahedron* **2002**, *58*, 4655; g) S. J. Oxenford, J. M. Wright, P. O'Brien, N. Panday, M. R. Shipton, *Tetrahedron: Asymmetry* **2005**, *46*, 8315.
- [72] a) M. Asami, T. Ishizaki, S. Inoue, *Tetrahedron: Asymmetry* **1994**, *5*, 793; b) M. Amadji, J. Vadecard, J. C. Plaquevent, L. Duhamel, P. Duhamel, *J. Am. Chem. Soc.* **1996**, *118*, 12483; c) M. Asami, T. Suga, K. Honda, S. Inoue, *Tetrahedron Lett.* **1997**, *38*, 6425; d) Y. Yamashita, K. Odashima, K. Koga, *Tetrahedron Lett.* **1999**, *40*, 2803; e) Y. Yamashita, Y. Emura, K. Odashima, K. Koga, *Tetrahedron Lett.* **2000**, *41*, 209; f) P. C. Brookes, D. J. Milne, J. P. Murphy, B. Spolaore, *Tetrahedron* **2002**, *58*, 4675.
- [73] a) A. J. Edwards, S. Hockey, F. S. Mair, P. R. Raithby, R. Snaith, N. S. Simpkins, *J. Org. Chem.* **1993**, *58*, 6942; b) P. C. Andrews, P. J. Duggan, M. Maguire, P. J. Nichols, *Chem. Commun.* **2001**, 53.
- [74] a) G. Hilmersson, Ö. Davidsson, *J. Org. Chem.* **1995**, *489*, 175; b) G. Hilmersson, Ö. Davidsson, *J. Org. Chem.* **1995**, *60*, 7660; c) G. Hilmersson, P. I. Arvidsson, Ö. Davidsson, *Organometallics* **1997**, *16*, 3352; d) G. Hilmersson, P. I. Arvidsson, Ö. Davidsson, M. Håkansson, *J. Am. Chem. Soc.* **1998**, *120*, 8143; e) G. Hilmersson, *Chem.–Eur. J.* **2000**, *6*, 3069; f) P. I. Arvidsson, Ö. Davidsson, *Angew. Chem. Int. Ed.*

- 2000, 39, 1467; g) R. Sott, J. Granander, P. Dinér, G. Hilmersson, *Tetrahedron: Asymmetry* **2004**, 15, 267; h) G. Kagan, W. Li, D. Li, R. Hopson, P. G. Williard, *J. Am. Chem. Soc.* **2011**, 133, 6596.
- [75] A. Johansson, A. Pettersson, Ö. Davidsson, *J. Organomet. Chem.* **2000**, 608, 153.
- [76] a) P. I. Arvidsson, G. Hilmersson, P. Ahlberg, *J. Am. Chem. Soc.* **1999**, 121, 1883; b) R. I. Olsson, P. Ahlberg, *Tetrahedron: Asymmetry* **1999**, 10, 3991.
- [77] a) A. Corruble, J.-Y. Valnot, J. Maddaluno, Y. Prigent, D. Davoust, P. Duhamel, *J. Am. Chem. Soc.* **1997**, 119, 10042; b) Y. Yuan, S. Desjardins, A. Harrison-Marchand, H. Oulyadi, C. Fressigné, C. Giessner-Pettré, J. Maddaluno, *Tetrahedron* **2005**, 61, 3325.
- [78] C. Strohmann, V. H. Gessner, *Angew. Chem. Int. Ed.* **2007**, 46, 8281.
- [79] V. H. Gessner, C. Strohmann, *Organometallics* **2010**, 29, 1858.
- [80] a) K. W. Henderson, W. J. Kerr, J. H. Moir, *Chem. Commun.* **2000**, 479; b) K. W. Henderson, W. J. Kerr, J. H. Moir, *Synlett* **2001**, 1253; c) K. W. Henderson, W. J. Kerr, *Chem. – Eur. J.* **2001**, 7, 3430; d) J. D. Anderson, P. García García, D. Hayes, K. W. Henderson, W. J. Kerr, J. H. Moir, K. P. Fondekar, *Tetrahedron Lett.* **2001**, 42, 7111; e) K. W. Henderson, W. J. Kerr, J. H. Moir, *Tetrahedron* **2002**, 58, 4573; f) E. L. Carswell, D. Hayes, K. W. Henderson, W. J. Kerr, C. J. Russell, *Synlett* **2003**, 1017; g) M. J. Bassindale, J. J. Crawford, K. W. Henderson, W. J. Kerr, *Tetrahedron Lett.* **2004**, 45, 4175; h) W. J. Kerr, M. Middleditch, A. J. B. Watson, *Synlett* **2010**, 177; i) L. S. Bennie, W. J. Kerr, M. Middleditch, A. J. B. Watson, *Chem. Commun.* **2011**, 47, 2264.
- [81] a) G. E. Coates, D. Ridley, *J. Chem. Soc. (A)* **1967**, 56; b) W. Clegg, F. J. Craig, K. W. Henderson, A. R. Kennedy, R. E. Mulvey, P. A. O'Neil, D. Reed, *Inorg. Chem.* **1997**, 36, 6238.
- [82] W. Clegg, M. Frank, R. E. Mulvey, P. A. O'Neil, *J. Chem. Soc., Chem. Commun.* **1994**, 97.
- [83] in *Compact Oxford English Dictionary*, 3rd ed., Oxford University Press, Oxford, **2005**.
- [84] R. E. Mulvey, F. Mongin, M. Uchiyama, Y. Kondo, *Angew. Chem. Int. Ed.* **2007**, 46, 3802.
- [85] a) R. E. Mulvey, *Organometallics* **2006**, 25, 1060; b) R. E. Mulvey, *Acc. Chem. Res.* **2009**, 42, 743.
- [86] a) A. Krasovskiy, P. Knochel, *Angew. Chem. Int. Ed.* **2004**, 43, 3333; b) H. Ren, A. Krasovskiy, P. Knochel, *Org. Lett.* **2004**, 6, 4215; c) A. Krasovskiy, B. F. Straub, P. Knochel, *Angew. Chem. Int. Ed.* **2006**, 45, 159; d) A. Krasovskiy, V. Krasovskaya, P. Knochel, *Angew. Chem. Int. Ed.* **2006**, 45, 2958; e) W. Lin, O. Baron, P. Knochel, *Org. Lett.* **2006**, 8, 5673; f) A. H. Stoll, P. Mayer, P. Knochel, *Organometallics* **2007**, 26, 6694; g) G. C. Clososki, C. J. Rohbogner, P. Knochel, *Angew. Chem. Int. Ed.* **2007**, 46, 7681; h) C. J. Rohbogner, G. C. Clososki, P. Knochel, *Angew. Chem. Int. Ed.* **2008**, 47, 1503; i) M. Mosrin, P. Knochel, *Org. Lett.* **2008**, 10, 2497; j) F. M. Piller, P. Knochel, *Org. Lett.* **2009**, 11, 445; k) C. J. Rohbogner, S. H. Wunderlich, G. C. Clososki, P. Knochel, *Eur. J. Org. Chem.* **2009**, 1781; l) M. Mosrin, T. Bresser, P. Knochel, *Org. Lett.* **2009**, 11, 3406; m) L. Melzig, C. B. Rauhut, P. Knochel, *Chem. Commun.* **2009**, 3536; n) S. H. Wunderlich, C. J. Rohbogner, A. Unsinn, P. Knochel, *Org. Process Rev. Des.* **2010**, 14, 339; o) B. Haag, M. Mosrin, H. Ila, V. Malakhov, P. Knochel, *Angew. Chem. Int. Ed.* **2011**, 50, 9794.
- [87] a) O. Bayh, H. Awad, F. Mongin, C. Hoarau, F. Trécourt, G. Quéguiner, F. Marsais, F. Blanco, B. Abarca, R. Ballesteros, *Tetrahedron* **2005**, 61, 4779; b) O. Bayh, H. Awad, F. Mongin, C. Hoarau, L. Bischoff, F. Trécourt, G. Quéguiner, F. Marsais, F. Blanco, B. Abarca, R. Ballesteros, *J. Org. Chem.* **2005**, 70, 5190; c) F. Mongin, A. Bucher, J. P. Bazureau, O. Bayh, H. Awad, F. Trécourt, *Tetrahedron Lett.* **2005**, 46, 7989.

- [88] a) K. Kitagawa, A. Inoue, H. Shinokubo, K. Oshima, *Angew. Chem. Int. Ed.* **2000**, *39*, 2481; b) A. Inoue, K. Kitagawa, H. Shinokubo, K. Oshima, *J. Org. Chem.* **2001**, *66*, 4333.
- [89] a) Y. Kondo, M. Shilai, M. Uchiyama, T. Sakamoto, *J. Am. Chem. Soc.* **1999**, *121*, 3539; b) T. Imahori, M. Uchiyama, T. Sakamoto, Y. Kondo, *Chem. Commun.* **2001**, 2450; c) M. Uchiyama, T. Miyoshi, Y. Kajihara, T. Sakamoto, Y. Otani, T. Ohwada, Y. Kondo, *J. Am. Chem. Soc.* **2002**, *124*, 8514; d) M. Uchiyama, Y. Matsumoto, D. Nobuto, T. Furuyama, K. Yamaguchi, K. Morokuma, *J. Am. Chem. Soc.* **2006**, *128*, 8748.
- [90] a) W. Clegg, S. H. Dale, E. Hevia, G. W. Honeyman, R. E. Mulvey, *Angew. Chem. Int. Ed.* **2006**, *45*, 2370; b) W. Clegg, S. H. Dale, R. W. Harrington, E. Hevia, G. W. Honeyman, R. E. Mulvey, *Angew. Chem. Int. Ed.* **2006**, *45*, 2374.
- [91] a) A. Seggio, F. Chevallier, M. Vaultier, F. Mongin, *J. Org. Chem.* **2007**, *72*, 6602; b) A. Seggio, M.-I. Lannou, F. Chevallier, D. Nobuto, M. Uchiyama, S. Golhen, T. Roisnel, F. Mongin, *Chem.–Eur. J.* **2007**, *13*, 9982; c) J.-M. L'Helgoual'ch, A. Seggio, F. Chevallier, M. Yonehara, E. Jeanneau, M. Uchiyama, F. Mongin, *J. Org. Chem.* **2008**, *73*, 177; d) K. Snégaroff, S. Komagawa, F. Chevallier, P. C. Gros, S. Golhen, T. Roisnel, M. Uchiyama, F. Mongin, *Chem.–Eur. J.* **2010**, *16*, 8191; e) F. Chevallier, Y. S. Halauko, C. Pecceu, I. F. Nassar, T. U. Dam, T. Roisnel, V. E. Matulis, O. A. Ivashkevich, F. Mongin, *Org. Biomol. Chem.* **2011**, *9*, 4671.
- [92] P. García-Álvarez, R. E. Mulvey, J. A. Parkinson, *Angew. Chem. Int. Ed.* **2011**, *50*, 9668.
- [93] P. García-Álvarez, D. V. Graham, E. Hevia, A. R. Kennedy, J. Klett, R. E. Mulvey, C. T. O'Hara, S. Weatherstone, *Angew. Chem. Int. Ed.* **2008**, *47*, 8079.
- [94] H. L. Hsieh, *J. Pol. Sci.: Pol. Chem. Ed.* **1976**, *14*, 379.
- [95] H. L. Hsieh, I. W. Wang, *Macromolecules* **1986**, *19*, 299.
- [96] T. A. Antkowiak, J. E. Hall, in *Eur. Pat. Appl.*, 0 747 405 A1, **1996**.
- [97] H. G. Richey Jr., J. Farkas Jr., *Organometallics* **1990**, *9*, 1778.
- [98] R. E. Mulvey, *Chem. Commun.* **2001**, 1049.
- [99] W. Clegg, G. C. Forbes, A. R. Kennedy, R. E. Mulvey, S. T. Liddle, *Chem. Commun.* **2003**, 406.
- [100] A. R. Kennedy, R. E. Mulvey, R. B. Rowlings, *J. Am. Chem. Soc.* **1998**, *120*, 7816.
- [101] G. Gokel, *Crown Ethers and Cryptands*, The Royal Society of Chemistry Cambridge, **1991**.
- [102] a) A. R. Kennedy, R. E. Mulvey, R. B. Rowlings, *Angew. Chem. Int. Ed.* **1998**, *37*, 3180; b) A. R. Kennedy, R. E. Mulvey, C. L. Raston, B. A. Roberts, R. B. Rowlings, *Chem. Commun.* **1999**, 353; c) G. C. Forbes, A. R. Kennedy, R. E. Mulvey, R. B. Rowlings, W. Clegg, S. T. Liddle, C. C. Wilson, *Chem. Commun.* **2000**, 1759; d) A. R. Kennedy, J. G. MacLellan, R. E. Mulvey, *Acta. Crystallogr. Sect. C* **2003**, *C59*, m302.
- [103] J. Wu, X. Pan, N. Tang, C.-C. Lin, *Inorg. Chem.* **2010**, *49*, 5362.
- [104] a) D. J. Gallagher, K. W. Henderson, A. R. Kennedy, C. T. O'Hara, R. E. Mulvey, R. B. Rowlings, *Chem. Commun.* **2002**, 376; b) P. C. Andrikopoulos, D. R. Armstrong, A. R. Kennedy, R. E. Mulvey, C. T. O'Hara, R. B. Rowlings, *Eur. J. Inorg. Chem.* **2003**, 3354.
- [105] D. R. Armstrong, A. R. Kennedy, R. E. Mulvey, R. B. Rowlings, *Angew. Chem. Int. Ed.* **1999**, *38*, 131.
- [106] E. Hevia, D. J. Gallagher, A. R. Kennedy, R. E. Mulvey, C. T. O'Hara, C. Talmard, *Chem. Commun.* **2004**, 2422.
- [107] P. C. Andrikopoulos, D. R. Armstrong, D. V. Graham, E. Hevia, A. R. Kennedy, R. E. Mulvey, C. T. O'Hara, C. Talmard, *Angew. Chem. Int. Ed.* **2005**, *44*, 3459.

- [108] D. V. Graham, E. Hevia, A. R. Kennedy, R. E. Mulvey, C. T. O'Hara, C. Talmard, *Chem. Commun.* **2006**, 417.
- [109] a) W. Clegg, K. W. Henderson, A. R. Kennedy, R. E. Mulvey, C. T. O'Hara, R. B. Rowlings, D. M. Tooke, *Angew. Chem. Int. Ed.* **2001**, *40*, 3902; b) P. C. Andrikopoulos, D. R. Armstrong, W. Clegg, C. J. Gilfillan, E. Hevia, A. R. Kennedy, R. E. Mulvey, C. T. O'Hara, J. A. Parkinson, D. M. Tooke, *J. Am. Chem. Soc.* **2004**, *126*, 11612.
- [110] a) E. Hevia, G. W. Honeyman, A. R. Kennedy, R. E. Mulvey, D. C. Sherrington, *Angew. Chem. Int. Ed.* **2005**, *44*, 68; b) P. C. Andrikopoulos, D. R. Armstrong, E. Hevia, A. R. Kennedy, R. E. Mulvey, *Organometallics* **2006**, *25*, 2415.
- [111] P. C. Andrikopoulos, D. R. Armstrong, H. R. L. Barley, W. Clegg, S. H. Dale, E. Hevia, G. W. Honeyman, A. R. Kennedy, R. E. Mulvey, *J. Am. Chem. Soc.* **2005**, *127*, 6184.
- [112] W. Clegg, S. H. Dale, E. Hevia, L. M. Hogg, G. W. Honeyman, R. E. Mulvey, C. T. O'Hara, *Angew. Chem. Int. Ed.* **2006**, *45*, 6548.
- [113] D. R. Armstrong, V. L. Blair, W. Clegg, S. H. Dale, J. García-Álvarez, G. W. Honeyman, E. Hevia, R. E. Mulvey, L. Russo, *J. Am. Chem. Soc.* **2010**, *132*, 9480.
- [114] D. R. Armstrong, W. Clegg, S. H. Dale, E. Hevia, L. M. Hogg, G. W. Honeyman, R. E. Mulvey, *Angew. Chem. Int. Ed.* **2006**, *45*, 3775.
- [115] B. Conway, E. Hevia, A. R. Kennedy, R. E. Mulvey, *Chem. Commun.* **2007**, 2864.
- [116] D. R. Armstrong, J. García-Álvarez, D. V. Graham, G. W. Honeyman, E. Hevia, A. R. Kennedy, R. E. Mulvey, *Chem.–Eur. J.* **2009**, *15*, 3800.
- [117] L. Balloch, A. R. Kennedy, J. Klett, R. E. Mulvey, C. T. O'Hara, *Chem. Commun.* **2010**, *46*, 2319.
- [118] L. Balloch, A. R. Kennedy, R. E. Mulvey, T. Rantanen, S. D. Robertson, V. Snieckus, *Organometallics* **2011**, *30*, 145.
- [119] A. R. Kennedy, J. Klett, R. E. Mulvey, D. S. Wright, *Science* **2009**, *326*, 706.
- [120] W. Clegg, S. H. Dale, A. M. Drummond, E. Hevia, G. W. Honeyman, R. E. Mulvey, *J. Am. Chem. Soc.* **2006**, *128*, 7434.
- [121] a) M. Uchiyama, Y. Matsumoto, S. Usui, Y. Hashimoto, K. Morokuma, *Angew. Chem. Int. Ed.* **2007**, *46*, 926; b) Y. Kondo, J. V. Morey, J. C. Morgan, H. Naka, D. Nobuto, P. R. Raithby, M. Uchiyama, A. E. H. Wheatley, *J. Am. Chem. Soc.* **2007**, *129*, 12734.
- [122] D. Nobuto, M. Uchiyama, *J. Org. Chem.* **2008**, *73*, 1117.
- [123] W. Clegg, B. Conway, E. Hevia, M. D. McCall, L. Russo, R. E. Mulvey, *J. Am. Chem. Soc.* **2009**, *131*, 2375.
- [124] H. R. L. Barley, W. Clegg, S. H. Dale, E. Hevia, G. W. Honeyman, A. R. Kennedy, R. E. Mulvey, *Angew. Chem. Int. Ed.* **2005**, *44*, 6018.
- [125] D. R. Armstrong, W. Clegg, S. H. Dale, J. García-Álvarez, R. W. Harrington, E. Hevia, G. W. Honeyman, A. R. Kennedy, R. E. Mulvey, C. T. O'Hara, *Chem. Commun.* **2008**, 187.
- [126] J. F. Couch, *J. Am. Chem. Soc.* **1936**, *58*, 1296.
- [127] a) D. Hoppe, F. Hintze, P. Tebben, M. Paetow, H. Ahrens, J. Schwerdtfeger, P. Sommerfeld, J. Haller, W. Guarnieri, S. Kolczewski, T. Hense, I. Hoppe, *Pure Appl. Chem.* **1994**, *66*, 1479; b) J. C. Anderson, J. D. Osborne, T. J. Woltering, *Org. Biomol. Chem.* **2008**, *6*, 330; c) B. P. McDermott, A. D. Campbell, A. Ertan, *Synlett* **2008**, 875; d) U. Groth, P. Köttgen, P. Langenbach, A. Lindenmaier, T. Schütz, M. Wiegand, *Synlett* **2008**, 1301; e) J. Clayden, L. Lemiègre, M. Pickworth, *Tetrahedron: Asymmetry* **2008**, *19*, 2218.
- [128] A. L. Hogan, D. O'Shea, *Chem. Commun.* **2008**, 3839.
- [129] a) P. Beak, A. Basu, D. J. Gallagher, Y. S. Park, S. Thayumanavan, *Acc. Chem. Res.* **1996**, *29*, 552; b) D. Hoppe, T. Hense, *Angew. Chem. Int. Ed. Engl.* **1997**, *36*, 2282; c)

- P. O'Brien, *J. Chem. Soc., Perkin Trans. 1* **1998**, 1439; d) T. Schütz, *Synlett* **2003**, 901; e) J.-C. Kizirian, *Chem. Rev.* **2008**, *108*, 140; f) M. R. Lauderer, W. F. Bailey, M. R. Lauderer, J. D. Fair, R. J. Dancer, M. B. Sommer, *Tetrahedron: Asymmetry* **2009**, *20*, 981.
- [130] N. Nozaki, T. Aratani, T. Toraya, *Tetrahedron Lett.* **1968**, *9*, 4097.
- [131] M. Guetté, J. Capillon, J.-P. Guetté, *Tetrahedron* **1973**, *29*, 3659.
- [132] Y. Okamoto, K. Suzuki, T. Kitayama, H. Yuki, H. Kageyama, K. Miki, N. Tanaka, N. Kasai, *J. Am. Chem. Soc.* **1982**, *104*, 4618.
- [133] D. Hoppe, F. Hintze, P. Tebben, *Angew. Chem. Int. Ed. Engl.* **1990**, *29*, 1422.
- [134] a) S. T. Kerrick, P. Beak, *J. Am. Chem. Soc.* **1991**, *113*, 9708; b) P. Beak, S. T. Kerrick, S. Wu, J. Chu, *J. Am. Chem. Soc.* **1994**, *116*, 3231.
- [135] M. Tsukazaki, M. Tinkl, A. Roglans, B. J. Chapell, N. J. Taylor, V. Snieckus, *J. Am. Chem. Soc.* **1996**, *118*, 685.
- [136] D. M. Hodgson, G. P. Lee, *Chem. Commun.* **1996**, 1015.
- [137] a) K. R. Campos, A. Klapars, J. H. Waldman, P. G. Dormer, C. Chen, *J. Am. Chem. Soc.* **2006**, *128*, 3538; b) A. Klapars, K. R. Campos, J. H. Waldman, D. Zewge, P. G. Dormer, C.-Y. Chen, *J. Org. Chem.* **2008**, *73*, 4986; c) G. Barker, J. L. McGrath, A. Klapars, D. Stead, G. Zhou, K. R. Campos, P. O'Brien, *J. Org. Chem.* **2011**, *76*, 5936.
- [138] J. J. Gammon, P. O'Brien, B. Kelly, *Org. Lett.* **2009**, *11*, 5022.
- [139] S. J. Canipa, P. O'Brien, S. Taylor, *Tetrahedron: Asymmetry* **2009**, *20*, 2407.
- [140] J. Granander, F. Secci, P. O'Brien, B. Kelly, *Tetrahedron: Asymmetry* **2009**, *20*, 2432.
- [141] J. J. Gammon, V. H. Gessner, G. R. Barker, J. Granander, A. C. Whitwood, C. Strohmman, P. O'Brien, B. Kelly, *J. Am. Chem. Soc.* **2010**, *132*, 13922.
- [142] J. Granander, F. Secci, S. J. Canipa, P. O'Brien, B. Kelly, *J. Org. Chem.* **2011**, *76*, 4794.
- [143] W. Tang, X. Zhang, *Chem. Rev.* **2003**, *103*, 3029.
- [144] a) B. D. Vineyard, W. S. Knowles, M. J. Sabacky, G. L. Bachman, O. J. Weinkauff, *J. Am. Chem. Soc.* **1977**, *99*, 5946; b) W. S. Knowles, *Acc. Chem. Res.* **1983**, *16*, 106.
- [145] W. S. Knowles, *Angew. Chem. Int. Ed.* **2002**, *41*, 1998.
- [146] W. S. Knowles, *J. Chem. Educ.* **1986**, *63*, 222.
- [147] in *Parkinson's disease: national clinical guideline for diagnosis and management in primary and secondary care*, Royal College of Physicians, London, **2006**, pp. 59-100.
- [148] V. H. Gessner, C. Däschlein, C. Strohmman, *Chem.–Eur. J.* **2009**, *15*, 3320.
- [149] C. Strohmman, T. Seibel, K. Strohfeltdt, *Angew. Chem. Int. Ed.* **2003**, *42*, 4531.
- [150] C. Strohmman, K. Strohfeltdt, D. Schildbach, *J. Am. Chem. Soc.* **2003**, *125*, 13672.
- [151] M. Vestergren, J. Eriksson, G. Hilmersson, M. Håkansson, *J. Organomet. Chem.* **2003**, *682*, 172.
- [152] C. Strohmman, S. Dilsky, K. Strohfeltdt, *Organometallics* **2006**, *25*, 41.
- [153] F. Marr, R. Fröhlich, D. Hoppe, *Tetrahedron: Asymmetry* **2002**, *13*, 2587.
- [154] C. Strohmman, C. Däschlein, D. Auer, *J. Am. Chem. Soc.* **2006**, *128*, 704.
- [155] C. Däschlein, C. Strohmman, *Eur. J. Inorg. Chem.* **2009**, 43.
- [156] T. Tatic, O. Holger, D. Stalke, *Eur. J. Inorg. Chem.* **2008**, 3765.
- [157] a) R. Sott, M. Håkansson, G. Hilmersson, *Organometallics* **2006**, *25*, 6047; b) G. Carbone, P. O'Brien, G. Hilmersson, *J. Am. Chem. Soc.* **2010**, *132*, 15445.
- [158] J. L. Rutherford, D. Hoffmann, D. B. Collum, *J. Am. Chem. Soc.* **2002**, *124*, 264.
- [159] a) D. J. Gallagher, S. T. Kerrick, P. Beak, *J. Am. Chem. Soc.* **1992**, *114*, 5872; b) D. J. Gallagher, P. Beak, *J. Org. Chem.* **1995**, *60*, 7092.
- [160] J.-C. Kizirian, *Top. Stereochem.* **2010**, *26*, 189.
- [161] a) I. Hoppe, M. Marsch, K. Harms, G. Boche, D. Hoppe, *Angew. Chem. Int. Ed. Engl.* **1995**, *34*, 2158; b) S. Wu, S. Lee, P. Beak, *J. Am. Chem. Soc.* **1996**, *118*, 715; c) Y. S. Park, M. S. Boys, P. Beak, *J. Am. Chem. Soc.* **1996**, *118*, 3757; d) K. M. Bertini Gross, Y. M. Jun, P. Beak, *J. Org. Chem.* **1997**, *62*, 7679; e) Z. Pakulski, M.



- Koprowski, K. M. Pietrusiewicz, *Tetrahedron* **2003**, *59*, 8219; f) J. Huang, P. O'Brien, *Chem. Commun.* **2005**, 5696; g) S. V. Kessar, P. Singh, K. Nain Singh, P. Venugopalan, A. Kaur, P. V. Bharatam, A. K. Sharma, *J. Am. Chem. Soc.* **2007**, *129*, 4506; h) D. M. Hodgson, J. Kloesges, *Angew. Chem. Int. Ed.* **2010**, *49*, 2900.
- [162] A. R. Kennedy, C. T. O'Hara, *Dalton Trans.* **2008**, *37*, 4975.
- [163] a) D. A. Fletcher, R. F. McMeeking, D. Parkin, *J. Chem. Inf. Comput. Sci.* **1996**, *36*, 746; b) F. H. Allen, *Acta. Crystallogr. Sect. B* **2002**, *B58*, 380; c) I. J. Bruno, J. C. Cole, P. R. Edgington, M. Kessler, C. F. Macrae, P. McCabe, J. Pearson, R. Taylor, *Acta. Crystallogr. Sect. B* **2002**, *B58*, 389.
- [164] a) T. Ebner, M. Eichelbaum, P. Fischer, C. O. Messe, *Arch. Pharm.* **1989**, 322, 399; b) T. B. Smith, J. A. Wendt, J. Aubé, *Org. Lett.* **2002**, *4*, 2577.
- [165] N. J. Leonard, R. E. Beyler, *J. Am. Chem. Soc.* **1950**, *72*, 1316.
- [166] a) J.-C. Kizirian, N. Cabello, A. Alexakis, *Tetrahedron Lett.* **2003**, *44*, 8893; b) N. Cabello, J.-C. Kizirian, S. Gille, A. Alexakis, G. Bernardinelli, L. Pinchard, J.-C. Caille, *Eur. J. Org. Chem.* **2005**, 4835; c) J.-C. Kizirian, N. Cabello, L. Pinchard, J.-C. Caille, A. Alexakis, *Tetrahedron* **2005**, *61*, 8939; d) S. Gille, N. Cabello, J.-C. Kizirian, A. Alexakis, *Tetrahedron: Asymmetry* **2006**, *17*, 1045.
- [167] a) J. R. Harrison, P. O'Brien, D. W. Porter, N. M. Smith, *Chem. Commun.* **2001**, 1202; b) M. J. Dearden, C. R. Firkin, J.-P. R. Hermet, P. O'Brien, *J. Am. Chem. Soc.* **2002**, *124*, 11870; c) J.-P. R. Hermet, D. W. Porter, M. J. Dearden, J. R. Harrison, T. Koplin, P. O'Brien, J. Parmene, V. Tyurin, A. C. Whitwood, J. Gilday, N. M. Smith, *Org. Biomol. Chem.* **2003**, *1*, 3977; d) M. J. Dearden, M. J. McGrath, P. O'Brien, *J. Org. Chem.* **2004**, *69*, 5789; e) P. O'Brien, K. B. Wilberg, W. F. Bailey, J.-P. R. Hermet, M. J. McGrath, *J. Am. Chem. Soc.* **2004**, *126*, 15480; f) M. J. McGrath, P. O'Brien, *J. Am. Chem. Soc.* **2005**, *127*, 16378; g) C. Genet, M. J. McGrath, P. O'Brien, *Org. Biomol. Chem.* **2006**, *4*, 1376; h) J.-P. R. Hermet, A. Viterisi, J. M. Wright, M. J. McGrath, P. O'Brien, A. C. Whitwood, J. Gilday, *Org. Biomol. Chem.* **2007**, *5*, 3614; i) P. O'Brien, *Chem. Commun.* **2008**, 655; j) D. Stead, P. O'Brien, A. Sanderson, *Org. Lett.* **2008**, *10*, 1409; k) D. Stead, G. Carbone, P. O'Brien, K. R. Campos, I. Coldham, A. Sanderson, *J. Am. Chem. Soc.* **2010**, *132*, 7260.
- [168] a) D. J. Gallagher, S. Wu, N. A. Nikolic, P. Beak, *J. Org. Chem.* **1995**, *60*, 8148; b) E.-U. Würthwein, K. Behrens, D. Hoppe, *Chem.–Eur. J.* **1999**, *5*, 3459; c) M. J. McGrath, J. L. Bilke, P. O'Brien, *Chem. Commun.* **2006**, 2607.
- [169] C. Strohmam, V. H. Gessner, *J. Am. Chem. Soc.* **2007**, *129*, 8952.
- [170] C. Strohmam, V. H. Gessner, *J. Am. Chem. Soc.* **2008**, *130*, 11719.
- [171] V. H. Gessner, B. Fröhlich, C. Strohmam, *Eur. J. Inorg. Chem.* **2010**, 5640.
- [172] V. H. Gessner, C. Strohmam, *Dalton Trans.* **2012**, 3452.
- [173] V. H. Gessner, S. Dilsky, C. Strohmam, *Chem. Commun.* **2010**, *46*, 4719.
- [174] D. Hoffman, D. B. Collum, *J. Am. Chem. Soc.* **1998**, *120*, 5810.
- [175] H. Doi, T. Sakai, M. Iguchi, K.-I. Yamada, K. Tomioka, *J. Am. Chem. Soc.* **2003**, *125*, 2886.
- [176] a) D. Seebach, *Angew. Chem. Int. Ed. Engl.* **1988**, *27*, 1624; b) B. Tchoubar, A. Loupy, *Salt Effects in Organic and Organometallic Chemistry*, Wiley-VCH, New York, **1992**; c) B. J. Bunn, N. S. Simpkins, *J. Org. Chem.* **1993**, *58*, 533; d) P. Caubère, *Chem. Rev.* **1993**, *93*, 2317; e) A. Yanagisawa, T. Kikuchi, H. Yamamoto, *Synlett* **1998**, 174; f) G. Asensio, P. Aleman, J. Gil, L. R. Domingo, M. Medio-Simon, *J. Org. Chem.* **1998**, *63*, 9342; g) D. Simoni, M. Roberti, R. Rondanin, A. P. Kozikowski, *Tetrahedron Lett.* **1999**, *40*, 4425; h) F. Cottet, M. Schlosser, *Eur. J. Org. Chem.* **2004**, 3793; i) E. Hevia, R. E. Mulvey, *Angew. Chem. Int. Ed.* **2011**, *50*, 6448.
- [177] a) E. C. Ashby, S. A. Noding, *J. Org. Chem.* **1979**, *44*, 4371; b) Y. Yamamoto, J.-I. Yamada, *J. Chem. Soc., Chem. Commun.* **1988**, 802; c) A. S. Galiano Roth, Y.-J. Kim, J. H. Gilchrist, A. T. Harrison, D. J. Fuller, D. B. Collum, *J. Am. Chem. Soc.* **1991**,

- 113, 5053; d) P. L. Hall, J. H. Gilchrist, D. B. Collum, *J. Am. Chem. Soc.* **1991**, *113*, 9571; e) F. S. Mair, W. Clegg, P. A. O'Neil, *J. Am. Chem. Soc.* **1993**, *115*, 3388; f) D. Seebach, A. K. Beck, A. Studer, *Mod. Synth. Methods* **1995**, *7*, 1; g) B. H. Lipschutz, M. R. Wood, C. W. Lindsley, *Tetrahedron Lett.* **1995**, *36*, 4385; h) K. W. Henderson, A. E. Dorigo, Q.-Y. Liu, P. G. Williard, P. v. R. Schleyer, P. R. Bernstein, *J. Am. Chem. Soc.* **1996**, *118*, 1339.
- [178] a) A. Krasovskiy, V. Malakhov, A. Gavryushin, P. Knochel, *Angew. Chem. Int. Ed.* **2006**, *45*, 6040; b) H. Ren, G. Dunet, P. Mayer, P. Knochel, *Angew. Chem. Int. Ed.* **2007**, *129*, 5376; c) F. Paté, N. Duguet, H. Oulyadi, A. Harrison-Marchand, C. Fressigné, J.-Y. Valnot, M.-C. Lasne, J. Maddaluno, *J. Org. Chem.* **2007**, *72*, 6982; d) S. H. Wunderlich, P. Knochel, *Angew. Chem. Int. Ed.* **2007**, *46*, 7685; e) N. Boudet, S. Sase, P. Sinha, C.-Y. Liu, A. Krasovskiy, P. Knochel, *J. Am. Chem. Soc.* **2007**, *129*, 12358; f) A. Metzger, M. A. Schade, P. Knochel, *Org. Lett.* **2008**, *10*, 1107; g) H. Ochiai, M. Jang, K. Hirano, H. Yorimitsu, K. Oshima, *Org. Lett.* **2008**, *10*, 2681; h) S. Wunderlich, P. Knochel, *Org. Lett.* **2008**, *10*, 4705; i) A. M. Dyke, D. M. Gill, J. N. Harvey, A. J. Hester, G. C. Lloyd-Jones, M. P. Muñoz, I. R. Shepperson, *Angew. Chem. Int. Ed.* **2008**, *47*, 5067; j) S. Wunderlich, P. Knochel, *Chem. Commun.* **2008**, 6387; k) D. A. Kummer, W. J. Chain, M. R. Morales, O. Quiroga, A. G. Myers, *J. Am. Chem. Soc.* **2008**, *130*, 13231; l) Z. Dong, G. C. Clososki, S. H. Wunderlich, A. Unsinn, J. Li, P. Knochel, *Chem.–Eur. J.* **2009**, *15*, 457; m) K. Koszinowski, P. Böhler, *Organometallics* **2009**, *28*, 771; n) L. Gupta, A. C. Hoepker, K. L. Singh, D. B. Collum, *J. Org. Chem.* **2009**, *74*, 2231; o) L. Salvi, J. G. Kim, P. J. Walsh, *J. Am. Chem. Soc.* **2009**, *131*, 12483; p) L. Jin, C. Liu, J. Liu, F. Hu, Y. Lan, A. S. Batsanov, J. A. K. Howard, T. B. Marder, A. Lei, *J. Am. Chem. Soc.* **2009**, *131*, 16656; q) M. Hatano, O. Ito, S. Suzuki, K. Ishihara, *Chem. Commun.* **2010**, *46*, 2674; r) D. R. Armstrong, P. García-Álvarez, A. R. Kennedy, R. E. Mulvey, J. A. Parkinson, *Angew. Chem. Int. Ed.* **2010**, *49*, 3185; s) G. T. Achonduh, N. Hadei, C. Valente, S. Avola, C. J. O'Brien, M. G. Organ, *Chem. Commun.* **2010**, *46*, 4109; t) M. Hatano, O. Ito, S. Suzuki, K. Ishihara, *J. Org. Chem.* **2010**, *75*, 5008; u) B. Lecachey, H. Oulyadi, P. Lameiras, A. Harrison-Marchand, H. Gérard, J. Maddaluno, *J. Org. Chem.* **2010**, *75*, 5976; v) Y. Ma, A. C. Hoepker, L. Gupta, M. F. Faggin, D. B. Collum, *J. Am. Chem. Soc.* **2010**, *132*, 15610; w) D. Stern, N. Finkelmeier, D. Stalke, *Chem. Commun.* **2011**, *47*, 2113; x) A. C. Hoepker, L. Gupta, Y. Ma, M. F. Faggin, D. B. Collum, *J. Am. Chem. Soc.* **2011**, *133*, 7135; y) A. C. Hoepker, D. B. Collum, *J. Org. Chem.* **2011**, *76*, 7985; z) B. Lecachey, C. Fressigné, H. Oulyadi, A. Harrison-Marchand, J. Maddaluno, *Chem. Commun.* **2011**, *47*, 9915.
- [179] F. Schmidt, R. T. Stemmler, J. Rudolph, C. Bolm, *Chem. Soc. Rev.* **2006**, *35*, 454.
- [180] E. Hevia, J. Z. Chua, P. García-Álvarez, A. R. Kennedy, M. D. McCall, *Proc. Nat. Acad. Sci. USA* **2010**, *107*, 5294.
- [181] R. Campbell, B. Conway, G. S. Fairweather, P. García-Álvarez, A. R. Kennedy, J. Klett, R. E. Mulvey, C. T. O'Hara, G. M. Robertson, *Dalton Trans.* **2010**, *39*, 511.
- [182] K. W. Henderson, A. E. Dorigo, Q.-L. Liu, P. G. Williard, *J. Am. Chem. Soc.* **1997**, *119*, 11855.
- [183] A. R. Kennedy, J. Klett, C. T. O'Hara, R. E. Mulvey, G. M. Robertson, *Eur. J. Inorg. Chem.* **2009**, 5029.
- [184] A. R. Kennedy, R. E. Mulvey, S. D. Robertson, *Dalton Trans.* **2010**, *39*, 9091.
- [185] a) A. R. Kennedy, R. E. Mulvey, R. B. Rowlings, *Angew. Chem. Int. Ed.* **1999**, *37*, 3180; b) P. C. Andrews, A. R. Kennedy, R. E. Mulvey, C. L. Raston, B. A. Roberts, R. B. Rowlings, *Angew. Chem. Int. Ed.* **2000**, *39*, 1960; c) L. Barr, A. R. Kennedy, J. G. MacLellan, J. H. Moir, R. E. Mulvey, P. J. A. Rodger, *Chem. Commun.* **2000**, 1757; d) K. W. Henderson, A. R. Kennedy, R. E. Mulvey, C. T. O'Hara, R. B. Rowlings, *Chem. Commun.* **2001**, 1678; e) A. M. Drummond, L. T. Gibson, A. R.

- Kennedy, R. E. Mulvey, C. T. O'Hara, R. B. Rowlings, T. Weightman, *Angew. Chem. Int. Ed.* **2002**, *41*, 2382.
- [186] B. Conway, E. Hevia, A. R. Kennedy, R. E. Mulvey, S. Weatherstone, *Dalton Trans.* **2005**, 1532.
- [187] D. R. Armstrong, W. Clegg, S. H. Dale, D. V. Graham, E. Hevia, L. M. Hogg, G. W. Honeyman, A. R. Kennedy, R. E. Mulvey, *Chem. Commun.* **2007**, 598.
- [188] W. Clegg, S. H. Dale, E. Hevia, L. M. Hogg, G. W. Honeyman, R. E. Mulvey, C. T. O'Hara, L. Russo, *Angew. Chem. Int. Ed.* **2008**, *47*, 731.
- [189] W. Clegg, J. García-Álvarez, P. García-Álvarez, D. V. Graham, R. W. Harrington, E. Hevia, A. R. Kennedy, R. E. Mulvey, L. Russo, *Organometallics* **2008**, *27*, 2654.
- [190] M. Westerhausen, B. Rademacher, W. Schwarz, *Z. Naturforsch., B: Chem. Sci.* **1994**, *49*, 199.
- [191] D. R. Armstrong, E. Herd, D. V. Graham, E. Hevia, A. R. Kennedy, W. Clegg, L. Russo, *Dalton Trans.* **2008**, 1323.
- [192] W. Clegg, D. V. Graham, E. Herd, E. Hevia, A. R. Kennedy, M. D. McCall, L. Russo, *Inorg. Chem.* **2009**, *48*, 5320.
- [193] a) D. Theonnes, E. Weiss, *Chem. Ber.* **1978**, *111*, 3726; b) T. Greiser, J. Kopf, D. Theonnes, E. Weiss, *Chem. Ber.* **1981**, *114*, 209; c) B. Schubert, E. Weiss, *Chem. Ber.* **1984**, *117*, 366; d) K. M. Waggoner, P. P. Power, *Organometallics* **1992**, *11*, 3209; e) W. Clegg, K. W. Henderson, R. E. Mulvey, P. A. O'Neil, *J. Chem. Soc., Chem. Commun.* **1994**, 769; f) G. C. Forbes, A. R. Kennedy, R. E. Mulvey, P. J. A. Rodger, *Chem. Commun.* **2001**, 1400; g) G. C. Forbes, A. R. Kennedy, R. E. Mulvey, B. A. Roberts, R. B. Rowlings, *Organometallics* **2002**, *21*, 5115; h) E. Hevia, F. R. Kenley, A. R. Kennedy, R. E. Mulvey, R. B. Rowlings, *Eur. J. Inorg. Chem.* **2003**, 3347; i) G. W. Honeyman, A. R. Kennedy, R. E. Mulvey, D. C. Sherrington, *Organometallics* **2004**, *23*, 1197; j) H. Awad, F. Mongin, F. Trécourt, G. Quéguiner, F. Marsais, F. Blanco, B. Abarca, R. Ballesteros, *Tetrahedron Lett.* **2004**, *45*, 6697; k) H. Awad, F. Mongin, F. Trécourt, G. Quéguiner, F. Marsais, *Tetrahedron Lett.* **2004**, *45*, 7873; l) P. C. Andrikopoulos, D. R. Armstrong, E. Hevia, A. R. Kennedy, R. E. Mulvey, C. T. O'Hara, *Chem. Commun.* **2005**, 1131; m) P. C. Andrikopoulos, D. R. Armstrong, A. R. Kennedy, R. E. Mulvey, C. T. O'Hara, R. B. Rowlings, S. Weatherstone, *Inorg. Chim. Acta.* **2007**, *360*, 1370; n) J. J. Morris, B. C. Noll, G. W. Honeyman, C. T. O'Hara, A. R. Kennedy, R. E. Mulvey, K. W. Henderson, *Chem.–Eur. J.* **2007**, *13*, 4418; o) J. García-Álvarez, D. V. Graham, E. Hevia, A. R. Kennedy, R. E. Mulvey, *Dalton Trans.* **2008**, 1481; p) V. L. Blair, A. R. Kennedy, J. Klett, R. E. Mulvey, *Chem. Commun.* **2008**, 5426; q) R. E. Mulvey, V. L. Blair, W. Clegg, A. R. Kennedy, J. Klett, L. Russo, *Nature Chemistry* **2010**, *2*, 588; r) V. L. Blair, A. R. Kennedy, R. E. Mulvey, C. T. O'Hara, *Chem.–Eur. J.* **2010**, *16*, 8600; s) M. S. Hill, G. Kociok-Kohn, D. J. MacDougall, *Inorg. Chem.* **2011**, *50*, 5234.
- [194] a) S. A. Couper, R. E. Mulvey, D. C. Sherrington, *Eur. Polym. J.* **1998**, *34*, 1877; b) W. Clegg, L. Horsburgh, S. A. Couper, R. E. Mulvey, *Acta. Crystallogr. Sect. C* **1999**, *C55*, 867.
- [195] C. Klein, H. Nöth, M. Tacke, M. Thomann, *Angew. Chem. Int. Ed. Engl.* **1993**, *32*, 886.
- [196] B. Conway, P. García-Álvarez, A. R. Kennedy, J. Klett, R. E. Mulvey, S. D. Robertson, *New J. Chem.* **2010**, *34*, 1707.
- [197] E. Hevia, G. W. Honeyman, A. R. Kennedy, R. E. Mulvey, *J. Am. Chem. Soc.* **2005**, *127*, 13106.
- [198] Prepared by PhD student Ross Campbell.
- [199] P. G. Williard, M. J. Hintze, *J. Am. Chem. Soc.* **1992**, *112*, 8602.
- [200] L. M. Carrella, C. Förster, A. R. Kennedy, J. Klett, R. E. Mulvey, E. Rentschler, *Organometallics* **2010**, *29*, 4756.

- [201] W. Clegg, S. Kleditzsch, R. E. Mulvey, P. O'Shaughnessy, *J. Organomet. Chem.* **1998**, 558, 193.
- [202] a) C. Knapp, E. Lork, T. Borrmann, W.-D. Stohrer, R. Mews, *Z. Anorg. Allg. Chem.* **2005**, 631, 1885; b) W. Clegg, S. H. Dale, D. V. Graham, R. W. Harrington, E. Hevia, L. M. Hogg, A. R. Kennedy, R. E. Mulvey, *Chem. Commun.* **2007**, 1641; c) M. S. Denning, M. Irwin, J. M. Goicoechea, *Inorg. Chem.* **2008**, 47, 6118; d) R. Campbell, D. Cannon, P. García-Álvarez, A. R. Kennedy, R. E. Mulvey, S. D. Robertson, J. Sassmanshausen, T. Tuttle, *J. Am. Chem. Soc.* **2011**, 133, 13706.
- [203] a) U. Schumann, U. Behrens, E. Weiss, *Angew. Chem. Int. Ed. Engl.* **1989**, 28, 476; b) R. Forret, A. R. Kennedy, J. Klett, R. E. Mulvey, S. D. Robertson, *Organometallics* **2010**, 29, 1436; c) J. J. Crawford, B. J. Fleming, A. R. Kennedy, J. Klett, C. T. O'Hara, S. A. Orr, *Chem. Commun.* **2011**, 47, 3772; d) D. R. Armstrong, A. R. Kennedy, R. E. Mulvey, S. D. Robertson, *Chem.–Eur. J.* **2011**, 17, 8820.
- [204] a) B. Teclé, W. H. Ilsley, J. P. Oliver, *Organometallics* **1982**, 1, 875; b) S. Harder, J. Boersma, L. Brandsma, *J. Organomet. Chem.* **1988**, 339, 7; c) M. A. Nichols, P. G. Williard, *J. Am. Chem. Soc.* **1993**, 115, 1568; d) N. D. R. Barnett, R. E. Mulvey, W. Clegg, P. A. O'Neil, *J. Am. Chem. Soc.* **1993**, 115, 1573; e) D. Hoffman, A. Dorigo, P. v. R. Schleyer, H. Reif, D. Stalke, G. M. Sheldrick, E. Weiss, M. Geissler, *Inorg. Chem.* **1995**, 34, 262.
- [205] F. T. Edelmann, F. Pauer, M. Wedler, D. Stalke, *Inorg. Chem.* **1992**, 31, 4143.
- [206] M. Karl, G. Seybert, W. Massa, K. Harms, S. Agarwal, R. Maleika, W. Stelter, A. Greiner, W. Heitz, B. Neumüller, K. Dehnicke, *Z. Anorg. Allg. Chem.* **1999**, 625, 1301.
- [207] P. C. Andrews, N. D. R. Barnett, R. E. Mulvey, W. Clegg, P. A. O'Neil, D. Barr, L. Cowton, A. J. Dawson, B. J. Wakefield, *J. Organomet. Chem.* **1996**, 518, 85.
- [208] A search of the CCDC reveals 105 examples of the lithium cation, 9 examples of the sodium cation and 19 examples of the magnesium anion (see references within section 2.3 for representative examples).
- [209] M. Westerhausen, W. Schwarz, *Z. Anorg. Allg. Chem.* **1992**, 609, 39.
- [210] a) K. R. Pörschke, W. Kleimann, G. Wilke, K. H. Claus, C. Krüger, *Angew. Chem. Int. Ed. Engl.* **1983**, 22, 991; b) R. Goddard, C. Krüger, K. R. Pörschke, G. Wilke, *J. Organomet. Chem.* **1986**, 308, 85; c) C. L. Raston, B. W. Skelton, C. R. Whitaker, A. H. White, *Aust. J. Chem.* **1988**, 41, 1621; d) P. J. Bonasia, J. Arnold, *J. Chem. Soc., Chem. Commun.* **1990**, 1299; e) N. S. Hosmane, K.-J. Lu, H. Zhang, J. A. Maguire, *Organometallics* **1997**, 16, 5163; f) A. Caselli, E. Solari, R. Scopelliti, C. Floriani, N. Re, C. Rizzoli, A. Chiesi-Villa, *J. Am. Chem. Soc.* **2000**, 122, 3652.
- [211] L. T. Wendell, J. Bender, X. He, B. C. Noll, K. W. Henderson, *Organometallics* **2006**, 25, 4953.
- [212] R. J. Morris, G. S. Girolami, *Organometallics* **1991**, 10, 792.
- [213] C. P. Gerlach, J. Arnold, *Organometallics* **1997**, 16, 5148.
- [214] M. M. Andrianarison, A. G. Avent, M. C. Ellerby, I. B. Gorrell, P. B. Hitchcock, J. D. Smith, D. R. Stanley, *J. Chem. Soc., Dalton Trans.* **1998**, 249.
- [215] R. K. Minhas, L. Scoles, S. Wong, S. Gambarotta, *Organometallics* **1996**, 15, 1113.
- [216] a) L. Xie, K. M. Isenberger, G. Held, L. M. Dahl, *J. Org. Chem.* **1997**, 62, 7516; b) L. Xie, K. Vanlandeghem, K. M. Isenberger, C. Bernier, *J. Org. Chem.* **2003**, 68, 641; c) T. Abe, C. Sato, H. Ushiroguchi, K. Sato, T. Takasaki, T. Isoda, A. Mihira, I. Yamamura, K. Hayashi, T. Kumagai, S. Tamai, M. Shiro, A. M. Venkatesan, T. S. Mansour, *J. Org. Chem.* **2004**, 69, 5850; d) X.-X. Yan, C.-G. Liang, Y. Zhang, W. Hong, B.-X. Cao, L.-X. Dai, X.-L. Hou, *Angew. Chem. Int. Ed.* **2005**, 44, 6544; e) M. E. Jung, T.-H. Zhang, *Org. Lett.* **2008**, 10, 137.
- [217] a) H. Fujisawa, T. Mukaiyama, *Chem. Lett.* **2002**, 182; b) T. Mukaiyama, H. Fujisawa, T. Nakagawa, *Helv. Chim. Acta.* **2002**, 85, 4518.

- [218] a) T. Satoh, M. Yoshida, Y. Takahashi, H. Ota, *Tetrahedron: Asymmetry* **2003**, *14*, 281; b) T. Satoh, T. Kawashima, S. Takahashi, K. Sakai, *Tetrahedron* **2003**, *59*, 9599.
- [219] a) Z. Gebeyehu, F. Weller, B. Neumüller, K. Dehnicke, *Z. Anorg. Allg. Chem.* **1991**, *593*, 99; b) F. Preuss, M. Vogel, U. Fischbeck, J. Perner, G. Overhoff, E. Fuchslocher, F. Tabellion, B. Geiger, G. Wolmershäuser, *Z. Naturforsch., B* **2001**, *56*, 1100; c) Y. Yao, Y. Zhang, Q. Shen, K. Yu, *Organometallics* **2002**, *21*, 819; d) F. Amor, J. Sánchez-Nieves, P. Royo, H. Jacobsen, O. Blacque, H. Berke, M. Lanfranchi, M. A. Pellinghelli, A. Tiripicchio, *Eur. J. Inorg. Chem.* **2002**, 2810; e) H. Link, P. Reiss, S. Chitsaz, H. Pfistner, D. Fenske, *Z. Anorg. Allg. Chem.* **2003**, *629*, 755; f) G. Mund, D. Vidovic, R. J. Batchelor, J. F. Britten, R. D. Sharma, C. H. W. Jones, D. B. Leznoff, *Chem.–Eur. J.* **2003**, *9*, 4757; g) A. Friedrich, U. Radius, *Eur. J. Inorg. Chem.* **2004**, 4300; h) T. A. Betley, J. C. Peters, *J. Am. Chem. Soc.* **2004**, *126*, 6252; i) M. Silva, M. Augusta Antunes, M. Dias, Â. Domingos, I. Corderio dos Santos, J. Marçalo, N. Marques, *Dalton Trans.* **2005**, 3353; j) M. Xue, Y. Yao, Q. Shen, Y. Zhang, *J. Organomet. Chem.* **2005**, *690*, 4685; k) M. A. Antunes, M. Dias, B. Monterio, Â. Domingos, I. C. Santos, N. Marques, *Dalton Trans.* **2006**, 3368; l) A. Sinha, R. R. Schrock, P. Müller, A. H. Hoveyda, *Organometallics* **2006**, *25*, 4621; m) Z. J. Tonzetich, Y. C. Lam, P. Müller, R. R. Schrock, *Organometallics* **2007**, *26*, 475.
- [220] S. Conejero, Y. Canac, F. S. Tham, G. Bertrand, *Angew. Chem. Int. Ed.* **2004**, *43*, 4089.
- [221] E. Ihara, T. Todaka, K. Inoue, *J. Polym. Sci., Part A* **2004**, *42*, 31.
- [222] a) J. S. DePue, D. B. Collum, *J. Am. Chem. Soc.* **1988**, *110*, 5518; b) J. S. DePue, D. B. Collum, *J. Am. Chem. Soc.* **1988**, *110*, 5524.
- [223] a) H. Hope, M. M. Olmstead, B. D. Murray, P. P. Power, *J. Am. Chem. Soc.* **1985**, *107*, 712; b) J. Guan, S. Jin, Y. Lin, Q. Shen, *Organometallics* **1992**, *11*, 2483; c) J.-I. Song, S. Gambarotta, *Chem.–Eur. J.* **1996**, *2*, 1258; d) M. Tayebani, S. Gambarotta, G. Yap, *Organometallics* **1998**, *17*, 3639; e) Y. Yao, X. Lu, Q. Shen, K. Yu, *J. Chem. Crystallogr.* **2004**, *34*, 275.
- [224] a) H. Schumann, E. Palamidis, J. Loebel, *J. Organomet. Chem.* **1990**, *390*, 45; b) L. Mao, Q. Shen, S. Jin, *Polyhedron* **1994**, *13*, 1023; c) J. Guan, Q. Shen, S. Jin, Y. Lin, *Polyhedron* **1994**, *13*, 1695; d) W.-K. Wong, L. Zhang, F. Xue, T. C. W. Mak, *Polyhedron* **1997**, *16*, 345; e) W.-K. Wong, L. Zhang, F. Xue, T. C. W. Mak, *Polyhedron* **1997**, *16*, 2013.
- [225] J. G. Reynolds, A. Zalkin, D. H. Templeton, N. M. Edelstein, *Inorg. Chem.* **1977**, *16*, 1090.
- [226] a) J. Kim, S. J. Bott, D. M. Hoffman, *Inorg. Chem.* **1998**, *37*, 3835; b) J. Pauls, B. Neumüller, *Inorg. Chem.* **2001**, *40*, 121.
- [227] a) R. K. Minhas, Y. Ma, J.-I. Song, S. Gambarotta, *Inorg. Chem.* **1996**, *35*, 1866; b) M. Karl, A. Dashti-Mommertz, B. Neumüller, K. Dehnicke, *Z. Anorg. Allg. Chem.* **1998**, *624*, 355; c) M. Karl, K. Harms, K. Dehnicke, *Z. Anorg. Allg. Chem.* **1999**, *625*, 1774; d) Y. Wang, Q. Shen, F. Xue, K. Yu, *Organometallics* **2000**, *19*, 357; e) P. Reiss, D. Fenske, *Z. Anorg. Allg. Chem.* **2000**, *626*, 1317; f) M. T. Gamer, P. W. Roesky, *Inorg. Chem.* **2005**, *44*, 5963.
- [228] W. Clegg, A. J. Edwards, F. S. Mair, P. M. Nolan, *Chem. Commun.* **1998**, 23.
- [229] R. P. Davies, P. R. Raithby, R. Snaith, *Angew. Chem. Int. Ed.* **1997**, *36*, 1215.
- [230] a) F. Becke, F. W. Heinemann, T. Rüffer, P. Wiegeleben, R. Boese, D. Blaeser, D. Steinborn, *J. Organomet. Chem.* **1997**, *548*, 205; b) U. Braun, T. Haberer, H. Nöth, H. Piotrowski, M. Warchhold, *Eur. J. Inorg. Chem.* **2002**, 1132; c) M. Gärtner, H. Görls, M. Westerhausen, *Acta. Crystallogr. Sect. E* **2007**, *E63*, m2287; d) M. Gärtner, H. Görls, M. Westerhausen, *Acta. Crystallogr. Sect. E* **2007**, *E63*, m2289.
- [231] E. R. Hurley, X. He, S. N. Brown, K. W. Henderson, *J. Am. Chem. Soc.* **2009**, *131*, 6056.

- [232] C. Glock, H. Görls, M. Westerhausen, *Eur. J. Inorg. Chem.* **2011**, 5288.
- [233] P. B. Hitchcock, A. V. Khvostov, M. F. Lappert, A. V. Protchenko, *J. Organomet. Chem.* **2002**, 647, 198.
- [234] B. J. Fleming, P. García-Álvarez, E. Keating, A. R. Kennedy, C. T. O'Hara, *Inorg. Chim. Acta.* **2012**, 384, 154.
- [235] W. Clegg, B. Conway, P. García-Álvarez, A. R. Kennedy, R. E. Mulvey, L. Russo, J. Sassmanshausen, T. Tuttle, *Chem.–Eur. J.* **2009**, 15, 10702.
- [236] a) V. L. Blair, L. M. Carrella, W. Clegg, B. Conway, R. W. Harrington, L. M. Hogg, J. Klett, R. E. Mulvey, E. Rentschler, L. Russo, *Angew. Chem. Int. Ed.* **2008**, 47, 6208; b) S. E. Baillie, W. Clegg, P. García-Álvarez, E. Hevia, A. R. Kennedy, J. Klett, L. Russo, *Chem. Commun.* **2011**, 47, 388.
- [237] J. Barker, D. Barr, N. D. R. Barnett, W. Clegg, I. Cragg-Hine, M. G. Davidson, R. P. Davies, S. M. Hodgson, J. A. K. Howard, M. Kilner, C. W. Lehmann, I. Lopez-Solera, R. E. Mulvey, P. R. Raithby, R. Snaith, *J. Chem. Soc., Dalton Trans.* **1997**, 951.
- [238] A. M. Belostotskii, H. E. Gottlieb, P. Aped, A. Hassner, *Chem.–Eur. J.* **1999**, 5, 449.
- [239] J. F. Allan, K. W. Henderson, A. R. Kennedy, S. J. Teat, *Chem. Commun.* **2000**, 1059.
- [240] C. A. Zechmann, T. J. Boyle, M. A. Rodriguez, R. A. Kemp, *Polyhedron* **2000**, 19, 2557.
- [241] C. A. Zechmann, T. J. Boyle, M. A. Rodriguez, R. A. Kemp, *Inorg. Chim. Acta.* **2001**, 319, 137.
- [242] M. Veith, D. Käfer, J. Koch, P. May, L. Stahl, V. Huch, *Chem. Ber.* **1992**, 125, 1033.
- [243] T.-Y. Her, C.-C. Chang, G.-H. Lee, S.-M. Peng, Y. Wang, *Inorg. Chem.* **1994**, 33, 99.
- [244] C.-C. Chang, W.-H. Lee, T.-Y. Her, G.-H. Lee, S.-M. Peng, Y. Wang, *J. Chem. Soc., Dalton Trans.* **1994**, 315.
- [245] E. Hevia, K. W. Henderson, A. R. Kennedy, R. E. Mulvey, *Organometallics* **2006**, 25, 1778.
- [246] M. Veith, M. Burkhart, V. Huch, *Angew. Chem. Int. Ed.* **2006**, 45, 5544.
- [247] S. S. Berg, D. T. Cowling, *J. Chem. Soc. (C)* **1971**, 1653.
- [248] P. García-Álvarez, A. R. Kennedy, C. T. O'Hara, K. Reilly, G. M. Robertson, *Dalton Trans.* **2011**, 5332.
- [249] N. M. Clark, P. García-Álvarez, A. R. Kennedy, C. T. O'Hara, G. M. Robertson, *Chem. Commun.* **2009**, 5835.
- [250] a) B. Conway, D. V. Graham, E. Hevia, A. R. Kennedy, J. Klett, R. E. Mulvey, *Chem. Commun.* **2008**, 2638; b) W. Clegg, B. Conway, D. V. Graham, E. Hevia, A. R. Kennedy, R. E. Mulvey, L. Russo, D. S. Wright, *Chem.–Eur. J.* **2009**, 15, 7074; c) W. Clegg, B. Conway, P. García-Álvarez, A. R. Kennedy, J. Klett, R. E. Mulvey, L. Russo, *Dalton Trans.* **2010**, 62.
- [251] B. Teclé, A. F. M. M. Rahman, J. P. Oliver, *J. Organomet. Chem.* **1986**, 317, 267.
- [252] D. M. Cousins, M. G. Davidson, C. J. Frankis, D. García-Vivo, M. F. Mahon, *Dalton Trans.* **2010**, 39, 8278.
- [253] B. L. Lucht, D. B. Collum, *Acc. Chem. Res.* **1999**, 32, 1035.
- [254] J. L. Dye, R. H. Huang, *Pure Appl. Chem.* **1993**, 65, 435.
- [255] M. Veith, S. Wiczorek, K. Fries, V. Huch, *Z. Anorg. Allg. Chem.* **2000**, 626, 1237.
- [256] T. W. Hudnall, C. W. Bielawski, *J. Am. Chem. Soc.* **2009**, 131, 16039.
- [257] a) H. Hao, H. W. Roesky, Y. Ding, C. Cui, M. Schormann, H.-G. Schmidt, M. Noltemeyer, B. Žemva, *J. Fluorine Chem.* **2002**, 115, 143; b) N. D. R. Barnett, W. Clegg, A. R. Kennedy, R. E. Mulvey, S. Weatherstone, *Chem. Commun.* **2005**, 375; c) M. Reinmuth, U. Wild, D. Rudolf, E. Kaifer, M. Enders, H. Wadepohl, H.-J. Himmel, *Eur. J. Inorg. Chem.* **2009**, 4795; d) J. Spielmann, D. F.-J. Piesik, S. Harder, *Chem.–Eur. J.* **2010**, 16, 8307.
- [258] D. V. Graham, E. Hevia, A. R. Kennedy, R. E. Mulvey, *Organometallics* **2006**, 25, 3297.

- [259] M. Geissler, J. Kopf, E. Weiss, *Chem. Ber.* **1989**, *122*, 1395.
- [260] A. R. Kennedy, R. E. Mulvey, C. T. O'Hara, G. M. Robertson, S. D. Robertson, *Angew. Chem. Int. Ed.* **2011**, *50*, 8375.
- [261] a) N. H. Buttrus, C. Eaborn, P. B. Hitchcock, J. D. Smith, J. G. Stamper, A. C. Sullivan, *J. Chem. Soc., Chem. Commun.* **1986**, 969; b) T. A. Bazhenova, A. V. Kulikov, A. F. Shestakov, A. E. Shilov, M. Y. Antipin, K. A. Lyssenko, Y. T. Struchkov, V. D. Makhaev, *J. Am. Chem. Soc.* **1995**, *117*, 12176.
- [262] D. Barr, R. Snaith, D. S. Wright, R. E. Mulvey, K. Wade, *J. Am. Chem. Soc.* **1987**, *109*, 7891.
- [263] a) D. Barr, W. Clegg, R. E. Mulvey, R. Snaith, *J. Chem. Soc., Chem. Commun.* **1984**, 226; b) W. Clegg, S. T. Liddle, R. E. Mulvey, A. Robertson, *Chem. Commun.* **2000**, 223; c) T. S. De Vries, A. Goswami, L. R. Liou, J. M. Gruver, E. Jayne, D. B. Collum, *J. Am. Chem. Soc.* **2009**, *131*, 13142.
- [264] T. Chivers, A. Downard, M. Parvez, *Inorg. Chem.* **1999**, *38*, 4347.
- [265] D. Woodruff, M. Bodensteiner, D. A. Sells, R. E. P. Winpenny, R. A. Layfield, *Dalton Trans.* **2011**, *40*, 10918.
- [266] Prepared by postdoc Dr. Stuart Robertson.
- [267] a) G. Ferguson, M. Parvez, *Acta Crystallogr. Sect. B* **1979**, *B35*, 2207; b) C. Slugovcl, C. Gemel, J.-Y. Shen, D. Doberer, R. Schmid, K. Kirchner, K. Mereiter, *Monatsh. Chem.* **1999**, *130*, 363.
- [268] A. G. Blackman, *Polyhedron* **2005**, *24*, 1.
- [269] G. J. P. Britovsek, J. England, A. J. P. White, *Inorg. Chem.* **2005**, *44*, 8125.
- [270] M. G. Davidson, D. Garcia-Vivo, A. R. Kennedy, R. E. Mulvey, S. D. Robertson, *Chem.–Eur. J.* **2011**, *17*, 3364.
- [271] a) A. Schnepf, G. Stösser, H. Schnöckel, *J. Am. Chem. Soc.* **2000**, *122*, 9178; b) A. Schnepf, B. Jee, H. Schnöckel, *Inorg. Chem.* **2003**, *42*, 7731; c) J. Steiner, G. Stöber, H. Schnöckel, *Angew. Chem. Int. Ed.* **2004**, *43*, 302; d) A. Schnepf, R. Köppe, E. Weckert, H. Schnöckel, *Chem.–Eur. J.* **2004**, *10*, 1977.
- [272] K. W. Henderson, A. E. Dorigo, P. G. Williard, P. R. Bernstein, *Angew. Chem. Int. Ed. Engl.* **1996**, *35*, 1322.
- [273] M. C. Copey, M. S. Balakrishna, T. Chivers, *Acta Crystallogr. Sect. E* **2006**, *E62*, m1680.
- [274] H. Riffel, B. Neumüller, E. Fluck, *Z. Anorg. Allg. Chem.* **1993**, *619*, 1682.
- [275] H. Nöth, R. Waldhör, *Z. Naturforsch., B: Chem. Sci.* **1998**, *53*, 1525.
- [276] C. L. Raston, B. W. Skelton, C. R. Whitaker, A. H. White, *J. Chem. Soc., Dalton Trans.* **1988**, 987.
- [277] Prepared by Erasmus student Maria Àngels Subirana Manzanares.
- [278] D. Barr, M. J. Doyle, R. E. Mulvey, P. R. Raithby, R. Snaith, D. S. Wright, *J. Chem. Soc., Chem. Commun.* **1988**, 145.
- [279] W. M. Boesveld, P. B. Hitchcock, M. F. Lappert, D.-S. Liu, S. Tian, *Organometallics* **2000**, *19*, 4030.
- [280] a) F. Gingl, W. Hiller, J. Strähle, H. Borgholte, K. Dehnjcke, *Z. Anorg. Allg. Chem.* **1991**, *606*, 91; b) T. Morawitz, H.-W. Lerner, M. Bolte, *Acta Crystallogr. Sect. E* **2007**, *E63*, m1923.
- [281] a) S. T. Liddle, W. Clegg, *J. Chem. Soc., Dalton Trans.* **2001**, 402; b) S. T. Liddle, W. Clegg, C. A. Morrison, *Dalton Trans.* **2004**, 2514.
- [282] D. F. Shriver, M. A. Drezdson, in *The Manipulation of Air-sensitive Compounds*, 2nd ed., Wiley-Blackwell, New York, **1986**, p. 88.
- [283] W. L. F. Armarego, D. D. Perrin, *Purification of Laboratory Chemicals*, 4th ed., Butterworth-Heinemann, Oxford, **1996**.
- [284] G. M. Sheldrick, *Acta Crystallogr. Sect. A* **2008**, *A64*, 112.
- [285] C. Schade, W. Bauer, P. v. R. Schleyer, *J. Organomet. Chem.* **1985**, *295*, c25.

- [286] D. Hoffmann, W. Bauer, F. Hampel, N. J. R. van Eikema Hommes, P. v. R. Schleyer, P. Otto, U. Pieper, D. Stalke, D. S. Wright, R. Snaith, *J. Am. Chem. Soc.* **1994**, *116*, 528.
- [287] R. Sott, J. Granander, C. Williamson, G. Hilmersson, *Chem.–Eur. J.* **2005**, *11*, 4785.
- [288] A. Johansson, Ö. Davidsson, *Chem.–Eur. J.* **2001**, *7*, 3461.
- [289] a) D. Catel, F. Chevallier, F. Mongin, P. C. Gros, *Eur. J. Org. Chem.* **2012**, 53; b) D. Catel, O. Payen, F. Chevallier, F. Mongin, P. C. Gros, *Tetrahedron* **2012**, *68*, 4018.
- [290] R. Noyori, S. Suga, K. Kawai, S. Okada, M. Kitamura, *Pure Appl. Chem.* **1988**, *60*, 1597.
- [291] C. V. Cárdenas, M. Á. M. Hernández, J.-M. Grévy, *Dalton Trans.* **2010**, 39, 6441.
- [292] P. D. Beer, P. A. Gale, *Angew. Chem. Int. Ed.* **2001**, *40*, 486.
- [293] *Chem. Soc. Rev.* **2010**, 39, 3581.
- [294] H. Chen, R. A. Bartlett, H. V. R. Dias, M. M. Olmstead, P. P. Power, *J. Am. Chem. Soc.* **1989**, *111*, 4338.
- [295] U. Pieper, S. Walter, U. Klingebiel, D. Stalke, *Angew. Chem. Int. Ed. Engl.* **1990**, *29*, 209.
- [296] K. Dippel, U. Klingebiel, D. Schmidt-Base, *Z. Anorg. Allg. Chem.* **1993**, *619*, 836.
- [297] M. Jendras, U. Klingebiel, J. Niesmann, M. Noltemeyer, *Phosphorus, Sulfer, Silicon, Relat. Elem.* **1998**, *142*, 1.
- [298] J. Niesmann, U. Klingebiel, C. Ropken, M. Noltemeyer, R. Herbst-Irmer, *Main Group Chem.* **1998**, *2*, 297.
- [299] L. Marcus, U. Klingebiel, L. Lameyer, D. Stalke, *Z. Anorg. Allg. Chem.* **1998**, *624*, 1041.
- [300] P. Neugebauer, U. Klingebiel, M. Noltemeyer, *Z. Naturforsch., B: Chem. Sci.* **2000**, *55*, 913.
- [301] C. Reiche, U. Klingebiel, M. Noltemeyer, *Z. Naturforsch., B: Chem. Sci.* **2003**, *58*, 939.
- [302] F. Antolini, B. Gehrhus, P. B. Hitchcock, M. F. Lappert, J. C. Sloatweg, *Dalton Trans.* **2004**, 3288.
- [303] H.-W. Lerner, I. Sanger, F. Schodel, K. Polborn, M. Bolte, M. Wagner, *Z. Naturforsch., B: Chem. Sci.* **2007**, *62*, 1285.
- [304] M. Veith, F. Goffing, V. Huch, *Chem. Ber.* **1988**, *121*, 943.
- [305] B. Tecklenburg, U. Klingebiel, D. Schmidt-Base, *J. Organomet. Chem.* **1992**, *426*, 287.
- [306] M. D. Fryzuk, J. B. Love, S. J. Rettig, *Chem. Commun.* **1996**, 2783.
- [307] L. Grocholl, L. Stahl, R. Staples, *Inorg. Chem.* **1998**, *37*, 5036.
- [308] M. D. Fryzuk, C. M. Kozak, M. R. Bowdridge, W. Jin, D. Tung, B. O. Patrick, S. J. Rettig, *Organometallics* **2001**, *20*, 3752.
- [309] U. Klingebiel, C. Matthes, A. Ringe, J. Magull, *Z. Naturforsch., B: Chem. Sci.* **2009**, *64*, 525.
- [310] M. Veith, A. Rammo, R. Heim, V. Huch, *Z. Anorg. Allg. Chem.* **2010**, *636*, 320.
- [311] I. Hemme, M. Schäfer, R. Herbst-Irmer, U. Klingebiel, *J. Organomet. Chem.* **1995**, *493*, 223.
- [312] T. Kaehler, F. Olbrich, *Private Communication to CCDC* **2002**, CCDC code: VABFIO.
- [313] M. Veith, O. Schutt, V. Huch, *Z. Anorg. Allg. Chem.* **1999**, *625*, 1155.
- [314] I. Hemme, U. Klingebiel, S. Freitag, D. Stalke, *Z. Anorg. Allg. Chem.* **1995**, *621*, 2093.
- [315] P. G. Williard, Q.-Y. Liu, *J. Org. Chem.* **1994**, *59*, 1596.
- [316] L. T. J. Evans, F. Geoffrey, N. Cloke, M. P. Coles, P. B. Hitchcock, *Inorg. Chim. Acta.* **2007**, *360*, 1258.
- [317] M. Haase, G. M. Sheldrick, *Acta Crystallogr. Sect. C* **1986**, *C42*, 1009.



- [318] E. Egert, U. Kliebisch, U. Klingebiel, D. Schmidt, *Z. Anorg. Allg. Chem.* **1987**, 548, 89.
- [319] K. Dippel, U. Klingebiel, G. M. Sheldrick, D. Stalke, *Chem. Ber.* **1987**, 120, 611.
- [320] P. G. Williard, Q.-Y. Liu, L. Lochmann, *J. Am. Chem. Soc.* **1992**, 114, 348.
- [321] S. Walter, U. Klingebiel, M. Noltemeyer, *Chem. Ber.* **1992**, 125, 783.
- [322] G. Boche, I. Langlotz, M. Marsch, K. Harms, G. Frenking, *Angew. Chem. Int. Ed. Engl.* **1993**, 32, 1171.
- [323] L. M. Atagi, D. M. Hoffman, D. C. Smith, *Inorg. Chem.* **1993**, 32, 5084.
- [324] D. Grosskopf, L. Marcus, U. Klingebiel, M. Noltemeyer, *Phosphorus, Sulfer, Silicon, Relat. Elem.* **1994**, 97, 113.
- [325] M. Veith, M. Zimmer, K. Fries, J. Bohnlein-Maus, V. Huch, *Angew. Chem. Int. Ed. Engl.* **1996**, 35, 1529.
- [326] D. R. Armstrong, M. G. Davidson, R. P. Davies, H. J. Mitchell, R. M. Oakley, P. R. Raithby, R. Snaith, S. Warren, *Angew. Chem. Int. Ed. Engl.* **1996**, 35, 1942.
- [327] M. D. Fryzuk, V. Hoffman, E. J. Kickham, S. J. Rettig, S. Gambarotta, *Inorg. Chem.* **1997**, 36, 3480.
- [328] C. F. Caro, P. B. Hitchcock, M. F. Lappert, M. Layh, *Chem. Commun.* **1998**, 1297.
- [329] K. W. Henderson, P. G. Williard, *Organometallics* **1999**, 18, 5620.
- [330] B. Jaschke, N. Helmold, I. Muller, T. Pape, M. Noltemeyer, R. Herbst-Irmer, U. Klingebiel, *Z. Anorg. Allg. Chem.* **2002**, 628, 2071.
- [331] S. Kliem, U. Klingebiel, M. Noltemeyer, S. Schmatz, *J. Organomet. Chem.* **2005**, 690, 1100.
- [332] J. F. Eichler, O. Just, W. S. Rees Junior, *ACS. Sym. Ser.* **2006**, 917, 122.
- [333] S. Aharonovich, M. Kapon, M. Botoshanski, M. S. Eisen, *Organometallics* **2008**, 27, 1869.
- [334] T. Chen, W. Hunks, P. S. Chen, G. T. Stauf, T. M. Cameron, C. Xu, A. G. DiPasquale, A. L. Rheingold, *Eur. J. Inorg. Chem.* **2009**, 2047.
- [335] K. Dippel, U. Klingebiel, M. Noltemeyer, F. Pauer, G. M. Sheldrick, *Angew. Chem. Int. Ed. Engl.* **1988**, 27, 1074.
- [336] K. Dippel, U. Klingebiel, T. Kottke, F. Pauer, G. M. Sheldrick, D. Stalke, *Chem. Ber.* **1990**, 123, 237.
- [337] I. Hemme, B. Tecklenburg, M. Noltemeyer, U. Klingebiel, *Chem. Ber.* **1995**, 128, 351.
- [338] U. Klingebiel, S. Schmatz, E. Gellermann, C. Drost, M. Noltemeyer, *Monatsh. Chem.* **2001**, 132, 1105.
- [339] Q. Li, J. Rong, S. Wang, S. Zhou, L. Zhang, X. Zhu, F. Wang, S. Yang, Y. Wei, *Organometallics* **2011**, 30, 992.
- [340] U. Klingebiel, M. Noltemeyer, H.-J. Rakebrandt, *Z. Anorg. Allg. Chem.* **1997**, 623, 281.
- [341] M. K. Rofouei, G. A. Lawless, A. Morsali, P. B. Hitchcock, *Inorg. Chim. Acta.* **2006**, 359, 3815.
- [342] M. Veith, J. Böhnlein, V. Huch, *Chem. Ber.* **1989**, 122, 841.
- [343] Y. Sarazin, S. J. Coles, D. L. Hughes, M. B. Hursthouse, M. Bochmann, *Eur. J. Inorg. Chem.* **2006**, 3211.
- [344] M. Veith, J. Böhnlein, *Chem. Ber.* **1989**, 122, 603.
- [345] W. J. Evans, D. B. Rego, J. W. Ziller, *Inorg. Chem.* **2006**, 45, 3437.
- [346] A. M. Domingos, G. M. Sheldrick, *Acta. Crystallogr. Sect. B* **1974**, B30, 517.
- [347] J. Schneider, E. Popowski, H. Reinke, *Z. Anorg. Allg. Chem.* **2003**, 629, 55.
- [348] R. W. Alder, M. E. Blake, C. Bortolotti, S. Bufali, C. P. Butts, E. Linehan, J. M. Oliva, A. G. Orpen, M. J. Quayle, *Chem. Commun.* **1999**, 241.
- [349] P. L. Arnold, I. J. Casely, Z. R. Turner, R. Bellabarba, R. B. Tooze, *Dalton Trans.* **2009**, 7236.

- [350] J.-C. Buffet, J. Okuda, *Dalton Trans.* **2011**, 40, 7748.